

Results of Blind Testing for the Program to Assess the Reliability of Emerging Nondestructive Techniques

AVAILABILITY OF REFERENCE MATERIALS IN NRC PUBLICATIONS

NRC Reference Material

As of November 1999, you may electronically access NUREG-series publications and other NRC records at the NRC's Public Electronic Reading Room at <http://www.nrc.gov/reading-rm.html>. Publicly released records include, to name a few, NUREG-series publications; *Federal Register* notices; applicant, licensee, and vendor documents and correspondence; NRC correspondence and internal memoranda; bulletins and information notices; inspection and investigative reports; licensee event reports; and Commission papers and their attachments.

NRC publications in the NUREG series, NRC regulations, and Title 10, "Energy," in the *Code of Federal Regulations* may also be purchased from one of these two sources.

1. The Superintendent of Documents

U.S. Government Publishing Office
Mail Stop SSOP
Washington, DC 20402-0001
Internet: <http://bookstore.gpo.gov>
Telephone: 1-866-512-1800
Fax: (202) 512-2104

2. The National Technical Information Service

5301 Shawnee Road
Alexandria, VA 22161-0002
<http://www.ntis.gov>
1-800-553-6847 or, locally, (703) 605-6000

A single copy of each NRC draft report for comment is available free, to the extent of supply, upon written request as follows:

U.S. Nuclear Regulatory Commission

Office of Administration
Publications Branch
Washington, DC 20555-0001
E-mail: distribution_resource@nrc.gov
Facsimile: (301) 415-2289

Some publications in the NUREG series that are posted at the NRC's Web site address <http://www.nrc.gov/reading-rm/doc-collections/nuregs> are updated periodically and may differ from the last printed version. Although references to material found on a Web site bear the date the material was accessed, the material available on the date cited may subsequently be removed from the site.

Non-NRC Reference Material

Documents available from public and special technical libraries include all open literature items, such as books, journal articles, transactions, *Federal Register* notices, Federal and State legislation, and congressional reports. Such documents as theses, dissertations, foreign reports and translations, and non-NRC conference proceedings may be purchased from their sponsoring organization.

Copies of industry codes and standards used in a substantive manner in the NRC regulatory process are maintained at—

The NRC Technical Library

Two White Flint North
11545 Rockville Pike
Rockville, MD 20852-2738

These standards are available in the library for reference use by the public. Codes and standards are usually copyrighted and may be purchased from the originating organization or, if they are American National Standards, from—

American National Standards Institute

11 West 42nd Street
New York, NY 10036-8002
<http://www.ansi.org>
(212) 642-4900

Legally binding regulatory requirements are stated only in laws; NRC regulations; licenses, including technical specifications; or orders, not in NUREG-series publications. The views expressed in contractor-prepared publications in this series are not necessarily those of the NRC.

The NUREG series comprises (1) technical and administrative reports and books prepared by the staff (NUREG-XXXX) or agency contractors (NUREG/CR-XXXX), (2) proceedings of conferences (NUREG/CP-XXXX), (3) reports resulting from international agreements (NUREG/IA-XXXX), (4) brochures (NUREG/BR-XXXX), and (5) compilations of legal decisions and orders of the Commission and Atomic and Safety Licensing Boards and of Directors' decisions under Section 2.206 of NRC's regulations (NUREG-0750).

DISCLAIMER: This report was prepared as an account of work sponsored by an agency of the U.S. Government. Neither the U.S. Government nor any agency thereof, nor any employee, makes any warranty, expressed or implied, or assumes any legal liability or responsibility for any third party's use, or the results of such use, of any information, apparatus, product, or process disclosed in this publication, or represents that its use by such third party would not infringe privately owned rights.

Results of Blind Testing for the Program to Assess the Reliability of Emerging Nondestructive Techniques

Manuscript Completed: February 2016

Date Published: June 2017

Prepared by:

R. M. Meyer and P. G. Heasler

Pacific Northwest National Laboratory

P.O. Box 999

Richland, WA 99352

I. Prokofiev and B. Lin, NRC Project Managers

NRC Job Code V6286

Office of Nuclear Regulatory Research

ABSTRACT

The U.S. Nuclear Regulatory Commission (NRC) has established the Program to Assess the Reliability of Emerging Nondestructive Techniques (PARENT) whose goal was to investigate the performance of current emerging and perspective novel nondestructive examination (NDE) procedures and techniques to find flaws in nickel-alloy welds and base materials. This was performed by conducting a series of open and blind international round-robin tests on a set of nickel alloy piping components that include large-bore dissimilar metal welds (LBDMW), small-bore dissimilar metal welds (SBDMW), and bottom-mounted instrumentation (BMI) penetration welds. The project was divided into open and blind testing portions for the purpose of separating the evaluation of novel techniques that are at a stage of relative immaturity for field testing and which were implemented by teams that may not have significant experience in conducting field examinations (open testing) from the evaluation of more established techniques implemented by commercial inspection vendors (blind testing). The objective of blind testing was to address a cross-cutting need identified as a goal by all international collaborators of PARENT to obtain quantitative estimates of the performance of the latest nondestructive evaluation inspection techniques used commercially in the field for detection and accurate sizing of primary water stress corrosion cracks (PWSCC) or interdendritic stress corrosion cracks (IDSCC). The data generated by this effort provides empirical bases that can support regulatory positions and which can inform analyses of the effectiveness of NDE and in-service inspection, more generally, by each country based on each country's specific laws, codes, standards, and regulations.

PARENT was a follow-on to the Program for Inspection of Nickel Alloy Components (PINIC), which was based on the Bilateral International Agreements with participants and the in-kind contribution of resources from organizations of Finland, Japan, Republic of Korea, Sweden, and the United States of America to evaluate several nondestructive techniques for detection and characterization of PWSCC and IDSCC in SBDMW and BMI components. In February 2012, the NRC conducted new agreements with VTT Technical Research Centre of Finland, Nuclear Regulation Authority of Japan, Korea Institute of Nuclear Safety, Swedish Radiation Safety Authority, and Swiss Federal Nuclear Safety Inspectorate to establish PARENT to conduct a series of round-robin tests on SBDMWs, BMIs, and LBDMWs. In PARENT blind testing, inspections were performed on two SBDMWs, six LBDMWs, five BMIs, and one weld overlay test block. All of the simulated flaws in SBDMWs and LBDMWs were cracks; mostly tightened solidification cracks and a few laboratory-grown SCC flaws. The inspection procedures employed in blind testing included combinations and variations of conventional ultrasonic testing (UT), phased-array UT (PAUT), UT time-of-flight diffraction (TOFD), and eddy current testing techniques.

Round-robin testing was performed in PARENT to build on the experience in PINIC. Whereas PINIC obtained data for SBDMW components, PARENT obtained data from both SBDMW and LBDMW components so that an estimate in the difference in performance for each type of component could be obtained and to obtain estimates of performance for techniques applied to the inner diameter (I.D.) and outer diameter (O.D.) surfaces of LBDMWs. In PARENT, LBDMW and SBDMW test blocks had near ideal surface conditions. Thus, the results obtained from these test blocks provide a quantitative measure of performance that can be achieved by I.D. access of components with I.D. surface preparation, relative to performance that can be achieved by O.D. surface access.

FOREWORD

Leakage events due to primary water stress corrosion cracking (PWSCC) or interdendritic stress corrosion cracking (IDSCC) have been recorded in the United States and internationally. This cracking has been observed at several weld locations in reactor coolant systems including penetrations to the reactor vessel (e.g., control rod drive mechanism (CRDM) penetrations, bottom-mounted instrumentation (BMI) penetrations, and nozzle penetrations), and nozzle penetrations on steam generator and pressurizer components. In-service inspections (ISI) are conducted at nuclear power plants to detect cracks before leakage occurs. The effectiveness of ISI is dependent on several factors such as the frequency with which periodic examinations occur, human factors, the performance capability of the nondestructive examination (NDE) procedures and techniques used, etc. Leakage events, both domestic and international, have indicated a need for additional research to evaluate the performance of NDE procedures and techniques for the detection and sizing of PWSCC and IDSCC flaws in reactor components.

In February 2012, the U.S. Nuclear Regulatory Commission executed agreements with organizations in Finland, Japan, Republic of Korea, Sweden, Switzerland, and the United States to establish the Program to Assess the Reliability of Emerging Nondestructive Techniques (PARENT) to investigate the performance of current and emerging NDE techniques to find flaws in nickel-alloy welds and base material. This assessment was performed by conducting a series of open and blind international round-robin tests on a set of component mock-ups. The project was divided into open and blind testing to separate the evaluation of novel techniques implemented by nonqualified teams from the evaluation of more established techniques implemented by commercial inspection service providers. The objective of the blind test was to obtain quantitative empirical estimates of the performance of contemporary NDE inspection procedures and techniques used within the industry to determine which of these may be more reliable for detecting and accurate sizing of PWSCC or IDSCC flaws. The objective of the open testing was to evaluate the performance of novel NDE procedures and techniques that have not yet reached the maturity appropriate for field testing.

The purpose of this report is to publish the results of the detection and sizing analyses performed on data collected in blind testing for PARENT. The results from open testing are documented in another report that is under preparation. The PARENT blind test results provide quantified estimates for the performance of various NDE procedures as applied to DMW test blocks with crack defects. The data generated from PARENT provides empirical evidence of the impact of test block size and procedure variables on NDE performance. Although the test conditions were less challenging than field conditions, data were collected for all test blocks and procedures under consistent conditions. Thus, conclusions may be derived regarding relative performances that should also be applicable under field conditions. The results generated from blind testing can also be used to inform analyses of the effectiveness of NDE and ISI performed in nuclear power plants. The data generated by the PARENT blind testing provides insight into capabilities of current nondestructive methods used to detect cracks in reactor components and the data from the open testing will provide insight into capabilities of more experimental nondestructive methods. These insights can be used in developing regulatory positions and to help direct additional research activities.

TABLE OF CONTENTS

ABSTRACT	iii
FOREWORD	v
LIST OF FIGURES	xi
LIST OF TABLES	xvii
EXECUTIVE SUMMARY	xxi
ACKNOWLEDGMENTS	xxv
ACRONYMS	xxvii
DEFINITIONS	xxix
1 INTRODUCTION	1-1
1.1 Quick-Blind Study.....	1-2
1.2 Bottom-Mounted Instrumentation Test Blocks	1-2
1.3 Weld Overlay Test Block.....	1-2
1.4 PWSCC/IDSCC Nomenclature	1-2
1.5 PARENT Organization	1-3
1.6 Organization of This Report	1-3
2 TEST BLOCK DESCRIPTIONS	2-1
2.1 Bottom-Mounted Instrumentation Test Blocks	2-1
2.2 Small-Bore Dissimilar Metal Weld Test Blocks	2-6
2.3 Large-Bore Dissimilar Metal Weld Test Blocks	2-7
2.4 Weld Overlay Test Block.....	2-8
2.5 Simulated Flaw Types.....	2-9
2.5.1 Laboratory-Grown SCC [P13, P15, P16, and P17]	2-10
2.5.2 Thermal Fatigue Cracks [P6, P8, and P9].....	2-12
2.5.3 Weld Solidification Cracks [P35, P40, and P33]	2-13
2.5.4 Electrical Discharge Machined Notches [P27]	2-13
2.5.5 Mechanical Fatigue Cracks [P27]	2-14
2.5.6 Welding Defects [P25, P26, P27, and P40]	2-14
2.6 True-State Determination	2-14
3 TECHNIQUES AND PROCEDURES DESCRIPTIONS	3-1
3.1 Procedure Summary Data Sheets	3-1
3.2 Ultrasonic Testing Background	3-3
3.2.1 Conventional Ultrasonic Testing Concepts	3-4
3.2.2 Time-of-Flight Diffraction.....	3-6
3.2.3 Phased-Array UT	3-7
3.3 Eddy Current Techniques	3-11
4 DATA OVERVIEW	4-1
4.1 Data Reporting.....	4-1

4.2	Records Collection Overview Summary	4-5
4.3	Scoring Procedure Used for PARENT Blind Round Robin	4-7
4.4	Multiple Indications Associated with One Flaw	4-9
4.5	Multiple Flaws Associated with One Indication	4-10
4.6	Probability of Detection Representation.....	4-14
4.7	Sizing Analysis for PARENT Blind Round-Robin Test.....	4-16
5	DATA RESULTS	5-1
5.1	Results for DMW Test Blocks	5-1
5.1.1	Quick-Blind Testing Results	5-1
5.1.2	DMW Detection and False Call Rate Summary	5-4
5.1.3	DMW Depth Sizing Summary	5-16
5.1.4	DMW Length Sizing Summary	5-32
5.2	Results for BMI Test Blocks.....	5-47
5.2.1	BMI Detection and False Call Rate Summary.....	5-47
5.2.2	BMI Depth Sizing Summary	5-48
5.2.3	BMI Length Sizing Summary	5-49
5.3	Results for WOL Test Blocks (P27)	5-49
6	ANALYSIS OF PARENT RESULTS	6-1
6.1	Influence of Variables on Detection and Sizing Performance.....	6-1
6.2	Comparison of Procedures and Procedure Type Performances	6-8
6.3	Quick-Blind Test Comparison.....	6-11
6.4	Influence of Tolerance Bounds on Detection Results	6-12
6.5	ASME Procedure for Combining Flaws	6-14
7	COMPARISON OF PARENT VS. PINC	7-1
7.1	Comparison of Performance on PARENT and PINC DMW Test Blocks	7-1
7.2	Comparison of Performance on PARENT and PINC BMI Test Blocks.....	7-3
7.3	Review of PINC Conclusions and Recommendations	7-8
7.3.1	Probability of Detection Performance	7-8
7.3.2	Sizing Performance.....	7-8
8	SUMMARY OF PISC III AND PINC OUTCOMES	8-1
8.1	PISC III.....	8-1
8.2	PINC	8-1
9	CONCLUSIONS	9-1
10	REFERENCES	10-1
	APPENDIX A – TEST BLOCK INFORMATION.....	A-1
	APPENDIX B – SUMMARY OF BLIND TESTING PROCEDURES/TECHNIQUES	B-1
	APPENDIX C – PROCEDURE SUMMARY SHEETS	C-1
	APPENDIX D – SCORING PROCEDURE USED FOR PINC	D-1
	APPENDIX E – INDICATION PLOTS	E-1

APPENDIX F – PROBABILITY OF DETECTION CURVES	F-1
APPENDIX G – SIZING REGRESSION PLOTS	G-1
APPENDIX H – EFFECTIVENESS EVOLUTION OF DMW INSPECTION TECHNIQUES ASSESSED THROUGH THREE INTERNATIONAL RRTs	H-1

LIST OF FIGURES

Figure 1.1	Organization Chart for Steering Committee and Task Groups	1-3
Figure 2.1	Coordinate System Used for BMI Test Blocks: P6, P8, P9, P25, P26	2-2
Figure 2.2	Depiction of Configuration for BMI Test Block P25 with Labeled Dimensions	2-3
Figure 2.3	Depiction of Configuration for BMI Test Block P26 with Labeled Dimensions	2-4
Figure 2.4	Depiction of Configuration for BMI Test Blocks P6, P8, and P9 with Labeled Dimensions	2-5
Figure 2.5	Coordinate System Definition for SBDMW Test Blocks P35 and P40, and LBDMW Test Block P33	2-6
Figure 2.6	Coordinate System for LBDMW Test Blocks P15, P16, P17, and P45.....	2-7
Figure 2.7	Coordinate System for LBDMW Test Block P13.....	2-8
Figure 2.8	Coordinate System for WOL Test Block P37.....	2-9
Figure 2.9	Depiction of the Approach Used to Produce a Laboratory-Grown PWSCC/IDSCC	2-11
Figure 2.10	Flowchart of the Process Used to Produce a Laboratory-Grown PWSCC/IDSCC	2-11
Figure 2.11	Illustration of Typical Flaw Morphology in P13, P15, P16, and P17	2-12
Figure 2.12	Eddy Current Response from Flaw 2 of Test Block P9 Showing Evidence of Flaw Cluster Formation	2-13
Figure 3.1	Example of a Completed Procedure Summary Sheet for Illustration Purposes.....	3-3
Figure 3.2	Illustration of Pulse-Echo UT Applied at Refracted Angle, θ , for Examination of I.D. Cracks	3-4
Figure 3.3	Illustration of Pitch/Catch UT Applied for Examination of I.D. Cracks.....	3-4
Figure 3.4	Illustration of a Transmit-Receive Transducer	3-5
Figure 3.5	Illustration of Crack Tip Diffraction and Crack Depth Sizing Based on Tip Diffraction Signal and Corner Reflection.....	3-5
Figure 3.6	Illustration of Amplitude Drop Method for Flaw Sizing	3-6
Figure 3.7	Diagram of Time-of-Flight Diffraction Technique	3-7
Figure 3.8	Illustration of Time Delay Sequencing of Excitation of PAUT Transducer Elements to Achieve Beam Steering and Focusing.....	3-8
Figure 3.9	Illustration of Beam Skew and Beam Refraction Directions for Matrix PAUT Probe.....	3-8
Figure 3.10	Depiction of Sectorial Scanning with PAUT	3-9
Figure 3.11	Illustration of B-scan, C-scan, and D-scan Views for Displaying PAUT Data Responses	3-10
Figure 3.12	PAUT Data Represented as A-scan (top left), C-scan (top right), B- scan (bottom left), and D-scan (bottom right)	3-10
Figure 3.13	PAUT Data Represented as Sectorial Scan	3-11

Figure 3.14	Depiction of a Single Coil Eddy Current Probe with an Alternating Current Excitation, Induced Magnetic Fields, and Induced Eddy Currents. Disturbance of eddy current flow can be caused by existence of a defect.	3-12
Figure 3.15	Schematic Illustration of an Eddy Current Probe with Separate Coils for Field Excitation and for Signal Detection	3-12
Figure 3.16	Depiction of the Cross-Coil Eddy Current Probe Configuration	3-13
Figure 4.1	Technique Data Sheets for Techniques ET400Hz and TOFD.Ax for Fictitious Inspection 12.P89.1	4-3
Figure 4.2	Technique Data Sheet for Technique TOFD.Circ for Fictitious Inspection 12.P89.1	4-4
Figure 4.3	Inspection Summary Data Sheet for Fictitious Inspection 12.P89.1	4-4
Figure 4.4	Illustration of Tolerance (δX and δY) Applied Flaw True-State (in red) Dimensions for the Purpose of Scoring in PARENT	4-8
Figure 4.5	Probability of Detection versus Scoring Tolerance for DMW Test Data	4-8
Figure 4.6	Probability of Detection versus Scoring Tolerance for BMI Test Data	4-9
Figure 4.7	Depiction of Indication Plot Illustrating 2-D Representation of Test Block. The red filled rectangles represent the true-state (actual flaws), while red empty rectangles surrounding the flaws depict the scoring tolerance. Indications are shown as black empty rectangles.....	4-9
Figure 4.8	Indication Plot for ECT.135 Applied to P33 from X = 2000 mm to X = 2800 mm Illustrating Two Indications Intersecting the Region Bounded by the Tolerance Box	4-10
Figure 4.9	Illustration of Tolerance Divided Between Flaw and Multiple Indications Intersecting the Region Bounded by the Flaw Tolerance Box	4-10
Figure 4.10	Indication Plot for Procedure PAUT.108 Applied to Test Block P35 in PARENT Blind Testing (X – Y view, 0 mm–300 mm)	4-11
Figure 4.11	Indication Plot for Procedure UT.108 Applied to Test Block P35 in PARENT Blind Testing (X – Y view, 0 mm–300 mm)	4-12
Figure 4.12	Indication Plot for Procedure PAUT.115 Applied to Test Block P35 in PARENT Blind Testing (X – Y view, 0 mm–300 mm)	4-12
Figure 4.13	Indication Plot for Procedure UT.TOFD.117 Applied to Test Block P35 in PARENT Blind Testing (X – Y view, 0 mm–300 mm)	4-13
Figure 4.14	Indication Plot for Procedure PAUT.128 Applied to Test Block P35 in PARENT Blind Testing (X – Y view, 0 mm–300 mm)	4-13
Figure 4.15	Indication Plot for Procedure UT.134 Applied to Test Block P35 in PARENT Blind Testing (X – Y view, 0 mm–300 mm)	4-14
Figure 4.16	POD versus Depth (mm) for PAUT Procedures Applied to LBDMW Test Blocks with O.D. Access (w/o Quick-blind).....	4-15
Figure 4.17	Example of Sizing Regression Plot for Depth Sizing Results Obtained on LBDMW Test Blocks by Access to the I.D. Surface (dimensions are in mm).....	4-17
Figure 4.18	Length Sizing Fit (in mm) for UT.PAUT Procedures Applied to LBDMWs (O.D. Access – Quick-blind)	4-18

Figure 4.19	Depth Sizing Fit (in mm) for PAUT Procedures Applied to LBDMWs (I.D. Access – Quick-blind)	4-19
Figure 5.1	Probability of Detection versus Flaw Depth	5-2
Figure 5.2	Probability of Detection versus Flaw Length.....	5-2
Figure 5.3	POD versus Depth (mm) for All Procedures Applied to LBDMW Test Blocks with I.D. Access.....	5-6
Figure 5.4	POD versus Depth (mm) for All Procedures Applied to LBDMW Test Blocks with O.D. Access	5-7
Figure 5.5	POD versus Depth (mm) for All Procedures Applied to SBDMW Test Blocks with O.D. Access	5-7
Figure 5.6	POD versus Depth (mm) for PAUT Procedures Applied to LBDMW Test Blocks with O.D. Access	5-9
Figure 5.7	POD versus Depth (mm) for Conventional UT Procedures Applied to LBDMW Test Blocks with O.D.	5-9
Figure 5.8	POD versus Depth (mm) for PAUT Procedures Applied to SBDMW Test Blocks	5-10
Figure 5.9	POD versus Depth (mm) for Conventional UT Procedures Applied to SBDMW Test Blocks.....	5-10
Figure 5.10	POD versus Length (mm) for All Procedures Applied to LBDMW Test Blocks with I.D. Access.....	5-12
Figure 5.11	POD versus Length (mm) for All Procedures Applied to LBDMW Test Blocks with O.D. Access	5-13
Figure 5.12	POD versus Length (mm) for All Procedures Applied to SBDMW Test Blocks	5-13
Figure 5.13	Depth Sizing Fit (in mm) for PAUT Procedures Applied to LBDMWs (I.D. Access – Quick-blind)	5-20
Figure 5.14	Depth Sizing Fit (in mm) for UT.ECT Procedures Applied to LBDMWs (I.D. Access)	5-21
Figure 5.15	Depth Sizing Fit (in mm) for UT.ECT Procedures Applied to LBDMWs (I.D. Access – Blind + Quick-blind)	5-22
Figure 5.16	Depth Sizing Fit (in mm) for UT.PAUT Procedures Applied to LBDMWs (I.D. Access)	5-23
Figure 5.17	Depth Sizing Fit (in mm) for UT.PAUT Procedures Applied to LBDMWs (I.D. Access – Blind + Quick-blind)	5-24
Figure 5.18	Depth Sizing Fit (in mm) for UT.TOFD.ECT Procedures Applied to LBDMWs (I.D. Access)	5-25
Figure 5.19	Depth Sizing Fit (in mm) for PAUT Procedures Applied to LBDMWs (O.D. Access).....	5-26
Figure 5.20	Depth Sizing Fit (in mm) for Conventional UT Procedures Applied to LBDMWs (O.D. Access)	5-27
Figure 5.21	Depth Sizing Fit (in mm) for Conventional UT Procedures Applied to LBDMWs (O.D. Access – Blind + Quick-blind)	5-28
Figure 5.22	Depth Sizing Fit (in mm) for UT.PAUT Procedures Applied to LBDMWs (O.D. Access – Quick-blind).....	5-29

Figure 5.23	Depth Sizing Fit (in mm) for PAUT Procedures Applied to SBDMWs (O.D. Access).....	5-30
Figure 5.24	Depth Sizing Fit (in mm) for Conventional UT Procedures Applied to SBDMWs (O.D. Access).....	5-31
Figure 5.25	Depth Sizing Fit (in mm) for UT.TOFD Procedures Applied to SBDMWs (O.D. Access).....	5-32
Figure 5.26	Length Sizing Fit (in mm) for ECT Procedures Applied to LBDMWs (I.D. Access).....	5-35
Figure 5.27	Length Sizing Fit (in mm) for UT.ECT Procedures Applied to LBDMWs (I.D. Access; all dimensions are in mm).....	5-36
Figure 5.28	Length Sizing Fit (in mm) for UT.ECT Procedures Applied to LBDMWs (I.D. Access – Blind + Quick-blind; all dimensions are in mm).....	5-37
Figure 5.29	Length Sizing Fit (in mm) for UT.PAUT Procedures Applied to LBDMWs (I.D. Access; all dimensions are in mm).....	5-38
Figure 5.30	Length Sizing Fit (in mm) for UT.PAUT Procedures Applied to LBDMWs (I.D. Access – Blind + Quick-blind; all dimensions are in mm).....	5-39
Figure 5.31	Length Sizing Fit (in mm) for UT.TOFD.ECT Procedures Applied to LBDMWs (I.D. Access; all dimensions are in mm).....	5-40
Figure 5.32	Length Sizing Fit (in mm) for PAUT Procedures Applied to LBDMWs (O.D. Access; all dimensions are in mm).....	5-41
Figure 5.33	Length Sizing Fit (in mm) for UT Procedures Applied to LBDMWs (O.D. Access; all dimensions are in mm).....	5-42
Figure 5.34	Length Sizing Fit (in mm) for UT Procedures Applied to LBDMWs (O.D. Access – Blind + Quick-blind; all dimensions are in mm).....	5-43
Figure 5.35	Length Sizing Fit (in mm) for UT.PAUT Procedures Applied to LBDMWs (O.D. Access – Quick-blind; all dimensions are in mm).....	5-44
Figure 5.36	Length Sizing Fit (in mm) for PAUT Procedures Applied to SBDMWs (O.D. Access; all dimensions are in mm).....	5-45
Figure 5.37	Length Sizing Fit (in mm) for UT Procedures Applied to SBDMWs (O.D. Access; all dimensions are in mm).....	5-46
Figure 5.38	Length Sizing Fit (in mm) for UT.TOFD Procedures Applied to SBDMWs (O.D. Access; all dimensions are in mm).....	5-47
Figure 5.39	Depth Sizing Results for the WOL Test Block with Results for Surface Breaking (Triangles) and Non-Surface Breaking (Circles) Flaws Identified.....	5-51
Figure 5.40	Length Sizing Results for the WOL Test Block with Results for Surface Breaking (Triangles) and Non-Surface Breaking (Circles) Flaws Identified.....	5-52
Figure 5.41	Indication Plot for Procedure PAUT.108 Applied to WOL Test Block (P27) [theta – R view].....	5-52
Figure 5.42	Indication Plot for Procedure PAUT.108 Applied to WOL Test Block (P27) [theta – Y view].....	5-53
Figure 5.43	Indication Plot for Procedure PAUT.126 Applied to WOL Test Block (P27) [theta – R view].....	5-53

Figure 5.44	Indication Plot for Procedure PAUT.126 Applied to WOL Test Block (P27) [theta – Y view].....	5-54
Figure 6.1	Depth Sizing Fit for Axial Flaws in LBDMWs (I.D. Access; all dimensions are in mm).....	6-3
Figure 6.2	Depth Sizing Fit for Circumferential Flaws in LBDMWs (I.D. Access; all dimensions are in mm).....	6-4
Figure 6.3	Depth Sizing Fit for Axial Flaws in LBDMWs (O.D. Access; all dimensions are in mm).....	6-5
Figure 6.4	Depth Sizing Fit for Circumferential Flaws in LBDMWs (O.D. Access; all dimensions are in mm).....	6-6
Figure 6.5	Depth Sizing Fit for Axial Flaws in SBDMWs (O.D. Access; all dimensions are in mm).....	6-7
Figure 6.6	Depth Sizing Fit for Circumferential Flaws in SBDMWs (O.D. Access; all dimensions are in mm).....	6-8
Figure 6.7	Indication Plot for UT.ECT.144 Applied to P33 from X = 0 mm to X = 1000 mm.....	6-13
Figure 6.8	Indication Plot for UT.ECT.144 Applied to P33 from X = 1000 mm to X = 2000 mm.....	6-13
Figure 6.9	Indication Plot for UT.ECT.144 Applied to P33 from X = 2000 mm to X = 2800 mm.....	6-14
Figure 6.10	Methodology for Determining Singularity or Multiplicity of Linear Surface Flaws. Reprinted from ASME 2007 BPVC Section XI, Figure IWA-3400-1, by permission of The American Society of Mechanical Engineers. All rights reserved.....	6-15
Figure 6.11	Indication Plot for ECT.135 Applied to P33 from X = 2000 mm to X = 2800 mm.....	6-16
Figure 7.1	POD Regression with 95% Confidence Bounds for TOFD.ECT.126 Procedure Applied to BMI Tube I.D. Examinations in Test Blocks P25 and P26.....	7-4
Figure 7.2	POD Regressions for BMI Tube I.D. Examinations in PINC (Figure 4.12 from NUREG/CR-7019).....	7-5
Figure 7.3	POD Regression with 95% Confidence Bounds for ECT.124 and ECT.108 Procedures Applied to BMI J-groove Weld Examinations in Test Blocks P6, P8, P9, and P26.....	7-5
Figure 7.4	Indication Plot for Procedure ECT.124 Applied to P26 [theta – R view].....	7-6
Figure 7.5	Indication Plot for Procedure ECT.108 Applied to P26 [theta – R view].....	7-7
Figure 7.6	Indication Plot for Procedure TOFD.ECT.126 Applied to P26 [theta – R view].....	7-7
Figure 7.7	Indication Plot for Procedure TOFD.ECT.126 Applied to P26 [theta – Z view].....	7-8

LIST OF TABLES

Table 1.1	Summary of Members of the PARENT Steering Committee, NDE Task Group, Atlas Task Group, and Invigator/DAG	1-5
Table 2.1	Summary of Categories into which Test Blocks for Blind Testing are Classified	2-1
Table 2.2	Tabulation of BMI Test Block Dimensions	2-5
Table 2.3	Summary of Dimensions for SBDMW Test Blocks	2-7
Table 2.4	Summary of Dimensions for LBDMW Test Blocks.....	2-8
Table 2.5	Summary of Dimensions for WOL Test Block P27	2-9
Table 2.6	Summary of Flaw Simulation Methods Used and Quantities of Each Type of Simulated Flaw	2-10
Table 3.1	Definitions of Data Fields in the “Procedure Summary Data Sheet”	3-2
Table 4.1	Definitions of Data Fields for “Technique Data Sheets” and “Inspection Summary Data Sheets”	4-2
Table 4.2	Number Inspection Summary Data Sheets Collected for Each Procedure	4-6
Table 4.3	Number of Inspections by Access.....	4-6
Table 4.4	Number of Flaw Observations by Flaw Type	4-7
Table 4.5.	Number of Flaw Observations by Flaw Orientation	4-7
Table 4.6	Summary of POD (%) versus Depth for Procedure Types for LBDMWs (O.D. Access).....	4-15
Table 4.7	Summary of POD (%) by Access, Orientation, and Block Type versus Flaw Depth.....	4-16
Table 5.1	Flaw Depth Sizing Error by Procedure.....	5-3
Table 5.2	Flaw Depth Sizing Error by I.D./O.D. Access.....	5-3
Table 5.3	Flaw Length Sizing Error by Procedures ^(a)	5-3
Table 5.4	Flaw Length Sizing Error Summary	5-3
Table 5.5	DMW Detection and False Call Rate Summary Organized by Procedure	5-5
Table 5.6	Detection and False Call Rate Summary for Each DMW Test Block.....	5-5
Table 5.7	Summary of POD (%) versus Depth for Procedure Types for LBDMWs (I.D. Access)	5-8
Table 5.8	Summary of POD (%) versus Depth for Procedure Types for LBDMWs (O.D. Access).....	5-8
Table 5.9	Summary of POD (%) versus Depth for Procedure Types for SBDMWs (O.D. Access).....	5-8
Table 5.10	Summary of POD (%) versus Depth for Procedures Applied to LBDMWs (I.D. Access)	5-11
Table 5.11	Summary of POD (%) versus Depth for Procedures Applied to LBDMWs (O.D. Access)	5-11

Table 5.12	Summary of POD (%) versus Depth for Procedures Applied to SBDMWs (O.D. Access)	5-11
Table 5.13	Summary of POD (%) by Flaw Length in LBDMW Test Blocks by Procedure Type (I.D. Access).....	5-14
Table 5.14	Summary of POD (%) by Flaw Length in LBDMW Test Blocks by Procedure Type (O.D. Access).....	5-14
Table 5.15	Summary of POD (%) by Flaw Length in SBDMW Test Blocks by Procedure Type	5-14
Table 5.16	Summary of POD (%) by Flaw Length in LBDMW Test Blocks for Each Procedure (I.D. Access).....	5-15
Table 5.17	Summary of POD (%) by Flaw Length in LBDMW Test Blocks for Each Procedure (O.D. Access).....	5-15
Table 5.18	Summary of POD (%) by Flaw Length in SBDMW Test Blocks for Each Procedure	5-15
Table 5.19	Summary of Depth Sizing Errors for Procedure Types Applied to LBDMWs with I.D. Access	5-16
Table 5.20	Summary of Depth Sizing Errors for Procedure Types Applied to LBDMWs with O.D. Access	5-16
Table 5.21	Summary of Depth Sizing Errors for Procedures Types on SBDMWs with O.D. Access.....	5-17
Table 5.22	Summary of Depth Sizing Errors for Procedures on LBDMWs (I.D. Access).....	5-17
Table 5.23	Summary of Depth Sizing Errors for Procedures on LBDMWs (O.D. Access).....	5-18
Table 5.24	Summary of Depth Sizing Errors for Procedures on SBDMWs (O.D. Access).....	5-19
Table 5.25	Summary of Length Sizing Errors for Procedure Types Applied to LBDMWs (I.D. Access – Outliers Omitted) ^(a)	5-33
Table 5.26	Summary of Length Sizing Errors for Procedure Types Applied to LBDMWs (O.D. Access)	5-33
Table 5.27	Summary of Length Sizing Errors for Procedure Types Applied to SBDMWs (O.D. Access).....	5-33
Table 5.28	Summary of Length Sizing Errors for Procedures Applied to LBDMWs (I.D. Access – Outliers Omitted) ^(a)	5-34
Table 5.29	Summary of Length Sizing Errors for Procedures Applied to LBDMWs (O.D. Access).....	5-34
Table 5.30	Summary of Length Sizing Errors for Procedures Applied to SBDMWs (O.D. Access).....	5-34
Table 5.31	Length Sizing Outliers.....	5-35
Table 5.32	BMI Detection and False Call Rate Summary Organized by Procedure	5-48
Table 5.33	Detection and False Call Rate Summary for Each BMI Test Block	5-48
Table 5.34	Summary of POD (%) by Flaw Depth in BMI Test Blocks for Each Procedure Type	5-48

Table 5.35	Summary of POD (%) by Flaw Length in BMI Test Blocks for Each Procedure Type	5-48
Table 5.36	BMI Depth Sizing Results	5-48
Table 5.37	BMI Length Sizing Results	5-49
Table 5.38	WOL Test Block Sizing Results	5-50
Table 5.39	Summary of Sizing RMSEs for the WOL Test Block	5-50
Table 6.1	Summary of POD (%) by Access, Orientation, and Block Type versus Flaw Depth.....	6-2
Table 6.2	Depth Sizing Results by Access, Orientation, and Block Type.....	6-2
Table 6.3	Length Sizing Results by Access, Orientation and Block Type (Outliers Omitted)	6-2
Table 6.4	Summary of POD (%) versus Depth for PAUT and UT Procedure Types for SBDMWs (O.D. Access).....	6-9
Table 6.5	Summary of POD (%) versus Depth for PAUT and UT Procedure Types for LBDMWs (O.D. Access)	6-9
Table 6.6	Summary of Depth Sizing Errors for PAUT and UT Procedures Types on SBDMWs with O.D. Access	6-9
Table 6.7	Summary of Depth Sizing Errors for PAUT and UT Procedure Types Applied to LBDMWs with O.D. Access	6-9
Table 6.8	Summary of Length Sizing Errors for Procedure Types that do and do not incorporate an ECT technique Applied to LBDMWs (I.D. Access – Outliers Omitted).....	6-9
Table 6.9	Summary of Procedures PAUT.115, PAUT.128, PAUT.108, and PAUT.126	6-10
Table 6.10	Summary of Procedures UT.108, UT.126, UT.134, and UT.25	6-11
Table 6.11	Comparison of Blind and Quick-blind Sizing Results for UT.PAUT.113	6-12
Table 6.12	Comparison of UT.ECT.144 (Blind) and UT.ECT.106 (Quick-blind) Sizing Results	6-12
Table 6.13	Detection and False Call Comparison for 10 mm and 15 mm Tolerances Applied for Procedure UT.ECT.144	6-14
Table 6.14	Depth Sizing Error Comparison for 10 mm and 15 mm Tolerances Applied for Procedure UT.ECT.144.	6-14
Table 6.15	Length Sizing Error Comparison for 10 mm and 15 mm Tolerances Applied for Procedure UT.ECT.144	6-14
Table 6.16	X1, X2, Y1, and Y2 Coordinates for Indications No. 10 and 11 in Test Block P33 by Procedure ECT.135	6-15
Table 7.1	Comparison of PINC and PARENT Detection Results [POD (%)] versus Depth for DMW Test Blocks.....	7-1
Table 7.2	Comparison on Sizing Performances (Depth and Length) for PINC and PARENT for DMW Test Blocks.....	7-2
Table 7.3	Summary of PARENT Procedures that Produced Depth Sizing RMSEs of Less Than the ASME Code Requirement for Depth Sizing Accuracy (3.2 mm).....	7-3

Table 7.4	Comparison of PINC and PARENT Detection Results [POD (%)] versus Length on BMI Test Blocks for J-groove Weld Surface Examinations	7-4
Table 7.5	Comparison of PINC and PARENT Length Sizing Results on BMI Test Blocks	7-6
Table 7.6	Subset of Flaws for Test Block P26	7-6

EXECUTIVE SUMMARY

The U.S. Nuclear Regulatory Commission executed agreements with VTT Technical Research Centre of Finland, Nuclear Regulation Authority of Japan (NRA), Korea Institute of Nuclear Safety (KINS), Swedish Radiation Safety Authority (SSM), and Swiss Federal Nuclear Safety Inspectorate (ENSI) to establish the Program to Assess the Reliability of Emerging Nondestructive Techniques (PARENT) in February of 2012 to investigate the performance of current emerging and perspective novel nondestructive examination procedures and techniques to find flaws in nickel-alloy welds and base material. This assessment was performed by conducting a series of open and blind international round-robin tests on a set of nickel alloy piping components. The blind testing portion of PARENT collected data from 71 inspections performed on 6 large-bore dissimilar metal weld (LBDMW) test blocks, 2 small-bore dissimilar metal weld (SBDMW) test blocks, 5 bottom-mounted instrumentation (BMI) test blocks, and 1 weld overlay (WOL) test block. The data was collected by 14 teams using 23 different inspection procedures. The objective of the blind testing is to obtain quantitative estimates of the performance of the latest commercially used nondestructive evaluation (NDE) inspection procedures to determine which may be more reliable for detecting and accurate sizing of primary water stress corrosion cracks (PWSCC) or interdendritic stress corrosion cracking (IDSCC). The inspection procedures employed in blind testing included combinations and variations of conventional ultrasonic testing (UT), phased-array UT (PAUT), UT time-of-flight diffraction (TOFD), and eddy current testing techniques (ECT). Quantitative NDE performance data for the latest procedures applied to inspect dissimilar metal weld (DMW) components in the field represents a cross-cutting need identified as a goal by all international collaborators of PARENT. The data generated by this effort provides empirical bases that can support regulatory positions and which can inform analyses of the effectiveness of NDE and in-service inspection, more generally, by each country based on each country's specific laws, codes, standards, and regulations.

PARENT is a follow-on to the Program for Inspection of Nickel Alloy Components (PINC) (Cumblidge et al. 2010). In PINC, a study was conducted to quantitatively estimate the performance of NDE methods of nickel-alloy SBDMW components. PARENT incorporates both SBDMWs and LBDMWs so that the difference in performance for each type of component can be observed and quantitatively estimated. In addition, LBDMWs were included in PARENT to allow quantitative comparison of NDE performance obtained from procedures that access the inner diameter (I.D.) and those that access the outer diameter (O.D.) surfaces of LBDMWs. In PARENT, LBDMW and SBDMW test blocks had near ideal surface conditions. Thus, the results obtained from these test blocks provide a quantitative measure of performance that can be achieved by I.D. access of components with I.D. surface preparation, relative to performance that can be achieved by O.D. surface access. Finally, PARENT blind testing was restricted to teams and procedures developed by commercial inspection vendors so that the results of aggregate analysis provide a better representation of NDE field performance within the industry.

The primary objective of this report is to publish the results of the detection and sizing analyses performed on data collected in blind testing for PARENT. Another report in preparation will document the results of PARENT open testing. The purpose of the open testing was to perform an evaluation of novel techniques that have not yet reached the maturity level for field testing. In open testing, test teams are provided information regarding the locations of flaws in test blocks. Most of the teams and procedures included in open testing were not formally qualified. The objective of open testing was to assess the basic performance capability of emerging techniques by reviewing signal responses for both flaws and noise.

Significant conclusions of PARENT blind testing data analysis include the following:

- I.D. procedures exhibited superior performance over O.D. procedures for LBDMWs as measured by probability of detection (POD) and length sizing root means squared error (RMSE).
- Better performance is observed for inspections performed from the O.D. of SBDMWs in comparison to inspections performed from the O.D. of LBDMWs based on POD and depth sizing RMSE results.
- Flaw orientation exhibited an influence on detection performance with circumferential flaws being easier to detect than axial flaws.
- Flaw orientation did not have an influence on depth sizing performance.
- I.D. procedures that include ECT performed better at length sizing than I.D. procedures that do not include ECT in the blind test.
- PAUT procedures exhibit better performance than conventional UT procedures for O.D. examinations of SBDMWs as measured by POD and depth sizing RMSE.
- PAUT performance is similar to conventional UT performance for O.D. examinations of LBDMWs as measured by POD and depth sizing RMSE.
- PARENT results indicate substantial improvement in PAUT and TOFD performance compared with PINC performance data.
- PARENT results indicate that significant variability in performance can exist for conventional UT and PAUT procedures implementing similar techniques.
- For O.D. examinations of SBDMWs, one of the conventional UT procedures exhibiting lowest detection performance employed only one angle for inspection. This conventional UT procedure was also the only non-qualified procedure that participated in blind testing. All other conventional UT procedures incorporated multiple angles for inspection.
- One of five procedures applied for length sizing on LBDMW test blocks by O.D. surface access in the Blind test exhibited length sizing performance that did **not** meet the intent of the American Society of Mechanical Engineers (ASME) Boiler and Pressure Vessel Code (ASME Code), Section XI requirement of RMSE within 19 mm.
- One of nine procedures applied for length sizing on SBDMW test blocks by O.D. surface access in the Blind test exhibited length sizing performance that did **not** meet the intent of the ASME Code, Section XI requirement of RMSE within 19 mm.
- Two of three procedures applied for depth sizing on LBDMW test blocks by I.D. surface access in the Blind test exhibited depth sizing performance that met the intent of the ASME Code, Section XI requirement of RSME within 3.2 mm. However, the flaw depth size distribution in these test blocks tended to be shallower than ASME Code, Section XI requirements for flaw size distribution and it was not the intent of the PARENT test blocks to meet ASME Code flaw size distribution requirements.

- Two of nine procedures applied for depth sizing on SBDMW test blocks by O.D. surface access in the Blind test exhibited depth sizing performance that met the intent of the ASME Code, Section XI requirement of RSME within 3.2 mm. However, the flaw depth size distribution in these test blocks tended to be shallower than ASME Code, Section XI requirements for flaw size distribution and it was not the intent of the PARENT test blocks to meet ASME Code flaw size distribution requirements.
- ECT POD data is higher for PINC than PARENT.
- In general, it was felt that insufficient data was collected on BMI test blocks to draw firm conclusions regarding detection and length sizing performance. No data was provided to assess depth sizing performance for flaws in J-groove welds. In addition, many of the flaws implanted in BMI test blocks were considered to have limited relevance to flaws expected in the field.

Recommendations for future work are presented here based on the conclusions from PARENT blind testing outlined above and the summary of outcomes from PISC III (Program for the Inspection of Steel Components) and PINC. An outline of the recommendations to be addressed in the future is provided below:

- **Recommendation 1:** Limited data was collected on BMI test blocks in PINC and PARENT, so future work could focus on collecting new BMI data for performance quantification and consider combining PINC and PARENT BMI data for analysis.
- **Recommendation 2:** ECT performance in PARENT is lower than reported for PINC. However, the ECT procedures in PARENT were applied to LBDMWs; in PINC, they were applied to SBDMWs. Therefore, further evaluation using laboratory parametric studies of ECT procedures applied to SBDMW and LBDMW test blocks to assess and understand the results in PINC and PARENT is recommended.
- **Recommendation 3:** Further work is needed to understand the source of performance variability observed for PAUT and conventional UT procedures implementing similar techniques in PARENT and to quantify the relative influence of equipment, human factors, etc. on performance for procedures employing similar techniques.
- **Recommendation 4:** Further work is needed to understand and quantify the influence of specific PAUT and conventional UT procedure variables, such as number of inspection angles and sectorial versus linear scanning, on detection and sizing performance.
- **Recommendation 5:** The flaw simulations used in PARENT approximate PWSCC and IDSCC degradation processes but are not actual field PWSCC or field IDSCC flaws. The limitations of SCC flaw simulation techniques with respect to their relevance to representing field PWSCC and IDSCC flaw NDE responses should be further evaluated. In addition, improving the relevance of simulated flaws to field PWSCC and IDSCC flaws, based on such an evaluation, should also be investigated.

ACKNOWLEDGMENTS

There have been significant contributions made by a number of people and organizations to accomplish this study. The authors express appreciation to Aladar Csontos, Iouri Prokofiev, and Stephen Cumblidge of the U.S. Nuclear Regulatory Commission (NRC) for their leadership in helping to organize and start the PARENT program; to David Rudland of the NRC for his continued commitment to PARENT; to Stephen Cumblidge for continuing to provide technical and philosophical input to PARENT; and to Iouri Prokofiev for his continuous leadership of PARENT. Brett Braatz was the original Project Manager for PARENT and was responsible for the complex task of organizing and executing test block shipping and data collection, including the Quick-blind testing. The authors also acknowledge the tireless efforts of the PARENT investigators—Tommy Zetterwall (Europe), Ichiro Komura (Japan), and Kyung Cho Kim (South Korea)—who reviewed inspection procedures and monitored the work of inspection teams in their respective regions. Without their efforts, PARENT could not have been conducted.

The following companies participated in the PARENT blind round-robin test and should be acknowledged for their significant contributions:

- European Inspection Teams
 - Alstom Power Products
 - VTT Technical Research Centre of Finland
 - Swiss Association for Technical Inspections, Nuclear Inspectorate (SVTI)
 - Dekra Industrial
 - Nuclear Research and Consultancy Group (NRG)
 - FORCE Technology
- Korean Inspection Teams
 - Doosan Heavy Industries & Construction
 - Korea Plant Service (KPS)
 - Universal Monitoring Inspection (UMI)
 - Advanced NDE Service Company (ANSCO)
 - SAE-AN Engineering Corporation
- Japanese Inspection Teams
 - Mitsubishi Heavy Industries, Ltd. (MHI)
- United States Inspection Teams
 - IHI Southwest Technologies

The authors acknowledge the following organizations who have participated in the PARENT.

Organizations from Japan

- Nuclear Regulation Authority (NRA)
- Japan Power Engineering and Inspection Corporation (JAPEIC)
- Japanese PWR Industry Group
 - Kansai Electric Power Company
 - Shikoku Electric Power Company
 - Kyushu Electric Power Company
 - Hokkaido Electric Power Company
 - Japan Atomic Power Company (JAPC)

Organizations from Europe

- Swedish Radiation Safety Authority (SSM)
- Swedish Qualification Centre (SQC)
- VTT Technical Research Centre of Finland
- Swiss Association for Technical Inspections, Nuclear Inspectorate (SVTI)
- Swiss Federal Nuclear Safety Inspectorate (ENSI)

Organizations from South Korea

- Korea Institute of Nuclear Safety (KINS)
- Korea Hydro & Nuclear Power (KHNP)

Organization from the United States

- U.S. Nuclear Regulatory Commission (NRC)

Finally, the authors thank Ms. Kay Hass for typing and editing versions and revisions of this document.

ACRONYMS

ASME	American Society of Mechanical Engineers
ASME Code	ASME Boiler and Pressure Vessel Code
Ax	axial
BMI	bottom-mounted instrumentation
BWR	boiling water reactor
Circ	circumferential
CRDM	control rod drive mechanism
DAG	Data Analysis Group
DMW	dissimilar metal weld
ECT	eddy current testing
EDM	electrical discharge machining
FCP	false call probability
FCR	false call rate
I.D.	inner diameter
ID	identification
IDSCC	interdendritic stress corrosion cracking
ISI	in-service inspection
LBDMW	large-bore dissimilar metal weld
MFC	mechanical fatigue crack
NDE	nondestructive examination
NOBS	number of observations
NRC	U.S. Nuclear Regulatory Commission
O.D.	outer diameter
PARENT	Program for Assessing the Reliability of Emerging Nondestructive Technologies
PAUT	phased-array ultrasonic testing
PC	pitch/catch
PE	pulse-echo
PINC	Program for Inspection of Nickel Allow Components
PISC	Program for the Inspection of Steel Components
PNNL	Pacific Northwest National Laboratory
POD	probability of detection
PWR	pressurized water reactor
PWSCC	primary water stress corrosion cracking
RMSE	root mean square error
RRT	round-robin testing

SBDMW	small-bore dissimilar metal weld
SC	solidification crack
SCC	stress corrosion cracking
SI	slag inclusion
TFC	thermal fatigue crack
TOFD	time-of-flight diffraction
TR	transmit-receive
TRL	transmit-receive-longitudinal
UT	ultrasonic testing
WOL	weld overlay

DEFINITIONS

Bottom-mounted instrumentation (BMI)	A cylindrical penetration in the bottom head of a nuclear reactor pressure vessel, into which a tube is welded. Typical inside diameters are a few centimeters.
Dendrite	weld grain (columnar or tree-like)
Dissimilar metal weld (DMW)	Weldments joining components made of different alloys. In the context of PINC, refers primarily to nozzle welds.
Heat-affected zone	a volume of base metal, adjacent to the fusion zone, changed by the heat of welding
Interdendritic	between the tree-like grains, such as can form in castings or weld metal
Intergranular	between the metal crystals rather than through them
J-groove weld	a weld with profile shaped as the letter "J," the seal weld of a CRDM or BMI penetration
Lack of fusion	missing metallic bond either between the sidewall of a weld with the base metal or between weld passes (inter-run)
Partial penetration weld	the weld preformed to eliminate leakage paths, also called a seal weld
Primary water stress corrosion cracking (PWSCC)	The intergranular or interdendritic cracking of nickel-base alloys that occurs in service and originates from the surfaces of a component that are wetted by the primary water of a pressurized water reactor (PWR)
Program for the Inspection of Nickel-Alloy Components (PINC)	An international cooperative research program, The purpose of PINC is to assess the capabilities of current and emerging NDE techniques to detect and size flaws associated with PWSCC in nuclear reactors. This information tool is the definitive source of information on PINC.
Round-robin test (RRT)	a test performed independently several times (usually at multiple testing facilities)

1 INTRODUCTION

The U.S. Nuclear Regulatory Commission (NRC) executed agreements with VTT Technical Research Centre of Finland, Nuclear Regulation Authority of Japan (NRA), Korea Institute of Nuclear Safety (KINS), Swedish Radiation Safety Authority (SSM), and Swiss Federal Nuclear Safety Inspectorate (ENSI) to establish the Program to Assess the Reliability of Emerging Nondestructive Techniques (PARENT) in February of 2012 to investigate the performance of current emerging and perspective novel nondestructive examination procedures and techniques to find flaws in nickel-alloy welds and base material. This assessment was performed by conducting a series of open and blind international round-robin tests on a set of nickel alloy piping components. The blind testing portion of PARENT collected data from 71 inspections performed on 6 large-bore dissimilar metal weld (LBDMW) test blocks, 2 small-bore dissimilar metal weld (SBDMW) test blocks, 5 bottom-mounted instrumentation (BMI) test blocks, and 1 weld overlay (WOL) test block. The data was collected by 14 teams using 23 different inspection procedures. The objective of the blind testing was to obtain quantitative estimates of the performance of the latest commercially used nondestructive evaluation (NDE) inspection procedures to determine which may be more reliable for detecting and accurate sizing of primary water stress corrosion cracks (PWSCC) or interdendritic stress corrosion cracking (IDSCC). Quantitative NDE performance data for the latest procedures applied to inspect dissimilar metal weld (DMW) components in the field represents a cross-cutting need identified as a goal by all international collaborators of PARENT. The data generated by this effort provides empirical bases that can support regulatory positions and which can inform analyses of the effectiveness of NDE and in-service inspection (ISI), more generally, by each country based on each country's specific laws, codes, standards, and regulations.

PARENT was a follow-on to the Program for Inspection of Nickel Alloy Components (PINC) (Cumblidge et al. 2010). In PINC, a study was conducted to quantitatively estimate the performance of NDE methods of nickel-alloy SBDMW components. PARENT incorporates both SBDMWs and LBDMWs so that the difference in performance for each type of component can be observed and quantitatively estimated. In addition, LBDMWs were included in PARENT to allow quantitative comparison of NDE performance obtained from procedures that access the inner diameter (I.D.) and those that access the outer diameter (O.D.) surfaces of LBDMWs. In PARENT, LBDMW and SBDMW test blocks had near ideal surface conditions. Thus, the results obtained from these test blocks provide a quantitative measure of performance that can be achieved by I.D. access of components with I.D. surface preparation, relative to performance that can be achieved by O.D. surface access. Finally, PARENT blind testing was restricted to teams and procedures developed by commercial inspection vendors so that the results of aggregate analysis provide a better representation of NDE field performance within the industry. All teams and procedures participating in blind testing were formally qualified with the exception of one conventional ultrasonic testing procedure (UT). The teams and procedures were qualified according to the qualification requirements of their country of residence.

The primary objective of this report was to publish the results of the detection and sizing analyses performed on data collected in blind testing for PARENT. Another report in preparation will document the results of PARENT open testing. The purpose of the open testing was to perform an evaluation of novel techniques that have not yet reached the maturity level for field testing. In open testing, test teams are provided information regarding the locations of flaws in test blocks. Most of the teams and procedures included in open testing were not formally qualified. The objective of open testing was to assess the basic performance capability of emerging techniques by reviewing signal responses for flaws and noise.

1.1 Quick-Blind Study

Some LBDMW test blocks with laboratory-grown stress corrosion cracking (SCC) flaws, contributed by Japan, were immediately available at the start of PARENT and tested separately before they were scheduled to undergo destructive evaluation (Braatz et al. 2014). This portion of testing is referred to as the “Quick-blind” test to distinguish it from the rest of the blind testing (referred to as the “Blind” test). The Quick-blind test allowed PARENT to collect additional data from these test blocks but it was not clear how the expedited timetable might impact results relative to the rest of the blind testing. During a June 2014 workshop with PARENT invigilators, a decision was made to compare Quick-blind results with the rest of the blind testing results to determine if there were significant differences in the results. Data analysis results for Quick-blind test blocks are presented separately from results for other test blocks in this regard. In addition, LBDMW testing results are presented in this report both with and without Quick-blind data included in the analysis so that the impact of Quick-blind data on results can be observed. Test blocks used in the Quick-blind study include LBDMW test blocks P15, P16, P17, and P45. In Section 5, Section 6, Appendix F, and Appendix G, “Blind + Quick-blind” is used to highlight results that are based on data from both Blind and Quick-blind tests and “Quick-blind” is used to highlight results based only on Quick-blind data. Red text color is also used to emphasize results that include data from Quick-blind testing.

1.2 Bottom-Mounted Instrumentation Test Blocks

Five BMI test blocks were employed in PARENT including P25, P26, P6, P8, and P9. Test blocks P6, P8, and P9 were contributed for evaluation of J-groove weld inspections and included thermal fatigue cracks (TFCs) in the J-groove weld region. Test blocks P25 and P26 included several weld defects and were contributed for the evaluation of inspections from the tube inner diameter (I.D.) surface. However, some examinations of the J-groove weld were also performed on these test blocks.

1.3 Weld Overlay Test Block

A WOL test block (P27) is also incorporated into the blind test matrix for PARENT. Weld overlays are a common repair practice in which additional material is welded to the surface of a component’s original base material to maintain structural and leak-tight integrity. WOLs are of interest for an NDE study because flaws in repairs can continue to grow and repairs can be subject to degradation themselves. Also, the repair can result in unusual geometric features to consider for an examination. Two inspections were performed on P27 in PARENT.

1.4 PWSCC/IDSCC Nomenclature

Throughout this report, reference is frequently made to PWSCC/IDSCC as being the target degradation mode for this study. Here, PWSCC is defined as:

The intergranular or interdendritic cracking of nickel-base alloys that occurs in service and originates from the surfaces of a component that are wetted by the primary water of a pressurized water reactor (PWR).

IDSCC (interdendritic stress corrosion cracking) refers to SCC in which crack growth propagates between the tree-like grains that can form in castings or weld metal. The term PWSCC implies applicability limited to PWR-type components, while the test blocks used in this study represent PWR and boiling water reactor (BWR) configurations. The convention adopted in this report is to refer to the target degradation as PWSCC/IDSCC because the intended focus of the PARENT investigation is to address SCC that occurs in nickel alloy components exposed to light water

reactor conditions, inclusive of both PWR and BWR conditions. The methods used to simulate PWSCC/IDSCC in PARENT blind testing are briefly described in Section 2. For the SBDMW and LBDMW test blocks, all of the flaws introduced to simulate PWSCC/IDSCC are manufactured cracks.

1.5 PARENT Organization

PARENT is organized with a Steering Committee, a Task Group on NDE, a Task Group on the PARENT Atlas, and an Invigilator/Data Analysis Group (DAG) following a convention used in PINC and as shown in **Error! Reference source not found.**. The objectives of these groups for PINC are described in Section 1.0 of NUREG-7019 (Cumblidge et al. 2010) and are similar to PARENT, although personnel have changed. A summary of the members of the Steering Committee, Task Group on NDE, Task Group on the PARENT Atlas, and the Invigilator/DAG, is provided in Table 1.1. PARENT participants met twice per year with one meeting in the United States and the other meeting rotated among the remaining participant countries. The first PARENT meeting was held June 1–3, 2010, at Pacific Northwest National Laboratory (PNNL) in Richland, Washington.

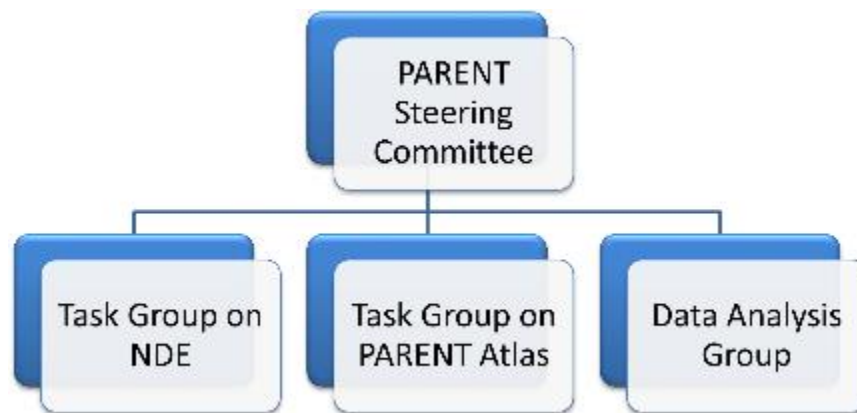


Figure 1.1 Organization Chart for Steering Committee and Task Groups

1.6 Organization of This Report

Section 2 of this report includes a description of the test blocks used in PARENT blind testing, including a description of true states and types of flaws used in each test block. Section 3 provides a summary of the procedures applied in PARENT blind testing and some background technical information so that readers can understand terminology associated with the NDE procedures applied in blind testing. Section 4 provides an overview of how data was recorded and a breakdown of inspections by procedure, test block, flaw type, and flaw orientation. Section 4.0 also provides an overview of the scoring procedure used in PARENT. Results of data analysis are presented in Section 5. The presentation of the results is organized by block type and access (LBDMW I.D., LBDMW O.D., SBDMW, BMI, and WOL) and sub-organized by detection analysis results, depth sizing results, and length sizing results. Section 6 includes a discussion of the results in Section 5 including a discussion on the influence of parameters on performance in PARENT, a comparison of the performance of procedures, and a comparison of Quick-blind and blind results. In Section 7, PARENT results are compared to PINC results and the conclusions and recommendations from PINC are revisited in the context of the additional information obtained from PARENT. Section 8 provides a summary of outcomes from PISC III (Program for the Inspection of Steel Components) and PINC round-robin testing outcomes based on a review

of these studies prepared by some of the participants, which is included in Appendix H. Finally, additional conclusions from PARENT and recommendations for future work are provided in Section 9.

Table 1.1 Summary of Members of the PARENT Steering Committee, NDE Task Group, Atlas Task Group, and Invigilator/DAG

Member Name		PARENT Committee Members				
		Organization	Steering	NDE Task Group	Atlas Task Group	Invigilator/Data Analysis Task Group
Finland	VTT	Esa Leskelä	Esa Leskelä	Esa Leskelä	Esa Leskelä	
	Aalto University				Hannu Hänninen	
Japan	NRAJNES	Kazunobu Sakamoto Kikuo Takeshima	Kazunobu Sakamoto Kikuo Takeshima	Kazunobu Sakamoto Kikuo Takeshima	Kenjiro Aono Kikuo Takeshima	Kensaku Arai Kikuo Takeshima
	JAPEIC		Ichiro Komura Toshihiro Yamamoto	Ichiro Komura Toshihiro Yamamoto		Ichiro Komura Toshihiro Yamamoto
	Japanese PWR Industry Group		Yusuke Kono (MHI) Takehiko Yamaguchi (MHI) Takayoshi Tsuruta (MHI)	(Rotating Member) Tomonori Shichida (MHI) Yasuto Nagoshi (MHI) Takehiko Sera (Kansai) Yasukazu Takada (Kansai) Seiji Asada (MHI) Junichiro Nishida (MHI)		
	Tohoku University		Tetsuya Uchimoto		Kyung Cho Kim	Kyung Cho Kim
	KINS		Sung-Sik Kang			
Korea	KPS		ES Doh			
	KHNP					
	KAERI				Hong-Pyo Kim	Yong-Sik Kim
	DOOSAN			DS Lee, Joo Youl Hong Hak-Joon Kim		
Sweden	SSM	Richard Sundberg Giselle Garcia Roldán				
	SQC		Tommy Zetterwall			Tommy Zetterwall (all of Europe) Ulf Hjerm (only invigilation)
Switzerland	ENSI		Klaus Germerdonk		Klaus Germerdonk	
	SVTI		Hardy Ernst			
USA	PNNL (Non-Voting)	Brett Braatz, Rob Harris Ryan M. Meyer	Brett Braatz, Ryan M. Meyer		Darren Curtis, Robert Harris Ryan M. Meyer	Steven Doctor, Brett Braatz Jack Spanner – DAG (Open Only) Ryan M. Meyer
	NRC	louri Prokofiev	Stephen Cumbilidge			
	EPRI	Jack Spanner	Jack Spanner			
	DOOSAN – Doosan Heavy Industries & Construction ENSI – Swiss Federal Nuclear Safety Inspectorate EPRI – Electric Power Research Institute JAPEIC – Japan Power Engineering and Inspection Corporation JNES – Japan Nuclear Energy Safety Organization	KAERI – Korea Atomic Energy Research Institute Kansai – The Kansai Electric Power Company, Inc. KHNP – Korea Hydro & Nuclear Power KINS – Korea Institute of Nuclear Safety KPS – Korea Plant Service MHI – Mitsubishi Heavy Industries, Ltd. NRC – US Nuclear Regulatory Commission	KAERI – Korea Atomic Energy Research Institute Kansai – The Kansai Electric Power Company, Inc. KHNP – Korea Hydro & Nuclear Power KINS – Korea Institute of Nuclear Safety KPS – Korea Plant Service MHI – Mitsubishi Heavy Industries, Ltd. NRC – US Nuclear Regulatory Commission	PNL – Pacific Northwest National Laboratory SKKU – Sungkyunkwan University SOC – Swedish Qualification Center SSM – Swedish Radiation Safety Authority SVTI – Swiss Association for Technical Inspections, Nuclear Inspectorate VTT – Technical Research Centre of Finland Ltd		

2 TEST BLOCK DESCRIPTIONS

The following section provides an overview of the test blocks used in the blind testing activity of PARENT. Four different categories of test blocks were used in the blind testing study and are summarized in Table 2.1. The four categories include BMI test blocks, SBDMW test blocks, LBDMW test blocks, and WOL specimens. A total of 14 test blocks were contributed for the blind testing. Table 2.1 also indicates the typical weldment in each test block category, test block diameter and wall thickness dimensions, and the identifications (IDs) of test blocks in each category. Descriptions of the test blocks in each category are provided in Sections 2.1–2.4, while the flaw fabrication methods are described in Section 2.5. True-state information for the flaws in each test block is summarized in Section 2.6.

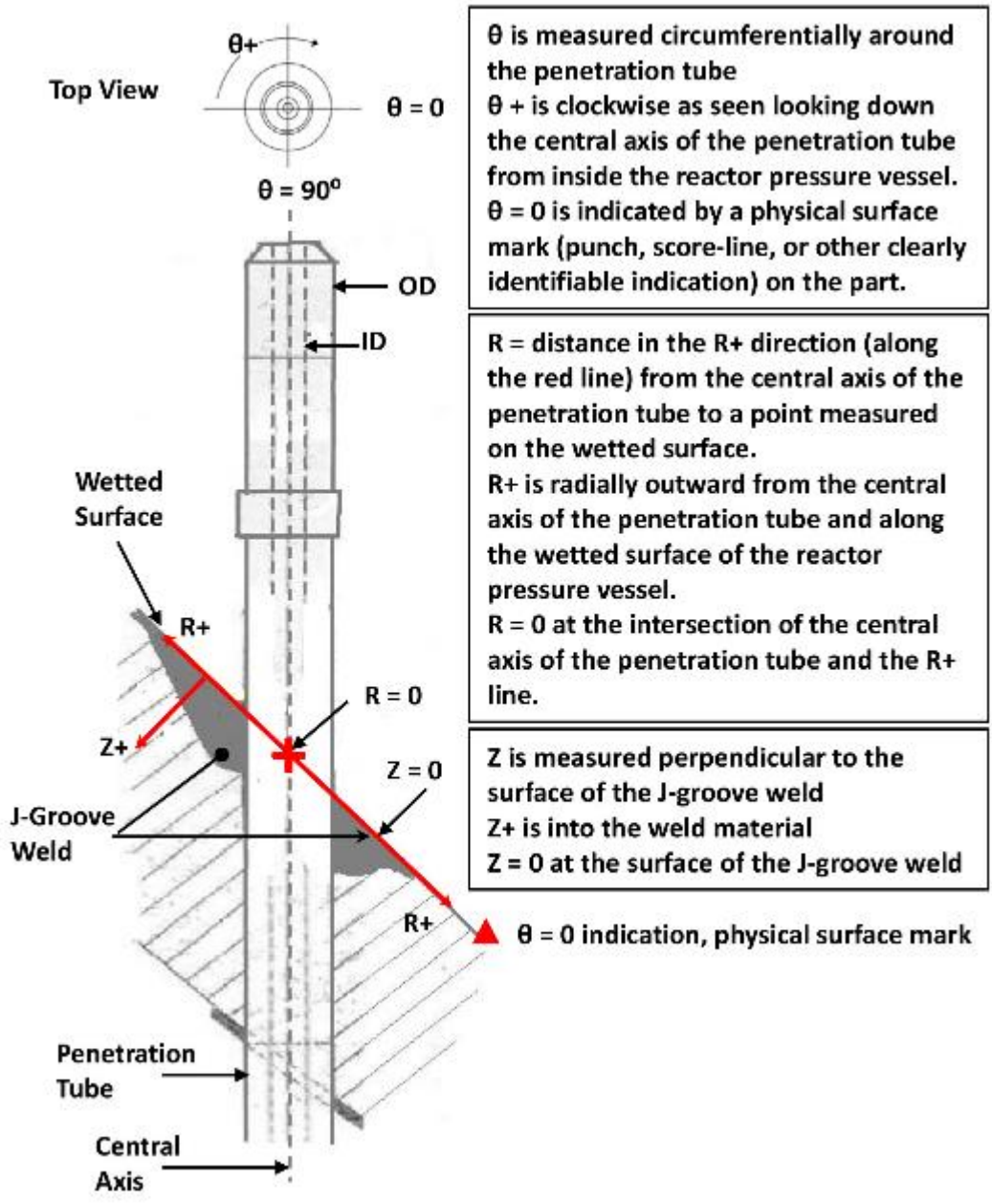
Table 2.1 Summary of Categories into which Test Blocks for Blind Testing are Classified

Category	Typical Weldment in Category	Diameter/Thickness Range	Test Block IDs	Test Block Photographs
BMI	J-groove weld	Tube O.D.: 38–45 mm	P25, P26, P6, P8, P9	Appendix A.1
SBDMW	DMW piping welds, BWR	Diameters: 289 mm, 815 mm (O.D.) Thickness range: 35 mm, 39.5 mm	P35, P40	Appendix A.2
LBDMW	DMW piping welds, PWR	Diameter range: 852–895 mm (O.D.) Thickness range: 68–78 mm	P15, P16, P17, P45, P13, P33	Appendix A.3
WOL		Pipe Diameter: 114 mm (O.D.) Overlay Diameter: 180 mm (O.D. – max) Pipe Thickness: 14 mm	P27	Appendix A.4

O.D. = outer diameter

2.1 Bottom-Mounted Instrumentation Test Blocks

As Table 2.1 indicates, five BMI test blocks were used in blind testing (P25, P26, P6, P8, and P9). The coordinate system defined for acquiring and reporting data on these test blocks is provided in Figure 2.1. Figure 2.1 shows that a cylindrical coordinate system is defined for BMI test blocks with the azimuthal coordinate, θ , increasing in the clockwise direction when viewed from the top of the test block (above the wetted surface) with the zero-point marked on the test block. The radial coordinate, R , is defined such that $R=0$ at the center of the penetration tube at the top (wetted) surface of the reactor pressure vessel material attached to the penetration tube. R increases outward from this point along a plane that is parallel with the top (wetted) surface. The Z coordinate is defined as perpendicular to the J-groove weld surface such that $Z=0$ at the top (wetted) surface and increases into the J-groove material. The dimensions of the BMI test blocks are labeled in Figures 2.2 to 2.4. The specific dimensions for each BMI test block are tabulated in Table 2.2. Figure 2.2 depicts the configuration for test block P25 and Figure 2.3 represents the configuration for test block P26. Test blocks P6, P8, and P9 are represented by Figure 2.4.



θ is measured circumferentially around the penetration tube
 $\theta +$ is clockwise as seen looking down the central axis of the penetration tube from inside the reactor pressure vessel.
 $\theta = 0$ is indicated by a physical surface mark (punch, score-line, or other clearly identifiable indication) on the part.

R = distance in the $R +$ direction (along the red line) from the central axis of the penetration tube to a point measured on the wetted surface.
 $R +$ is radially outward from the central axis of the penetration tube and along the wetted surface of the reactor pressure vessel.
 $R = 0$ at the intersection of the central axis of the penetration tube and the $R +$ line.

Z is measured perpendicular to the surface of the J-groove weld
 $Z +$ is into the weld material
 $Z = 0$ at the surface of the J-groove weld

Figure 2.1 Coordinate System Used for BMI Test Blocks: P6, P8, P9, P25, P26

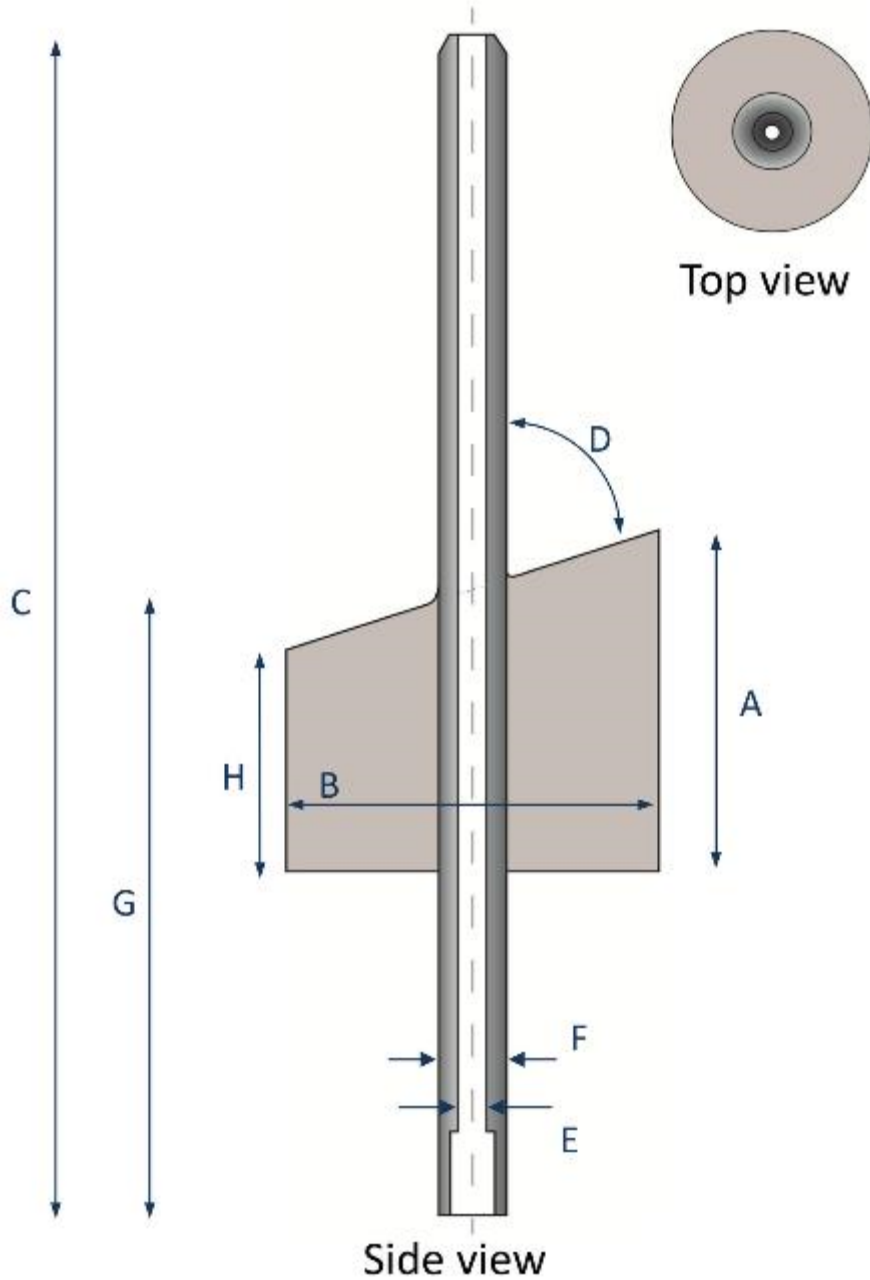


Figure 2.2 Depiction of Configuration for BMI Test Block P25 with Labeled Dimensions

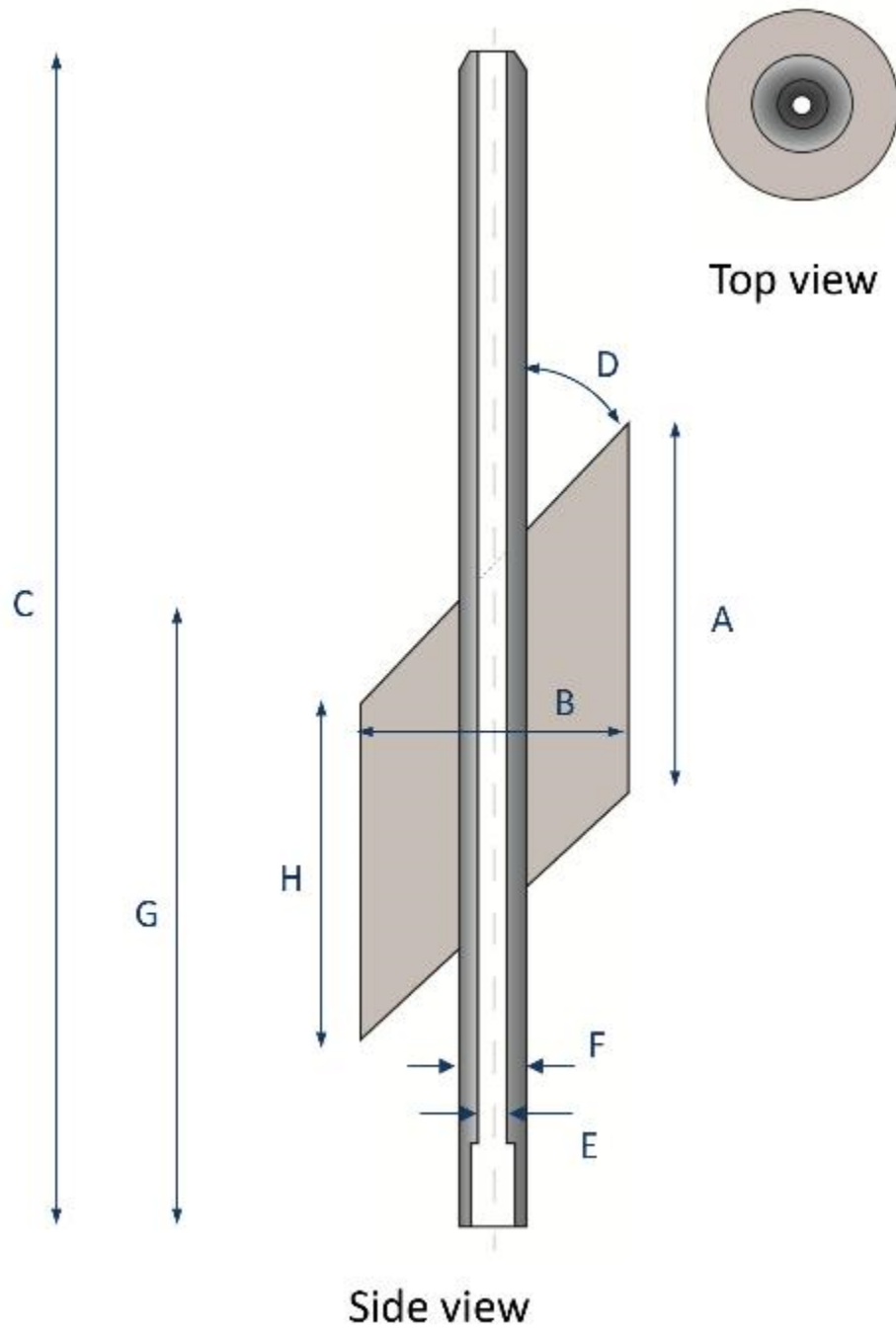


Figure 2.3 Depiction of Configuration for BMI Test Block P26 with Labeled Dimensions

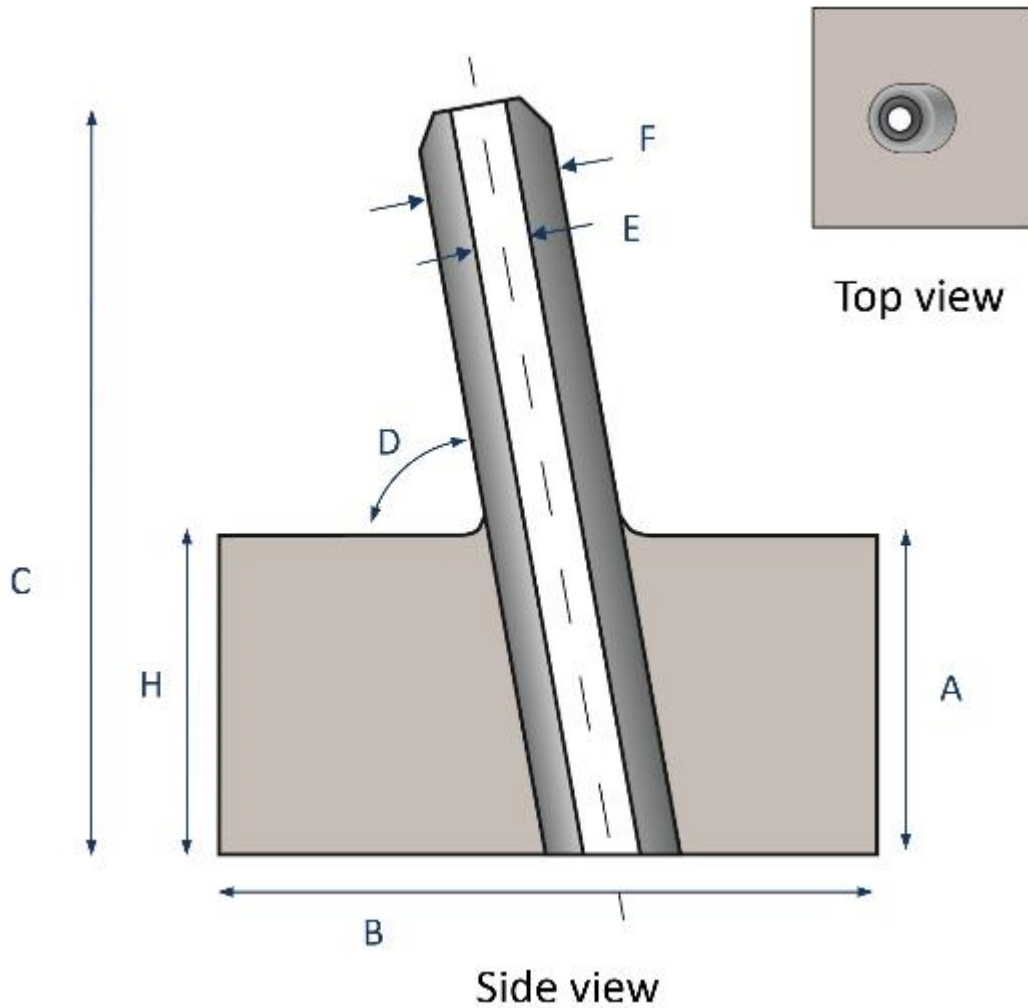


Figure 2.4 Depiction of Configuration for BMI Test Blocks P6, P8, and P9 with Labeled Dimensions

Table 2.2 Tabulation of BMI Test Block Dimensions

Test Block ID	Figure Ref.	A, mm	B, mm	C, mm	D (angle), degrees	E (I.D.), mm	F (O.D.), mm	G, mm	H, mm
P25	Figure 2.2	183.5	198.1 (dia.)	634	72.3	15.0	38.2	307.3	121.8
P26	Figure 2.3	198.1	146.1 (dia.)	634.5	44.0	15.0	38.2	330.2	183.4
P6	Figure 2.4	86.0	220 × 227	219	80.0	15.9	44.2	86.0	86.0
P8	Figure 2.4	110.0	224 × 228	243	75.0	15.9	44.2	110.0	110.0
P9	Figure 2.4	91.0	219 × 223	234	78.0	15.9	44.2	91.0	91.0

I.D. = inner/inside diameter
O.D. = outer/outside diameter

2.2 Small-Bore Dissimilar Metal Weld Test Blocks

Two SBDMW test blocks were utilized in PARENT (P35 and P40 – see Table 2.1). The coordinate system defined for acquiring and reporting data on these test blocks is provided in Figure 2.5. The zero point is defined as that location on the test block where $X=0$, $Y=0$, and $Z=0$. Figure 2.5 also provides the definitions for the directional vectors $X+$, $Y+$, and $Z+$ in relation to the zero point and with respect to the material construction of the test block. The location for $Z=0$, $Y=0$ is at the O.D. surface of the test block, at the center of the weld, and is located a distance “D” from the face edge of the carbon steel pipe. The $X=0$ location is indicated by a punch marking on the test block outer surface. A summary of dimensions for SBDMW test blocks is provided in Table 2.3. The diameter of test block P40 is actually similar to diameters of large-bore DMWs described in the next section. However, the thickness of the P40 test block is consistent with the SBDMW classification.

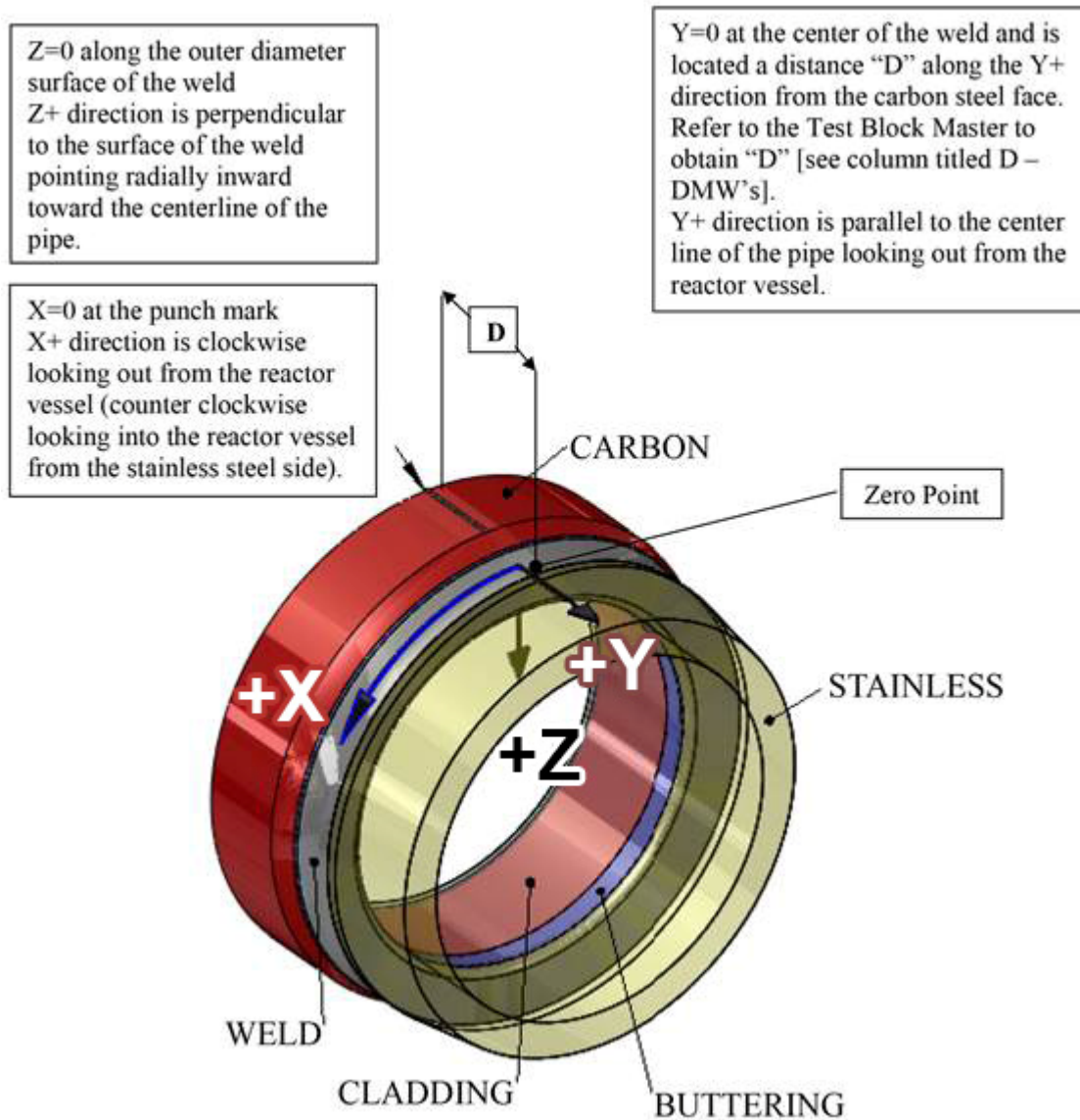


Figure 2.5 Coordinate System Definition for SBDMW Test Blocks P35 and P40, and LBDMW Test Block P33

Table 2.3 Summary of Dimensions for SBDMW Test Blocks

Test Block ID	Inner Diameter, mm	Outer Diameter, mm	Thickness, mm	D, mm	Axial Extent, mm	Circumferential Extent, degrees
P35	219.0	289.0	35.0	215.0	---	360.0
P40	736.0	815.0	39.5	170.0	---	360.0

2.3 Large-Bore Dissimilar Metal Weld Test Blocks

Six LBDMW test blocks (P15, P16, P17, P45, P13, and P33) were utilized in the blind testing activities as indicated in Table 2.1. These test blocks use a similar coordinate system definition as the SBDMWs. However, one difference for test blocks P13, P15, P16, P17, and P45 with respect to SBDMWs is that the test blocks are only sector portions of the DMW cut-out; whereas, the SBDMW test blocks are full circumference. Thus, the X=0 point is defined at a sector edge for those test blocks. Four of these test blocks (P15, P16, P17, and P45) were utilized in the Quick-blind study (Braatz et al. 2014). Figure 2.6 depicts the coordinate system defined for these test blocks. The coordinate system defined for test block P13 is shown in Figure 2.7. In this case, because the circumferential weld only covers half of the test block, the zero point is defined at the opposite end of the test block with respect to the zero-point definition for P15, P16, P17, and P45 in Figure 2.6 and X values are defined negative from this point. Finally, test block P33 is a full circumference specimen and its coordinate system definition is consistent with the definition for SBDMW test blocks, as depicted in Figure 2.5. A summary of dimensions for LBDMW test blocks is provided in Table 2.4.

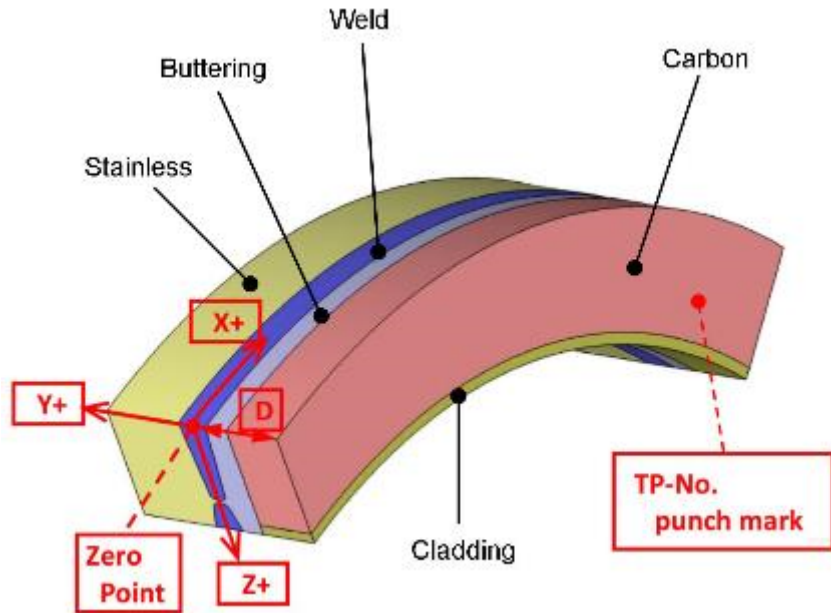


Figure 2.6 Coordinate System for LBDMW Test Blocks P15, P16, P17, and P45

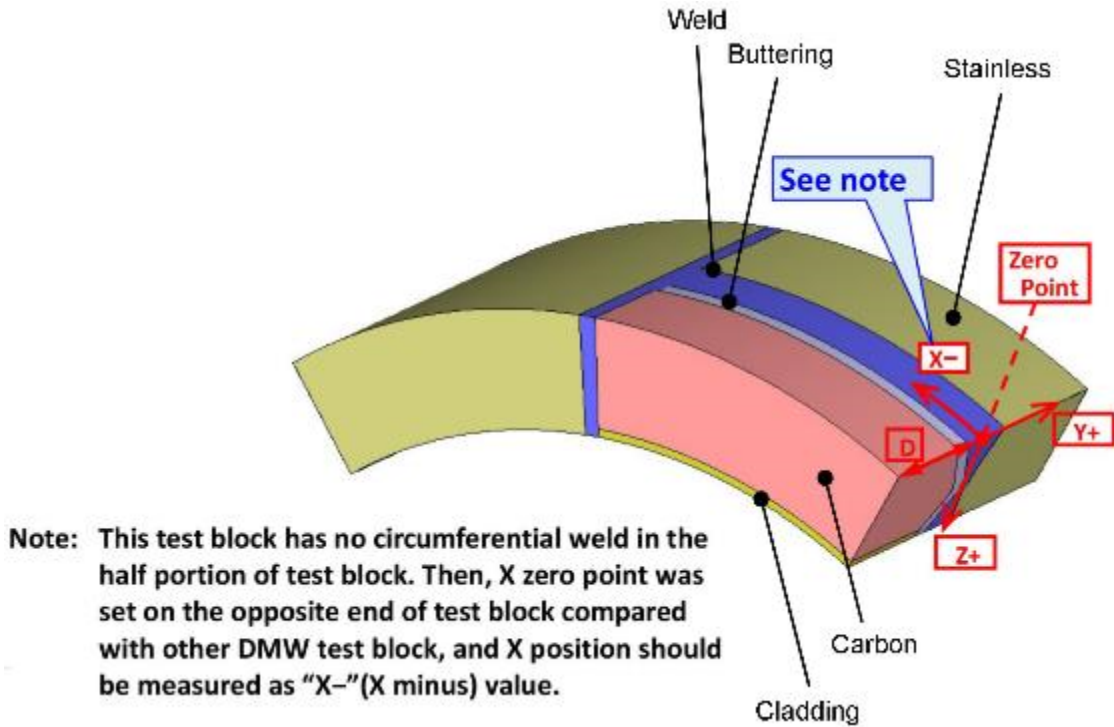


Figure 2.7 Coordinate System for LBDMW Test Block P13

Table 2.4 Summary of Dimensions for LBDMW Test Blocks

Test Block ID	Inner Diameter, mm	Outer Diameter, mm	Thickness, mm	D, mm	Axial Extent, mm	Circumferential Extent, degrees
P15	736.6	873.0	68.2	50.0	100.0	60.0
P16	736.6	873.0	68.2	50.0	100.0	60.0
P17	736.6	873.0	68.2	50.0	100.0	60.0
P45	736.6	873.0	68.2	51.5	105.0	60.0
P13	698.5	852.5	77.0	100.0	200.0	64.5
P33	741.0	895.0	77.0	300.0	---	360.0

2.4 Weld Overlay Test Block

One WOL test block was utilized in the blind portion of PARENT testing (block P27). The coordinate system defined for the test block is indicated in Figure 2.8. The dimensions of P27 are tabulated in Table 2.5.

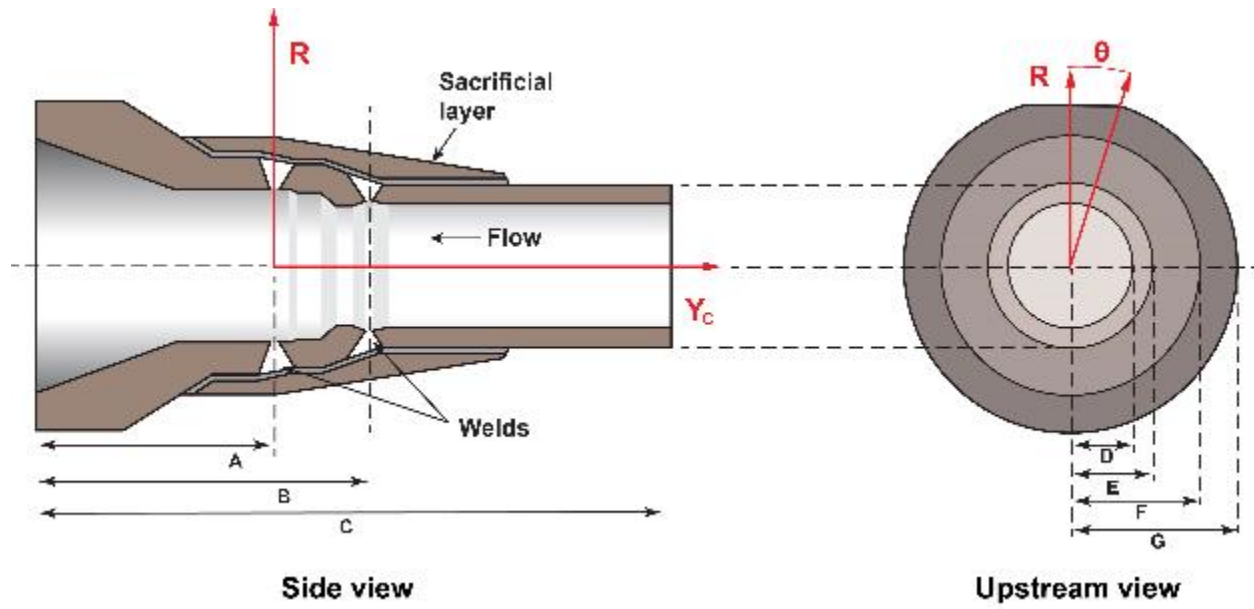


Figure 2.8 Coordinate System for WOL Test Block P37

Table 2.5 Summary of Dimensions for WOL Test Block P27

Test Block ID	A, mm	B, mm	C, mm	D, mm	E, mm	F, mm	G, mm
P27	167	233	443	43	57	90	215

2.5 Simulated Flaw Types

Field flaws were simulated in PARENT test blocks using similar methods as those used in PINC. Simulation flaw types include laboratory-grown SCC, tightened weld solidification cracks (SC), TFCs, electrical discharge machining (EDM), and implanted welding defects such as lack of fusion, slag inclusion (SI), porosity, and weld repair. A summary of the type and quantity of simulated flaws used in each test block is provided in Table 2.6. Brief descriptions of the flaw simulation types are provided in the following sections with the objective of highlighting some of the advantages and limitations of each flaw simulation type with respect to representing PWSCC/IDSCC for assessing NDE performance.

Table 2.6 Summary of Flaw Simulation Methods Used and Quantities of Each Type of Simulated Flaw

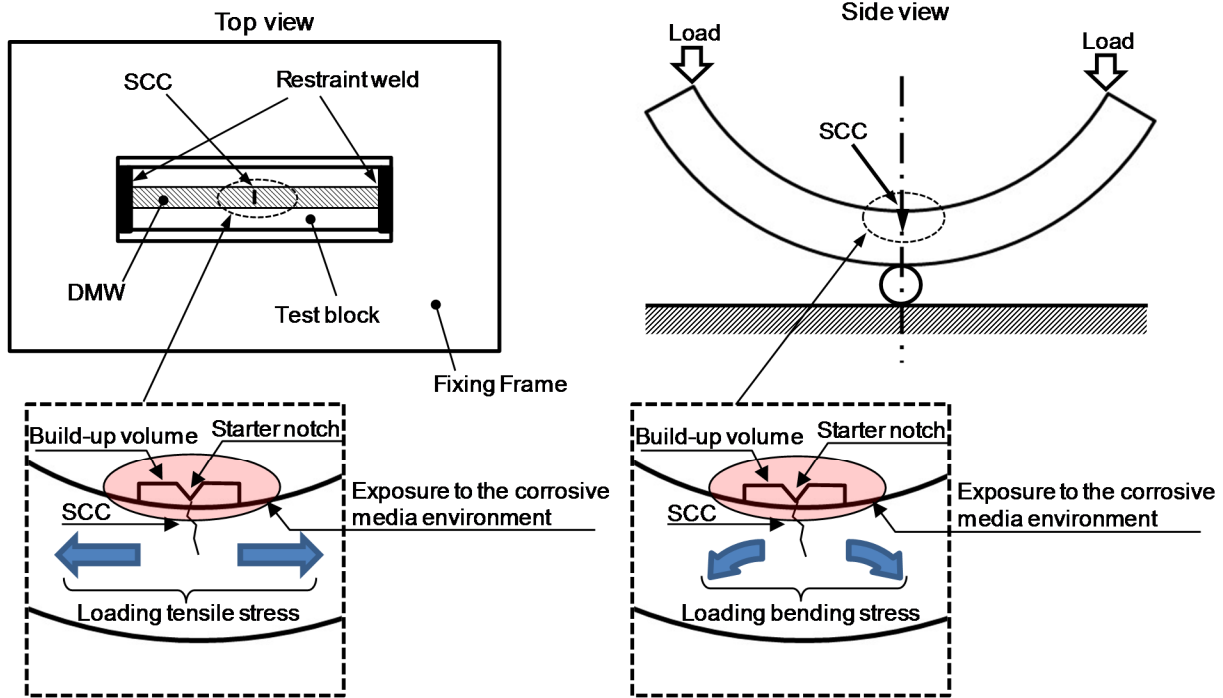
Flaw Type	Total Flaws
Laboratory-Grown SCC	4
Thermal Fatigue Cracks (TFC)	31
Tightened Weld Solidification Cracks (SC)	44
Welding Defects	10
Mechanical Fatigue Cracks (MFC)	5
Electrical Discharge Machining (EDM)	3
Total	97

2.5.1 Laboratory-Grown SCC [P13, P15, P16, and P17]

Laboratory methods for introducing SCC flaws allow for the deliberate introduction of realistic flaws into test pieces at desired locations. However, even under laboratory conditions, the dimensions of SCC flaws can be difficult to control. In addition, it can be difficult to grow SCC flaws into complex geometries as it can be difficult to generate the necessary stresses to promote SCC growth. Nonetheless, laboratory-grown SCC was introduced into four test blocks, as indicated in Table 2.6.

The two configurations shown in Figure 2.9(a) and (b) were used to fabricate laboratory-grown PWSCC in test blocks P13, P15, P16, and P17. In order to grow a deep SCC flaw and also avoid the large crack opening, which typically accompanies bending loading techniques, the tensile loading type setup shown in Figure 2.9(a) was used to produce the flaw in P15. A tensile stress was generated from the difference of shrinkage between restraint weld and fixing frame during a cooling process. The bending loading type setup shown in Figure 2.9(b) was used for P13, P16, and P17, with the intent to introduce SCC flaws of shallow and medium depth. The process used is depicted as a flowchart in Figure 2.10.

The morphology of the SCC flaws generated by this technique are clustered in nature. An illustration of the typical flaw morphology is shown in Figure 2.11. In this case, the flaws resemble a cluster of axially oriented cracks with varying depths.



(a) Tensile loading setup for P15

(b) Bending loading setup for P13, P16 and P17

Figure 2.9 Depiction of the Approach Used to Produce a Laboratory-Grown PWSCC/IDSCC

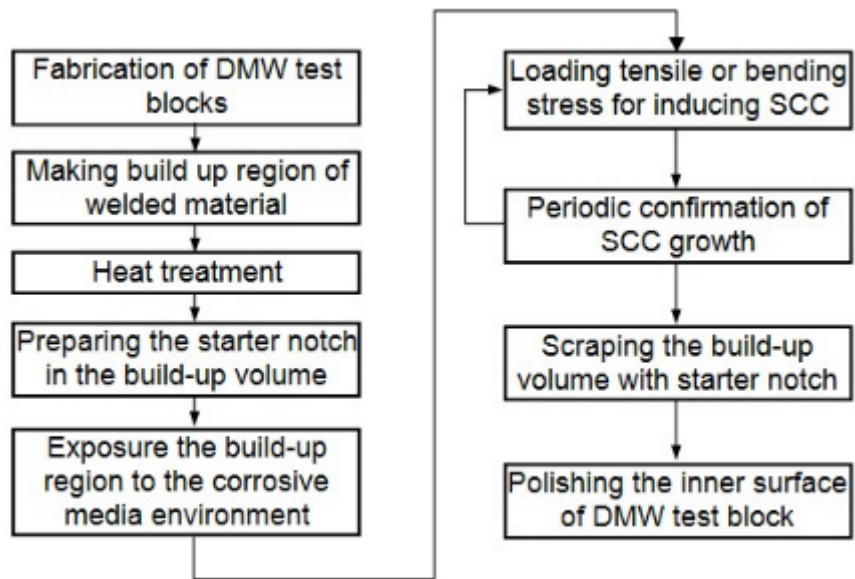


Figure 2.10 Flowchart of the Process Used to Produce a Laboratory-Grown PWSCC/IDSCC

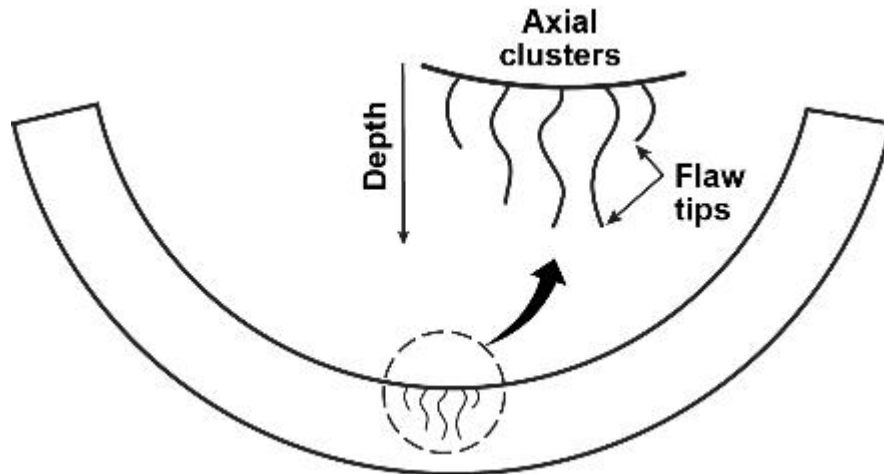


Figure 2.11 Illustration of Typical Flaw Morphology in P13, P15, P16, and P17

2.5.2 Thermal Fatigue Cracks [P6, P8, and P9]

Thermal fatigue cracks can be introduced directly into test blocks without welding or machining. TFCs can be grown directly into test specimens by placing the coil of a high-frequency inductive heater near the surface where the flaw is to be initiated and using water or gas jets to cool. A single crack or a network of cracks can be induced in the base material and welded areas without artificial crack initiators. An advantage of TFCs is that the location, orientation, and size of produced cracks can be accurately adjusted. In addition, TFCs are better at simulating the tightness between crack faces of PWSCC/IDSCC relative to mechanical fatigue cracks (MFCs) and EDM notches. A total of 31 TFCs were introduced into PARENT BMI specimens P6, P8, and P9. Fingerprinting of these flaws in test blocks P6, P8, and P9 indicated that the cracks are wider than a typical SCC flaw. Further, flaw clusters are actually observed at several locations. The clusters may make certain flaws easier to detect than they would be otherwise. In addition, flaw clusters can introduce difficulty in depth sizing because of the interference caused by several crack tips in close proximity. Flaw cluster formation is illustrated in the eddy current response from flaw 2 of test block P9, shown in Figure 2.12.

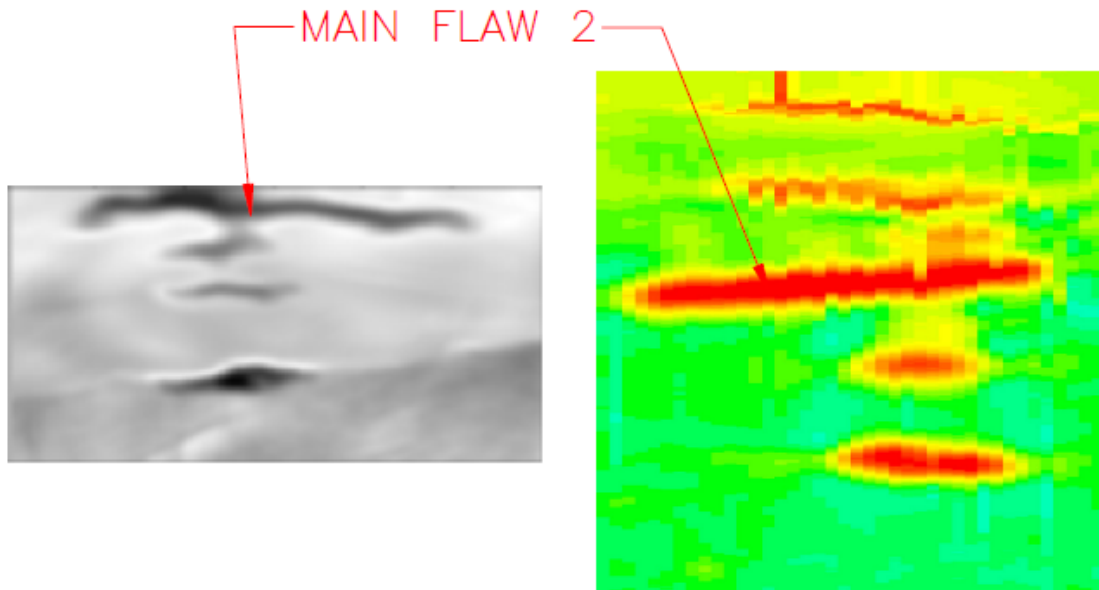


Figure 2.12 Eddy Current Response from Flaw 2 of Test Block P9 Showing Evidence of Flaw Cluster Formation

2.5.3 Weld Solidification Cracks [P35, P40, and P33]

Weld SCs may be used to simulate service-type defects such as IDSCC or PWSCC. The region where the cracks are fabricated are excised and filled with a “poisoned” weld metal that is designed to crack upon cooling. In this case, the SCs are tightened either through a welding process or through application of a mechanical pressure during fabrication to result in cracks with narrower width. Care must be taken when SCs are to be used to determine the capability of NDE methods because the region of flaw fabrication may be too obvious for the examination, similar to flaws that are implanted, especially in base metal. For this reason, SCs are recommended for simulating flaws in weld regions. A total of 44 tightened SCs were used to simulate service-induced SCC flaws in test blocks P35, P40, and P33.

2.5.4 Electrical Discharge Machined Notches [P27]

Three EDM notches are included in test block P27. Electrical discharge machining works by eroding the material in the path of electrical discharges that form between an electrode and the work piece. EDM notches are relatively easy to make and control the dimensions of, but they are often criticized for limited representation of real flaw features. In addition, the width of an EDM notch is dependent on the depth of the notch, with greater surface opening required with increasing depth.

2.5.5 Mechanical Fatigue Cracks [P27]

Test block P27 included five MFC flaws. MFCs are formed by cyclic mechanical loading of a test block or piece of material that is then implanted into a larger test block. MFCs typically have wider crack openings than SCC type flaws and the crack faces generally are not in contact except when under compression. Further, MFCs do not exhibit the branching behavior that is sometimes associated with SCC flaws.

2.5.6 Welding Defects [P25, P26, P27, and P40]

A total of ten welding defects are included in test blocks P25, P26, P27, and P40. The types of welding defects included lack of fusion, SI, porosity, and weld repairs.

2.6 True-State Determination

Information on flaw true states for each test block were documented on test block drawings by the test block contributors (PARENT participants) based on information documented in the flaw fabrication process and by fingerprinting, with the exception of P15, P16, and P17, which were destructively analyzed. In this case, the results of the destructive analysis were used to inform true-state determination.

3 TECHNIQUES AND PROCEDURES DESCRIPTIONS

This section describes the techniques/procedures used for testing in the blind portion of PARENT. The relationship between techniques and procedures is described in Section 3.1. Section 3.1 includes an overview of how relevant information on techniques and procedures used by participants was collected and organized. This is followed in Sections 3.2 and 3.3 with a brief technical background on the techniques used in blind testing, which includes variants of conventional UT, phased-array UT (PAUT), time-of-flight diffraction UT (TOFD), and eddy current testing (ECT). A tabulated summary of all of the techniques/ procedures applied in the blind round-robin testing (RRT) of PARENT is included in Appendix B based on information provided by teams in procedure summary data sheets, which are included in Appendix C. The objective of the descriptions provided in Sections 3.2 and 3.3 is to provide general descriptions of the techniques applied in blind testing and to define terminology used to specify details of the techniques in the information provided in Appendix C and summarized in Appendix B.

3.1 Procedure Summary Data Sheets

Teams submitted information describing the techniques and procedures used for inspections on a standardized form referred to as the “Procedure Summary Data Sheet.” A single inspection may require the application of several procedures and/or techniques to the test block. The description of the techniques used in a particular inspection is recorded on the “Procedure Summary Data Sheet.” This form also includes information describing how the results from individual technique applications are combined to provide the final inspection result. If a team used more than one procedure during the RRT, then a separate form for each procedure is submitted.

A summary of descriptions for all of the data fields in the “Procedure Summary Data Sheet” is provided in Table 3.1. An example of a completed “Procedure Summary Data Sheet” is also provided in Figure 3.1. In this example, a fictitious Team 12 has inspected test block P89 using Procedure 12.1. Procedure 12.1 uses three techniques in the inspection, identified as ET400kHz, TOFD.Ax, and TOFD.Circ. As indicated, the techniques are combined to obtain a final inspection result by using the ET400kHz technique for detection, length sizing, and defect position and using the TOFD.Ax and TOFD.Circ techniques for depth sizing and characterization.

A collection of Procedure Summary Data Sheets is provided in Appendix C. In addition to Procedure Summary Data Sheets, for each inspection, teams submitted an “Inspection Summary Data Sheet” and “Technique Data Sheets.” These will be described in Section 4.

Table 3.1 Definitions of Data Fields in the “Procedure Summary Data Sheet”

Field Name	Description
Procedure ID	This has format of Team-ID.seq-no and uniquely identifies this procedure in the round-robin test.
Team ID	This is a unique number assigned to each participating team in the test to maintain anonymity.
Procedure Type	Techniques utilized in the procedure are entered here (e.g., UT, ECT, PAUT). All of the techniques utilized in a procedure should be indicated in this field.
Scan Access	This field indicates if access is obtained from I.D. or O.D. If access is from both sides, “I.D. and O.D.” can be entered.
Scan Direction	This field indicates if scanning is performed in the axial or circumferential direction. If scanning is performed in both directions, it should be indicated.
Detection	This field should contain “yes” if at least one of the techniques in the procedure is able to detect flaws. Otherwise, it should contain “no.”
Length Sizing	This field should contain “yes” if at least one of the techniques in the procedure is able to length size flaws. Otherwise, it should contain “no.”
Depth Sizing	This field should contain “yes” if at least one of the techniques in the procedure is able to depth-size flaws. Otherwise, it should contain “no.”
Description for Combining Techniques	This field provides a description of how the results on the “Technique Data Sheets” are combined together to produce the results on the “Inspection Summary Data Sheet.”
Tech ID	This is a unique alpha-numeric Identifier assigned to each technique on the data form. The assignment is made by the invigilator/team.
Description	A short description of the technique equipment used.
Evaluation Method	Describe how data from equipment is used to detect or size flaws.

PARENT RRT-Procedure Summary Data Sheet

Procedure ID: 12.1	Team ID: 12
Procedure Type: UT & ET	Scan Access: ID
Scan Direction: Axial & Circ	Detection: yes
Length Sizing: yes	Depth Sizing: yes

Description for Combining Techniques: ET used for detection, length sizing, and positioning, TOFD techniques are used for characterization and depth sizing.

Detection

Tech-ID	Description	Evaluation Method
ET400kHz	400 KHz Eddy Current Raster Scan	Amplitude and phase

Characterization

Tech-ID	Description	Evaluation Method
TOFD.Ax	2MHz TOFD Axial Scan	Lateral wave break and tip diff.
TOFD.Circ	2MHz TOFD Circ. Scan	Lateral wave break and tip diff.

Length Sizing

Tech-ID	Description	Evaluation Method
ET400kHz	400 kHz Eddy Current Raster Scan	Amplitude and phase

Depth Sizing

Tech-ID	Description	Evaluation Method
TOFD.Ax	2MHz TOFD Axial Scan	Lateral wave break and tip diff.
TOFD.Circ	2MHz TOFD Circ. Scan	Lateral wave break and tip diff.

Defect Positioning

Tech-ID	Description	Evaluation Method
ET400kHz	400kHz Eddy Current Raster Scan	Amplitude and phase

Figure 3.1 Example of a Completed Procedure Summary Sheet for Illustration Purposes

3.2 Ultrasonic Testing Background

Several procedures utilized for blind testing in PARENT applied ultrasonic techniques. Specifically, the techniques applied included variations of conventional UT, TOFD, and PAUT. The following sections (3.2.1–3.2.3) provide a brief overview of these techniques to provide relevant background for specific techniques used in blind testing. A summary of these specific techniques is provided in Appendix B.

3.2.1 Conventional Ultrasonic Testing Concepts

Conventional UT usually refers to UT techniques based on application of single-element transducers applied for flaw detection or characterization through information provided by attenuation and/or velocity. In the blind testing portion of PARENT, conventional UT was applied in both pulse-echo (PE) and pitch/catch (PC) variations. Ultrasonic energy is introduced into the test specimen at an angle through the use of wedges to ensure sufficient interaction of the ultrasonic energy with planar flaws growing through the thickness of the test piece. Selection of the angle may depend on several factors including the material type, component thickness, and purpose of the examination. Illustrations of conventional UT applied in both PE and PC modes for examination of I.D. cracks are provided in Figures 3.2 and 3.3, respectively.

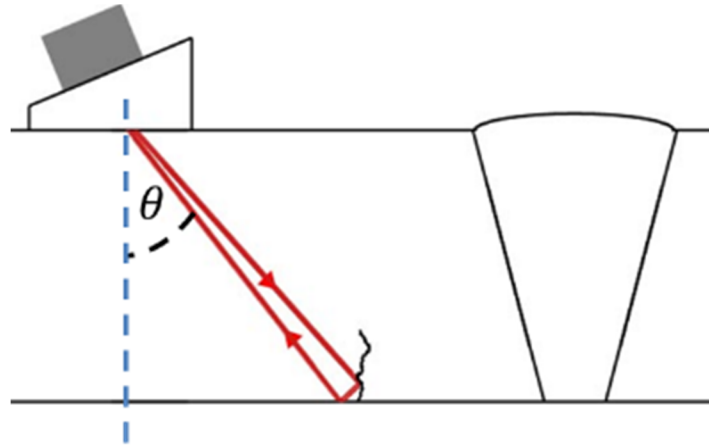


Figure 3.2 Illustration of Pulse-Echo UT Applied at Refracted Angle, θ , for Examination of I.D. Cracks

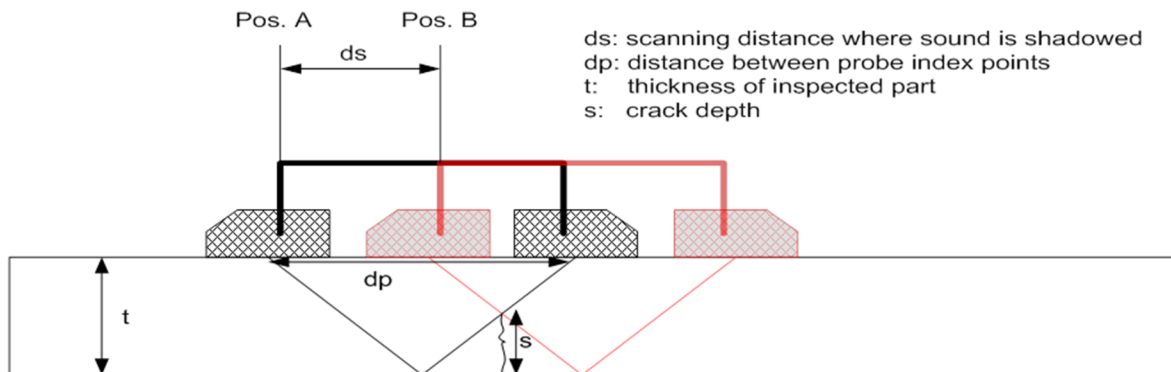


Figure 3.3 Illustration of Pitch/Catch UT Applied for Examination of I.D. Cracks

The PE mode of conventional UT can be implemented with a dual-mode transducer consisting of separate elements for transmitting and receiving signals. As such, these transducers are also referred to as transmit-receive (TR) transducers. In TR transducers, the transmit and receive sensors are electrically and acoustically isolated (see Figure 3.4) resulting in improved signal-to-noise ratio. Conventional UT performed with TR transducers and based on interrogation of test pieces with longitudinal waves is referred to as transmit-receive-longitudinal (TRL) testing.

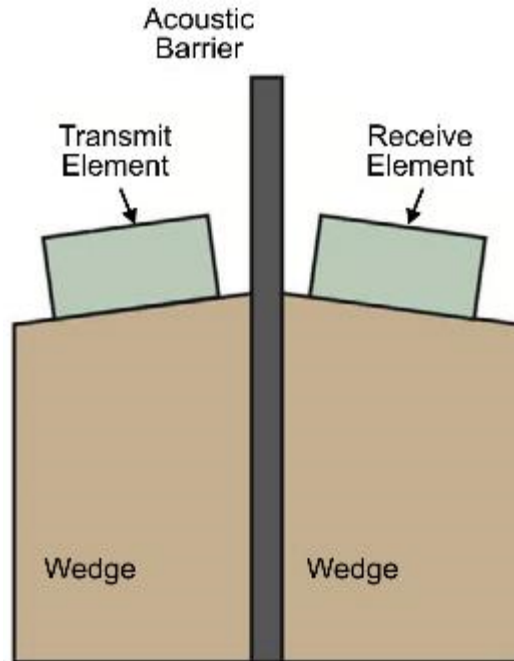


Figure 3.4 Illustration of a Transmit-Receive Transducer

Figure 3.2 illustrates that crack detection with PE mode can be based on the reflection of ultrasound by the corner where the crack plane intersects the component surface. Crack depth sizing can be performed based on both detection of a corner reflection signal and a phenomenon known as crack tip diffraction. Crack tip diffraction refers to the emission of a weak ultrasonic signal from the tip of an insonified crack, as depicted in Figure 3.5. Figure 3.5 also depicts an A-scan to illustrate how depth can be estimated from the difference in time of arrivals of the tip diffraction signal and corner reflection signal. In Figure 3.3, flaw evaluation (detection, sizing, characterization) is based on shadowing of the signal from the transmitter, resulting in a drop in the signal at the receiver. Sizing (both length and depth) can also be based on amplitude drop methods, as illustrated in Figure 3.6.

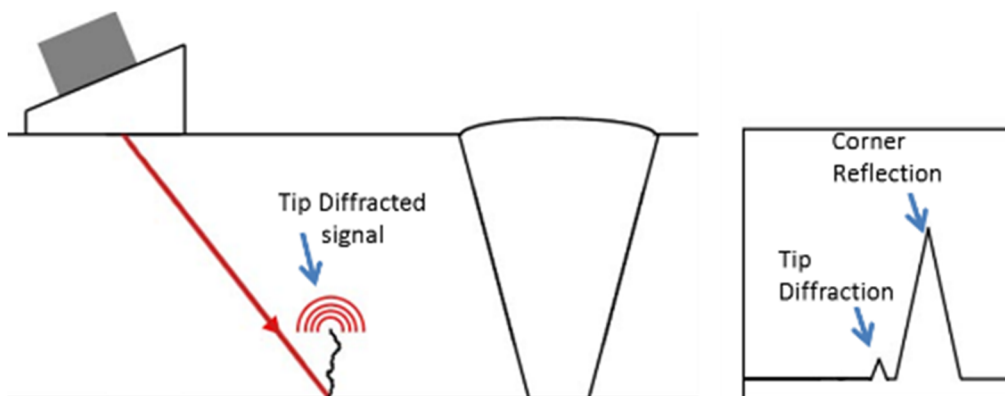


Figure 3.5 Illustration of Crack Tip Diffraction and Crack Depth Sizing Based on Tip Diffraction Signal and Corner Reflection

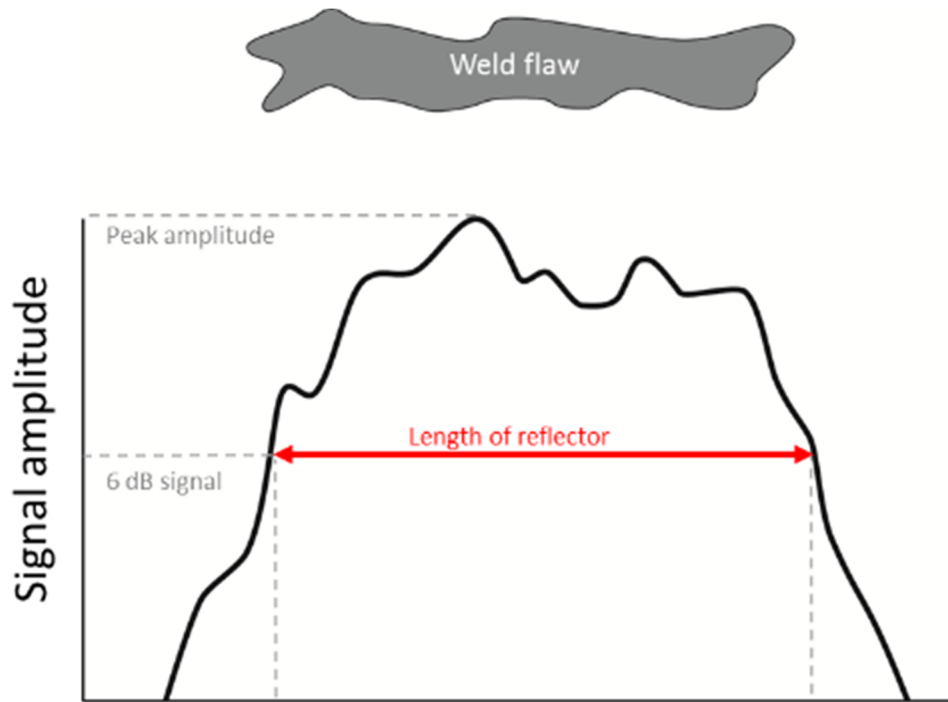


Figure 3.6 Illustration of Amplitude Drop Method for Flaw Sizing

3.2.2 Time-of-Flight Diffraction

The TOFD technique is a two-probe method using one probe for transmitting and the other probe for receiving (Figure 3.7). The transmitter introduces an L-mode beam at an angle and a so-called “lateral wave” that propagates along the component surface. With no flaws present, the receiver will pick up a back-wall echo and the transmitted lateral wave. The transit time information for the back-wall signal and lateral wave can enable crack detection and location. In the case of front-surface cracks, crack detection and location will be based on the lateral wave echo. For back-surface cracks, detection and location will be based on the back-wall signal. Depth sizing may be accomplished by detection and transit time analysis of a tip-diffracted signal.

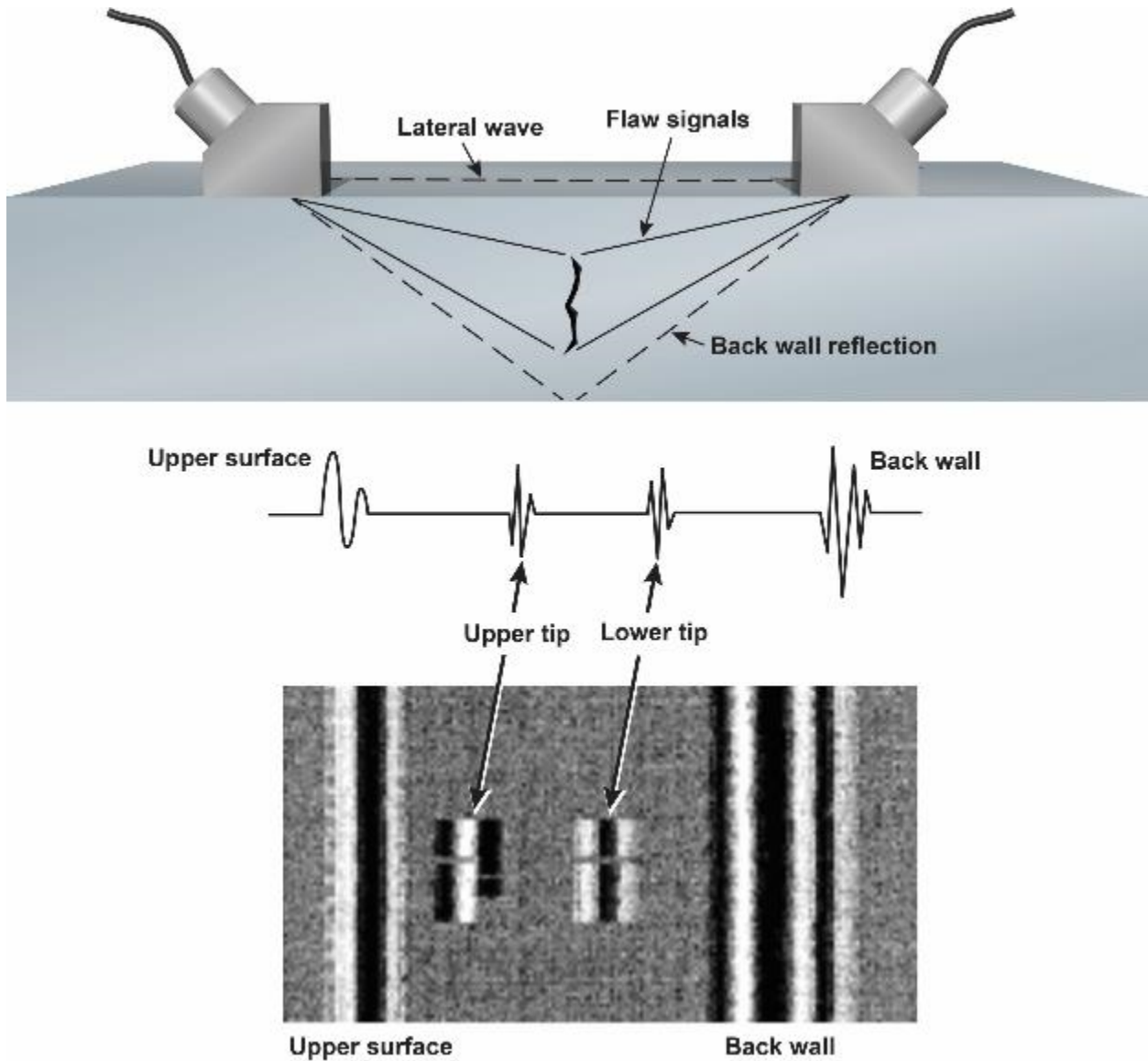


Figure 3.7 Diagram of Time-of-Flight Diffraction Technique

3.2.3 Phased-Array UT

Phased-array ultrasonic techniques have been gaining increased acceptance for performing ISI of nuclear power plants. PAUT uses a transducer consisting of multiple piezoelectric or piezocomposite elements in contrast to conventional UT, which uses transducers with only a single element. Electronic beam steering and focusing is achieved by careful time delay sequencing of excitation signals to the individual elements in the PAUT transducers to create complex constructive and destructive interference patterns to intensify the sound field in a desired location (see Figure 3.8). There are several types of phased-array transducers including a linear array transducer and 2-D matrix array transducers. A linear array transducer is only capable of steering the beam over a range of refraction angles within a single plane while a 2-D matrix array is capable of providing adjustments to both beam refraction angle and beam skew, as illustrated in Figure 3.9. Figure 3.9 also illustrates that PAUT can be implemented using a TR probe.

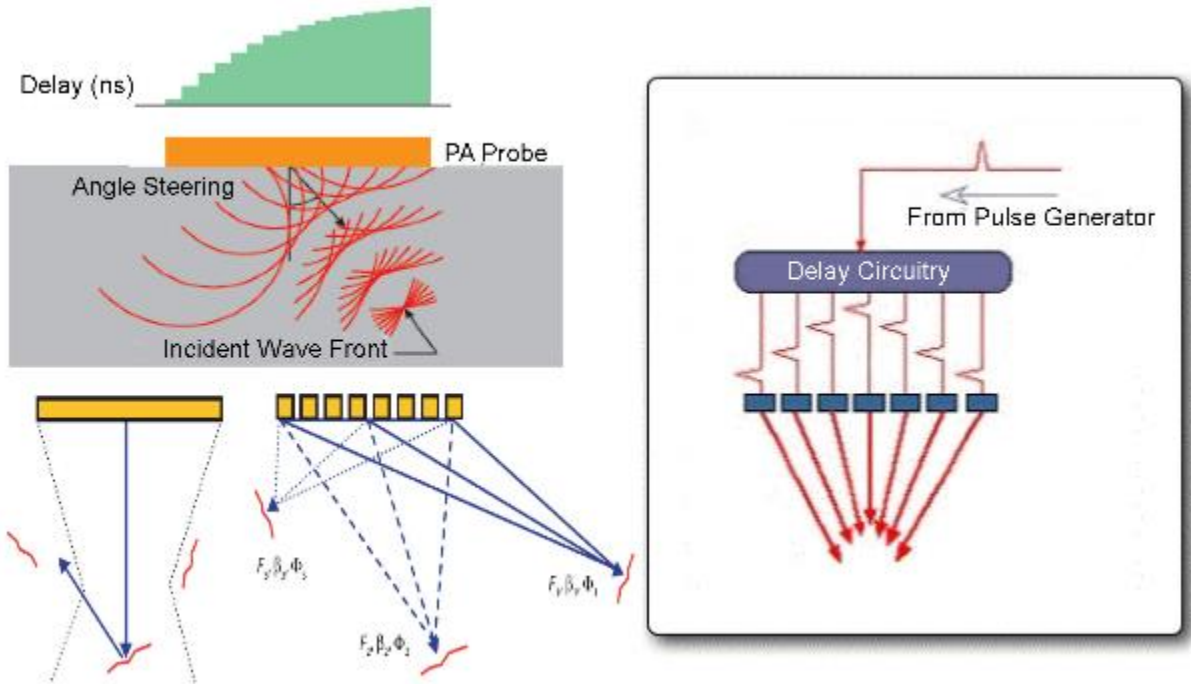


Figure 3.8 Illustration of Time Delay Sequencing of Excitation of PAUT Transducer Elements to Achieve Beam Steering and Focusing

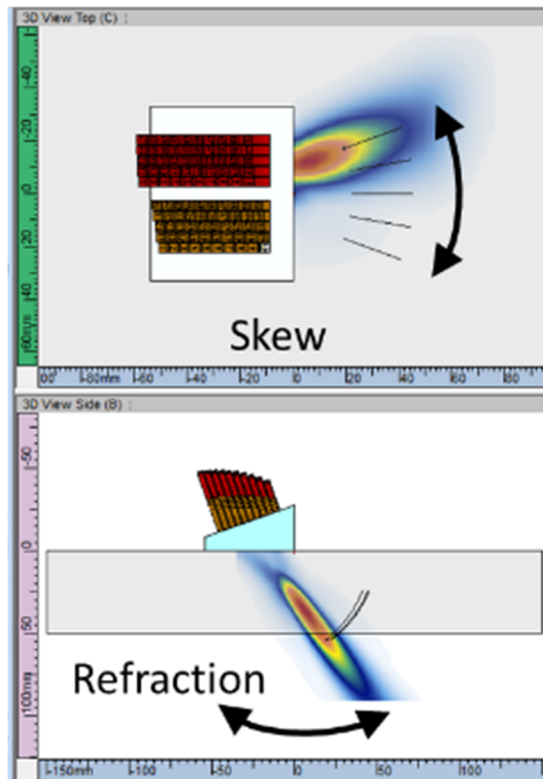


Figure 3.9 Illustration of Beam Skew and Beam Refraction Directions for Matrix PAUT Probe

One of the significant capabilities facilitated by the use of PAUT is that of sectorial scanning. Sectorial scanning refers to sweeping of the sound beam over a range of refraction angles. This allows data obtained from many angles to be collected quickly, enhancing flaw detection and characterization. This is in contrast to conventional UT, which require change out of transducers for each refraction angle desired, or to PAUT performed in linear scan mode, in which the refraction angle is fixed. An illustration of sectorial scanning is provided in Figure 3.10.

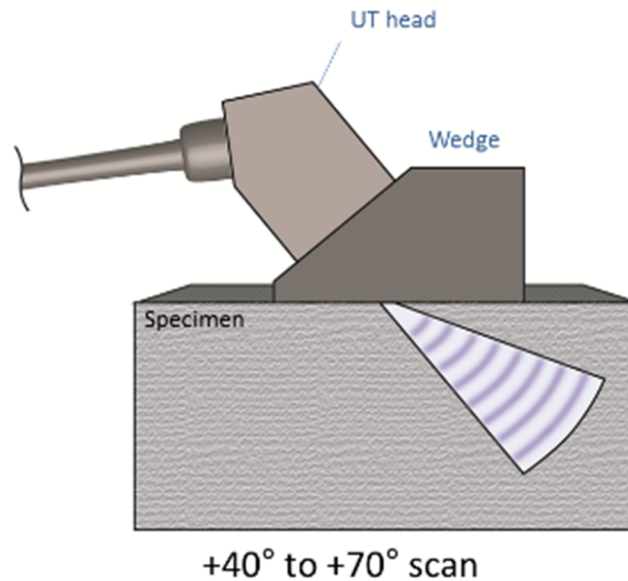


Figure 3.10 Depiction of Sectorial Scanning with PAUT

PAUT data is often presented in A-scan, B-scan, C-scan, and D-scan image form for analysis. An A-scan is a trace of the signal amplitude versus time and resembles a trace on an oscilloscope display. The A-scan is characterized by peaks at the location of reflectors. Illustrations depicting the B-scan, C-scan, and D-scan viewpoints are provided in Figure 3.11. The B-scan could represent a single index plane, a selected range of index planes, or all index planes in the scan volume. If more than one index plane is selected, the B-scan image is a composite view of all the planes. More specifically, the maximum response at each scan and depth position from all selected index planes is displayed. The D-scan end view corresponds to a plane along the index axis. Therefore, the image horizontal represents the index axis and the vertical represents the specimen thickness. Finally, a C-scan top view is a bird's eye view of the data volume with horizontal and vertical axes representing scan and index directions. Figure 3.12 shows an example of PAUT data representation as A-scan, B-scan, C-scan, and D-scan images. From these data representations, the linear dimensions of a flaw are characterized based on image analysis. In addition, data can be presented in a sectorial view (see Figure 3.13).

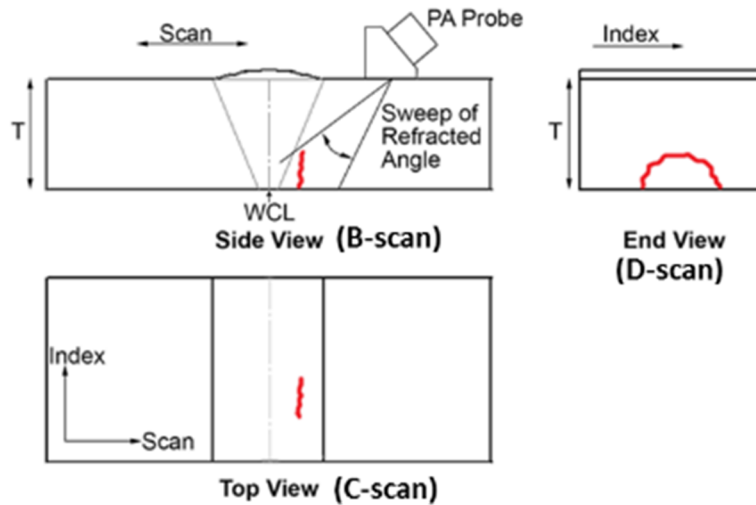


Figure 3.11 Illustration of B-scan, C-scan, and D-scan Views for Displaying PAUT Data Responses

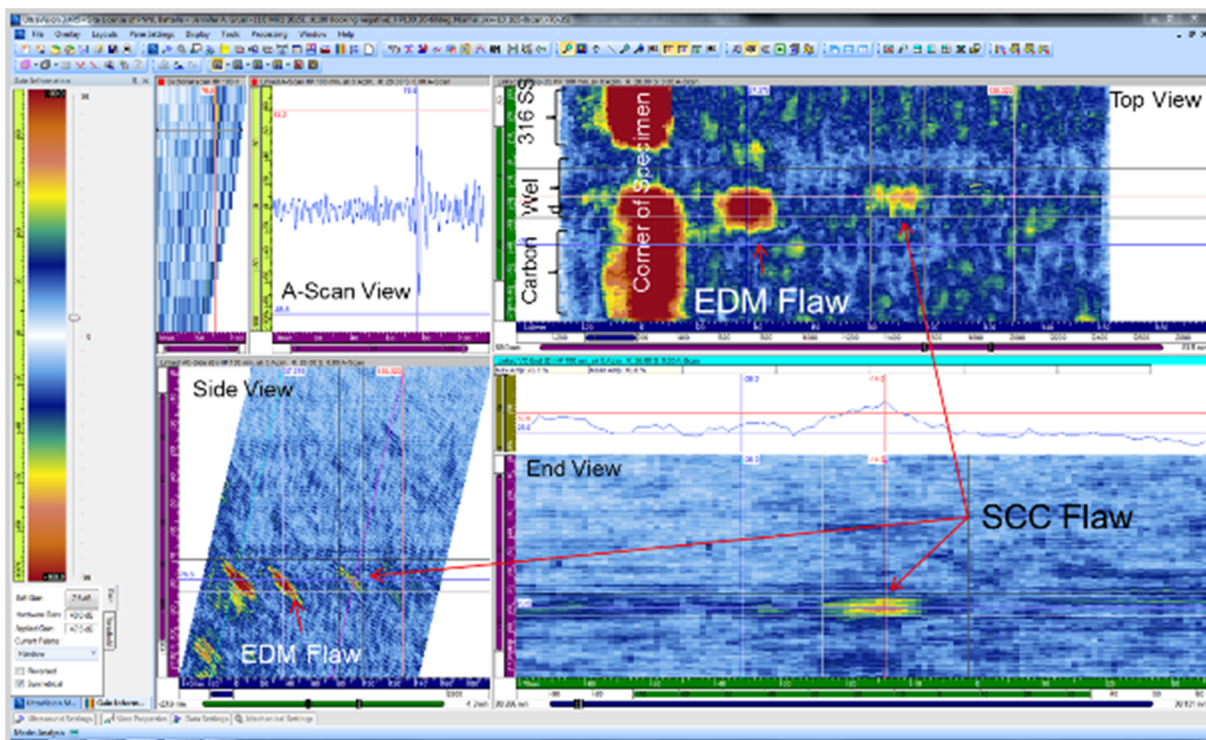


Figure 3.12 PAUT Data Represented as A-scan (top left), C-scan (top right), B-scan (bottom left), and D-scan (bottom right)

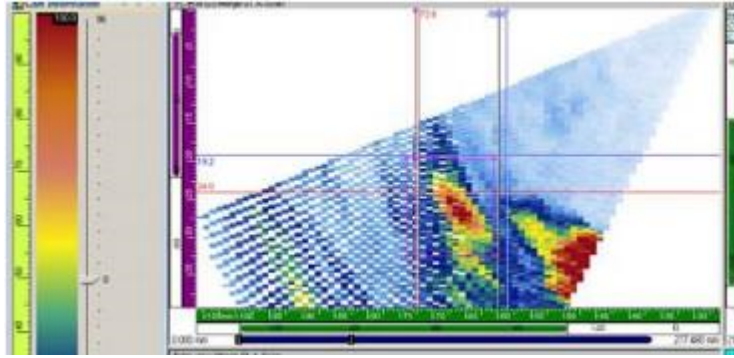


Figure 3.13 PAUT Data Represented as Sectorial Scan

3.3 Eddy Current Techniques

In practice, an eddy current probe consists of one or more coils with the axis alignment most often perpendicular or parallel to the inspection surface normal. An alternating current source is applied to the one or more coils, generating magnetic fields. These magnetic fields induce eddy currents in the conducting materials when the probe is positioned nearby (see Figure 3.14). Flaws and defects in the test material impede the flow of eddy currents manifesting as a change in the measurable eddy current coil impedance. An important parameter for ECT is the skin depth, δ ,

$$\delta = \sqrt{\frac{1}{\pi f \sigma \mu}} \quad (3.1)$$

which provides a measure of the depth to which eddy current fields can penetrate in a test material. As can be seen from Eq. (3.1), this quantity depends on the coil frequency, f , and electrical conductivity, σ , of the test material (μ is the magnetic permeability). Thus, in metal components, the depth of penetration is usually small and the eddy current technique is often limited to surface examinations. Multi-coil techniques can include separate coils for the generation of eddy current fields in the test material and for detection of the fields at the surface, as illustrated in Figure 3.15. These types of probes may also be referred to as reflection probes, driver-pickup, exciter-pickup, or send-receive probes. This contrasts with absolute coil ECT in which the same coil is used for both field generation and for signal reception as illustrated in Figure 3.14.

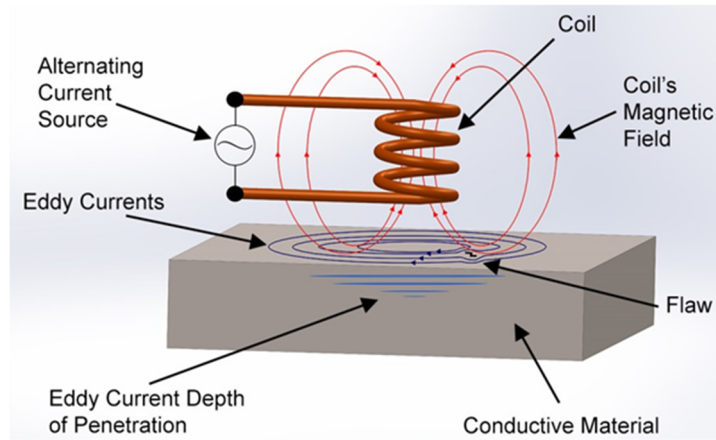


Figure 3.14 Depiction of a Single Coil Eddy Current Probe with an Alternating Current Excitation, Induced Magnetic Fields, and Induced Eddy Currents. Disturbance of eddy current flow can be caused by existence of a defect.

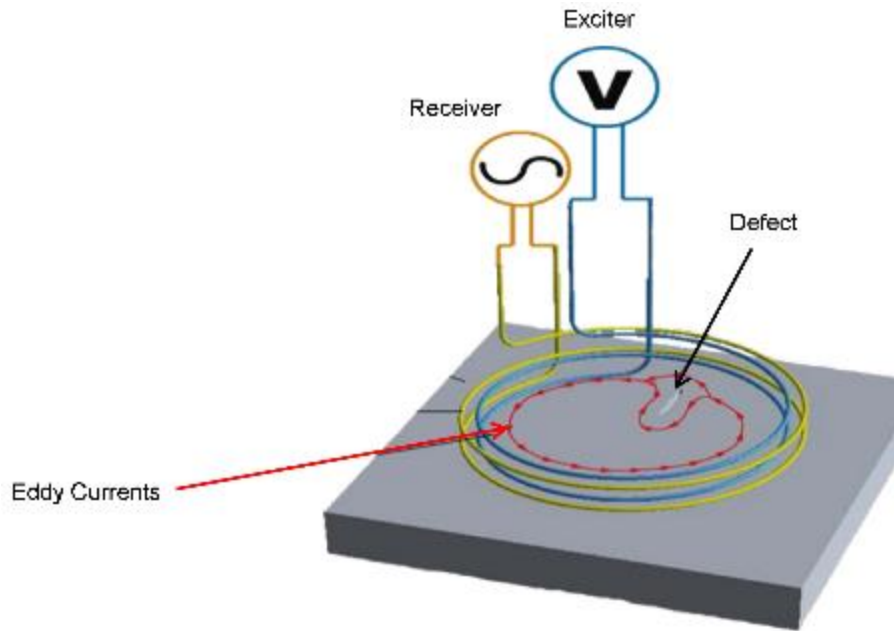


Figure 3.15 Schematic Illustration of an Eddy Current Probe with Separate Coils for Field Excitation and for Signal Detection

The cross-coil eddy current probe refers to a configuration with two orthogonal coils (OC) oriented relative to the test surface as shown in Figure 3.16. The cross-coil ECT technique is a differential eddy current technique meaning that the output of one coil is referenced to the output of the other coil. Differential eddy current probes are typically less sensitive to lift-off and surface irregularities. One advantage of cross-coil ECT is that it has directional sensitivity to flaws, making it possible to distinguish between axial and circumferential defects. The OC configuration helps minimize the influence of flaw orientation with respect to the probe performance as defects that are parallel to the current flow can be missed. Rotation of the OC-ECT probe can also be performed to further minimize the influence of flaw orientation.

In general, the advantage of ECT over conventional UT, PAUT, and TOFD is that it is more sensitive to small defects and the probes do not require coupling to the test material surface. As noted, a significant disadvantage of ECT is that it is usually relegated to surface inspections and is not very useful for characterizing the depth of flaws. In addition, the increased sensitivity of ECT can make it more prone to false calls from the pick up of signals from superficial surface imperfections (such as scratches) and ECT can be sensitive to lift-off variations and variations in material conductivity.

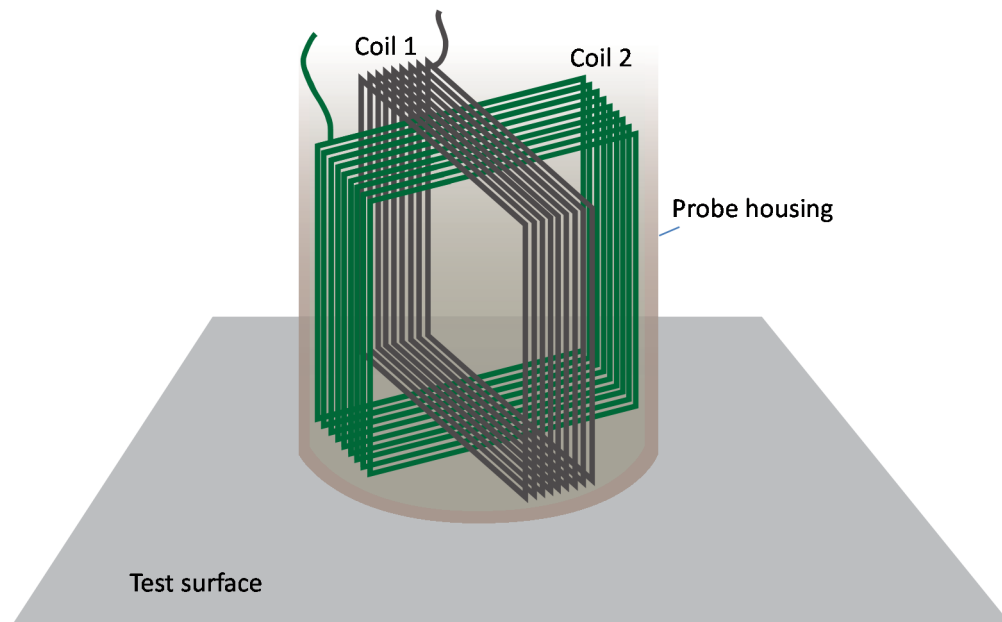


Figure 3.16 Depiction of the Cross-Coil Eddy Current Probe Configuration

4 DATA OVERVIEW

This section provides information on what data was recorded and reported during PARENT blind round-robin testing and how the data is scored for detection and sizing analysis. Section 4.1 provides a description of data reporting by describing the data sheets used to record and report test data. Section 4.2 provides an overview summary of inspection records collected, while Section 4.3 includes a discussion of how data is scored and how it is analyzed. Section 4.4 includes a discussion of how probability of detection (POD) is calculated and how it is presented throughout the report. Section 4.7 includes a discussion of how sizing analysis is performed and how sizing results are presented. PARENT utilizes the same procedures for scoring and analyzing test data that were used in PINC (Cumblidge et al. 2010) and the relevant description from PINC is provided in Appendix D for reference.

4.1 Data Reporting

This section provides an example of the completed data forms for one inspection. In this inspection, Team 12 has inspected test block P89 using Procedure 12.1. Procedure 12.1 uses three techniques in the inspection, identified as ET400kHz, TOFD.Ax, and TOFD.Circ. Consequently, this inspection generates three Technique Data Sheets, and one Inspection Summary Data Sheet. A Procedure Summary Data Sheet is also necessary to describe the inspection procedure, but it may apply to several inspections. Procedure Summary Data Sheets are described in Section 3.1.

Illustrations of Technique Data Sheets and an Inspection Summary Data Sheet are provided in Figures 4.1 through 4.3. Information in the Inspection Summary Data Sheets is based on data recorded in Technique Data Sheets. For the example provided, techniques TOFD.Ax and TOFD.Circ are used for depth sizing and characterization while technique ET400kHz is used for detection, length sizing, and positioning. This information is combined in completion of the Inspection Summary Data Sheet. Similar data fields are included in Technique Data Sheets and Inspection Summary Data Sheets. A summary of descriptions for all of the data fields is provided in Table 4.1. Figures 4.1 through 4.3 show that data sheets include a table where information about each observed indication is recorded. The information includes a series of coordinates (X1, X2, Y1, Y2, Z1, Z2) that describe a cuboid that envelopes an observed indication, allowing for comparison of its position and size to true-state information for both detection and sizing analysis. In addition, fields " Y_{max}/X_{max} ," "Amp dB," and "Surface Breaking" are included to allow recording of the location where a maximum signal response is observed, the value of that signal, and whether or not an observed indication is surface breaking.

Table 4.1 Definitions of Data Fields for “Technique Data Sheets” and “Inspection Summary Data Sheets”

Field Name	Description
Procedure ID	This has format of Team-ID.seq-no and uniquely identifies this procedure in the round-robin test. This ID originates from the Procedure Summary Data Sheet that describes this technique.
Team ID	This is a unique number assigned to each participating team in the test to maintain anonymity.
Tech ID	This is a unique alpha-numeric identifier assigned to each technique on the data form. This ID originates from the Procedure Summary Data Sheet and identifies the technique being applied.
Inspection ID	This ID identifies each unique inspection performed. One inspection ID is common to all inspections made on a specific test block, by a specific test team, for all the Technique IDs applied within a specific Procedure ID. Format: Team-id.Block-id.seq-no.
Test Block ID	ID of the test block being inspected.
Access	This field indicates if access is obtained from I.D. or O.D. If access is from both sides, “I.D. and O.D.” can be entered.
Date	Date of inspection.
Detection	This field should contain “yes” if at least one of the techniques in the procedure is able to detect flaws. Otherwise, it should contain “no.”
Length Sizing	This field should contain “yes” if at least one of the techniques in the procedure is able to length size flaws. Otherwise, it should contain “no.”
Depth Sizing	This field should contain “yes” if at least one of the techniques in the procedure is able to depth-size flaws. Otherwise, it should contain “no.”
Weld Volume Inspected	Coordinates of the volume of material inspected.
Defect No.	Uniquely identifies each observed indications.
X1, X2, Y1, Y2, Z1, Z2	These coordinates describe a cuboid that contains the observed indication.
Y_{max}/X_{max}	This identifies the location at which a maximum signal is observed.
Amp dB	The amplitude of the signal observed at Y_{max}/X_{max} is recorded here.
Surface Breaking	Indicate whether or not a flaw is surface breaking.
Comments	To include useful information about each indication found.

PARENT RRT- DMW TECHNIQUE Data Sheet

Procedure ID:12.1
 Inspection ID:12.P89.1
 Test Block ID:P89
 Team ID:12

Tech ID: ET400Hz
 Access:ID
 Date:2010/01/01

Detection:*yes*
 Length Sizing:*yes*
 Depth Sizing:*no*

Weld Volume Inspected
 X1:0 X2:457
 Y1:-31 Y2:20
 Z1:0 Z2:68

Defect No	X1 mm	X2 mm	Y1 mm	Y2 mm	Z1 mm	Z2 mm	Y_{max} mm	Amp dB	Surface Breaking	Comments
1	230.2	235.5	-11	1	NA	NA	NA	NA	yes	
2	215.2	218.2	-12	5	NA	NA	NA	NA	yes	

PARENT RRT- DMW TECHNIQUE Data Sheet

Procedure ID:12.1
 Inspection ID:12.P89.1
 Test Block ID:P89
 Team ID:12

Tech ID: TOFD.Ax
 Access:ID
 Date:2010/01/01

Detection:*no*
 Length Sizing:*no*
 Depth Sizing:*yes*

Weld Volume Inspected
 X1:0 X2:457
 Y1:-31 Y2:20
 Z1:0 Z2:68

Defect No	X1 mm	X2 mm	Y1 mm	Y2 mm	Z1 mm	Z2 mm	Y_{max} mm	Amp dB	Surface Breaking	Comments
1	227.4	229.9	-12	-1	50.3	68.2	-6	-14	yes	
2	226.4	225.4	-11	2	51.7	68.2	-5	-12	yes	
3	224.8	227.7	-10	1	48.2	68.2	-3	-19	yes	
4	226.3	226.5	-12	1	50.3	68.2	-2	-16	yes	

Figure 4.1 Technique Data Sheets for Techniques ET400Hz and TOFD.Ax for Fictitious Inspection 12.P89.1

PARENT RRT-DMW TECHNIQUE Data Sheet										
Procedure ID:12.1					Tech ID: TOFD.Circ					
Inspection ID:12.P89.1					Access:ID					
Test Block ID:P89					Date:2010/01/01					
Team ID:12										
Detection: <i>no</i>					Weld Volume Inspected					
Length Sizing: <i>no</i>					X1:0		X2:457			
Depth Sizing: <i>yes</i>					Y1:-31		Y2:20			
					Z1:0		Z2:68			
Defect No	X1 mm	X2 mm	Y1 mm	Y2 mm	Z1 mm	Z2 mm	Y_{max} mm	Amp dB	Surface Breaking	Comments
1	219.8	220.6	-8	-1	62.5	68.2	-4	-8	yes	
2	233.0	234.2	-10	1	58.4	68.2	-8	-7	yes	

Figure 4.2 Technique Data Sheet for Technique TOFD.Circ for Fictitious Inspection 12.P89.1

PARENT RRT-DMW INSPECTION SUMMARY Data Sheet										
Inspection ID:12.P89.1					Procedure ID:12.1					
Test Block ID:P89					Date:2012/01/01					
Team ID:12					Access: ID					
Detection: <i>yes</i>					Weld Volume Inspected					
Length Sizing: <i>yes</i>					X1:0		X2:457			
Depth Sizing: <i>yes</i>					Y1:-31		Y2:20			
					Z1:0		Z2:68			
Defect No	X1 mm	X2 mm	Y1 mm	Y2 mm	Z1 mm	Z2 mm	Y_{max} mm	Amp dB	Surface Breaking	Comments
1	230.2	235.5	-11	1	48.2	68.2	-3	-19	yes	Detection: Tech-ID ET400kHz Length: Tech ID ET400kHz Depth: Tech-ID TOFD.Ax
2	#	#	#	#	#	#	#	#	entry	As was done for flaw 1, data could be entered for flaw 2

Figure 4.3 Inspection Summary Data Sheet for Fictitious Inspection 12.P89.1

4.2 Records Collection Overview Summary

The number of inspection summary data sheets collected (equivalent to the number of inspections) for each block type (i.e., BMI, DMW, and WOL) is tabulated in Table 4.2 according to procedure ID. Procedure ID is expressed here as “Tech1.Tech2...TechN.TeamID” where Tech1 through TechN represent all the techniques used for a given procedure ID. The possible techniques include conventional UT, PAUT, ECT, and TOFD, as mentioned in Section 3. For example, team 126 employs a procedure that includes a TOFD technique and an ECT technique; thus, its procedure name is TOFD.ECT.126. Table 4.3 breaks down the number of inspections by access type (i.e., O.D. vs. I.D.) for BMI, DMW, and WOL test blocks. Table 4.4 tabulates the number of flaws by flaw type and Table 4.5 tabulates number of flaws by flaw orientation. Flaw orientation is considered axial if the axial dimension of the flaw is 3x the circumferential dimension or greater. Flaw orientation is considered circumferential if the circumferential dimension of the flaw is 3x the axial dimension or greater. If neither of these criteria is met, the flaw is classified as diagonal. In this case, the term diagonal is used to distinguish from axial and circumferential orientation and reflect that the flaw does not have a dominant orientation in the axial or circumferential direction based on dimensions.

In these tables, an inspection refers to the application of a procedure to a test block. Thus, the number of inspections for BMI test blocks (tube I.D. access) for instance, refers to the number of procedures applied to all BMI test blocks by tube I.D. access. The number of flaw observations is the number of flaws times the number of times an attempt is made to detect them (equal to the number of inspections). For each inspection performed on a test block, it is assumed that an attempt is made to detect all of the flaws in the test block. For a given test block, the number of flaw observations is equal to the total number of flaws in the test block multiplied by the number of times the test block is inspected. For a test block type, such as BMIs, it is equal to the sum of the number of flaws in each BMI test block times the number of times each BMI test block is inspected. For ECT procedures, subsurface flaws are excluded.

Table 4.2 Number Inspection Summary Data Sheets Collected for Each Procedure

	BMI	DMW	WOL	Form Procedure ID (Appendix C)
ECT.108	4	0	0	108.6
ECT.124	4	0	0	124.1
ECT.135	0	1	0	135.1
PAUT.108.1	0	4	0	108.3
PAUT.108.2	0	0	1	108.4
PAUT.115	0	2	0	115.1
PAUT.126.1	0	4	0	126.2
PAUT.126.2	0	0	1	126.4
PAUT.128	0	2	0	128.1
PAUT.132	0	4	0	132.1
TOFD.ECT.126	2	0	0	126.5
UT.108	0	4	0	108.2
UT.126	0	4	0	126.3
UT.134.1	0	4	0	134.1
UT.134.2	0	4	0	134.2
UT.25	0	1	0	25.1
UT.ECT.106	0	4	0	106.1
UT.ECT.144	0	2	0	144.1
UT.PAUT.108	0	4	0	108.1
UT.PAUT.113	0	5	0	113.1
UT.PAUT.126	0	4	0	126.1
UT.TOFD.117	0	2	0	117.1
UT.TOFD.ECT.101	0	2	0	101.1
TOTAL	10	57	2	

UT = conventional UT

Table 4.3 Number of Inspections by Access

	I.D.	O.D.
BMI	2 (tube)	10 (j-groove)
DMW	18	39
WOL	0	2
Total	25	46

Table 4.4 Number of Flaw Observations by Flaw Type

	BMI	DMW	WOL
Mechanical Fatigue Crack (MFC)	0	0	10
Electric Discharge Machine (EDM) Notch	0	0	6
Solidification Crack (SC)	0	380	0
Stress Corrosion Crack (SCC)	0	25	0
Thermal Fatigue Crack (TFC)	62	0	0
Weld Defects	15	16	4
Total	77	421	20

Table 4.5. Number of Flaw Observations by Flaw Orientation

	BMI	DMW	WOL
Axial	21	124	0
Circumferential	43	271	12
Diagonal	13	26	8
Total	77	421	20

4.3 Scoring Procedure Used for PARENT Blind Round Robin

PARENT utilized the same scoring criteria as PINC which is described in Section 4.1 of NUREG/CR-7019 (Cumblidge et al. 2010) and also included in Appendix D of this report for reference. Similar to PINC, a tolerance was added to flaw true-state dimensions in PARENT to limit systematic positioning error resulting in legitimate detections being classified as misses. Once the tolerance is defined, δX and δY , then the flaw cuboid, $X_1, X_2; Y_1, Y_2; Z_1, Z_2$, becomes,

$$(X_1 - \delta X, X_2 + \delta X, Y_1 - \delta Y, Y_2 + \delta Y, Z_1, Z_2) \quad (4.1)$$

An illustration of tolerance applied to flaw true-state (solid red) dimensions is provided in Figure 4.4 resulting in an enlarged region represented by white space with a red border. Indications that intersect any portion of this enlarged region are classified as hits. A tolerance analysis was performed for PARENT data to determine the appropriate tolerance for both DMW and BMI test blocks in PARENT. The POD versus scoring tolerance is plotted in Figure 4.5 for DMW test blocks and Figure 4.6 for BMI test blocks. These figures indicate that the POD begins to level off with a scoring tolerance of approximately $\delta X = \delta Y = 10$ mm. This observation is consistent with PINC in which a 10-mm tolerance was applied to flaws for detection analysis. A collection of indication plots for all of the blind inspections performed in PARENT is included in Appendix E. An illustration of an indication plot is provided in Figure 4.7. The red rectangles represent the “true-state” (actual flaws) with the surrounding tolerance box. Indications are shown as empty rectangles.

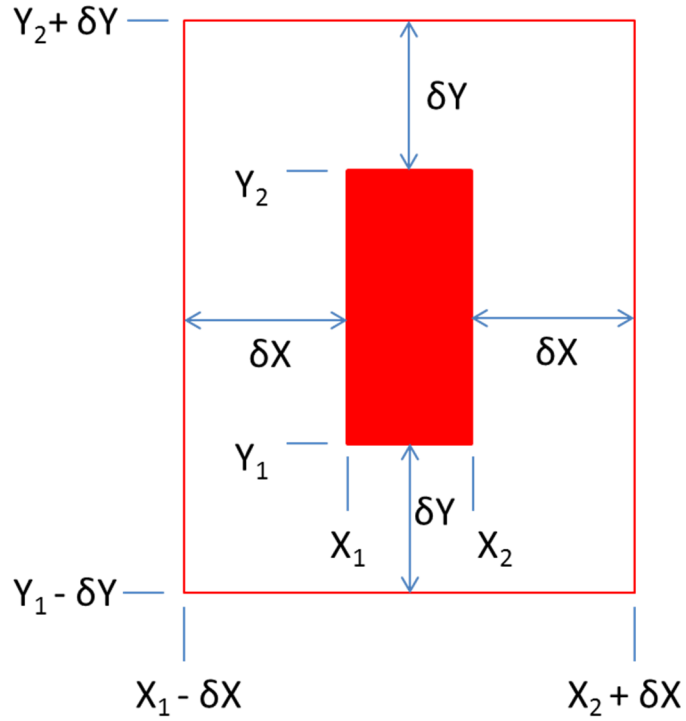


Figure 4.4 Illustration of Tolerance (δX and δY) Applied Flaw True-State (in red) Dimensions for the Purpose of Scoring in PARENT

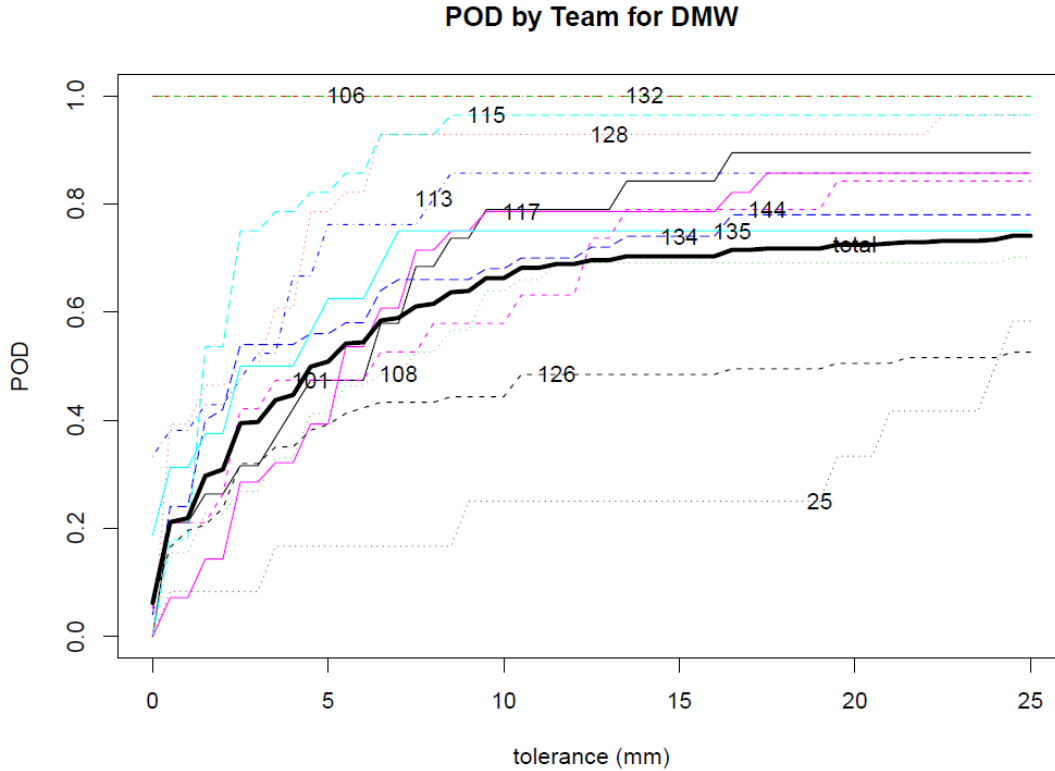


Figure 4.5 Probability of Detection versus Scoring Tolerance for DMW Test Data

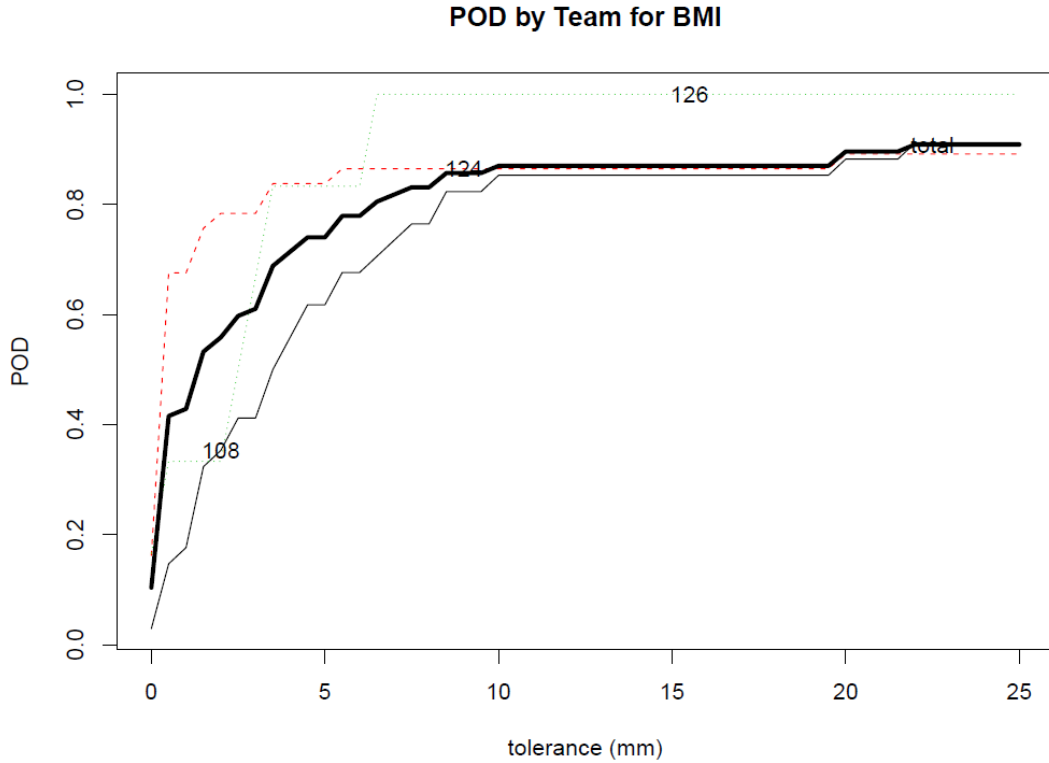


Figure 4.6 Probability of Detection versus Scoring Tolerance for BMI Test Data

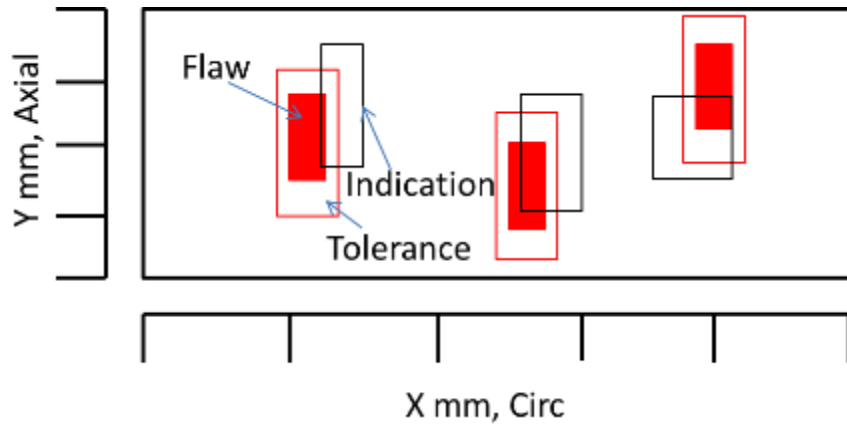


Figure 4.7 Depiction of Indication Plot Illustrating 2-D Representation of Test Block. The red filled rectangles represent the true-state (actual flaws), while red empty rectangles surrounding the flaws depict the scoring tolerance. Indications are shown as black empty rectangles.

4.4 Multiple Indications Associated with One Flaw

In a few cases, multiple indications may intersect the region bounded by the tolerance box for the same flaw. An example is provided in Figure 4.8 for procedure ECT.135 inspection on test block P33. For these scenarios, it is necessary to select one of the indications for performing the sizing analysis. The selection is based on the indication with the largest intersecting area with the tolerance region. To accommodate indications that may have no width defined in one dimension

(i.e., X or Y), and thus have no area, the tolerance is divided between the flaw and the indications with values of $\delta X/2$ and $\delta Y/2$ (refer to Figure 4.4). This is illustrated in Figure 4.9. The indication whose tolerance boundaries form the largest region of intersection with the area defined by the flaw tolerance boundaries is selected as the indication to associate with the flaw for sizing analysis purposes.

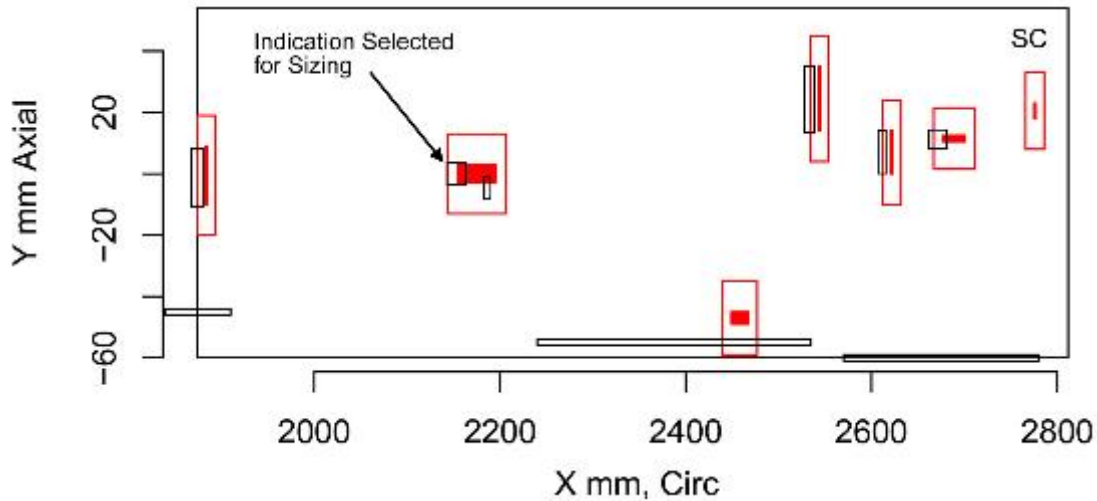


Figure 4.8 Indication Plot for ECT.135 Applied to P33 from X = 2000 mm to X = 2800 mm Illustrating Two Indications Intersecting the Region Bounded by the Tolerance Box

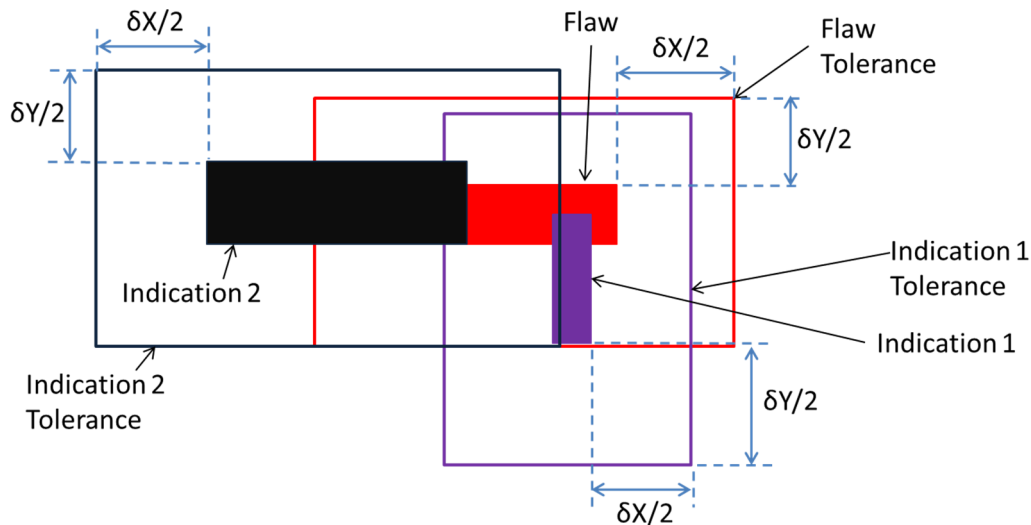


Figure 4.9 Illustration of Tolerance Divided Between Flaw and Multiple Indications Intersecting the Region Bounded by the Flaw Tolerance Box

4.5 Multiple Flaws Associated with One Indication

SBDMW test block P35 had a circumferentially oriented flaw and axially oriented flaw with overlapping tolerance bounds. These flaws did not meet the criteria for combining flaws as defined by the description of the “Scoring Process for Multiple Closely Spaced Cracks” in

Appendix D.5. Six indication plots in Figures 4.10 through 4.15 highlight six inspections in which an indication overlapped the tolerance boundaries of the flaws with overlapping tolerance boundaries. In this analysis, the indications were scored as a hit for both flaws, and each flaw was considered detected. In addition, sizing analysis was performed by comparing the dimensions of the indication with the dimensions of each flaw. It is conceivable that the analysis could have been performed by associating the indication with just one of the flaws by comparing the orientation of the indication with the orientation of the flaws. For instance, it appears that in Figures 4.10 and 4.11 the indications overlapping the two flaw boundaries have circumferential orientations and could be associated with only the circumferential flaw. Conversely, Figures 4.12, 4.13, and 4.15 have indications that appear to have an axial orientation. Thus, the indication could be associated with the axial flaws in these inspections. In Figure 4.14, the flaw orientation is ambiguous and it would be difficult to determine which flaw the indication should be assigned to. If the analysis were performed in this way, the PODs would be slightly lower because there would be one less hit for each inspection represented in Figures 4.10 through 4.15. The results of sizing analysis may be influenced positively, assuming the indication is only compared with the flaw that has the most similar dimensions.

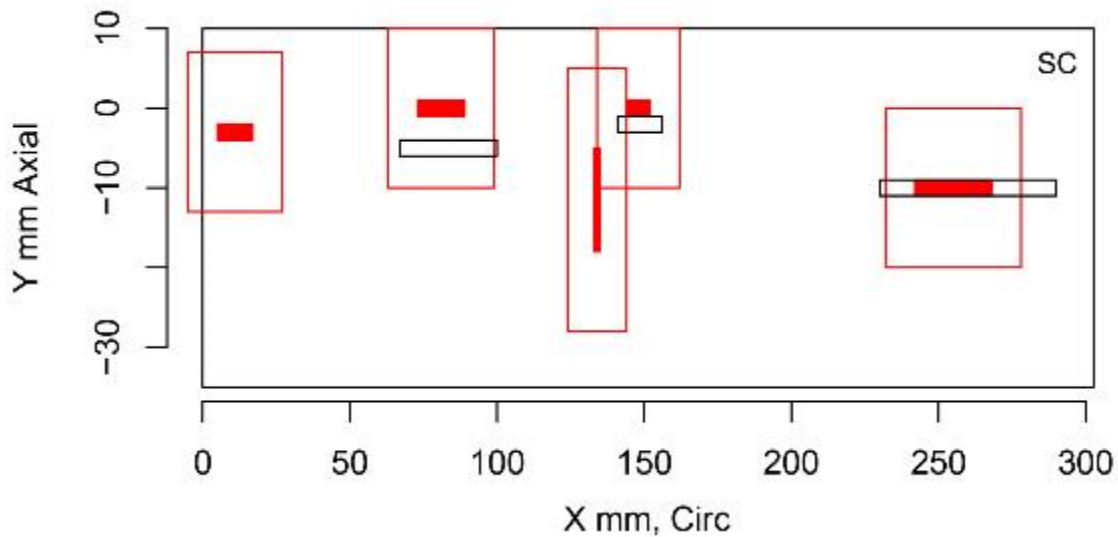


Figure 4.10 Indication Plot for Procedure PAUT.108 Applied to Test Block P35 in PARENT Blind Testing (X – Y view, 0 mm–300 mm)

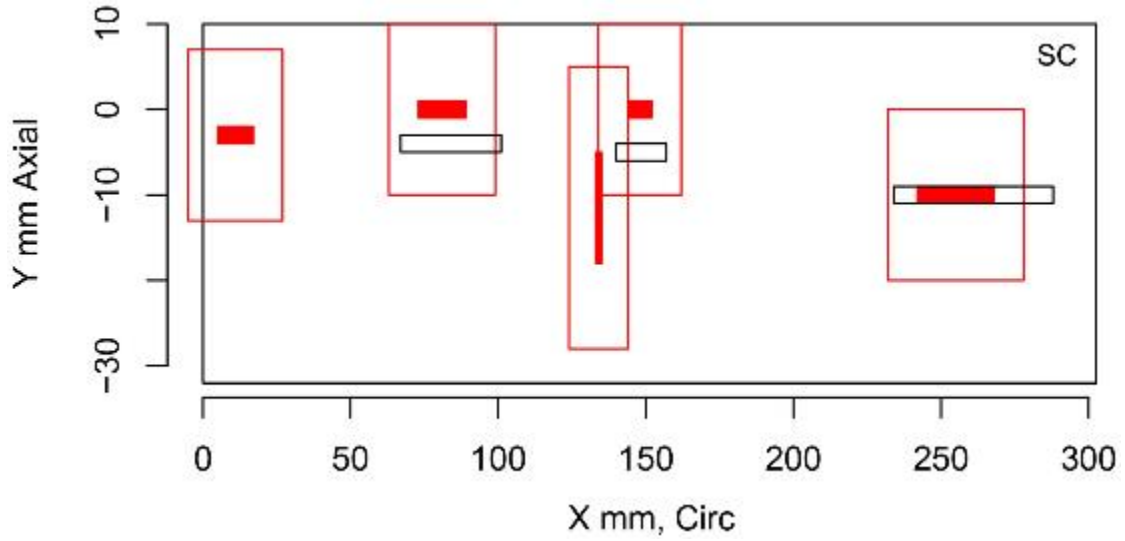


Figure 4.11 Indication Plot for Procedure UT.108 Applied to Test Block P35 in PARENT Blind Testing (X – Y view, 0 mm–300 mm)

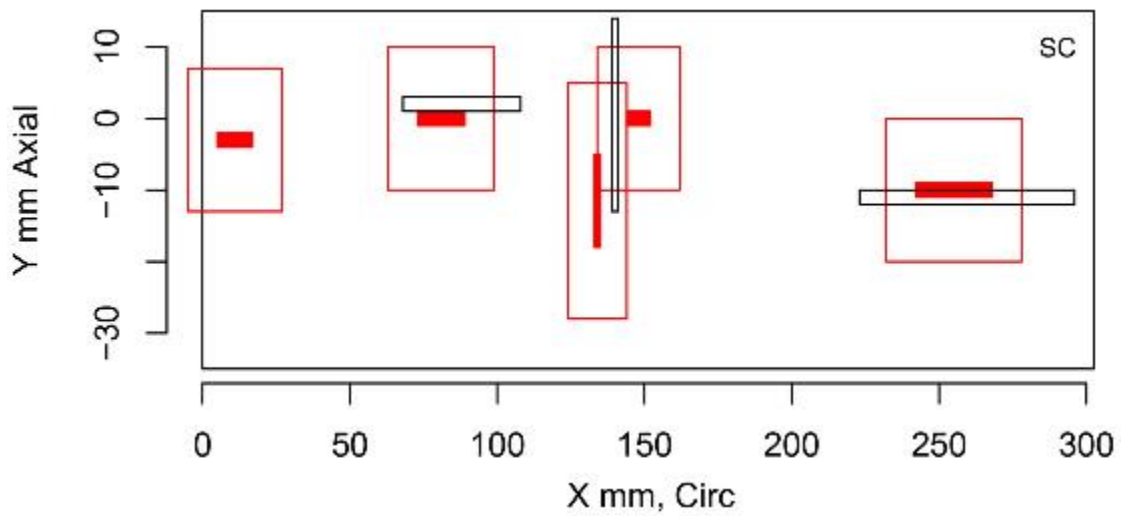


Figure 4.12 Indication Plot for Procedure PAUT.115 Applied to Test Block P35 in PARENT Blind Testing (X – Y view, 0 mm–300 mm)

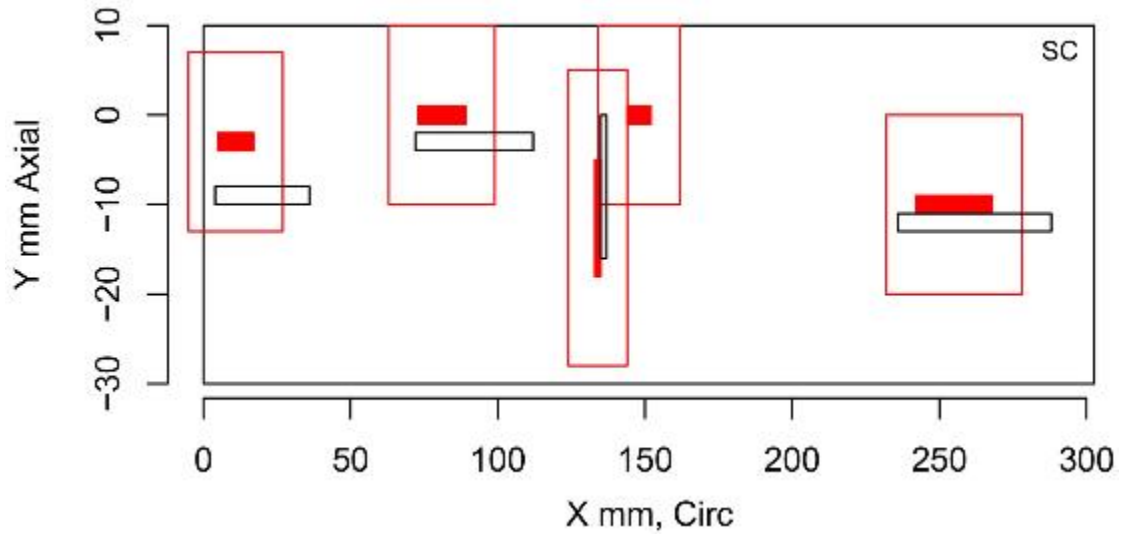


Figure 4.13 Indication Plot for Procedure UT.TOFD.117 Applied to Test Block P35 in PARENT Blind Testing (X – Y view, 0 mm–300 mm)

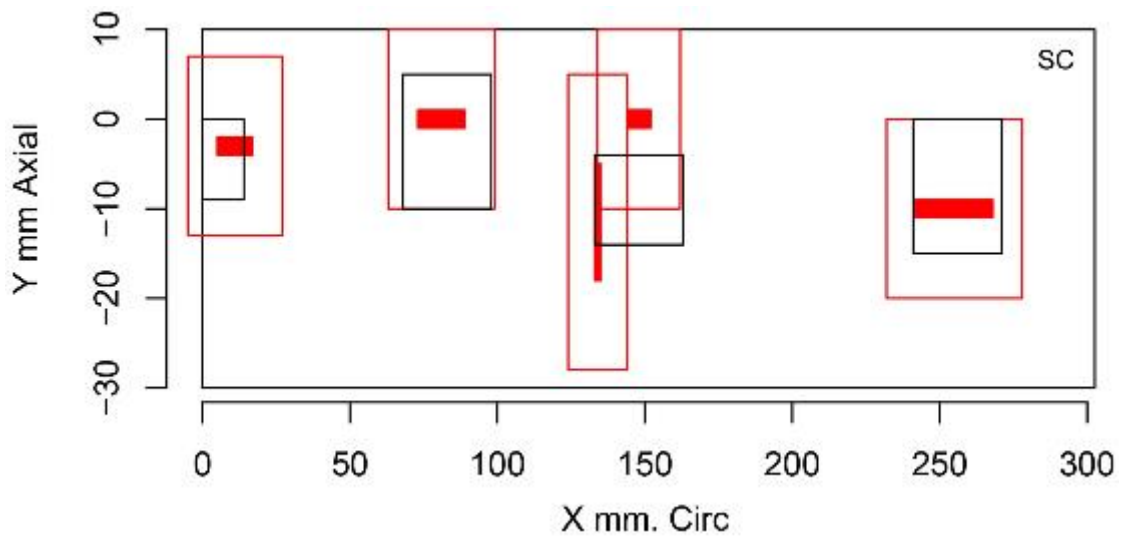


Figure 4.14 Indication Plot for Procedure PAUT.128 Applied to Test Block P35 in PARENT Blind Testing (X – Y view, 0 mm–300 mm)

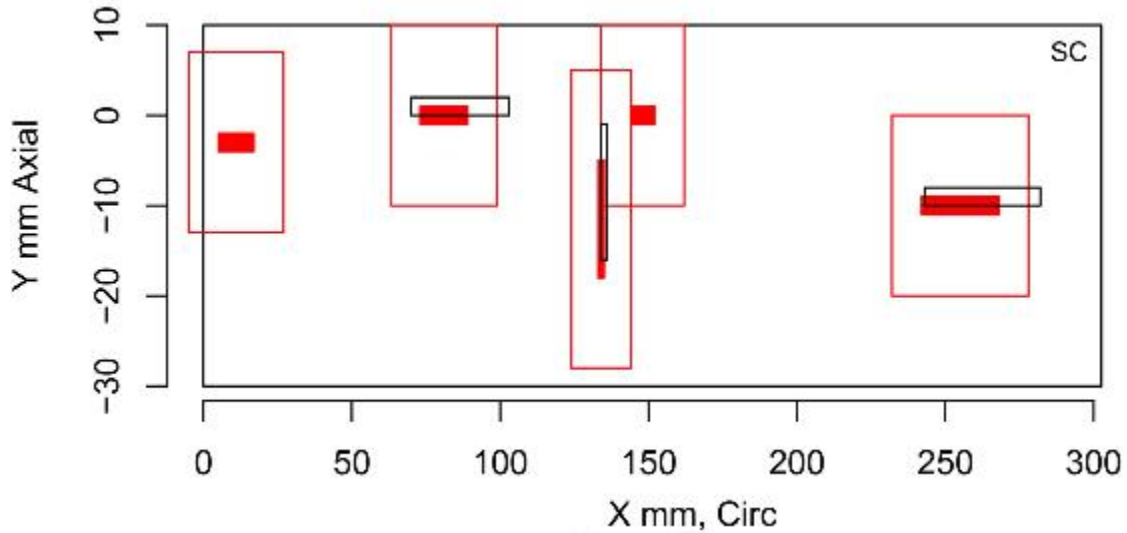


Figure 4.15 Indication Plot for Procedure UT.134 Applied to Test Block P35 in PARENT Blind Testing (X – Y view, 0 mm–300 mm)

4.6 Probability of Detection Representation

A logistic regression model was used to relate POD to flaw size, S. Flaw size represents either depth or length. The logistic regression model is given by,

$$\text{POD}(S) = \text{logistic}(\beta_1 + \beta_2 S), \quad (4.2)$$

where $\beta = (\beta_1, \beta_2)$ are unknown parameters to be determined by the regression algorithm and the function, $\text{logistic}(x)$ is defined as

$$\text{logistic}(x) = \frac{1}{1 + e^{-x}} \quad (4.3)$$

Estimates produced by the algorithm are maximum-likelihood estimates.

In Section 5.1.2, detection performance is presented in a tabular format with POD values provided at discrete flaw sizes (i.e., at 0 mm, 5 mm, 10 mm, 15 mm, etc.). The values of POD at these discrete flaw sizes are the values estimated by the logistic regression model expressed by Eqs. (4.2) and (4.3). This is represented by an example of PAUT procedures applied to the O.D. of LBDMW test blocks in Table 4.6 and by a plot of the corresponding logistic regression model in Figure 4.16. Table 4.6 includes a column with heading “NOBS,” which refers to the number of flaw observations in the sample that POD data in the row is calculated from. In addition, the first column includes POD data for flaws that are 0 mm deep. In this case, the value at 0 mm [POD(0)] can also be interpreted as the false call probability (FCP) determined by the regression fit. The value of the regression fit at 0 mm is influenced by the measured FCP, which is calculated from the false call rate (FCR) with Eq. (D.3) in Appendix D. FCR has units of number of false calls per meter. Further definitions of the measured FCP and POD can be found in Appendix D.1. Figure 4.16 also illustrates 95% confidence intervals for the logistic regression curve.

Section 6.1 includes an analysis of the effect of variables on detection performance, particularly with respect to surface access, flaw orientation, and block type. In this case, POD data is again

provided in tabular format. However, in this case, the flaw size is binned into ranges of 0–5 mm, 5–10 mm, 10–20 mm, and > 20 mm; and POD values are provided for data included in each of these bins, as illustrated with Table 4.7. In this case, the POD values represent the mean POD and the standard deviation for data included in these bins. In each bin, the data is fit with a binomial distribution.

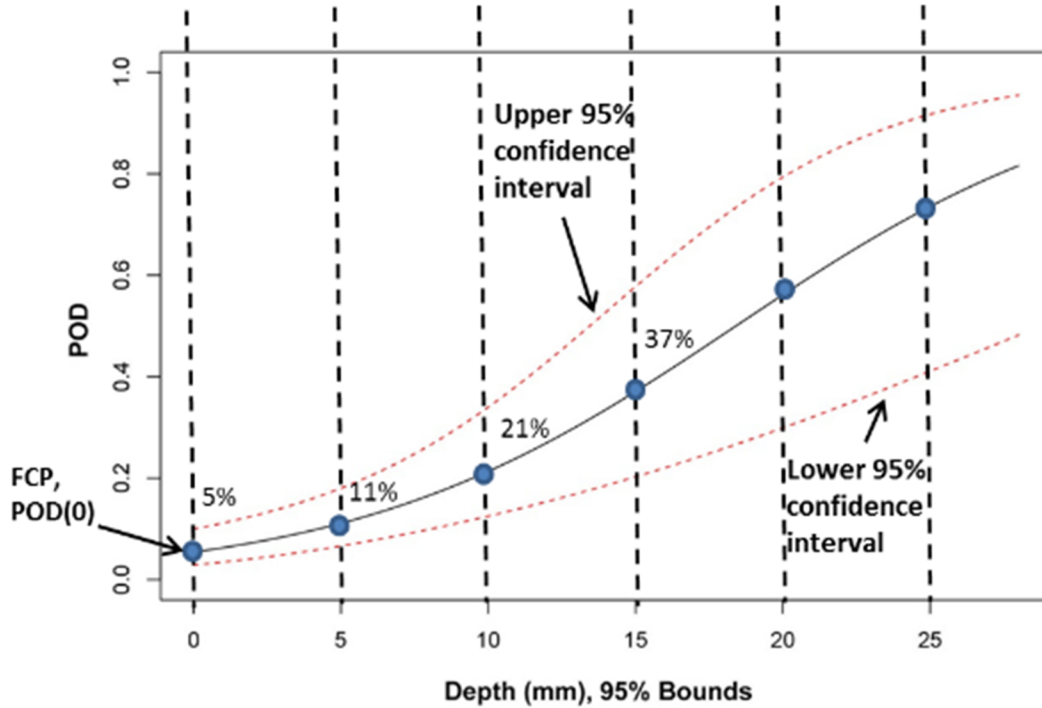


Figure 4.16 POD versus Depth (mm) for PAUT Procedures Applied to LBDMW Test Blocks with O.D. Access (w/o Quick-blind)

Table 4.6 Summary of POD (%) versus Depth for Procedure Types for LBDMWs (O.D. Access)

	NOBS	0 mm	5 mm	10 mm	15 mm
PAUT	38	5	11	21	37
⋮	⋮	⋮	⋮	⋮	⋮

UT = conventional UT

Table 4.7 Summary of POD (%) by Access, Orientation, and Block Type versus Flaw Depth

Access	Orientation	Block Type	0–5 mm	5–10 mm	10–20 mm	>20 mm
I.D.	Axial	LBDMW	25 ± 23	75 ± 13	83 ± 17	75 ± 13
O.D.	Axial	LBDMW	0 ± 12	20 ± 11	10 ± 11	67 ± 12
⋮	⋮	⋮	⋮	⋮	⋮	⋮

4.7 Sizing Analysis for PARENT Blind Round-Robin Test

Linear regression was used to analyze sizing data (depth and length) in PARENT Blind testing. An error relation between the measured and true sizes of the flaws is defined by the following regression formula:

$$M_i = B1 + B2 \times T_i + E_i \quad (4.4)$$

where M_i represents the measured size associated with flaw i
 T_i represents the true size of flaw i
 E_i represents the measurement error in sizing flaw i

$B1$ and $B2$ are the regression parameters usually associated with the Y intercept and slope of the linear regression. Ideal performance for sizing would occur when $B1 = 0$, $B2 = 1$, and $E_i = 0$. To compare two different regressions, and to order a set of regression fits (from most accurate to least accurate as an example), the metric of root mean square error (RMSE) is used. RMSE is a statistic that summarizes the three deviations of regression analyses from their respective ideals. RMSE is defined by

$$RMSE^2 = \frac{\sum_i (M_i - T_i)^2}{n} \quad (4.5)$$

where all the variables are the same as in the preceding descriptions and n is the total number of measurements. RMSE can also be represented in terms of bias and standard deviation as,

$$RMSE^2 = bias^2 + StDev^2 \quad (4.6)$$

In this formula, standard deviation is represented with the variable $StDev$. The bias and $StDev$ represent systematic and random components to the error and are calculated with the following formulas,

$$bias = \frac{\sum_i (M_i - T_i)}{n} \quad (4.7)$$

$$StDev = \sqrt{\frac{\sum_i [(M_i - T_i) - bias]^2}{n}} \quad (4.8)$$

An example of a sizing regression curve is provided in Figure 4.17 for depth sizing performed on axial flaws in LBDMW test blocks from the I.D. surface. The dark line represents the regression fit while the red dashed lines above and below the regression fit are the 95% confidence intervals for the regression fit. In this case, the “A’s” represent the data and represent axially oriented flaws, “C” would be used to represent circumferentially oriented flaws, and “D” represents diagonally oriented flaws which are flaws that do not have a dominant orientation based on dimensions.

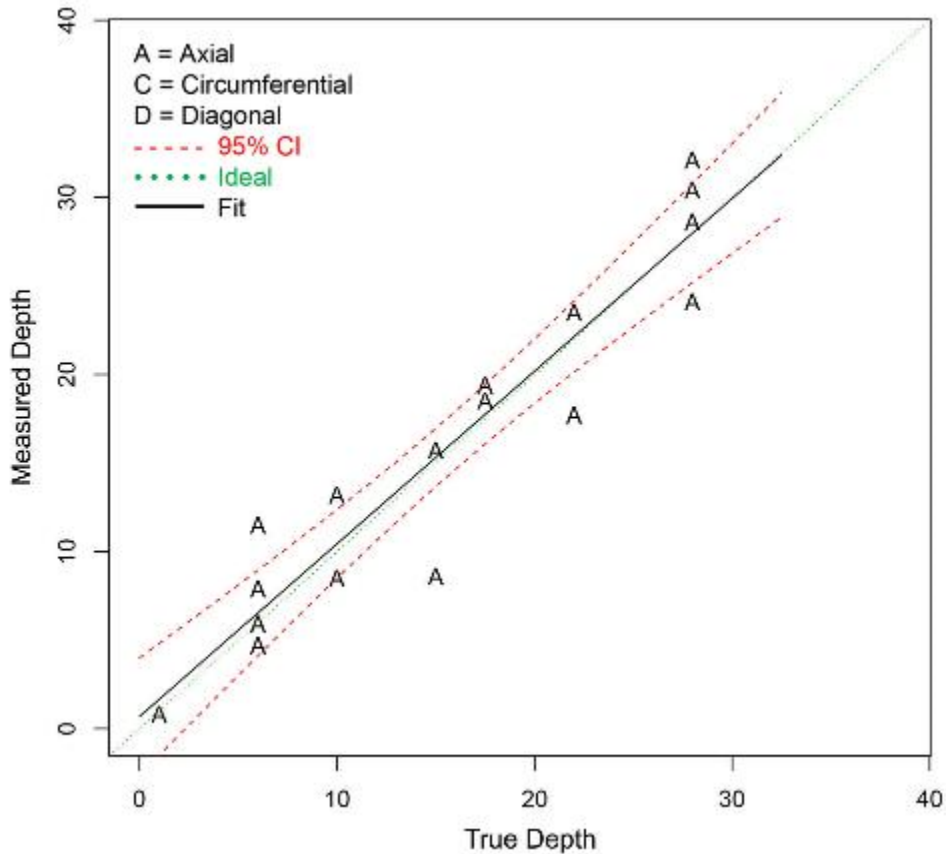


Figure 4.17 Example of Sizing Regression Plot for Depth Sizing Results Obtained on LBDMW Test Blocks by Access to the I.D. Surface (dimensions are in mm)

In some scenarios, the sizing regression analysis for procedures applied to Quick-blind test blocks resulted in counterintuitive outcomes. An example is provided in Figure 4.18 below which shows a regression curve for the length sizing performance of UT.PAUT procedures applied to Quick-blind test blocks with a negative slope. This result is most likely an artifact of the limited sample size, the sizing analysis, and/or possibly the morphology of flaws in the Quick-blind test blocks (see Figure 2.11), which consist of a cluster of parallel axially oriented cracks with varying depth. From the 95% confidence intervals (red dashed lines), it appears that both negative and positive slope curves could fit within the bounds of uncertainty. Further, the clustered nature of the flaws in Quick-blind test blocks introduces complexity in length sizing of flaws that is not representative of what is expected in the field for PWSCC/IDSCC flaws. Therefore, the sizing results represented in Figure 4.18 are likely not a good representation of the actual length sizing capability of UT.PAUT procedures.

In addition, for some presentations of sizing results for Quick-blind test blocks, plots such as Figure 4.19 are provided. In this case, no regression fit is displayed because four data points are required to provide a fit for the model in Eq. (4.4).

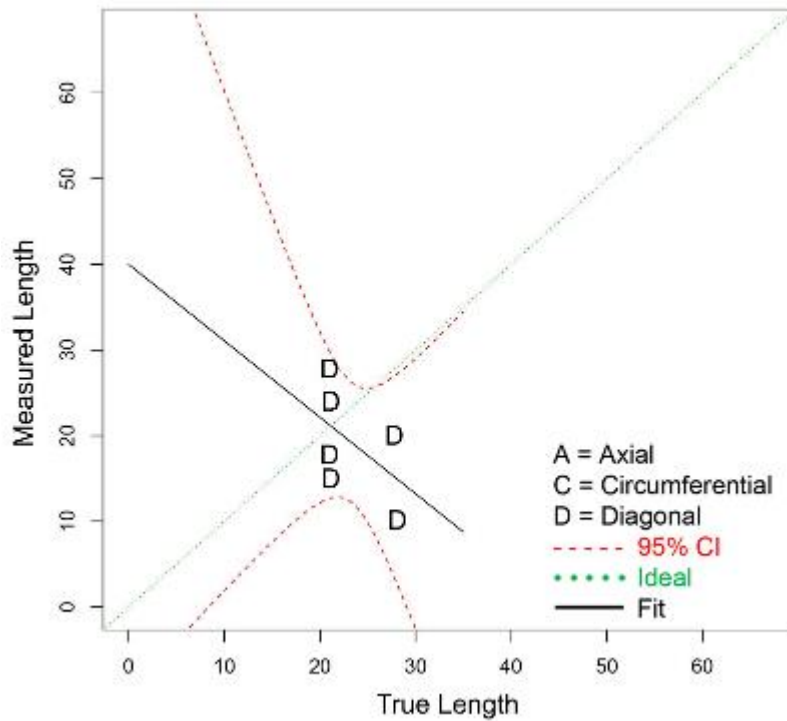


Figure 4.18 Length Sizing Fit (in mm) for UT.PAUT Procedures Applied to LBDMWs (O.D. Access - Quick-blind)

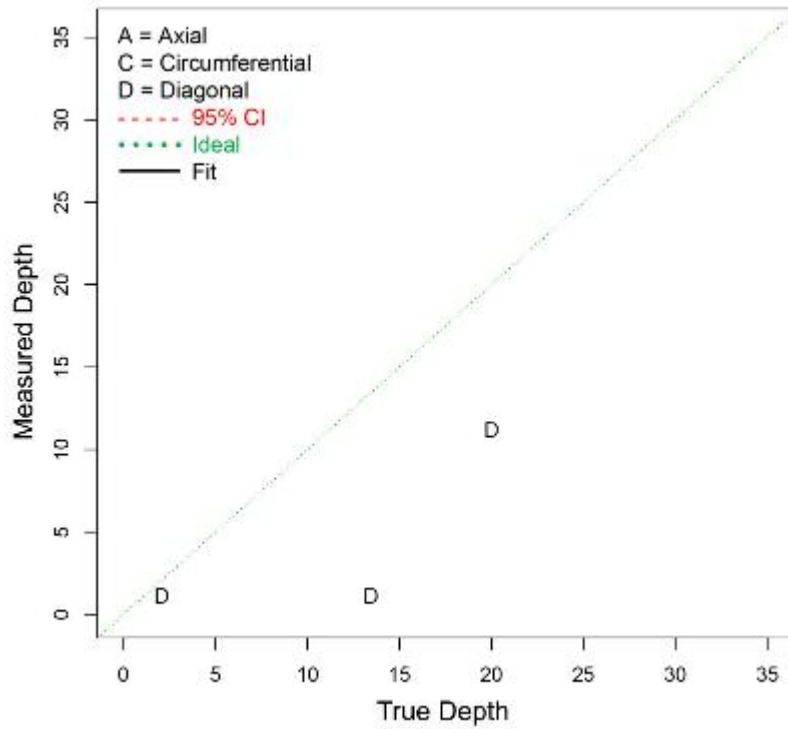


Figure 4.19 Depth Sizing Fit (in mm) for PAUT Procedures Applied to LBDMWs (I.D. Access – Quick-blind)

5 DATA RESULTS

This section presents the results of data analysis performed for blind test data collected in PARENT. The primary data analyses performed includes detection and false call rate analysis, length sizing analysis, and depth sizing analysis. Section 5.1 includes the data analysis results for DMW test blocks, while Sections 5.2 and 5.3 include results for BMI and WOL test blocks, respectively. Additional analysis is performed to compare performance by procedure type, flaw type, access type, and flaw orientation in Section 6. The data results presented in this section serve as a reference to support analyses and conclusions presented in later sections. The reader may wish to skip over this section to Sections 6–9, referring back to this section, as needed.

5.1 Results for DMW Test Blocks

This section includes a summary of data analysis results for inspections performed on DMW test blocks. This includes detection and FCR results and depth and length sizing results. These results are presented for the Quick-blind test in Section 5.1.1 and for the Blind and Quick-blind test data in Sections 5.1.2 and 5.1.3. Results from an earlier analysis of the Quick-blind data were presented in a report on the Quick-blind testing (Braatz et al. 2014). In the earlier analysis, length sizing is performed based on the axial dimensions of the flaws because all flaws in Quick-blind test blocks were intended to have axial orientation. However, destructive analysis revealed that the flaws in P16 and P17 had circumferential dimensions that were greater than their axial dimensions. In this section, the largest flaw dimension in the axial or circumferential direction is used as the basis for length sizing analysis of Quick-blind data to be consistent with the analysis of Blind data.

5.1.1 Quick-Blind Testing Results

Figures 5.1 and 5.2 provide POD curves as a function of flaw depth and length, respectively. These were developed from the combined detection and false call data of the six test teams. The dashed red lines represent the upper and lower 95% confidence bounds. The wide confidence interval is a result of the limited number of data points available. Three flaws were included in Quick-blind testing (one in each test block), and all flaws were inspected by each team (total of six teams). All the teams detected all flaws in all test blocks.

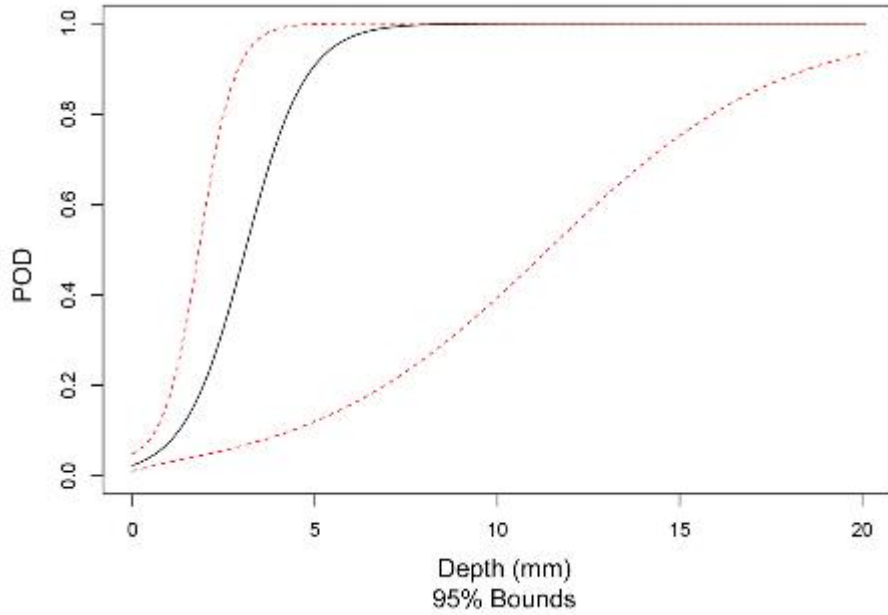


Figure 5.1 Probability of Detection versus Flaw Depth

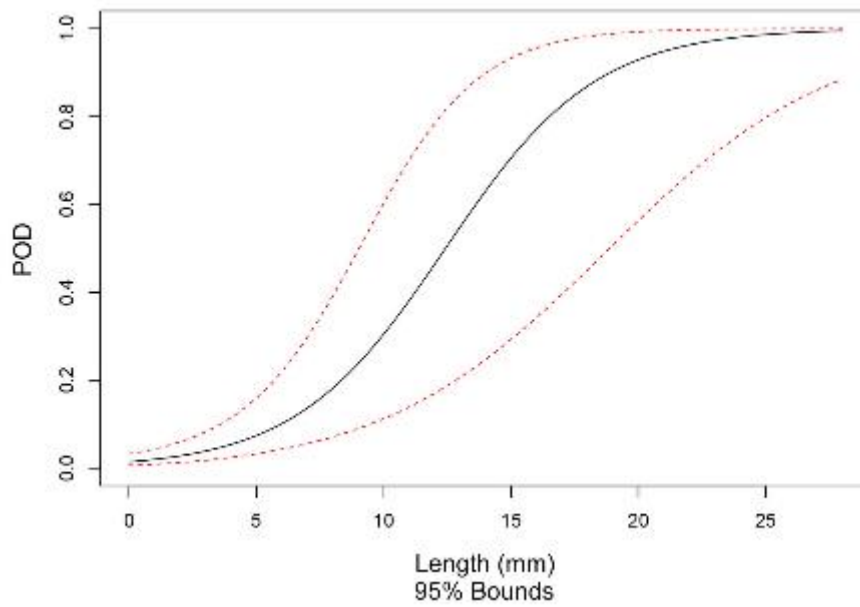


Figure 5.2 Probability of Detection versus Flaw Length

Table 5.1 shows the depth sizing error by procedure and by I.D. or O.D. access for combined data taken on Quick-blind test blocks. Teams 113 and 106 had the lowest RMSE, both having accessed the test block from the I.D.

Table 5.1 Flaw Depth Sizing Error by Procedure

Procedure	Access	Bias, mm	RMSE, mm
UT.134.1	O.D.	-6.5	10.0
PAUT.132	I.D.	-7.5	8.8
UT.PAUT.108	O.D.	-9.1	11.4
UT.PAUT.126	O.D.	-3.5	6.2
UT.PAUT.113	I.D.	0.9	1.2
UT.ECT.106	I.D.	0.0	3.3

UT = conventional UT

Table 5.2 shows how the depth sizing error differs for I.D. and O.D. access. The RMSE values indicate that those procedures that accessed the test block from the I.D. outperformed procedures that accessed from the O.D. Table 5.3 shows the length sizing error by test team for data collected from Quick-blind test blocks. Table 5.4 provides a summary of the length sizing errors for I.D. and O.D. access inspections from Quick-blind testing.

Table 5.2 Flaw Depth Sizing Error by I.D./O.D. Access

Access	NOBS	Bias, mm	RMSE, mm
I.D.	9	-2.2	5.5
O.D.	9	-6.4	9.4

Table 5.3 Flaw Length Sizing Error by Procedures^(a)

Procedure	Access	Bias, mm	RMSE, mm
UT.134.1	O.D.	-9.0	12.2
UT.PAUT.108	O.D.	-9.0	11.1
UT.PAUT.126	O.D.	0.7	6.4
UT.PAUT.113	I.D.	-11.7	12.8
UT.ECT.106	I.D.	-9.3	10.0

(a) Procedure PAUT.132 was not qualified for length sizing and this data is not included in the summary.

UT = conventional UT

Table 5.4 Flaw Length Sizing Error Summary

Access	NOBS	Bias, mm	RMSE, mm
I.D.	6	-10.5	11.5
O.D.	9	-5.8	10.2

5.1.2 DMW Detection and False Call Rate Summary

Table 5.5 provides a summary of detection and FCR results for each procedure applied to DMW test blocks. The column headings are: number of observations (NOBS), POD, FCP, FCR, and access (I.D vs. O.D.). Table 5.6 provides a summary of detection and FCR results for each DMW test block inspected in the blind testing. A collection of indication plots for all of the blind inspections performed in PARENT is included in Appendix E. In this section and throughout the remainder of this report, “Blind + Quick-blind” is used to highlight results that are based on data from both Blind and Quick-blind tests and “Quick-blind” is used to highlight results based only on Quick-blind data. Red text color is also used to emphasize results that include data from Quick-blind testing. Also, several tables include overall statistics for rows in the tables associated with only Blind test data or associated with Blind + Quick-blind data. This includes Table 5.5, Table 5.7, Table 5.8, Table 5.13, Table 5.14, Table 5.19, Table 5.20, Table 5.25, and Table 5.26. In this case, the symbol “*” is used to denote a row that is included in the calculation of overall statistics for Blind data only, and the symbol “+” is used to denote a row that is included in the calculation of overall statistics for Blind + Quick-blind data. A row can include both symbols; in which case, this denotes the row is used in the calculation of overall statistics for both scenarios.

Table 5.5 DMW Detection and False Call Rate Summary Organized by Procedure

	NOBS	POD, %	FCP, %	FCR, #/m	Access	LBDMW	SBDMW
ECT.135*.*+	16	75	1	0.4	I.D.	P33	
PAUT.108.1*.*+	47	64	1	0.6	O.D.	P13, P33	P35, P40
PAUT.115*.*+	28	96	0	0.0	O.D.		P35, P40
PAUT.126.1*.*+	47	51	3	1.2	O.D.	P13, P33	P35, P40
PAUT.128*.*+	28	93	6	2.4	O.D.		P35, P40
PAUT.132 (Quick-blind)*.*+	3	100	0	0.0	I.D.	P15, P16, P17, P45	
UT.108*.*+	47	62	2	0.8	O.D.	P13, P33	P35, P40
UT.126*.*+	47	34	6	2.3	O.D.	P13, P33	P35, P40
UT.134.1 (Quick-blind)*.*+	3	100	0	0.0	O.D.	P15, P16, P17, P45	
UT.134.2*.*+	47	66	4	1.7	O.D.	P13, P33	P35, P40
UT.25*.*+(a)	12	25	10	4.3	O.D.		P35
UT.ECT.106 (Quick-blind)*.*+	3	100	0	0.0	I.D.	P15, P16, P17, P45	
UT.ECT.144*.*+	19	58	6	2.3	I.D.	P13, P33	
UT.PAUT.108 (Quick-blind)*.*+	3	100	0	0.0	O.D.	P15, P16, P17, P45	
UT.PAUT.113 (Blind + Quick-blind)*.*+	21	86	0	0.0	I.D.	P33 P15, P16, P17, P45	
UT.PAUT.113*	18	83	0	0.0	I.D.	P33	
UT.PAUT.126 (Quick-blind)*.*+	3	100	7	2.9	O.D.	P15, P16, P17, P45	
UT.TOFD.117*.*+	28	82	1	0.4	O.D.		P35, P40
UT.TOFD.ECT.101*.*+	19	79	3	1.1	I.D.	P13, P33	
*All (Blind)	403	65	3	1.2			
+All (Blind + Quick-blind)	421	67	3	1.1			

(a) UT.25 was not a qualified procedure.
UT = conventional UT

Table 5.6 Detection and False Call Rate Summary for Each DMW Test Block

	Number of Flaws	Number of Inspections	FCR, #/m	FCP, %	POD, %
P13	1	7	3.65	8.7	42.9
P15 (Quick-blind)	1	6	0.41	1.0	100.0
P16 (Quick-blind)	1	6	0.42	1.0	100.0
P17 (Quick-blind)	1	6	0.43	1.1	100.0
P33	18	9	1.24	3.1	52.5
P35	12	9	1.44	3.5	61.1
P40	16	8	0.81	2.0	84.4
P45 (Quick-blind)	0	6	0.78	1.9	

POD versus depth curves for all inspections performed on LBDMWs are provided in Figures 5.3 and 5.4 for I.D. and O.D. access, respectively. The POD versus depth curve for all inspections performed on SBDMWs is provided in Figure 5.5. Tables 5.7 through 5.9 provide results of POD versus depth for procedure types applied to LBDMW test blocks with I.D. access, LBDMW test blocks with O.D. access, and SBDMW test blocks (all O.D. access), respectively. Figures 5.6 and 5.7 include POD versus depth curves for PAUT and conventional UT procedures applied to LBDMWs with O.D. access, respectively. Figures 5.8 and 5.9 include POD versus depth curves for PAUT and conventional UT procedures applied to SBDMWs with O.D. access, respectively. Tables 5.10 through 5.12 provide POD as a function of flaw depth for individual procedures applied to LBDMW test blocks with I.D. access, LBDMW test blocks with O.D. access, and SBDMW test blocks, respectively.

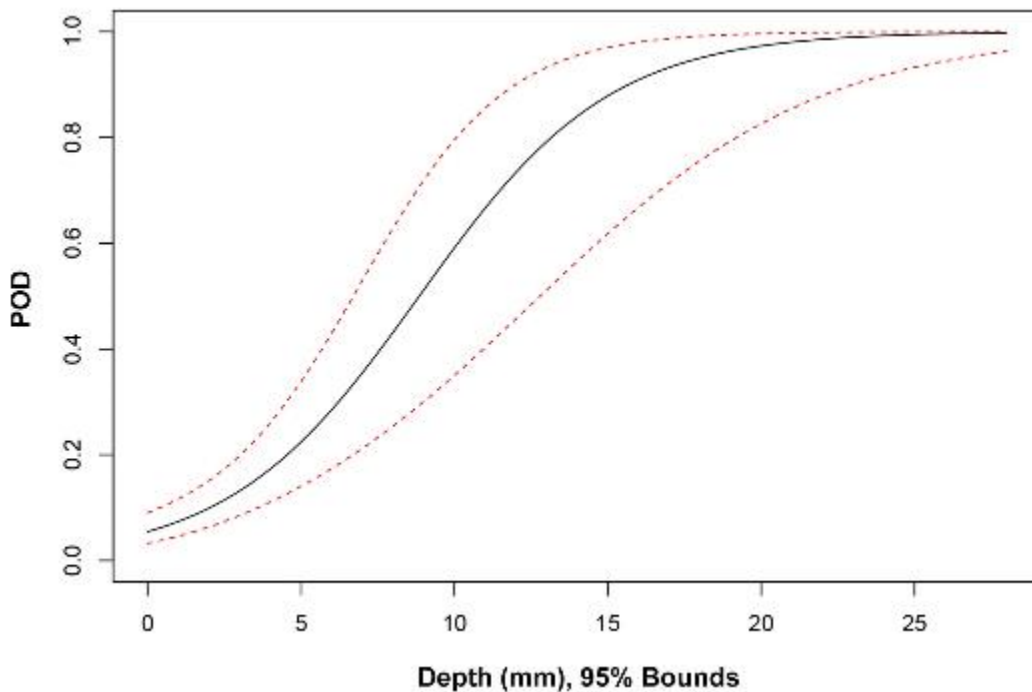


Figure 5.3 POD versus Depth (mm) for All Procedures Applied to LBDMW Test Blocks with I.D. Access

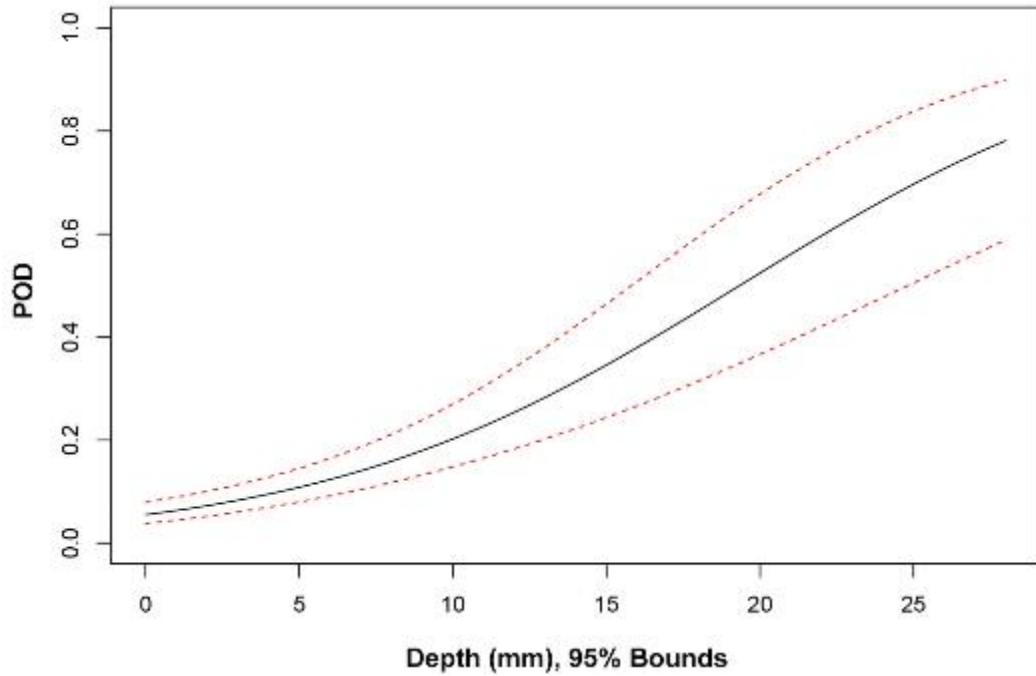


Figure 5.4 POD versus Depth (mm) for All Procedures Applied to LBDMW Test Blocks with O.D. Access

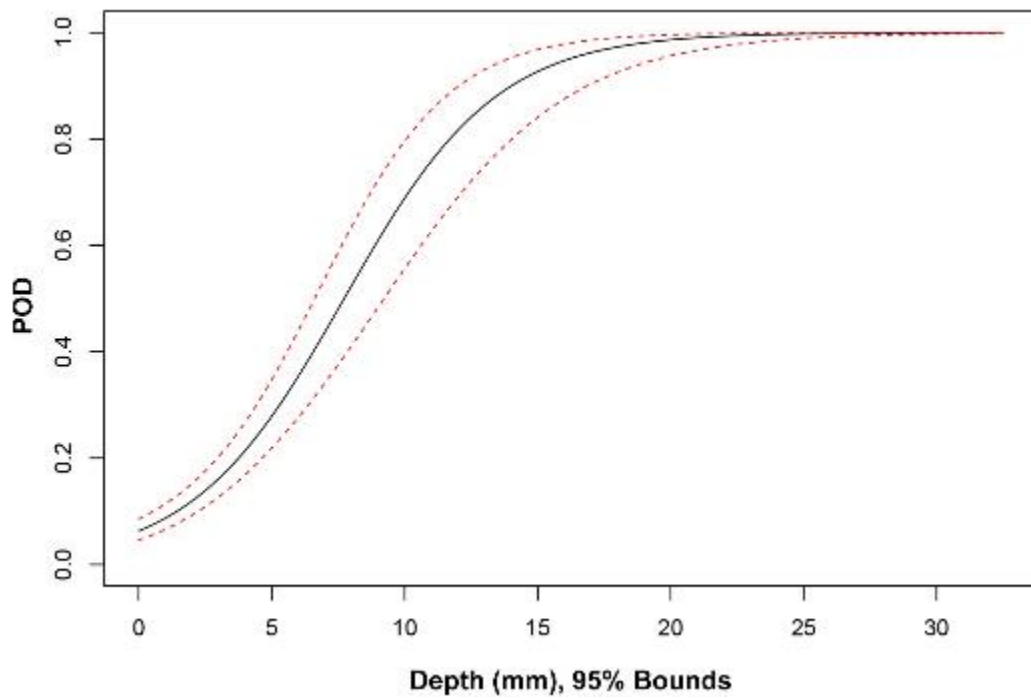


Figure 5.5 POD versus Depth (mm) for All Procedures Applied to SBDMW Test Blocks with O.D. Access

Table 5.7 Summary of POD (%) versus Depth for Procedure Types for LBDMWs (I.D. Access)

	NOBS	0 mm	5 mm	10 mm	15 mm	30 mm
PAUT (Quick-blind) ⁺	3	3	9	26	56	97
ECT ^{*,+}	16	3	23	76	97	100
UT.ECT [*]	19	9	17	30	46	84
UT.ECT (Blind + Quick-blind) ⁺	22	7	15	31	52	92
UT.PAUT [*]	18	3	42	94	100	100
UT.PAUT (Blind + Quick-blind) ⁺	21	2	47	97	100	100
UT.TOFD.ECT ^{*,+}	19	7	22	48	76	99
*All (Blind)	72	5	22	59	88	100
⁺ All (Blind + Quick-blind)	81	4	22	64	92	100

UT = conventional UT

Table 5.8 Summary of POD (%) versus Depth for Procedure Types for LBDMWs (O.D. Access)

	NOBS	0 mm	5 mm	10 mm	15 mm	30 mm
PAUT ^{*,+}	38	5	10	21	37	82
UT [*]	57	5	10	19	32	74
UT (Blind + Quick-blind) ⁺	60	5	10	19	34	79
UT.PAUT (Quick-blind) ⁺	6	5	19	49	80	99
*All (Blind)	95	5	10	20	34	79
⁺ All (Blind + Quick-blind)	104	5	11	22	39	85

UT = conventional UT

Table 5.9 Summary of POD (%) versus Depth for Procedure Types for SBDMWs (O.D. Access)

	NOBS	0 mm	5 mm	10 mm	15 mm	30 mm
PAUT	112	6	39	87	99	100
UT	96	8	20	43	69	98
UT.TOFD	28	4	42	92	99	100
All	236	6	28	69	93	100

UT = conventional UT

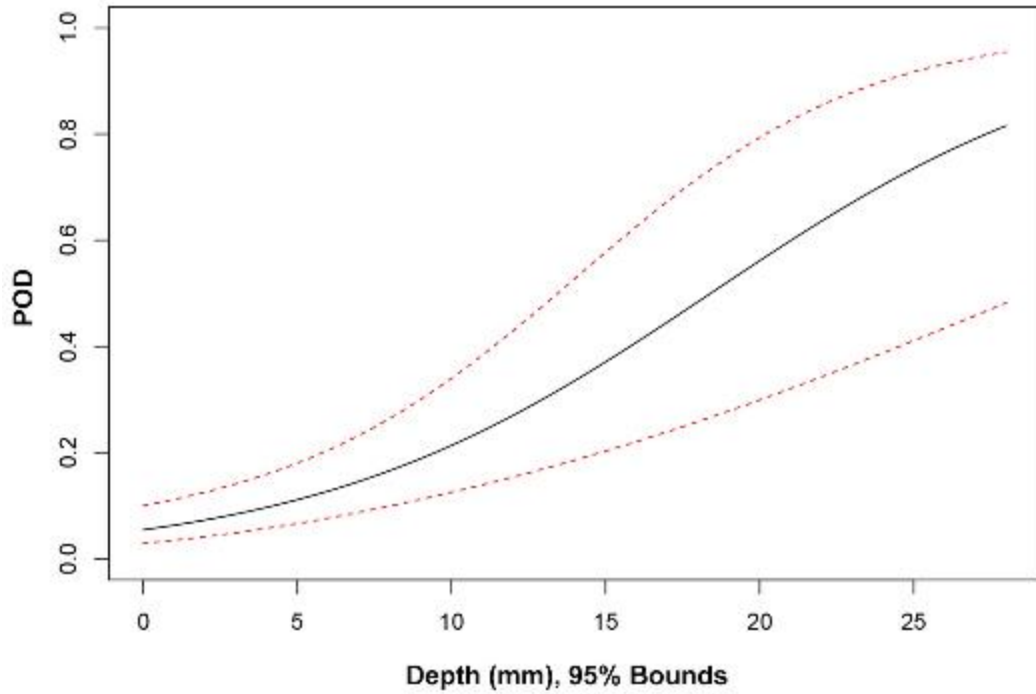


Figure 5.6 POD versus Depth (mm) for PAUT Procedures Applied to LBDMW Test Blocks with O.D. Access

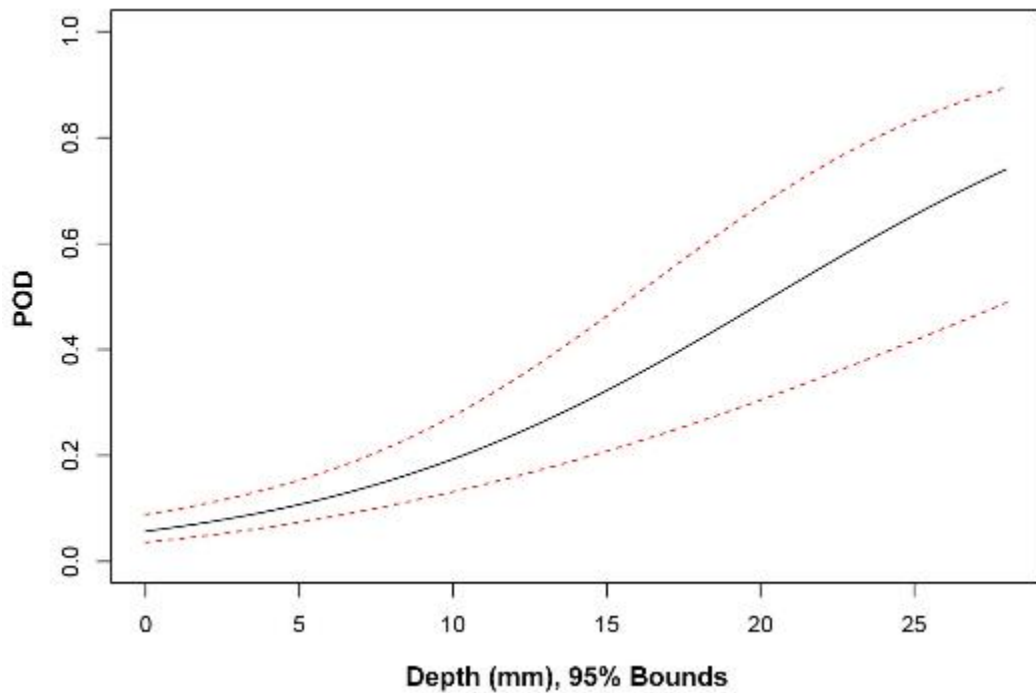


Figure 5.7 POD versus Depth (mm) for Conventional UT Procedures Applied to LBDMW Test Blocks with O.D.

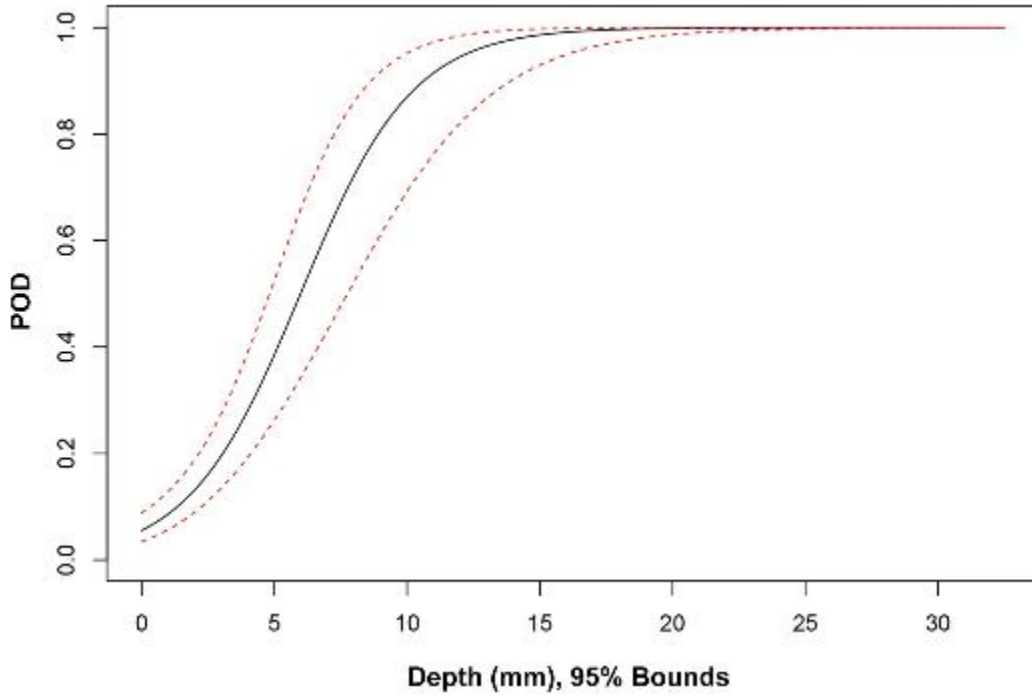


Figure 5.8 POD versus Depth (mm) for PAUT Procedures Applied to SBDMW Test Blocks

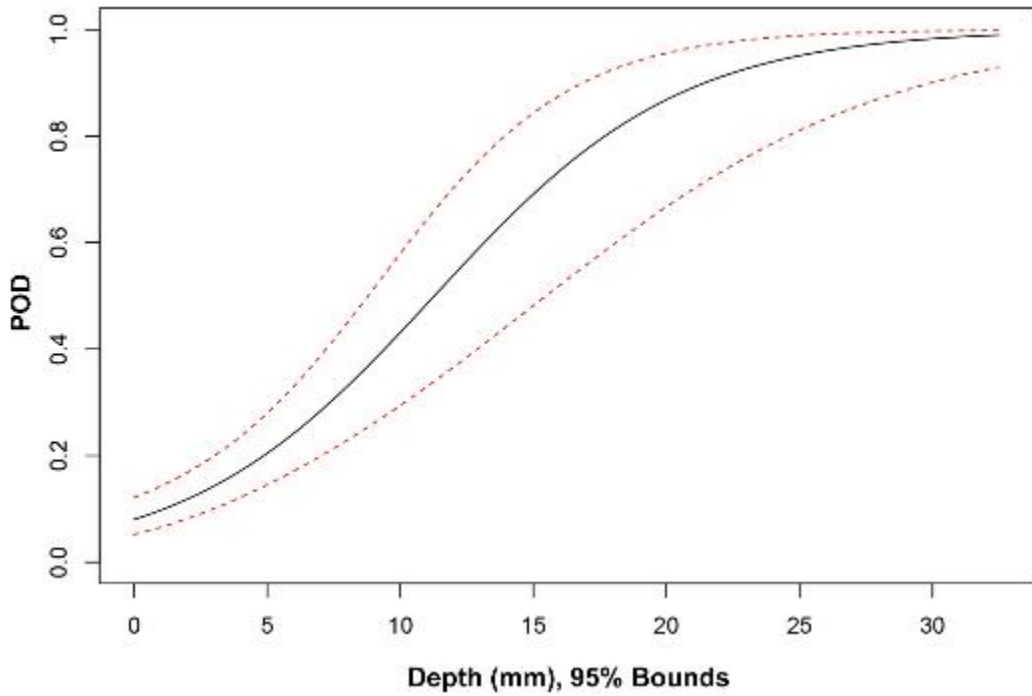


Figure 5.9 POD versus Depth (mm) for Conventional UT Procedures Applied to SBDMW Test Blocks

Table 5.10 Summary of POD (%) versus Depth for Procedures Applied to LBDMWs (I.D. Access)

	NOBS	0 mm	5 mm	10 mm	15 mm	30 mm
PAUT.132 (Quick-blind)	3	3	9	26	56	97
ECT.135	16	3	23	76	97	100
UT.ECT.106 (Quick-blind)	3	3	10	27	56	97
UT.ECT.144	19	9	17	30	46	84
UT.PAUT.113	18	3	42	94	100	100
UT.PAUT.113 (Blind + Quick-blind)	21	2	47	97	100	100
UT.TOFD.ECT.101	19	7	22	48	76	99

UT = conventional UT

Table 5.11 Summary of POD (%) versus Depth for Procedures Applied to LBDMWs (O.D. Access)

	NOBS	0 mm	5 mm	10 mm	15 mm	30 mm
PAUT.108.1	19	3	8	16	30	79
PAUT.126.1	19	7	14	24	40	81
UT.108	19	3	8	16	30	79
UT.126	19	7	11	15	20	40
UT.134.2	19	6	14	28	49	91
UT.134.1 (Quick-blind)	3	2	10	35	73	93
UT.PAUT.108 (Quick-blind)	3	2	8	25	55	97
UT.PAUT.126 (Quick-blind)	3	9	20	39	61	94

UT = conventional UT

Table 5.12 Summary of POD (%) versus Depth for Procedures Applied to SBDMWs (O.D. Access)

	NOBS	0 mm	5 mm	10 mm	15 mm	30 mm
PAUT.108.1	28	5	35	84	98	100
PAUT.115	28	6	58	97	100	100
PAUT.126.1	28	3	12	33	65	99
PAUT.128	28	11	51	89	99	100
UT.108	28	6	33	81	97	100
UT.126	28	8	14	23	35	76
UT.134.2	28	9	28	59	84	100
UT.25 ^(a)	12	11	17	26	37	74
UT.TOFD.117	28	4	42	92	99	100

(a) UT.25 was not a qualified procedure.
 UT = conventional UT

Figures 5.10 through 5.12 include POD versus flaw length curves for all inspections performed on LBDMWs with I.D. access, LBDMWs with O.D. access, and SBDMWs, respectively. Tables 5.13 through 5.15 summarize POD versus flaw length for procedure types applied to LBDMW test blocks with I.D. access, LBDMW test blocks with O.D. access, and SBDMW test blocks, respectively. Finally, Tables 5.16 through 5.18 provide a summary of POD versus flaw length for individual procedures applied to LBDMW test blocks with I.D. access, LBDMW test blocks with O.D. access, and SBDMW test blocks, respectively. The results have been presented with and without Quick-blind data included, and this is indicated in the tables and figure captions where necessary. POD curves without and with Quick-blind data are provided in Appendix F.1 and F.2, respectively, as a function of flaw depth and flaw length.

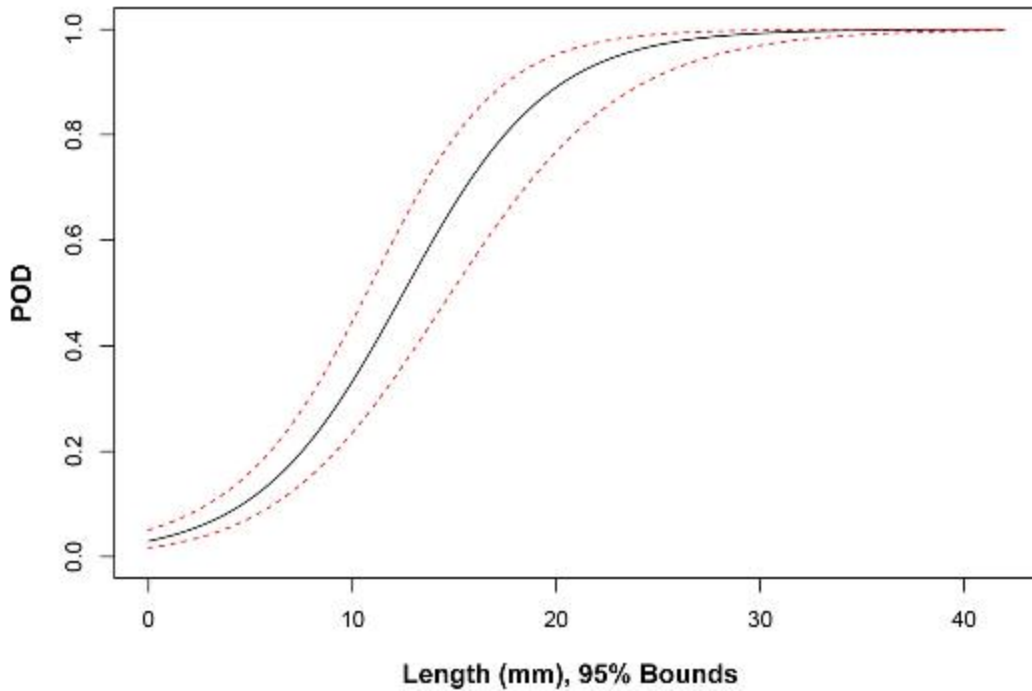


Figure 5.10 POD versus Length (mm) for All Procedures Applied to LBDMW Test Blocks with I.D. Access

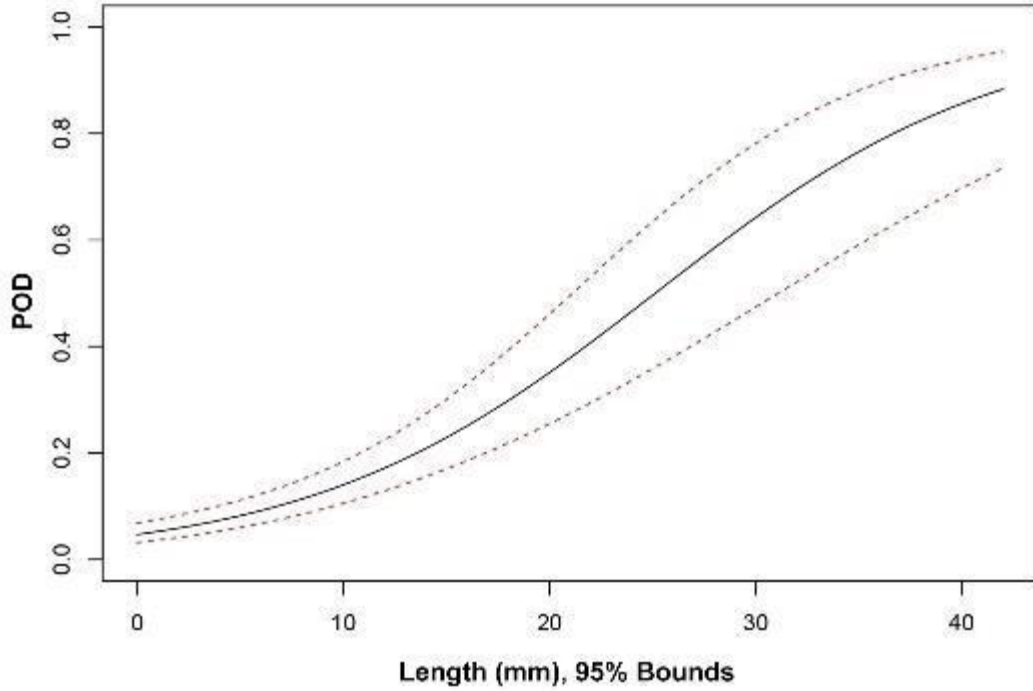


Figure 5.11 POD versus Length (mm) for All Procedures Applied to LBDMW Test Blocks with O.D. Access

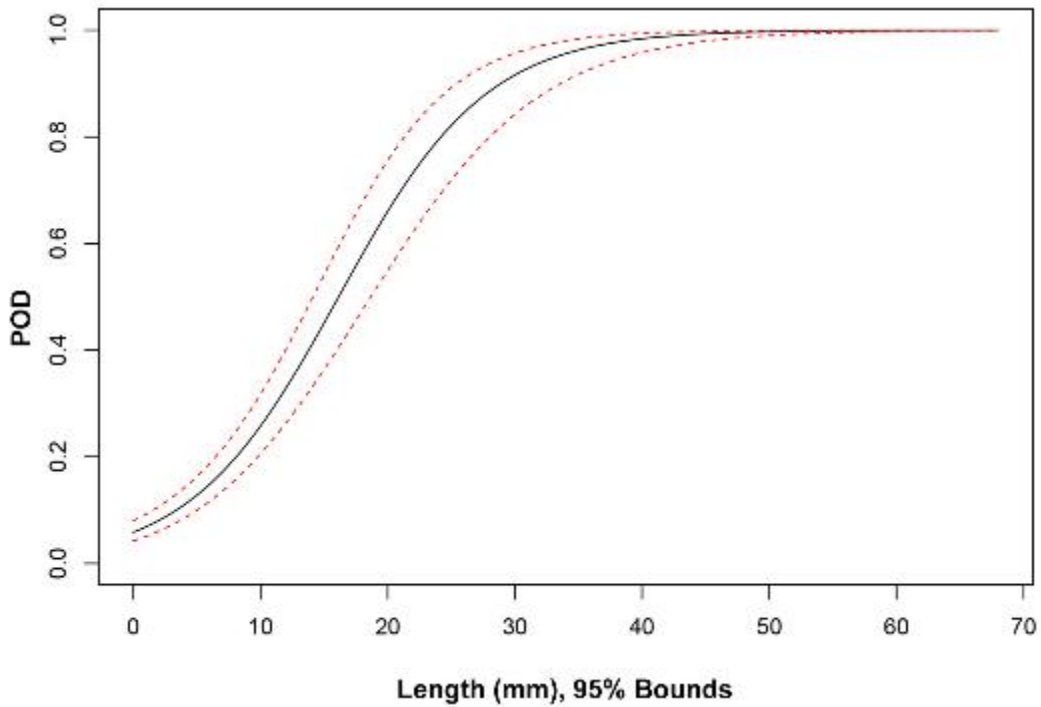


Figure 5.12 POD versus Length (mm) for All Procedures Applied to SBDMW Test Blocks

Table 5.13 Summary of POD (%) by Flaw Length in LBDMW Test Blocks by Procedure Type (I.D. Access)

	NOBS	0 mm	5 mm	10 mm	15 mm	30 mm
PAUT (Quick-blind) ⁺	3	1	4	13	32	94
ECT ^{*,+}	16	2	10	37	76	100
UT.ECT [*]	19	7	14	26	44	89
UT.ECT (Blind + Quick-blind) ⁺	22	5	11	25	46	94
UT.PAUT [*]	18	1	9	46	88	100
UT.PAUT (Blind + Quick-blind) ⁺	21	1	7	44	89	100
UT.TOFD.ECT [*]	19	4	14	38	69	99
*All (Blind)	72	3	12	38	73	100
⁺ All (Blind + Quick-blind)	78	2	10	36	75	100

UT = conventional UT

Table 5.14 Summary of POD (%) by Flaw Length in LBDMW Test Blocks by Procedure Type (O.D. Access)

	NOBS	0 mm	5 mm	10 mm	15 mm	30 mm
PAUT ^{*,+}	38	4	8	16	28	78
UT [*]	57	5	8	15	25	70
UT (Blind + Quick-blind) ⁺	60	4	8	14	26	75
UT.PAUT (Quick-blind) ⁺	6	4	12	29	55	97
*All (Blind)	95	4	8	15	26	74
⁺ All (Blind + Quick-blind)	104	4	8	16	29	81

UT = conventional UT

Table 5.15 Summary of POD (%) by Flaw Length in SBDMW Test Blocks by Procedure Type

	NOBS	0 mm	5 mm	10 mm	15 mm	30 mm
PAUT	112	6	16	37	65	98
UT	96	8	14	24	37	80
UT.TOFD	28	4	15	41	75	100
All	236	6	14	30	53	95

UT = conventional UT

Table 5.16 Summary of POD (%) by Flaw Length in LBDMW Test Blocks for Each Procedure (I.D. Access)

	NOBS	0 mm	5 mm	10 mm	15 mm	30 mm
PAUT.132 (Quick-blind)	3	1	4	13	32	94
ECT.135	16	2	10	37	76	100
UT.ECT.106 (Quick-blind)	3	1	4	13	32	94
UT.ECT.144	19	7	14	26	44	89
UT.PAUT.113	18	1	9	46	88	100
UT.PAUT.113 (Blind + Quick-blind)	22	1	7	44	89	100
UT.TOFD.ECT.101	19	4	14	38	69	99

UT = conventional UT

Table 5.17 Summary of POD (%) by Flaw Length in LBDMW Test Blocks for Each Procedure (O.D. Access)

	NOBS	0 mm	5 mm	10 mm	15 mm	30 mm
PAUT.108.1	19	2	5	11	23	80
PAUT.126.1	19	6	11	19	30	72
UT.108	19	2	5	11	23	80
UT.126	19	7	9	13	18	39
UT.134.2	19	6	11	20	33	80
UT.134.1 (Quick-blind)	3	1	3	12	35	95
UT.PAUT.108 (Quick-blind)	3	1	4	12	31	94
UT.PAUT.126 (Quick-blind)	3	8	16	30	48	91

UT = conventional UT

Table 5.18 Summary of POD (%) by Flaw Length in SBDMW Test Blocks for Each Procedure

	NOBS	0 mm	5 mm	10 mm	15 mm	30 mm
PAUT.108.1	28	5	14	33	60	97
PAUT.115	28	6	21	53	83	100
PAUT.126.1	28	3	7	14	25	76
PAUT.128	28	11	27	52	76	99
UT.108	28	6	15	33	59	97
UT.126	28	9	11	15	20	39
UT.134.2	28	9	17	31	48	89
UT.25 ^(a)	12	13	16	19	22	35
UT.TOFD.117	28	4	15	41	75	100

(a) UT.25 was not a qualified procedure.

UT = conventional UT

5.1.3 DMW Depth Sizing Summary

Depth sizing errors are provided in terms of bias and RMSE in Tables 5.19 through 5.21 for procedure types applied to LBDMW test blocks with I.D. access, LBDMW test blocks with O.D. access, and SBDMW test blocks, respectively. Depth sizing errors are provided in terms of bias and RMSE in Tables 5.22 through 5.24 for individual procedures applied to LBDMW test blocks with I.D. access, LBDMW test blocks with O.D. access, and SBDMW test blocks, respectively. Depth sizing data, along with regression curve fits for LBDMW test blocks with I.D. access, are provided in Figures 5.13 through 5.18. For LBDMW test blocks with O.D. access, depth sizing data along with regression curve fits are provided in Figures 5.19 through 5.22. Finally, depth sizing data along with regression curve fits for SBDMW test blocks are provided in Figures 5.23 through 5.25. Depth sizing regression plots are provided in Appendix G.1.1 and Appendix G.2.1 for Blind and Blind + Quick-blind results, respectively.

Table 5.19 Summary of Depth Sizing Errors for Procedure Types Applied to LBDMWs with I.D. Access

	NOBS	Bias, mm	RMSE, mm
PAUT (Quick-blind) ⁺	3	-7.5	8.8
UT.ECT*	9	0.7	2.2
UT.ECT (Blind + Quick-blind) ⁺	12	0.5	2.5
UT.PAUT*	15	2.0	2.9
UT.PAUT (Blind + Quick-blind) ⁺	18	1.8	2.7
UT.TOFD.ECT* ⁺	15	-1.0	3.4
*All	39	0.6	3.0
⁺ All (Blind + Quick-blind)	48	0.0	3.6
UT = conventional UT			

Table 5.20 Summary of Depth Sizing Errors for Procedure Types Applied to LBDMWs with O.D. Access

	NOBS	Bias, mm	RMSE, mm
PAUT* ⁺	15	0.1	9.7
UT*	16	-4.4	9.8
UT (Blind + Quick-blind) ⁺	19	-4.7	9.9
UT.PAUT (Quick-blind) ⁺	6	-6.3	9.2
*All	31	-2.2	9.8
⁺ All (Blind + Quick-blind)	40	-3.2	9.7
UT = conventional UT			

Table 5.21 Summary of Depth Sizing Errors for Procedures Types on SBDMWs with O.D. Access

	NOBS	Bias, mm	RMSE, mm
PAUT	84	-0.9	3.6
UT	54	-3.5	7.9
UT.TOFD	19	0.6	4.1
All	157	-1.6	5.5
UT = conventional UT			

Table 5.22 Summary of Depth Sizing Errors for Procedures on LBDMWs (I.D. Access)

	NOBS	Bias, mm	RMSE, mm
PAUT.132 (Quick-blind)	3	-7.5	8.8
UT.ECT.106 (Quick-blind)	3	0.0	3.3
UT.ECT.144	9	0.7	2.2
UT.PAUT.113	15	2.0	2.9
UT.PAUT.113 (Blind + Quick-blind)	18	1.8	2.7
UT.TOFD.ECT.101	15	-1.0	3.4
UT = conventional UT			

Table 5.23 Summary of Depth Sizing Errors for Procedures on LBDMWs (O.D. Access)

	NOBS	Bias, mm	RMSE, mm
PAUT.108.1	7	-2.8	5.0
PAUT.126.1	8	2.6	12.5
UT.108	4	-0.3	9.0
UT.126	4	0.6	6.8
UT.134.2	8	-8.9	11.4
UT.134.1 (Quick-blind)	3	-6.2	11.3
UT.PAUT.108 (Quick-blind)	3	-9.1	11.4
UT.PAUT.126 (Quick-blind)	3	-3.5	6.2

UT = conventional UT

Table 5.24 Summary of Depth Sizing Errors for Procedures on SBDMWs (O.D. Access)

	NOBS	Bias, mm	RMSE, mm
PAUT.108.1	21	-1.7	2.4
PAUT.115	25	-0.3	1.8
PAUT.126.1	14	-5.0	5.9
PAUT.128	24	1.4	4.2
UT.108	20	-1.0	4.2
UT.126	10	-4.1	7.1
UT.134.2	21	-4.9	9.5
UT.25 ^(a)	3	-8.8	13.9
UT.TOFD.117	19	0.6	4.1

(a) UT.25 was not a qualified procedure.
UT = conventional UT

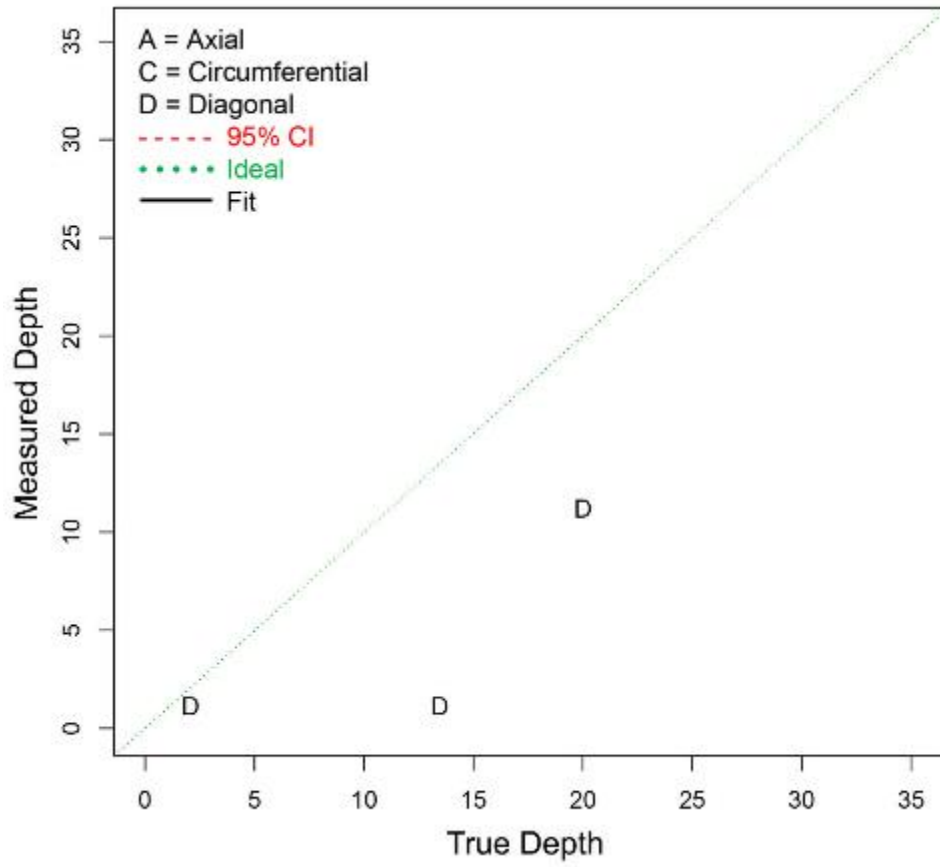


Figure 5.13 Depth Sizing Fit (in mm) for PAUT Procedures Applied to LBDMWs (I.D. Access – Quick-blind)

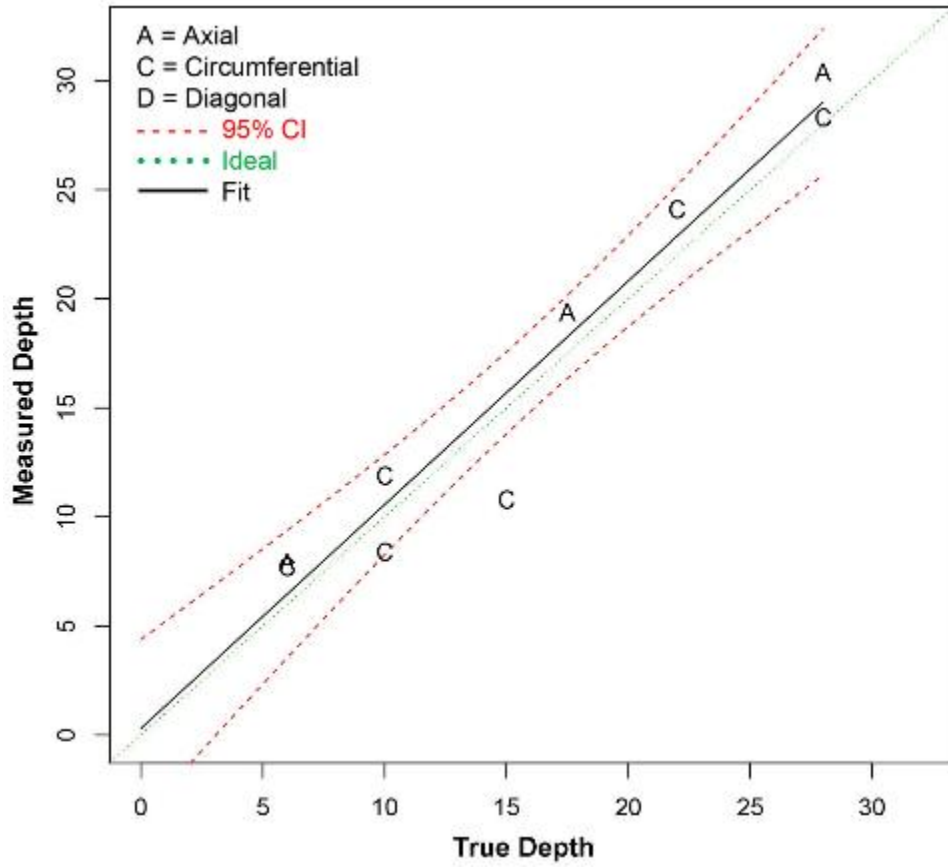


Figure 5.14 Depth Sizing Fit (in mm) for UT.ECT Procedures Applied to LBDMWs (I.D. Access)

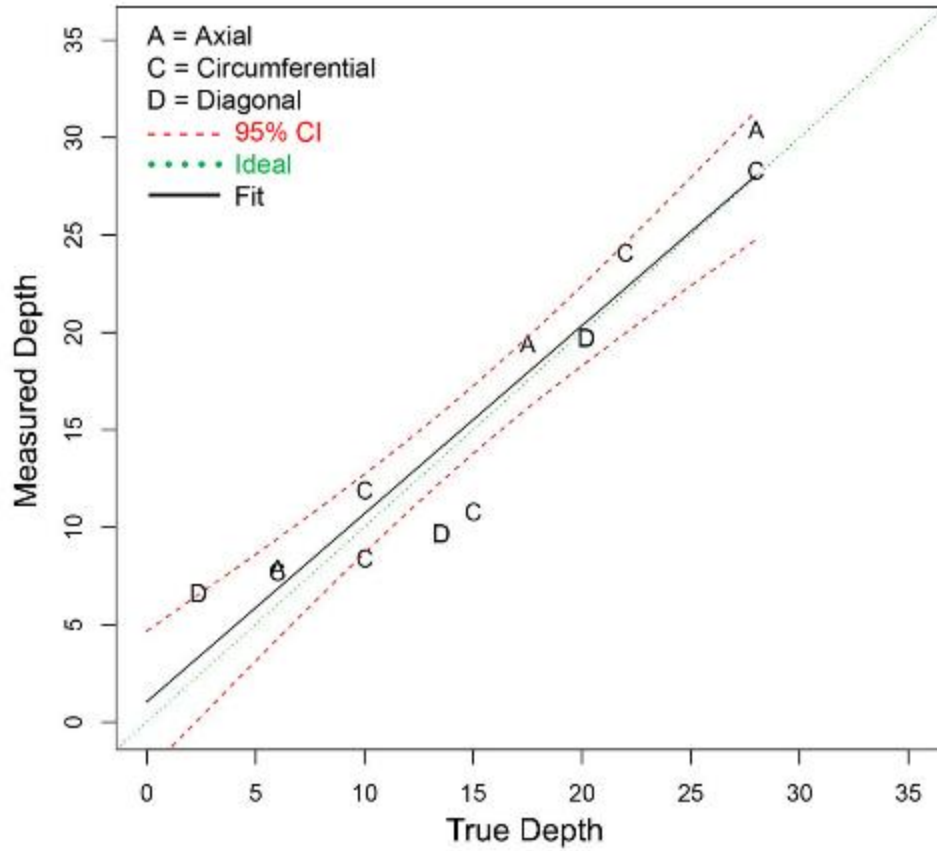


Figure 5.15 Depth Sizing Fit (in mm) for UT.ECT Procedures Applied to LBDMWs (I.D. Access – **Blind + Quick-blind**)

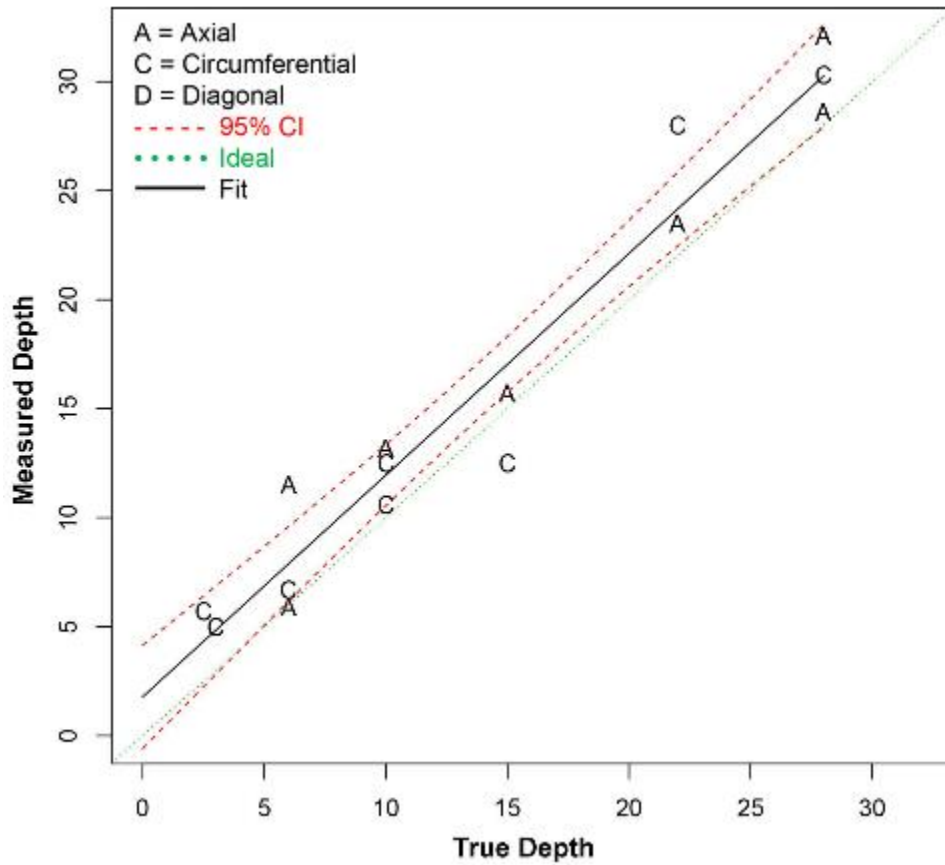


Figure 5.16 Depth Sizing Fit (in mm) for UT.PAUT Procedures Applied to LBDMWs (I.D. Access)

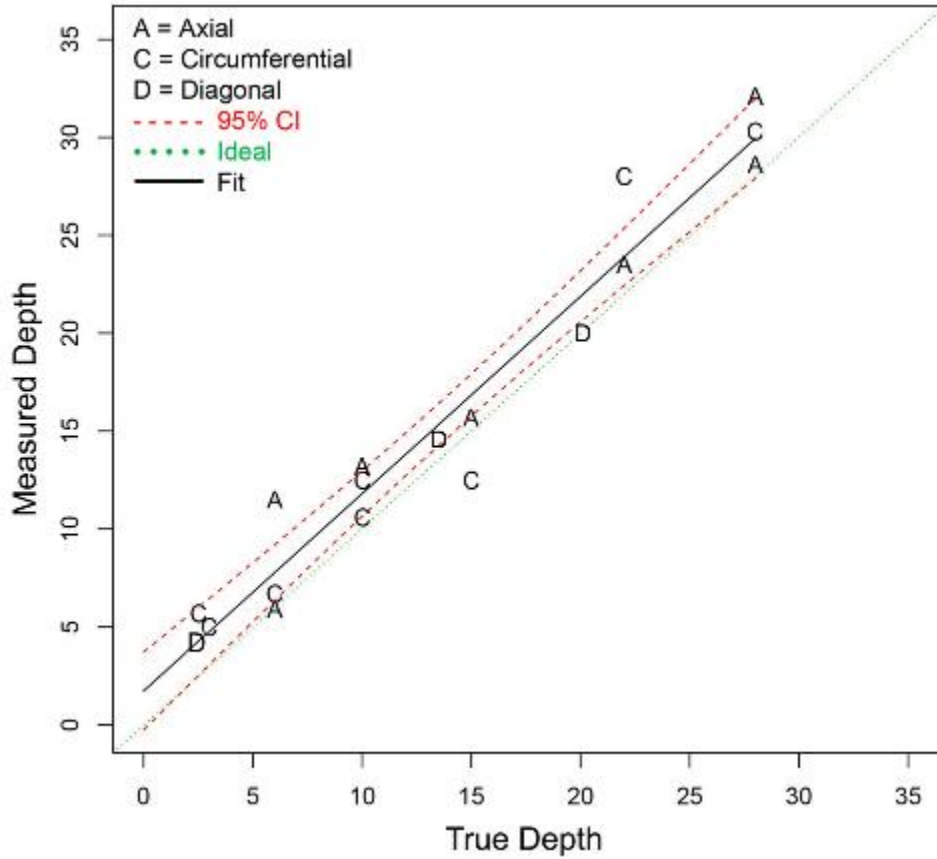


Figure 5.17 Depth Sizing Fit (in mm) for UT.PAUT Procedures Applied to LBDMWs (I.D. Access – **Blind + Quick-blind**)

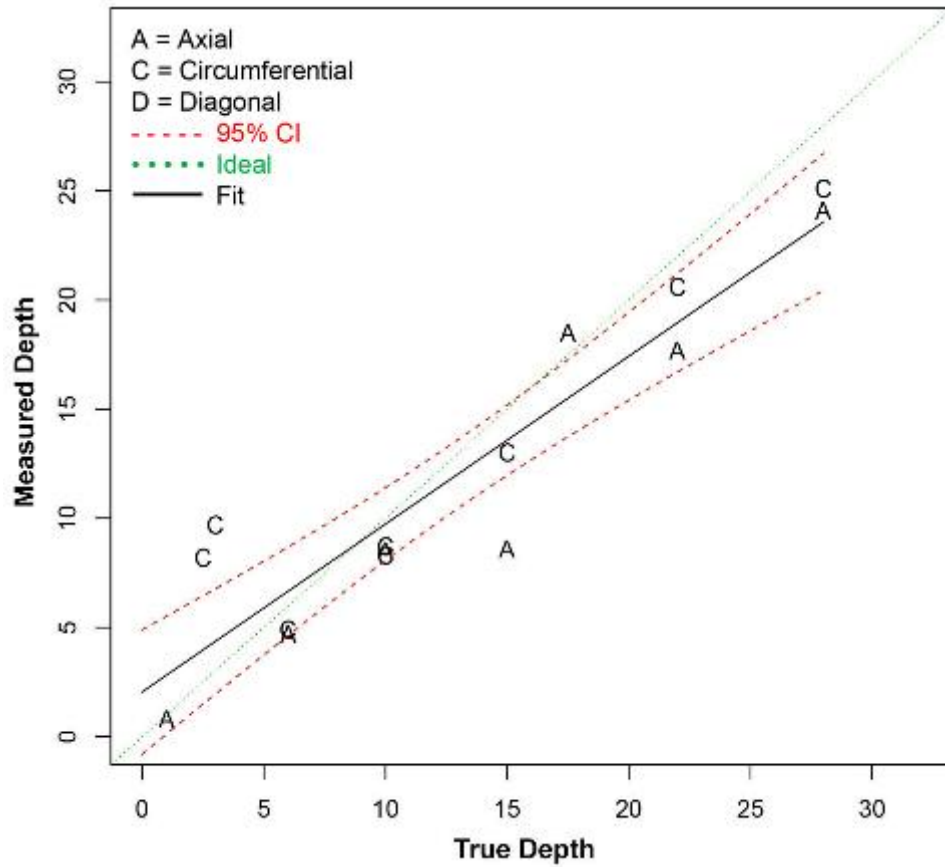


Figure 5.18 Depth Sizing Fit (in mm) for UT, TOFD, ECT Procedures Applied to LBDMWs (I.D. Access)

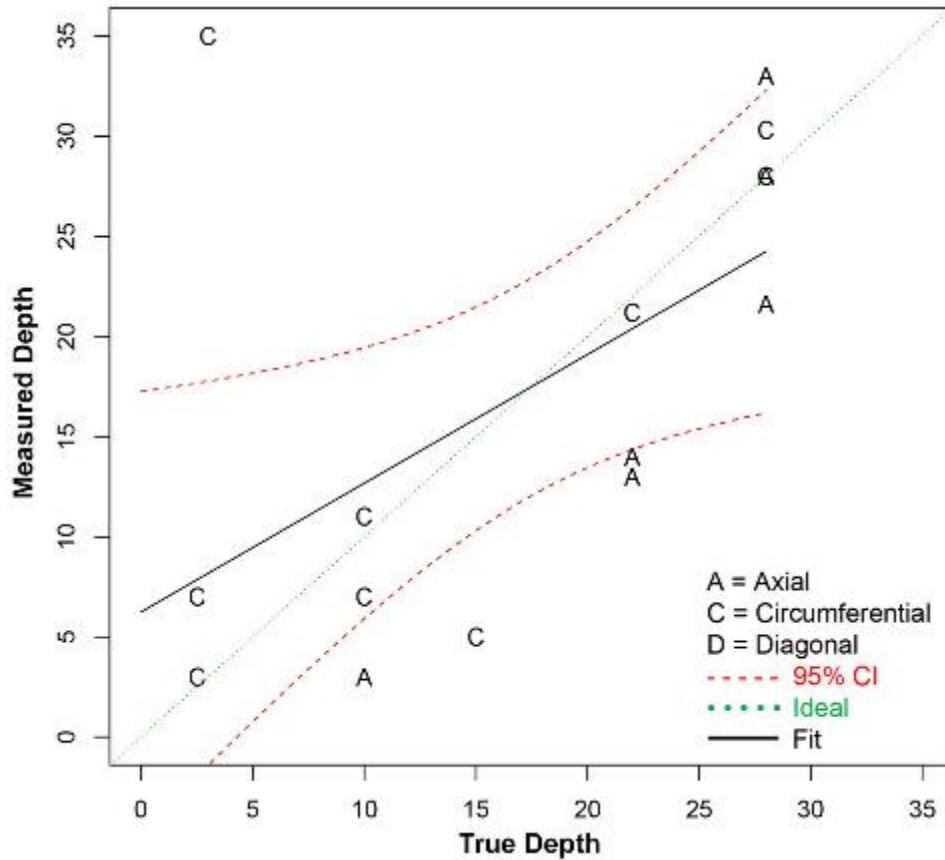


Figure 5.19 Depth Sizing Fit (in mm) for PAUT Procedures Applied to LDMWs (O.D. Access)

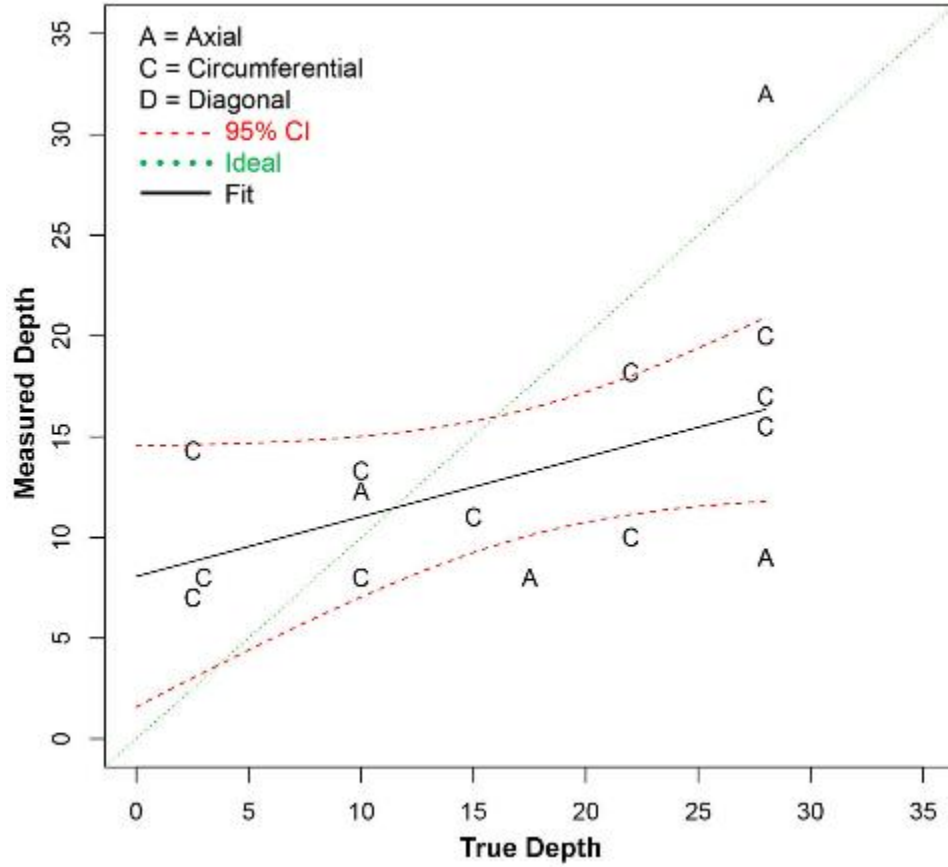


Figure 5.20 Depth Sizing Fit (in mm) for Conventional UT Procedures Applied to LBDMWs (O.D. Access)

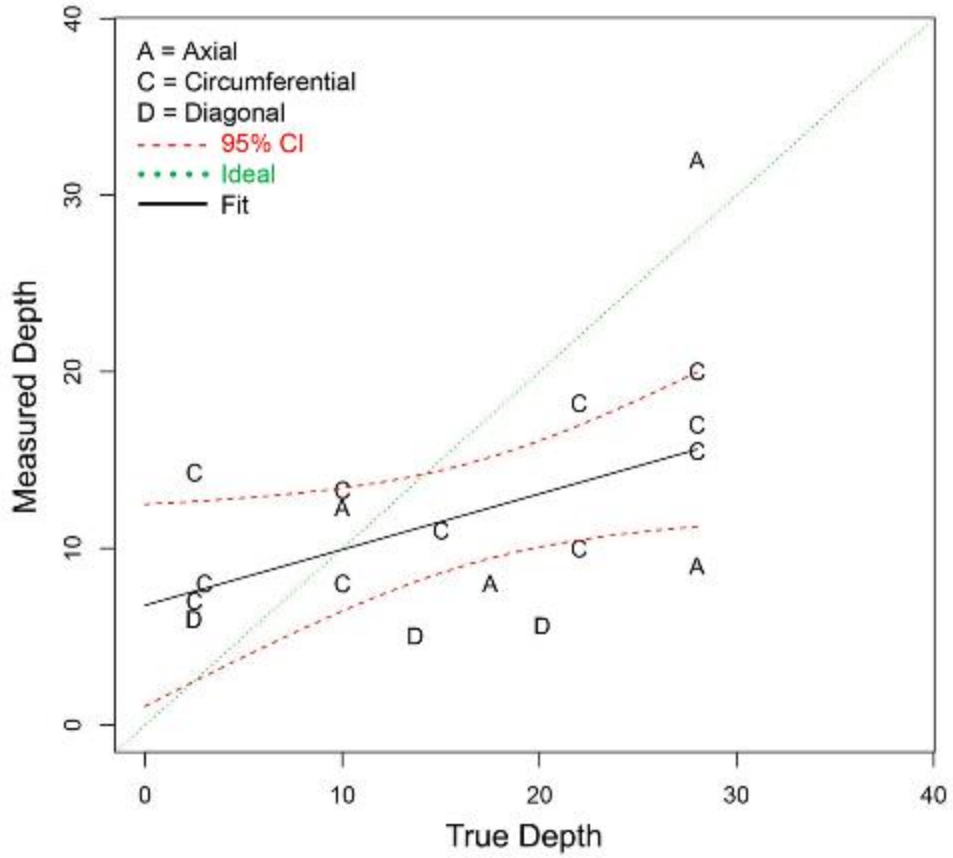


Figure 5.21 Depth Sizing Fit (in mm) for Conventional UT Procedures Applied to LBDMWs (O.D. Access – **Blind + Quick-blind**)

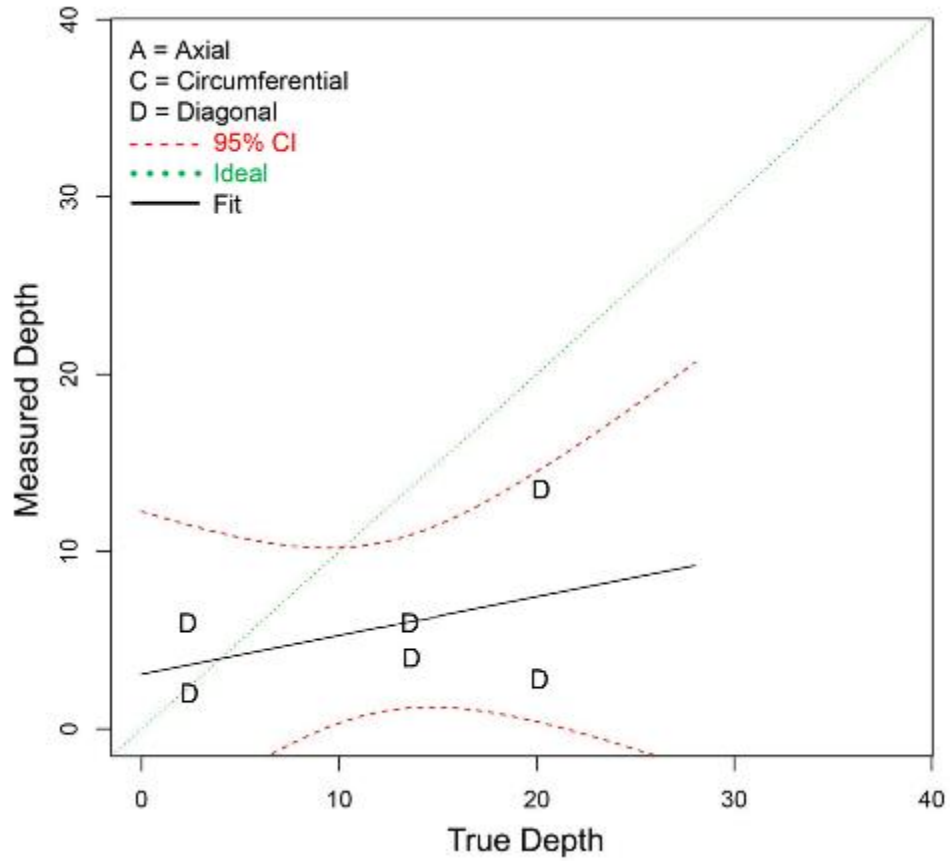


Figure 5.22 Depth Sizing Fit (in mm) for UT.PAUT Procedures Applied to LBDMWs (O.D. Access – Quick-blind)

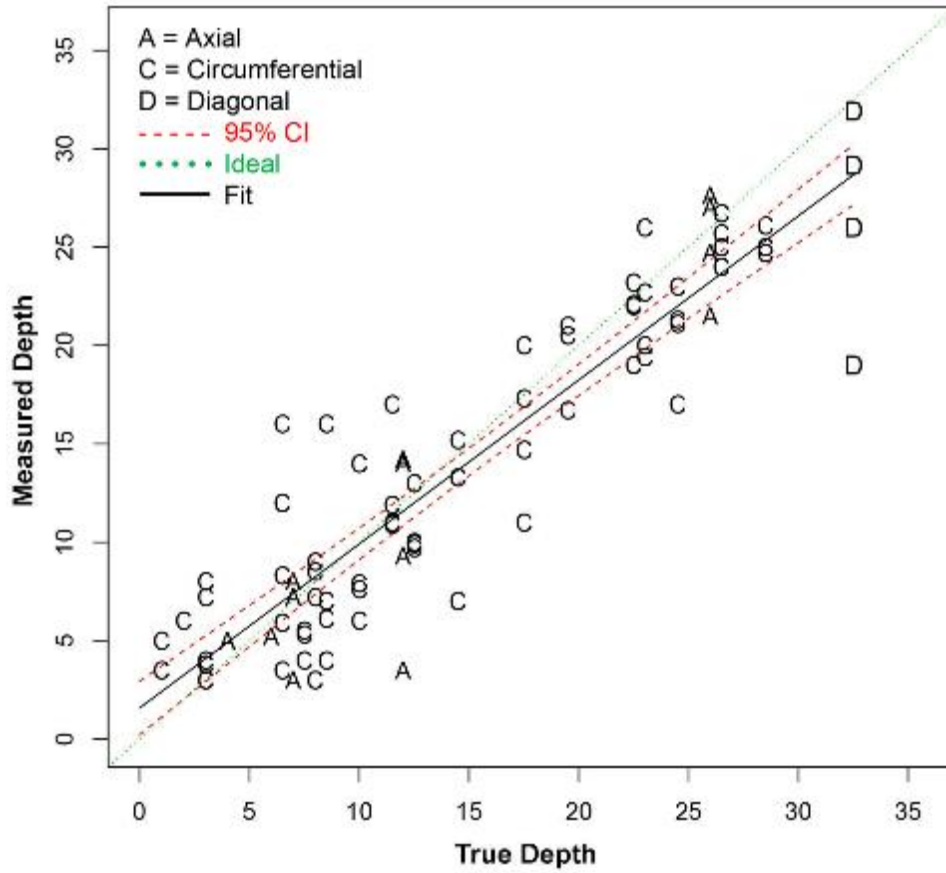


Figure 5.23 Depth Sizing Fit (in mm) for PAUT Procedures Applied to SBDMWs (O.D. Access)

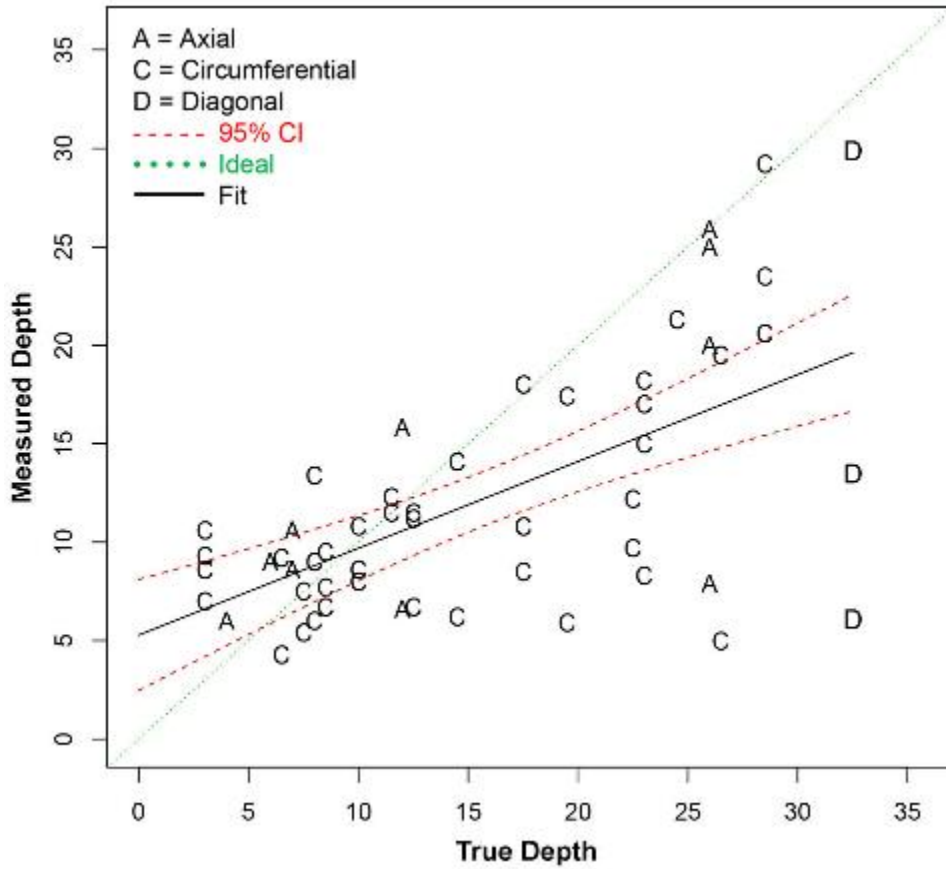


Figure 5.24 Depth Sizing Fit (in mm) for Conventional UT Procedures Applied to SBDMWs (O.D. Access)

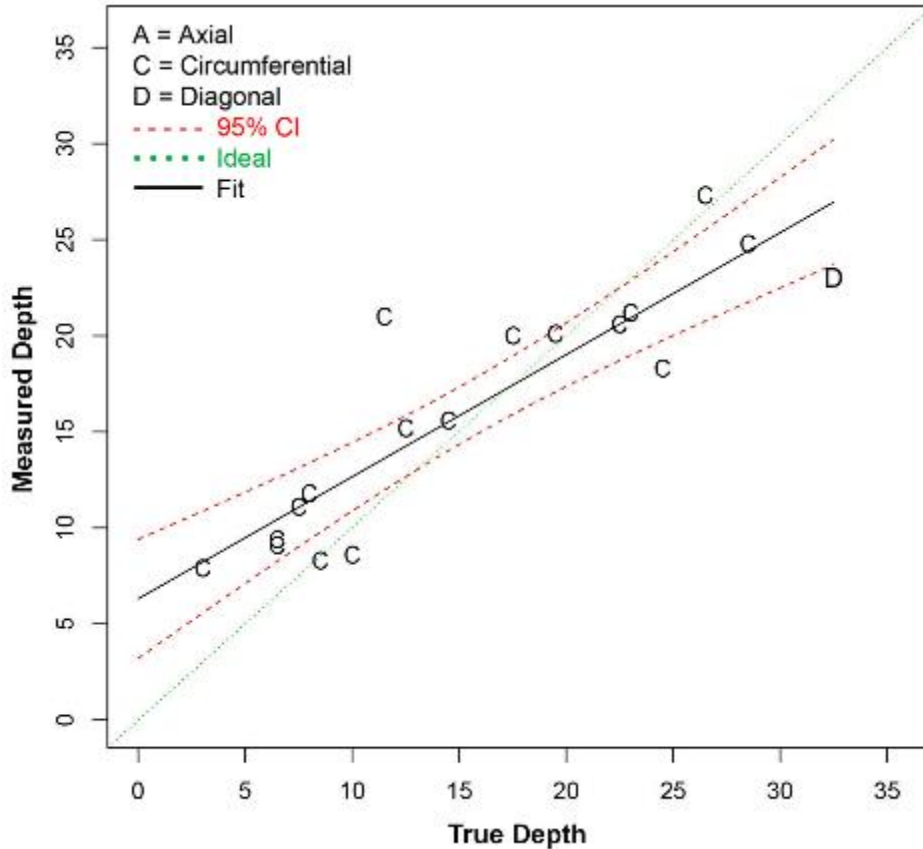


Figure 5.25 Depth Sizing Fit (in mm) for UT.TOFD Procedures Applied to SBDMWs (O.D. Access)

5.1.4 DMW Length Sizing Summary

Length sizing errors are provided in terms of bias and RMSE in Tables 5.25 through 5.27 for procedure types applied to LBDMW test blocks with I.D. access, LBDMW test blocks with O.D. access, and SBDMW test blocks, respectively. Length sizing errors are provided in terms of bias and RMSE in Tables 5.28 through 5.30 for individual procedures applied to LBDMW test blocks with I.D. access, LBDMW test blocks with O.D. access, and SBDMW test blocks, respectively. A list of the sizing outliers is included in Table 5.31 and these were excluded from the analysis. Length sizing data, along with regression curve fits for LBDMW test blocks with I.D. access, are provided in Figures 5.26 through Figure 5.31. For LBDMW test blocks with O.D. access, length sizing data along with regression curve fits are provided in Figure 5.32 through 5.35. Finally, length sizing data along with regression curve fits for SBDMW test blocks are provided in Figures 5.36 through 5.38. Length sizing regression plots are provided in Appendix G.1.2 and Appendix G.2.2 for Blind and Blind + Quick-blind data, respectively.

Table 5.25 Summary of Length Sizing Errors for Procedure Types Applied to LBDMWs (I.D. Access – Outliers Omitted)^(a)

	NOBS	Bias, mm	RMSE, mm
ECT*,+	12	-2.2	6.2
UT.ECT*	11	2.9	4.2
UT.ECT (Blind + Quick-blind) ⁺	14	0.3	5.9
UT.PAUT*	15	10.6	13.3
UT.PAUT (Blind + Quick-blind) ⁺	18	6.9	13.2
UT.TOFD.ECT*,+	15	1.1	5.3
*All	53	3.4	8.4
+All (Blind + Quick-blind)	59	2.0	8.7

(a) Procedure PAUT.132 was not qualified for length sizing and this data is not included in the summary.
 UT = conventional UT

Table 5.26 Summary of Length Sizing Errors for Procedure Types Applied to LBDMWs (O.D. Access)

	NOBS	Bias, mm	RMSE, mm
PAUT*	14	3.1	8.9
UT*,+	18	6.9	15.9
UT (Blind + Quick-blind) ⁺	21	4.7	15.4
UT.PAUT (Blind + Quick-blind) ⁺	6	-4.2	9.0
*All	32	5.2	13.3
+All (Blind + Quick-blind)	41	2.8	12.7

UT = conventional UT

Table 5.27 Summary of Length Sizing Errors for Procedure Types Applied to SBDMWs (O.D. Access)

	NOBS	Bias, mm	RMSE, mm
PAUT	84	6.6	11.8
UT	54	6.0	12.8
UT.TOFD	23	4.3	11.7
All	161	6.1	12.1

UT = conventional UT

Table 5.28 Summary of Length Sizing Errors for Procedures Applied to LBDMWs (I.D. Access – Outliers Omitted)^(a)

	NOBS	Bias, mm	RMSE, mm
ECT.135	12	-2.2	6.2
UT.ECT.106 (Quick-blind)	3	-9.3	10.0
UT.ECT.144	11	2.9	4.2
UT.PAUT.113	15	10.6	13.3
UT.PAUT.113 (Blind + Quick-blind)	18	6.9	13.2
UT.TOFD.ECT.101	15	1.1	5.3

(a) Procedure PAUT.132 was not qualified for length sizing and this data is not included in the summary.
 UT = conventional UT

Table 5.29 Summary of Length Sizing Errors for Procedures Applied to LBDMWs (O.D. Access)

	NOBS	Bias, mm	RMSE, mm
PAUT.108.1	7	-0.4	7.2
PAUT.126.1	7	6.6	10.3
UT.108	7	4.9	8.1
UT.126	3	12.3	17.1
UT.134.2	8	6.8	20.0
UT.134.1 (Quick-blind)	3	6.6	8.2
UT.PAUT.108 (Quick-blind)	3	-9.0	11.1
UT.PAUT.126 (Quick-blind)	3	-0.7	6.4

UT = conventional UT

Table 5.30 Summary of Length Sizing Errors for Procedures Applied to SBDMWs (O.D. Access)

	NOBS	Bias, mm	RMSE, mm
PAUT.108.1	21	1.0	9.2
PAUT.115	25	8.2	13.1
PAUT.126.1	14	5.7	12.4
PAUT.128	24	10.5	12.0
UT.108	20	3.9	8.0
UT.126	10	18.6	22.6
UT.134.2	21	1.4	9.9
UT.25 ^(a)	3	10.0	12.7
UT.TOFD.117	23	4.3	11.7

(a) UT.25 was not a qualified procedure.
 UT = conventional UT

Table 5.31 Length Sizing Outliers

Procedure	Flaw ID	Indication ID	Length Size Error, mm
UT.126	P33.14	12	374
PAUT.126	P33.14	9	229

UT = conventional UT

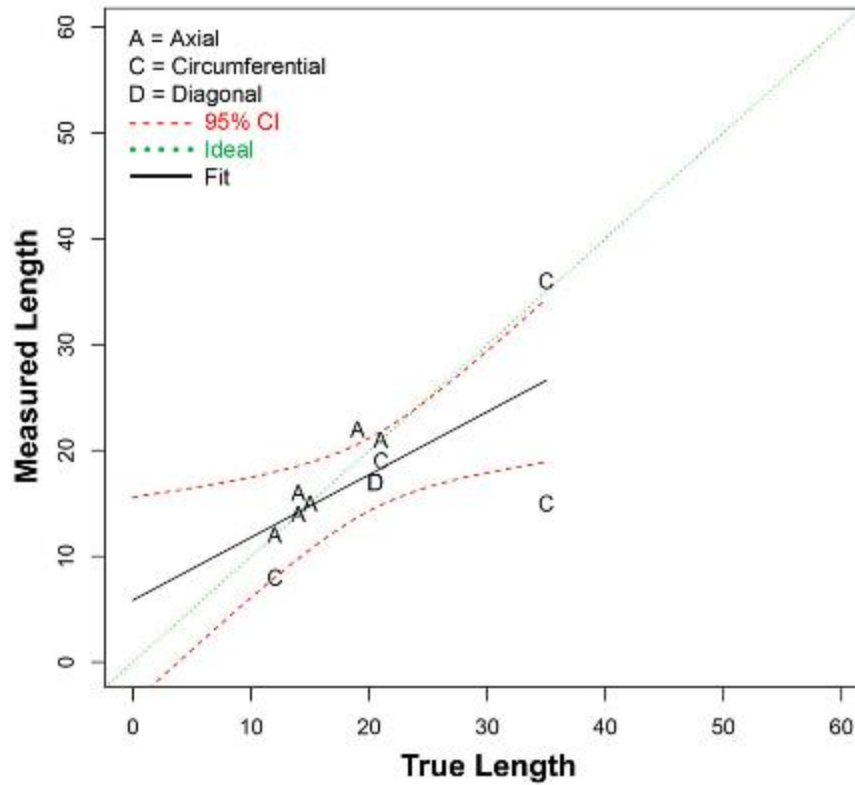


Figure 5.26 Length Sizing Fit (in mm) for ECT Procedures Applied to LBDMWs (I.D. Access)

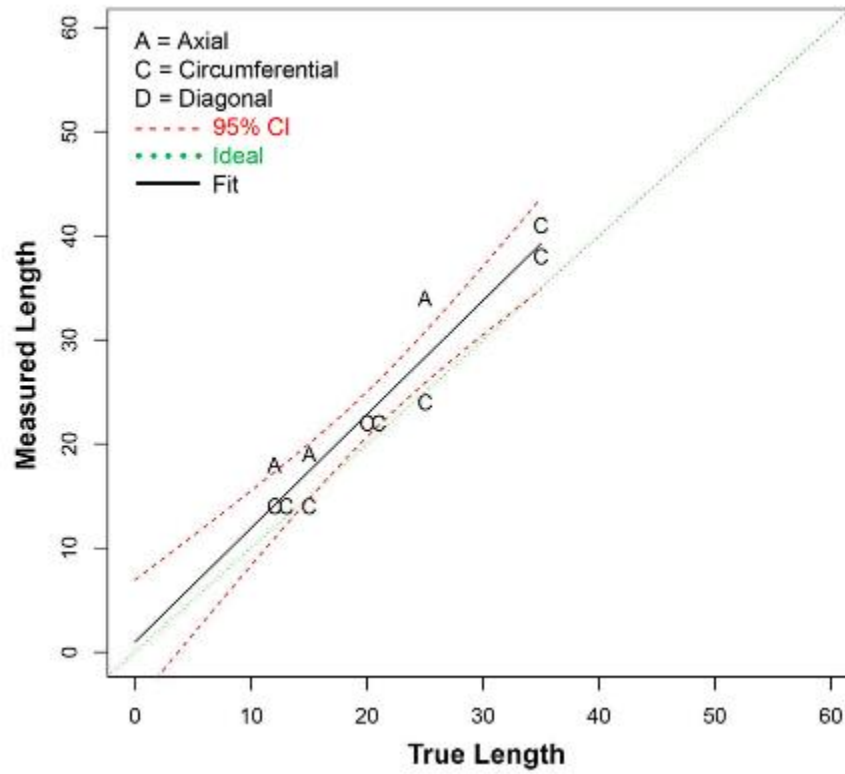


Figure 5.27 Length Sizing Fit (in mm) for UT.ECT Procedures Applied to LBDMWs (I.D. Access; all dimensions are in mm)

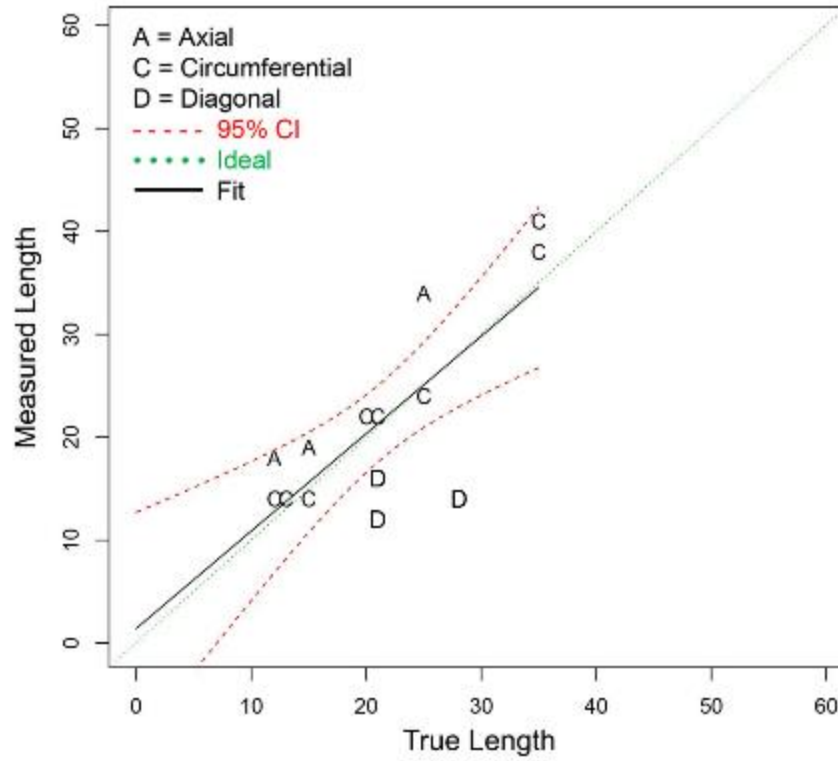


Figure 5.28 Length Sizing Fit (in mm) for UT.ECT Procedures Applied to LBDMWs (I.D. Access – **Blind + Quick-blind**; all dimensions are in mm)

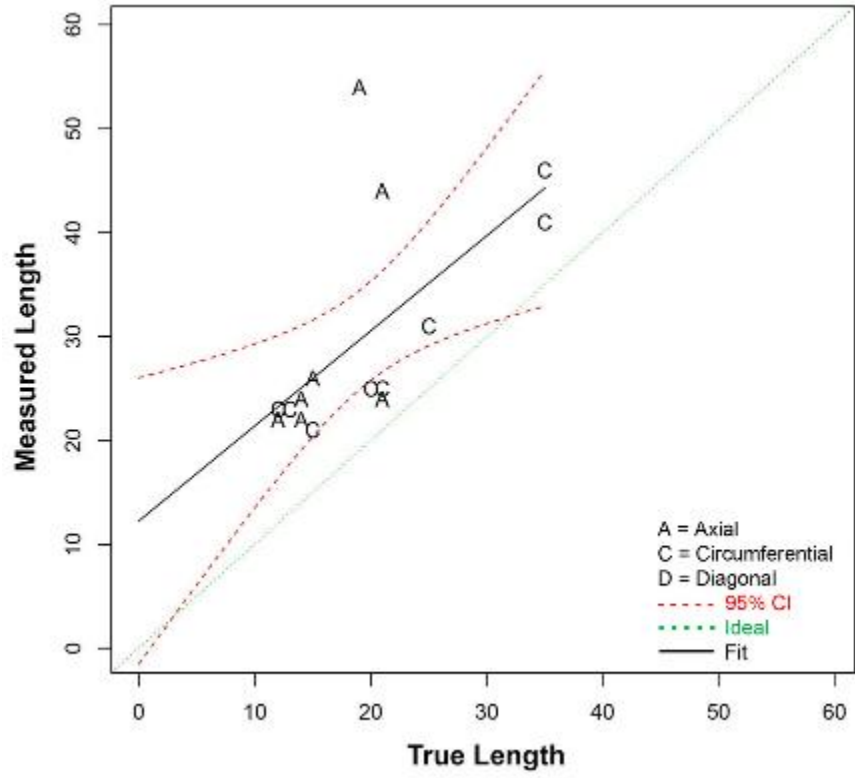


Figure 5.29 Length Sizing Fit (in mm) for UT.PAUT Procedures Applied to LBDMWs (I.D. Access; all dimensions are in mm)

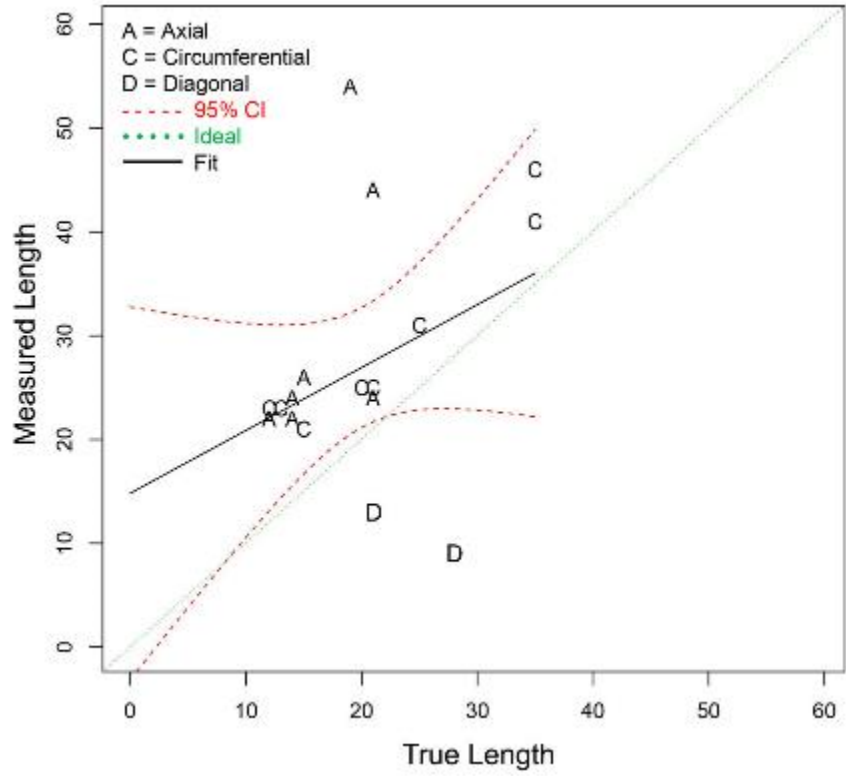


Figure 5.30 Length Sizing Fit (in mm) for UT.PAUT Procedures Applied to LBDMWs (I.D. Access – **Blind + Quick-blind**; all dimensions are in mm)

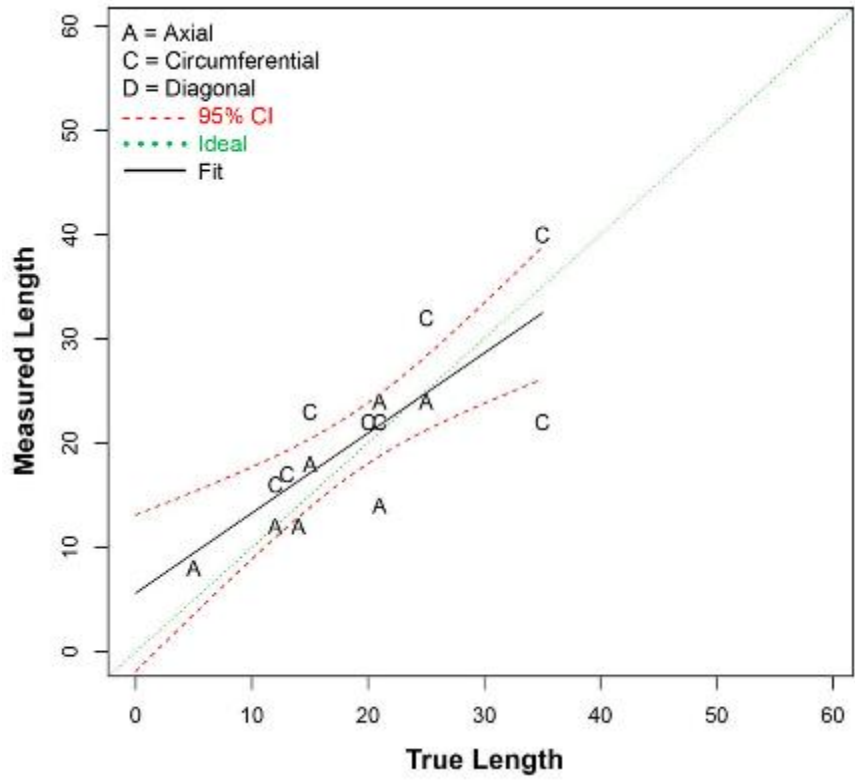


Figure 5.31 Length Sizing Fit (in mm) for UT, TOFD, ECT Procedures Applied to LBDMWs (I.D. Access; all dimensions are in mm)

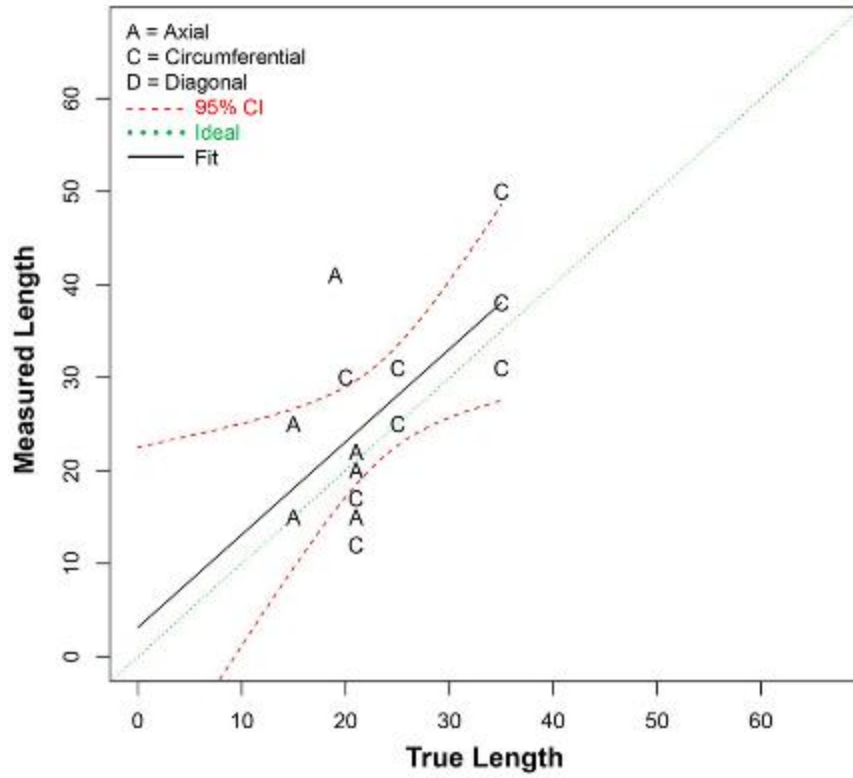


Figure 5.32 Length Sizing Fit (in mm) for PAUT Procedures Applied to LBDMWs (O.D. Access; all dimensions are in mm)

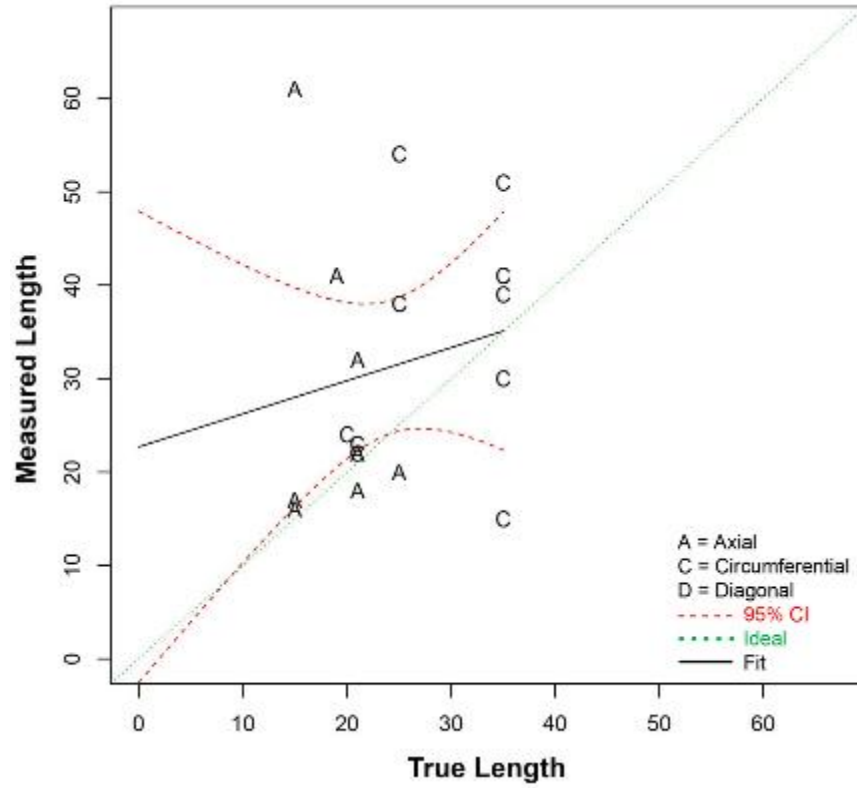


Figure 5.33 Length Sizing Fit (in mm) for UT Procedures Applied to LBDMWs (O.D. Access; all dimensions are in mm)

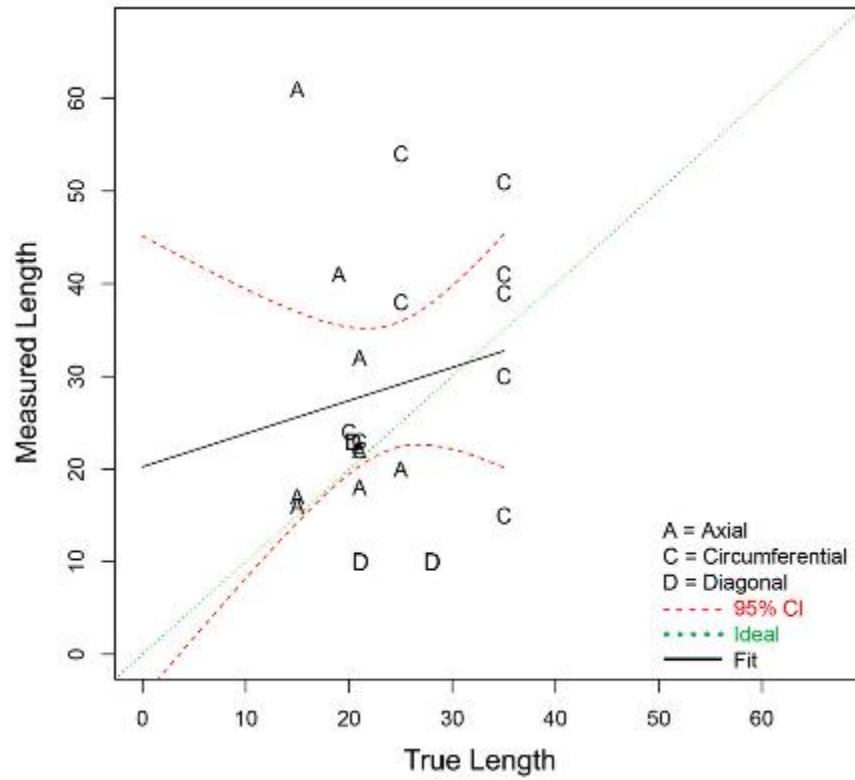


Figure 5.34 Length Sizing Fit (in mm) for UT Procedures Applied to LBDMWs (O.D. Access – **Blind + Quick-blind**; all dimensions are in mm)

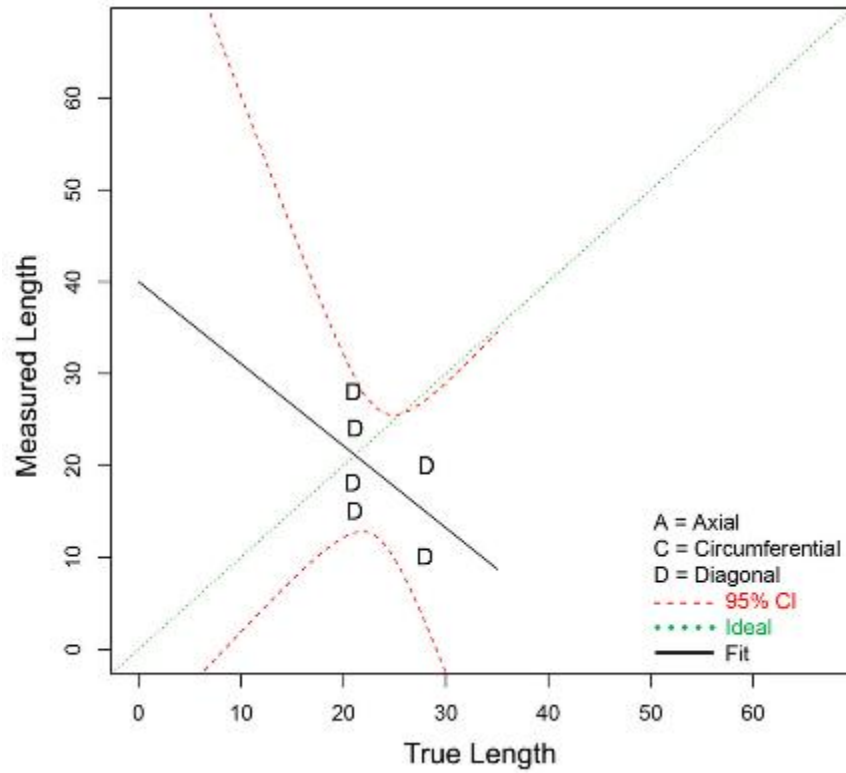


Figure 5.35 Length Sizing Fit (in mm) for UT.PAUT Procedures Applied to LBDMWs (O.D. Access – Quick-blind; all dimensions are in mm)

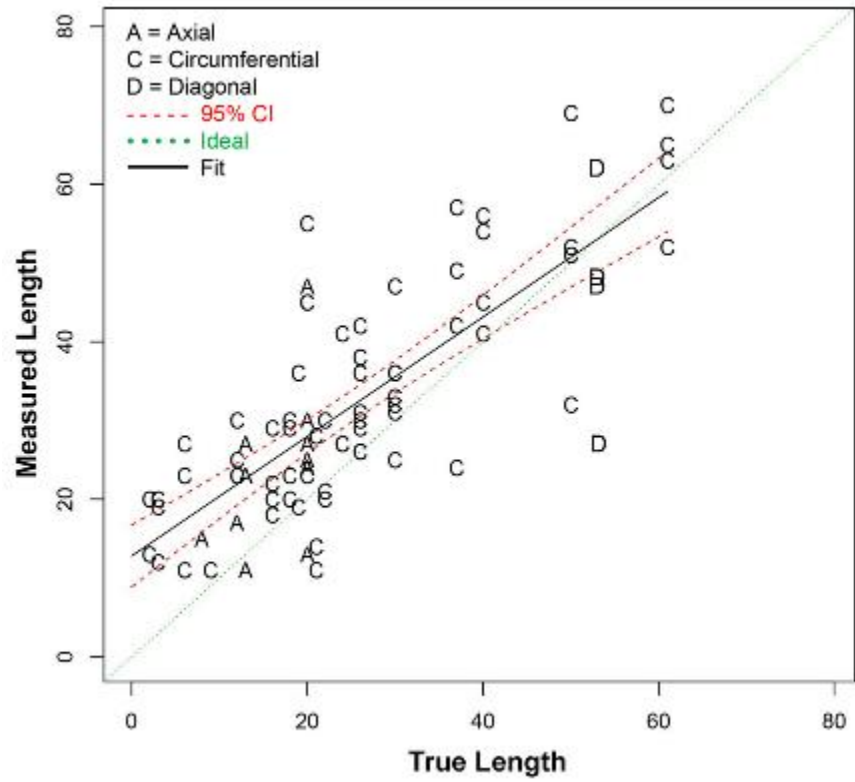


Figure 5.36 Length Sizing Fit (in mm) for PAUT Procedures Applied to SBDMWs (O.D. Access; all dimensions are in mm)

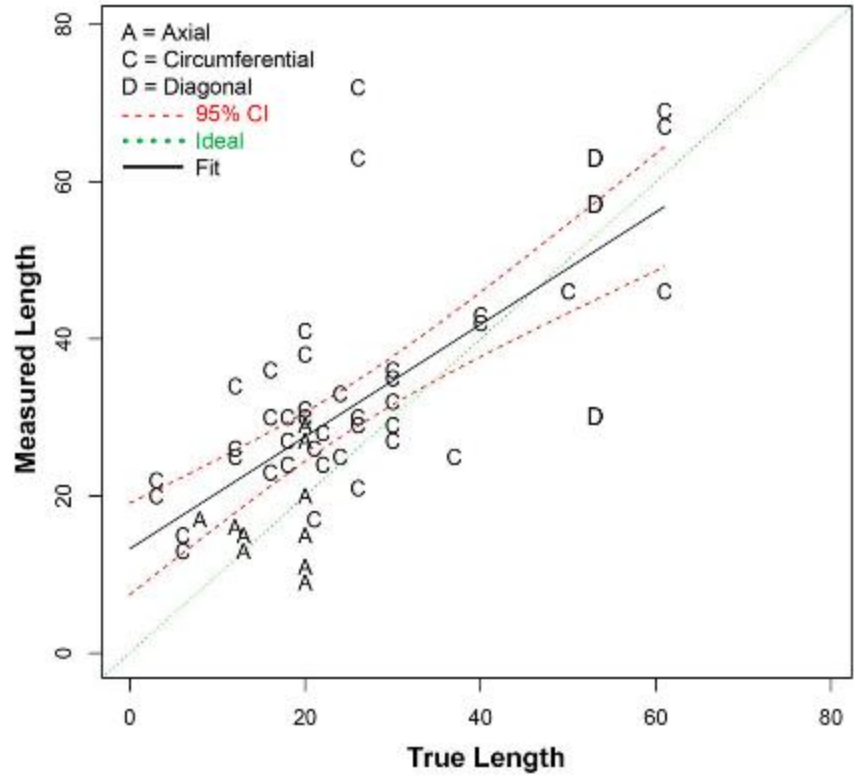


Figure 5.37 Length Sizing Fit (in mm) for UT Procedures Applied to SBDMWs (O.D. Access; all dimensions are in mm)

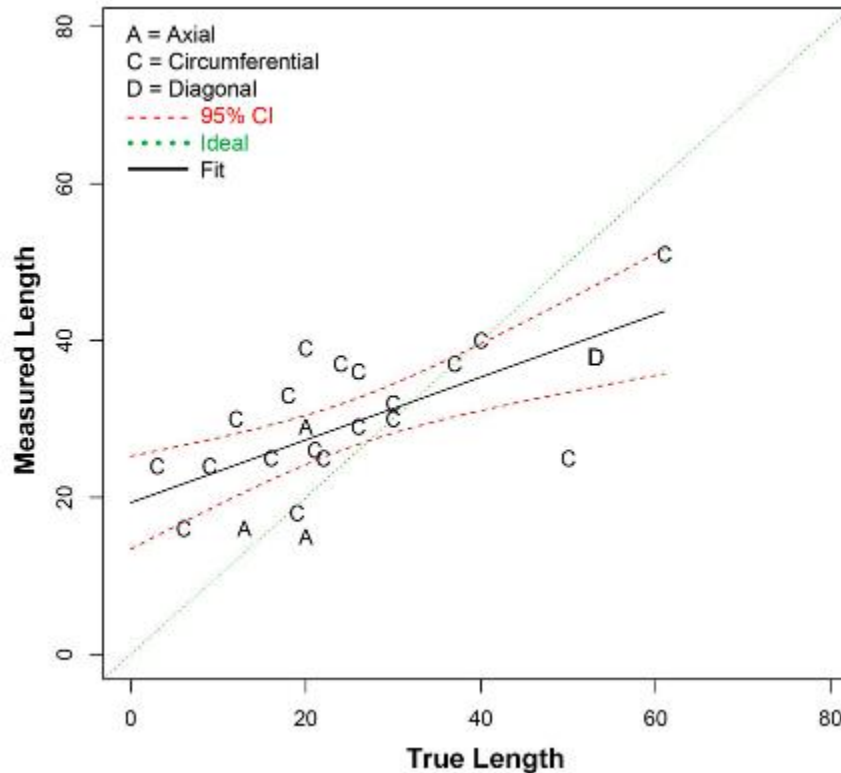


Figure 5.38 Length Sizing Fit (in mm) for UT.TOFD Procedures Applied to SBDMWs (O.D. Access; all dimensions are in mm)

5.2 Results for BMI Test Blocks

This section includes a summary of data analysis results for inspections performed on BMI test blocks. This includes detection and FCR results (Section 5.2.1) and depth and length sizing results (Section 5.2.2 and 5.2.3, respectively). Two types of inspections were performed on BMI test blocks: a) surface examinations of J-groove welds and b) I.D. examinations of penetration tubes. Procedures ECT.108 and ECT.124 were used to examine J-groove welds while TOFD.ECT.126 was used for the BMI tube I.D. examination.

5.2.1 BMI Detection and False Call Rate Summary

Table 5.32 provides a summary of detection and FCR results for each procedure applied to BMI test blocks. The column headings are similar to those used in Table 5.5 except access refers to either the BMI J-groove weld surface or the BMI tube I.D. surface. Table 5.32 summarizes the detection probability for all flaws in BMI test blocks, while Table 5.33 provides a summary of detection and FCR results for each BMI test block. Tables 5.34 and 5.35 tabulate detection performance versus flaw depth and flaw length, respectively, for each procedure type. From Table 5.33, it is evident that only test blocks P26 and P6 have a POD of less than 100%. Test blocks P6, P8, and P9 consisted of TFC flaws, many of which exhibited unintentional clustering as mentioned in Section 2.5.2. It is also worth noting that test blocks P25 and P26 were contributed for tube I.D. examinations even though examinations of the J-groove weld surface were also performed. POD curves for BMI inspections are included in Appendix F.1.1.4 as a function of depth and Appendix F.1.2.4 as a function of length.

Table 5.32 BMI Detection and False Call Rate Summary Organized by Procedure

	NOBS	POD, %	FCP, %	FCR, #/m	Access	Test Blocks
ECT.108	34	79	15	7	J-groove	P26, P6, P8, P9
ECT.124	34	94	5	2	J-groove	P26, P6, P8, P9
TOFD.ECT.126	6	83	18	8	Tube I.D.	P25, P26

Table 5.33 Detection and False Call Rate Summary for Each BMI Test Block

	No. of Flaws	No. of Inspections	FCR, #/m	FCP, %	POD, %
P25	2	1	4.36	10.3	100.0
P26	4	3	2.82	6.8	50.0
P6	9	2	15.09	31.4	72.2
P8	9	2	0.00	0.0	100.0
P9	13	2	6.36	14.7	100.0

Table 5.34 Summary of POD (%) by Flaw Depth in BMI Test Blocks for Each Procedure Type

	NOBS	POD 0-mm	POD 5-mm	POD 10-mm	POD 15-mm	Access
ECT	68	27	82	98	99	J-groove
TOFD.ECT	6	34	56	76	79	Tube I.D.

Table 5.35 Summary of POD (%) by Flaw Length in BMI Test Blocks for Each Procedure Type

	NOBS	POD 0 mm	POD 5 mm	POD 10 mm	POD 15 mm	Access
ECT	68	41	57	73	84	J-groove
TOFD.ECT	6	41	44	48	51	Tube I.D.

5.2.2 BMI Depth Sizing Summary

Only one procedure was applied for depth sizing in BMI test blocks. Sizing results for procedure TOFD.ECT.126 are provided in Table 5.36. Procedure TOFD.ECT.126 was only applied to test blocks P25 and P26 and was applied to the tube I.D. Therefore, no attempts were made to depth-size clustered flaws in test blocks P6, P8 and P9. The depth sizing regression plot is included in Appendix G.1.1.4.

Table 5.36 BMI Depth Sizing Results

	NOBS	Bias, mm	RMSE, mm	Test Blocks
TOFD.ECT.126	5	-0.5	1.7	P25, P26

5.2.3 BMI Length Sizing Summary

Length sizing results for BMI test blocks are summarized in Table 5.37. Length sizing regression plots are included in Appendix G.1.2.4.

Table 5.37 BMI Length Sizing Results

	NOBS	Bias, mm	RMSE, mm	Access	Test Blocks
ECT.108	27	3.9	8.1	J-groove	P25, P26, P6, P8, P9
ECT.124	32	11.2	15.6	J-groove	P25, P26, P6, P8, P9
TOFD.ECT.126	5	-4.0	7.0	Tube I.D.	P25, P26
All	64	6.9	12.4		

5.3 Results for WOL Test Blocks (P27)

Two inspections were performed on P27 for a total of 20 flaw observations. All flaws in the test block were detected. A summary of depth and length sizing results for procedures PAUT.108 and PAUT.126 for the individual flaws in P27 is provided in Table 5.38. A summary of the RMSE errors for depth and length sizing on test block P27 is provided in Table 5.39, and plots of depth and length sizing data for P27 are included in Figures 5.39 and 5.40, respectively. Finally, indication plots for the PAUT.108 inspection on P27 are included in Figures 5.41 and 5.42, and indication plots for PAUT.126 are included in Figures 5.43 and 5.44.

Table 5.38 WOL Test Block Sizing Results

Procedure	Flaw ID	Orientation	Flaw Type	Surface Breaking	Depth-Size Error, mm	Length Size Error, mm
PAUT.108.2	P27.1	Diagonal	MFC	Yes	-1.8	-1.9
PAUT.108.2	P27.2	Diagonal	EDM	Yes	-1	1.5
PAUT.108.2	P27.3	Diagonal	EDM	Yes	0	-5
PAUT.108.2	P27.4	Circumferential	MFC	Yes	-0.5	-8.6
PAUT.108.2	P27.5	Diagonal	EDM	Yes	-1.5	-1
PAUT.108.2	P27.6	Circumferential	MFC	Yes	-1.1	-8
PAUT.108.2	P27.7	Circumferential	LOB	No	-3.2	7.1
PAUT.108.2	P27.8	Circumferential	LOB	No	-3	-6.8
PAUT.108.2	P27.9	Circumferential	MFC	No	1.5	-5.4
PAUT.108.2	P27.10	Circumferential	MFC	No	2.8	-6.4
PAUT.126.2	P27.1	Diagonal	MFC	Yes	0.2	-1.3
PAUT.126.2	P27.2	Diagonal	EDM	Yes	-0.3	-0.5
PAUT.126.2	P27.3	Diagonal	EDM	Yes	0.4	1
PAUT.126.2	P27.4	Circumferential	MFC	Yes	0.2	11.7
PAUT.126.2	P27.5	Diagonal	EDM	Yes	0.4	0
PAUT.126.2	P27.6	Circumferential	MFC	Yes	0.7	6.3
PAUT.126.2	P27.7	Circumferential	LOB	No	-5.2	-8.4
PAUT.126.2	P27.8	Circumferential	LOB	No	-5	2.3
PAUT.126.2	P27.9	Circumferential	MFC	No	0.6	-7.7
PAUT.126.2	P27.10	Circumferential	MFC	No	1.1	-10.7

LOB = lack of bond
 UT = conventional UT

Table 5.39 Summary of Sizing RMSEs for the WOL Test Block

	NOBS	RMSE, mm
Depth	20	2.1
Length	20	6.2

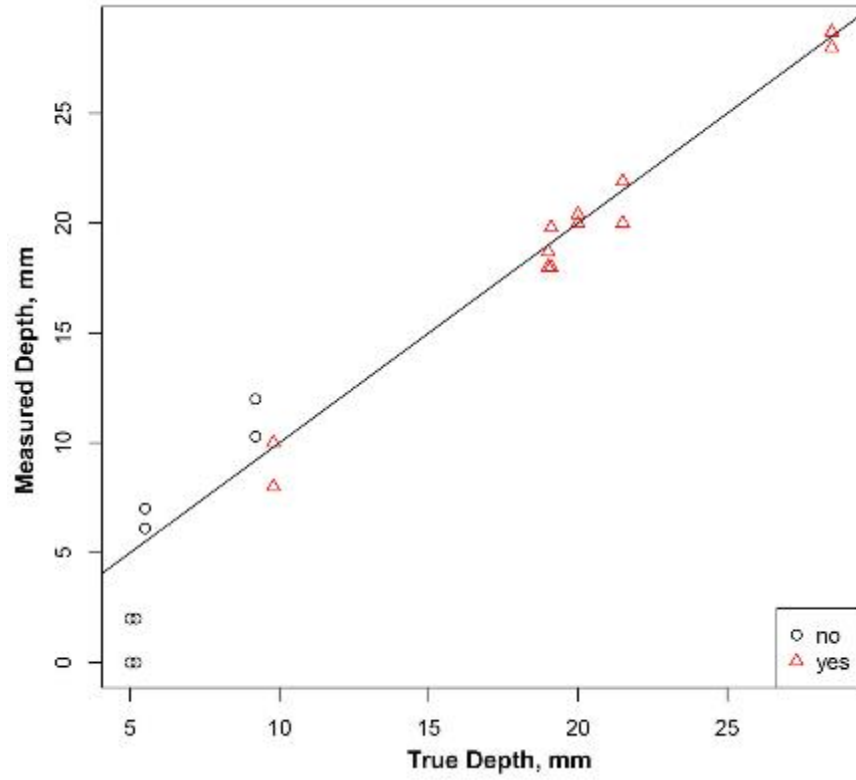


Figure 5.39 Depth Sizing Results for the WOL Test Block with Results for Surface Breaking (Triangles) and Non-Surface Breaking (Circles) Flaws Identified

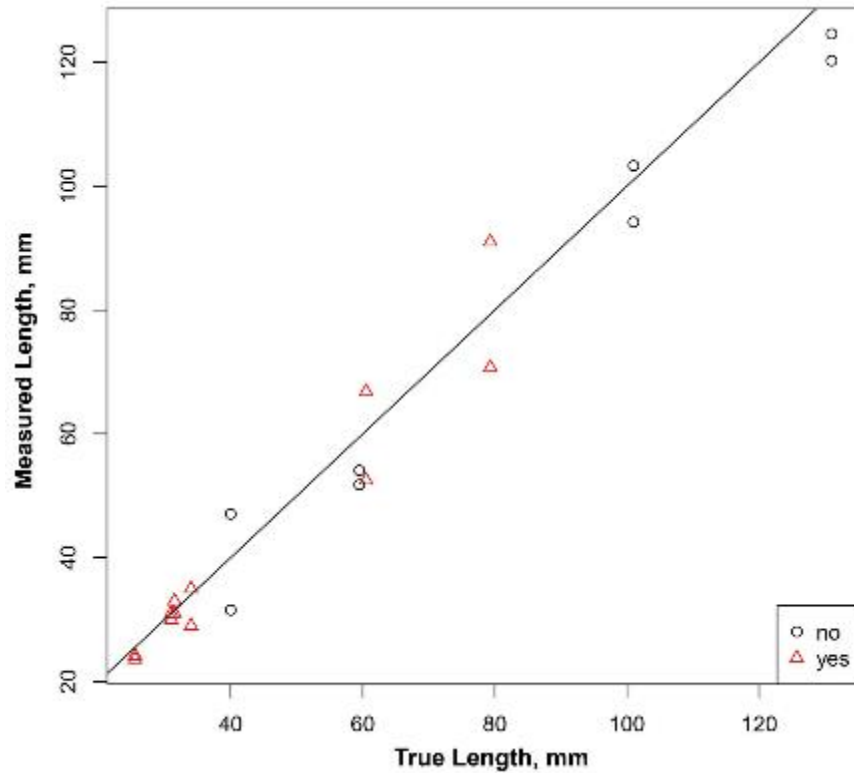


Figure 5.40 Length Sizing Results for the WOL Test Block with Results for Surface Breaking (Triangles) and Non-Surface Breaking (Circles) Flaws Identified

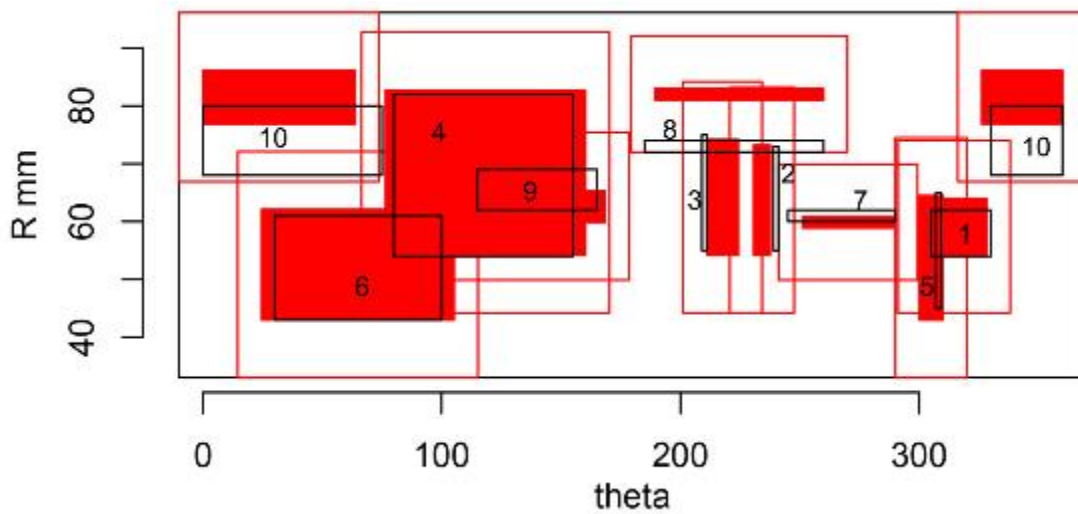


Figure 5.41 Indication Plot for Procedure PAUT.108 Applied to WOL Test Block (P27) [theta – R view]

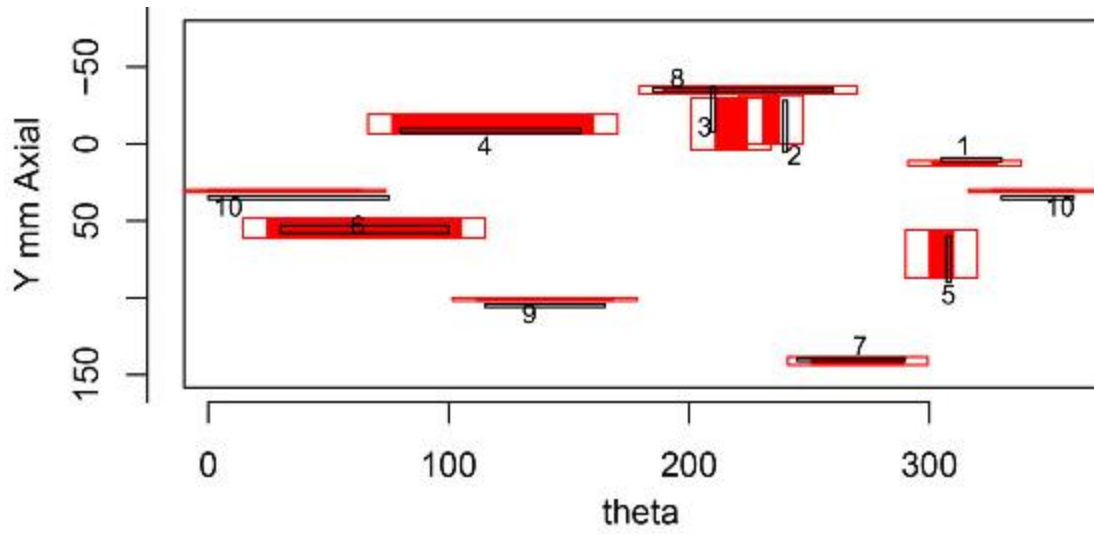


Figure 5.42 Indication Plot for Procedure PAUT.108 Applied to WOL Test Block (P27) [theta – Y view]

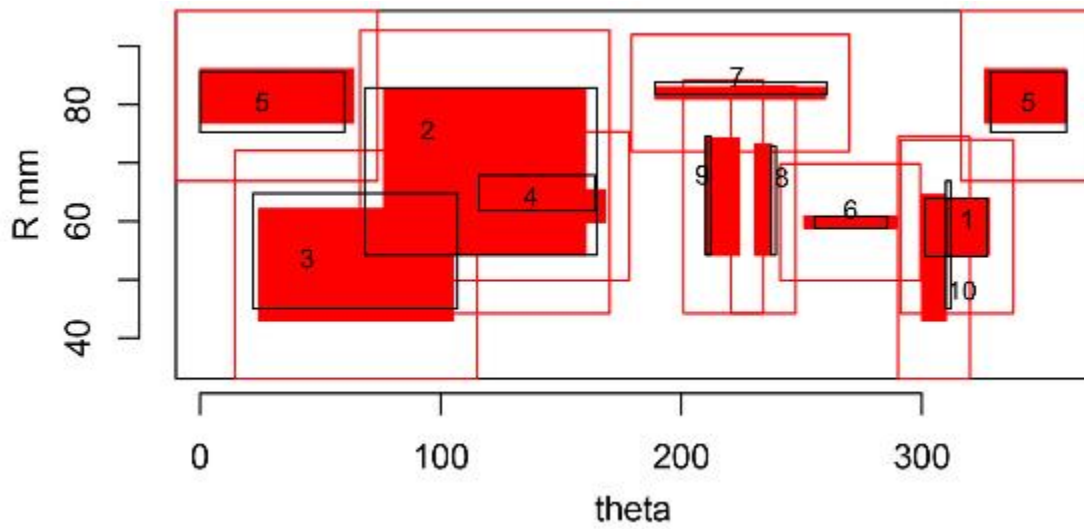


Figure 5.43 Indication Plot for Procedure PAUT.126 Applied to WOL Test Block (P27) [theta – R view]

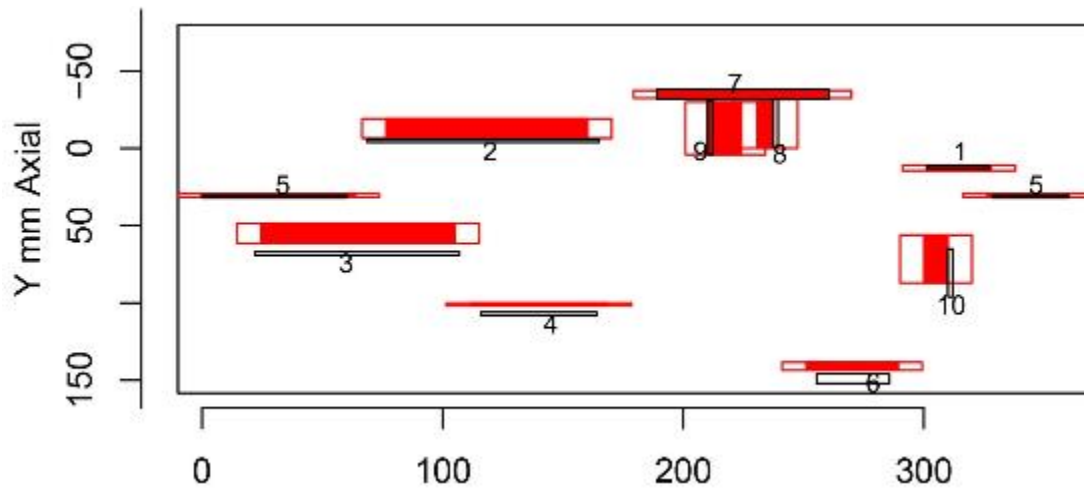


Figure 5.44 Indication Plot for Procedure PAUT.126 Applied to WOL Test Block (P27) [theta – Y view]

6 ANALYSIS OF PARENT RESULTS

This section includes a discussion of PARENT results presented in Section 5. The influence of several test block variables on performance as measured by POD, depth sizing error, and length sizing error is provided in Section 6.1. A comparison of PAUT and UT procedures is provided in Section 6.2, followed by a comparison of the Quick-blind test results with the blind testing results in Section 6.3. Section 6.4 includes a discussion of the influence of the defined tolerance box on detection analysis performed in PARENT; and finally, Section 6.5 includes a discussion of the influence of following the ASME Code, Section XI IWA-3400 rules for combining multiple closely spaced flaws on the results.

6.1 Influence of Variables on Detection and Sizing Performance

Table 6.1 provides POD results as a function of depth, flaw orientation, and access for LBDMW and SBDMW test blocks. This table indicates that access (O.D. versus I.D.) and block type (SBDMW vs. LBDMW) do influence detection performance with better performance observed for I.D. access versus O.D. access (with the exception of Quick-blind test blocks) and better performance observed for SBDMW test blocks than LBDMW test blocks for a given flaw size. For flaw orientation, the general trend observed in Table 6.1 indicates that circumferential flaws are easier to detect than axial flaws, although this appears to be dependent of flaw size for SBDMW test blocks with the effect diminishing with increasing flaw depth. This is likely an artifact caused by saturation of POD with flaw depth in SBDMW test blocks.

Depth and length sizing performance as measured by RMSE and bias is provided in Tables 6.2 and 6.3, respectively, for each combination of access, block type, and flaw orientation variables. Table 6.2 indicates that block type and access variables influence depth sizing performance with better depth sizing performance observed for I.D. versus O.D. access and better depth sizing performance observed on SBDMW versus LBDMW test blocks. Flaw orientation does not appear to have an influence on depth sizing performance. The data in Table 6.3 indicates that length sizing performance is better for I.D. access than O.D. access, and it appears that length sizing performance for axial flaws is better for SBDMW than LBDMW test blocks. Otherwise, there does not appear to be an effect of block type or flaw orientation on length sizing performance.

A review of Figures 6.1 through 6.6 indicates a tendency to oversize the depth of shallow flaws and undersize the depth of deep flaws, especially with O.D. access procedures. These plots show the depth sizing regression fits for axial and circumferential flaws considering I.D. and O.D. access on LBDMWs and O.D. access on SBDMWs. Better sizing performance by I.D. access procedures is indicated by these plots. In this case, not only is the overall RMSE for I.D. access smaller, but the error is more consistent for all flaw depths. Figures 6.1 through 6.6 support the conclusion that flaw orientation does not appear to have an influence on depth sizing performance based in data in Table 6.2.

Table 6.1 Summary of POD (%) by Access, Orientation, and Block Type versus Flaw Depth

Access	Orientation	Block Type	0–5 mm	5–10 mm	10–20 mm	>20 mm
I.D.	Axial	LBDMW	25±23	75±13	83±17	75±13
O.D.	Axial	LBDMW	0±12	20±11	10±11	67±12
O.D.	Axial	SBDMW	22±14	44±12	78±14	100±7
I.D.	Circumferential	LBDMW	43±13	92±9	100±15	100±8
O.D.	Circumferential	LBDMW	30±10	27±12	40±22	80±13
O.D.	Circumferential	SBDMW	58±7	78±6	88±5	90±5
I.D.	Diagonal	LBDMW (Quick-blind)	69±13		85±11	93±8
O.D.	Diagonal	LBDMW (Quick-blind)	75±16		100±8	88±13

Table 6.2 Depth Sizing Results by Access, Orientation, and Block Type

Access	Orientation	Block Type	Bias, mm	RMSE, mm	
I.D.	Axial	LBDMW	0.3	3.0	
I.D.	Axial	SBDMW			
I.D.	Circumferential	LBDMW	0.8	3.0	
I.D.	Circumferential	SBDMW			
I.D.	Diagonal	LBDMW	-2.2	5.5	Quick-blind
O.D.	Axial	LBDMW	-6.1	10.0	
O.D.	Axial	SBDMW	-1.3	5.0	
O.D.	Circumferential	LBDMW	-0.1	9.7	
O.D.	Circumferential	SBDMW	-1.2	4.7	
O.D.	Diagonal	LBDMW	-6.4	9.4	Quick-blind

Table 6.3 Length Sizing Results by Access, Orientation and Block Type (Outliers Omitted)

Access	Orientation	Block Type	Bias, mm	RMSE, mm	
I.D.	Axial	LBDMW	5.0	10.0	
I.D.	Axial	SBDMW			
I.D.	Circumferential	LBDMW	2.1	6.8	
I.D.	Circumferential	SBDMW			
I.D.	Diagonal	LBDMW	-10.5	11.5	Quick-blind
O.D.	Axial	LBDMW	7.2	15.5	
O.D.	Axial	SBDMW	3.9	8.7	
O.D.	Circumferential	LBDMW	3.7	11.2	
O.D.	Circumferential	SBDMW	7.3	12.6	
O.D.	Diagonal	LBDMW	-5.8	10.2	Quick-blind

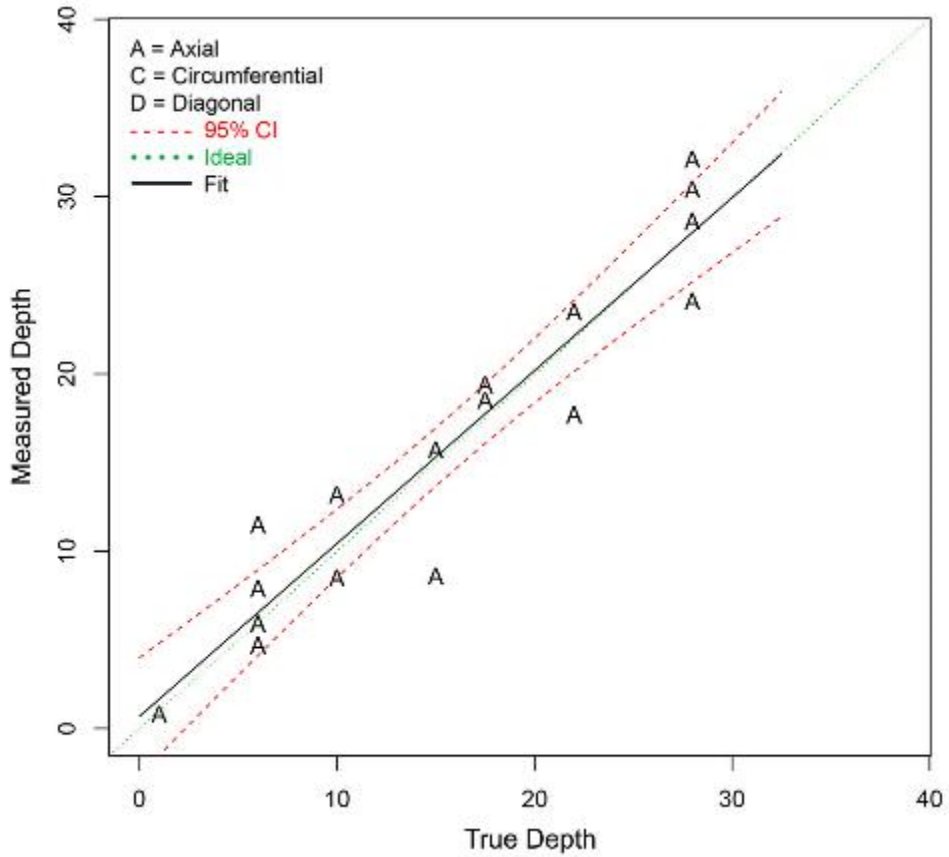


Figure 6.1 Depth Sizing Fit for Axial Flaws in LBDMWs (I.D. Access; all dimensions are in mm)

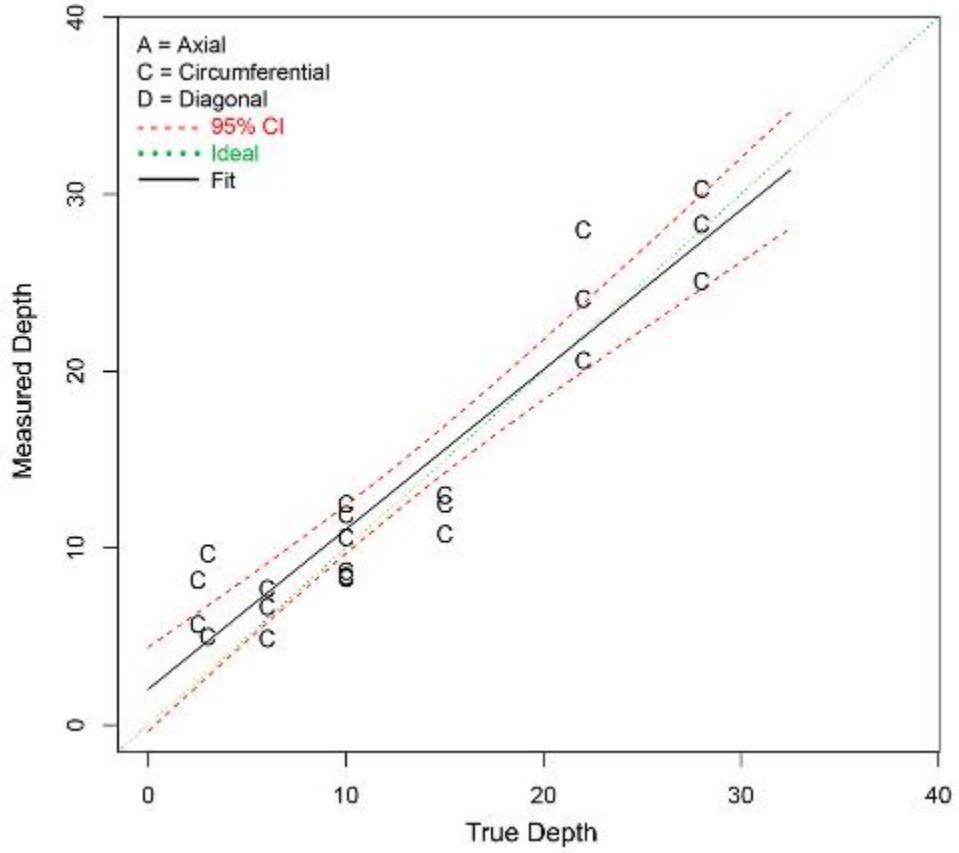


Figure 6.2 Depth Sizing Fit for Circumferential Flaws in LBDMWs (I.D. Access; all dimensions are in mm)

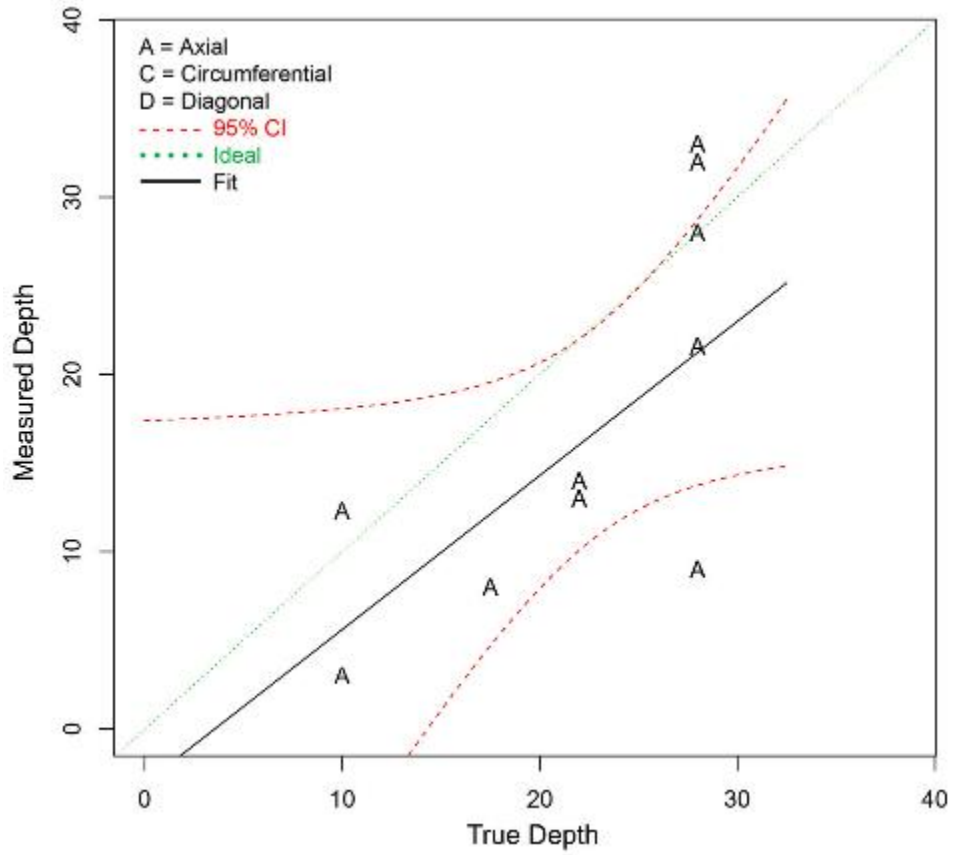


Figure 6.3 Depth Sizing Fit for Axial Flaws in LBDMWs (O.D. Access; all dimensions are in mm)

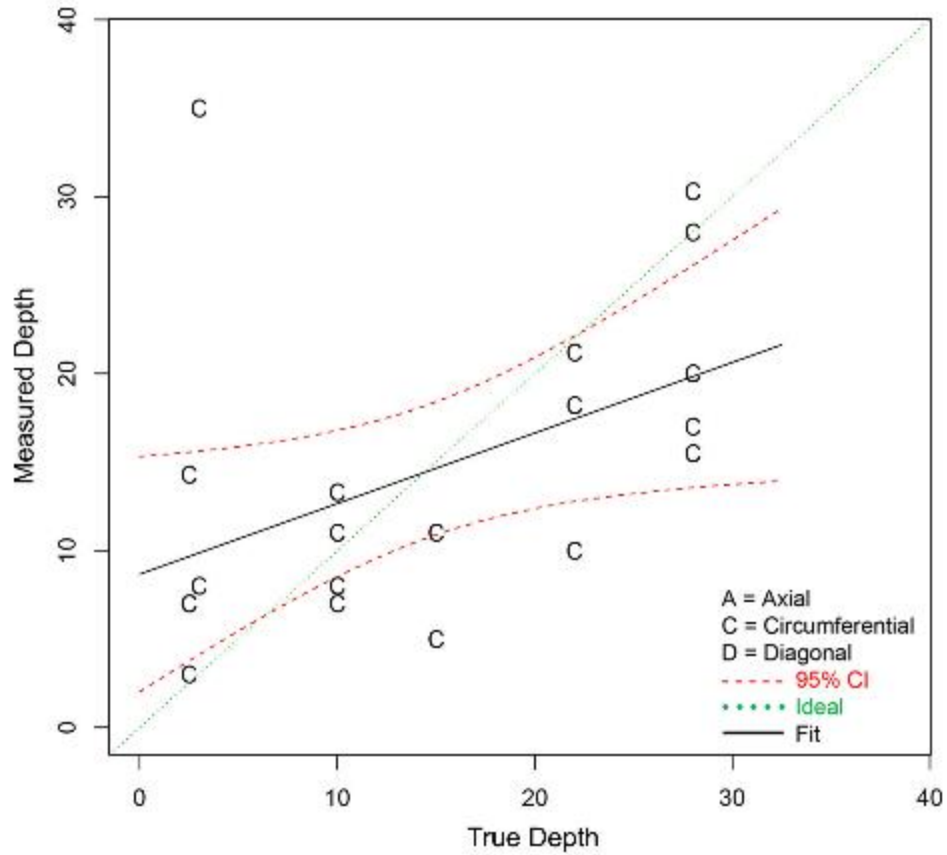


Figure 6.4 Depth Sizing Fit for Circumferential Flaws in LBDMWs (O.D. Access; all dimensions are in mm)

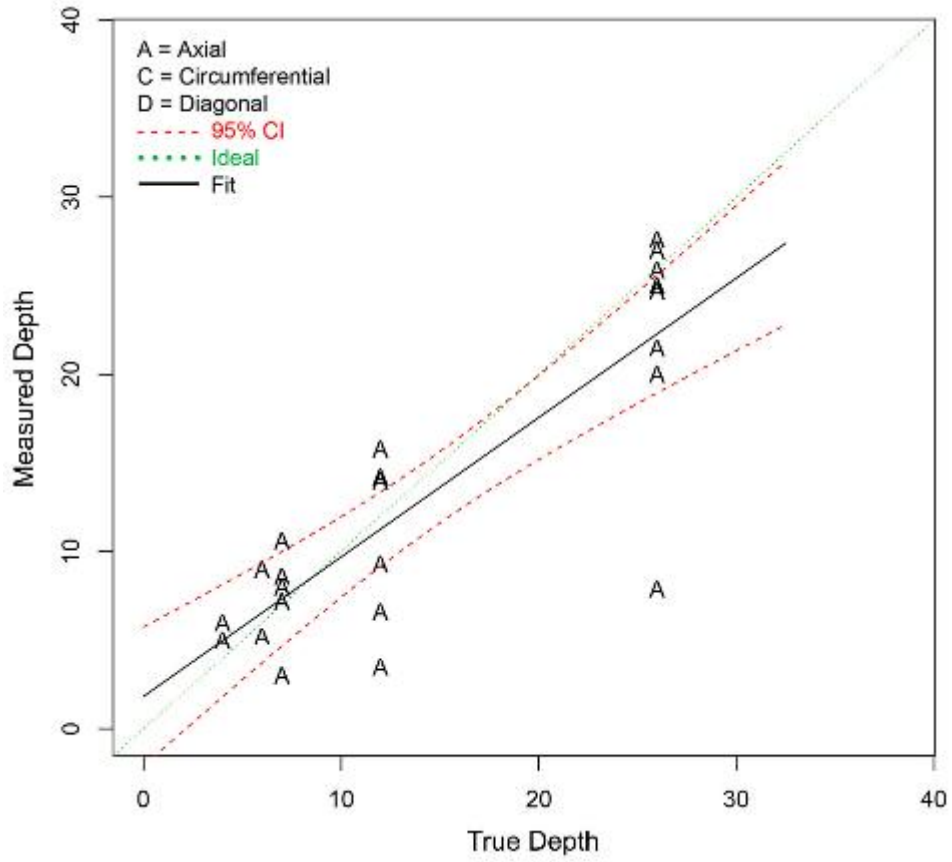


Figure 6.5 Depth Sizing Fit for Axial Flaws in SBDMWs (O.D. Access; all dimensions are in mm)

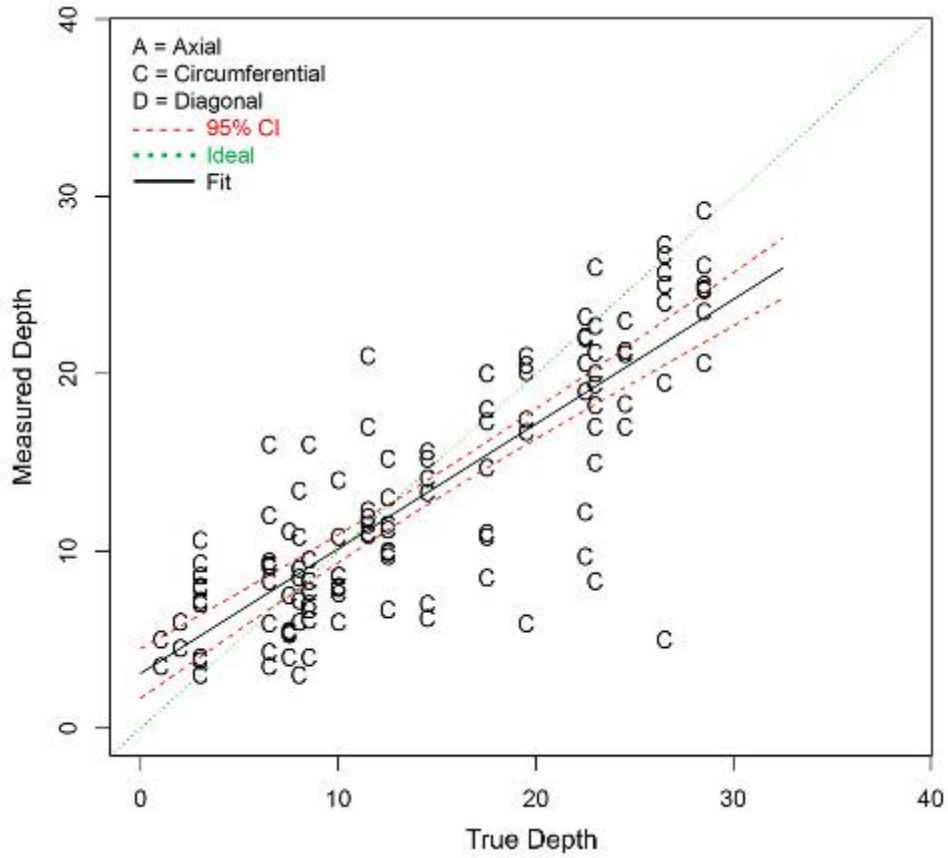


Figure 6.6 Depth Sizing Fit for Circumferential Flaws in SBDMWs (O.D. Access; all dimensions are in mm)

6.2 Comparison of Procedures and Procedure Type Performances

A review of Table 6.4 indicates that PAUT performance is better than conventional UT performance on SBDMW test blocks. However, Table 6.5 indicates that any difference between PAUT and conventional UT performance is marginal for LBDMW test blocks (O.D. access). A similar trend is observed in the summaries of depth sizing performances for SBDMW and LBDMW (O.D. access) test blocks in Tables 6.6 and 6.7, respectively, where it is observed in Table 6.6 that PAUT depth sizing performance is better than conventional UT depth sizing performance for SBDMW test blocks and in Table 6.7 where it appears that the difference in depth sizing performance for PAUT and conventional UT applied to LBDMW test blocks (O.D. access) is marginal.

A review of Table 6.8 indicates that procedure types that include ECT exhibit better length sizing performance than procedure types that do not include ECT on LBDMW test blocks (I.D. access), particularly for axially oriented flaws.

Table 6.4 Summary of POD (%) versus Depth for PAUT and UT Procedure Types for SBDMWs (O.D. Access)

	NOBS	0 mm	5 mm	10 mm	15 mm	30 mm
PAUT	112	6	39	87	99	100
UT	96	8	20	43	69	98

UT = conventional UT

Table 6.5 Summary of POD (%) versus Depth for PAUT and UT Procedure Types for LBDMWs (O.D. Access)

	NOBS	0 mm	5 mm	10 mm	15 mm	30 mm
PAUT	38	5	10	21	37	82
UT	57	5	10	19	32	74
UT (Blind + Quick-blind)	60	5	10	19	34	79

UT = conventional UT

Table 6.6 Summary of Depth Sizing Errors for PAUT and UT Procedures Types on SBDMWs with O.D. Access

Procedure Type	NOBS	RMSE, mm
PAUT	84	3.6
UT	54	7.9

UT = conventional UT

Table 6.7 Summary of Depth Sizing Errors for PAUT and UT Procedure Types Applied to LBDMWs with O.D. Access

Procedure Type	NOBS	RMSE, mm
PAUT	15	9.7
UT	16	9.8
UT (Blind + Quick-blind)	19	9.9

UT = conventional UT

Table 6.8 Summary of Length Sizing Errors for Procedure Types that do and do not incorporate an ECT technique Applied to LBDMWs (I.D. Access – Outliers Omitted)

Block Type	Orientation	Access	ECT?	NOBS	RMSE, mm
LBDMW	Axial	I.D.	ECT	17	3.8
LBDMW	Axial	I.D.	No ECT	7	17.5
LBDMW	Circumferential	I.D.	ECT	21	6.3
LBDMW	Circumferential	I.D.	No ECT	8	7.8

The detection data for PAUT.108, PAUT.115, PAUT.126, and PAUT.128 is compared by considering only data collected from SBDMW test blocks in Table 5.12. This table indicates that the performance of PAUT.126 is much worse than the performance observed for PAUT.108, PAUT.115, and PAUT.128. Details regarding these procedures are summarized in Table 6.9. Overall, this table indicates substantial similarities between the procedures and that PAUT.126 is most similar to PAUT.128 with the exception that PAUT.128 is automated while PAUT.126 is manual. The variability in performance could be caused by several factors including differences in the equipment used, human factors, etc.

Table 6.9 Summary of Procedures PAUT.115, PAUT.128, PAUT.108, and PAUT.126

	Frequency	Interrogation Modes/Angles for Circumferential Defects	Interrogation Modes/Angles for Axial Defects	Manual or Automated?	Encoded?
PAUT.115	2.0 MHz	L25° to L70° (Step 1°) S35° to S65° (Step 1°)	L25° to L70° (Step 1°) S35° to S65° (Step 1°)	Manual	No
PAUT.128	1.5 MHz	L45°, L60°, L70°, S45°, S60°	L25°, L35°, L45°, L55°; S35°, S45°, S55°, Skew -25° to +25°, step 2.5°	Automated	Yes
PAUT.108	2.0 MHz	L0° to L70°	L0° to L70°	Manual	No
PAUT.126	1.5 MHz	L30°, L45°, L60°, S45°, S60° (Nozzle Side) L45°, L60°, L70°, S45°, S60° (Pipe Side)	L22.5°, L30°, L37.5°, L45° for SBDMWs L25°, L35°, L45°, L55° for LBDMWs	Manual	Yes

UT = conventional UT

Detection results for conventional UT procedures (UT.108, UT.126, UT.134, and UT.25) can also be compared in Table 5.12 for SBDMWs. A disparity in performance is observed in the table. To gather insight, procedures UT.108, UT.126, UT.134, and UT.25 are summarized in Table 6.10. This table indicates that UT.25 employs automated data collection and encoding, while the other procedure types are all manual and not encoded. However, UT.25 employs a relatively low frequency (0.5 MHz) and only longitudinal waves at one angle, which may contribute to its relatively low performance. In addition, UT.25 was also the only non-qualified procedure participating in blind testing. However, UT.126 performance is also low despite the procedure being substantially similar to UT.108 and UT.134. The variability in performance observed for conventional UT procedures could also be caused by several factors including differences in the equipment used, human factors, etc.

Table 6.10 Summary of Procedures UT.108, UT.126, UT.134, and UT.25

	Frequency	Interrogation Modes/Angles for Circumferential Defects	Interrogation Modes/Angles for Axial Defects	Manual or Automated?	Encoded?
UT.108	1–5 MHz	L30°, L45°, L60° CW/CCW scan	L30°, L45°, L60° raster scan	Manual	No
UT.126	1–1.5 MHz base metal 1–2.25 MHz weld or butter material	S45° CW/CCW scan L30°, L45°, L60° CW/CCW scan	S45° raster scan L30°, L45°, L60° raster scan	Manual	No
UT.134	1–5 MHz	L30°, L45°, L60°, L70° CW/CCW scan	L30°, L45°, L60°, L70° skewed scan	Manual	No
UT.25 ^(a)	0.5 MHz	L45° relying on back-wall reflection	L45° relying on back-wall reflection	Automated	Yes

(a) UT.25 was not a qualified procedure.
UT = conventional UT

6.3 Quick-Blind Test Comparison

Blind test results are compared to Quick-blind test results by comparing sizing results for common procedures applied in both tests. In this case, UT.PAUT.113 depth sizing and length sizing results are summarized for blind testing and Quick-blind testing in Table 6.11. The most significant observation is the large negative bias observed for length sizing in Quick-blind testing in comparison to the large positive bias observed in blind testing, indicating that there was a tendency to significantly undersize flaws in Quick-blind test blocks. Table 6.11 indicates the difference in depth sizing error observed for blind testing versus Quick-blind testing is not large and that the length sizing error is essentially the same. Another comparison is made of the sizing performances of UT.ECT.106 applied in Quick-blind testing to UT.ECT.144 applied in blind testing in Table 6.12. These procedures are substantially similar. As in the case of UT.PAUT.113, the results do not indicate a large difference in depth sizing performance. The most significant observation is the large negative bias for length sizing in Quick-blind testing. Further, Table 6.12 indicates that the length sizing error is much larger for Quick-blind testing than blind testing.

Table 6.11 Comparison of Blind and Quick-blind Sizing Results for UT.PAUT.113

Depth Sizing		
	Bias, mm	RMSE, mm
Quick-blind	0.9	1.2
Blind	2.0	2.9
Length Sizing		
	Bias, mm	RMSE, mm
Quick-blind	-11.7	12.8
Blind	10.6	13.3

Table 6.12 Comparison of UT.ECT.144 (Blind) and UT.ECT.106 (Quick-blind) Sizing Results

Depth Sizing		
	Bias, mm	RMSE, mm
UT.ECT.106 (Quick-blind)	0.0	3.3
UT.ECT.144 (Blind)	0.7	2.2
Length Sizing		
	Bias, mm	RMSE, mm
UT.ECT.106 (Quick-blind)	-9.3	10.0
UT.ECT.144 (Blind)	2.9	4.2

UT = conventional UT

6.4 Influence of Tolerance Bounds on Detection Results

In Section 4.3, tolerance bounds are described that are used to determine if an indication should be classified as a hit or miss based on how close the indication is to a flaw. A 10 mm tolerance is applied to flaw true states as forgiveness for positioning error. The nature of a collaborative test, such as PARENT, requires a more rigid conformance to an agreed upon tolerance to ensure all participants are evaluated consistently. However, this also resulted in several genuine detections

being classified as misses by procedure UT.ECT.144 on test block P33. In this case, there were five indications located 10 mm to 20 mm from the flaw true states and four of these indications were located within 15 mm of the true state. These misses are highlighted in Figures 6.7 through 6.9 as “Probable Detections.”

A comparison of performance results obtained as a result of using a 10 mm tolerance versus a 15 mm tolerance for UT.ECT.144 is presented in Table 6.13 through Table 6.15. Table 6.13 is a comparison of detection and false call performance for a 10 mm tolerance versus a 15 mm tolerance and shows that the overall POD increases from 58% for a 10 mm tolerance to 79% for a 15 mm tolerance. Table 6.14 provides a comparison of depth sizing error obtained for both tolerance considerations and shows that the depth sizing RMSE for UT.ECT.144 is modestly impacted. Finally, Table 6.15 provides a comparison of length sizing errors and indicates a slight increase in length sizing RMSE as a consequence of increasing the tolerance from 10 mm to 15 mm.

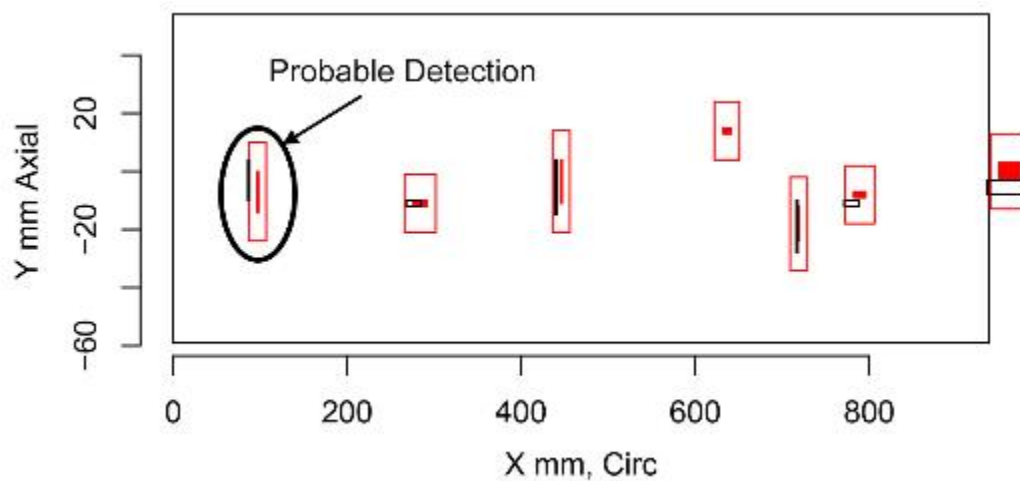


Figure 6.7 Indication Plot for UT.ECT.144 Applied to P33 from X = 0 mm to X = 1000 mm

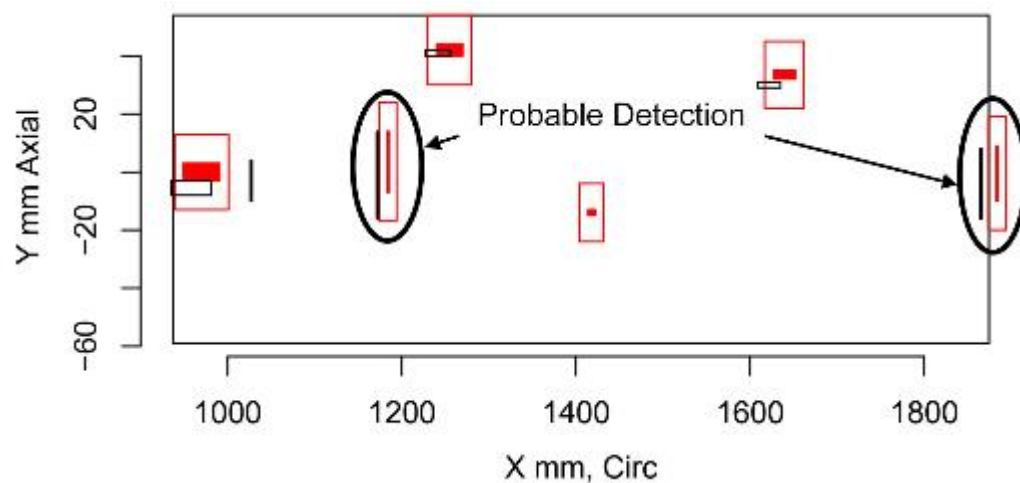


Figure 6.8 Indication Plot for UT.ECT.144 Applied to P33 from X = 1000 mm to X = 2000 mm

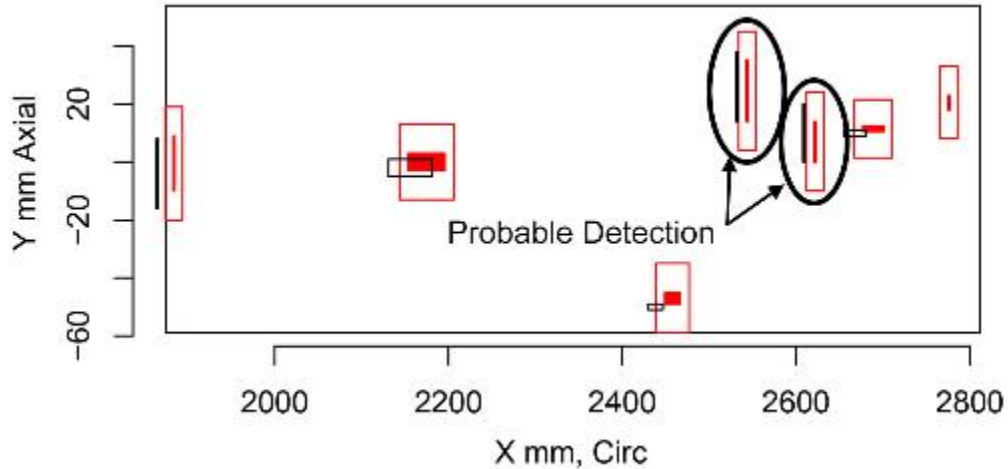


Figure 6.9 Indication Plot for UT.ECT.144 Applied to P33 from X = 2000 mm to X = 2800 mm

Table 6.13 Detection and False Call Comparison for 10 mm and 15 mm Tolerances Applied for Procedure UT.ECT.144

	NOBS	POD, %	FCP, %	FCR, #/m	Access	Test Blocks (LBDMWs)
10 mm tolerance	19	58	6	2.3	I.D.	P13, P33
15 mm tolerance	19	79	2	0.8	I.D.	P13, P33

Table 6.14 Depth Sizing Error Comparison for 10 mm and 15 mm Tolerances Applied for Procedure UT.ECT.144.

	NOBS	Bias, mm	RMSE, mm
10 mm tolerance	9	0.7	2.2
15 mm tolerance	13	0.4	2.1

Table 6.15 Length Sizing Error Comparison for 10 mm and 15 mm Tolerances Applied for Procedure UT.ECT.144

	NOBS	Bias, mm	RMSE, mm
10 mm tolerance	11	2.9	4.2
15 mm tolerance	15	3.3	4.6

6.5 ASME Procedure for Combining Flaws

The Data Analysis Task Group (DAG) used the ASME Section XI IWA-3400 rules for linear surface flaws to account for multiple flaws that are in close proximity.

Section XI, IWA-3400 of the ASME Code states the following:

(a) Linear flaws detected by surface (PT/MT) or volumetric (RT) examination methods shall be considered single linear surface flaws provided the separation distance between flaws is equal to or less than the dimension S, where S is determined as shown in Figure IWA-3400-1.

(b) The overall length of a single and discontinuous linear flaw shall be determined as shown in Figure IWA-3400-1.

Figure 6.10 is a reproduction of part of IWA-3400-1 to show the methodology used to determine whether multiple flaws should be combined as one flaw with length or whether the flaws should be considered as single individual flaws.

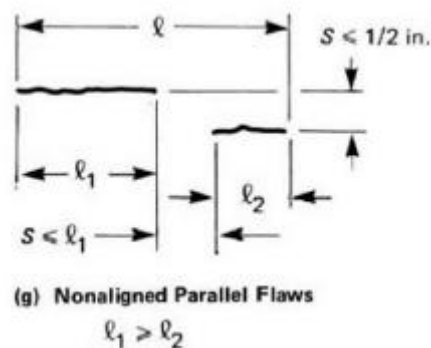


Figure 6.10 Methodology for Determining Singularity or Multiplicity of Linear Surface Flaws. Reprinted from ASME 2007 BPVC Section XI, Figure IWA-3400-1, by permission of The American Society of Mechanical Engineers. All rights reserved.

An example of the effect of the application of the ASME procedures for combining flaws is illustrated by the inspection of test block P33 by procedure ECT.135. Two indications (no. 10 and 11) are depicted in Figure 6.11 and have the X1, X2, Y1, and Y2 coordinates as indicated in Table 6.16. If these two indications were combined, they will have length of $2187.1 - 2142.4 = 44.7$ mm which is very close to the true length of a nearby flaw. However, according to the procedure for combining flaws indicated in Figure 6.10, these indications should not be combined because the distance, S, separating the flaws is greater than the longest flaw. In this case, $S = 20.6$ mm, and the longer of the two indications has a length of 18.6 mm. As a result, the two indications must be treated individually and the calculated length sizing error is greater than if the two indications were combined.

Table 6.16 X1, X2, Y1, and Y2 Coordinates for Indications No. 10 and 11 in Test Block P33 by Procedure ECT.135

Indication No.	X1, mm	X2, mm	Y1, mm	Y2, mm
10	2142.4	2161.0	-3.0	3.9

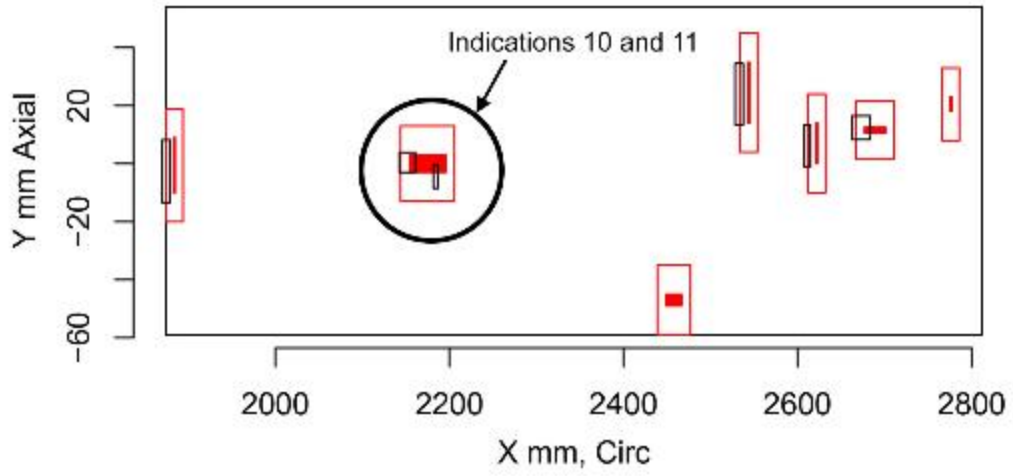


Figure 6.11 Indication Plot for ECT.135 Applied to P33 from X = 2000 mm to X = 2800 mm

7 COMPARISON OF PARENT VS. PINC

This section provides a comparison of results of conclusions from PARENT with the results and conclusions from PINC. A comparison of the performance results in PARENT and PINC on DMW and BMI test blocks is included in Sections 7.1 and 7.2, respectively. Conclusions and recommendations from PINC are reviewed in the context of the information provided by PARENT in Section 7.3.

7.1 Comparison of Performance on PARENT and PINC DMW Test Blocks

Table 7.1 compares PINC results to the current PARENT round robin for SBDMW test blocks. PINC DMW test blocks ranged in thickness from 41 to 47 mm (Cumblidge et al. 2010) while PARENT SBDMW test blocks are 35 and 39.5 mm thick (see Table 2.1). Thus, comparable procedure types between PINC and PARENT include PAUT, conventional UT, and UT.TOFD, which were all applied to SBDMWs in PARENT. PAUT and UT.TOFD procedures employed in PARENT appear to have performed better than similar procedures in PINC. In addition, ECT procedure performance from PINC can be compared to the performance of I.D. access procedures in Table 5.7. It can be seen that the performance of ECT procedures in PINC is much better than the performance of I.D. access procedures in PARENT, including the ECT procedure. Although I.D. access procedures are applied to LBDMW test blocks in PARENT, test block thickness should not have a significant influence on procedures for which detection is based on ECT applied to the I.D. The false call probability [FCP, POD(0)] was consistent between PINC and PARENT for all procedure types with the exception of UT.TOFD. In this case, FCP was defined in terms of a 100 mm long grading unit for PINC and in terms of a 25 mm long grading unit for PARENT. The values of POD(0) for PINC procedures are calculated by dividing the values for FCP in Table 4.9 of NUREG/CR-7019 (Cumblidge et al. 2010) by 4 to normalize the values with PARENT data. This calculation is performed based on the Taylor series expansion of Eq. (D.3), which produces a linear proportional relationship between FCP and the grading unit length.

Table 7.1 Comparison of PINC and PARENT Detection Results [POD (%)] versus Depth for DMW Test Blocks

	0 mm	5 mm	10 mm	15 mm	
PINC UT	6	36	51	67	Table 4.9 (NUREG/CR-7019)
PARENT UT	8	20	43	69	Table 5.9 (SBDMWs)
PINC PAUT	6	36	51	66	Table 4.9 (NUREG/CR-7019)
PARENT PAUT	6	39	87	99	Table 5.9 (SBDMWs)
PINC UT.TOFD	9	44	53	61	Table 4.9 (NUREG/CR-7019)
PARENT UT.TOFD	4	42	92	99	Table 5.9 (SBDMWs)
PINC ECT	4	88	100	100	Table 4.9 (NUREG/CR-7019)
PARENT ECT (LBDMW)	3	23	76	97	Table 5.7 (LBDMWs – I.D. Access)

UT = conventional UT

Sizing results on SBDMW test blocks are also compared for both PINC and PARENT (refer to Table 7.2). Overall depth sizing RMSE is improved for PARENT, although the spread between best and worst sizing performers is larger for PARENT than PINC. Length sizing also appears to have improved in PARENT relative to PINC (25 mm RMSE for PINC and 12.1 mm for PARENT) and the spread between best and worst length sizing performers is narrower for PARENT relative to PINC. However, two gross “outlier” measurements were not included in the length sizing analysis for PARENT and are listed in Table 5.31.

Table 7.2 Comparison on Sizing Performances (Depth and Length) for PINC and PARENT for DMW Test Blocks

	Depth Sizing (RMSE), mm			
	All	Best	Worst	
PINC	7.07	3.18	10.09	Table 4.20 (NUREG/CR-7019)
PARENT	5.5	1.8	13.9	Table 5.21 and Table 5.24
	Length Sizing (RMSE)			
	All	Best	Worst	
PINC	25	3.56	91	Table 4.20 (NUREG/CR-7019)
PARENT	12.1	8.0	22.6	Table 5.27 and Table 5.30 ^(a)
(a) For PARENT evaluation, two “outlier” measurements were excluded from length sizing (see Table 5.31).				

Overall depth sizing RMSE for I.D. access to LBDMWs (see Table 5.19) is 3.0 mm (3.6 mm for Blind + Quick-blind). Thus, it would appear that the depth sizing results for I.D. access of LBDMWs (excluding the Quick-blind data) meet the intent of the ASME Code requirement (less than 3.2 mm). All of the procedures that produced depth sizing results that meet the intent of the ASME Code requirement are listed in Table 7.3. In PARENT, the flaw depth size distribution in test blocks tended to be shallower than ASME Code, Section XI requirements for flaw size distribution and it was not the intent of the test blocks to meet this flaw size distribution requirement. This is significant for I.D. procedures for which depth sizing becomes more challenging with increasing crack depth. Thus, the results obtained for depth sizing by I.D. procedures could be optimistic. In all, there are four procedures with two procedures associated with I.D. access inspections of LBDMWs and two procedures associated with SBDMW inspections. None of the procedures applied to O.D. inspections of LBDMWs produced sizing results that would meet the intent of the ASME Code requirements. In PINC, no procedures exhibited depth sizing accuracy that would meet the intent of the ASME Code requirement, so PARENT results do represent improvement in depth sizing performance compared to PINC based on SBDMW data. However, the flaws used in PARENT and PINC were not necessarily selected to meet the sizing requirements in ASME Code, Section XI, Division 1, Appendix VIII, so having a small RMSE value is insightful but does not necessarily reflect that desired performance has been met.

Table 7.3 Summary of PARENT Procedures that Produced Depth Sizing RMSEs of Less Than the ASME Code Requirement for Depth Sizing Accuracy (3.2 mm)

Procedure	Block Type	Access	NOB	Bias, mm	RMSE, mm
UT.ECT.144	LBDMW	I.D.	9	0.7	2.2
UT.PAUT.113	LBDMW	I.D.	15	2.0	2.9
UT.PAUT.113 (Blind + Quick-blind)	LBDMW	I.D.	18	1.8	2.7
PAUT.108.1	SBDMW	O.D.	21	-1.7	2.4
PAUT.115	SBDMW	O.D.	25	-0.3	1.8

UT = conventional UT

A review of Tables 5.28 to 5.30 indicates that only two O.D. access procedures (UT.126 and UT.134) produced length sizing results that would not satisfy the intent of the ASME Code length sizing requirement of 19 mm.

7.2 Comparison of Performance on PARENT and PINC BMI Test Blocks

Comparisons of PINC and PARENT BMI results for J-groove weld surface examinations are included in Table 7.4, and by Figure 7.3, and for tube I.D. examinations in Figures 7.1 and 7.2. The comparisons illustrate that PARENT inspections performed from the J-groove weld surface and from the BMI tube I.D. have higher FCPs in comparison to the FCPs observed in PINC for these access conditions. The ECT procedures used for J-groove weld surface examinations are ECT.124 and ECT.108. ECT.124 utilizes a single sensor excited at 100 kHz. ECT.108 includes an array probe operated at 500 kHz. Similar to PINC, the limited amount of data acquired on BMIs limits the ability to draw many definitive conclusions. However, the FCPs [POD(0)] of PARENT ECT procedures in Table 7.4 are high relative to the ECT procedures used in PINC. This can be analyzed by focusing on the subset of flaws for P26. This flaw subset is provided in Table 7.6 for convenience. In addition, indication plots for procedures ECT.124, ECT.108, and TOFD.ECT.126 applied to P26 are provided in Figures 7.4 through 7.7. These plots indicate that flaw P26.6 is a large flaw exhibiting low POD, which would have an effect raising the curve for low defect sizes and increasing FCP. From Figures 7.4 through 7.6, it is apparent that P26.6 has a small dimension in the theta direction, which may contribute to difficulty in detection by a I.D. tube examination performed by TOFD.ECT.126. Further, a review of Figures 7.4 and 7.5 indicates that flaw P26.6 was actually detected by both ECT.124 and ECT.108, but only one procedure (ECT.124) was given credit for the detection because the indication recorded for ECT.108 is just outside of the scoring tolerance.

A comparison of length sizing performance for J-groove weld surface examinations in PINC and PARENT is provided in Table 7.5. It appears that the average length sizing performances between PINC and PARENT are similar although a smaller spread between the best and worst performances are observed in PARENT in comparison to PINC. However, the “worst” RMSE from PINC (Table 4.27 of NUREG/CR-7019) appears to be a significant outlier as the second “worst” RMSE is reported as 5.46 mm. If this outlier is removed, then the average RMSE is 4.1 mm,

which represents significantly better length sizing performance for PINC in comparison to PARENT.

Table 7.4 Comparison of PINC and PARENT Detection Results [POD (%)] versus Length on BMI Test Blocks for J-groove Weld Surface Examinations

	PINC				
	0 mm	5 mm	10 mm	15 mm	
ECT 300 kHz	0.03	0.31	0.83	0.98	From Table 4.18 on pg. 4.26 of NUREG/CR- 7019
ECT 400 kHz	0.01	0.80	1.00	1.00	
Array ECT 100 kHz	0.34	0.44	0.55	0.65	
Array ECT 200 kHz	0.21	0.37	0.58	0.76	
	PARENT				
	0 mm	5 mm	10 mm	15 mm	
ECT	0.41	0.57	0.73	0.84	From Table 5.35

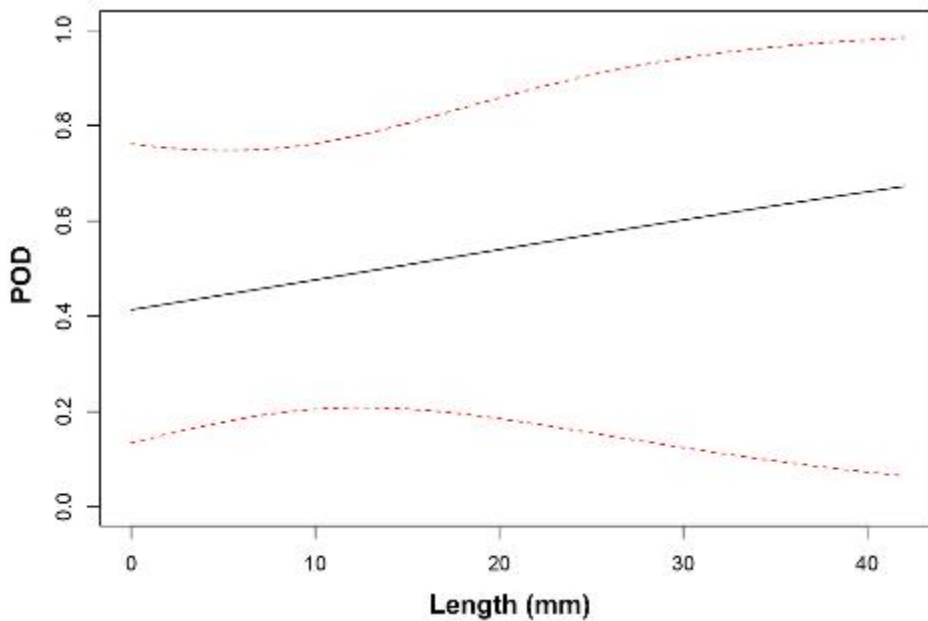


Figure 7.1 POD Regression with 95% Confidence Bounds for TOFD.ECT.126 Procedure Applied to BMI Tube I.D. Examinations in Test Blocks P25 and P26

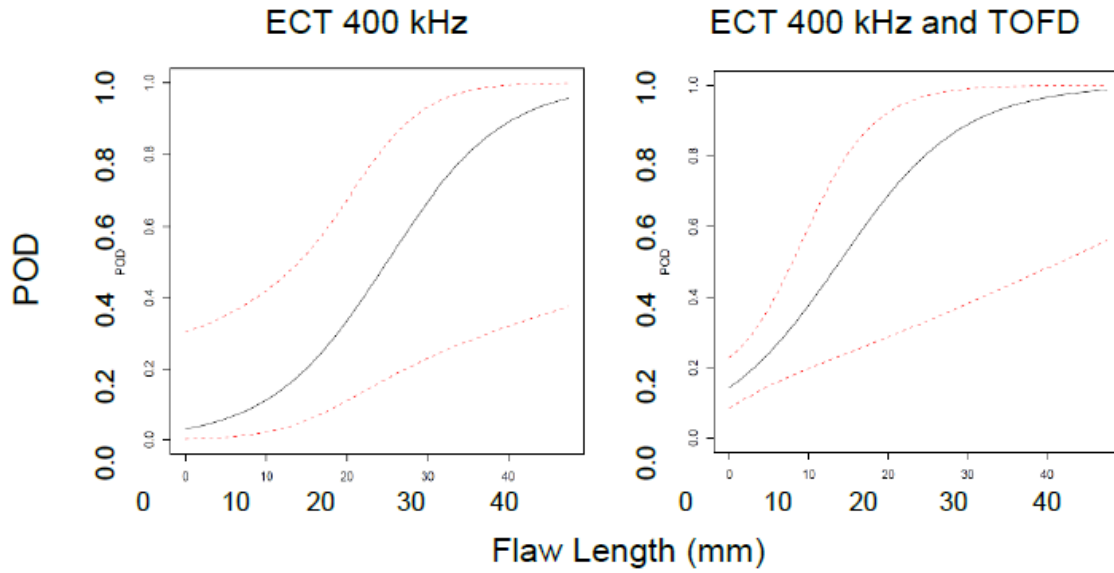


Figure 7.2 POD Regressions for BMI Tube I.D. Examinations in PINC (Figure 4.12 from NUREG/CR-7019)

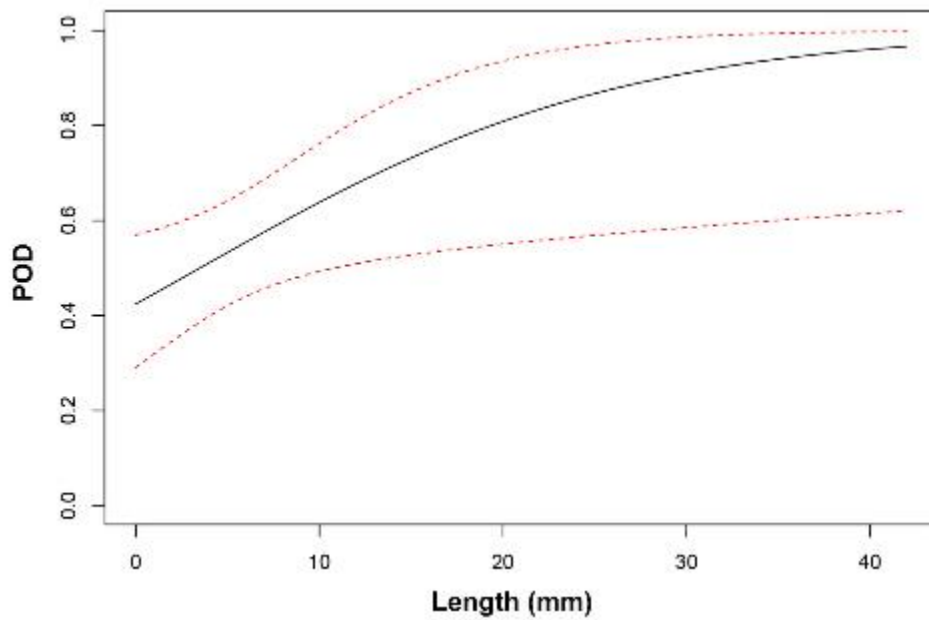


Figure 7.3 POD Regression with 95% Confidence Bounds for ECT.124 and ECT.108 Procedures Applied to BMI J-groove Weld Examinations in Test Blocks P6, P8, P9, and P26

Table 7.5 Comparison of PINC and PARENT Length Sizing Results on BMI Test Blocks

	All	Best	Worst	
PINC	11.7 mm	2.45 mm	32.28 mm	From Table 4.27 of NUREG/CR-7019
PINC [RMSE=32.28 mm Outlier removed]	4.1 mm	2.45 mm	5.46 mm	From Table 4.27 of NUREG/CR-7019
PARENT	12.7 mm	8.1 mm	15.6 mm	From Table 5.37

Table 7.6 Subset of Flaws for Test Block P26

	Flaw Type	NOBS	POD, %
P26.2	Weld Defect	1	100
P26.3	Weld Defect	3	67
P26.5	Weld Defect	3	33
P26.6	Weld Defect	3	33

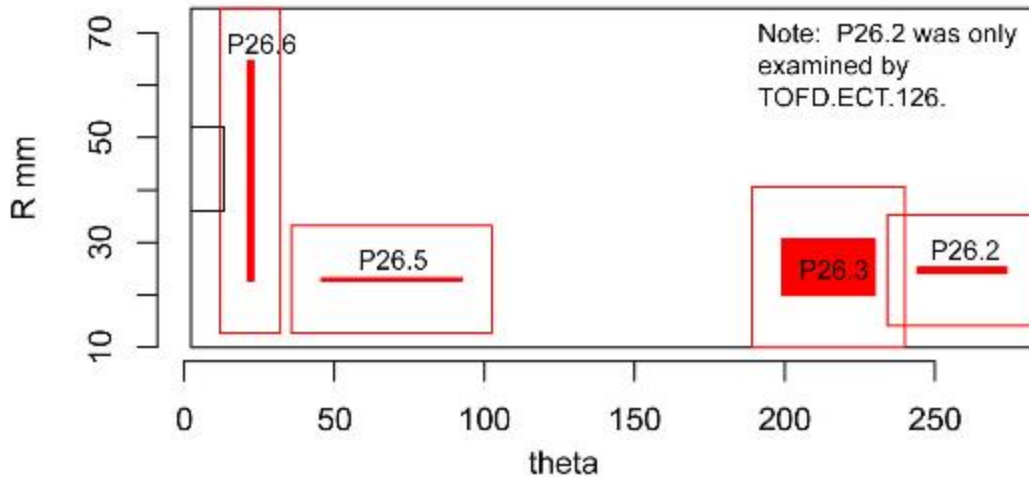


Figure 7.4 Indication Plot for Procedure ECT.124 Applied to P26 [theta – R view]

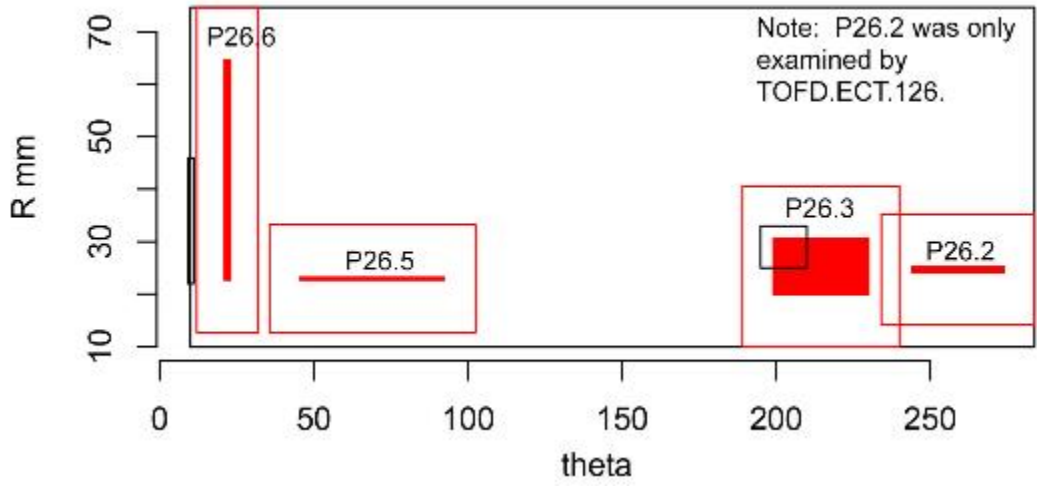


Figure 7.5 Indication Plot for Procedure ECT.108 Applied to P26 [theta - R view]

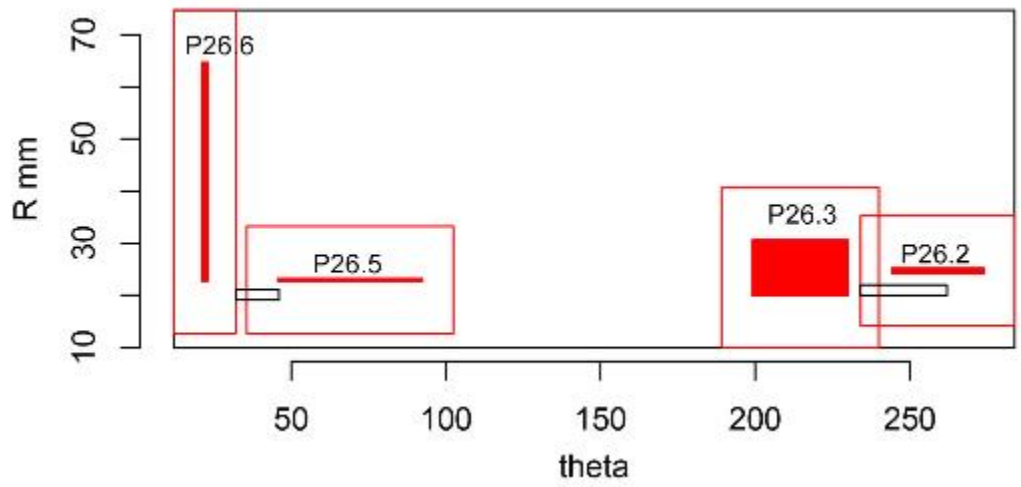


Figure 7.6 Indication Plot for Procedure TOFD.ECT.126 Applied to P26 [theta - R view]

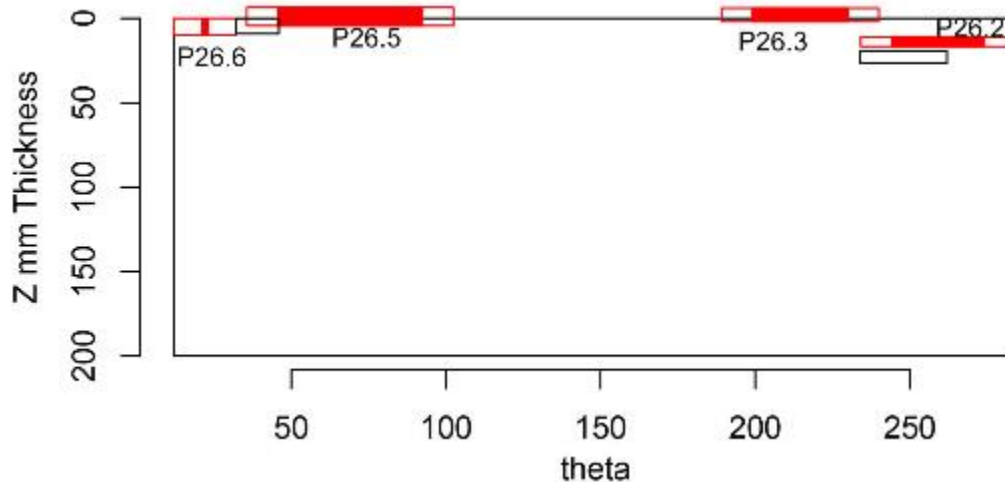


Figure 7.7 Indication Plot for Procedure TOFD.ECT.126 Applied to P26 [theta – Z view]

7.3 Review of PINC Conclusions and Recommendations

Several conclusions and recommendations are documented in the PINC report (Cumblidge et al. 2010) based on the results of testing in PINC. It is appropriate to review those conclusions and recommendations in light of additional testing results provided by PARENT.

7.3.1 **Probability of Detection Performance**

PINC Conclusion 1: Eddy current inspection from the cracked surface demonstrated the highest POD for all flaws in the DMW round robin.

PARENT Observation 1: I.D. procedures exhibit higher POD than O.D. procedures for LBDMW inspections in PARENT.

- **PINC Recommendation 1:** The results of this study show that eddy current inspection is the preferred detection technique for DMWs, where conditions allow access to the same surface from which the crack originates and where the surface conditions allow for ECT testing.
- **PARENT Informed Response 1:** The results of this study indicate that I.D. procedures are preferred for detection technique for LBDMWs when access and conditions allow.

7.3.2 **Sizing Performance**

PINC Conclusion 6: Eight teams length-sized flaws with an RMSE within the ASME Section XI standard of 0.75 inch (19 mm). Teams that used phased-array UT and eddy current achieved higher accuracy than teams that used conventional UT and potential-drop techniques.

PARENT Observation 6: All but two of the procedures employed in PARENT length-sized flaws in DMWs with an RMSE within the ASME Section XI standard of 0.75 inch (19 mm). Overall, procedures tended to oversize the length of flaws. Four of the top five best length sizing performances included procedures incorporating ECT. Four of the top five best length sizing performances included hybrid procedures incorporating multiple techniques.

- **PINC Recommendation 6:** *Phased-array UT or a combination of eddy current techniques and conventional UT are the preferred method for length sizing.*
- **PARENT Informed Response 6:** PARENT data suggests that hybrid procedures combining ECT with conventional UT, PAUT, and/or TOFD are preferred for length sizing from the I.D.

8 SUMMARY OF PISC III AND PINC OUTCOMES

This section provides a summary of PISC III (Program for the Inspection of Steel Components) and PINC round-robin testing outcomes based on a review of these studies prepared by some of the participants, which is included in Appendix H. In Section 9, the conclusions of PARENT blind testing are presented. The conclusions of PARENT blind testing along with the review in Appendix H and this summary can be used to provide guidance to future efforts.

8.1 PISC III

The PISC Program had the general objective of assessing procedures and techniques in use for the inspection of nuclear power plant pressurized components. The third phase of PISC III was conducted from 1986 into the early 1990s and consisted of eight actions and Action No. 3 was dealing with the evaluation of the effectiveness and reliability of NDE procedures on, at that time, realistic defects in dissimilar metal weldments. The study evaluated detection and sizing performance and largely focused on what would be considered conventional UT techniques, although some X-ray techniques were also evaluated.

The results of PISC III established the limited reliability of NDE as it was performed at that time as evidenced by high FCRs. In addition, the results demonstrated significant variability in performance. The study highlighted that there were many potential sources to this variability, including parameters associated with techniques and procedures and the surface that is accessed for inspection. Some of the parameters associated with techniques and procedures included whether the technique was manual or automated and the threshold level for rejecting noise. In addition, PISC III results showed that results obtained with longitudinal wave techniques were better than results obtained with shear wave techniques. Finally, procedures that employed multiple techniques for sizing tended to perform better than procedures that relied on only one technique for sizing.

8.2 PINC

The PINC program was executed between 2005 and 2008 with the objectives to address the problem of PWSCC/IDSCC in pressurized nuclear reactor components (Cumblidge et al. 2010). The research was designed to understand the morphology of PWSCC/IDSCC and to assess NDE techniques for detection, characterization, and sizing cracks with such morphology. PINC was focused on two areas—BMI penetration and DMWs. In PINC, a more diverse set of procedure types was evaluated in comparison to PISC III. PINC evaluated ECT, conventional UT, and advanced ultrasonic techniques such as PAUT, as well as less established procedure types such as potential drop.

The results of PINC indicated that ECT performed from surface of crack initiation exhibited the best detection performance and that none of the procedures exhibited depth sizing performance that would meet ASME Code requirements, although a couple of procedures were close. The results of PINC also showed that circumferential flaws were easier to detect than axial flaws and that PAUT performance did not appear better than conventional UT performance for detection. Finally, variability of performance within procedure types was observed in PINC, and the qualification of teams and procedures was observed to have an influence on performance.

9 CONCLUSIONS

This section includes a summary of several conclusions that may be obtained from PARENT blind testing results and recommendations for future work. All of the data collected on SBDMW and LBDMW test blocks was based on manufactured cracks that were introduced to simulate PWSCC/IDSCC. Future work recommendations are based on the conclusions presented here and the summary of PISC III and PINC outcomes in Section 8. Conclusions that can be obtained from PARENT blind testing results are:

- **PARENT Conclusion 1:** I.D. procedures exhibited superior performance over O.D. procedures for LBDMWs as measured by POD and length sizing RMSE based on data in Tables 6.1 and 6.3, respectively.
- **PARENT Conclusion 2:** O.D. inspections performed on SBDMW test blocks exhibit better performance than O.D. inspections performed on LBDMW test blocks based on POD and depth sizing RMSE, according to data in Tables 6.1 and 6.2, respectively. Further, length sizing RMSE of axial flaws is also better for SBDMW test blocks in comparison to O.D. access of LBDMW test blocks based on Table 6.3.
- **PARENT Conclusion 3:** Flaw orientation exhibits an influence on detection performance with circumferential flaws exhibiting a greater likelihood of detection than axial flaws, as a function of depth, based on data in Table 6.1 for LBDMW and SBDMW test blocks.
- **PARENT Conclusion 4:** Flaw orientation did not show an influence on depth sizing performance based on depth sizing RMSE results in Table 6.2 and regression plots in Figures 6.1 through 6.6 for LBDMW and SBDMW test blocks.
- **PARENT Conclusion 5:** I.D. procedures that include ECT performed better at length sizing than I.D. procedures that do not include ECT, particularly for axial flaws, as indicated by RMSE values in Table 6.8 for LBDMW test blocks.
- **PARENT Conclusion 6:** O.D. PAUT procedures exhibit better performance than O.D. conventional UT procedures for SBDMWs as measured by POD and depth sizing RMSE based on data in Tables 6.4 and 6.6, respectively.
- **PARENT Conclusion 7:** O.D. PAUT performance is similar to O.D. conventional UT performance for LBDMWs as measured by POD and depth sizing RMSE based on data in Tables 6.5 and 6.7, respectively.
- **PARENT Conclusion 8:** PARENT results indicate substantial improvement in O.D. PAUT performance for SBDMWs, compared with PINC performance data, based on data in Table 7.1.
- **PARENT Conclusion 9:** PARENT results indicate significant variability in performance for UT procedures employing similar techniques and for PAUT procedures employing similar techniques on SBDMWs by O.D. access. This is based on detection performance data versus depth and depth sizing data in Tables 5.12 and 5.24, respectively, and tabulation of procedure information in Tables 6.9 and 6.10.

- **PARENT Conclusion 10:** One of the conventional UT procedures exhibiting the poorest performance for O.D. examinations of SBDMWs employed only one angle for inspection. This conventional UT procedure was also the only non-qualified procedure that participated in blind testing. All other conventional UT procedures incorporated multiple angles for inspection. This is based on detection performance data versus depth and depth sizing data in Tables 5.12 and 5.24, respectively, and tabulation of procedure information in Table 6.10.
- **PARENT Conclusion 11:** One of five procedures applied for length sizing on LBDMW test blocks by O.D. surface access in the Blind test exhibited length sizing performance that did **not** meet the intent of ASME Code, Section XI requirement of RMSE within 19 mm based on data in Table 5.29.
- **PARENT Conclusion 12:** One of nine procedures applied for length sizing on SBDMW test blocks by O.D. surface access in the Blind test exhibited length sizing performance that did **not** meet the intent of ASME Code, Section XI requirement of RMSE within 19 mm based on data in Table 5.30.
- **PARENT Conclusion 13:** Two of three procedures applied for depth sizing on LBDMW test blocks by I.D. surface access in the Blind test exhibited depth sizing performance that met the intent of the ASME Code Section XI requirement of RSME within 3.2 mm and these are included in the summary in Table 7.3. However, the flaw depth size distribution in these test blocks tended to be shallower than ASME Code, Section XI requirements for flaw size distribution and it was not the intent of the PARENT test blocks to meet ASME Code flaw size distribution requirements.
- **PARENT Conclusion 14:** Two of nine procedures applied for depth sizing on SBDMW test blocks by O.D. surface access in the Blind test exhibited depth sizing performance that met the intent of the ASME Code, Section XI requirement of RSME within 3.2 mm and these are included in the summary in Table 7.3. However, the flaw depth size distribution in these test blocks tended to be shallower than ASME Code, Section XI requirements for flaw size distribution and it was not the intent of the PARENT test blocks to meet ASME Code flaw size distribution requirements.
- **PARENT Conclusion 15:** ECT performance results are better for PINC than PARENT based on POD information in Table 7.1.
- **PARENT Conclusion 16:** In general, it was felt that insufficient data was collected on BMI test blocks to draw firm conclusions regarding detection and length sizing performance. No data was provided to assess depth sizing performance for flaws in J-groove welds. In addition, many of the flaws implanted in BMI test blocks were considered to have limited relevance to flaws expected in the field.

As previously mentioned, recommendations for future work are presented here based on the conclusions from PARENT blind testing outlined above and the summary of PISC III and PINC outcomes in Section 8. Thus, an outline of recommendations for future work is provided below:

- **Recommendation 1:** Limited data was collected on BMI test blocks in PINC and PARENT so future work could focus on collecting new BMI data for performance quantification and consider combining PINC and PARENT BMI data for analysis.

- **Recommendation 2:** ECT performance in PARENT is lower than reported for PINC. However, the ECT procedures in PARENT were applied to LBDMWS; in PINC, they were applied to SBDMWs. Therefore, further evaluation using laboratory parametric studies of ECT procedures applied to SBDMW and LBDMW test blocks to assess and understand the results in PINC and PARENT is recommended.
- **Recommendation 3:** PARENT conclusion 9 states that significant variability is observed for some conventional UT and PAUT procedures that employ similar techniques. Additional study could help determine and quantify the relative influence of equipment, human factors, etc. on performance for procedures employing similar techniques.
- **Recommendation 4:** Further work is needed to understand and quantify the influence of specific PAUT and conventional UT procedure variables, such as number of inspection angles and sectorial versus linear scanning, on detection and sizing performance.
- **Recommendation 5:** The flaw simulations used in PARENT approximate PWSCC and IDSCC degradation processes but are not actual field PWSCC or field IDSCC flaws. The limitations of SCC flaw simulation techniques with respect to their relevance to representing field PWSCC and IDSCC flaw NDE responses should be further evaluated. In addition, improving the relevance of simulated flaws to field PWSCC and IDSCC flaws, based on such an evaluation, should also be investigated.

10 REFERENCES

Braatz BG, PG Heasler and RM Meyer. 2014. *PARENT Quick Blind Round-Robin Test Report*. PNNL-22677, Pacific Northwest National Laboratory, Richland, Washington. ADAMS Accession No. ML14276A052.

Cumblidge SE, SR Doctor, PG Heasler and TT Taylor. 2010. *Results of the Program for the Inspection of Nickel Alloy Components*. NUREG/CR-7019; PNNL-18713, Rev. 1, U.S. Nuclear Regulatory Commission, Washington, D.C.

APPENDIX A
TEST BLOCK INFORMATION

APPENDIX A
TEST BLOCK INFORMATION

A.1 BMI Test Blocks



Figure A.1 BMI Test Block P6



Figure A.2 BMI Test Block P8



Figure A.3 BMI Test Block P9



Figure A.4 BMI Test Block P25



Figure A.5 BMI Test Block P26

A.2 SBDMW Test Blocks



Figure A.6 SBDMW Test Block P35



Figure A.7 SBDMW Test Block P40

A.3 LBDMW Test Blocks

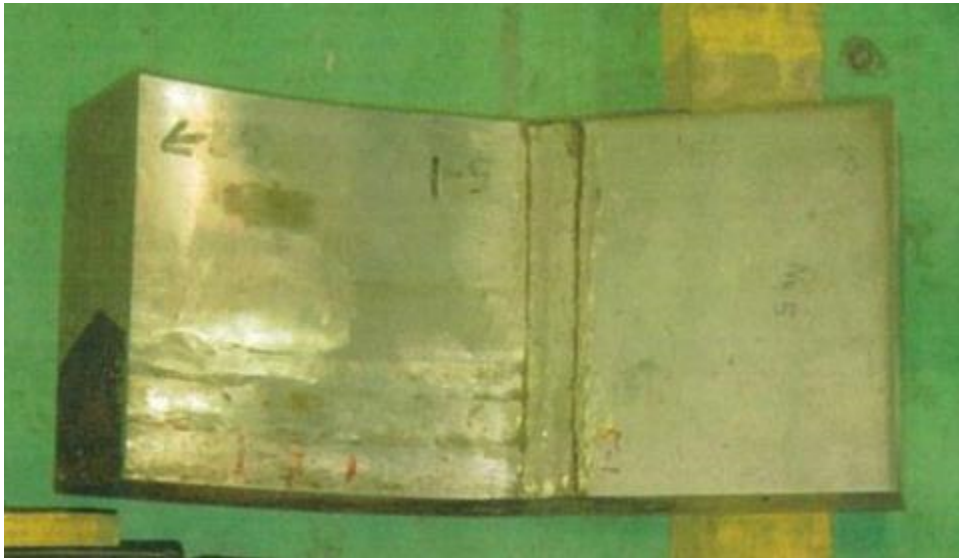


Figure A.8 LBDMW Test Block P13



Figure A.9 LBDMW Test Block P15



Figure A.10 LBDMW Test Block P16



Figure A.11 LBDMW Test Block P17



Figure A.12 LBDMW Test Block P33



Figure A.13 LBDMW Test Block P45

A.4 WOL Test Block



Figure A.14 WOL Test Block P27

APPENDIX B

SUMMARY OF BLIND TESTING PROCEDURES/TECHNIQUES

APPENDIX B

SUMMARY OF BLIND TESTING PROCEDURES/TECHNIQUES

B.1 Summary of Techniques Applied to Quick-blind Test Blocks

Team#	NDE Technique Description	Form Procedure ID	Procedure ID Used in Formal Documentation	Technique ID	Manual or Automated	Encoded (Y/N)	Exam Surface	Probe Frequency (MHz)/Inspection Angle (Deg.)/ Skew (Deg.)	Technique Comment
106	Mechanized UT pulse-echo	106.1	UT.ECT.106	106-UT0	Automated	Y	I.D.	2 MHz	Detection, Length, Depth
106	Mechanized ECT	106.1	UT.ECT.106	106-ECT0	Automated	Y	I.D.	200 kHz	Detection, Characterization, Length
108	Conventional ultrasonic	108.1	UT.PAUT.108	108-UT0	Manual	N	O.D.	1.0 MHz/L45° 1.0 MHz/L60° 1.5 MHz/L35° 1.5 MHz/L45° 2.0 MHz/L33° 2.0 MHz/L45	Detection, Characterization, Length, Depth, Positioning
108	Phased array UT (sectorial)	108.1	UT.PAUT.108	108-PA0	Manual	N	O.D.	2.0 MHz/L0°~L85°	Detection, Characterization, Length, Depth, Positioning
134	Conventional ultrasonic	134.1	UT.134.1	134-UT0	Manual	N	O.D.	1.5 MHz/L35° 1.5 MHz/L45° 2.0 MHz/L33°	Detection, Characterization, Length, Depth, Positioning
126	Conventional ultrasonic	126.1	UT.PAUT.126	126-UT0	Manual	N	O.D.	2.0 MHz/L45° 2.0 MHz/L60°	Detection, Characterization, Length, Depth, Positioning

Team#	NDE Technique Description	Form Procedure ID	Procedure ID Used in Formal Documentation	Technique ID	Manual or Automated	Encoded (Y/N)	Exam Surface	Probe Frequency (MHz)/Inspection Angle (Deg.)/ Skew (Deg.)	Technique Comment
126	Phased array UT (linear)	126.1	UT.PAUT.126	126-PA0	Manual	Y	O.D.	1.5 MHz/L25° 1.5 MHz/L35° 1.5 MHz/L45° 1.5 MHz/L55°	Detection, Characterization, Length, Depth, Positioning
113	Ultrasonic, TRL	113.1	UT.PAUT.113	113-UT2	Automated	Y	I.D.	3 MHz/ LAD70°(Transmitter)– 50°(Receiver) Longitudinal	Characterization, Detection, Positioning
113	Phased array ultrasonic, matrix	113.1	UT.PAUT.113	113-PA1	Automated	Y	I.D.	2 MHz/45°, 55° Longitudinal	Characterization, Detection, Positioning, Length Sizing, Depth Sizing
113	Phased array ultrasonic, TRL	113.1	UT.PAUT.113	113-PA2	Automated	Y	I.D.	5 MHz/TRL35°–55° 5° increments Longitudinal	Characterization, Detection, Positioning, Length Sizing, Depth Sizing
132	Linear phased array ultrasonic	132.1	PAUT.132	132.PA0			I.D.	1.5 MHz/L60°–L82°; L40°–L46°; L30°– L70° azimuthal scans	Detection, Characterization, Length, Depth, Positioning

B.2 Summary of Techniques Applied to SBDMW Test Blocks

Team#	NDE Technique Description	Form Procedure ID	Procedure ID Used in Formal Documentation	Technique ID	Manual or Automated	Encoded (Y/N)	Exam Surface	Probe Frequency (MHz)/Inspection Angle (Deg.)/ Skew (Deg.)	Technique Comment
25	Mechanized UT through transmission pitch-catch	25.1	UT.25	25-UT-P/C0	Automated	Y	O.D.	0.5 MHz (1.5 in. aperture)/L45°	Detection, Characterization, Length, Depth, Positioning

Team#	NDE Technique Description	Form Procedure ID	Procedure ID Used in Formal Documentation	Technique ID	Manual or Automated	Encoded (Y/N)	Exam Surface	Probe Frequency (MHz)/Inspection Angle (Deg.)/Skew (Deg.)	Technique Comment
115	Manual linear TR UT-PA	115.1	PAUT.115	115-PA1	Manual	N	O.D.	2.0 MHz/2x16 elements	Detection, Characterization, Length, Depth, Positioning
128	Encoded TR UT-PA linear (circ. flaws), sectorial (axial flaws)	128.1	PAUT.128	128-PA1	Automated	Y	O.D.	Circ. flaws 1.5 MHz / L45°, L60°, L70°, S45°, S60° Axial flaws 1.5 MHz / L25°, L35°, L45°, L55°, S35°, S45°, S55°, skew -25° to +25°, step 2.5°	Detection, Characterization, Length (circ. flaws), Depth, Positioning
117	Mechanized UT pulse-echo and TOFD	117.1	UT.TOFD.117	117-UT0	Automated	Y	O.D.	1-2 MHz	Detection, Characterization, Length, Positioning
117	Mechanized UT TOFD	117.1	UT.TOFD.117	117-TOFD0	Automated	Y	O.D.	3 MHz	Depth
108	Conventional ultrasonic	108.2	UT.108	108-UT1	Manual	N	O.D.	1.5 MHz/L30° L45°, L60° 2.0 MHz/L30°, L45°, L60°	Detection, Characterization, Length, Depth, Positioning
108	Phased array UT (sectorial)	108.3	PAUT.108.1	108-PA1	Manual	N	O.D.	2.0 MHz/ L0°~L85°	Detection, Characterization, Length, Depth, Positioning
134	Conventional ultrasonic	134.2	UT.134.2	134-UT1	Manual	N	O.D.	1~5MHz L35°, L45°, L60°, L70° CW/CCW scan for circ. flaws Raster scan for axial flaws	Detection, Characterization, Length, Depth, Positioning

Team#	NDE Technique Description	Form Procedure ID	Procedure ID Used in Formal Documentation	Technique ID	Manual or Automated	Encoded (Y/N)	Exam Surface	Probe Frequency (MHz)/Inspection Angle (Deg.)/ Skew (Deg.)	Technique Comment
126	Conventional ultrasonic	126.3	UT.126	126-UT1	Manual	N	O.D.	1~1.5 MHz/S45° base metal 1~2.25 MHz/ L30°, L45°, L60° weld or butter material CW/CCW scan for circ. flaws Raster scan for axial flaws	Detection, Characterization, Length, Depth, Positioning
126	Phased array UT (linear)	126.2	PAUT.126.1	126-PA1	Manual	Y	O.D.	Circ. Scan 1.5 MHz/L22.5° 1.5 MHz/L25° 1.5 MHz/L35° 1.5 MHz/L37.5° 1.5 MHz/L45° 1.5 MHz/L55° Axial Scan 1.5 MHz/L45° 1.5 MHz/L60° 1.5 MHz/L70°	Detection, Characterization, Length, Depth, Positioning

B.3 Summary of Techniques Applied to LBDMW Test Blocks

Team#	NDE Technique Description	Form Procedure ID	Procedure ID Used in Formal Documentation	Technique ID	Manual or Automated	Encoded (Y/N)	Exam Surface	Probe Frequency (MHz)/ Inspection Angle (Deg.)/Skew (Deg.)	Technique Comment
101	Mechanized ECT	101.1	UT.TOFD.ECT.101	101-ECT1	Automated	Y	I.D.	300 kHz	Detection, Length
101	Mechanized UT pulse-echo and TOFD	101.1	UT.TOFD.ECT.101	101-UT0	Automated	Y	I.D.	2 MHz	Detection, Characterization, Length, Depth, Positioning
144	Mechanized UT pulse-echo	144.1	UT.ECT.144	144-UT0	Automated	Y	I.D.	2 MHz	Detection, Length, Depth
144	Mechanized ECT	144.1	UT.ECT.144	144-ECT0	Automated	Y	I.D.	200 kHz	Detection, Characterization, Length
108	Conventional ultrasonic	108.2	UT.108	108-UT1	Manual	N	O.D.	1.5 MHz/L30° L45°, L60° 2.0 MHz/L30°, L45°, L60°	Detection, Characterization, Length, Depth, Positioning
108	Phased array UT (sectorial)	108.3	PAUT.108.1	108-PA1	Manual	N	O.D.	2.0 MHz/L0°~L85°	Detection, Characterization, Length, Depth, Positioning
134	Conventional ultrasonic	134.2	UT.134.2	134-UT1	Manual	N	O.D.	1~5MHz L35°, L45°, L60°, L70° CW/CCW scan for circ. flaws Raster scan for axial flaws	Detection, Characterization, Length, Depth, Positioning

Team#	NDE Technique Description	Form Procedure ID	Procedure ID Used in Formal Documentation	Technique ID	Manual or Automated	Encoded (Y/N)	Exam Surface	Probe Frequency (MHz)/ Inspection Angle (Deg.)/Skew (Deg.)	Technique Comment
126	Conventional ultrasonic	126.3	UT.126	126-UT1	Manual	N	O.D.	1~1.5 MHz/S45° base metal 1~2.25 MHz/L30°, L45°, L60° weld or butter material CW/CCW scan for circ. flaws Raster scan for axial flaws	Detection, Characterization, Length, Depth, Positioning
126	Phased array UT (linear)	126.2	PAUT.126.1	126-PA1	Manual	Y	O.D.	Circ. Scan 1.5 MHz/L22.5° 1.5 MHz/L25° 1.5 MHz/L35° 1.5 MHz/L37.5° 1.5 MHz/L45° 1.5 MHz/L55° Axial Scan 1.5 MHz/L45° 1.5 MHz/L60° 1.5 MHz/L70°	Detection, Characterization, Length, Depth, Positioning
113	Ultrasonic, TRL	113.1	UT.PAUT.113	113-UT1	Automated	Y	I.D.	2.25 MHz/ LAD70° (Transmitter)– 50° (Receiver) Longitudinal	Detection, Positioning, Characterization
113	Ultrasonic, TRL	113.1	UT.PAUT.113	113-UT2	Automated	Y	I.D.	3 MHz/ LAD70° (Transmitter)– 50° (Receiver) Longitudinal	Detection, Positioning, Characterization, Length Sizing, Depth Sizing
113	Phased array ultrasonic, matrix	113.1	UT.PAUT.113	113-PA1	Automated	Y	I.D.	2 MHz/45°, 55° Longitudinal	Detection, Positioning, Characterization, Length Sizing, Depth Sizing

Team#	NDE Technique Description	Form Procedure ID	Procedure ID Used in Formal Documentation	Technique ID	Manual or Automated	Encoded (Y/N)	Exam Surface	Probe Frequency (MHz)/ Inspection Angle (Deg.)/Skew (Deg.)	Technique Comment
113	Phased array ultrasonic, TRL	113.1	UT.PAUT.113	113-PA2	Automated	Y	I.D.	5 MHz/TRL35° -55° 5° increments Longitudinal	Detection, Positioning, Characterization, Length Sizing, Depth Sizing
135	Cross-coil ECT	135.1	ECT.135	135-ECT1	Manual	Y	I.D.	50 kHz-1 MHz/ 3 mm-8x2 ch 400 kHz dominant	Detection, Characterization, Length, Positioning

B.4 Summary of Techniques Applied to BMI Test Blocks

Team#	NDE Technique Description	Form Procedure ID	Procedure ID Used in Formal Documentation	Technique ID	Manual or Automated	Encoded (Y/N)	Exam Surface	Probe Frequency (MHz)/ Inspection Angle (Deg.)/Skew (Deg.)	Technique Comment
124	Mechanized ECT	124.1	ECT.124	124-ECT0	Automated	Y	I.D.	100 kHz	Detection, Characterization, Length, Positioning
108	Eddy current	108.6	ECT.108	108-ECT0	Auto	Y	O.D.	32 channel array 500 kHz Pancake coil probe Flexible array	Examine Only J-Groove Weld [Detection, Characterization, Length, Positioning]
126	Eddy current ECT	126.5	TOFD.ECT.126	126-ECT0	Automated	Y	Tube I.D.	400 kHz	Detection, Characterization, Positioning
126	Time of flight diffraction TOFD	126.5	TOFD.ECT.126	126-TOFD0	Automated	Y	Tube I.D.	6 MHz	Detection, Characterization, Length, Depth, Positioning

B.5 Summary of Techniques Applied to WOL Test Blocks

Team#	NDE Technique Description	Form Procedure ID	Procedure ID Used in Formal Documentation	Technique ID	Manual or Automated	Encoded (Y/N)	Exam Surface	Probe Frequency (MHz)/ Inspection Angle (Deg.)/Skew (Deg.)	Technique Comment
108	Phased array UT (sectorial)	108.4	PAUT.108.2	108-PA2	Manual	N	O.D.	2 MHz/L0°~L85°	Detection, Characterization, Length, Depth, Positioning
126	Phased array UT (sectorial)	126.4	PAUT.126.2	126-PA2	Manual	N	O.D.	2 MHz/ L0°~L85°	Detection, Characterization, Length, Depth, Positioning

APPENDIX C
PROCEDURE SUMMARY SHEETS

APPENDIX C

PROCEDURE SUMMARY SHEETS

C.1 Procedure 25.1

Procedure ID: **25.1**

Team ID: **25**

Procedure Type: **UT**

Scan Access: **O.D.**

Scan Direction: **CIRC**

Detection: **YES**

Length Sizing: **YES**

Depth Sizing: **YES**

C.1.1 Description for Combining Techniques

Detection

Tech-ID	Description	Evaluation Method
25.1	<p>Pitch and catch configuration with reflection on back wall and inspection angle of approximately 45° long. Probe separation will be 70 mm (approximately twice the wall thickness).</p> <p>Probe frequency will be 0.5 MHz (aperture diameter 1.5 Inch, with tapered Rexolite wedge, contact area to test block with approximately 10 mm diameter).</p> <p>Probe index points have to be measured and their distance will then be used for evaluation.</p> <p>Knowledge of the delay of the wedges will allow calculating the wall thickness (in case of changing wall thicknesses).</p> <p>Area where cracks are expected will be scanned with sound direction perpendicular to the crack. Therefore more than 1 direction may be necessary.</p>	<p>C-scan of 45° LL reflection of back wall will be evaluated:</p> <p>Where no (perpendicular) crack is present the back wall will be detected with high amplitude. At positions where the sound path from sender to receiver is affected by the crack the amplitude will drop. 6 dB drop compared to sound material will be used. Additionally pattern recognition will be used.</p>

Characterization

Tech-ID	Description	Evaluation Method
25.1	See description for detection technique.	A crack connected to the inner surface will result in a C-scan where the area with amplitude drop will be continuous whereas an inclusion or lack of fusion will result in two individual (mirrored) areas with amplitude drop). 6 dB drop compared to sound material will be used. Additionally pattern recognition will be used.

Length Sizing

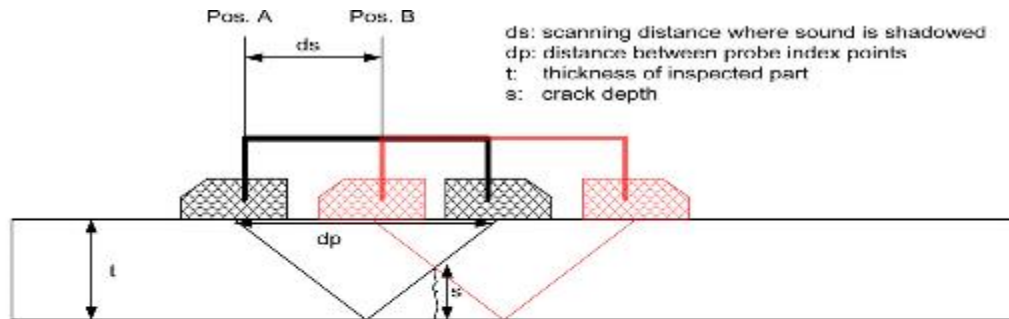
Tech-ID	Description	Evaluation Method
25.1	See description for detection technique.	Length of the crack corresponds to the scanning index distance where the crack will be detected. 6 dB drop compared to sound material will be used. Additionally pattern recognition will be used.

Depth Sizing

Tech-ID	Description	Evaluation Method
25.1	See description for detection technique.	Crack depth is calculated from the scanning distance where a drop of amplitude is detected. For calculation of crack depth compare attached sketch and formula. 6 dB drop compared to sound material will be used. Additionally pattern recognition will be used.

Defect Positioning

Tech-ID	Description	Evaluation Method
25.1	See description for detection technique.	Sizing technique will be used. Centerline (perpendicular to scanning direction) of the area with amplitude drop will be used as defect position whereas the mechanical reference of the C-scan will be the center of the probe assembly. 6 dB drop compared to sound material will be used. Additionally pattern recognition will be used.



Set-up:

- Two identical probes (aperture, frequency, angle) with an angle of about 40° to 45° (long), fixed in a probe holder.
- Distance between probe index points is optimized to receive the reflected longitudinal wave from the backwall (LL)
- Probe holder is moved over the surface and the distance where sound is shadowed by the crack will be stored (B-scan of the received signal)

Crack depth is given by the following formula:

$$s = ds * t / dp$$

Figure C.1

C.2 Procedure 101.1

Procedure ID: **101.1**

Team ID: **101**

Procedure Type: **ET**

Scan Access: **ID**

Scan Direction: **CIRC**

Detection: **YES**

Length Sizing: **YES**

Depth Sizing: **NO**

C.2.1 Description for Combining Techniques

- ET 300 kHz is used for detection and length sizing.
- This procedure is used combined with procedure ID: 101.2. ET 50 KHz or 300 KHz is used as a complement to the evaluation.

Detection

Tech-ID	Description	Evaluation Method
ET 300 KHz Circ. and Axial defects	Zetec Z001003-2 probe Cross point probe, transmit receive Frequency 300 KHz (50 or 150 KHz for defects in areas detected with UT)	<ul style="list-style-type: none"> • Defect signal to noise ratio 2:1 (50%) • Maximum amplitude phase between 80°-130° • Defect like signal pattern • Defect pattern for at least 8 consecutive scan lines (axial) and 4 consecutive scan lines (circ) For UT defect location phase angle restriction do not apply. Defect indications are considered separate if they are separated by at least 6 mm in length

Characterization

Tech-ID	Description	Evaluation Method
ET 300 KHz Circ. and Axial defects	Zetec Z001003-2 probe Cross point probe, transmit receive Frequency 300 KHz	All defects detected with ET are characterized as surface breaking.

Length Sizing

Tech-ID	Description	Evaluation Method
ET 300 KHz Circ. and Axial defects	Zetec Z001003-2 probe Cross point probe, transmit receive Frequency 300 KHz (50 or 150 KHz for defects in areas detected with UT)	The defect signal is followed down to noise level.

Depth Sizing

Tech-ID	Description	Evaluation Method
N/A	N/A	N/A

Defect Positioning

Tech-ID	Description	Evaluation Method
ET 300 KHz Circ. and Axial defects	Zetec Z001003-2 probe Cross point probe, transmit receive Frequency 300 KHz (50 or 150 KHz for defects in areas detected with UT)	Based on previous described methodology for detection, length and height sizing <ul style="list-style-type: none"> • X positions are as per position from length sizing for defects along weld • Y positions, across defect, is taken from length sizing technique at max amplitude for defects along weld • Y positions are as per position from detection for defects with axial orientation

C.3 Procedure 101.2

Procedure ID: **101.2**

Team ID: **101**

Procedure Type: **UT PE and TOFD**

Scan Access: **I.D.**

Scan Direction: **CIRC**

Detection: **YES**

Length Sizing: **YES**

Depth Sizing: **YES**

C.3.1 Description for Combining Techniques

- UT PE for detection, characterization, length sizing and positioning. TOFD or PE A-scans for depth sizing
- Used together with ET procedure (101.1)

Detection

Tech-ID	Description	Evaluation Method
UT PE 70° TRL2-F and 70° TRL2 B	Circumferential defects	Cal+DAC, registration to noise level
UT PE 70° TRL2CW and 70° TRL2 AC	Transverse defects, Z max to be used for evaluation is 20 mm	Cal + DAC registration to noise level. Separate setting without DAC for areas with high noise level.
UT PE 65° TRL2-F and 65° TRL2-B	Longitudinal defects	Cal+DAC, registration to noise level
UT PE 65° TRL2-CW and 65° TRL2-AC	Transverse defects	Cal+DAC, registration to noise level
UT PE Adept 42/55° TRL2 F and Adept 42/55° TRL2 B	Longitudinal defects	Cal + DAC + 4 dB Registration to noise level
UT PE Adept 42/55° TRL2 CW and Adept 42/55° TRL2 AW	Transverse defects	Cal + DAC + 4 dB Registration to noise level
UT PE 0° TRL	Laminar defects	Cal

Characterization

Tech-ID	Description	Evaluation Method
UT PE TRL and Adept probes	Volumetric or Planar	Volumetric: The echo shape shall be smooth without tip reflections also not detected with ET Planar: Tip reflection or ET-detected
TOFD ET (Proc. 101.1)	Surface breaking near inner surface	ET detected Ligament 3 mm or smaller with TOFD
UT PE TRL and Adept probes, TOFD	Embedded	Ligament greater than 3 mm

Length Sizing

Tech-ID	Description	Evaluation Method
UT PE TRL/Adept F/B	The greatest length taken from forward or backward probe	Sizing down noise level
UT PE TRL/Adept AC/CW	The greatest length taken from clockwise or anti clockwise probe	Sizing down noise level

Depth Sizing

Tech-ID	Description	Evaluation Method
UT PE A-scan and TOFD	<ul style="list-style-type: none"> • Defects detected with ET (101.1) = inner surface breaking • Defects only detected with ET are sized with TOFD PSD 9 • No sizing are performed if defects are characterized as volumetric • TOFD In case tip reflections are present in the A-scan use these Z values for probe choice and PSD distance. PSD 9 Z ≤ 5 mm PSD 18 Z > 5 mm < 15 mm PSD 35 Z > 10 mm for transverse defects 	<p>A-scan tip reflection in combination with TOFD</p> <p>Longitudinal defects: TOFD PSD 9, PSD 18 and PSD ≥35</p> <ul style="list-style-type: none"> • TOFD at a flat surface using the lateral wave as reference <p>TOFD PSD ≥ 35</p> <ul style="list-style-type: none"> • TOFD at a flat surface using the surface or bottom reflection as reference <p>Transverse defects: TOFD PSD 9, PSD 18 and PSD ≥35</p> <ul style="list-style-type: none"> • TOFD at a surface with radius R using the lateral wave as a reference <p>TOFD PSD ≥ 35</p> <ul style="list-style-type: none"> • TOFD at a surface with radius R using the surface or bottom reflection as a reference

Defect Positioning

Tech-ID	Description	Evaluation Method
UT PE TRL/Adept F/B	Longitudinal defects Y position max amplitude and min X and max X position	Max amplitude of probe with highest signal Min and max X signal to noise level
UT PE TRL/Adept CW/AW	Transverse defects X position max amplitude and min Y and max Y position	Max amplitude of probe with highest signal Min and max Y signal to noise level

C.4 Procedure 106.1

Procedure ID: **106.1**

Team ID: **106**

MPP-01 Procedure for mechanized Ultrasonic (UT) and Eddy Current (ET) Inspection of the Inlet and Outlet Nozzle Connection Welds.

Procedure Type: **ET and UT Pulse Echo**

Scan Access: **I.D.**

Scan Direction: **AXIAL** and **CIRC**

Detection: **YES**

Length Sizing: **YES**

Depth Sizing: **YES (not of embedded flaws)**

C.4.1 Description for Combining Techniques

- **Detection** shall be performed using a combination of both UT and ET techniques. ET will be used for detection of fatigue type defects and those clearly open to the surface and both ET and UT will be used for detection of those defects with partially intact ligaments, namely interdendritic stress corrosion cracking (IDSCC).
- **Characterization** between surface breaking and embedded will be performed using ET.
- **Sizing:** Any defect that is characterized as surface breaking shall be *sized for length* using ET and/or UT. Any defect that is characterized as surface breaking shall also be *sized for height* using UT.

Detection

Tech-ID	Description	Evaluation Method	
ET Circ and axial	ET 200 KHz driver/pickup cross wound probe with ferrite core	Has an amplitude ≥ 0.9 V on at least one scan line Has a phase of $90^\circ \pm 20^\circ$ or $270^\circ \pm 20^\circ$ Has a crack like signal (refer to calibration signal)	
UT Pulse Echo Circ and axial	UT 55° TRL FD 10 as a complement in case of partially intact ligaments, named IDSCC.	Long defects: Trans defects:	Amplitude ≥ 4 dB on 3 or more consecutive scan lines. (equivalent to 4 mm) Amplitude above noise on 3 or more consecutive scan lines. (equivalent to 6 mm)

Characterization

Tech-ID	Description	Evaluation Method	
ET Circ and axial	ET 200 KHz Driver/Pickup cross wound probe with ferrite core.	Has an amplitude ≥ 0.9 V on at least one scan line Has a phase of $90^\circ \pm 20^\circ$ or $270^\circ \pm 20^\circ$ Has a crack like signal (refer to calibration signal) Only characterization made is surface breaking or not. The orientation of the defect shall also be determined. All defects that are surface breaking shall be sized for length and height.	

Length Sizing

Tech-ID	Description	Evaluation Method
ET Circ and axial	ET 200 KHz Driver/Pickup cross wound probe with ferrite core.	<p>Down to noise level</p> <p>The length of a defect shall be determined by measuring the distance between the first and last crack like signal in the direction of the defect.</p> <p>Indications along the same line with a distance smaller than the measured length of the shortest indication shall be regarded as one single defect.</p>
UT Pulse Echo Circ and axial	55°TRL2-Aust FD 10 mm	<p>Down to noise level</p> <p>The length of a defect shall be determined by measuring the distance between the first and last position where the defect-like signal is discernible from the noise.</p> <p>Where the length measurements from two beam directions differ, the longest length shall be reported.</p> <p>Indications along the same defect axis with a distance between them of ≤ 10 mm shall be regarded as one single defect.</p>

Depth Sizing

Tech-ID	Description	Evaluation Method
UT Pulse Echo Circ and axial	55°TRL2-Aust FD 10 mm 45°TRL2-Aust FD 25 mm	<p>Pulse Echo Tip Diffraction. If a clear lower tip is identified at a depth of < 16 mm, the results from the 55TRL FD10 shall be reported. Where the depth is measured from both beam directions the deepest depth shall be used.</p> <p>If a clear lower tip is identified at a depth of ≥ 16 mm, the results from the 45TRL FD25 shall be reported. Where the depth is measured from both beam directions the deepest depth shall be used.</p> <p>Where depth measurements from both probe types are just within their applicable depth zones, the depth from the probe with the focal depth closest to the measured depth shall be used.</p> <p>If no tip responses are evident in the zone specified for the applicable probe, tip responses from the other probe shall be reported.</p>

Defect Positioning

Tech-ID	Description	Evaluation Method
ET circ and axial	ET 200 KHz Driver/Pickup cross wound probe with ferrite core.	<p>X-axis Position: For longitudinal defects, the start and end X co-ordinates are the positions obtained during the length sizing process. The X co-ordinates shall be reported from the probe/technique used to report the defect length. For transverse defects, the X co-ordinate of the maximum response obtained during the ET detection / characterization process shall be reported.</p> <p>Y-axis Position: For transverse defects, the start and end Y co-ordinates are the positions obtained during the length sizing process. The Y co-ordinates shall be reported from the probe/technique used to report the defect length. For longitudinal defects, the Y co-ordinate of the maximum response obtained during the ET detection / characterization process shall be reported</p>
UT pulse echo Circ and axial	55°TRL2-Aust FD 10 mm	

C.5 Procedure 108.1 and 108.2

Procedure ID: **108.1 and 108.2**

Team ID: **108**

Procedure Type: **UT**

Scan Access: **O.D.**

Scan Direction: **AXIAL** and **CIRC**

Detection: **YES**

Length Sizing: **YES**

Depth Sizing: **YES**

C.5.1 Description for Combining Techniques

- Manual conventional contact pulse echo UT used for detection and length/depth sizing of DMW.

Detection

Tech-ID	Description	Evaluation Method
Focused RL-Dual Probe	<p>The primary mode of propagation is longitudinal waves.</p> <p>(1~5 MHz, 30,45,60°)</p> <p>For I.D. connected flaw select focusing within 75 to 125% T.</p> <p>Perform Raster scan for axial flaw and CW/CCW Scan for circum flaw</p>	<p>According to Figure C.2.</p> <p>Evaluation level is noise level.</p>

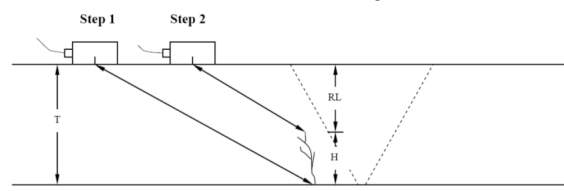
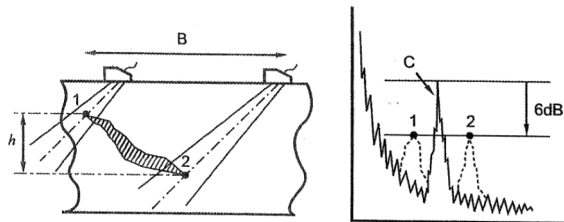
Characterization

Tech-ID	Description	Evaluation Method
Focused RL-Dual Probe	<p>All suspected flaw indications, regardless of amplitude, shall be investigated to the extent necessary to provide accurate characterization, identity, and location.</p> <p>Perform re-evaluations (relooks) with qualified equipment are acceptable.</p>	<p>-According to Figure C.2.</p> <p>-All suspected flaw indications shall be plotted on a cross sectional drawing of the weld. Indication plots shall accurately identify the specific origin of the reflector.</p>

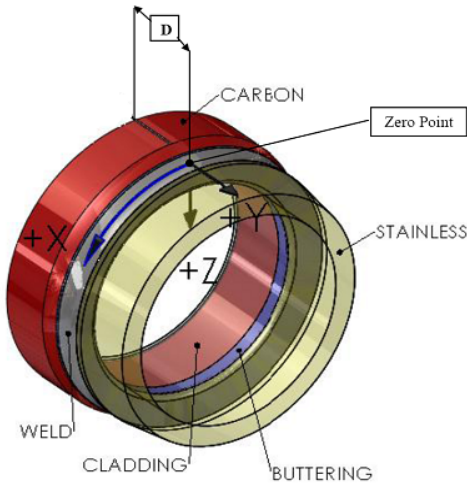
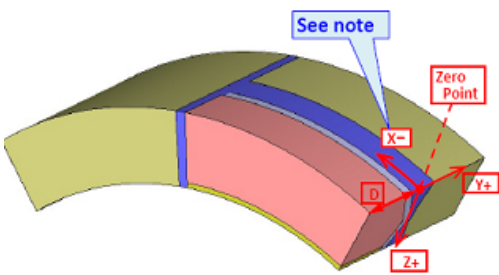
Length Sizing

Tech-ID	Description	Evaluation Method
Focused RL-Dual Probe	<p>Adjust the system gain as needed to optimize flaw responses.</p> <p>Maximize the signal response from the flaw indication. Adjust the system gain until this response is ~ 80 % FSH.</p>	<p>Even though detected with opposite beam direction, report length from near side of weld.</p> <p>The end points of flaw shall be determined in each direction until the signal response has diminished into the general background noise (full amplitude drop).</p>

Depth Sizing

Tech-ID	Description	Evaluation Method
<p>Focused RL-Dual Probe</p>	<p>If tip signal of flaw display, flaw depth is the calculated by subtracting the remaining ligament from the actual material thickness.</p> <p>If tip signal of flaw not display, the amplitude assessment level is 6 dB below the maximum echo height observed at any position along the flaw, rather than at a constant.</p>	<p>Absolute Arrival Time Technique</p>  <p>T = Material Thickness H = Flaw Height RL = Remaining Ligament</p> <p>Step 1. Locate base of flaw</p> <p>Step 2. Move forward up face of flaw to flaw tip</p> <p>-6 dB drop from maximum technique</p> 

Defect Positioning

Tech-ID	Description	Evaluation Method
<p>Focused RL-Dual Probe</p>	<p>Teams identifying on the reporting data sheets are projected position value from flaw.</p>	<p>P35, P40, P33</p>  <p>P13</p> 

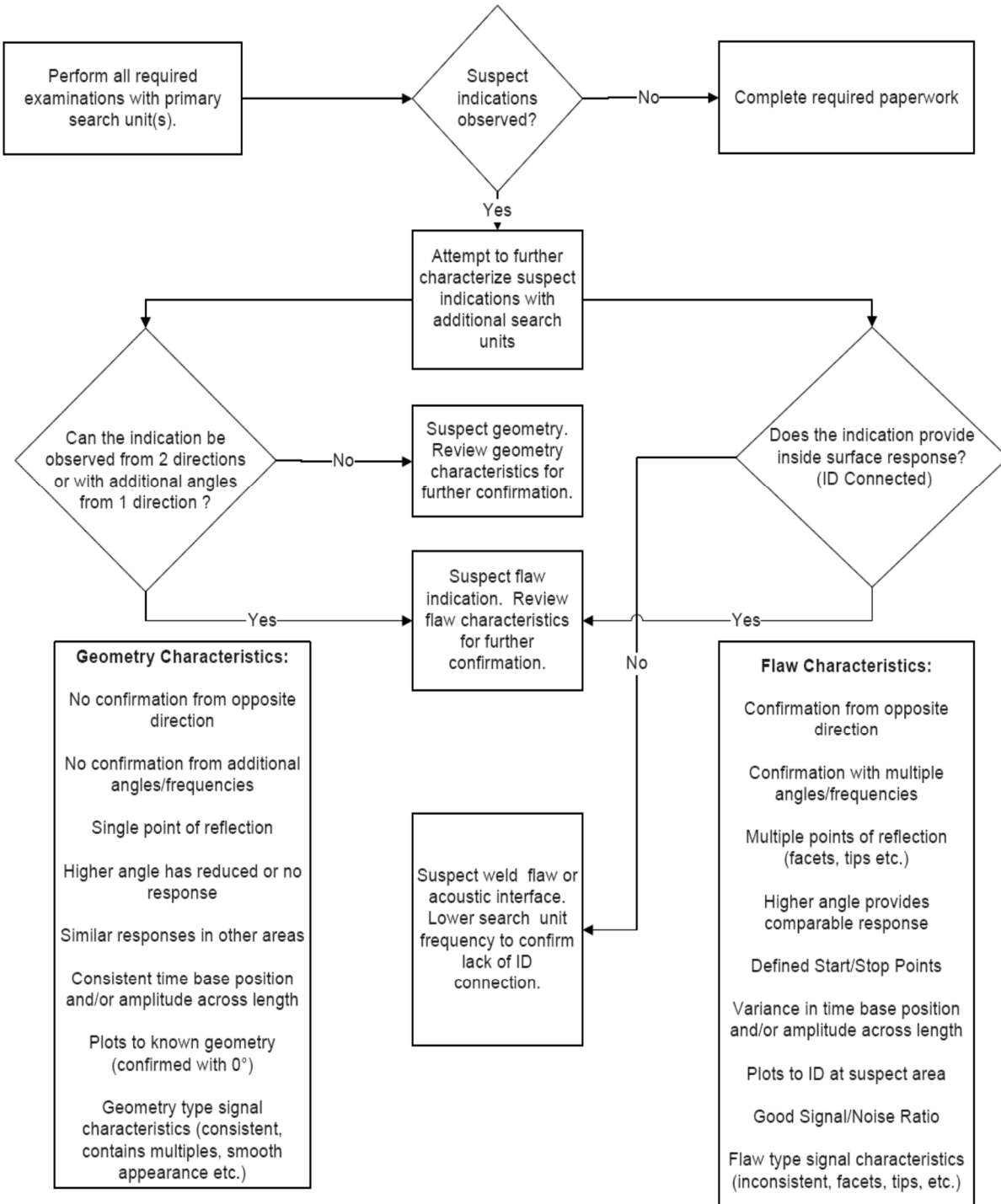


Figure C.2 Indication Evaluation Flow Chart

C.6 Procedure 108.3

Procedure ID: **108.3**

Team ID: **108**

Procedure Type: **UT**

Scan Access: **O.D.**

Scan Direction: **AXIAL** and **CIRC**

Detection: **YES**

Length Sizing: **YES**

Depth Sizing: **YES**

C.6.1 Description for Combining Techniques

- Phased array UT techniques are used for detection, length sizing, and depth sizing.

Detection

Tech-ID	Description	Evaluation Method
PA-01	Phased Array UT Using 2 MHz TRL Probe Axial Sectorial Scan	Amplitude
PA-02	Phased Array UT Using 2 MHz TRL Probe Circ. Sectorial Scan	Amplitude

Characterization

Tech-ID	Description	Evaluation Method
PA-01	Phased Array UT Using 2 MHz TRL Probe Axial Sectorial Scan	The indication provides responses identifying that the flaw initiates at or near the inside surface of weld.
PA-02	Phased Array UT Using 2 MHz TRL Probe Circ. Sectorial Scan	The indication has a high signal-to-noise ratio (> 2:1) with defined start and stop point. Raising the upper and lower amplitude thresholds of the color palette and observing signal-to-noise ratio contrast across the length of the component can support this.

Length Sizing

Tech-ID	Description	Evaluation Method
PA-01	Phased Array UT Using 2 MHz TRL Probe Axial Sectorial Scan	The flaw length shall be determined by scanning along the length of the flaw in each direction until the signal response has diminished onto the general background noise (full amplitude drop).
PA-02	Phased Array UT Using 2 MHz TRL Probe Circ. Sectorial Scan	

Depth Sizing

Tech-ID	Description	Evaluation Method
PA-01	Phased Array UT Using 2 MHz TRL Probe Axial Sectorial Scan	Absolute Arrival Time Technique. This technique relies upon obtaining direct signal responses (diffraction) from the flaw tip. The amount of unflawed material, or remaining ligament, is then read directly from either the A-Scan and/or S-Scan presentations.
PA-02	Phased Array UT Using 2 MHz TRL Probe Circ. Sectorial Scan	

Defect Positioning

Tech-ID	Description	Evaluation Method
PA-01	Phased Array UT Using 2 MHz TRL Probe Axial Sectorial Scan	As access allows, evaluate the flaw signal amplitude responses from each side of the weld. Observe if the signal response appears reduced due to weld volume sound attenuation from one side or another. Evaluate the ultrasonic responses from each side of the weld in both flawed and unflawed regions. If the flaw is only observable one direction, the location coordinates shall be determined from that observation. If the flaw is observable from two opposite directions, the flaw location coordinates shall be determined using an average from both observations.
PA-02	Phased Array UT Using 2 MHz TRL Probe Circ. Sectorial Scan	

C.7 Procedure 108.4

Procedure ID: **108.4**

Procedure Type: **UT**

Scan Direction: **AXIAL** and **CIRC**

Length Sizing: **YES**

Team ID: **108**

Scan Access: **O.D.**

Detection: **YES**

Depth Sizing: **YES**

C.7.1 Description for Combining Techniques

- Phased array UT techniques are used for detection, length sizing, and depth sizing (weld overlaid piping welds).

Detection

Tech-ID	Description	Evaluation Method
PAUT-AXIAL	Phased Array UT Using 2 MHz TRL Probe Axial Sectorial Scan	Amplitude. 0° to 25° angle range examinations for laminar defects. 25° to 85° angle range examinations for overlay material welding defects and original material defects.
PAUT-CIRC.	Phased Array UT Using 2 MHz TRL Probe Circ. Sectorial Scan	Amplitude. 25° to 85° angle range examinations for overlay material welding defects and original material defects.

Characterization

Tech-ID	Description	Evaluation Method
PAUT-AXIAL	Phased Array UT Using 2 MHz TRL Probe Axial Sectorial Scan	The indication has good signal-to-noise ratio (> 2:1) with defined start and stop points. Lack of Bond or Inter Bead Lack of Fusion <ul style="list-style-type: none"> • The indication has volumetric positioning at the weld overlay to base material interface (lack of bond) or within the volume of the weld overlay material (inter-bead lack of fusion). • The indication response is reduced or absent when viewing the 25°–85° angles Contamination Cracking <ul style="list-style-type: none"> • The indication provides volumetric positioning identifying that the entire flaw is contained within the volume of the weld overlay material. • The indication response is unobservable or substantially reduced from the 0° to 25° angle range. Original Material Defects <ul style="list-style-type: none"> • The indication provides responses identifying that the flaw initiates at or near the inside surface of the original base material. • The indication response is reduced or absent when viewing the 25°–85° angles
PAUT-CIRC.	Phased Array UT Using 2 MHz TRL Probe Circ. Sectorial Scan	The indication has good signal-to-noise ratio (> 2:1) with defined start and stop points. Contamination Cracking <ul style="list-style-type: none"> • The indication provides volumetric positioning identifying that the entire flaw is contained within the volume of the weld overlay material. • The indication response is unobservable or substantially reduced from the 0° to 25° angle range. Original Material Defects <ul style="list-style-type: none"> • The indication provides responses identifying that the flaw initiates at or near the inside surface of the original base material. • The indication response is reduced or absent when viewing the 25°–85° angles

Length Sizing

Tech-ID	Description	Evaluation Method
PAUT-AXIAL	Phased Array UT Using 2 MHz TRL Probe Axial Sectorial Scan	The length of flaws shall be determined by scanning along the length of the flaw in each direction until the signal response in the A-scan has diminished into the general background noise (full amplitude drop) or the image response in the S-scan has diminished into the general image background noise.
PAUT-CIRC.	Phased Array UT Using 2 MHz TRL Probe Circ. Sectorial Scan	

Depth Sizing

Tech-ID	Description	Evaluation Method
PAUT-AXIAL	Phased Array UT Using 2 MHz TRL Probe Axial Sectorial Scan	Absolute Arrival Time Technique. This technique relies upon obtaining direct signal responses (diffraction) from the flaw tip. The amount of unflawed material, or remaining ligament, is then read directly from either the A-scan and/or S-scan presentations.
PAUT-CIRC.	Phased Array UT Using 2 MHz TRL Probe Circ. Sectorial Scan	

Defect Positioning

Tech-ID	Description	Evaluation Method
PAUT-AXIAL	Phased Array UT Using 2 MHz TRL Probe Axial Sectorial Scan	Amplitude. If the flaw is only observable one direction, the location coordinates shall be determined from that observation. If the flaw is observable from two opposite directions, the flaw location coordinates shall be determined using an average from both observations.
PAUT-CIRC.	Phased Array UT Using 2 MHz TRL Probe Circ. Sectorial Scan	

C.8 Procedure 108.5

Procedure ID: **108.5**

Team ID: **108**

Procedure Type: **UT, ET**

Scan Access: **I.D.**

Scan Direction: **AXIAL**

Detection: **YES**

Length Sizing: **YES**

Depth Sizing: **YES**

C.8.1 Description for Combining Techniques

- ECT techniques are used for detection and length sizing
- UT techniques are used for detection, length sizing, and depth sizing

Detection

Tech-ID	Description	Evaluation Method
BMI-TUBE-TOFD-UT	UT Using 10 MHz TOFD UT Probe	TOFD Tip Signal Loss of Lateral Wave Loss of Backwall
BMI-TUBE-ECT	ECT Using X-Type Coil Probe	Phase Angle and C-scan image

Characterization

Tech-ID	Description	Evaluation Method
BMI-TUBE-TOFD-UT	UT Using 10 MHz TOFD UT Probe	I.D. Connected Defect: The lateral wave break and bottom tip signal present in the penetration. O.D. Connected Defect: The top tip signal from a defect emanating from the O.D. surface will have no lateral wave break, with back wall disturbance present.
BMI-TUBE-ECT	ECT Using X-Type Coil Probe	The indication provides responses identifying that the flaw exist at surface of Tube ID. The indication has a high signal-to-noise ratio (> 2:1) with defined start and stop point.

Length Sizing

Tech-ID	Description	Evaluation Method
BMI-TUBE-TOFD-UT	UT Using 10 MHz TOFD UT Probe	The start and stop position of the defect will be taken on the last scan line where the lateral/backwall disturbance or tip signal is evident.
BMI-TUBE-ECT	ECT Using X-Type Coil Probe	The 6 dB down measurement method

Depth Sizing

Tech-ID	Description	Evaluation Method
BMI-TUBE-TOFD-UT	UT Using 10 MHz TOFD UT Probe	TOFD Tip Signal
BMI-TUBE-ECT	ECT Using X-Type Coil Probe	N/A

Defect Positioning

Tech-ID	Description	Evaluation Method
BMI-TUBE-TOFD-UT	UT Using 10 MHz TOFD UT Probe	Location of lateral/backwall wave disturbance or crack tip signals
BMI-TUBE-ECT	ECT Using X-Type Coil Probe	Phase angle and C-scan image

C.9 Procedure 108.6

Procedure ID: **108.6**

Team ID: **108**

Procedure Type: **ET**

Scan Access: **I.D.**

Scan Direction: **CIRC**

Detection: **YES**

Length Sizing: **YES**

Depth Sizing: **NO**

C.9.1 Description for Combining Techniques

- ECT techniques are used for detection and length sizing of J-groove weld surface flaws.

Detection

Tech-ID	Description	Evaluation Method
BMI-WELD-ECT	Array ECT Using 32 CH Probe	Phase Angle and C-scan image

Characterization

Tech-ID	Description	Evaluation Method
BMI-WELD-ECT	Array ECT Using 32 CH Probe	The indication provides responses identifying that the flaw exist at surface of J-groove weld. The indication has a high signal-to-noise ratio (> 2:1) with defined start and stop point.

Length Sizing

Tech-ID	Description	Evaluation Method
BMI-WELD-ECT	Array ECT Using 32 CH Probe	The 6 dB down measurement method.

Depth Sizing

Tech-ID	Description	Evaluation Method
N/A	N/A	N/A

Defect Positioning

Tech-ID	Description	Evaluation Method
BMI-TUBE-ECT	ECT Using X-Type Coil Probe	Phase angle and C-scan image

C.10 Procedure 113.1

Procedure ID: **113.1**

Team ID: **113**

Procedure Type: **UT**

Scan Access: **I.D.**

Scan Direction: **AXIAL** and **CIRC**

Detection: **YES**

Length Sizing: **YES**

Depth Sizing: **YES**

C.10.1 Description for Combining Techniques

- The indications with SNR>2 are picked up. The evaluation is performed in consideration of the indication amplitude, the distribution of indication in B/C/D scope.

Detection

Tech-ID	Description	Evaluation Method
113-UT1	<p>Conventional UT contact technique based on reflection signal from a defect using probe 2.25C-LAD70-50.</p> <ul style="list-style-type: none"> • Frequency: 2.25 MHz. • Inspection angle: 55° (Transmitter: 70°, Receiver: 50°) <p>Data recording pitch</p> <ul style="list-style-type: none"> • For Axial defect: $\Delta X=0.2$ mm, $\Delta Y=4$ mm • For Circ. defect: $\Delta X=4$ mm, $\Delta Y=0.2$ mm 	<p>Based on Signal to Noise Ratio (SNR)</p> <p>Evaluation of signals with SNR larger than 2</p>
113-UT2	<p>Conventional UT contact technique based on reflection signal from a defect using probe 3C-LAD70-50.</p> <ul style="list-style-type: none"> • Frequency: 3 MHz. • Inspection angle: 55° (Transmitter: 70°, Receiver: 50°) <p>Data recording pitch</p> <ul style="list-style-type: none"> • For Axial defect: $\Delta X=0.2$ mm, $\Delta Y=2$ mm • For Circ. defect: $\Delta X=2$ mm, $\Delta Y=0.2$ mm 	<p>Based on Signal to Noise Ratio (SNR)</p> <p>Evaluation of signals with SNR larger than 2</p>
113-PA1	<p>PAUT contact technique based on reflection signal from a defect using probe 2C-96ch Matrix phased array probe.</p> <ul style="list-style-type: none"> • Frequency: 2 MHz. • Range of angle: 45° (two angles are used with probe scanning of forward and backward direction) <p>Data recording pitch</p> <ul style="list-style-type: none"> • For Axial defect: $\Delta X=0.2$ mm, $\Delta Y=2$ mm • For Circ. defect: $\Delta X=2$ mm, $\Delta Y=0.2$ mm 	<p>Based on Signal to Noise Ratio (SNR)</p> <ul style="list-style-type: none"> • Evaluation of signals with SNR larger than 2 • Final evaluation will be performed using 45° data.

113-PA2	<p>PAUT contact technique based on reflection signal from a defect using probe 5C-40ch phased array probe.</p> <ul style="list-style-type: none"> • Frequency: 5 MHz. • Range of angle: 35–55° • Increment of angle: 5° (five angles are used with probe scanning of forward and backward direction) <p>Data recording pitch</p> <ul style="list-style-type: none"> • For Axial defect: $\Delta X=0.2$ mm, $\Delta Y=2$ mm • For Circ. defect: $\Delta X=2$ mm, $\Delta Y=0.2$ mm 	<p>Based on Signal to Noise Ratio (SNR)</p> <ul style="list-style-type: none"> • Evaluation of signals with SNR larger than 2 • Final evaluation will be performed using 45° data.
---------	--	--

Characterization

Tech-ID	Description	Evaluation Method
113-UT1 113-UT2 113-PA1 113-PA2	<p>UT contact technique based on reflection from defect.</p> <ul style="list-style-type: none"> • All probes are used. 	<p>Characterization is carried out by considering signal amplitude and signal profile in B-scope, C-scope and D-scope. The Criteria of A/B/C/D scope to characterize an indication are as follows. At first, the indications with SNR>2 are picked up. Then, the evaluation is performed in consideration of the indication amplitude, the distribution of indication in B/C/D scope, and the movement of waveform with the forward and backward probe scanning.</p>

Length Sizing

Tech-ID	Description	Evaluation Method
113-UT2 113-PA1 113-PA2	<p>UT contact technique based on reflection from defect.</p> <ul style="list-style-type: none"> • Conventional UT probe for sizing and two phased array probes are used. (3C-LAD70-50, 2C-96ch Matrix and 5C-40ch TRL) <p>Data recording pitch for 113-UT1</p> <ul style="list-style-type: none"> • For Axial defect: $\Delta X=0.2$ mm, $\Delta Y=4$ mm • For Circ. defect: $\Delta X=4$ mm, $\Delta Y=0.2$ mm <p>Data recording pitch for other Tech.ID</p> <ul style="list-style-type: none"> • For Axial defect: $\Delta X=0.2$ mm, $\Delta Y=4$ mm • For Circ. defect: $\Delta X=4$ mm, $\Delta Y=0.2$ mm 	<p>Based on the signal amplitude exceed noise level.</p> <p>Length sizing is obtained from the difference of the maximum and the minimum.</p> <p>Length sizing is performed using the maximum value of length sizing data of three probes.</p>

Depth Sizing

Tech-ID	Description	Evaluation Method
113-UT2 113-PA1 113-PA2	<p>UT contact technique based on reflection from tip.</p> <ul style="list-style-type: none"> Conventional UT probe for sizing and two phased array probes are used. (3C-LAD70-50, 2C-96ch Matrix and 5C-40ch TRL) <p>Data recording pitch for 113-UT1</p> <ul style="list-style-type: none"> For Axial defect: $\Delta X=0.2$ mm, $\Delta Y=4$ mm For Circ. defect: $\Delta X=4$ mm, $\Delta Y=0.2$ mm <p>Data recording pitch for other Tech.ID</p> <ul style="list-style-type: none"> For Axial defect: $\Delta X=0.2$ mm, $\Delta Y=4$ mm For Circ. defect: $\Delta X=4$ mm, $\Delta Y=0.2$ mm 	<p>Evaluation of each scan line searching for diffraction from defect tip.</p> <p>Take the value which gives the greatest depth.</p>

Defect Positioning

Tech-ID	Description	Evaluation Method
113-UT1 113-UT2 113-PA1 113-PA2	<p>Based on technique for detection, length and depth sizing</p> <p>Data recording pitch for 113-UT1</p> <ul style="list-style-type: none"> For Axial defect: $\Delta X=0.2$ mm, $\Delta Y=4$ mm For Circ. defect: $\Delta X=4$ mm, $\Delta Y=0.2$ mm <p>Data recording pitch for other Tech.ID</p> <ul style="list-style-type: none"> For Axial defect: $\Delta X=0.2$ mm, $\Delta Y=4$ mm For Circ. defect: $\Delta X=4$ mm, $\Delta Y=0.2$ mm 	<p>Based on previously described methodology for detection, length and depth sizing:</p> <p>For axial defects</p> <ul style="list-style-type: none"> Y positions, along defect, are taken from length sizing. (Y position is determined based on maximum and minimum of Y axis value of defect signal.) Ymax is determined from depth sizing. X position, across defect, is taken from depth sizing. Z positions are directly taken from depth sizing. <p>For circumferential defects</p> <ul style="list-style-type: none"> X positions, along defect, are taken from length sizing. (X position is determined based on maximum and minimum of X axis value of defect signal.) Xmax is determined from depth sizing. Y position, across defect, is taken from depth sizing. Z positions are directly taken from depth sizing.

C.11 Procedure 115.1

Procedure ID: **115.1**

Procedure Type: **UT**

Scan Direction: **CIRC** and **AXIAL**

Length Sizing: **YES**

Team ID: **115**

Scan Access: **O.D.**

Detection: **YES**

Depth Sizing: **YES**

C.11.1 Description for Combining Techniques

Detection

Tech-ID	Description	Evaluation Method
115.1	<p>Detection is performed with phased array pulse echo techniques (TR Mode).</p> <p>The detection of surface breaking I.D. flaws relies upon the corner response being observed.</p> <p>The optimum technique to generate a corner response is the 45° shear angle. Since the PWSCC are in the anisotropic, heterogeneous DM weld material use of shear waves is seriously restricted (beam distortion). Therefore number of angled longitudinal waves shall also be used.</p>	<p>Axial scan direction (circumferential flaws)</p> <ul style="list-style-type: none">• 25° to 70° long (Step 1°)• 35° to 65° shear (Step 1°) <p>Circ scan direction (axial flaws)</p> <ul style="list-style-type: none">• 25° to 70° long (Step 1°)• 35° to 65° shear (Step 1°)

Characterization

Tech-ID	Description	Evaluation Method
115.1	The characterization is based on the identification of flaw like indications which cannot be attributed to the component geometry based on the supplied as built drawings, manufacturing defects (reported during previous inspections) or indications due to reflection's or scattering on the anisotropic und heterogeneous weld structure.	<p>Flaw Indications</p> <ul style="list-style-type: none"> • Good signal to noise ratio (variations along the length) • Plots to susceptible crack location • Substantial echo dynamic travel • Areas of unique amplitude • Inconsistent time base positions • Tip signals • Conformation from the opposite direction • Seen with many angles • Mode converted shear signal (only circ flaws with substantial depth) <p>Non relevant indications</p> <ul style="list-style-type: none"> • Near WCL or weld geometry • Seen continuously • Consistent time & amplitude • Weak echo dynamic travel

Length Sizing

Tech-ID	Description	Evaluation Method
115.1	Length of a flaw shall be determined by moving the probe along the flaw.	<p>On the same side of the weld as the indication</p> <p>Optimize the signal from the flaw indication</p> <p>Adjust the system gain until the response is ~ 80 % FSH</p> <p>Scan along the length of the flaw in each direction until the signal response has been reduced to:</p> <ul style="list-style-type: none"> • background noise for fare side indication • 20% FSH (12 dB drop) for near side indication <p>The length on outside diameter is longer than the actual inside diameter length. Calculate correct I.D. flaw length according t: (I.D./O.D.) x O.D. flaw length = I.D. flaw length</p>

Depth Sizing

Tech-ID	Description	Evaluation Method
115.1	<p>For flaw depth sizing the Absolute Arrival Time Technique (AATT) is used. The technique relies upon obtaining a direct signal response from the flaw tip using a material depth calibration. From the flaw tip response the amount of unflawed material or remaining ligament can be read directly from the Sector-scan. Flaw depth is calculated by subtracting the remaining ligament from the actual material thickness.</p> <p>The preferred propagation mode is longitudinal. Shear wave propagation is not as reliable through austenitic weld filler material. However, shear waves have better resolution for flaws that do not penetrate the DM weld material. This should be considered when analyzing the data.</p>	<p>Phasor technique:</p> <ul style="list-style-type: none"> • Find Tip-Diffraction Echo in Sector-scan (max. Depth) • Put vertical Cursor 1 (blue) to I.D. • Adjust Beam Cursor (A-scan) to maximum of tip diffraction dynamic • Put vertical Cursor 2 (red) to cross point • Value D1-2 corresponds to flaw depth

Defect Positioning

Tech-ID	Description	Evaluation Method
115.1	<p>Due to uncertainties associated with sound propagation in anisotropic, heterogeneous austenitic weld material indication positioning require detailed evaluation. The information provided under "Evaluation Method" may assist indication positioning.</p>	<p>Perform thickness and surface contour recordings at the indication position.</p> <p>Evaluate the flaw signal amplitude responses from each side of the weld. Observe if the signal response appears reduced due to weld volume sound attenuation from one side or another.</p> <p>Identify standard benchmark responses (weld root, weld noise, acoustic interfaces) and flaw indication responses.</p> <p>Coordinate and plot the information on a cross sectional drawing of the weld.</p>

C.12 Procedure 117.1 and 117.2

Procedure ID: **117.1 and 117.2**

Team ID: **117**

Detection: P6UP68087-UTC2h (117-1)

Characterization: P6UP68087-UTC2h (117-1)

Length Sizing: P6UP68087-UTC2h (117-1)

Height sizing: P6UP68087-UT-CSI (117-2)

Procedure Type: **UT**

Scan Access: **O.D.**

P-Scan system PS4 for data acquisition and analysis

Scan Direction: **CIRC** and **AXIAL**

Detection: **YES**

Automated scanner, X- and Y movement
Magnetic wheels

Length Sizing: **YES**

Depth Sizing: **YES (only circ. flaws)**

C.12.1 Description for Combining Techniques

- Inspection results are based on two procedures, one for detection, characterization and length sizing (117-1) and one for height sizing (117-2). Tip diffraction technique is used for height sizing. Different PCS (Probe Centre Separation) and angles depending on crack tip depth from O.D. surface.

Detection

Tech-ID	Description	Evaluation Method
117-1 UT Pulse-echo P6UP68087-UTC2h	Pulse-echo, projection images TRL-probes 2 MHz and 1 MHz 0°, 45°, 60° and 74° for circ. flaws 40° and 54° for axial flaws	Pattern recognition to noise level (S/N about ≥ 6dB)

Characterization

Tech-ID	Description	Evaluation Method
117-1 UT Pulse-echo P6UP68087-UTC2h	Position of indication or maximum amplitude in volume TRL-probes 2 MHz and 1 MHz 0°, 45°, 60° and 74° for circ. flaws 40° and 54° for axial flaws	Based on probe angle, beam direction and echo dynamics

Length Sizing

Tech-ID	Description	Evaluation Method
117-1 UT Pulse-echo P6UP68087-UTC2h	Measurement on images using cursor	10 dB-drop, alternatively down to noise if 10 dB cannot be used

Depth Sizing

Tech-ID	Description	Evaluation Method
117-2 UT Tip diffraction with pulse-echo P6UP68087-UTCSI	Tip diffraction using A-scan composite view 45° and 60° probes from detection	Identify tip signal and calculate depth from O.D. surface Only used for I.D.-surface cracks

Depth Sizing

Tech-ID	Description	Evaluation Method
117-2 UT Tip diffraction with TOFD P6UP68087-UTCSI	Tip diffraction using TOFD 3 MHz probes 45° and 60° with different PCS based on estimated depth from 117-2 A-scan, or fixed values of PCS depending on characterization result	Identify tip signal and calculate depth from O.D. surface TOFD result shall correlate with depth from A-scan tip depth measurement where applicable

Defect Positioning

Tech-ID	Description	Evaluation Method
117-1	Cursor measurement on scan images in connection with length sizing	Centre of indication in Y-direction and start of indication (lowest X-pos value) in X-direction for defects parallel to weld and vice versa for defects perpendicular to weld.

C.13 Procedure 124.1

Procedure ID: **115.1**

Team ID: **124**

MPP-08 Procedure for the Mechanized
Ultrasonic (UT) and Eddy Current (ET)

Inspection of Bottom Mounted
Instrumentation (BMI) J-Groove Weld

Procedure Type: ET and **UT pulse echo
and TOFD**

Scan Access: **I.D.**

Scan Direction: **AXIAL** and **CIRC**

Detection: **YES**

Length Sizing: **YES**

Depth Sizing: **YES**

C.13.1 Description for Combining Techniques

- **Detection:** ET is used for detection of transverse and longitudinal defects open to J-groove weld surface (IDSCC).
- **Characterization:** ET characterizes all defects to be surface breaking.
- **Sizing:** Any defect that is characterized as surface breaking shall be *sized for length* using ET. Any defect that is characterized as surface breaking shall also be *sized for height* using UT.

TOFD PCS 24 and PCS 10 are used for axial defects. 55TRL2 and TOFD PCS 10 are used for circumferential defects.

Detection

Tech-ID	Description	Evaluation Method
124.1 ET Circ and axial	ET 100 KHz X wound probe with ferrite core driven both in D/P and differential mode.	Has an amplitude ≥ 1 V on at least one scan line Has a phase of $90^\circ \pm 20^\circ$ or $270^\circ \pm 20^\circ$ Has a crack like signal (refer to calibration signal)

Characterization

Tech-ID	Description	Evaluation Method
124.1 ET Circ and axial	ET 100 KHz X wound probe with ferrite core driven both in D/P and differential mode	Has an amplitude ≥ 1 V on at least one scan line Has a phase of $90^\circ \pm 20^\circ$ or $270^\circ \pm 20^\circ$ Has a crack like signal (refer to calibration signal)

Length Sizing

Tech-ID	Description	Evaluation Method
124.1 ET Circ and axial	ET 100 KHz X wound probe with ferrite core driven both in D/P and differential mode.	Down to noise level The length of a defect shall be determined by measuring the distance between the first and last crack like signal in the direction of the defect. Indications along the same line with a distance smaller than the measured length of the shortest indication shall be regarded as one single defect.

Depth Sizing

Tech-ID	Description	Evaluation Method
124.1 UT Pulse Echo and TOFD for circular defects UT TOFD for axial defects	55°TRL2-Aust FD 8-10 mm TOFD PCS 10 6 MHz TOFD PCS 24 or PCS 10 6 MHz	Height sizing of J-groove surface breaking defects is performed with TOFD and/or 55TRL using tip diffraction: <ul style="list-style-type: none"> • Transverse defects will be sized with circumferential beam TOFD PCS 24 and/or PCS 10. • Longitudinal defects will be primarily sized with 55TRL. TOFD is used when possible with regards to the geometry of the defect position. Following evaluation of the data the defect height will reported as follows: <ul style="list-style-type: none"> • If a clear lower tip is identified the greatest depth along the defect length shall be reported. • If both 55TRL and TOFD measure an accurate depth, the deepest measurement shall be reported. • If the results show no evidence of a surface breaking defect at the location reported during detection, the defect height shall be reported as < 2 mm. Note: The height estimation is based upon the vertical distance from the surface to the tip and no correction for defect tilt will be applied.

Defect Positioning

Tech-ID	Description	Evaluation Method
124.1 ET Circ and axial	ET 100 KHz X wound probe with ferrite core driven both in D/P and differential mode.	<p>X-axis Position</p> <ul style="list-style-type: none"> • For axial defects, the X co-ordinates are the positions of the maximum response obtained during detection. • For circumferential defects, the X co-ordinate is the start point of the defect, obtained during length sizing. <p>Y-axis position</p> <ul style="list-style-type: none"> • For axial defects, the start Y co-ordinates are the positions obtained during the length sizing process. • For circumferential defects, the Y co-ordinate is the maximum response obtained during the detection process.

C.14 Procedure 126.1

Procedure ID: **126.1**

Team ID: **126**

Procedure Type: **ET and UT**

Scan Access: **I.D.**

Scan Direction: **AXIAL**

Detection: **YES**

Length Sizing: **YES**

Depth Sizing: **YES**

C.14.1 Description for Combining Techniques

- Automatic UT (TOFD) & ET used for detection and length/depth sizing of BMI

Detection

Tech-ID	Description	Evaluation Method
BMI	<p>BMI Nozzle I.D. side Inspection at Axial Scan</p> <p>TOFD technique shall be used lateral wave and back wall signal to detect the presence of O.D./I.D. defect.</p> <p>TOFD technique shall be used 6 MHz</p> <p>TOFD technique shall be used 2 channel (Axial shooting TOFD, Circumferential shooting TOFD)</p> <p>ET shall be detection for surface or near surface indications</p> <p>P6, P8, P9, P25, P26 for defects</p>	<p>TOFD Select channel, display mode to analyze (axial shooting the B-Scan (TOPS), circumferential shooting TOFD channel: D-Scan)</p> <p>Investigate any areas with a loss of the lateral wave for tip signals and or loss of back wall.</p> <p>ET probe shall be a cross wound driver pickup design.</p> <p>ET technique shall be used 400 KHz</p> <p>Detection with TOFD and ECT enough to consider as defect</p>

Characterization

Tech-ID	Description	Evaluation Method
BMI	<p>TOFD technique shall be used lateral wave and back wall signal to detect the presence of O.D./I.D. defect</p> <p>ET using the c-scan, impedance plane, and strip chart</p> <p>Scan index: circumferential clockwise (2 degree increment)</p>	<p>I.D. surface Indications: A break, or disturbance of the lateral wave</p> <p>I.D. surface Indications (ET): visual changes of C-scan</p> <p>O.D. surface Indications: A break, or perturbation of the back wall signal</p>

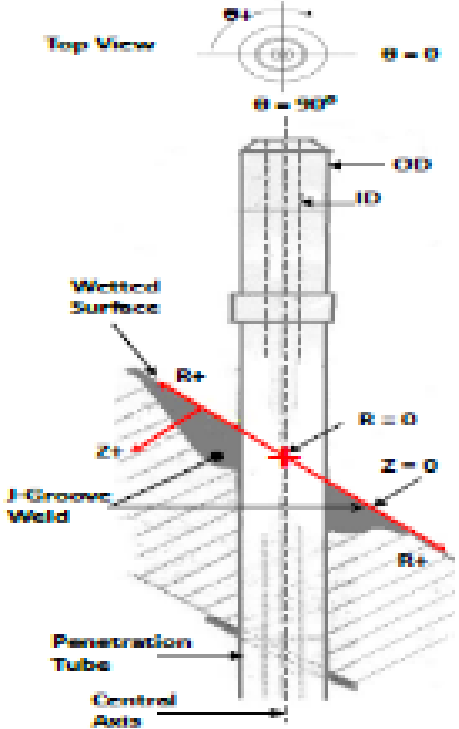
Length Sizing

Tech-ID	Description	Evaluation Method
BMI	<p>TOFD technique shall be used lateral wave and back wall signal to detect the presence of O.D./I.D. length sizing</p> <p>No use ET Technique</p>	<p>Flaw length sizing shall be determined as follows using TOFD techniques.</p> <p>In addition to the broken lateral wave, the diffracted flaw Arc and loss of back wall</p>

Depth Sizing

Tech-ID	Description	Evaluation Method
BMI	<p>Flaw length sizing shall be determined as follows using TOFD techniques.</p> <p>The measured tip response from a defect emanating from the O.D./I.D. surface of the lateral wave.</p>	<p>TOFD technique shall be used lateral wave and back wall signal to detect the presence of O.D./I.D. Depth sizing</p> <p>No use ET Technique</p>

Defect Positioning

Tech-ID	Description	Evaluation Method
BMI	Teams identifying on the reporting data sheets are projected position value from flaw.	<p>P6, P8, P9, P25, P26</p>  <p>θ is measured circumferentially around the Penetration tube</p> <p>R is distance in the R+ direction from the central axis of the penetration tube to a point measured on the wetted surface</p> <p>Z is measured perpendicular to the surface of the J-groove weld</p>

C.15 Procedure 126.2

Procedure ID: **126.2**

Procedure Type: **UT**

Scan Direction: **AXIAL, CIRC**

Length Sizing: **YES**

Team ID: **126**

Scan Access: **O.D.**

Detection: **YES**

Depth Sizing: **YES**

C.15.1 Description for Combining Techniques

- Manually driven, phased array UT used for detection and length/depth sizing of DMW.

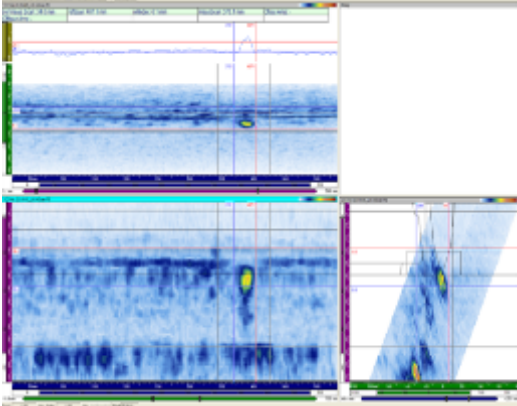
Detection

Tech-ID	Description	Evaluation Method
PA-DMW-Ax PA-DMW-Circ.	<p>Ultrasonic phased array 1.5 MHz, beam steering with fixed refraction angles.</p> <p>Used refraction angle</p> <ul style="list-style-type: none"> • L22.5°, L30°, L37.5°, L45° for axial defects (O.D.<12") • L25°, L35°, L45°, L55° for axial defects (O.D.<12" and O.D.<40") • L30°, L45°, L60° for circ (Nozzle Side) • S45°, S60° for circ (Nozzle Side) • L45°, L60°, L70° for circ (Pipe Side) • S4°5, S60° for circ (Pipe Side) 	<p>Pattern recognition: Stands out from geometrical echoes, has through wall characteristics</p> <p>Evaluation level is noise level</p> <p>Detection with one angle and one direction enough to consider as defect</p>

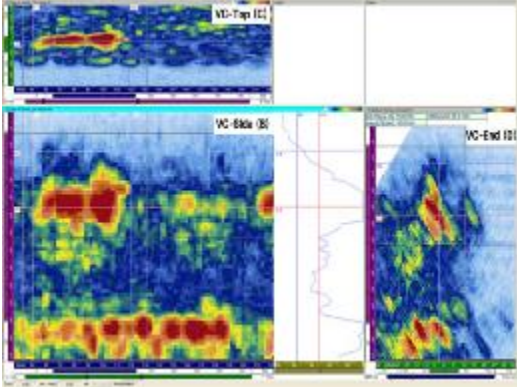
Characterization

Tech-ID	Description	Evaluation Method
PA-DMW-Ax PA-DMW-Circ.	<p>All suspected flaw indications, regardless of amplitude, shall be investigated to the extent necessary to provide accurate characterization, identity, and location.</p> <p>Perform re-evaluations (relooks) with qualified equipment are acceptable.</p>	<p>According to Figure C.2.</p> <p>All suspected flaw indications shall be plotted on a cross sectional drawing of the weld. Indication plots shall accurately identify the specific origin of the reflector.</p>

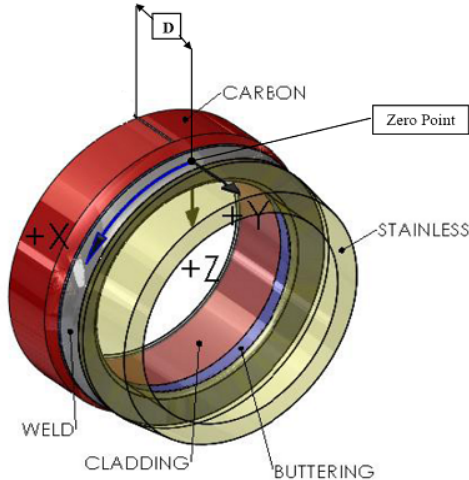
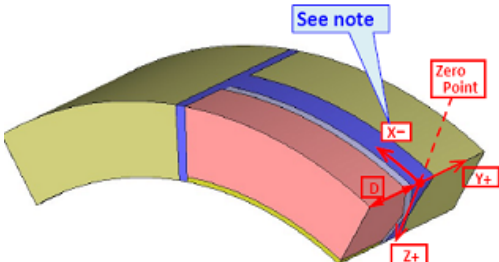
Length Sizing

Tech-ID	Description	Evaluation Method
PA-DMW-Ax PA-DMW-Circ.	<p>Circumferential Flaw</p> <ul style="list-style-type: none"> The technique (wave mode: SW, LW; beam angle: 45°, 60° or 70°) yielding the best response shall generally be used for length sizing. <p>Axial Flaw</p> <ul style="list-style-type: none"> L35 used for length sizing. If not detected with L35, take L25,L45,L55 	<p>Even though detected with opposite beam direction, report length from near side of weld. The end points of flaw shall be determined in each direction until the signal response has diminished into the general background noise (full amplitude drop).</p>  <p style="text-align: center;">Figure C.3 Length Sizing Layout</p>

Depth Sizing

Tech-ID	Description	Evaluation Method
PA-DMW-Ax PA-DMW-Circ.	<p>If tip signal of flaw display, flaw depth is the calculated by subtracting the remaining ligament from the actual material thickness.</p> <p>If tip signal of flaw not display, the amplitude assessment level is 6 dB below the maximum echo height observed at any position along the flaw, rather than at a constant.</p>	<p>Display the merged data groups using the Display Layout Depth Sizing (see Figure C.4) containing the VC-Top (C), VC-Side (B) and VC-End (D) views</p>  <p style="text-align: center;">Figure C.4 Depth Sizing Layout</p> <p>Max differences between extremities of defect in through wall direction</p> <p>Depth sizing for tip-diffraction signal</p> <p>Regardless of analysis method, confirmation of final flaw depth should generally be available with alternative beam angles, beam modes, and/or beam directions</p>

Defect Positioning

Tech-ID	Description	Evaluation Method
PA-DMW-Ax PA-DMW-Circ.	Teams identifying on the reporting data sheets are projected position value from flaw.	P35, P40, P33  P13 

C.16 Procedure 126.3

Procedure ID: **126.3**

Procedure Type: **UT**

Scan Direction: **AXIAL, CIRC**

Length Sizing: **YES**

Team ID: **126**

Scan Access: **O.D.**

Detection: **YES**

Depth Sizing: **YES**

C.16.1 Description for Combining Techniques

- Manual conventional contact pulse echo UT used for detection and length/depth sizing of DMW.

Detection

Tech-ID	Description	Evaluation Method
PE-DMW-Ax PE-DMW-Circ	<p>The primary mode of propagation is shear and longitudinal waves.</p> <ul style="list-style-type: none"> • Shear waves shall primarily be used for the detection of base material flaws (1~1.5 MHz , 45°) • Longitudinal waves shall be used for the detection of flaws within the weld or butter material (1~2.25 MHz, 30°,45°,60°) <p>If Search units with nominal angles $\leq 52^\circ$ designed to produce corner trap responses shall be focused within 75 to 125%T or else 60 to 110%T.</p> <p>Perform Raster scan for axial flaw and CW/CCW Scan for circum flaw.</p>	<p>According to Figure C.2.</p> <p>Evaluation level is noise level.</p>

Characterization

Tech-ID	Description	Evaluation Method
PE-DMW-Ax PE-DMW-Circ	<p>All suspected flaw indications, regardless of amplitude, shall be investigated to the extent necessary to provide accurate characterization, identity, and location.</p> <p>Perform re-evaluations (relooks) with qualified equipment are acceptable.</p>	<p>According to Figure C.2.</p> <p>All suspected flaw indications shall be plotted on a cross sectional drawing of the weld. Indication plots shall accurately identify the specific origin of the reflector.</p>

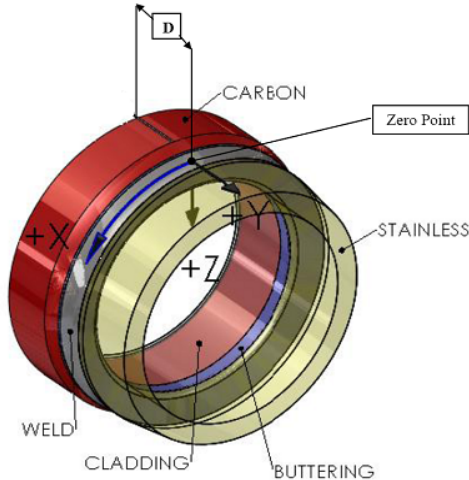
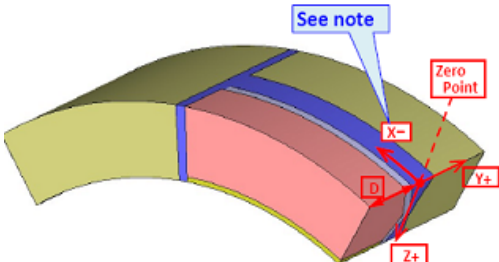
Length Sizing

Tech-ID	Description	Evaluation Method
PE-DMW-Ax PE-DMW-Circ	<p>Adjust the system gain as needed to optimize flaw responses.</p> <p>Maximize the signal response from the flaw indication. Adjust the system gain to 80% FSH.</p>	<p>Even though detected with opposite beam direction, report length from near side of weld.</p> <p>The end points of flaw shall be determined in each direction until the signal response has diminished into the general background noise (full amplitude drop).</p>

Depth Sizing

Tech-ID	Description	Evaluation Method
PE-DMW-Ax PE-DMW-Circ	<p>If tip signal of flaw display, flaw depth is the calculated by subtracting the remaining ligament from the actual material thickness.</p> <p>If tip signal of flaw not display, the amplitude assessment level is 6 dB below the maximum echo height observed at any position along the flaw, rather than at a constant.</p>	<p style="text-align: center;">Absolute Arrival Time Technique</p> <p style="text-align: center;"> T = Material Thickness H = Flaw Height RL = Remaining Ligament </p> <p style="text-align: center;"> Step 1. Locate base of flaw Step 2. Move forward up face of flaw to flaw tip </p> <p style="text-align: center;">-6 dB drop from maximum technique</p>

Defect Positioning

Tech-ID	Description	Evaluation Method
PE-DMW-Ax PE-DMW-Circ	Teams identifying on the reporting data sheets are projected position value from flaw.	P35, P40, P33  P13 

C.17 Procedure 126.4

Procedure ID: **126.4**

Procedure Type: **UT**

Scan Direction: **AXIAL, CIRC**

Length Sizing: **YES**

Team ID: **126**

Scan Access: **O.D.**

Detection: **YES**

Depth Sizing: **YES**

C.17.1 Description for Combining Techniques

- Manual Phased Array UT used for detection and length/depth sizing of WOL.

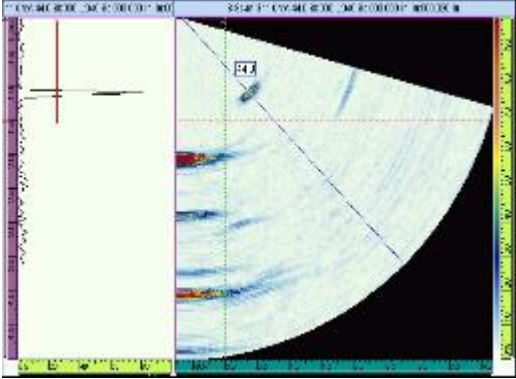
Detection

Tech-ID	Description	Evaluation Method
PA-WOL-Circ. PA-WOL-Ax	<p>Used Ultrasonic phased array 2.0 MHz, Sectorial Scan Exam Angle Range</p> <ul style="list-style-type: none"> • 0° to 25°: Searched the weld overlay to base material interface(lack of bond) or within the volume of the weld overlay material(lack of fusion) • 25° to 80°: Entire flaw within the volume of the weld overlay material or near the inside surface of the original base material. 	<p>According to Figure C.2. Evaluation level is noise level</p>

Characterization

Tech-ID	Description	Evaluation Method
PA-WOL-Circ. PA-WOL-Ax	<p>All suspected flaw indications, regardless of amplitude, shall be investigated to the extent necessary to provide accurate characterization, identity, and location.</p> <p>Perform re-evaluations (relooks) with qualified equipment are acceptable.</p>	<p>According to Figure C.2. All suspected flaw indications shall be plotted on a cross sectional drawing of the weld. Indication plots shall accurately identify the specific origin of the reflector.</p>

Length Sizing

Tech-ID	Description	Evaluation Method
PA-WOL-Circ. PA-WOL-Ax	<p>Circumferential Flaw</p> <ul style="list-style-type: none"> The technique (wave mode: LW, Sectorial scan of beam angle: 0°~ 75°) <p>Axial Flaw</p> <ul style="list-style-type: none"> The technique (wave mode: LW, Sectorial scan of beam angle: 0°~ 80°) 	<p>Maximize the signal response from the flaw indication.</p> <div style="text-align: center;">  </div> <p style="text-align: center;">Figure C.5. Sectorial Scan</p> <p>The length of flaws shall be determined by scanning along the length of the flaw in each direction until the signal response in the A-scan has diminished into the general background noise (full amplitude drop) or the image response in the S-scan has diminished into the general image background noise.</p>

Depth Sizing

Tech-ID	Description	Evaluation Method
PA-WOL-Ax PA-WOL-Circ.	<p>Flaw depth sizing shall be performed utilizing the Absolute Arrival Time Technique.</p> <p>This technique relies upon obtaining direct signal responses (diffraction) from the flaw tip. The amount of unflawed material, or remaining ligament, is then read directly from either the A-scan and/or S-scan presentations.</p>	<p>Prior to performing final depth sizing efforts, the time base accuracy for the angle(s) that provide the most favorable flaw tip responses should be verified at a depth comparable to the estimated flaw depth. Adjustments to the system probe delay should be performed as needed.</p> <p>Max differences between extremities of defect in through wall direction.</p> <p>Depth sizing for tip-diffraction signal.</p>

C.18.1 Description for Combining Techniques

- Automatic UT(TOFD) & ET used for detection and length/depth sizing of BMI.

Detection

Tech-ID	Description	Evaluation Method
BMI	<p>BMI nozzle I.D. side inspection at axial scan</p> <ul style="list-style-type: none"> • TOFD technique shall be used lateral wave and back wall signal to detect the presence of O.D./I.D. defect. • TOFD technique shall be used 6 MHz • TOFD technique shall be used 2 channel (Axial shooting TOFD, Circumferential shooting TOFD) • ET shall be detection for surface or near surface indications • P6, P8, P9, P25, P26 for defects 	<ul style="list-style-type: none"> • TOFD Select channel, display mode to analyze (axial shooting the B-scan (TOPS), circumferential shooting TOFD channel: D-scan) • Investigate any areas with a loss of the lateral wave for tip signals and or loss of back wall. • ET probe shall be a cross wound driver pickup design. • ET technique shall be used 400 kHz • Detection with TOFD and ECT enough to consider as defect

Characterization

Tech-ID	Description	Evaluation Method
BMI	<ul style="list-style-type: none"> • TOFD technique shall be used lateral wave and back wall signal to detect the presence of O.D./I.D. defect • ET using the S-scan, impedance plane, and strip chart • Scan index: circumferential clockwise (2 degree increment) 	<ul style="list-style-type: none"> • I.D. surface Indications: A break, or disturbance of the lateral wave • I.D. surface Indications (ET): visual changes of C-scan • O.D. surface Indications: A break, or perturbation of the back wall signal

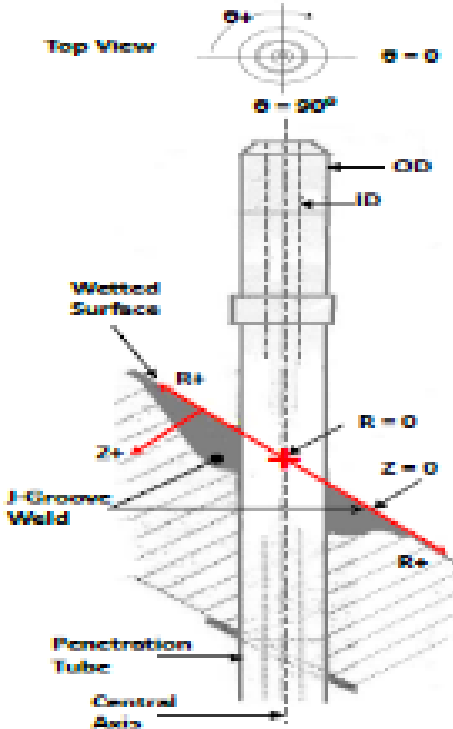
Length Sizing

Tech-ID	Description	Evaluation Method
BMI	<ul style="list-style-type: none"> • TOFD technique shall be used lateral wave and back wall signal to detect the presence of O.D./I.D. length sizing • No use ET Technique 	<ul style="list-style-type: none"> • Flaw length sizing shall be determined as follows using TOFD techniques. • In addition to the broken lateral wave, the diffracted flaw arc and loss of back wall

Depth Sizing

Tech-ID	Description	Evaluation Method
BMI	<ul style="list-style-type: none"> Flaw length sizing shall be determined as follows using TOFD techniques. The measured tip response from a defect emanating from the O.D./I.D. surface of the lateral wave. 	<ul style="list-style-type: none"> TOFD technique shall be used lateral wave and back wall signal to detect the presence of O.D./I.D. depth sizing No use ET Technique

Defect Positioning

Tech-ID	Description	Evaluation Method
BMI	Teams identifying on the reporting data sheets are projected position value form flaw.	<p>P6, P8, P9, P25, P26</p>  <ul style="list-style-type: none"> θ is measured circumferentially around the Penetration tube R is distance in the R+ direction from the central axis of the penetration tube to a point measured on the wetted surface Z is measured perpendicular to the surface of the J-groove weld

C.19 Procedure 128.1

Procedure ID: **128.1**
 Procedure for Encoded, Phased Array
 Ultrasonic Examination of Dissimilar
 Metal Piping Welds
 Zetec OmniScanPA-03-rev A

Team ID: **128**

Procedure Type: **UT Phased Array**

Scan Access: **O.D.**

Scan Direction: **CIRC** and **AXIAL**

Detection: **YES**

Length Sizing: **YES (only circ. flaws)**

Depth Sizing: **YES**

C.19.1 Description for Combining Techniques

- UT Phased Array for detection, characterization and sizing.
- Tip-diffraction for through-wall sizing (TWS) and “last maxima technique for TW-estimation” is used.

Detection

Tech-ID	Description	Evaluation Method
UT Phased Array Circ. and Axial	Ultrasonic phased array 1.5 MHz, beam steering with fixed refraction angles. Reflection technique. <ul style="list-style-type: none"> • Circumferential flaws linear scan L45°, L60°, L70°, S45°, and S60° • Axial flaws sectorial scan L25°, L35°, L45°, L55°, S35°, S45°, and S55°; skew -25° to +25°, step 2.5° 	Based on pattern recognition <ul style="list-style-type: none"> • Evaluation level is noise level • Pattern recognition: Stands out from geometrical echoes, has through wall characteristics • Detection with one angle and one direction enough to consider as defect

Characterization

Tech-ID	Description	Evaluation Method
UT Phased Array Circ. and Axial	Ultrasonic phased array 1.5 MHz, beam steering with fixed refraction angles. Reflection technique <ul style="list-style-type: none"> • L45° for circumferential flaws • L35° for axial flaws 	Based on TW position of corner echo/lower signal <ul style="list-style-type: none"> • Makes a difference between Geometrical-, Material- and Flaw Indications (section 9.3.1) • Characterized as surface breaking if corner echo/lower signal closer than 5 mm from nominal back wall

Length Sizing

Tech-ID	Description	Evaluation Method
UT Phased Array Circ.	Ultrasonic phased array 1.5 MHz, beam steering with fixed refraction angles. Reflection technique <ul style="list-style-type: none"> • Circumferential flaws SW and/or LW, 45°, 60°, 70° • The best signal response shall generally be used 	Differences between extremity of defect positions <ul style="list-style-type: none"> • “Full amplitude drop method”, Evaluation down to noise level for longitudinal defects. • No length sizing for Axial defects, because the procedure is not qualified for this.

Depth Sizing

Tech-ID	Description	Evaluation Method
UT Phased Array Circ. and Axial	Ultrasonic phased array 1.5 MHz, beam steering with fixed refraction angles. Diffraction technique or last maxima technique <ul style="list-style-type: none"> • Circumferential flaws L45°, L60°, and L70° • Angle that provides the best tip signal or L45° 	Evaluation of each scan line searching for diffracted signal or DRM (deeper relative maximum) <div style="text-align: center; margin: 10px 0;"> </div> <ul style="list-style-type: none"> • Circumferential flaws depth sizing with L45°, L60°, and L70°. Take for final value 1: Tip signal, 2: DRM • Axial flaws depth sizing with L25° and L45°. Take for final value 1: Tip signal, 2: DRM. If all angles/directions show same response take deepest size.

Defect Positioning

Tech-ID	Description	Evaluation Method
UT Phased Array Circ. and Axial	Ultrasonic phased array 1.5 MHz, beam steering with fixed refraction angles. Previous described techniques <ul style="list-style-type: none"> • Longitudinal defects plain geometry L45° and L60° • Axial defects L25° and L35° See Ref. 9.3.3 in IP	Based on previous described methodology for detection, length and height sizing <ul style="list-style-type: none"> • X positions are as per position from length sizing for defects along weld • Y positions, across defect, is taken from length sizing technique at max amplitude for defects along weld • Y positions are as per position from detection for defects with axial orientation • X positions, across defect, is taken from height sizing technique at max amplitude for defects with axial orientation • Z positions, through wall position is directly taken from height sizing and characterization, wall thickness

C.20 Procedure 134.1 and 134.2

Procedure ID: **134.1 and 134.2**

Team ID: **134**

Procedure Type: **UT**

Scan Access: **O.D.**

Scan Direction: **AXIAL, CIRC.**

Detection: **YES**

Length Sizing: **YES**

Depth Sizing: **YES**

C.20.1 Description for Combining Techniques

- Manual conventional contact pulse echo UT used for detection and length/depth sizing of DMW.

Detection

Tech-ID	Description	Evaluation Method
PE Axial & Circ.	The primary mode of propagation is longitudinal waves. (1~5MHz, 35,45,60,70°) Use of focusing transducers based on each thickness range (upper, middle, lower). Perform the skewed scan for axial flaw and CW/CCW Scan for circum flaw	In accordance with the Figure C.2. Evaluation of signals exceeding the the signal to noise ratio of 2:1.

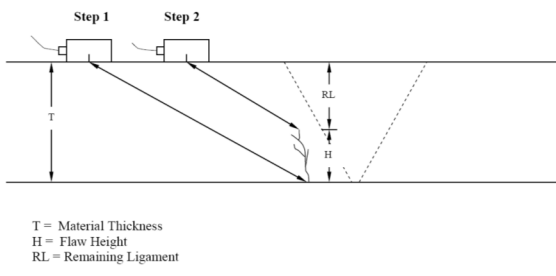
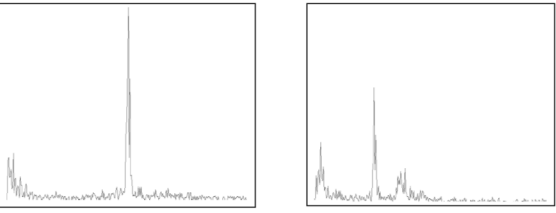
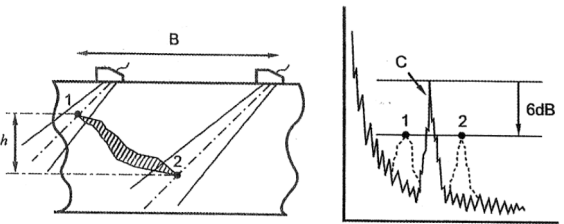
Characterization

Tech-ID	Description	Evaluation Method
PE Axial & Circ.	All suspected flaw indications, regardless of amplitude, were investigated to the extent necessary to provide accurate characterization, identity, and location.	In accordance with the Figure C.2. All suspected flaw indications were plotted on a cross sectional drawing of the weld. Indication plots were accurately identified the specific origin of the reflectors.

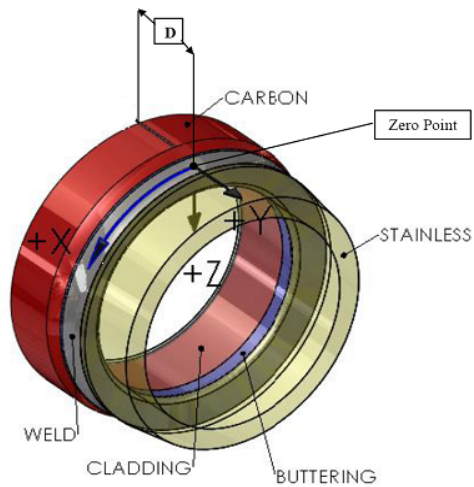
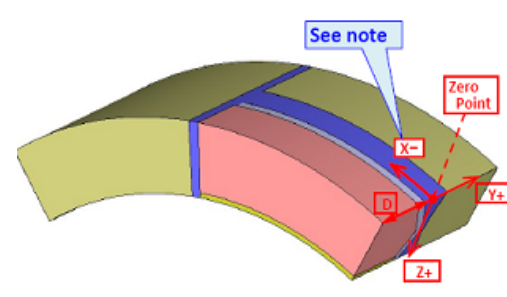
Length Sizing

Tech-ID	Description	Evaluation Method
PE Axial & Circ.	Adjust the system gain as needed to optimize the flaws. Maximize the signal response from the flaws. Adjust the system gain until this response is 80 % FSH.	Although the flaw is detected at both sides of weld, the length is reported from the near side of weld. The end points of flaws were determined in each direction until the signal response is diminished to 20% FSH (12drop).

Depth Sizing

Tech-ID	Description	Evaluation Method
PE Axial & Circ.	If the tip signal of flaw is displayed, flaw depth is calculated by subtracting the remaining ligaments from the actual material thickness. If the tip signal of flaws not displayed, the amplitude assessment level is 6 dB below the maximum echo height observed at any position along the flaw.	<p style="text-align: center;">Absolute Arrival Time Technique</p>  <p style="font-size: small;">T = Material Thickness H = Flaw Height RL = Remaining Ligament</p>  <p style="font-size: x-small;">Step 1. Locate base of flaw Step 2. Move forward up face of flaw to flaw tip</p> <p style="text-align: center;">-6 dB drop from maximum technique</p> 

Defect Positioning

Tech-ID	Description	Evaluation Method
PE Axial & Circ.	Identified data are reported from the reference position.	<p>P33, P35, P40</p>  <p>P13</p> 

C.21 Procedure 135.1

Procedure ID: **135.1**

Team ID: **135**

Procedure Type: ECT

Scan Access: **I.D.**

Scan Direction: **CIRC.**

Detection: **YES**

Length Sizing: **YES**

Depth Sizing: **NO**

C.21.1 Description for Combining Techniques

Detection

Tech-ID	Description	Evaluation Method
135-ECT1	<p>ECT technique based on eddy current signal from a defect using Multi cross coil probe (16 cross coils).</p> <ul style="list-style-type: none"> • Frequency: mainly 400 kHz • (Frequency range: 50 kHz ~ 1 MHz) <p>Sampling pitch along circumferential direction is less than 0.5 mm.</p> <p>Sampling pitch along axial direction is 2.75 mm.</p>	<p>Based on signal to noise ratio (SNR). Evaluation of signals with SNR larger than 2.</p> <p>400 kHz frequency data are mainly used for detection.</p>

Characterization

Tech-ID	Description	Evaluation Method
135-ECT1	<p>ECT technique based on eddy current signal from a defect using Multi cross coil probe (16 cross coils).</p> <ul style="list-style-type: none"> • Frequency: mainly 400 kHz • (Frequency range: 50 kHz ~ 1 MHz) <p>Sampling pitch along circumferential direction is less than 0.5 mm.</p> <p>Sampling pitch along axial direction is 2.75 mm.</p>	<p>Characterization is carried out by considering signal amplitude and phase of multi frequencies.</p>

Length Sizing

Tech-ID	Description	Evaluation Method
135-ECT1	<p>ECT technique based on eddy current signal from a defect using Multi cross coil probe (16 cross coils).</p> <ul style="list-style-type: none"> • Frequency: mainly 400 kHz • (Frequency range: 50 kHz ~ 1 MHz) <p>Sampling pitch along circumferential direction is less than 0.5 mm.</p> <p>Sampling pitch along axial direction is 2.75 mm.</p>	<p>Based on the signal amplitude exceed noise level.</p> <p>Defect length will be determined by measuring length of area with S/N ratio lager than 1.</p> <p>400 kHz frequency data are mainly used for length sizing.</p>

Depth Sizing

Tech-ID	Description	Evaluation Method
N/A	N/A	N/A

Defect Positioning

Tech-ID	Description	Evaluation Method
135-ECT1	<p>ECT technique based on eddy current signal from a defect using multi cross coil probe (16 cross coils).</p> <ul style="list-style-type: none"> • Frequency: mainly 400 kHz • (Frequency range: 50 kHz ~ 1 MHz) <p>Sampling pitch along circumferential direction is less than 0.5 mm.</p> <p>Sampling pitch along axial direction is 2.75 mm.</p>	<p>Based on previously described methodology for detection and length sizing:</p> <p>For axial defects;</p> <ul style="list-style-type: none"> • Y positions, along defect, are taken from length sizing. • Y position is determined based on maximum and minimum of Y-axis value of defect signal. • X positions, across defect, are taken from length sizing. • X position is determined based on maximum and minimum of X-axis value of defect signal. • Ymax is determined from maximum defect signal. • Xmax position, across defect, is taken from maximum defect signal. <p>For circumferential defects;</p> <ul style="list-style-type: none"> • X positions, along defect, are taken from length sizing. • X position is determined based on maximum and minimum of X-axis value of defect signal. • Y positions, across defect, are taken from length sizing. • Y position is determined based on maximum and minimum of Y-axis value of defect signal. • Xmax is determined from maximum defect signal. • Ymax position, across defect, is taken from maximum defect signal.

C.22 Procedure 144.1

Procedure ID: **144.1**

Team ID: **144**

MPP-01 Procedure for mechanized Ultrasonic (UT) and Eddy Current (ET) Inspection of the Inlet and Outlet Nozzle Connection Welds.

Procedure Type: **ET and UT Pulse Echo**

Scan Access: **I.D.**

Scan Direction: **AXIAL and CIRC.**

Detection: **YES**

Length Sizing: **YES**

Depth Sizing: **Yes (not of embedded flaws)**

C.22.1 Description for Combining Techniques

- **Detection** shall be performed using a combination of both UT and ET techniques. ET will be used for detection of fatigue type defects and those clearly open to the surface and both ET and UT will be used for detection of those defects with partially intact ligaments, namely IDSCC.
- **Characterization** between surface breaking and embedded will be performed using ET.
- **Sizing:** Any defect that is characterized as surface breaking shall be *sized for length* using ET and/or UT. Any defect that is characterized as surface breaking shall also be *sized for height* using UT.

Detection

Tech-ID	Description	Evaluation Method	
ET Circ and axial	ET 200 KHz Driver/Pickup probe with ferrite core	Has an amplitude ≥ 0.9 V on at least one scan line Has a phase of $90^\circ \pm 20^\circ$ or $270^\circ \pm 20^\circ$ Has a crack like signal (refer to calibration signal)	
UT Pulse Echo Circ and axial	55°TRL2-Aust FD 10 mm 45°TRL2-Aust FD 25 mm	Long defects:	Amplitude ≥ 4 dB above noise on 3 or more consecutive scan lines (equivalent to 4 mm)
		Trans defects:	Amplitude above noise on 7 or more consecutive scan lines (equivalent to 6 mm)

Characterization

Tech-ID	Description	Evaluation Method
ET Circ and axial	ET 200 KHz Driver/Pickup probe with ferrite core	<p>Has an amplitude ≥ 0.9 V on at least one scan line</p> <p>Has a phase of $90^\circ \pm 20^\circ$ or $270^\circ \pm 20^\circ$</p> <p>Has a crack like signal (refer to calibration signal)</p>

Length Sizing

Tech-ID	Description	Evaluation Method
ET Circ and axial	ET 200 KHz Driver/Pickup probe with ferrite core	<p>Down to noise level</p> <p>The length of a defect shall be determined by measuring the distance between the first and last crack like signal in the direction of the defect.</p> <p>Indications along the same line with a distance smaller than the measured length of the shortest indication shall be regarded as one single defect.</p>
UT Pulse Echo Circ and axial	55°TRL2-Aust FD 10 mm	<p>Down to noise level</p> <p>The length of a defect shall be determined by measuring the distance between the first and last position where the defect-like signal is discernible from the noise.</p> <p>Where the length measurements from two beam directions differ, the longest length shall be reported.</p> <p>Indications along the same defect axis with a distance between them of ≤ 10 mm shall be regarded as one single defect.</p>

Depth Sizing

Tech-ID	Description	Evaluation Method
UT Pulse Echo Circ and axial	55°TRL2-Aust FD 10 mm 45°TRL2-Aust FD 25 mm	Pulse Echo Tip Diffraction. <ul style="list-style-type: none"> • If a clear lower tip is identified at a depth of < 16 mm, the results from the 55TRL FD10 shall be reported. Where the depth is measured from both beam directions the deepest depth shall be used. • If a clear lower tip is identified at a depth of ≥ 16 mm, the results from the 45TRL FD25 shall be reported. Where the depth is measured from both beam directions the deepest depth shall be used. • Where depth measurements from both probe types are just within their applicable depth zones, the depth from the probe with the focal depth closest to the measured depth shall be used. If no tip responses are evident in the zone specified for the applicable probe, tip responses from the other probe shall be reported.

Defect Positioning

Tech-ID	Description	Evaluation Method
ET Circ and axial	ET 200 KHz Driver/Pickup probe with ferrite core.	X-axis Position <ul style="list-style-type: none"> • For longitudinal defects, the start and end X coordinates are the positions obtained during the length sizing process. • The X co-ordinates shall be reported from the probe/technique used to report the defect length. • For transverse defects, the X coordinate of the maximum response obtained during the ET detection/characterization process shall be reported. Y-axis Position <ul style="list-style-type: none"> • For transverse defects, the start and end Y coordinates are the positions obtained during the length sizing process. • The Y co-ordinates shall be reported from the probe/technique used to report the defect length. • For longitudinal defects, the Y coordinate of the maximum response obtained during the ET detection/characterization process shall be reported.
UT Pulse Echo Circ and axial	55°TRL2-Aust FD 10 mm 45°TRL2-Aust FD 25 mm	

APPENDIX D

SCORING PROCEDURE USED FOR PINC

APPENDIX D

SCORING PROCEDURE USED FOR PINC

This section describes how inspection results were compared to the true state of the DMW and BMI test blocks. Specifically, this section describes (1) the method used to determine whether or not an individual flaw was detected; (2) if the flaw was detected, what depth and length size should be assigned to it; (3) unintended defects (flaws that occurred during the test block fabrication process that were not intended to be part of the test block); and (4) the methodology used to determine false calls (i.e., indications not associated with any known flaw).

Scoring merges the inspection results with the true-state results by associating inspection indications with true-state flaws. The scoring procedure is summarized by the flowchart in Figure D.1.

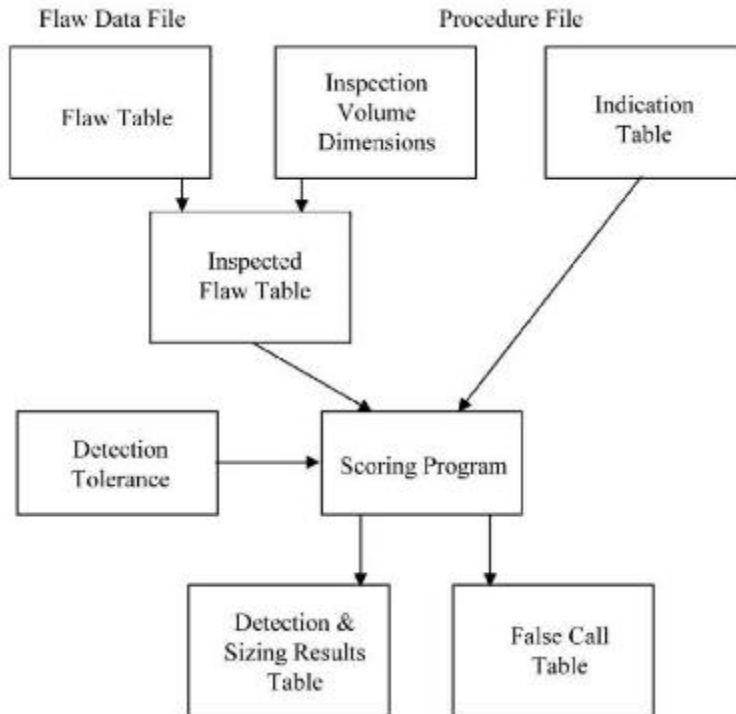


Figure D.1 Scoring Procedure for PINC Round Robins

The first step of the scoring process consisted of uniquely identifying the flaws in the inspected volume of the weld. For this analysis, a table of flaws was developed for each test specimen. The *inspection volume* field indicated in the portable document format file record for inspections was then compared with the flaw table for each specimen to determine which flaws fell within the inspected volume. These flaws are then placed in the *inspected flaw table*.

The next step of the scoring process compared the entries in the *inspected flaw table* to the entries in the *indication table* (the indications that were recorded on inspection data sheets) to determine which flaw cuboids intersected with which indication cuboids.

A tolerance box was defined around each flaw to account for possible location error. Figure D.2 shows the POD versus size of tolerance for the DMW round robin, and Figure D.3 shows the same information for the BMI round-robin results. As can be seen in Figures D.2 and D.3, there is not much improvement in detection for tolerances larger than 10 mm. The exception is for the tube examinations of the BMI samples, which have closely spaced flaws. Therefore, for the analysis used in this report, a tolerance box of 10 mm was used to score the DMW and BMI results. Without use of a tolerance box, location errors might be misclassified as non-detections. Once the tolerance is defined, AX, AY, and AZ, then the flaw cuboid, X1, X2; Y1, Y2; Z1, Z2, becomes

$$(X_1 - \delta X, X_2 + \delta X, Y_1 - \delta Y, Y_2 + \delta Y, Z_1, Z_2) \tag{D.1}$$

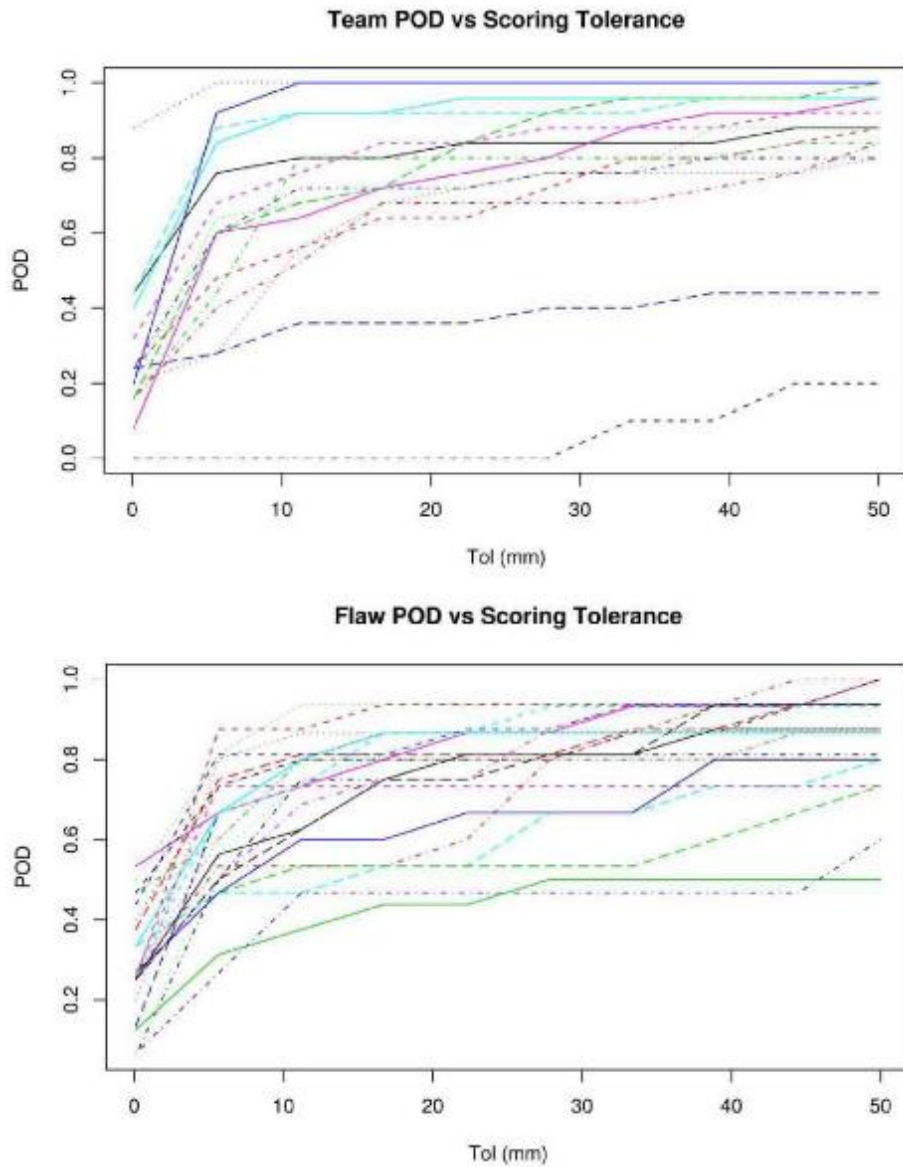


Figure D.2 Probability of Detection versus Scoring Tolerance for Teams and Flaws for DMW Round Robin

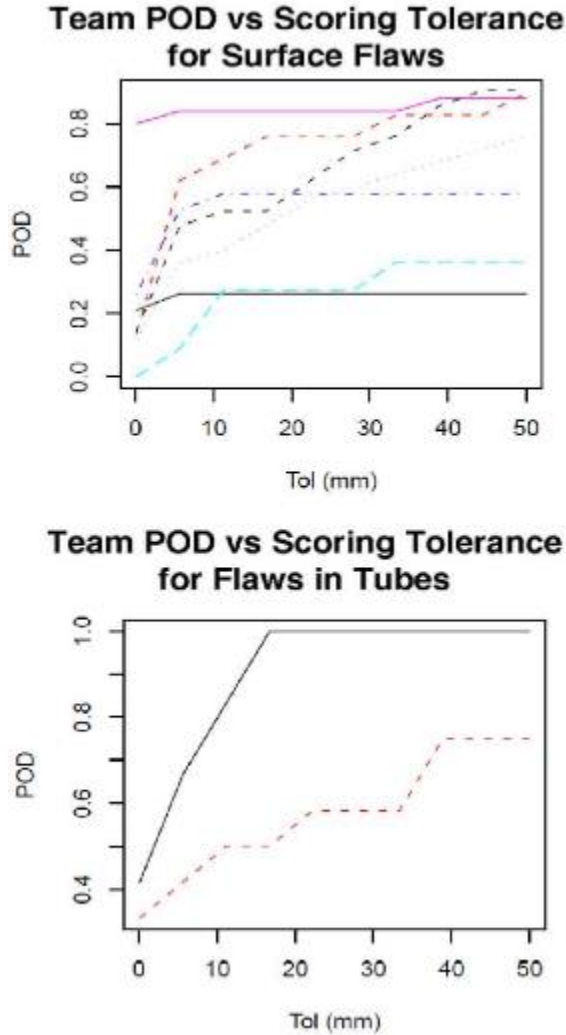


Figure D.3 Probability of Detection versus Scoring Tolerance for All Teams and Flaws in BMI Round Robin

A list of all indications not intersecting with any flaws was compiled and was termed the *false call table*. The *false call table* was compiled after the intersecting flaw-indication cuboids had been identified for each indication.

The scoring process therefore resulted in two outputs—the detection of flaws, including the length and through-wall depth determined for each flaw, and a list of false calls.

Finally, detection and sizing information were appended to all flaws in the *inspected flaw table*, using the intersection information, to produce the *detection and sizing results table*.

D.1 Definitions of False Call Probability and Probability of Detection

False call probability (FCP) and POD quantify inspection performance on blank (unflawed) versus flawed material. The FCP is the probability that an inspector will call a flaw in a blank unit of material, while POD is the probability that an inspector will call a flaw in a flawed unit of material. With these definitions, (FCP, POD) measure the capability for inspection to correctly classify units

of material as unflawed or flawed. Another equivalent term for FCP is false positive probability while POD is equivalent to 1 minus false negative probability.

POD is frequently expressed as a function of various flaw, material, or inspection variables that might affect detection performance. For example, in PINC, POD is considered to be a function of flaw size, so the expression POD(S) is used to represent the probability of calling a detection in a unit of material than contains a flaw of size S.

One would expect POD(S) to be a monotonically increasing function of flaw size S. Also, one should note that using the FCP as the POD for a flaw of size zero (POD(0) = FCP) follows from the definition of FCP and POD. When the S = 0 point is included on the POD curve, this curve provides the most basic description of inspection efficacy. An inspection that is no more effective than guessing will have a flat POD curve. More specifically, if the POD for flaws of size S is equal to FCP, (POD(S) = FCP) then flaws of this size aren't really being detected by the inspection procedure.

To be able to calculate FCP and POD, one has to define the applicable unit of material. We call this unit of material the grading unit; in other words, each grading unit in the round-robin study will generate a detection statistic when inspected. For inspection of dissimilar metal weldments, the ideal grading unit would be an entire weld, but a round-robin test that used whole weldments as the experimental unit would be too costly. Due to cost constraints, the grading unit used is the length of a flaw plus an allowance for sizing error.

To produce unbiased estimates of FCP and POD, the blank and flawed grading units must be identical in all important respects (except that the flawed grading units contain a flaw). Also, if multiple grading units are to be placed in a single weldment, they must be separated from each other by a sufficient distance. These constraints caused problems in defining blank grading units in the PINC specimens. Since reasonable blank grading units could not be defined, we constructed a probability model (described in the next section), to estimate FCP from available PINC false call statistics.

D.2 Calculation of FCP

In the PINC inspections, a false call is defined as a call that does not intersect with a flawed grading unit. These false calls were used to estimate a false call rate, λ_{fc} (false calls per meter)

$$\lambda_{fc} = \frac{\text{\#False Calls}}{\text{Length of Material Inspected}} \quad (\text{D.2})$$

Using this rate and the assumption that false calls are randomly (i.e., Poisson) distributed one can then calculate the probability that a call would intersect a blank grading unit of length L_{gu} . Assuming that the average length of a false call is L_{fc} , the probability of a false call intersecting the grading unit is

$$\text{FCP} = \text{Pr(Grading Unit Intersection)} = 1 - \exp\left(-\lambda_{fc} (L_{gu} + L_{fc})\right) \quad (\text{D.3})$$

D.3 Logistic Regression Model for POD

In PINC, a logistic regression model was used to relate POD to flaw size, S. Flaw size represents either depth or length. The logistic regression model is given by

$$\text{POD}(S) = \text{logistic}(\beta_1 + \beta_2 S) \quad (\text{D.4})$$

where $\beta = (\beta_1, \beta_2)$ are unknown parameters to be determined by the regression algorithm and the function, $\text{logistic}(x)$ is defined as

$$\text{logistic}(x) = \frac{1}{1 + \exp(-x)} \quad (\text{D.5})$$

Estimates produced by the algorithm are maximum-likelihood estimates. The regression fits included data for flaw size zero (i.e., the FCP estimates described in the last section). In the regression fit plots, you will sometimes see a data point at $S = 0$ and that represents false call data.

D.4 Scoring Example for Single Flaws

For all inspections of the DMW test blocks and the inspections of the weld surface of the BMI test blocks, the scoring was performed using a 10-mm scoring box. This section presents the scoring results for a single inspection, so the reader can more easily understand the scoring process. The example used is an inspection of test block 2.9.

This test block was selected because it contains each type of scoring situation, including missed flaws, false calls, and hits on poorly documented flaws. The team has inspected the entire block (and this is the case for almost all inspections in the round robin), so all flaws in the block should be included in the scoring procedure. The indications called by the inspection team (using their labeling system) are summarized in Table D.1.

The scoring result is summarized visually by Figure D.4. Figure D.4 shows the results in the X, Y plane, the plane most relevant to our scoring definition. The locations of the indications called by the inspection team are shown as black rectangles in Figure D.4. The test block contains 12 flaws used for scoring (shown in red) and 2 poorly documented flaws that were not intentionally placed in the test block for the PINC studies but still are detectable (shown in blue). When the intersections between the called indications and the actual flaw locations are compared, one can determine how well the team performed.

Table D.1 Test Block PINC 2.9 Inspection Results

Indication ID	X1, mm	X2, mm	Y1, mm	Y2, mm	Z1, mm	Z2, mm	X max, mm	Y max, mm	Z max, mm
1	51	86	-7	-7	16	43	75	1	51
1a	66	108	19	19	35	43	81	2	66
2	163	190	-19	-19	37	43	176	3	163
3	271	304	-18	-18	31	43	298	4	271
4	375	439	14	14	28	43	412	5	375
5	496	527	-1	-1	28	43	513	6	496
6	686	732	-9	-9	27	43	708	7	686
7	787	807	-18	-18	37	43	798	8	787
8	860	880	-5	-5	37	43	870	9	860
9	972	999	-4	-4	36	43	979	10	972
10	1047	1067	-18	-18	38	43	1058	11	1047
11	1105	1125	-4	-4	35	43	1111	12	1105
12	1173	1201	-6	-6	20	43	1180	13	1173

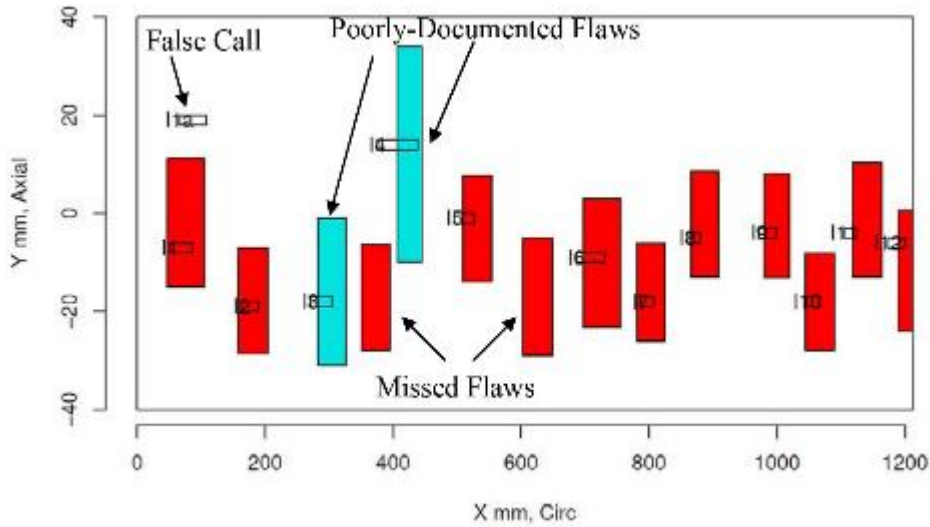


Figure D.4 Scoring Inspection Results of Test Block 2.9 with 10-mm Tolerance

The scored results are presented in Table D.2 (detection results). In Table D.2, each row describes a flaw in the block. From Table D.2, we see that Flaws 9.8 and 9.9 were not detected, while flaws 9.1–9.7 and 9.10–9.14 were detected and are scored as hits, and the supplied lengths and depths were used to evaluate the length and depth sizing capabilities of the technique. Both of the poorly documented flaws were detected but are not used for depth or length sizing. Missing the poorly documented flaws would not have been counted against the inspection because the exact locations of the poorly documented flaws are not known.

The team conducting the examination successfully detected ten of the flaws used for scoring and both poorly documented flaws. Additionally, the team missed two flaws and made one false call.

Table D.2 Detection Results for Sample Inspection of PINC Test Block 2.9

Flaw No.	Detection: 0 = no 1 = yes	X1, mm	X2, mm	Indication ID from Data Sheet of Team 67
F9.1	1	57.3	95.6	1
F9.2	1	518.7	544.3	5
F9.3	1	707.4	745.7	6
F9.4	1	875.8	898.8	8
F9.5	1	990.3	1010	9
F9.6	1	1128	1154	11
F9.7	1	168.4	194	2
F9.8	0	360.4	386	N/A
F9.9	0	613.1	638.6	N/A
F9.10	1	1054	1080	10
F9.11	1	791.6	814.6	7
F9.12	1	1199	1225	12
F9.13*	1	293	317	4
F9.14*	1	417	435	3

N/A = Not applicable.

*Not used for POD or sizing (see page 2.39 of NUREG/CR-7019).

D.5 Scoring Process for Multiple Closely Spaced Cracks

As the Data Analysis Task Group (DAG) reviewed the data from the PINC round-robin exercise, members of the DAG recognized that the test blocks used in the BMI did not contain a single crack; rather, the test blocks contained multiple cracks. In fact, many cracks in the test blocks used for the PINC BMI were close together. The DAG decided to analyze the PINC BMI data using a set of proximity rules that would account for the multiple flaws in the test blocks.

The DAG used the American Society of Mechanical Engineers (ASME) Section XI IWA-3400 rules for linear surface flaws to account for the multiple flaws that were close together. The scoring process was the same as that described in Section D.1.

Section XI, IWA-3400 of the ASME Code states the following:

- (a) Linear flaws detected by surface (PT/MT) or volumetric (RT) examination methods shall be considered single linear surface flaws provided the separation distance between flaws is equal to or less than the dimension S, where S is determined as shown in Figure IWA-3400-1.
- (b) The overall length of a single and discontinuous linear flaw shall be determined as shown in Figure IWA-3400-1.

Figure D.5 is a reproduction of IWA-3400-1 to show the methodology used to determine whether multiple flaws in a PINC BMI test block should be combined as one flaw with length or whether the flaws should be considered as single individual flaws.

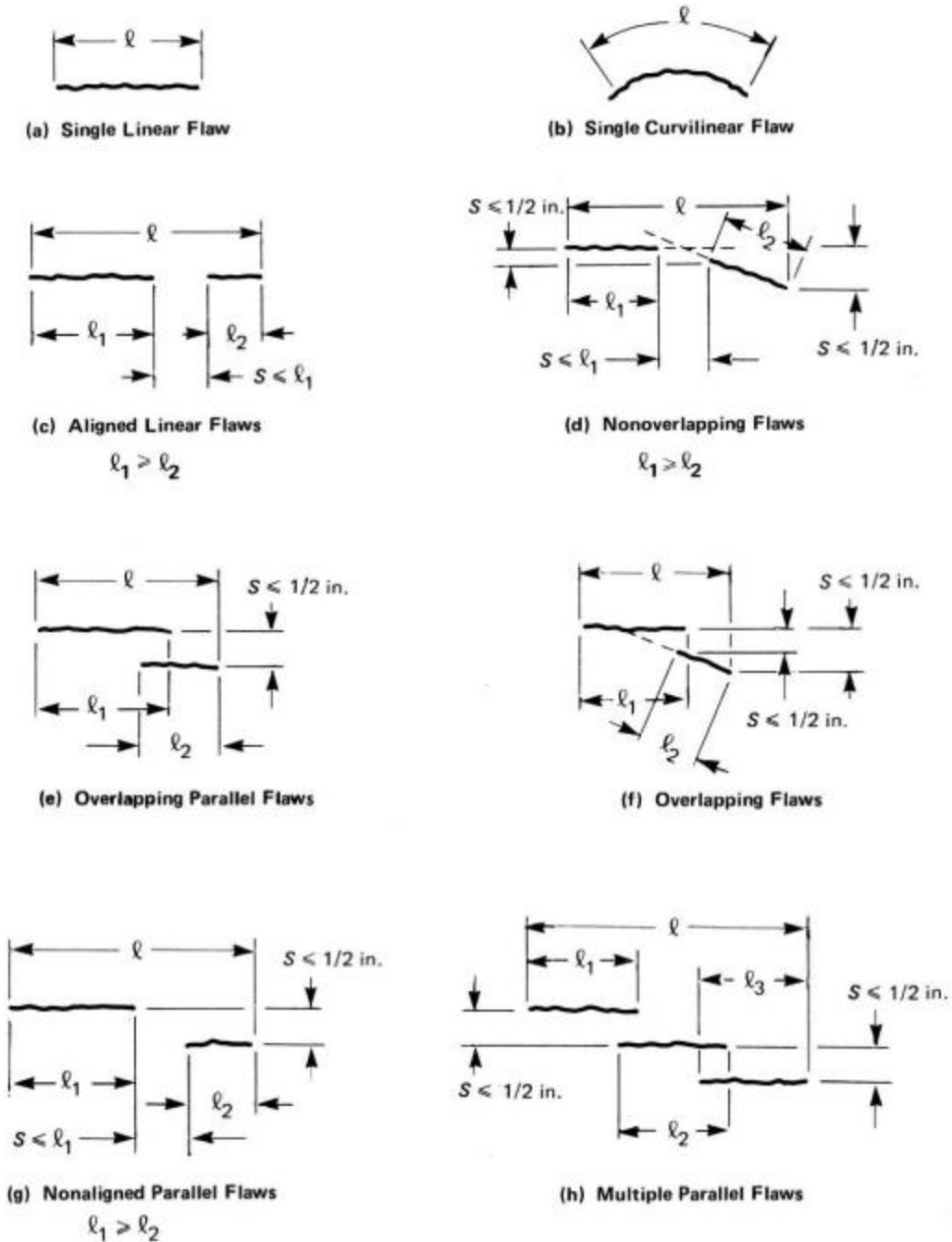


Figure D.5 Methodology for Determining Singularity or Multiplicity of Linear Surface Flaws. Reprinted from ASME 2015 Edition, Section XI, Figure IWA-3400-1, by permission of The American Society of Mechanical Engineers. All rights reserved.

Once the rules of IWA-3400 were applied to the test blocks, the scoring process described under Section D.1 was used on the test blocks.

One can see from Figure D.6 that test block 5.1 has six individual flaws that are very close in proximity. Figure D.7 shows that using the rules of IWA-3400, the six individual flaws in test block 5.1 could be considered as two.

This procedure was not carried out for Sample 5.2, based on the destructive evaluation results.

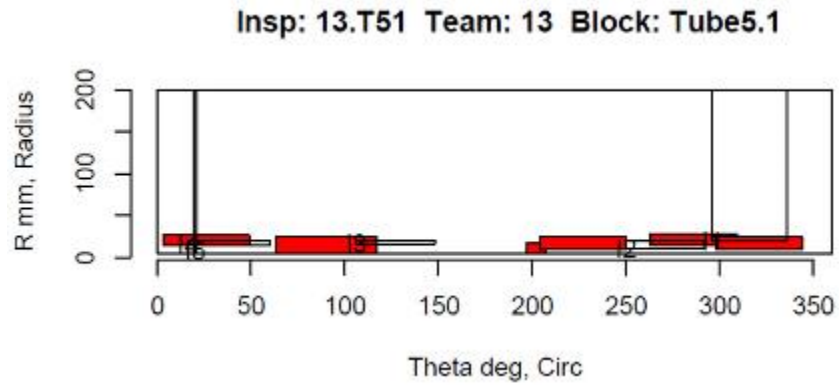


Figure D.6 Test Block 5.1 – Individual Flaws

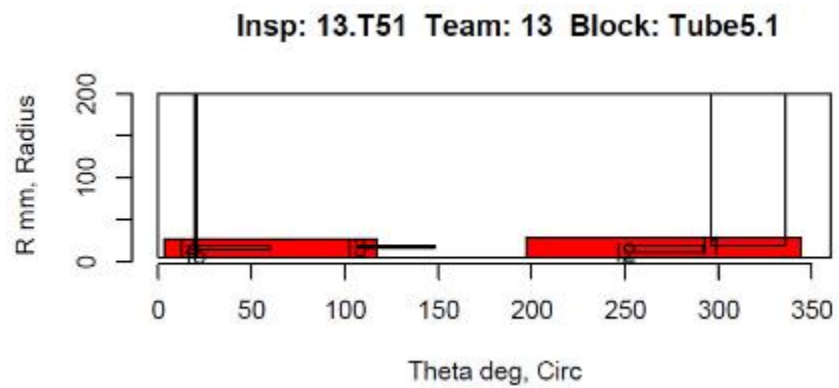


Figure D.7 Test Block 5.1 – Individual Flaws Combined Under Rules of IWA-3400

APPENDIX E
INDICATION PLOTS

APPENDIX E
INDICATION PLOTS

Contents

E.1	Quick-blind Inspection Summary Results	E-2
E.1.1	Plots for Team 106	E-2
E.1.2	Plots for Team 108	E-6
E.1.3	Plots for Team 113	E-10
E.1.4	Plots for Team 126	E-14
E.1.5	Plots for Team 132	E-18
E.1.6	Plots for Team 134	E-22
E.2	DMW Inspection Summary Results	E-26
E.2.1	Plots for Team 101	E-26
E.2.2	Plots for Team 108	E-30
E.2.3	Plots for Team 113	E-50
E.2.4	Plots for Team 115	E-53
E.2.5	Plots for Team 117	E-59
E.2.6	Plots for Team 126	E-65
E.2.7	Plots for Team 128	E-85
E.2.8	Plots for Team 134	E-91
E.2.9	Plots for Team 135	E-101
E.2.10	Plots for Team 144	E-104
E.3	BMI Inspection Summary Results	E-111
E.3.1	Plots for Team 108	E-111
E.3.2	Plots for Team 124	E-116
E.3.3	Plots for Team 126	E-121
E.4	WOL Inspection Summary Results	E-123
E.4.1	Plots for Team 108	E-123
E.4.2	Plots for Team 126	E-124

E.1 Quick-blind Inspection Summary Results

E.1.1 Plots for Team 106

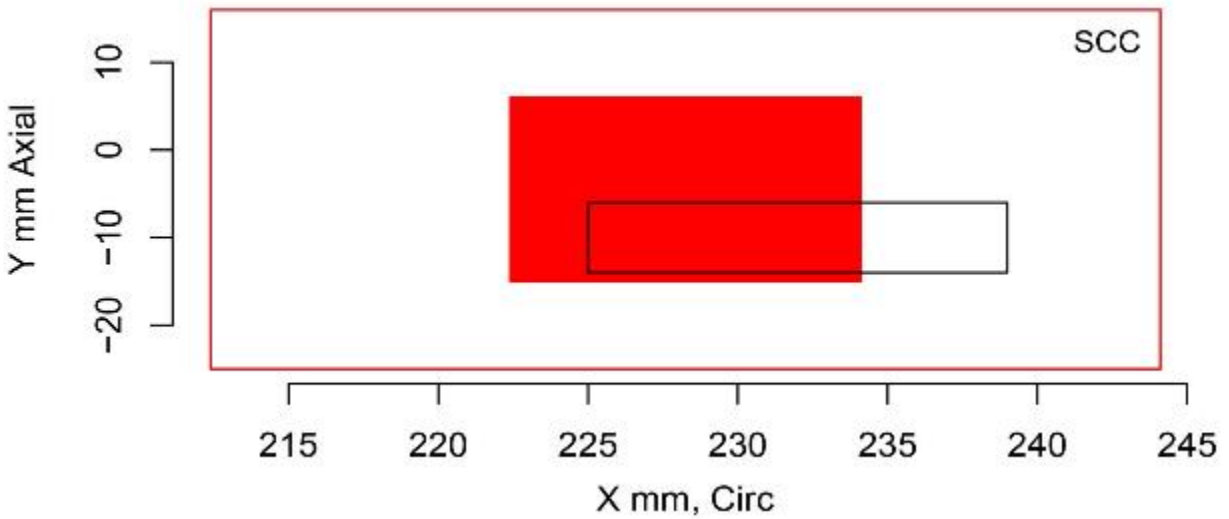


Figure E.1 Indication Plot for Procedure UT.ECT.106 Applied to Test Block P15 in PARENT Blind Testing (X - Y view)

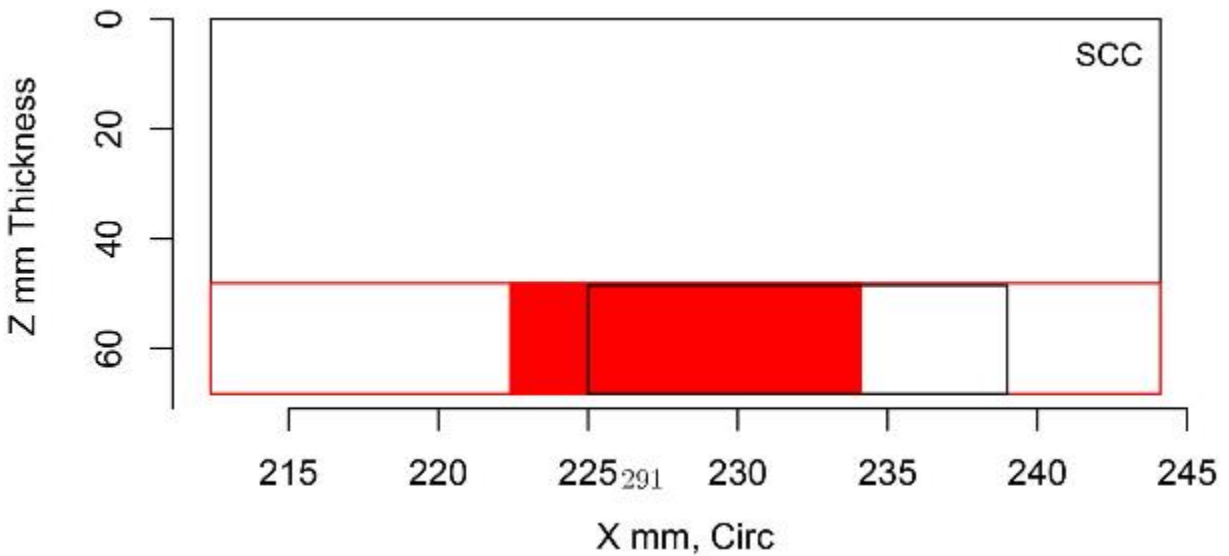


Figure E.2 Indication Plot for Procedure UT.ECT.106 Applied to Test Block P15 in PARENT Blind Testing (X - Z view)

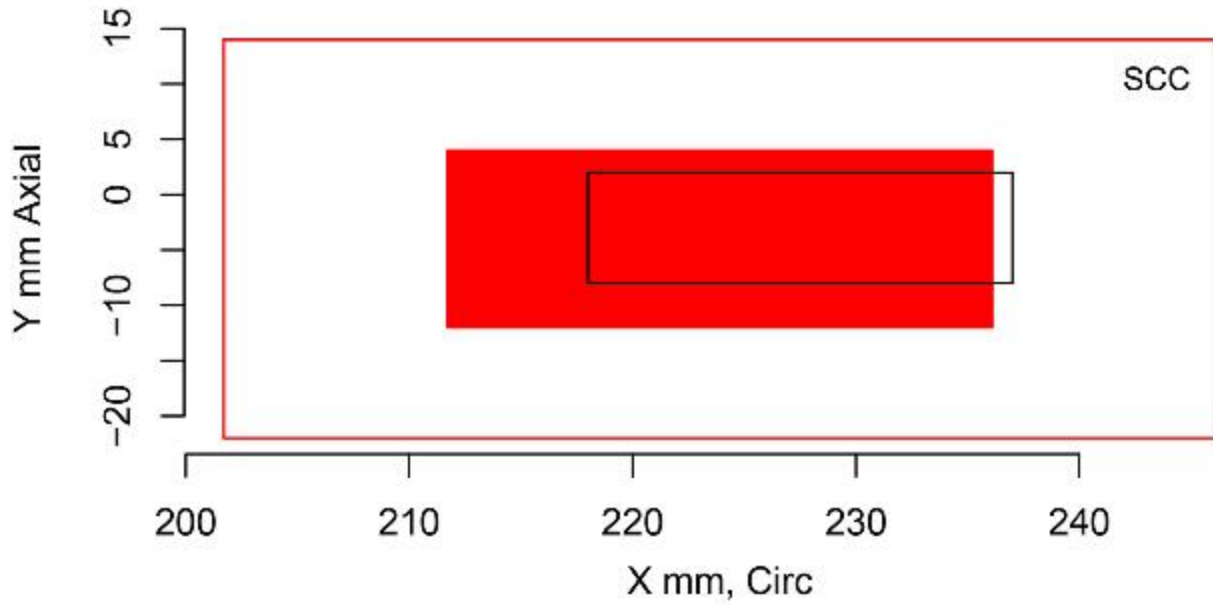


Figure E.3 Indication Plot for Procedure UT.ECT.106 Applied to Test Block P16 in PARENT Blind Testing (X – Y view)

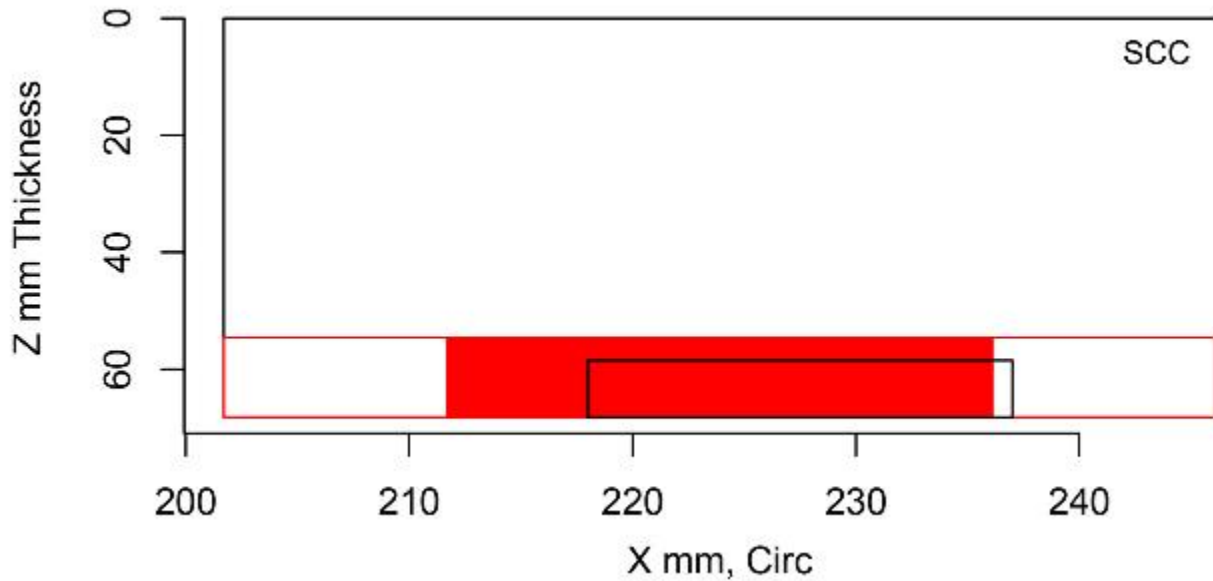


Figure E.4 Indication Plot for Procedure UT.ECT.106 Applied to Test Block P16 in PARENT Blind Testing (X – Z view)

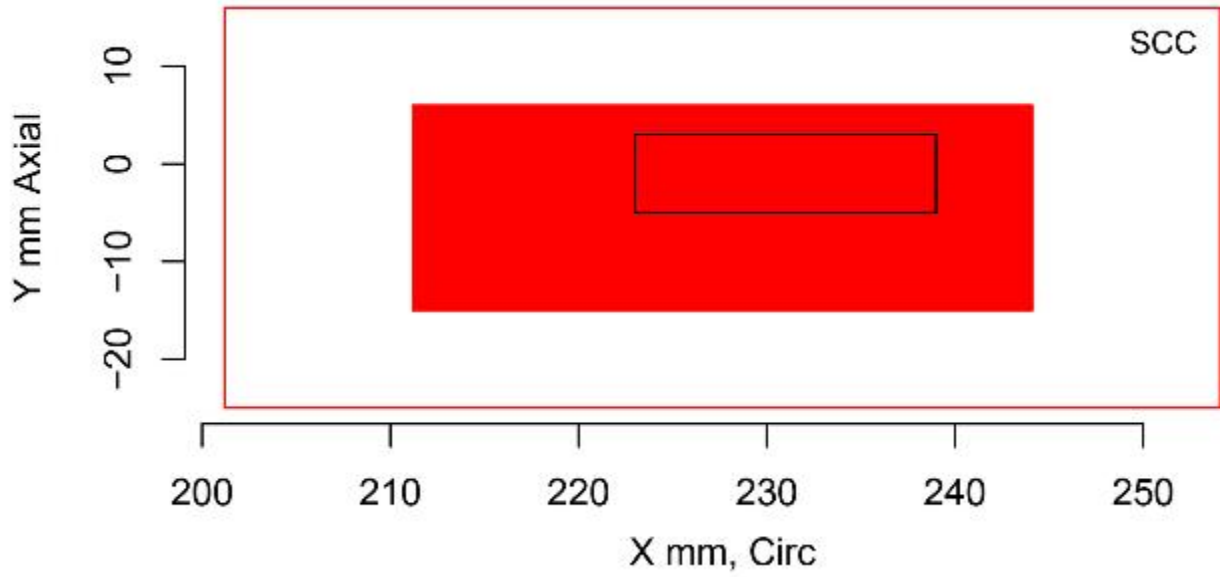


Figure E.5 Indication Plot for Procedure UT.ECT.106 Applied to Test Block P17 in PARENT Blind Testing (X – Y view)

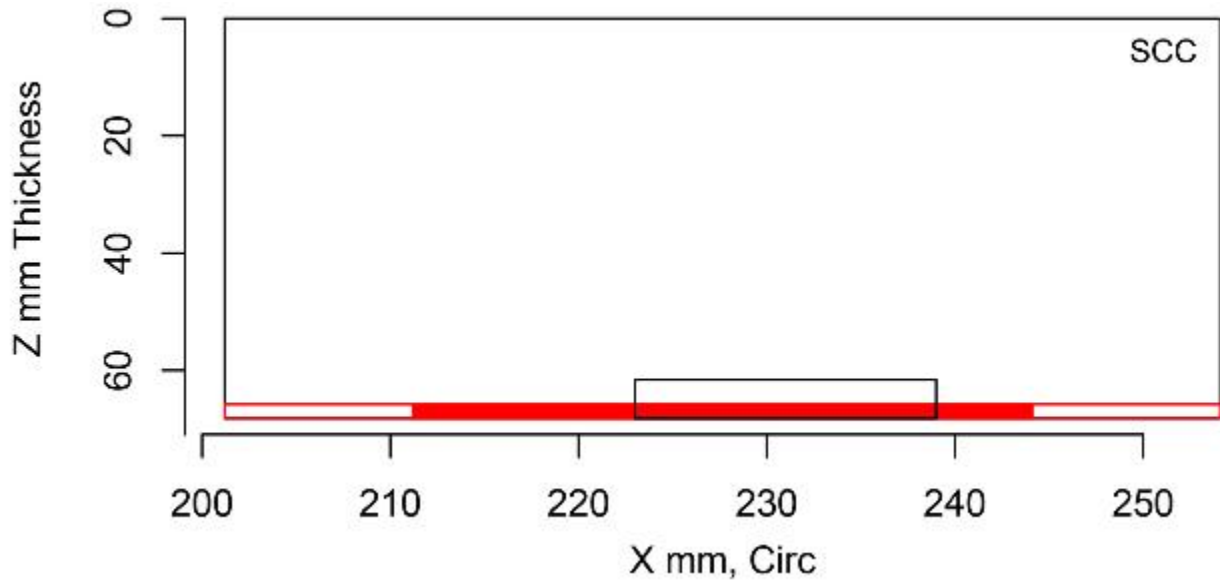


Figure E.6 Indication Plot for Procedure UT.ECT.106 Applied to Test Block P17 in PARENT Blind Testing (X – Z view)

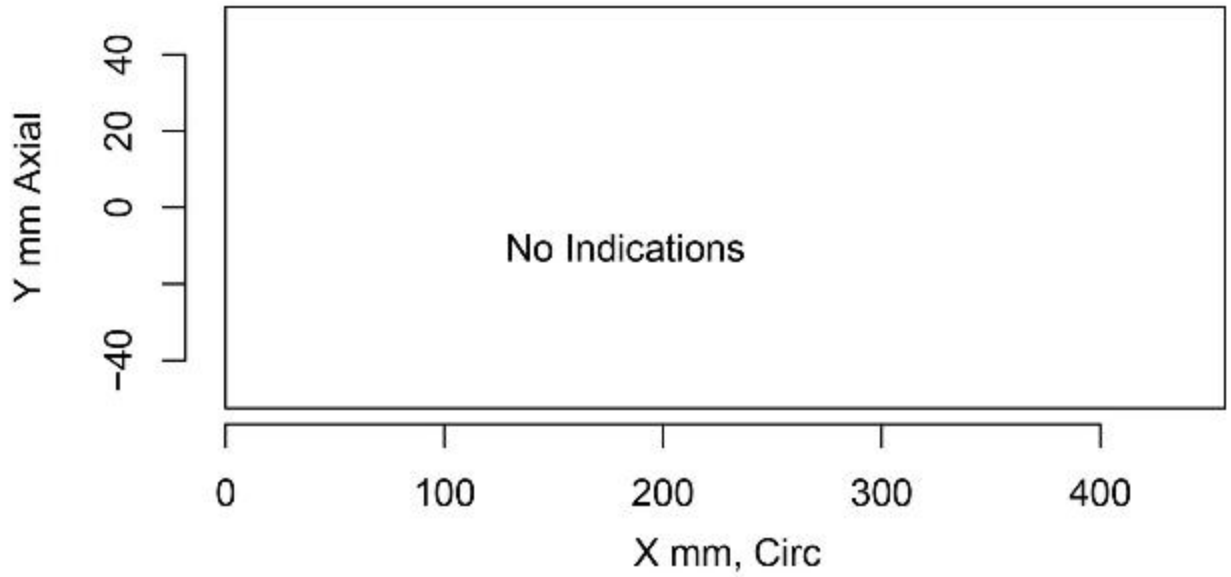


Figure E.7 Indication Plot for Procedure UT.ECT.106 Applied to Test Block P45 in PARENT Blind Testing (X – Y view)

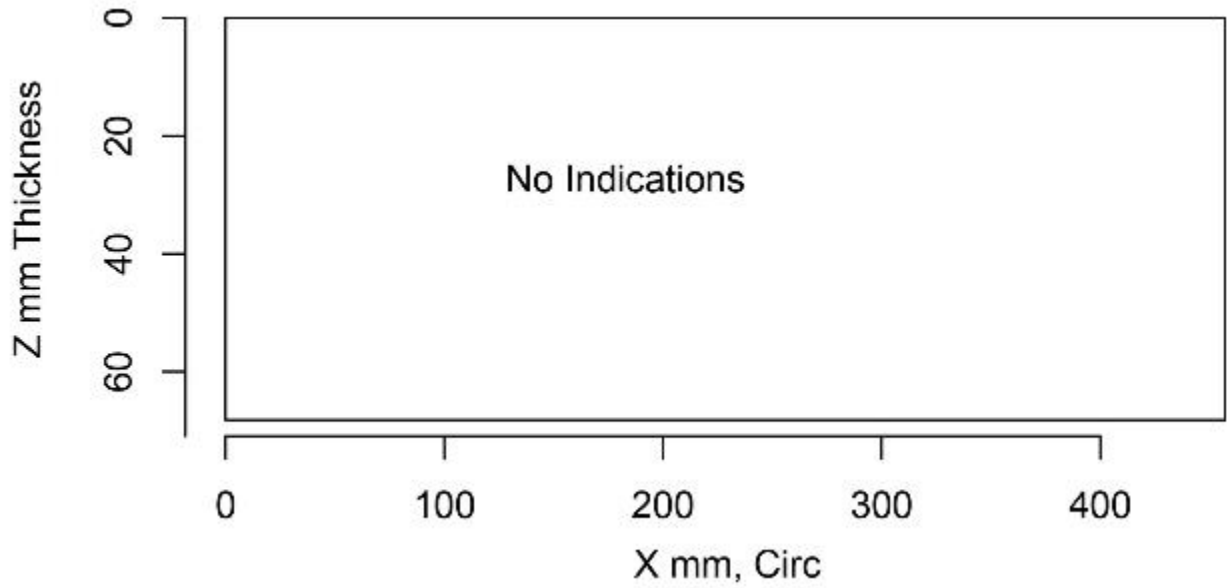


Figure E.8 Indication Plot for Procedure UT.ECT.106 Applied to Test Block P45 in PARENT Blind Testing (X – Z view)

E.1.2 Plots for Team 108

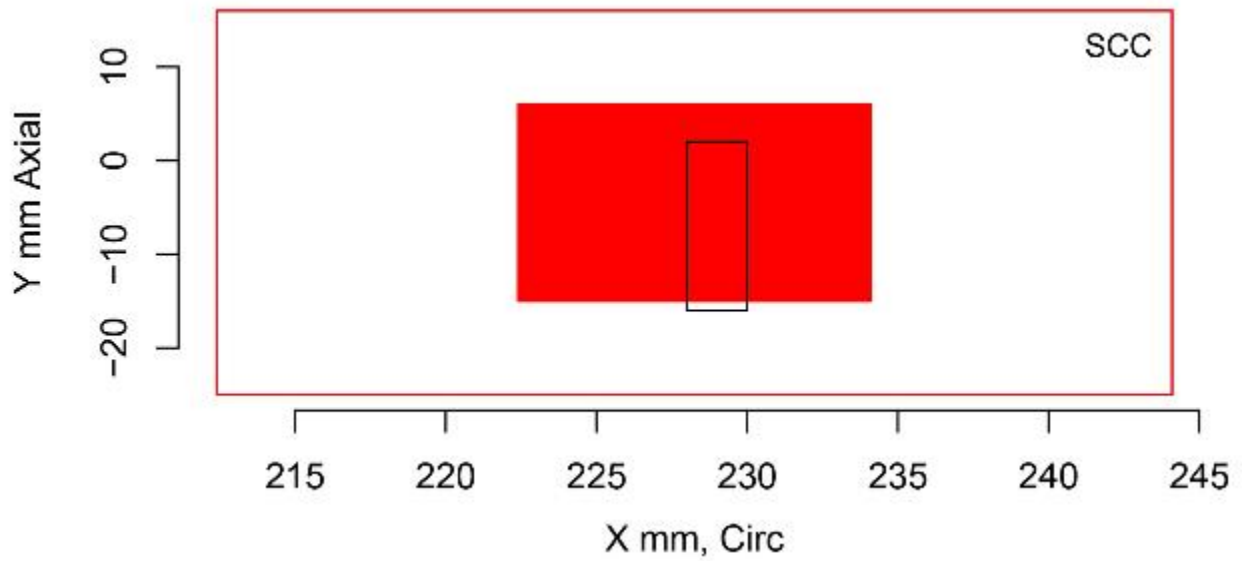


Figure E.9 Indication Plot for Procedure UT.PAUT.108 Applied to Test Block P15 in PARENT Blind Testing (X - Y view)

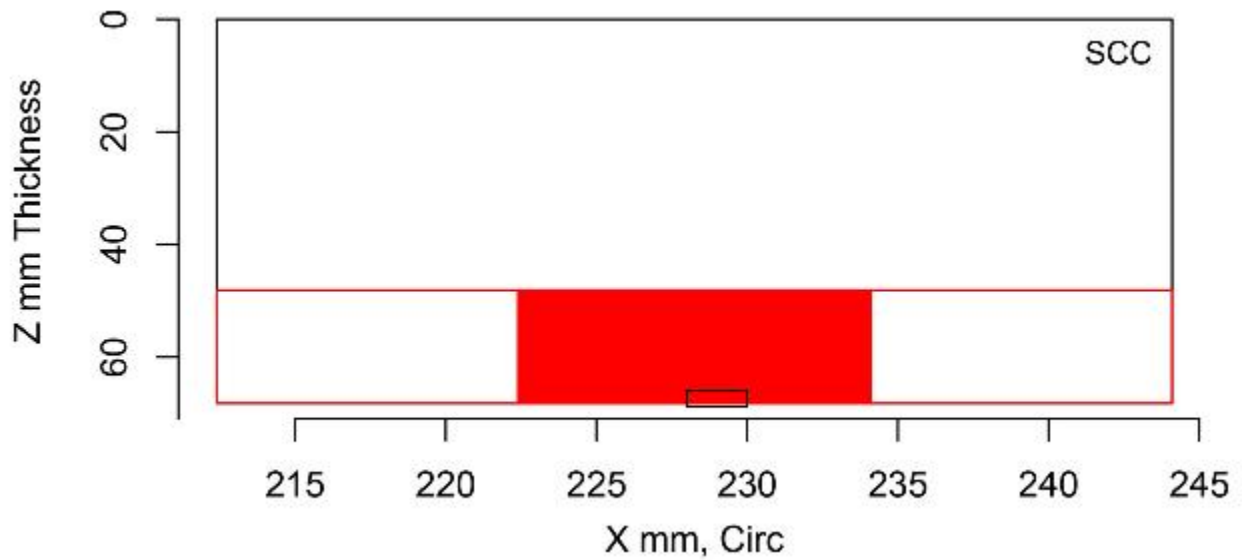


Figure E.10 Indication Plot for Procedure UT.PAUT.108 Applied to Test Block P15 in PARENT Blind Testing (X - Z view)

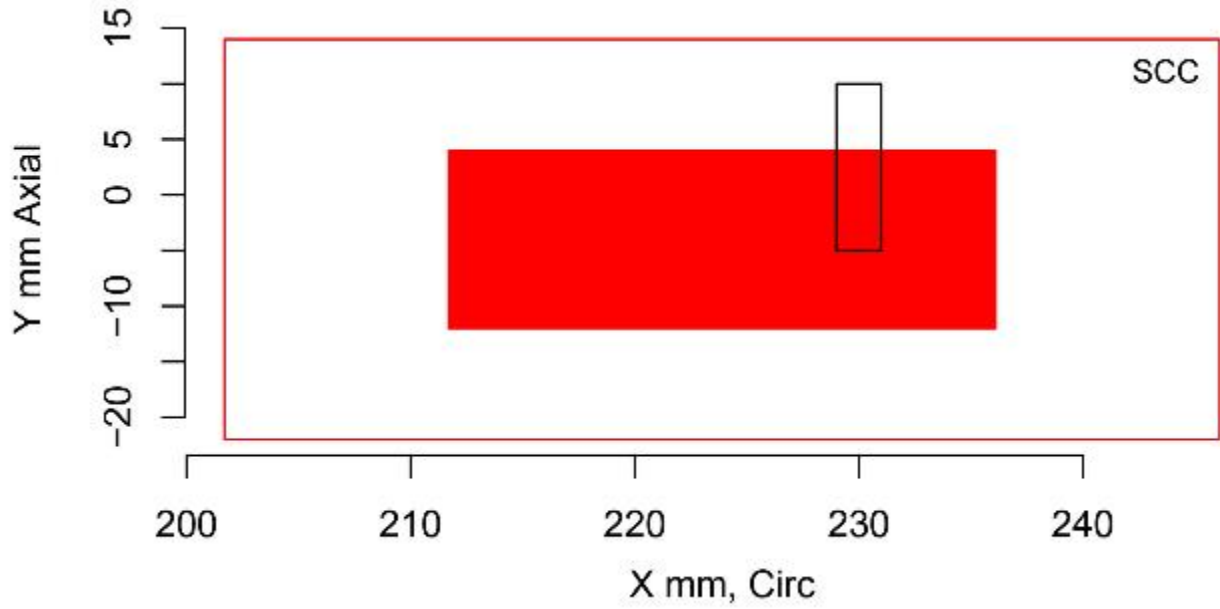


Figure E.11 Indication Plot for Procedure UT.PAUT.108 Applied to Test Block P16 in PARENT Blind Testing (X – Y view)

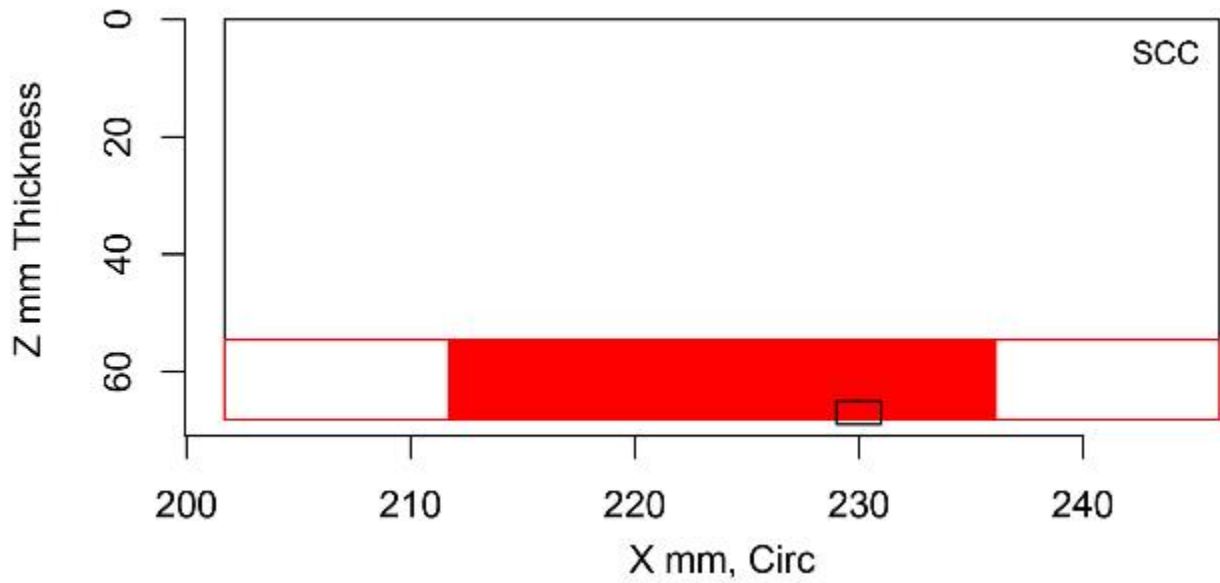


Figure E.12 Indication Plot for Procedure UT.PAUT.108 Applied to Test Block P16 in PARENT Blind Testing (X – Z view)

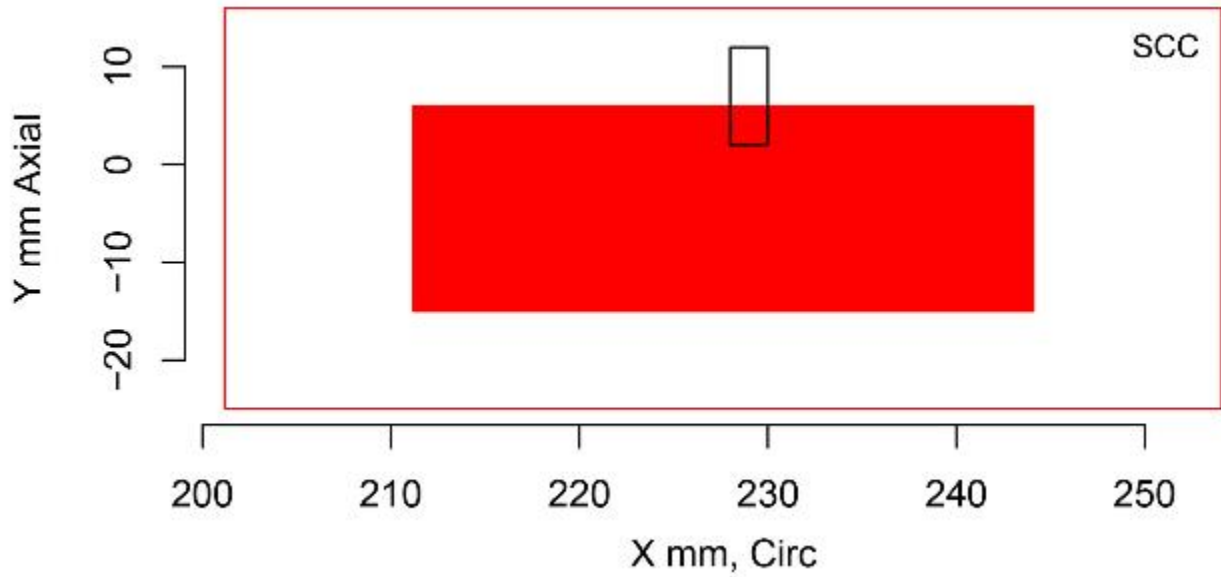


Figure E.13 Indication Plot for Procedure UT.PAUT.108 Applied to Test Block P17 in PARENT Blind Testing (X – Y view)

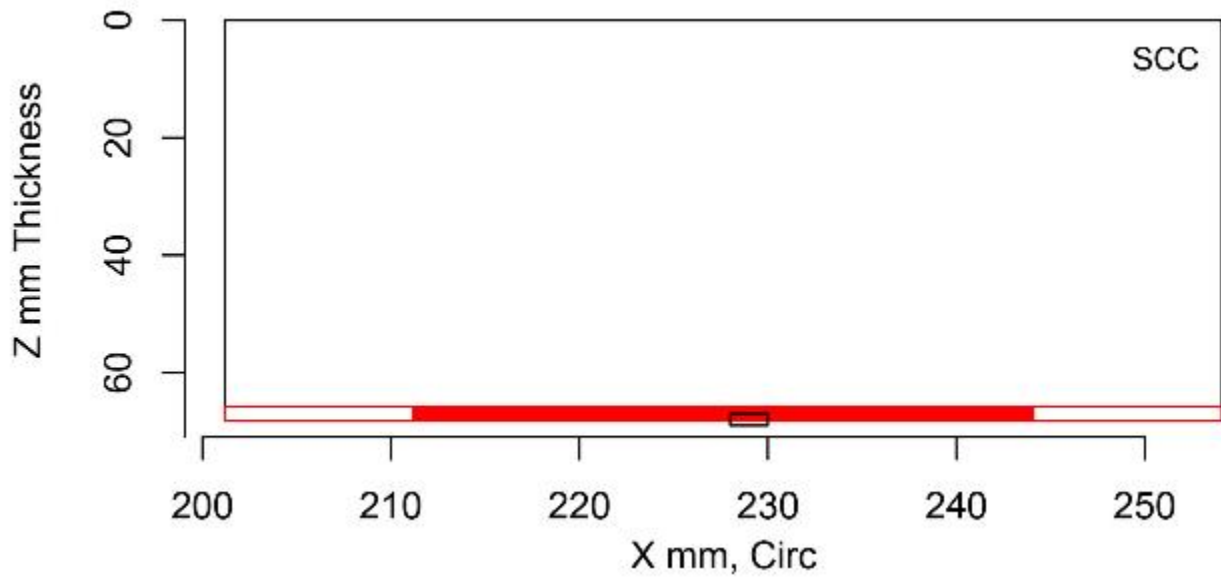


Figure E.14 Indication Plot for Procedure UT.PAUT.108 Applied to Test Block P17 in PARENT Blind Testing (X – Z view)

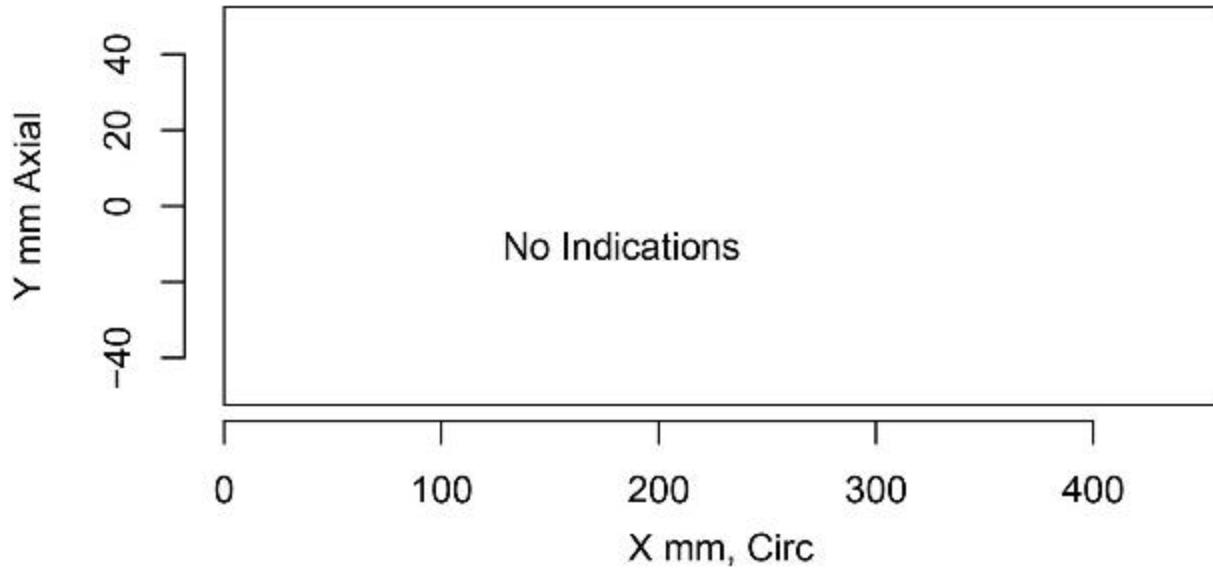


Figure E.15 Indication Plot for Procedure UT.PAUT.108 Applied to Test Block P45 in PARENT Blind Testing (X – Y view)

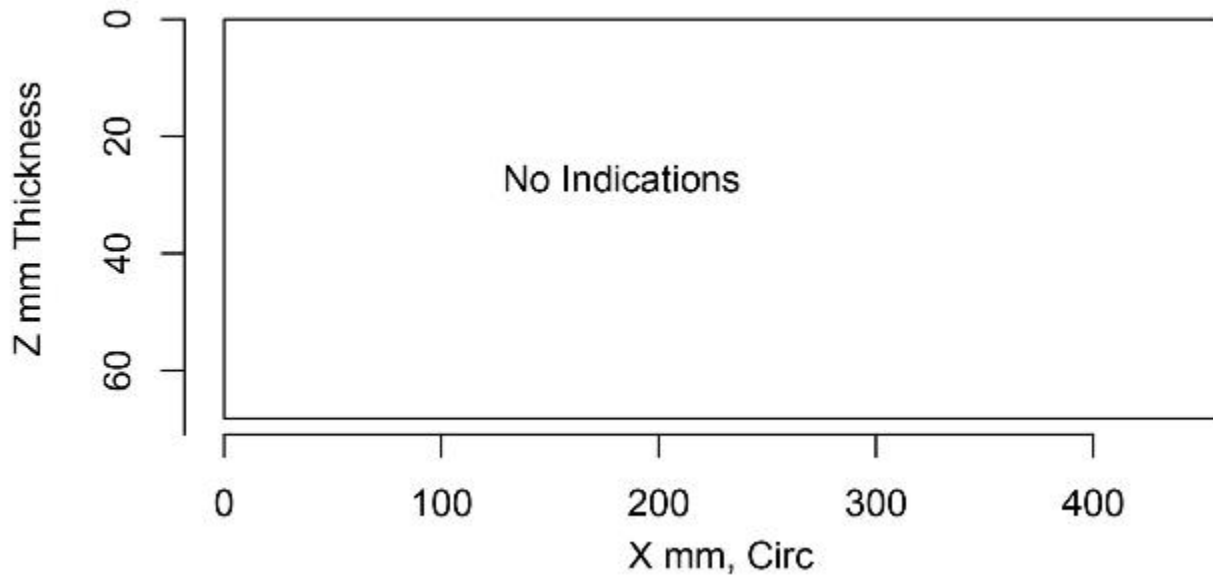


Figure E.16 Indication Plot for Procedure UT.PAUT.108 Applied to Test Block P45 in PARENT Blind Testing (X – Z view)

E.1.3 Plots for Team 113

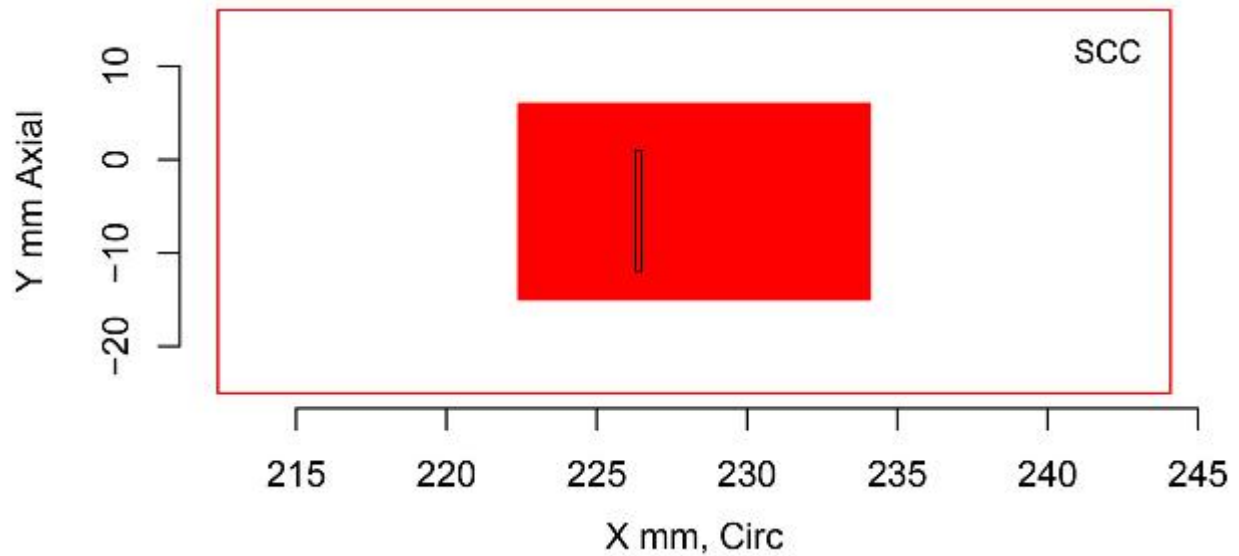


Figure E.17 Indication Plot for Procedure UT.PAUT.113 Applied to Test Block P15 in PARENT Blind Testing (X - Y view)

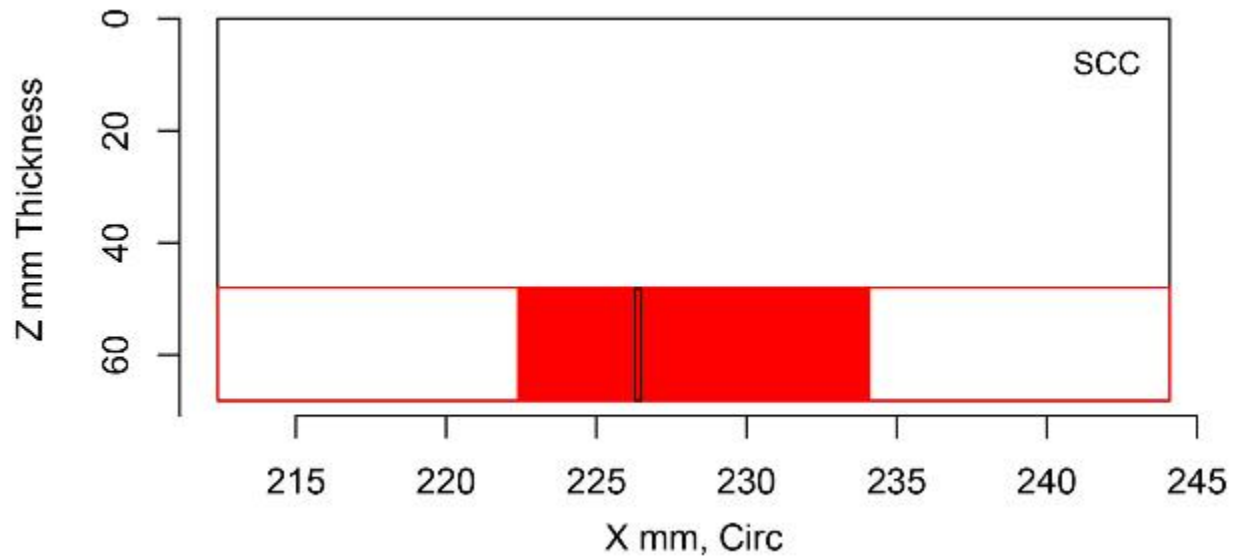


Figure E.18 Indication Plot for Procedure UT.PAUT.113 Applied to Test Block P15 in PARENT Blind Testing (X - Z view)

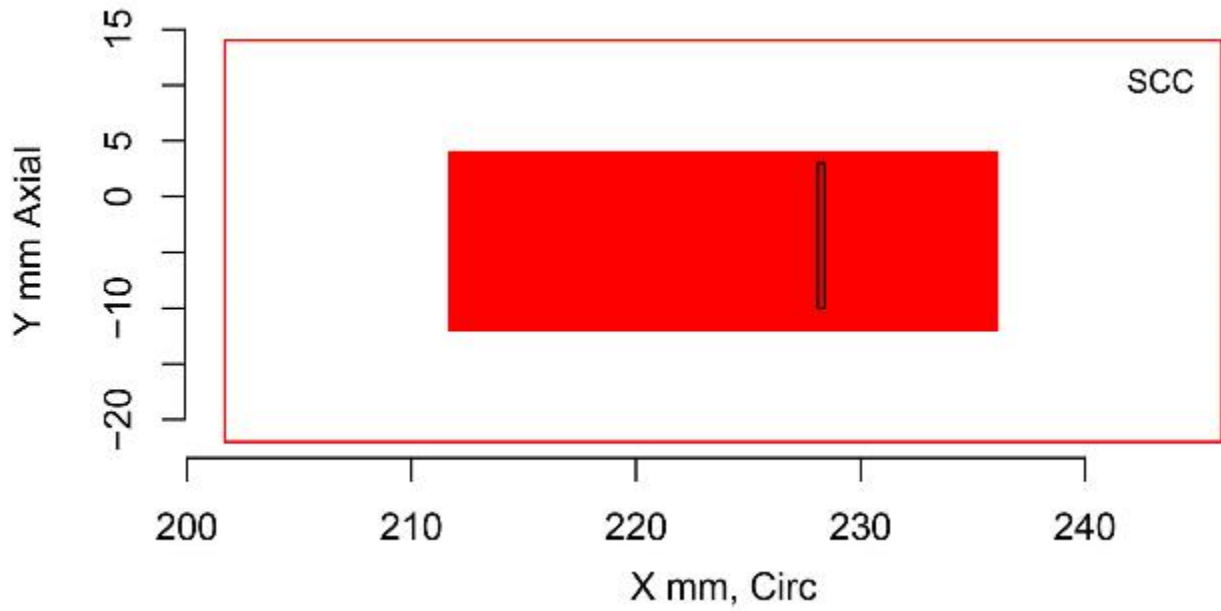


Figure E.19 Indication Plot for Procedure UT.PAUT.113 Applied to Test Block P16 in PARENT Blind Testing (X – Y view)

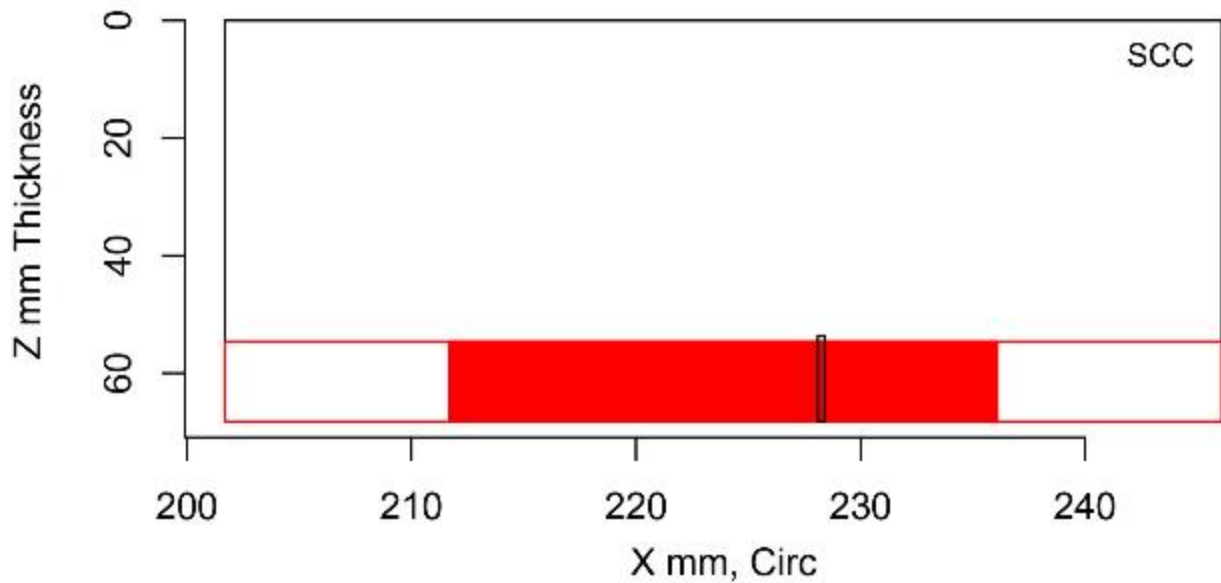


Figure E.20 Indication Plot for Procedure UT.PAUT.113 Applied to Test Block P16 in PARENT Blind Testing (X – Z view)

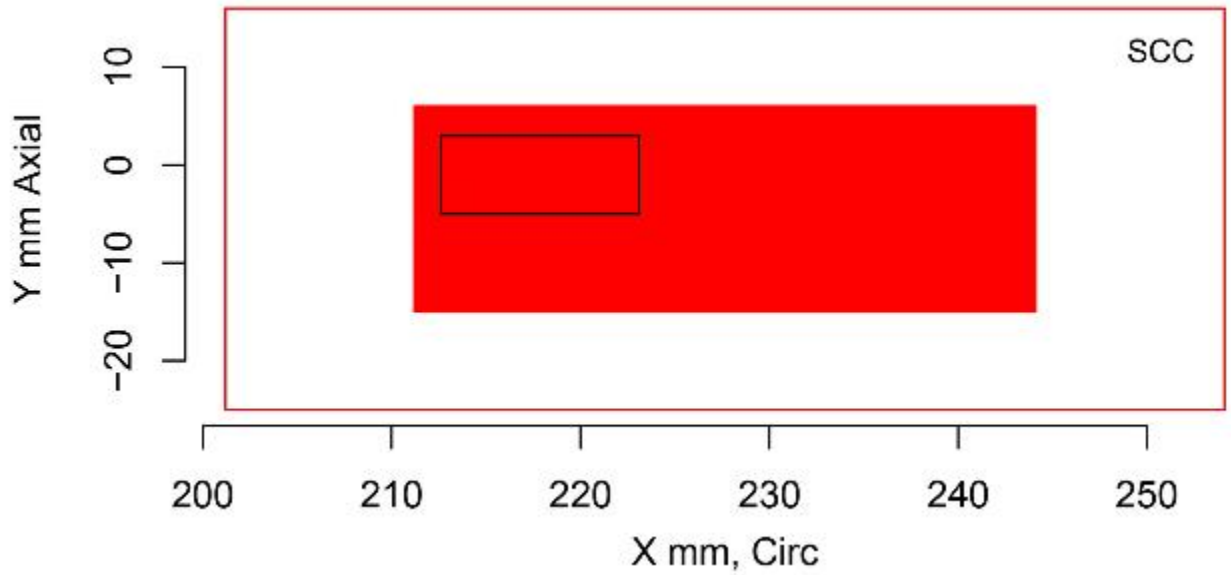


Figure E.21 Indication Plot for Procedure UT.PAUT.113 Applied to Test Block P17 in PARENT Blind Testing (X – Y view)

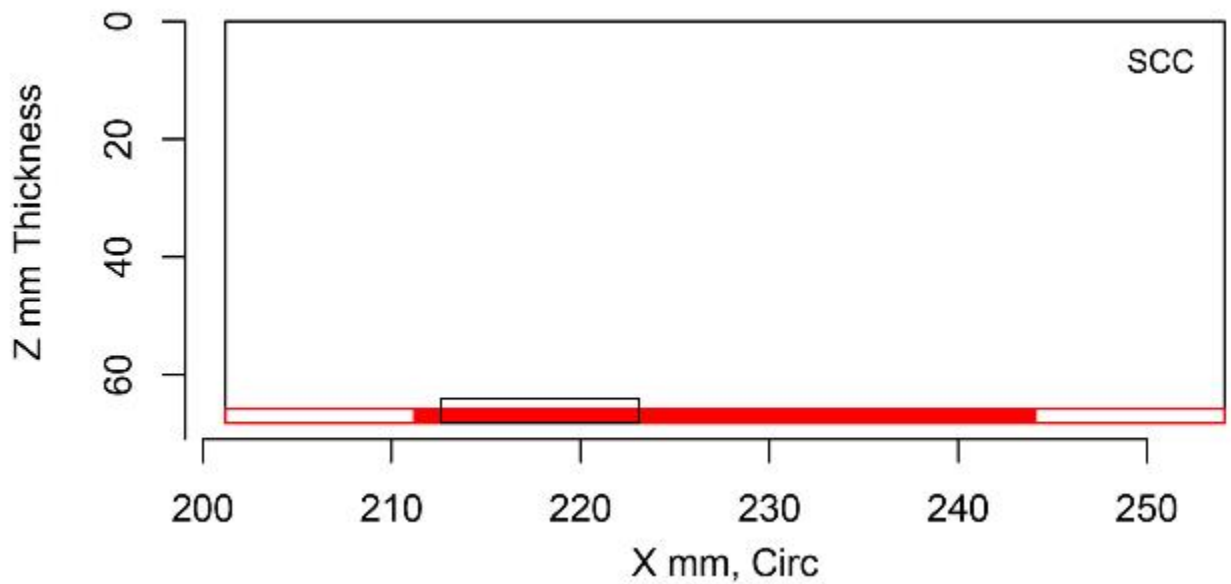


Figure E.22 Indication Plot for Procedure UT.PAUT.113 Applied to Test Block P17 in PARENT Blind Testing (X – Z view)

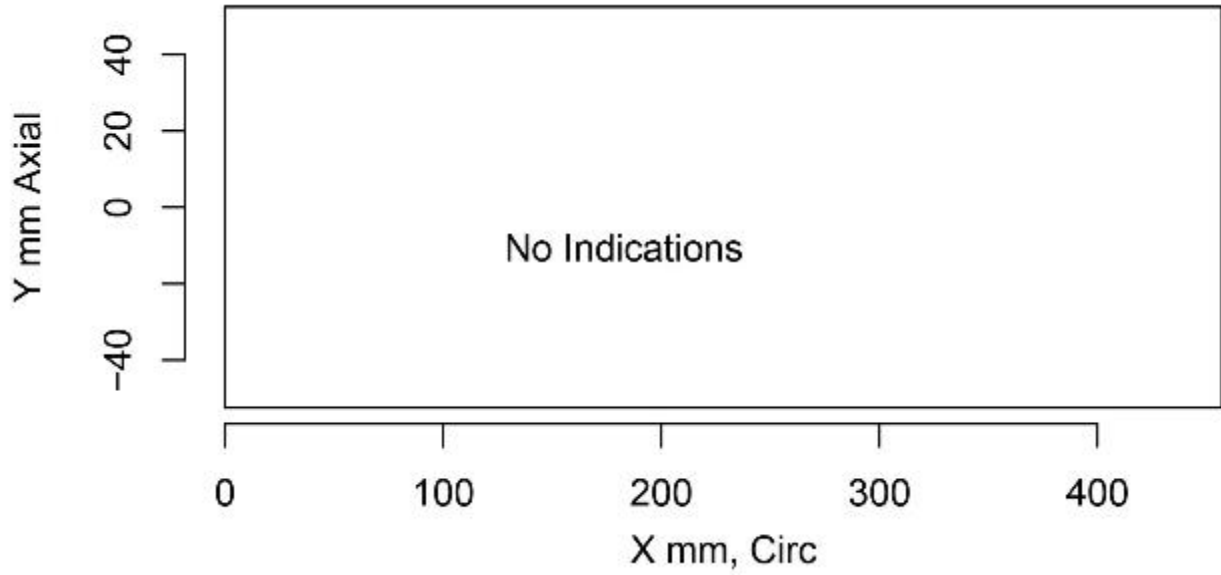


Figure E.23 Indication Plot for Procedure UT.PAUT.113 Applied to Test Block P45 in PARENT Blind Testing (X – Y view)

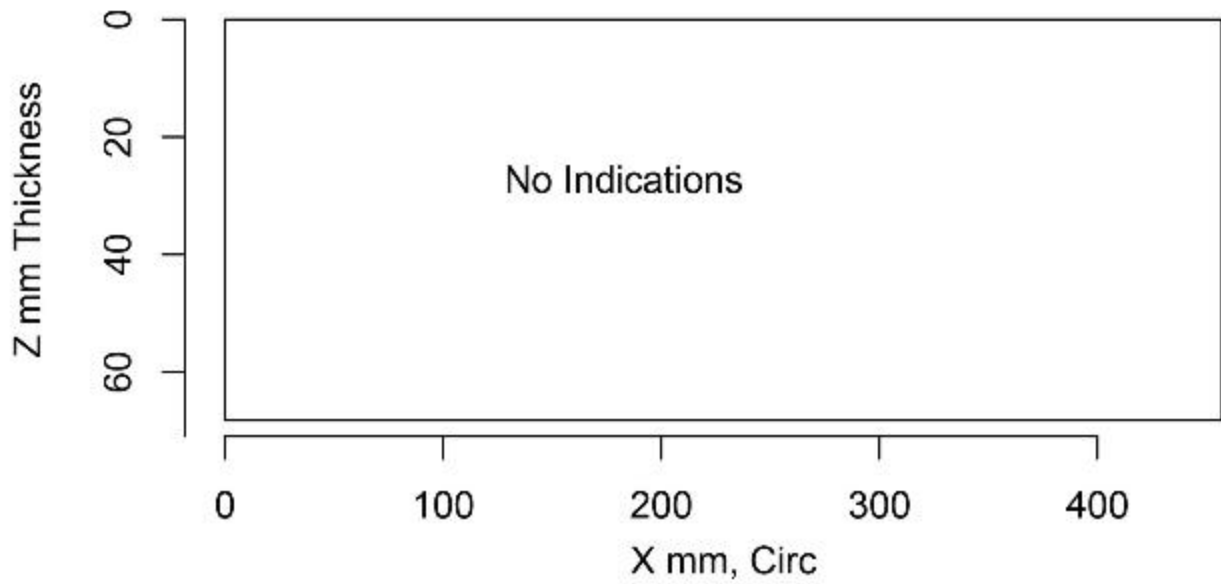


Figure E.24 Indication Plot for Procedure UT.PAUT.113 Applied to Test Block P45 in PARENT Blind Testing (X – Z view)

E.1.4 Plots for Team 126

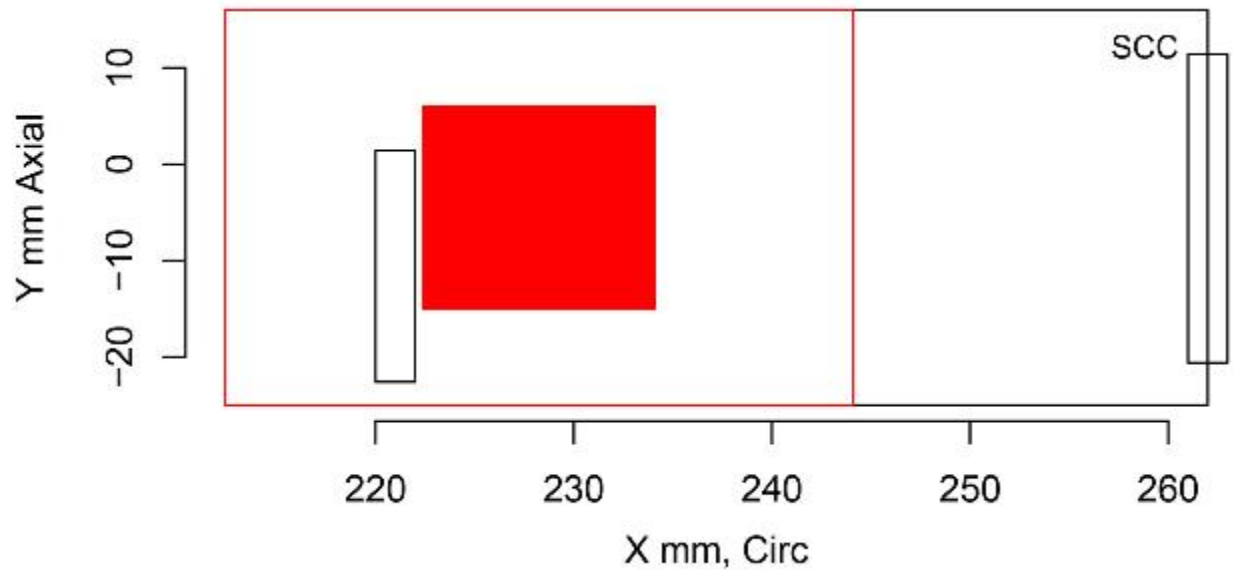


Figure E.25 Indication Plot for Procedure UT.PAUT.126 Applied to Test Block P15 in PARENT Blind Testing (X – Y view)

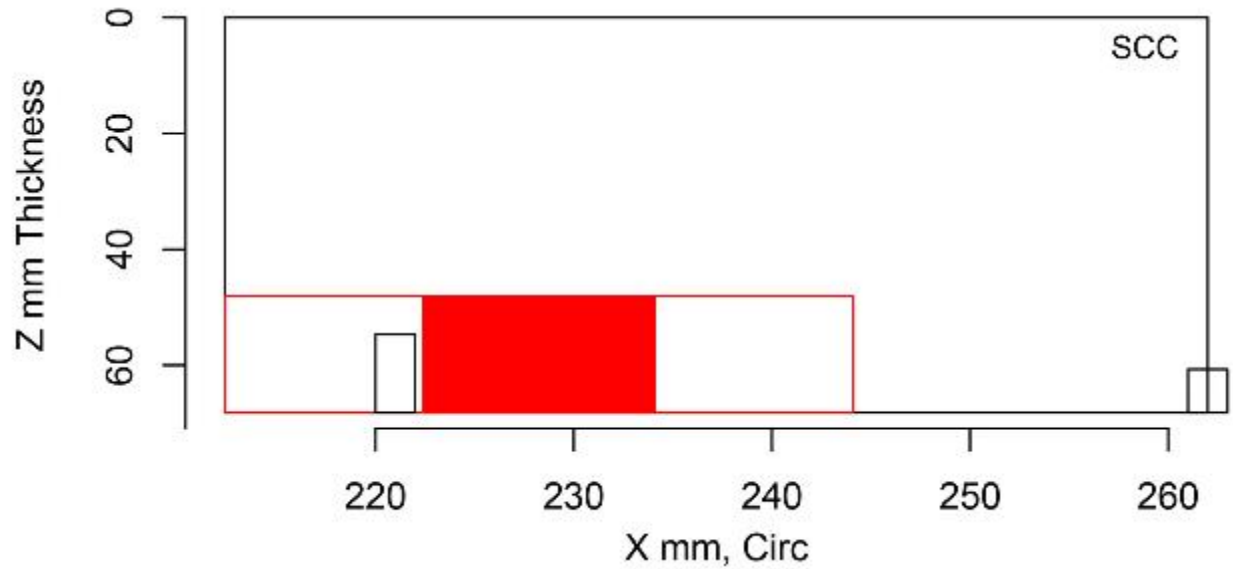


Figure E.26 I Indication Plot for Procedure UT.PAUT.126 Applied to Test Block P15 in PARENT Blind Testing (X – Z view)

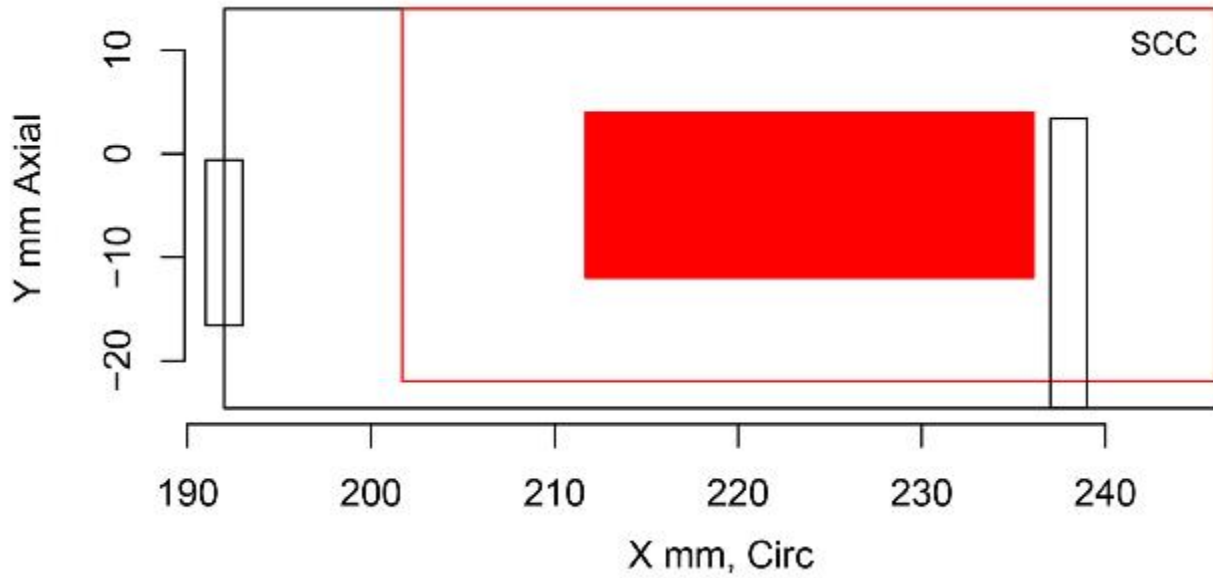


Figure E.27 Indication Plot for Procedure UT.PAUT.126 Applied to Test Block P16 in PARENT Blind Testing (X – Y view)

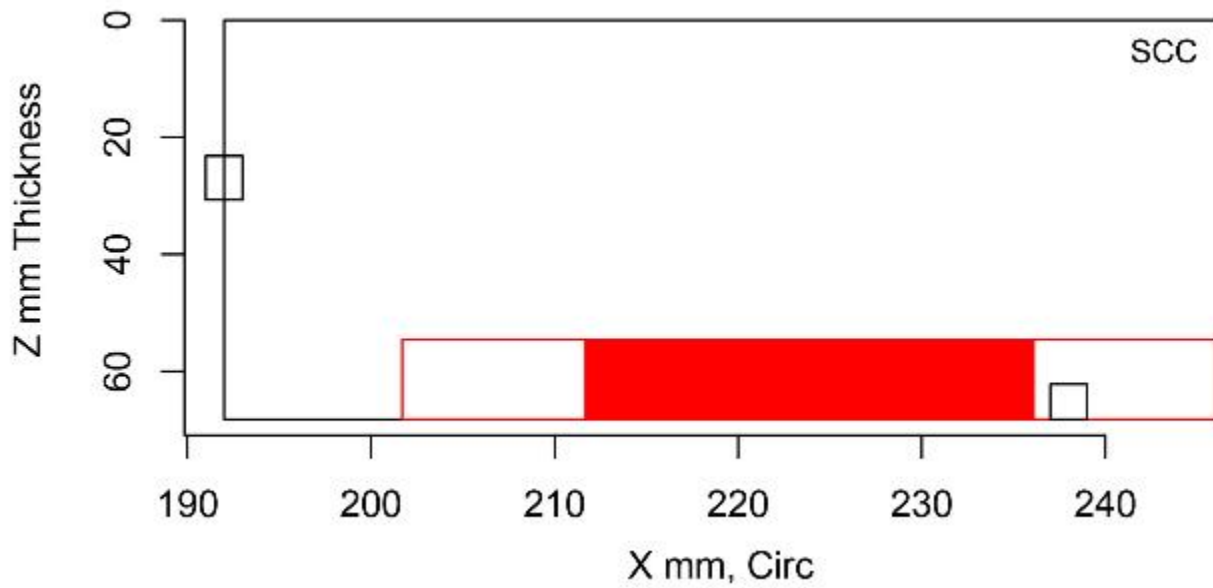


Figure E.28 Indication Plot for Procedure UT.PAUT.126 Applied to Test Block P16 in PARENT Blind Testing (X – Z view)

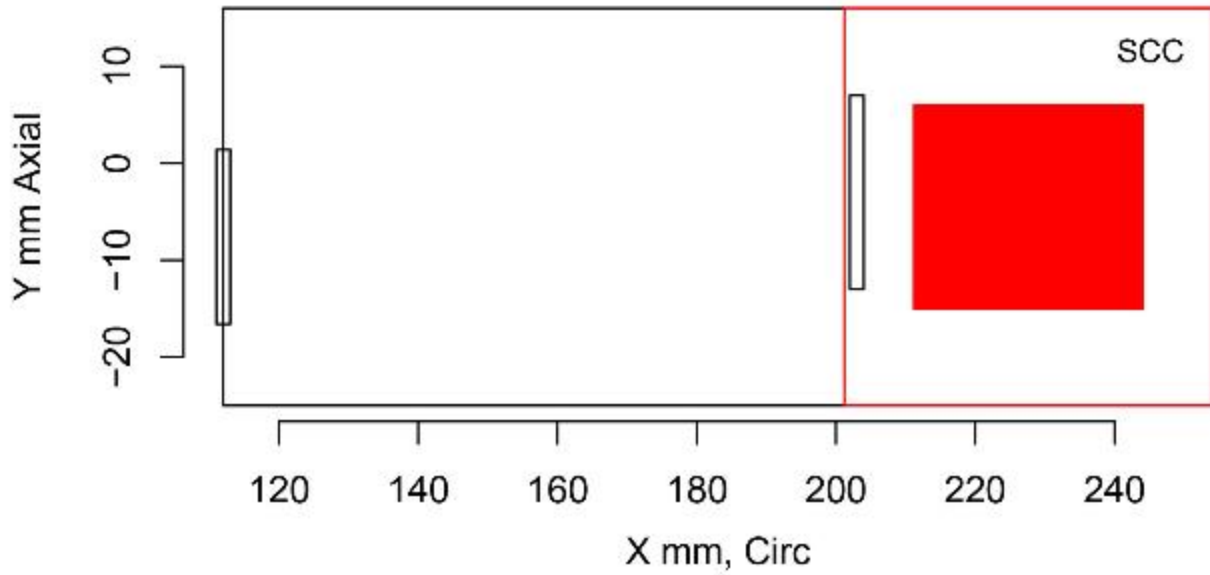


Figure E.29 Indication Plot for Procedure UT.PAUT.126 Applied to Test Block P17 in PARENT Blind Testing (X – Y view)

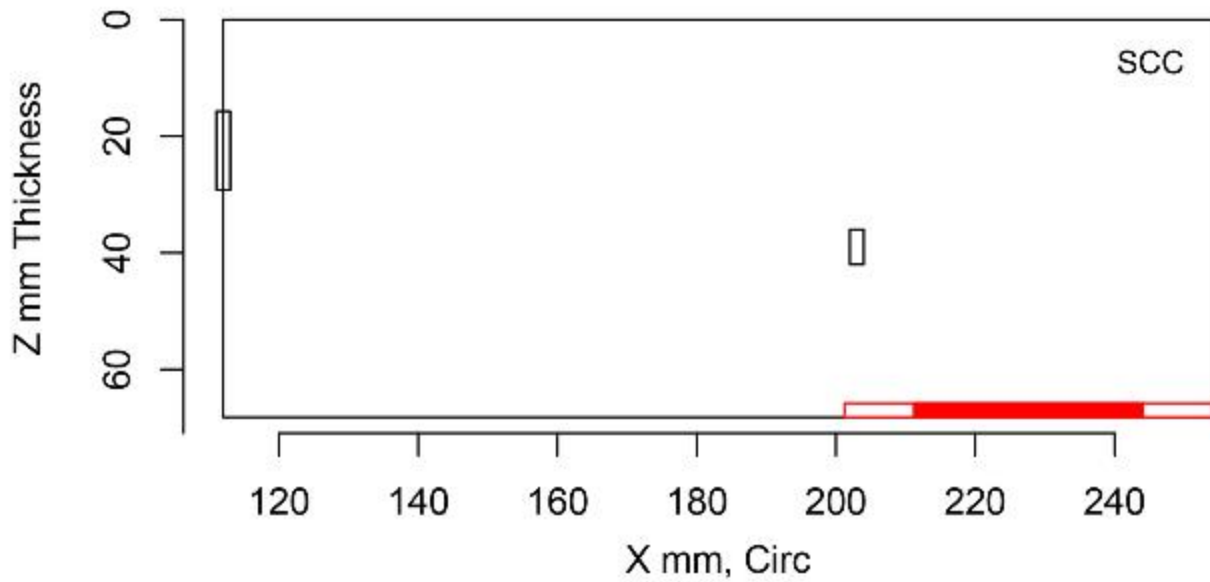


Figure E.30 Indication Plot for Procedure UT.PAUT.126 Applied to Test Block P17 in PARENT Blind Testing (X – Z view)

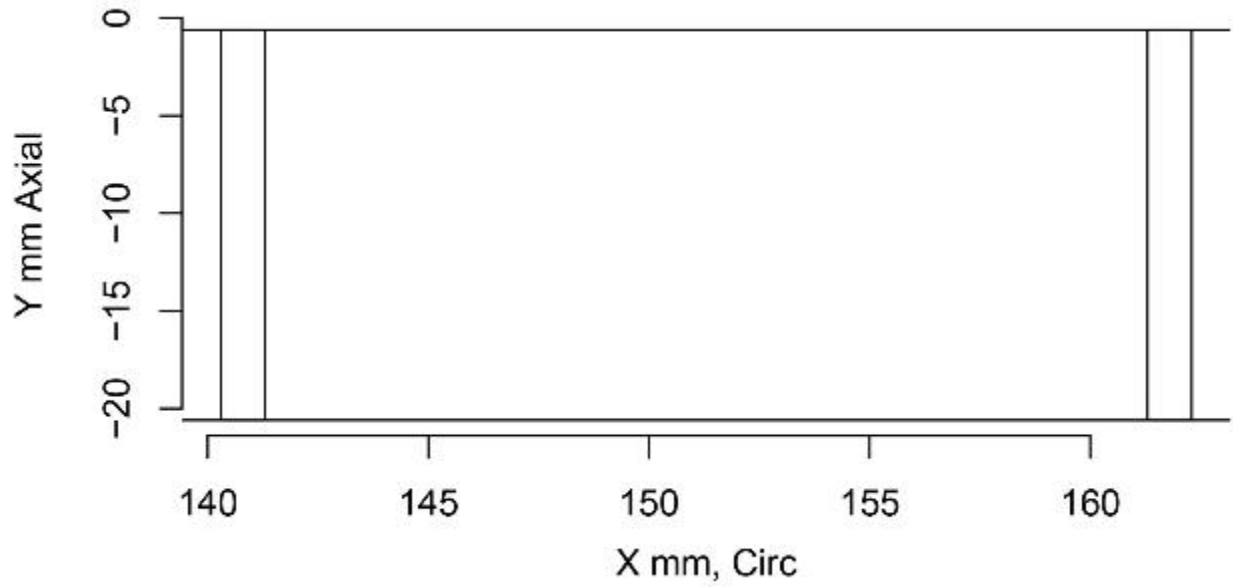


Figure E.31 Indication Plot for Procedure UT.PAUT.126 Applied to Test Block P45 in PARENT Blind Testing (X - Y view)

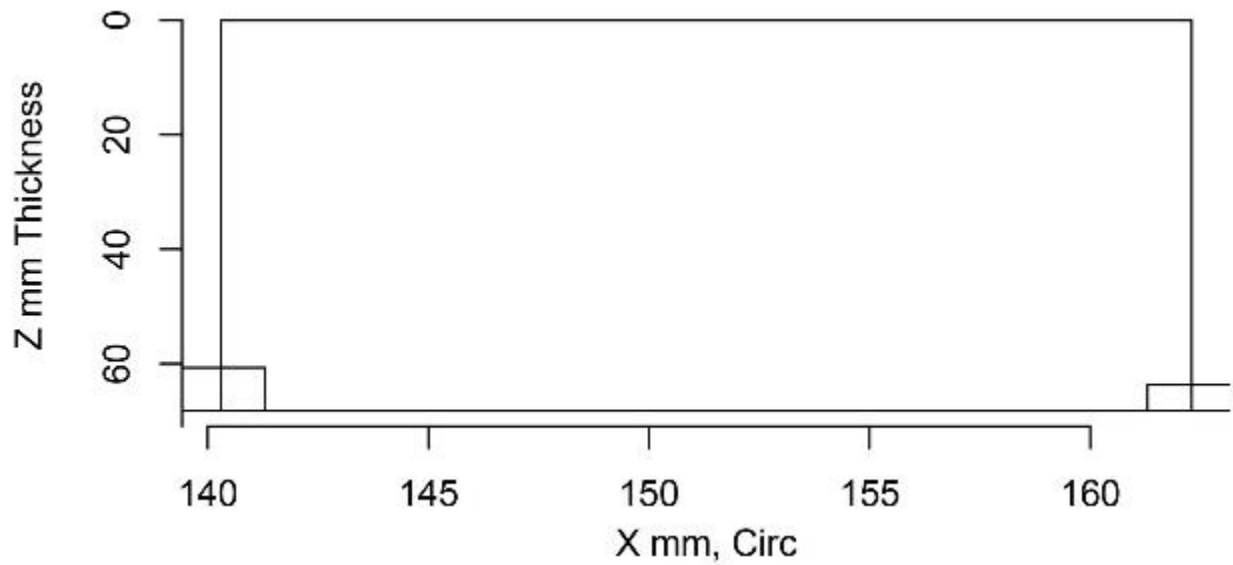


Figure E.32 Indication Plot for Procedure UT.PAUT.126 Applied to Test Block P45 in PARENT Blind Testing (X - Z view)

E.1.5 Plots for Team 132

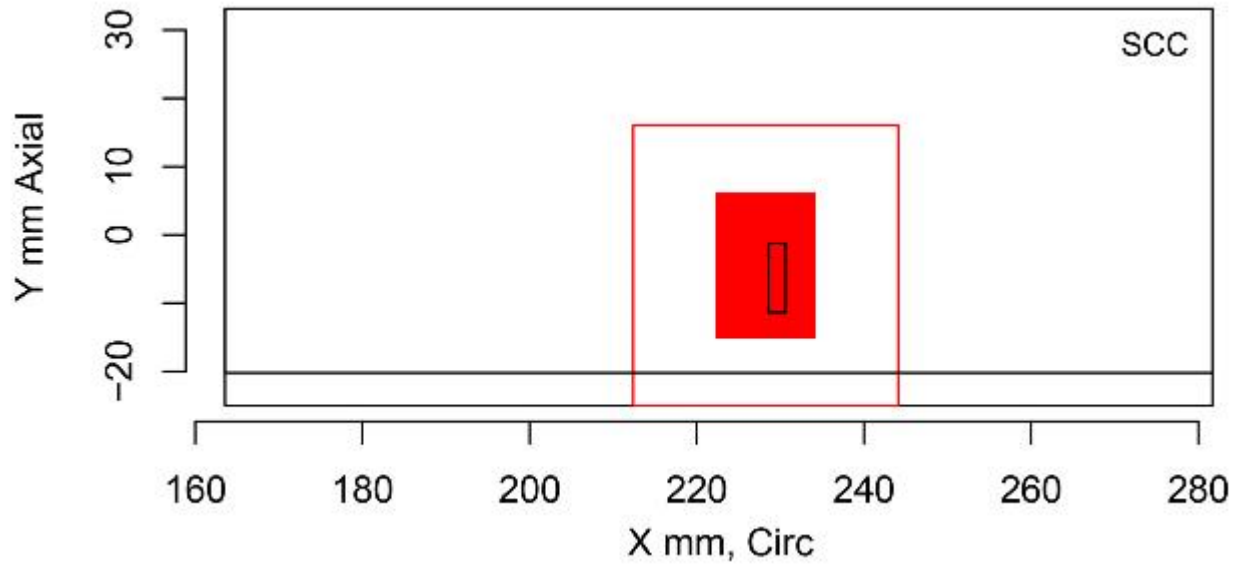


Figure E.33 Indication Plot for Procedure PAUT.132 Applied to Test Block P15 in PARENT Blind Testing (X – Y view)

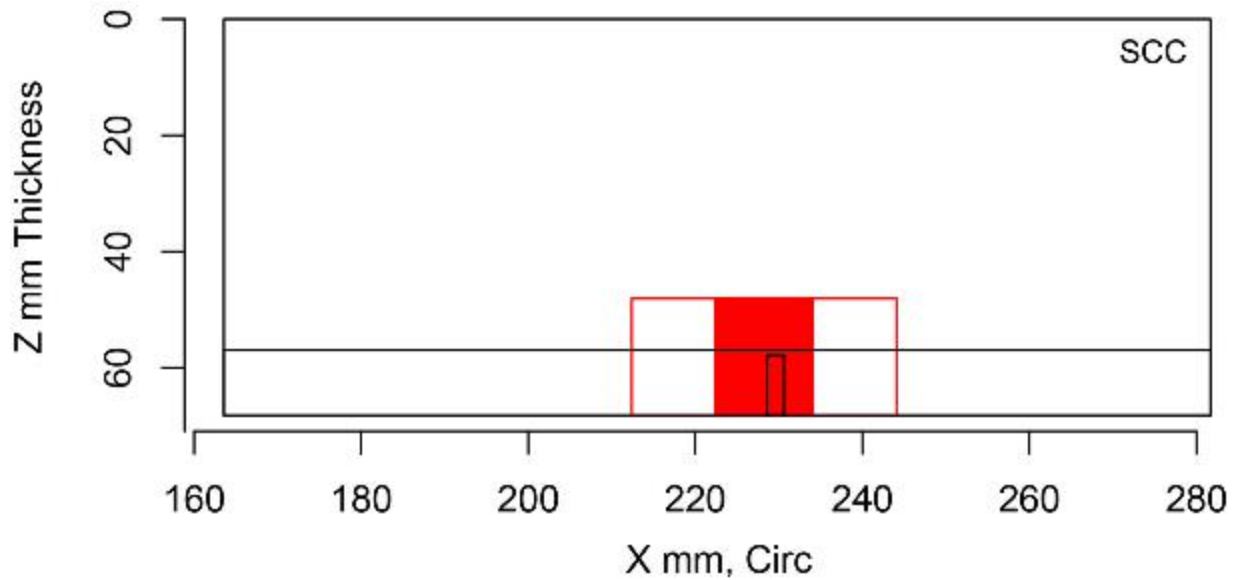


Figure E.34 Indication Plot for Procedure PAUT.132 Applied to Test Block P15 in PARENT Blind Testing (X – Z view)

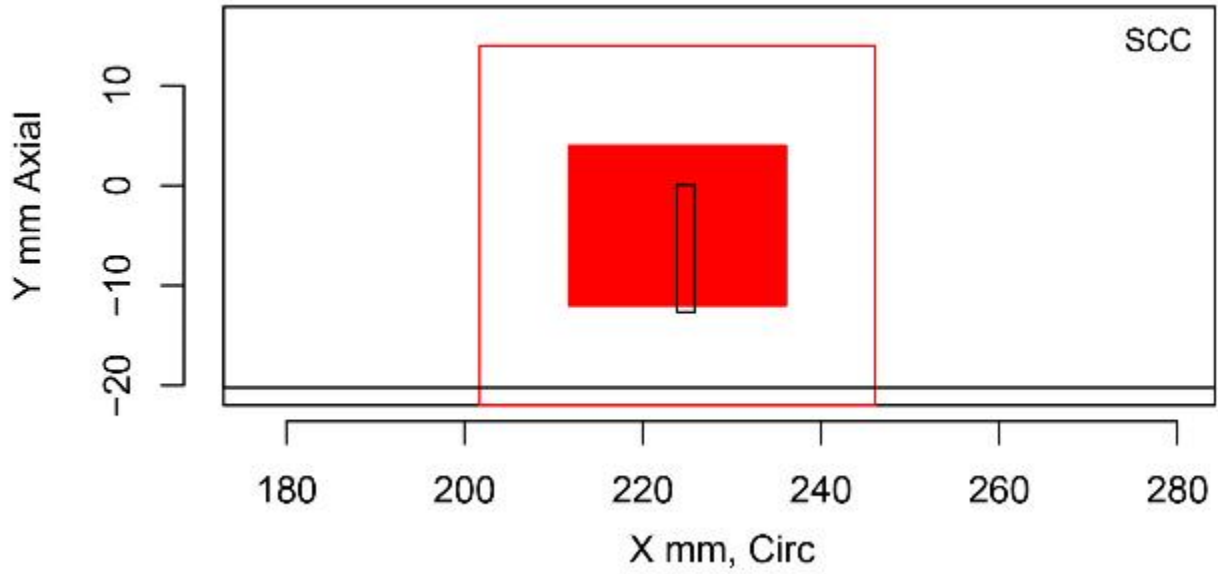


Figure E.35 Indication Plot for Procedure PAUT.132 Applied to Test Block P16 in PARENT Blind Testing (X – Y view)

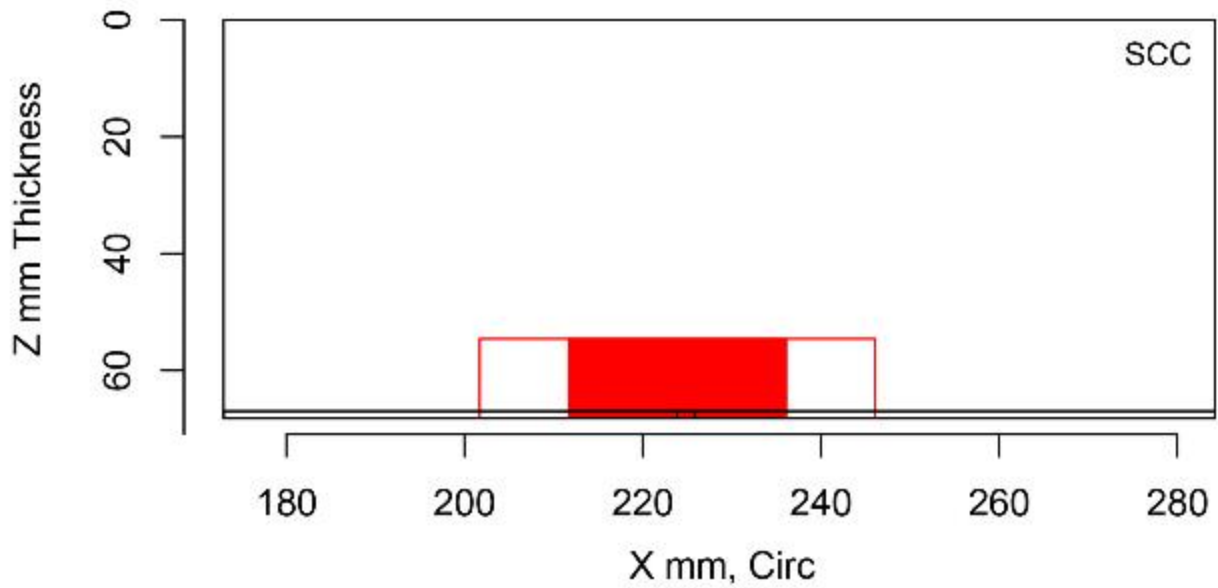


Figure E.36 Indication Plot for Procedure PAUT.132 Applied to Test Block P16 in PARENT Blind Testing (X – Z view)

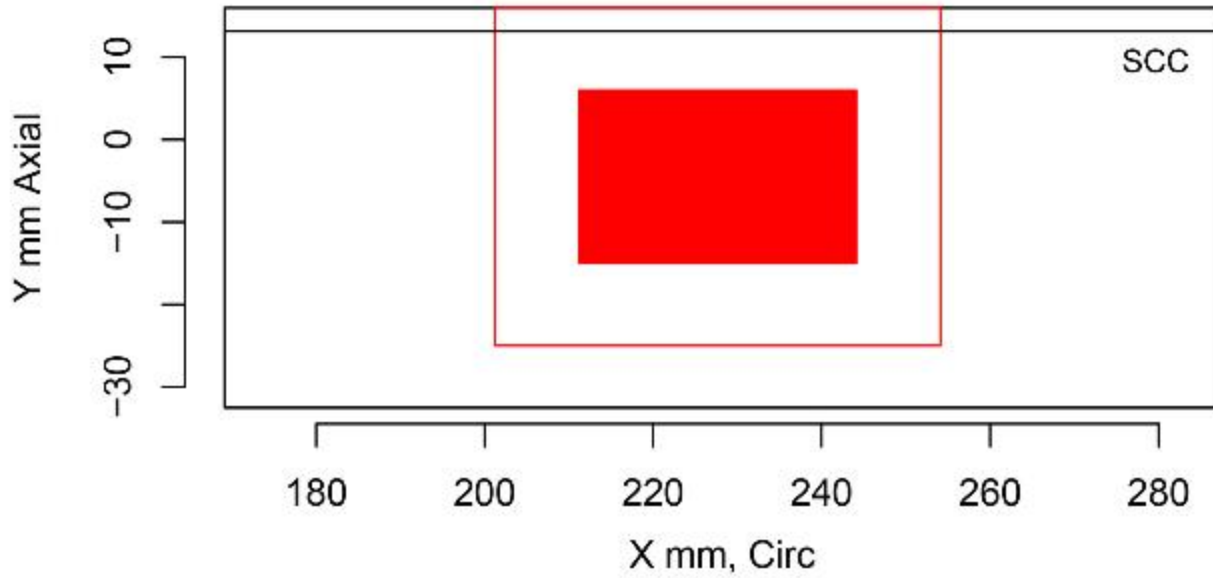


Figure E.37 Indication Plot for Procedure PAUT.132 Applied to Test Block P17 in PARENT Blind Testing (X – Y view)

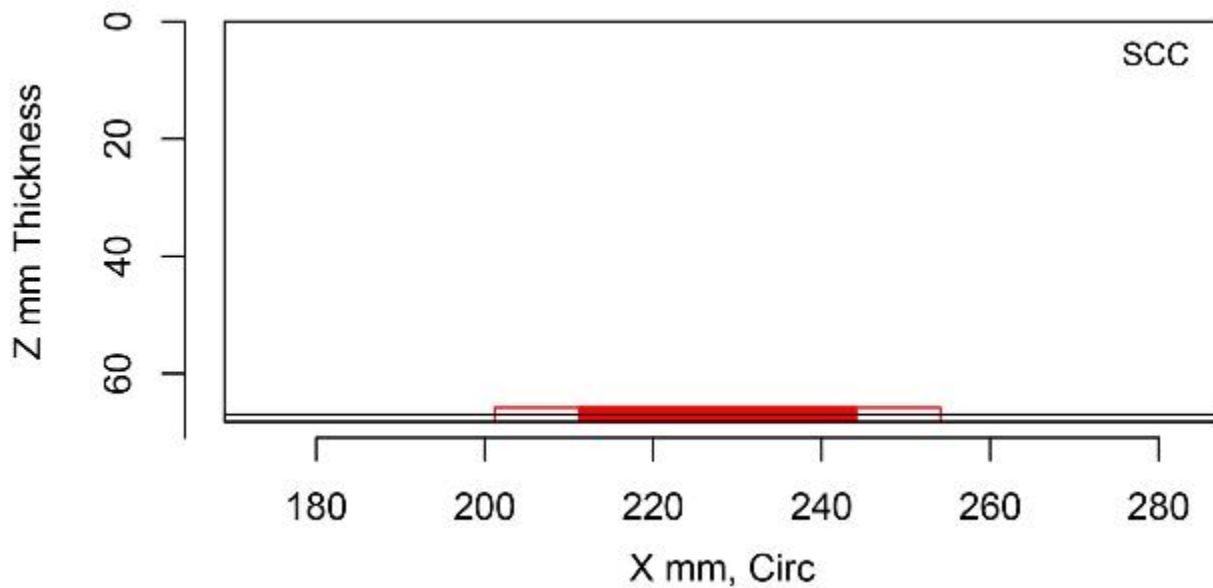


Figure E.38 Indication Plot for Procedure PAUT.132 Applied to Test Block P17 in PARENT Blind Testing (X – Z view)

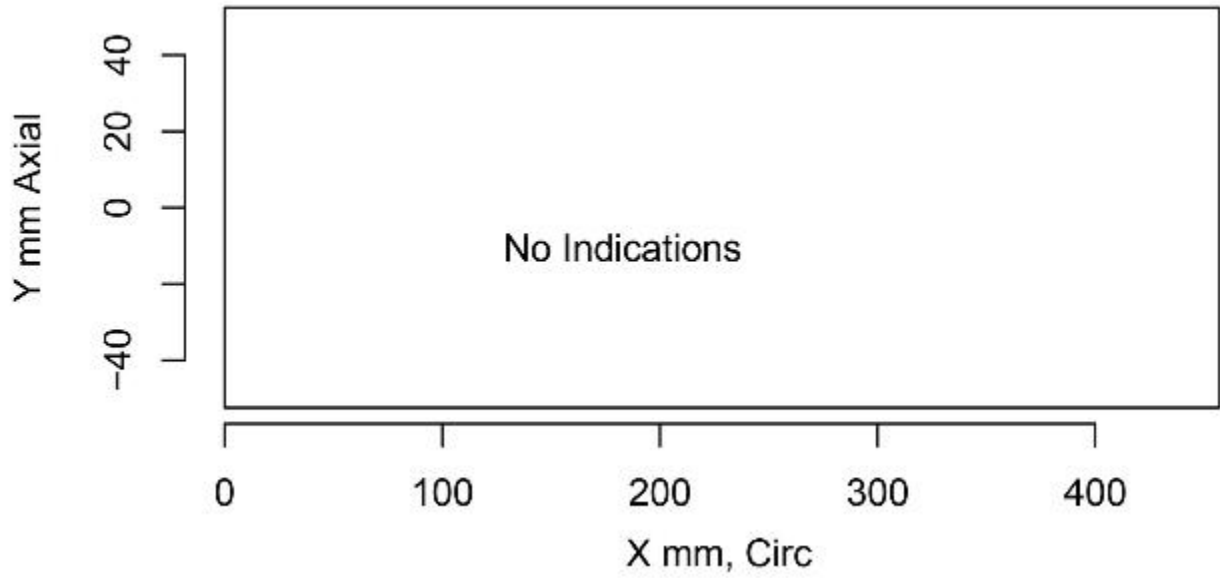


Figure E.39 Indication Plot for Procedure PAUT.132 Applied to Test Block P45 in PARENT Blind Testing (X – Y view)

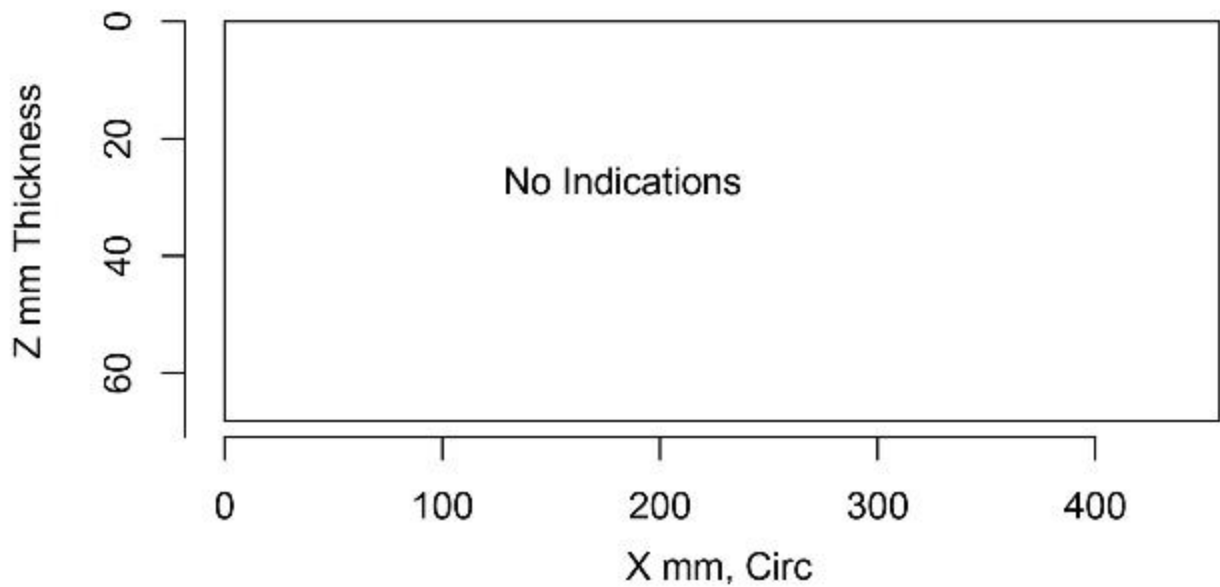


Figure E.40 Indication Plot for Procedure PAUT.132 Applied to Test Block P45 in PARENT Blind Testing (X – Z view)

E.1.6 Plots for Team 134

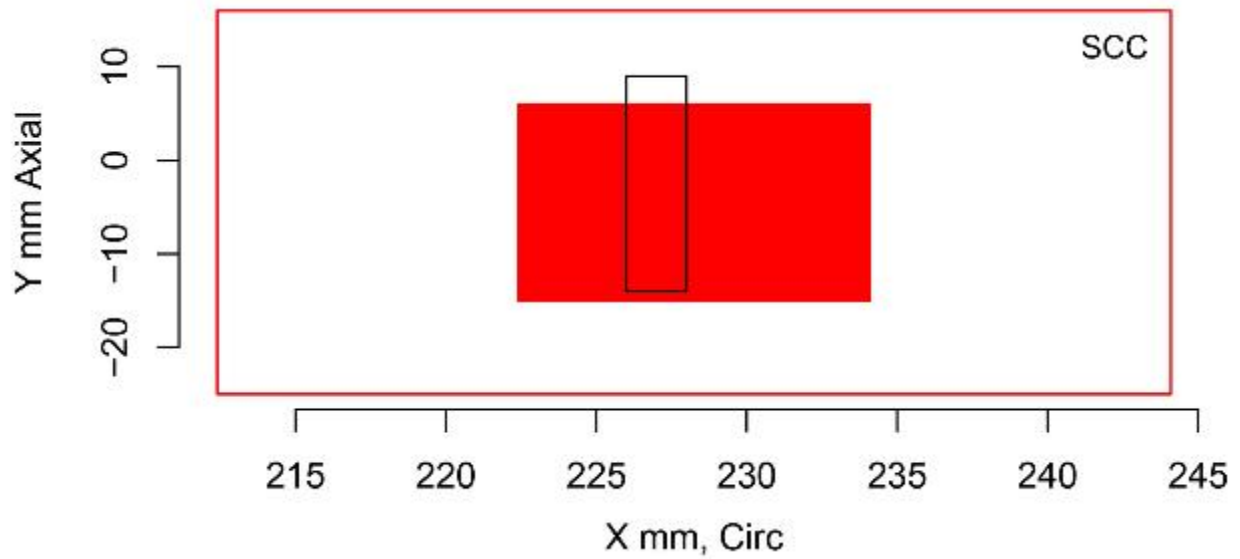


Figure E.41 Indication Plot for Procedure UT.134 Applied to Test Block P15 in PARENT Blind Testing (X - Y view)

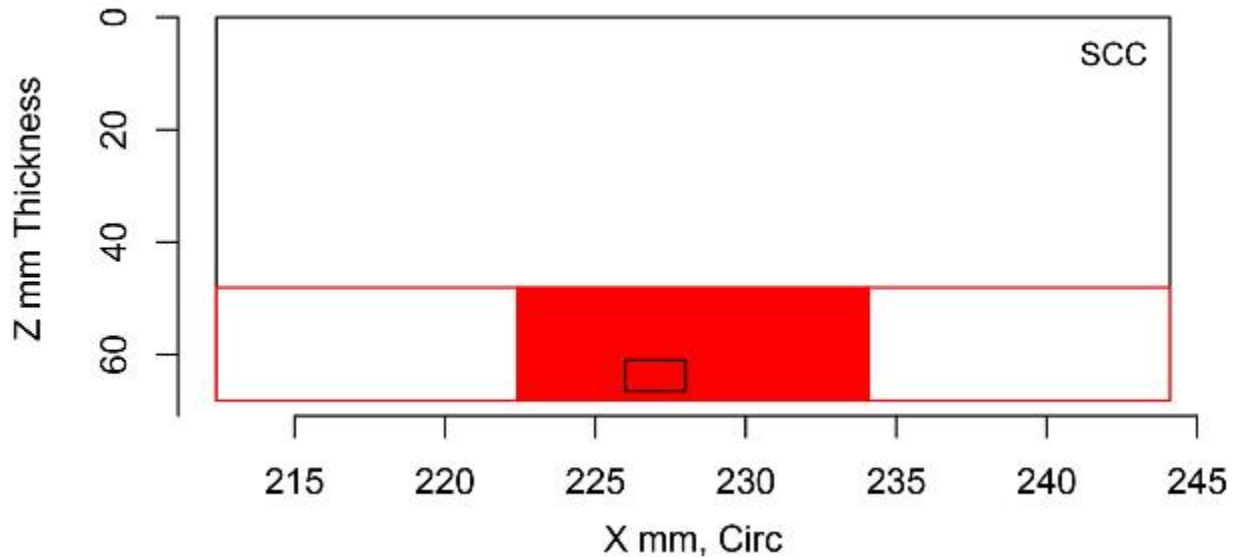


Figure E.42 Indication Plot for Procedure UT.134 Applied to Test Block P15 in PARENT Blind Testing (X - Z view)

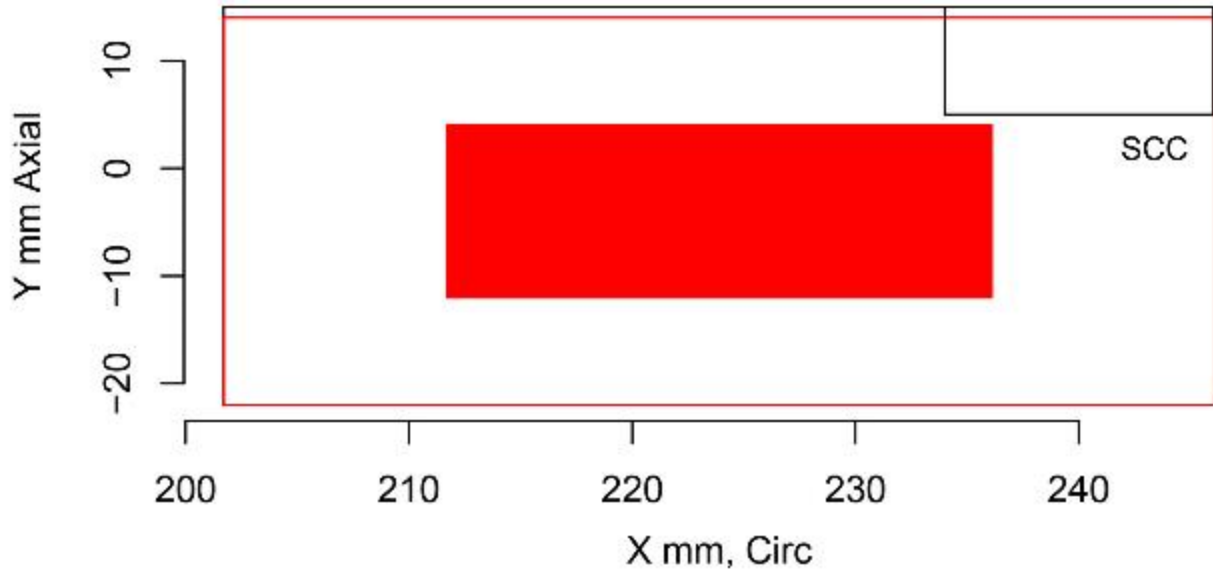


Figure E.43 Indication Plot for Procedure UT.134 Applied to Test Block P16 in PARENT Blind Testing (X – Y view)

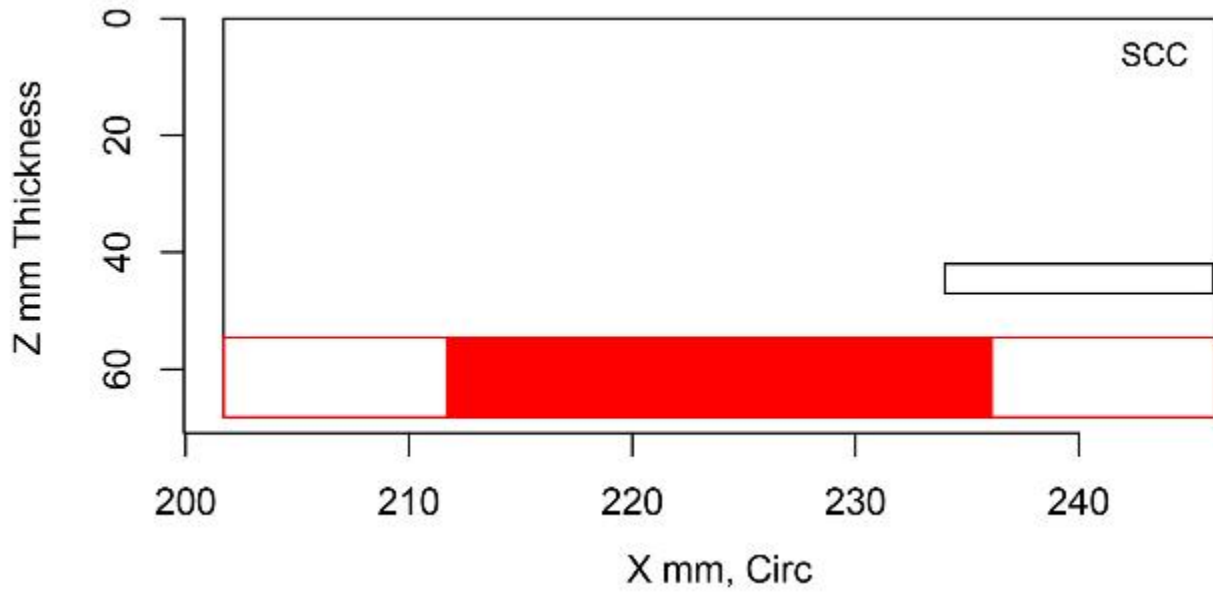


Figure E.44 Indication Plot for Procedure UT.134 Applied to Test Block P16 in PARENT Blind Testing (X – Z view)

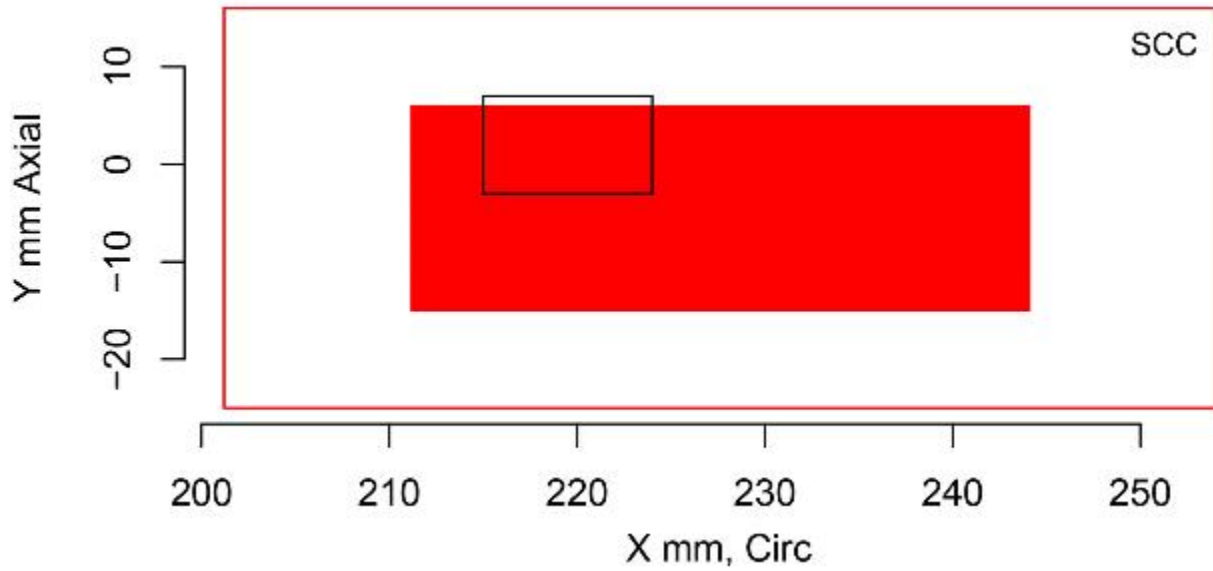


Figure E.45 Indication Plot for Procedure UT.134 Applied to Test Block P17 in PARENT Blind Testing (X – Y view)

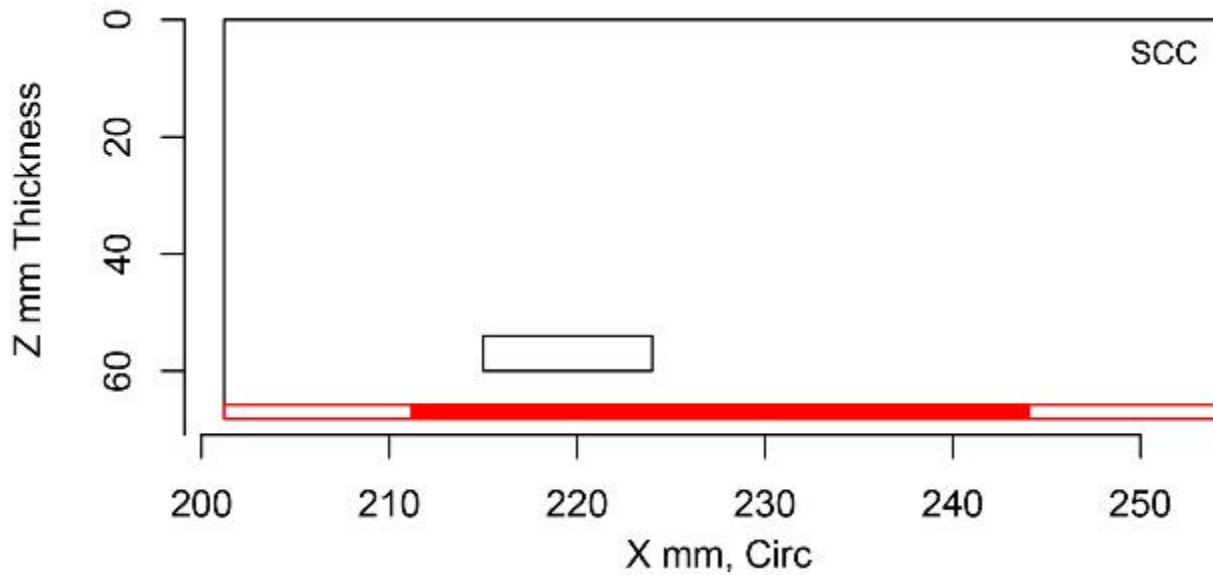


Figure E.46 Indication Plot for Procedure UT.134 Applied to Test Block P17 in PARENT Blind Testing (X – Z view)

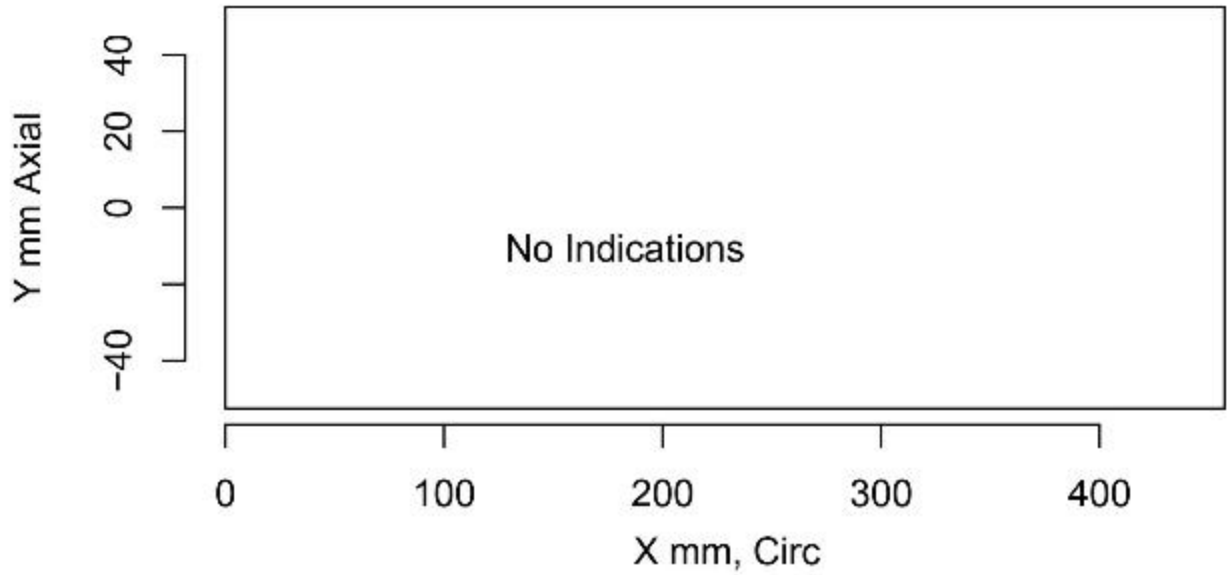


Figure E.47 Indication Plot for Procedure UT.134 Applied to Test Block P45 in PARENT Blind Testing (X – Y view)

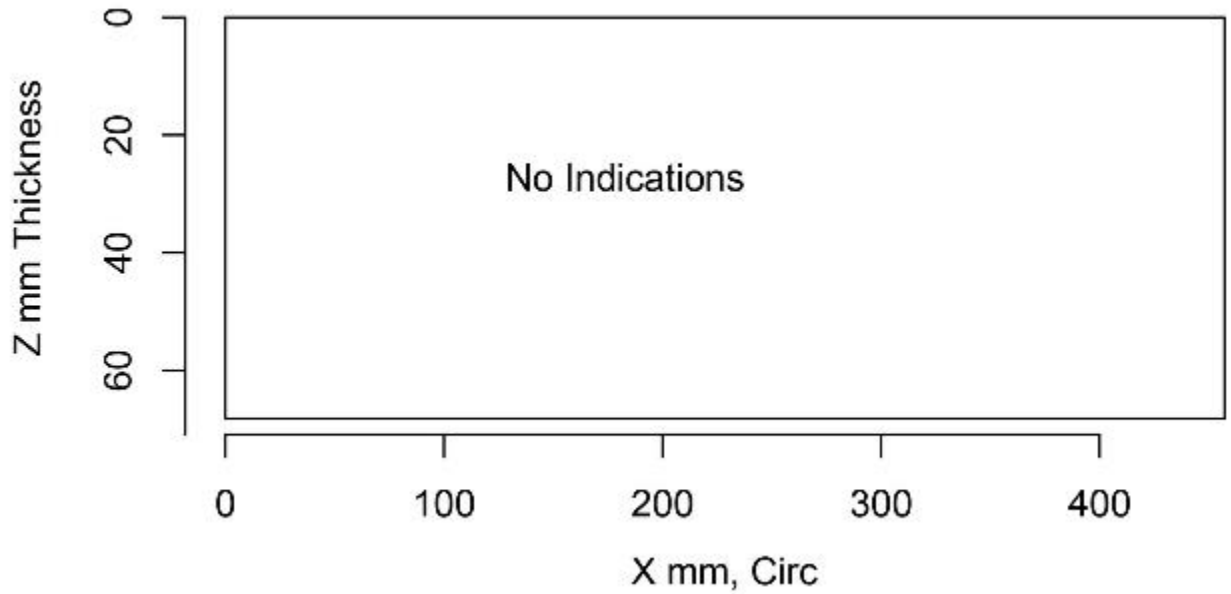


Figure E.48 Indication Plot for Procedure UT.134 Applied to Test Block P45 in PARENT Blind Testing (X – Z view)

E.2 DMW Inspection Summary Results

E.2.1 Plots for Team 101

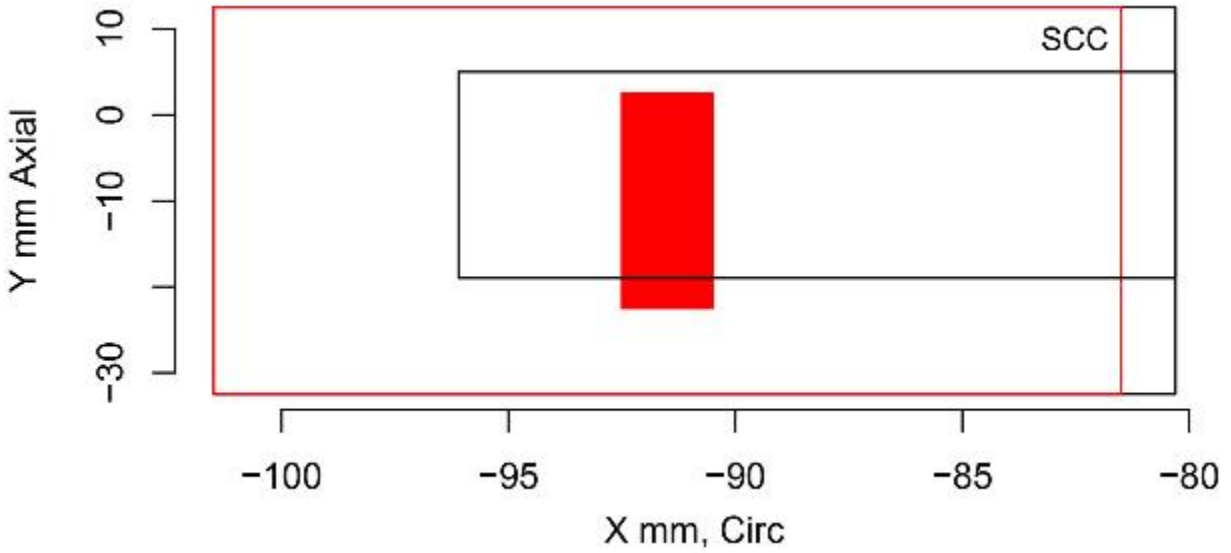


Figure E.49 Indication Plot for Procedure UT.TOFD.ECT.101 Applied to Test Block P13 in PARENT Blind Testing (X – Y view)

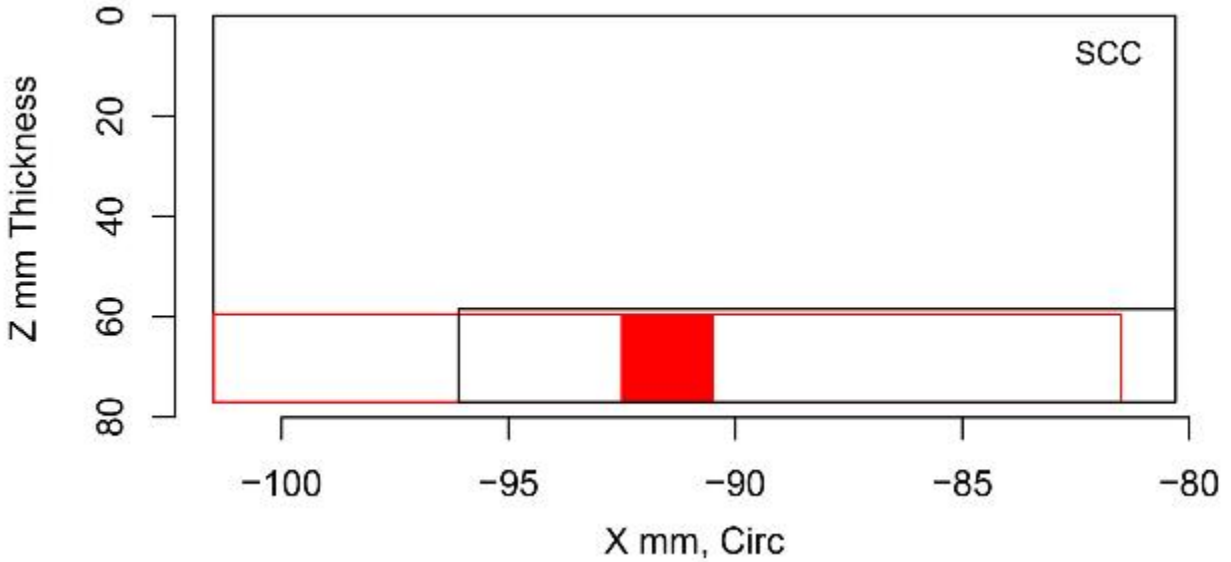


Figure E.50 Indication Plot for Procedure UT.TOFD.ECT.101 Applied to Test Block P13 in PARENT Blind Testing (X – Z view)

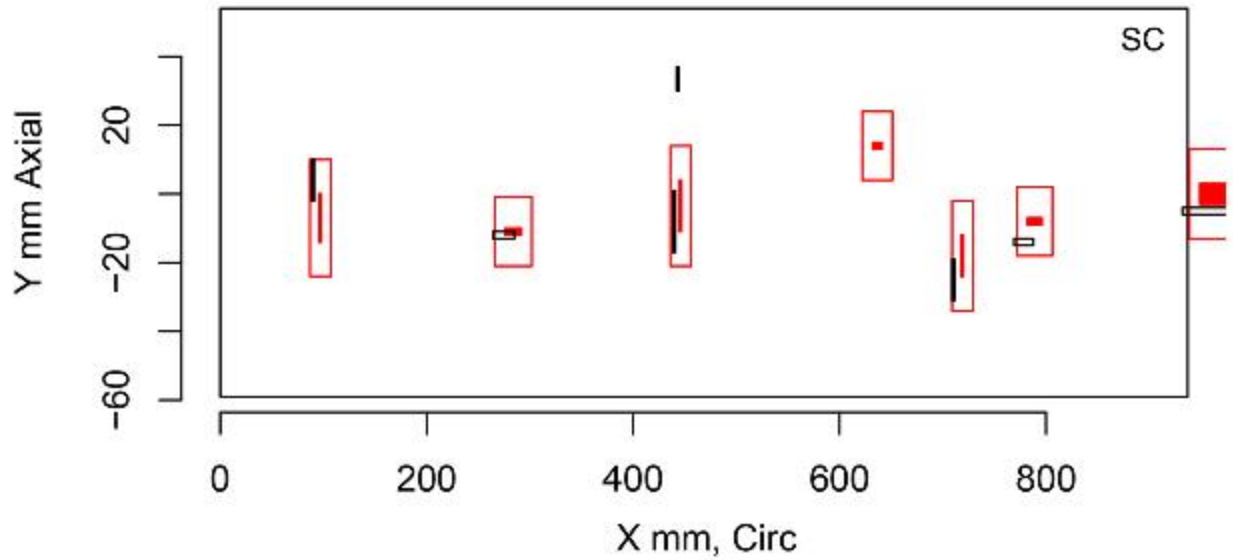


Figure E.51 Indication Plot for Procedure UT.TOFD.ECT.101 Applied to Test Block P33 in PARENT Blind Testing (X – Y view, 0 mm–800 mm)

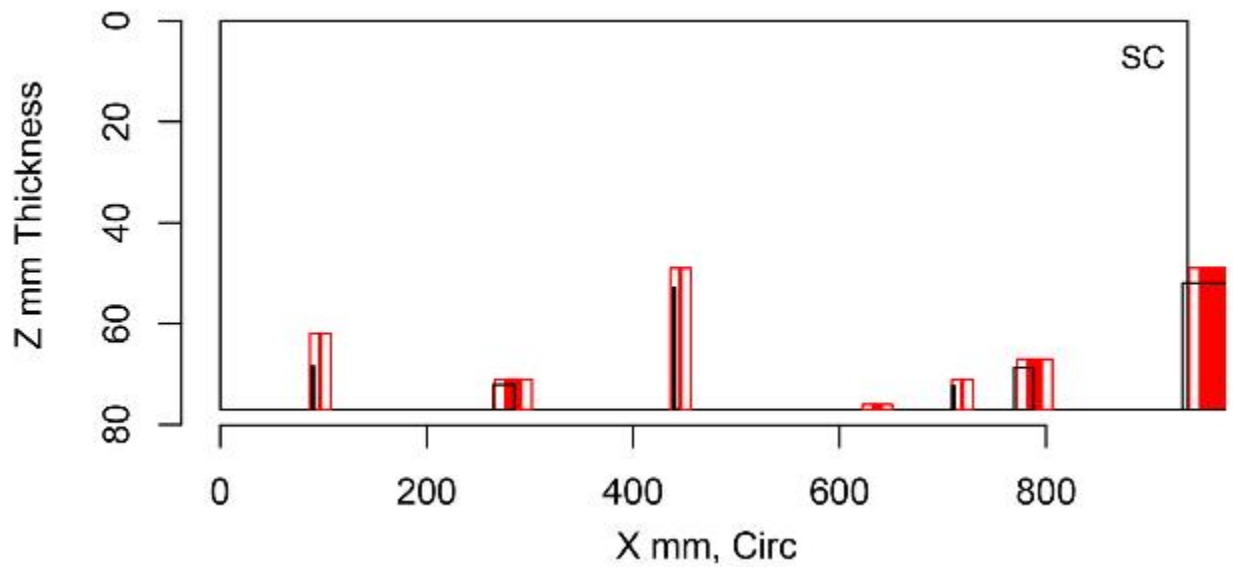


Figure E.52 Indication Plot for Procedure UT.TOFD.ECT.101 Applied to Test Block P33 in PARENT Blind Testing (X – Z view, 0 mm–800 mm)

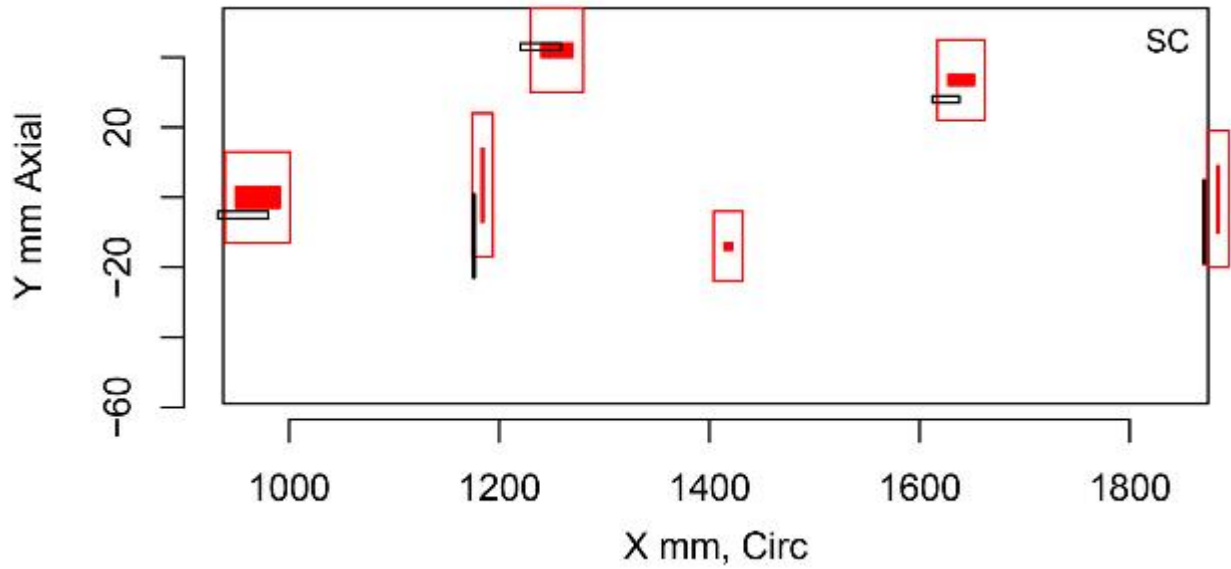


Figure E.53 Indication Plot for Procedure UT.TOFD.ECT.101 Applied to Test Block P33 in PARENT Blind Testing (X – Y view, 1000 mm–1800 mm)

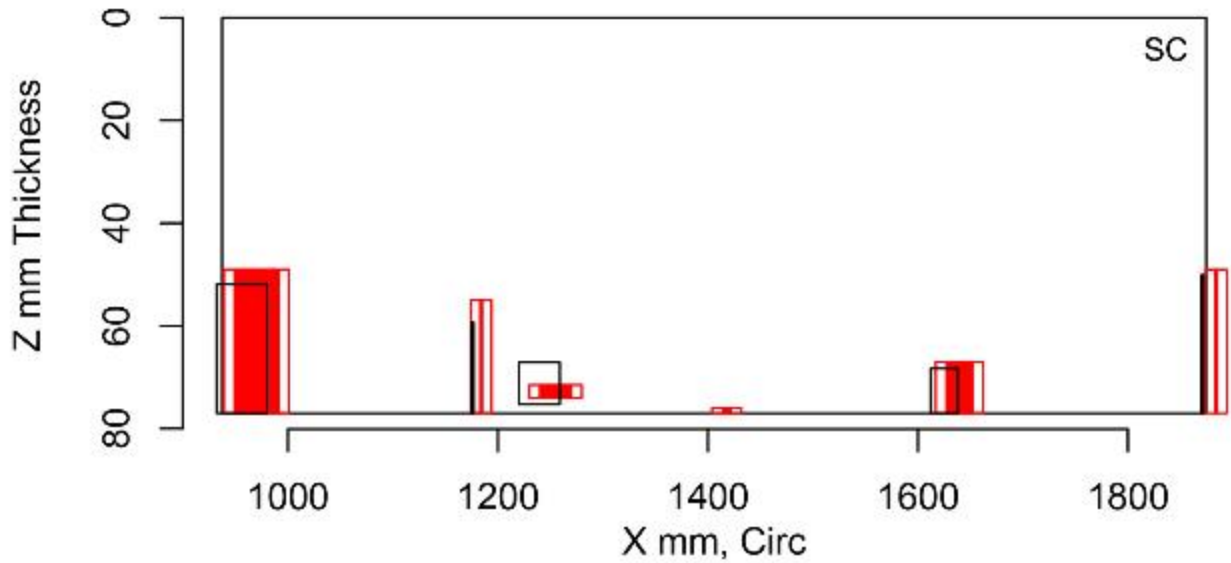


Figure E.54 Indication Plot for Procedure UT.TOFD.ECT.101 Applied to Test Block P33 in PARENT Blind Testing (X – Z view, 1000 mm–1800 mm)

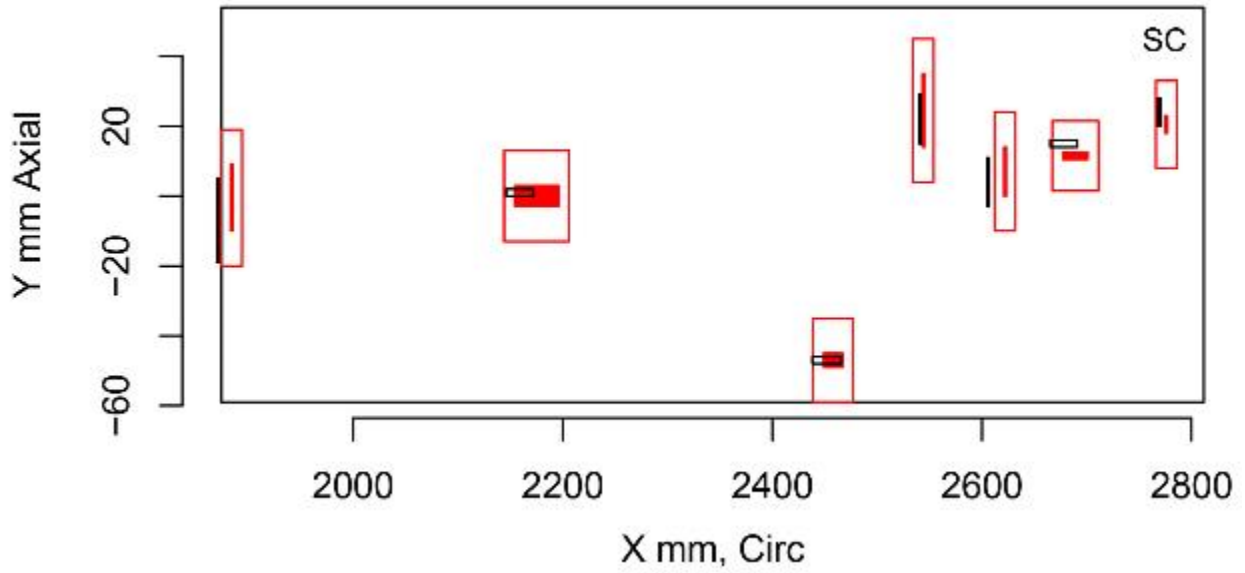


Figure E.55 Indication Plot for Procedure UT.TOFD.ECT.101 Applied to Test Block P33 in PARENT Blind Testing (X – Y view, 2000 mm–2800 mm)

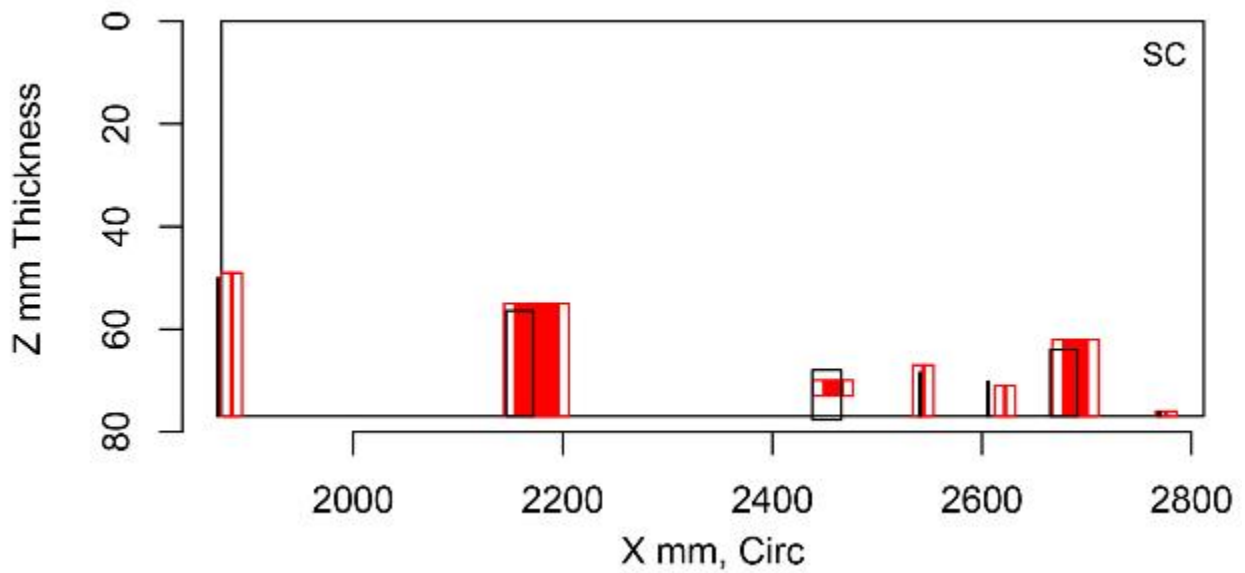


Figure E.56 Indication Plot for Procedure UT.TOFD.ECT.101 Applied to Test Block P33 in PARENT Blind Testing (X – Z view, 2000 mm–2800 mm)

E.2.2 Plots for Team 108

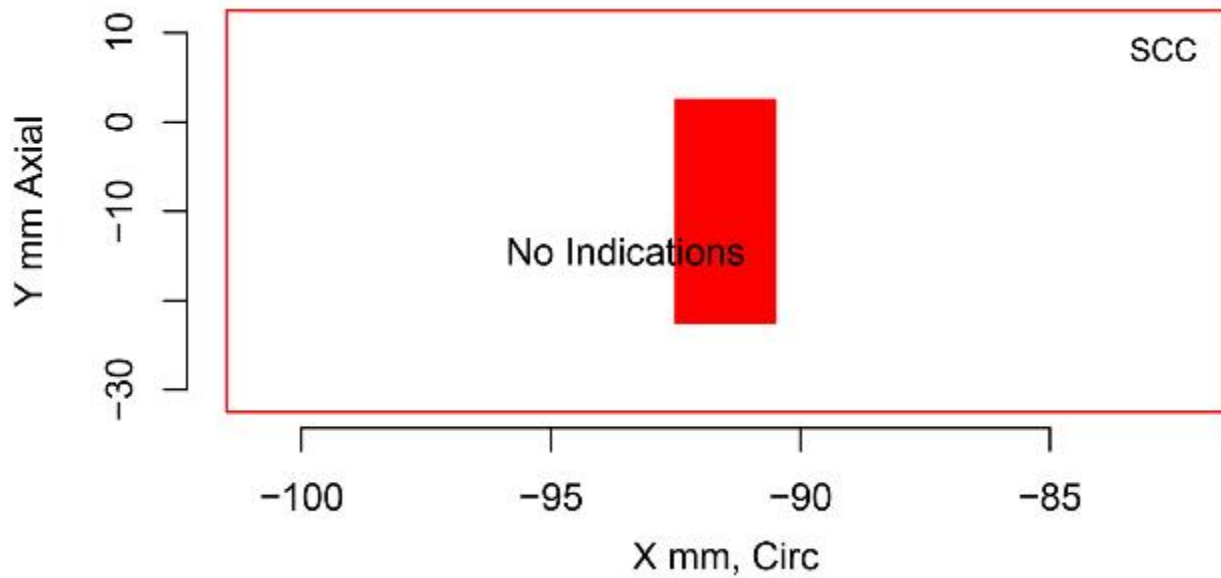


Figure E.57 Indication Plot for Procedure PAUT.108 Applied to Test Block P13 in PARENT Blind Testing (X – Y view)

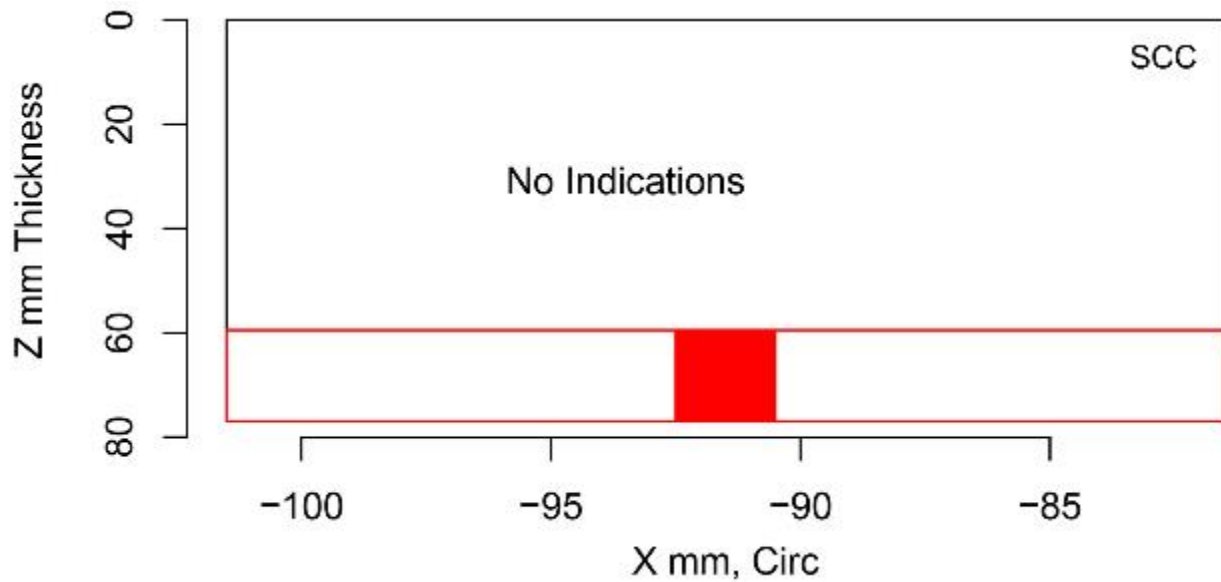


Figure E.58 Indication Plot for Procedure PAUT.108 Applied to Test Block P13 in PARENT Blind Testing (X – Z view)

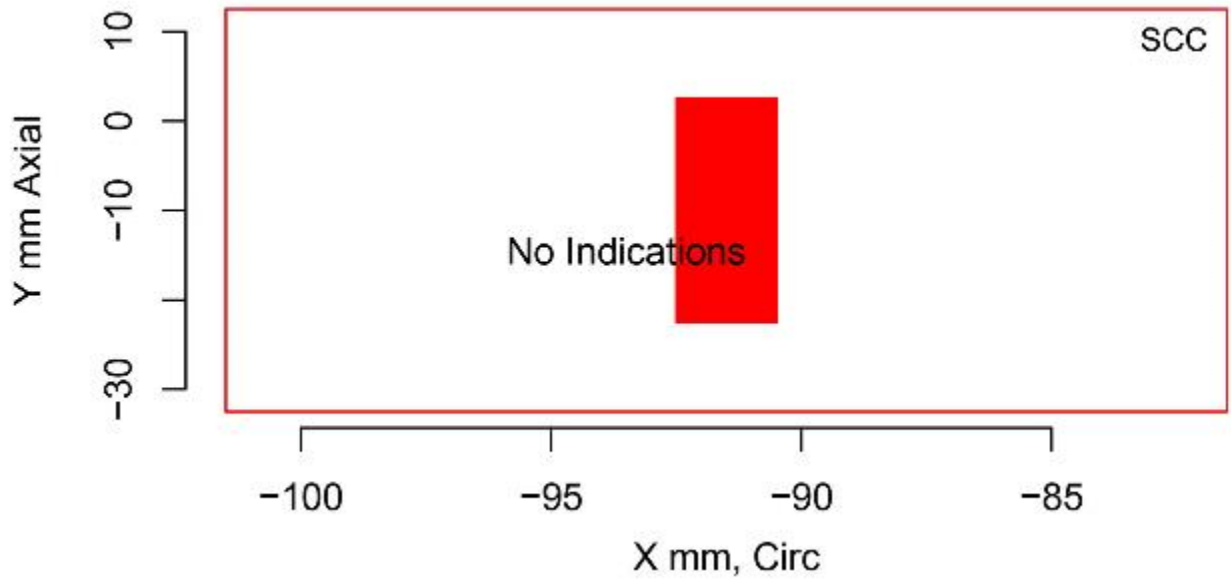


Figure E.59 Indication Plot for Procedure UT.108 Applied to Test Block P13 in PARENT Blind Testing (X – Y view)

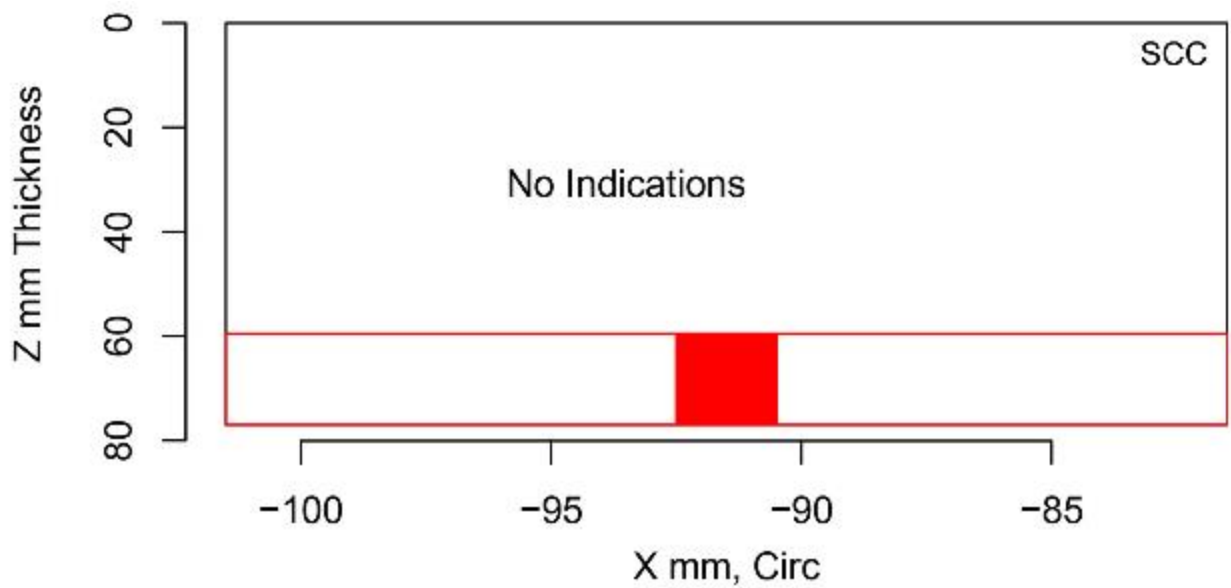


Figure E.60 Indication Plot for Procedure UT.108 Applied to Test Block P13 in PARENT Blind Testing (X – Z view)

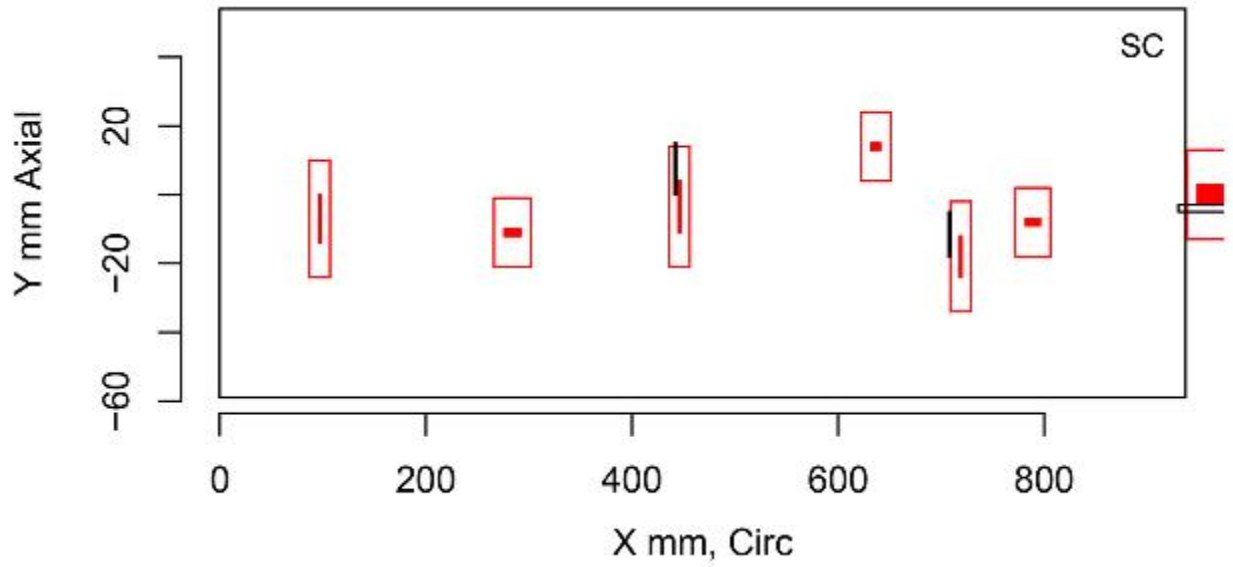


Figure E.61 Indication Plot for Procedure PAUT.108 Applied to Test Block P33 in PARENT Blind Testing (X – Y view, 0 mm–800 mm)

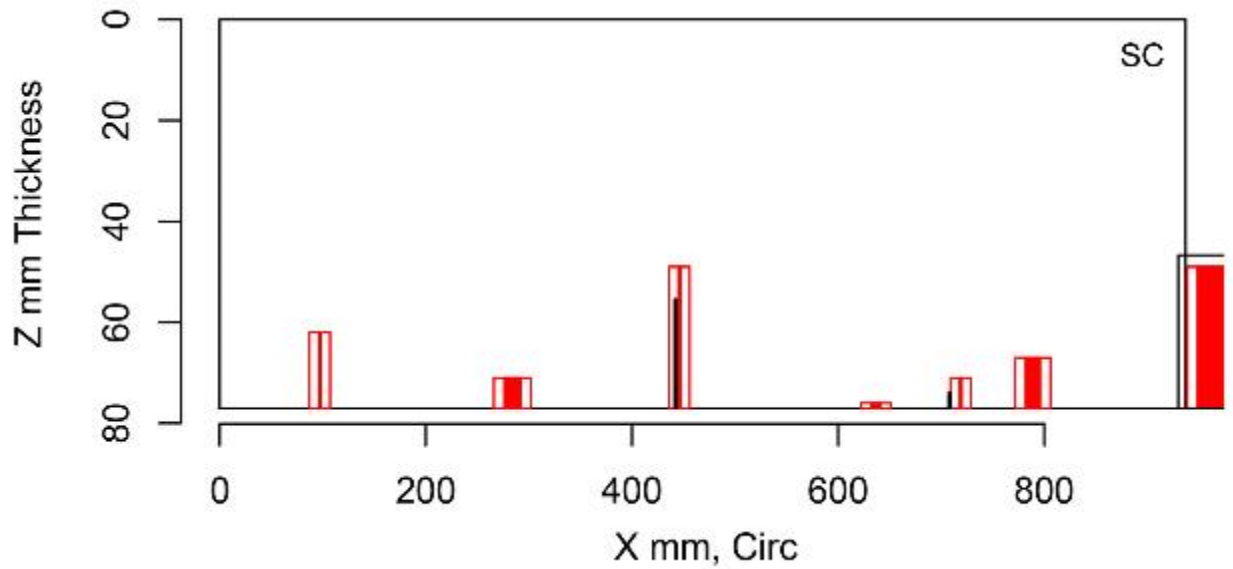


Figure E.62 Indication Plot for Procedure PAUT.108 Applied to Test Block P33 in PARENT Blind Testing (X – Z view, 0 mm–800 mm)

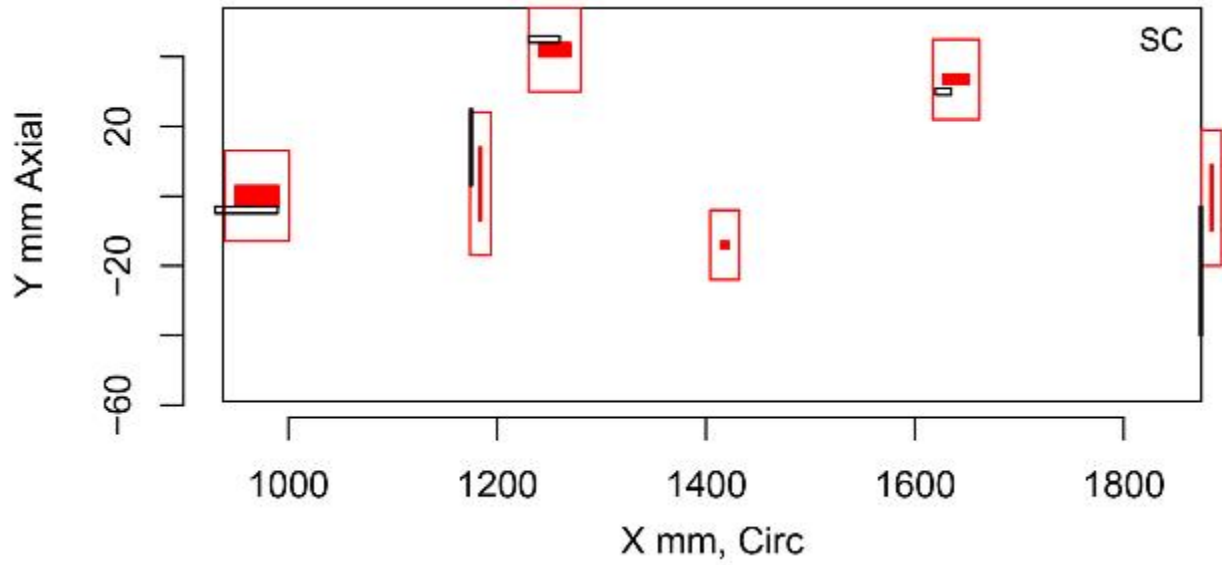


Figure E.63 Indication Plot for Procedure PAUT.108 Applied to Test Block P33 in PARENT Blind Testing (X - Y view, 1000 mm-1800 mm)

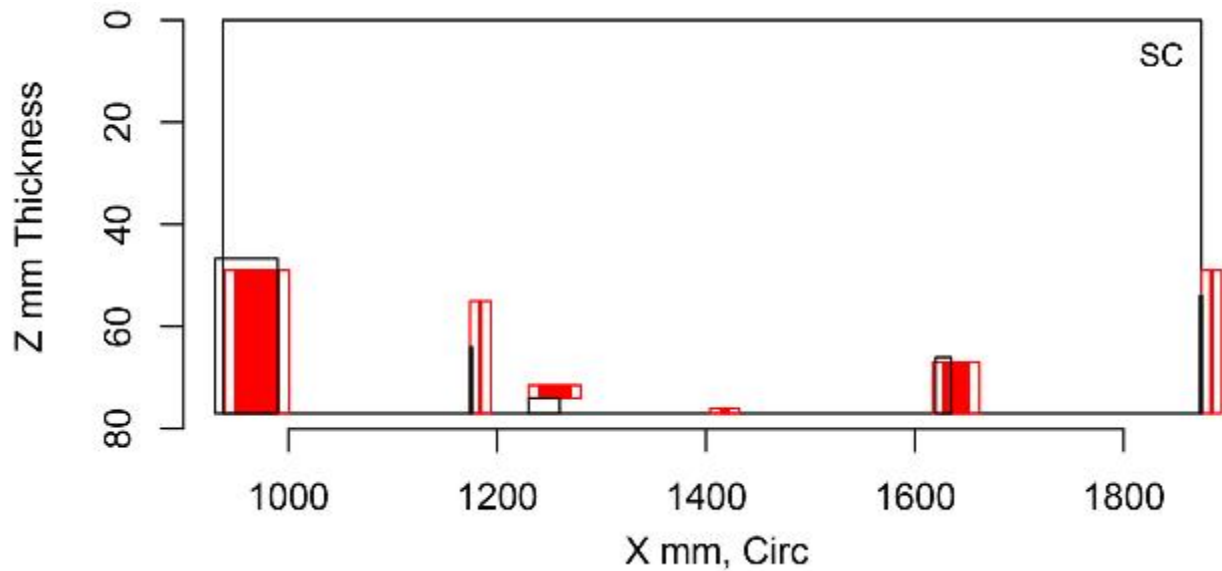


Figure E.64 Indication Plot for Procedure PAUT.108 Applied to Test Block P33 in PARENT Blind Testing (X - Z view, 1000 mm-1800 mm)

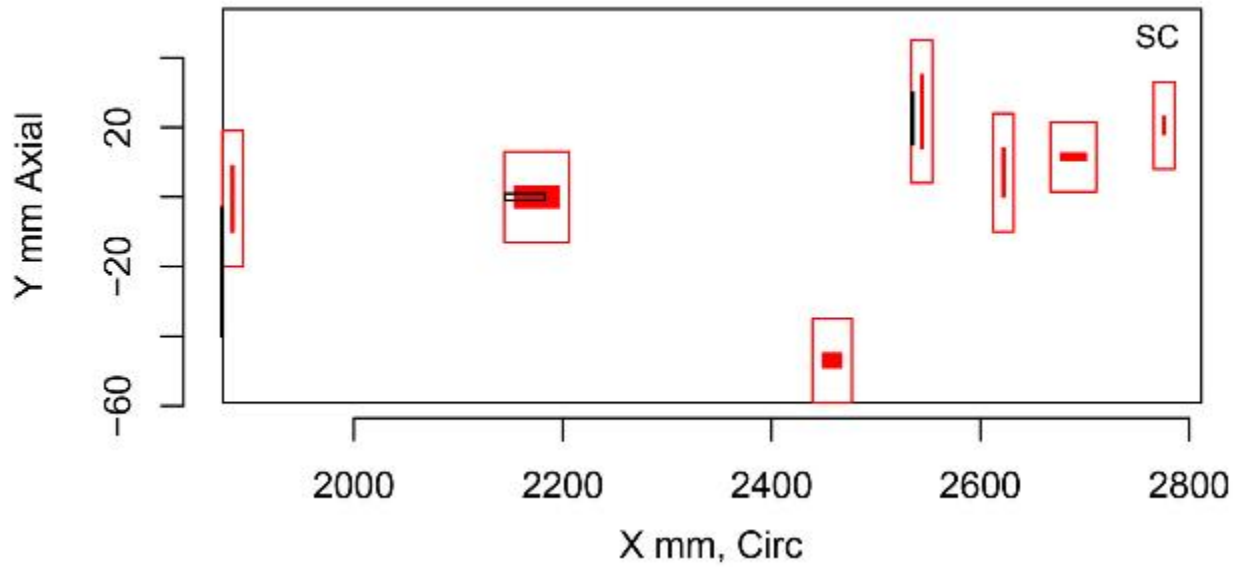


Figure E.65 Indication Plot for Procedure PAUT.108 Applied to Test Block P33 in PARENT Blind Testing (X – Y view, 2000 mm–2800 mm)

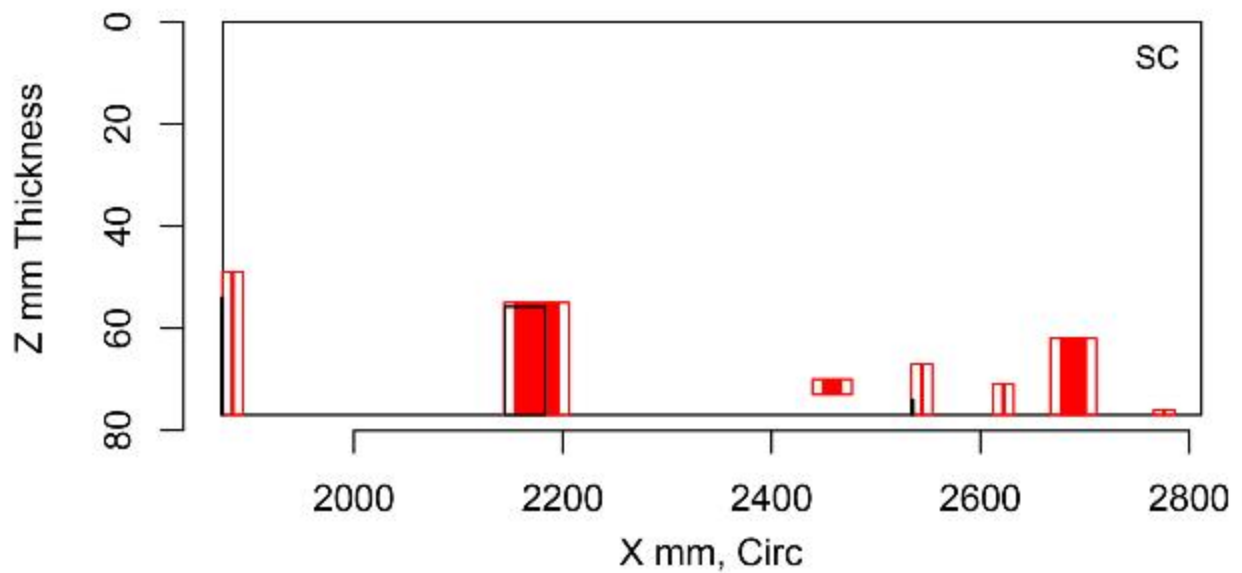


Figure E.66 Indication Plot for Procedure PAUT.108 Applied to Test Block P33 in PARENT Blind Testing (X – Z view, 2000 mm–2800 mm)

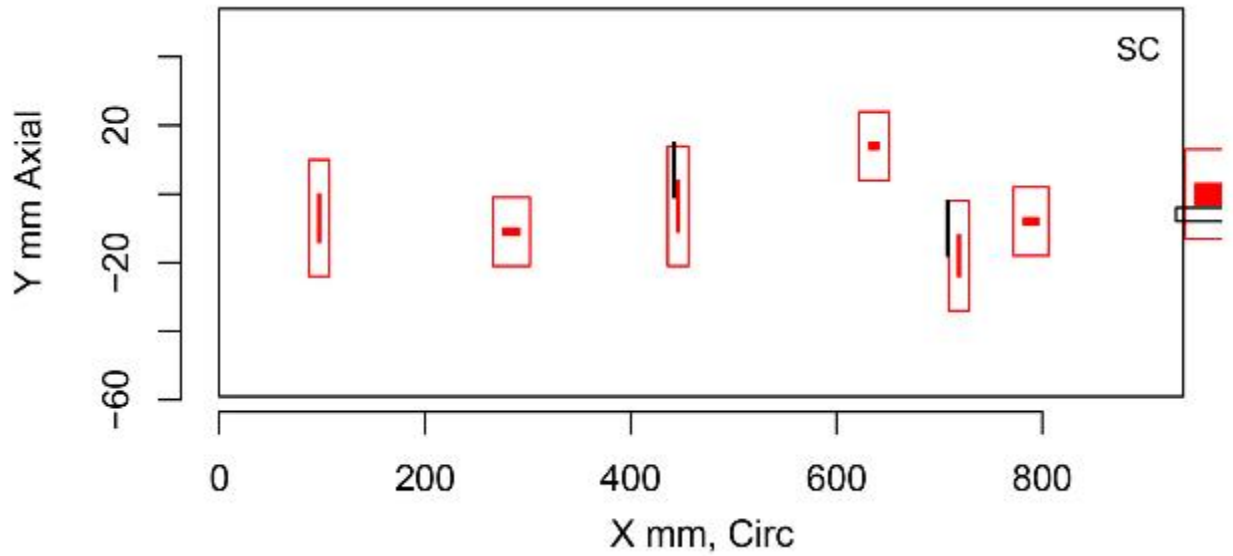


Figure E.67 Indication Plot for Procedure UT.108 Applied to Test Block P33 in PARENT Blind Testing (X – Y view, 0 mm–800 mm)

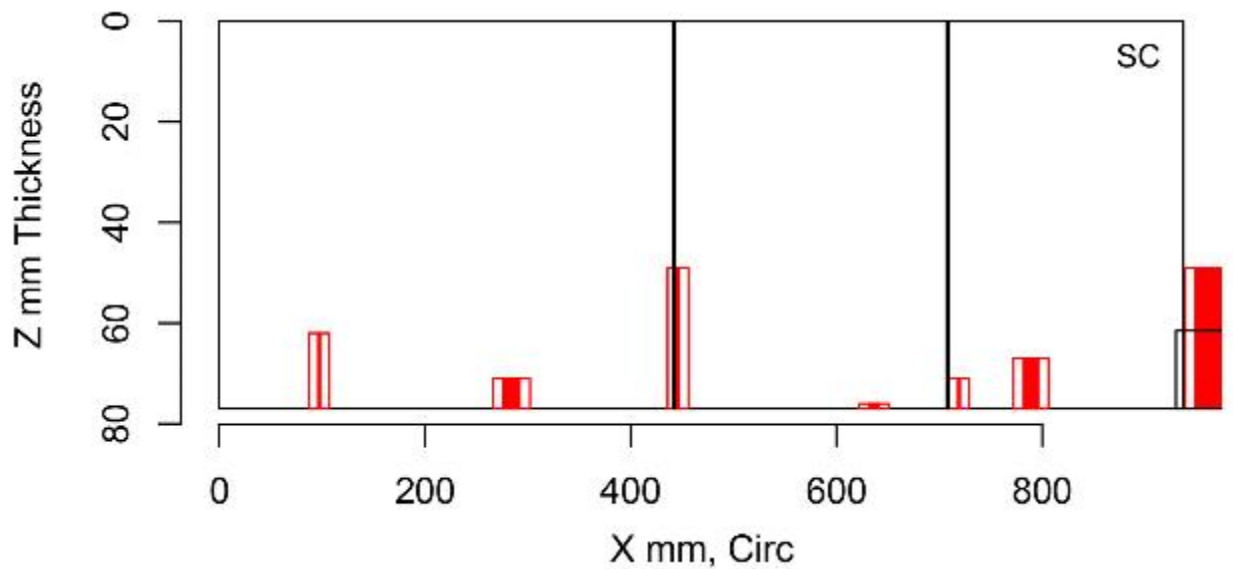


Figure E.68 Indication Plot for Procedure UT.108 Applied to Test Block P33 in PARENT Blind Testing (X – Z view, 0 mm–800 mm)

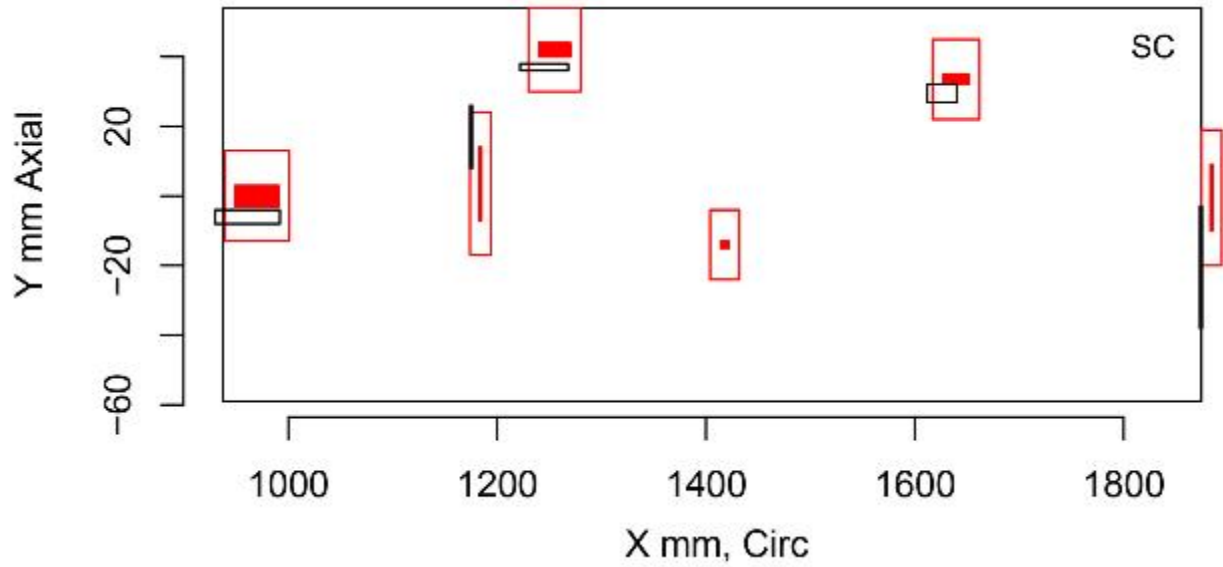


Figure E.69 Indication Plot for Procedure UT.108 Applied to Test Block P33 in PARENT Blind Testing (X – Y view, 1000 mm–1800 mm)

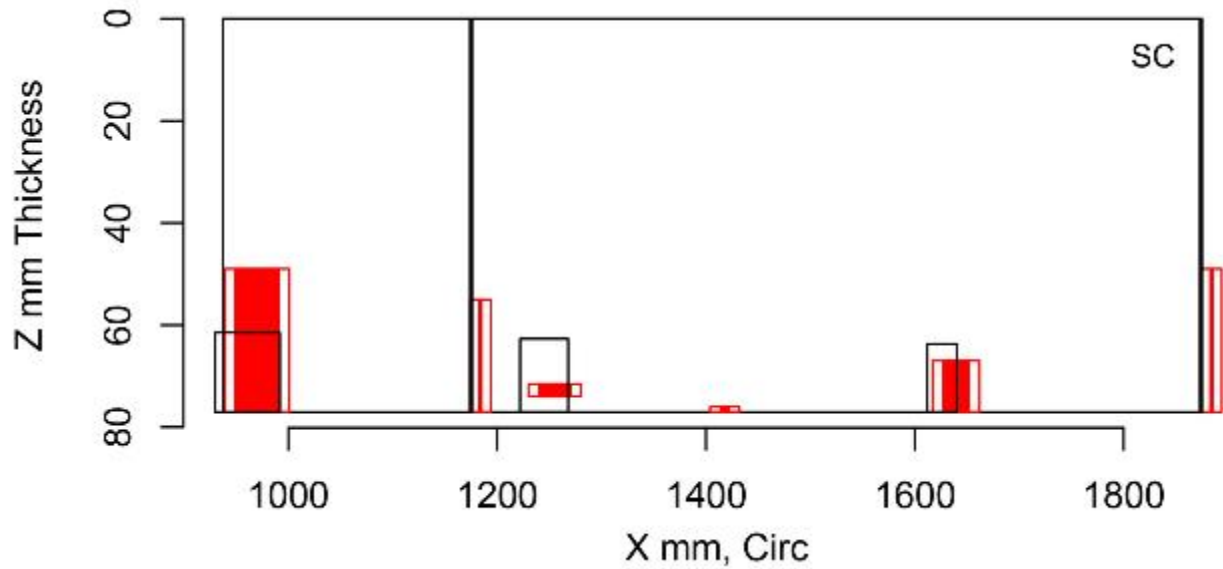


Figure E.70 Indication Plot for Procedure UT.108 Applied to Test Block P33 in PARENT Blind Testing (X – Z view, 1000 mm–1800 mm)

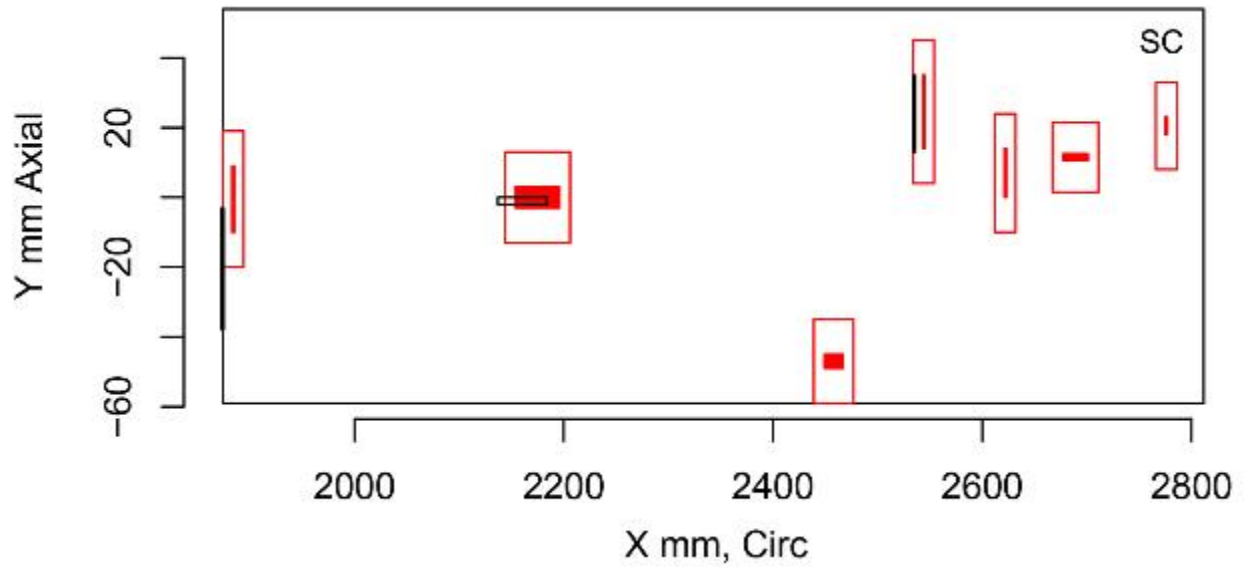


Figure E.71 Indication Plot for Procedure UT.108 Applied to Test Block P33 in PARENT Blind Testing (X – Y view, 2000 mm–2800 mm)

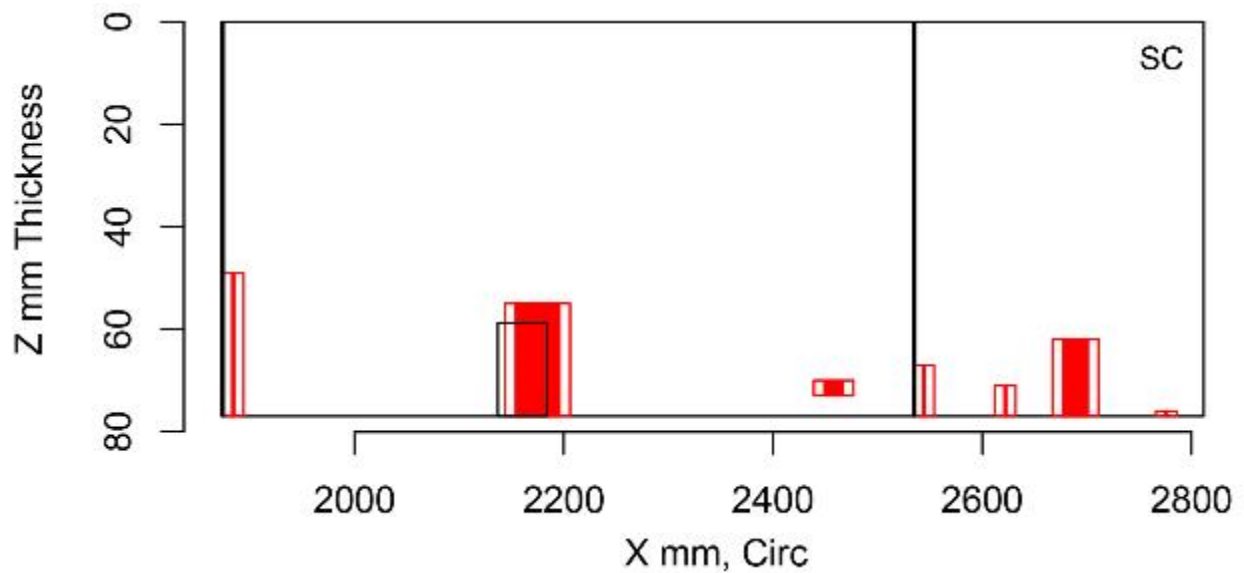


Figure E.72 Indication Plot for Procedure UT.108 Applied to Test Block P33 in PARENT Blind Testing (X – Z view, 2000 mm–2800 mm)

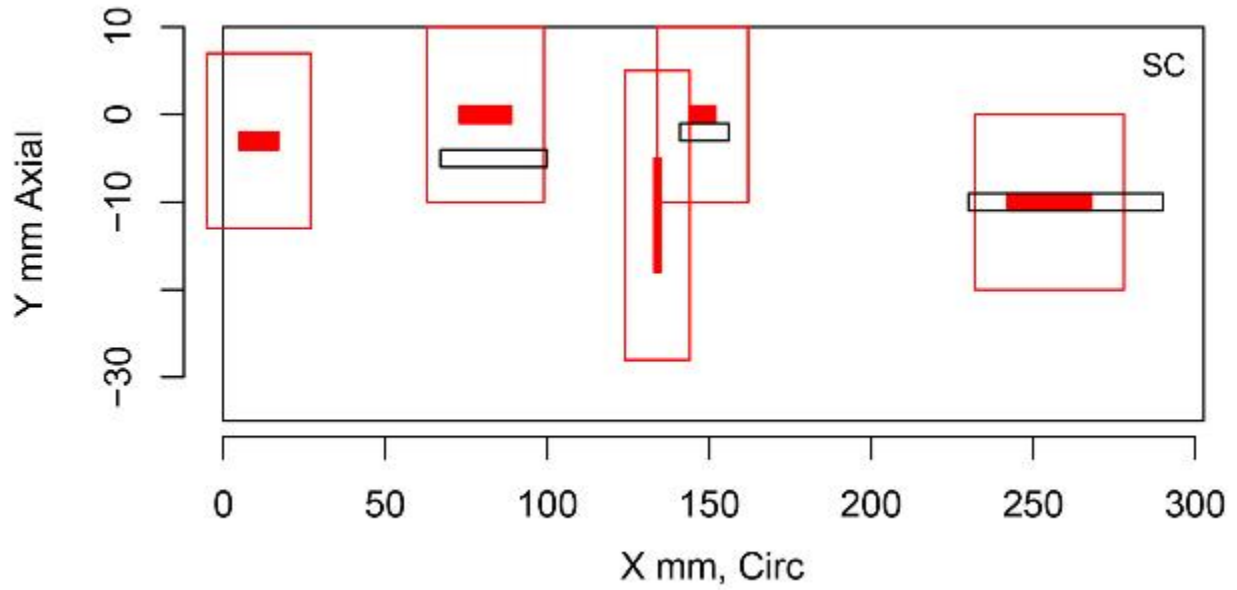


Figure E.73 Indication Plot for Procedure PAUT.108 Applied to Test Block P35 in PARENT Blind Testing (X - Y view, 0 mm-300 mm)

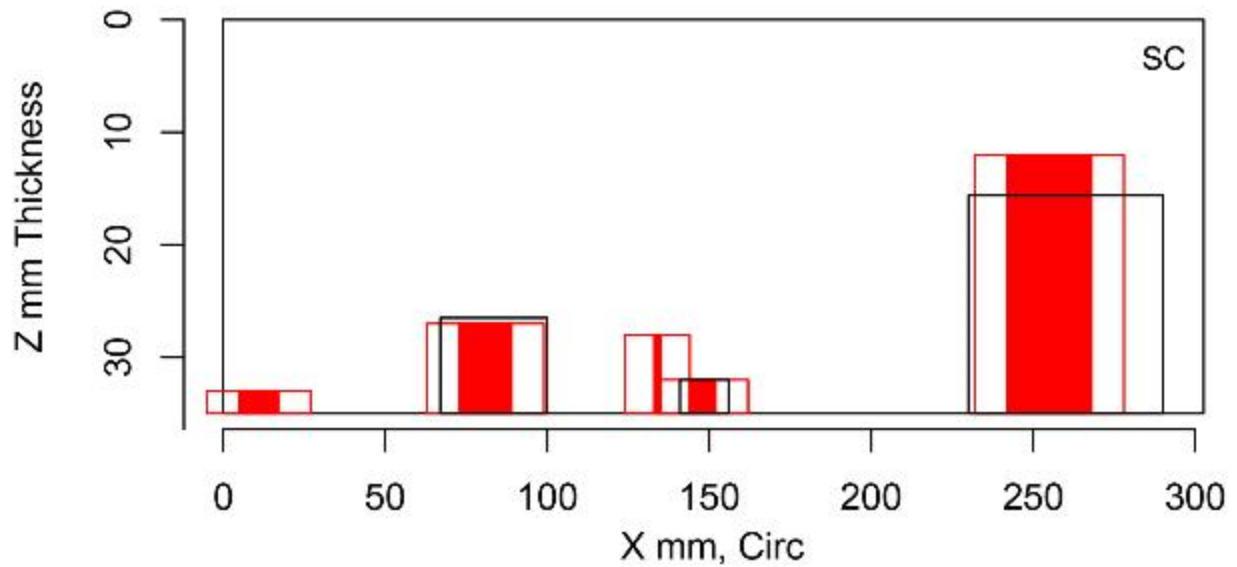


Figure E.74 Indication Plot for Procedure PAUT.108 Applied to Test Block P35 in PARENT Blind Testing (X - Z view, 0 mm-300 mm)

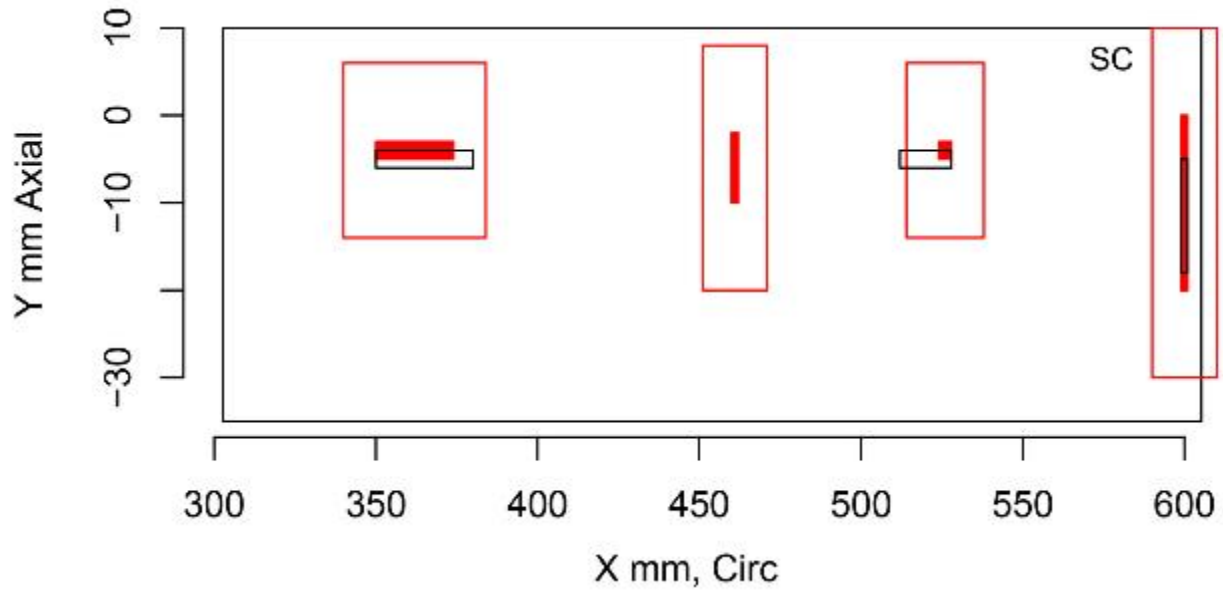


Figure E.75 Indication Plot for Procedure PAUT.108 Applied to Test Block P35 in PARENT Blind Testing (X – Y view, 300 mm–600 mm)

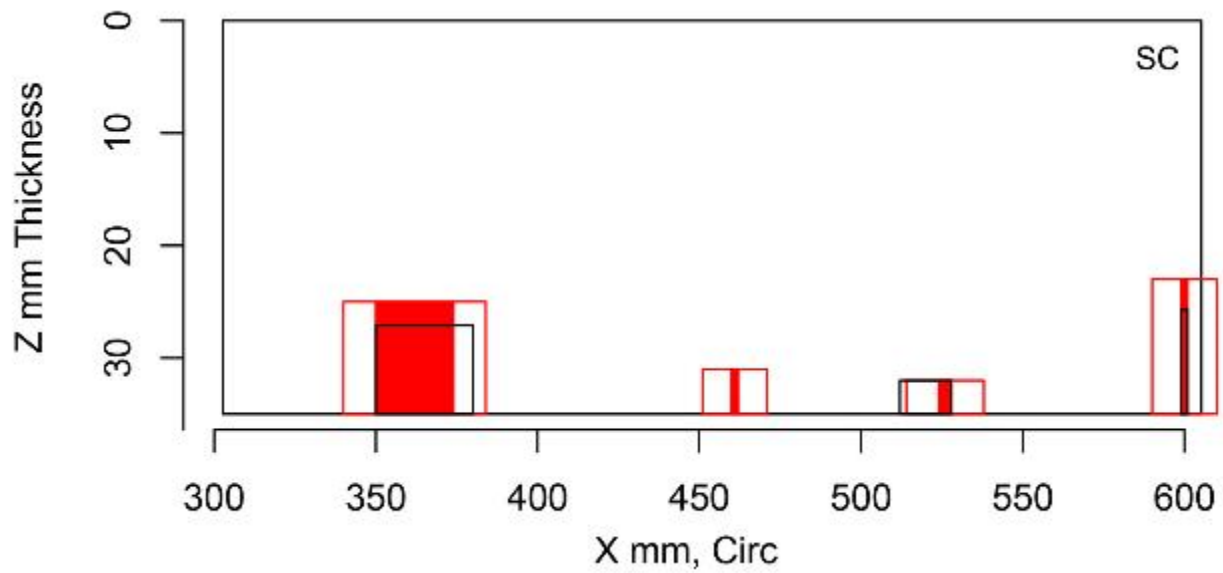


Figure E.76 Indication Plot for Procedure PAUT.108 Applied to Test Block P35 in PARENT Blind Testing (X – Z view, 300 mm–600 mm)

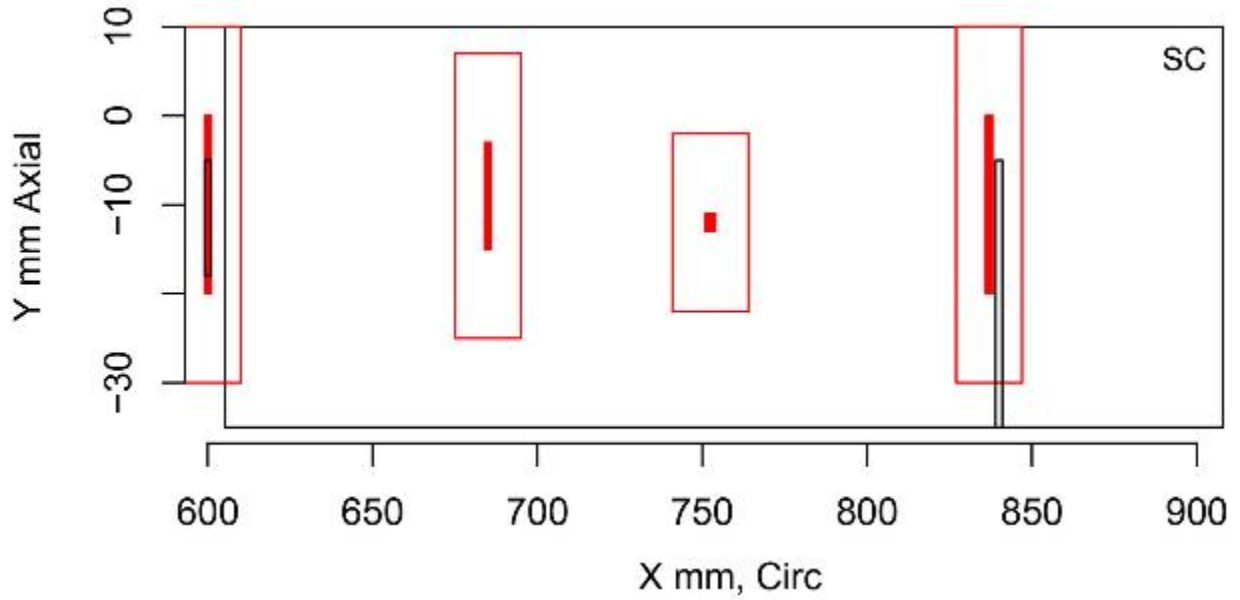


Figure E.77 Indication Plot for Procedure PAUT.108 Applied to Test Block P35 in PARENT Blind Testing (X - Y view, 600 mm-900 mm)

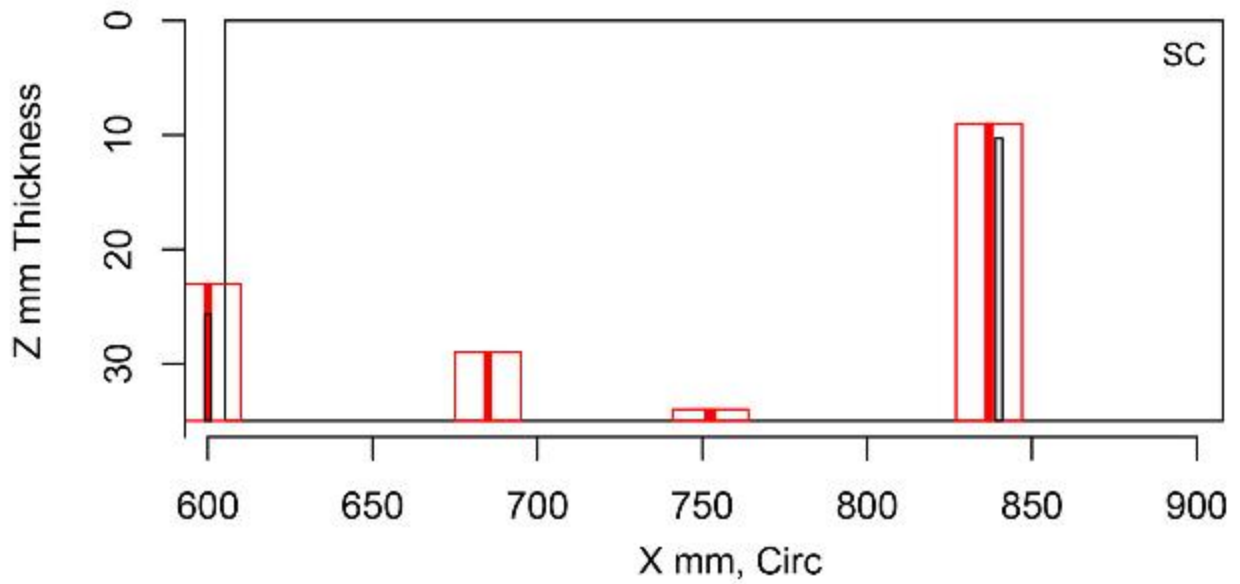


Figure E.78 Indication Plot for Procedure PAUT.108 Applied to Test Block P35 in PARENT Blind Testing (X - Z view, 600 mm-900 mm)

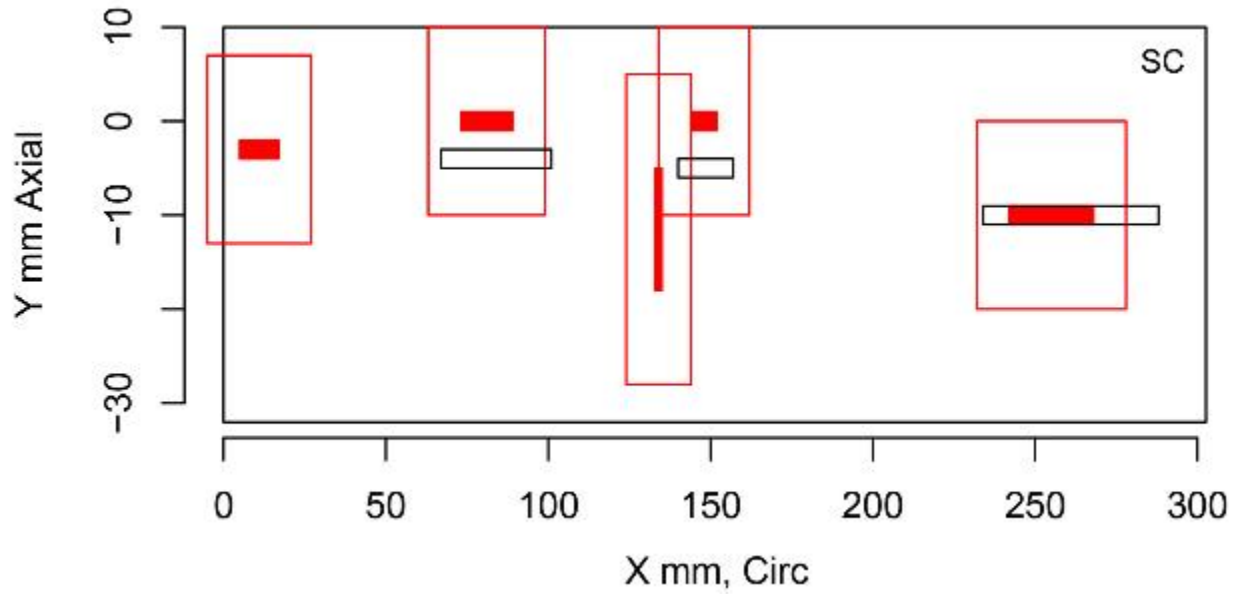


Figure E.79 Indication Plot for Procedure UT.108 Applied to Test Block P35 in PARENT Blind Testing (X - Y view, 0 mm-300 mm)

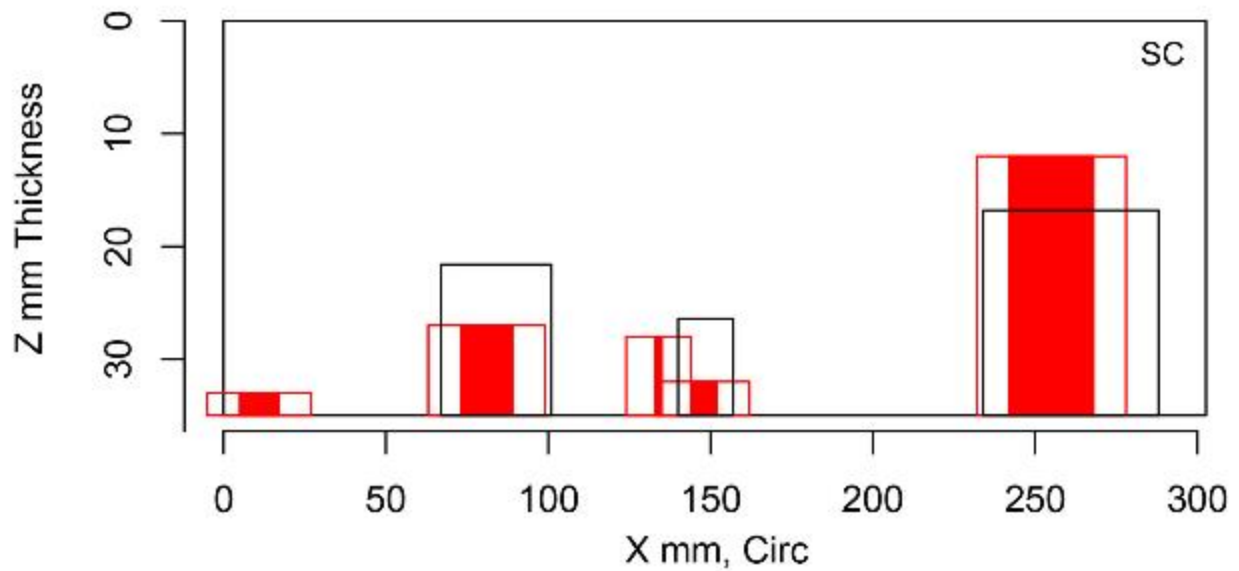


Figure E.80 Indication Plot for Procedure UT.108 Applied to Test Block P35 in PARENT Blind Testing (X - Z view, 0 mm-300 mm)

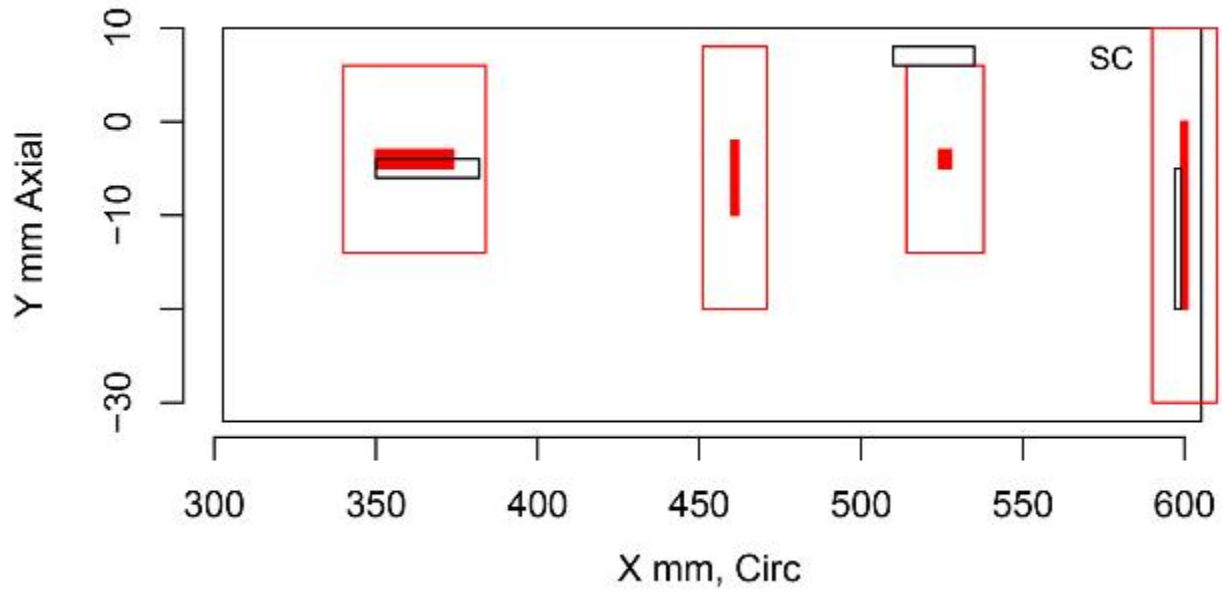


Figure E.81 Indication Plot for Procedure UT.108 Applied to Test Block P35 in PARENT Blind Testing (X – Y view, 300 mm–600 mm)

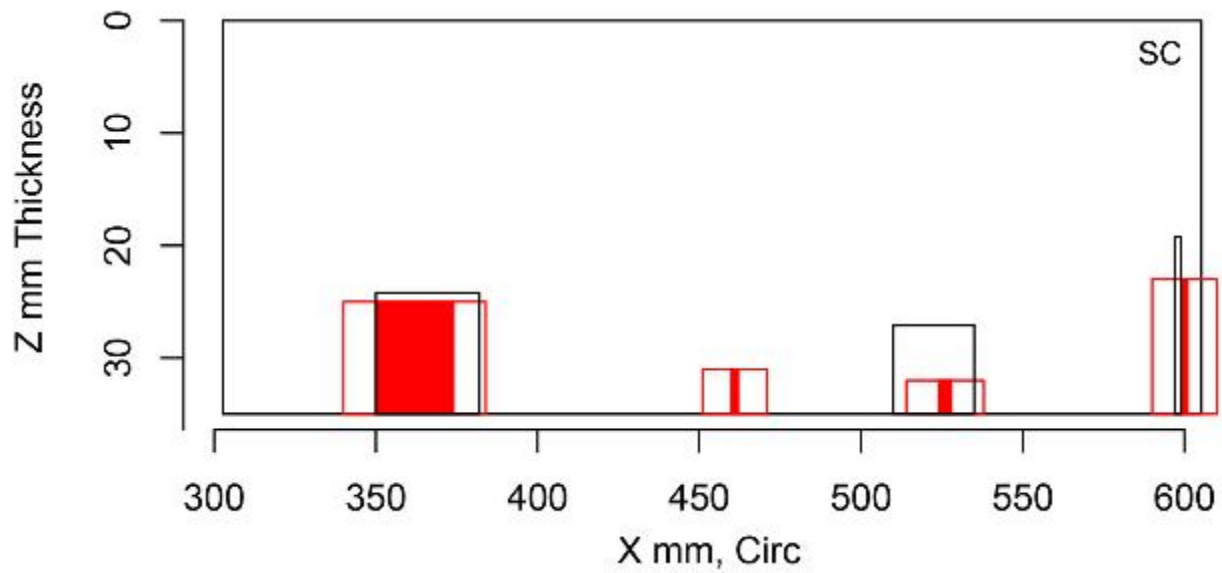


Figure E.82 Indication Plot for Procedure UT.108 Applied to Test Block P35 in PARENT Blind Testing (X – Z view, 300 mm–600 mm)

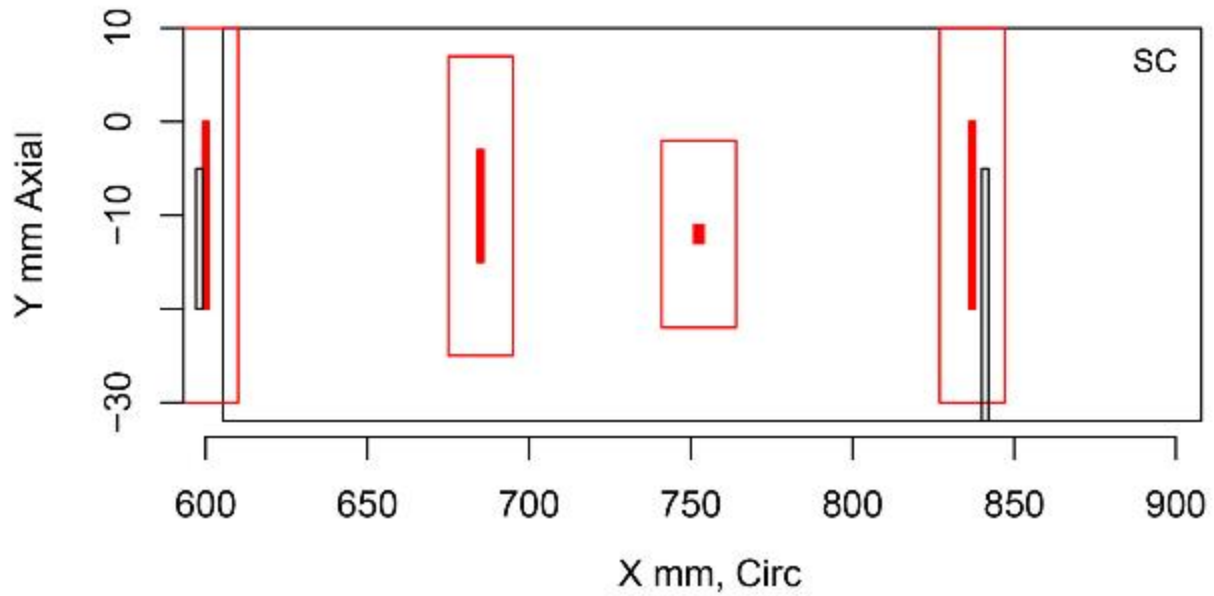


Figure E.83 Indication Plot for Procedure UT.108 Applied to Test Block P35 in PARENT Blind Testing (X - Y view, 600 mm-900 mm)

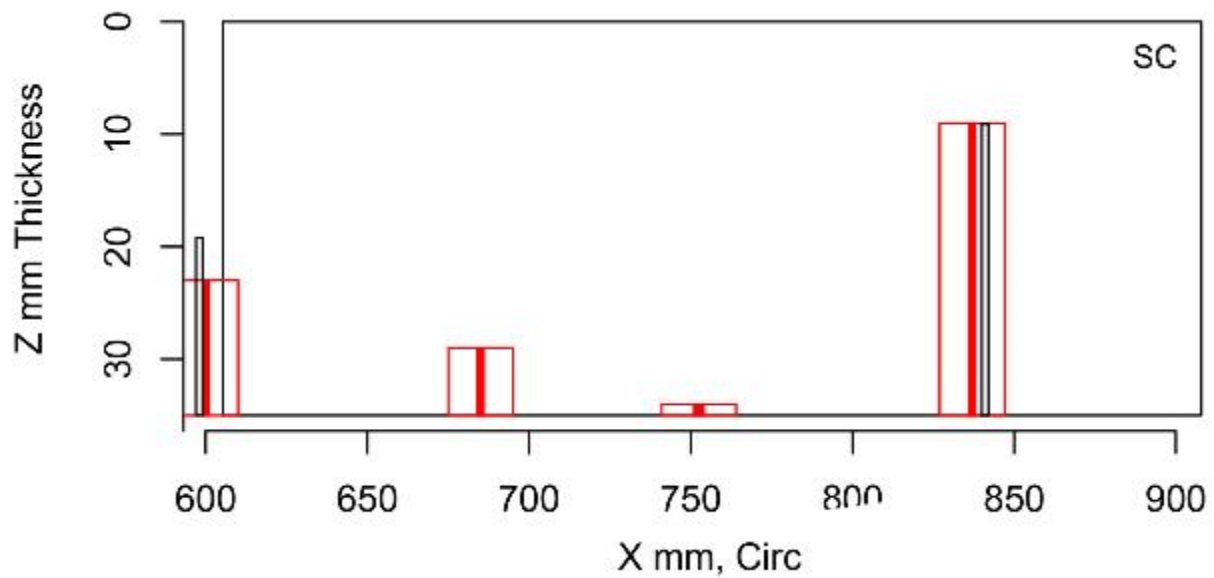


Figure E.84 Indication Plot for Procedure UT.108 Applied to Test Block P35 in PARENT Blind Testing (X - Z view, 600 mm-900 mm)

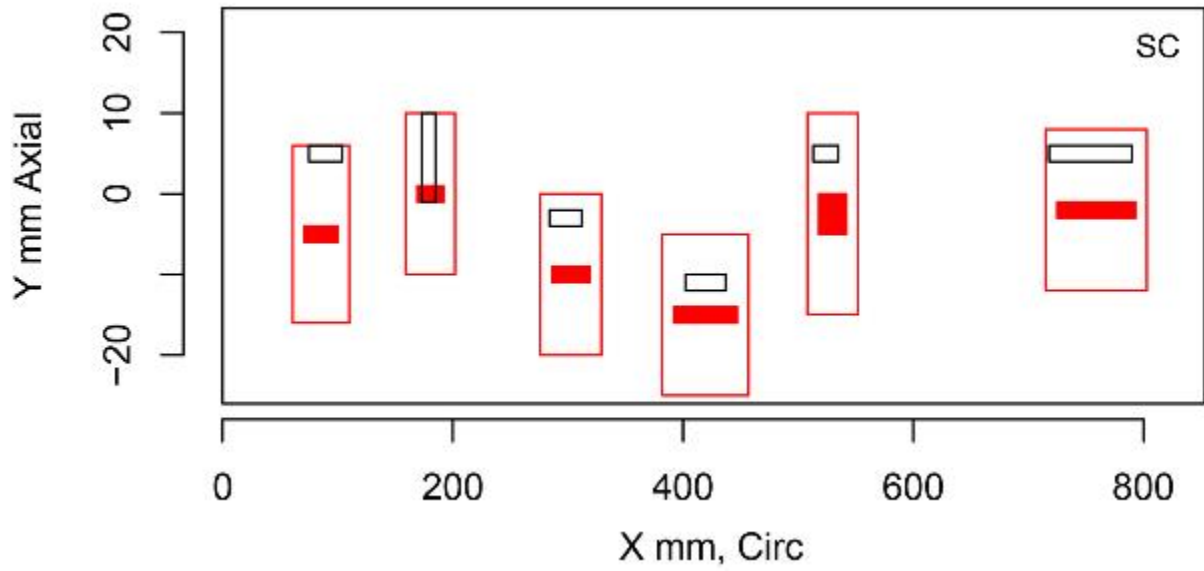


Figure E.85 Indication Plot for Procedure PAUT.108 Applied to Test Block P40 in PARENT Blind Testing (X – Y view, 0 mm–800 mm)

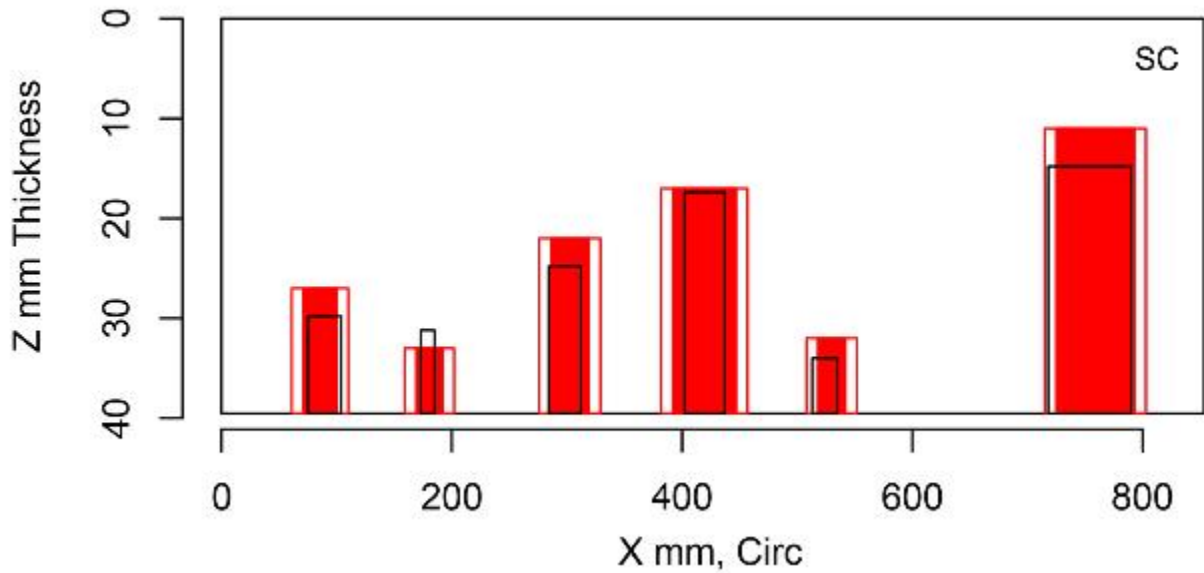


Figure E.86 Indication Plot for Procedure PAUT.108 Applied to Test Block P40 in PARENT Blind Testing (X – Z view, 0 mm–800 mm)

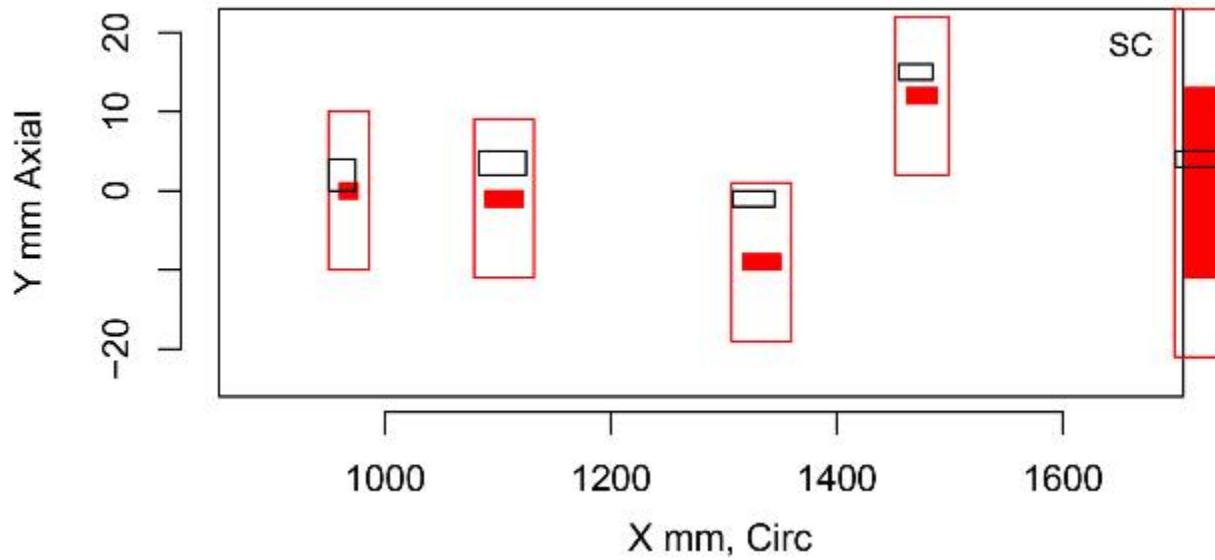


Figure E.87 Indication Plot for Procedure PAUT.108 Applied to Test Block P40 in PARENT Blind Testing (X – Y view, 1000 mm–1600 mm)

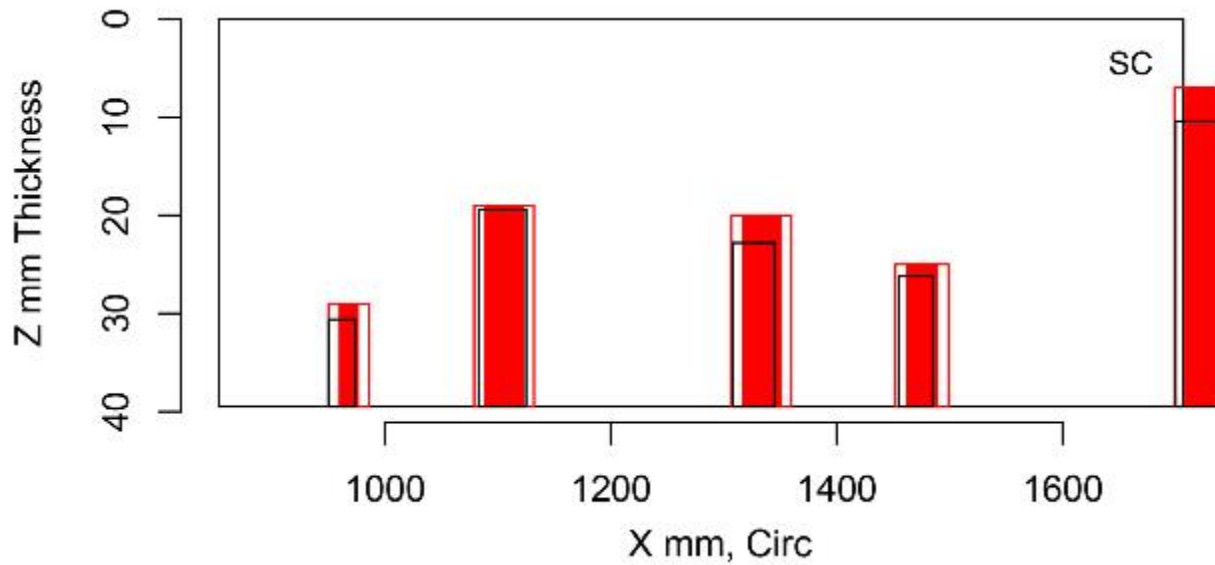


Figure E.88 Indication Plot for Procedure PAUT.108 Applied to Test Block P40 in PARENT Blind Testing (X – Z view, 1000 mm–1600 mm)

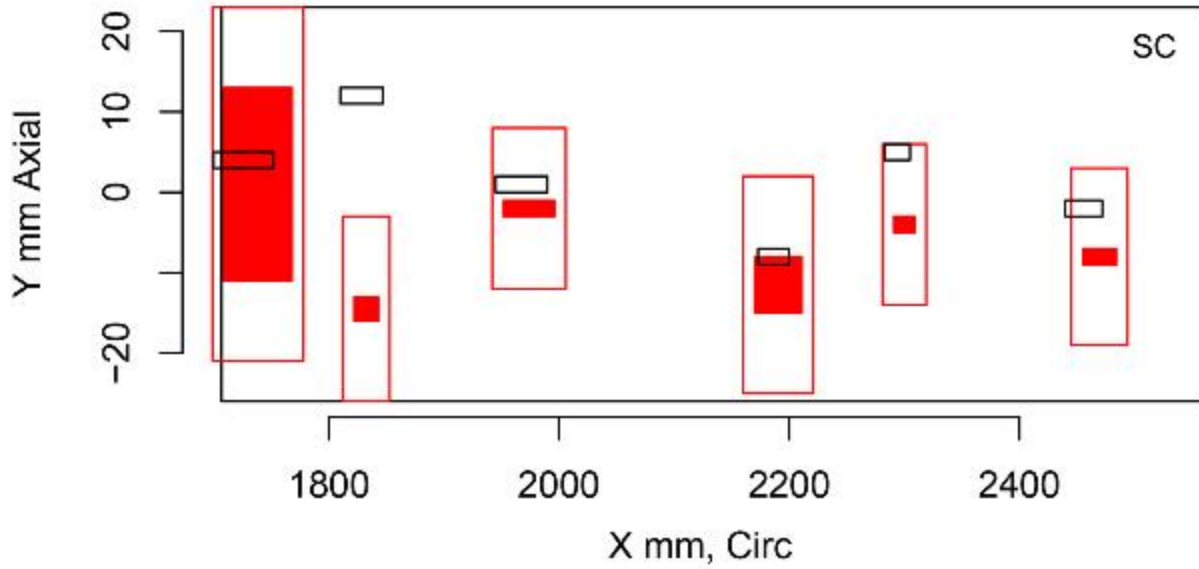


Figure E.89 Indication Plot for Procedure PAUT.108 Applied to Test Block P40 in PARENT Blind Testing (X – Y view, 1800 mm–2400 mm)

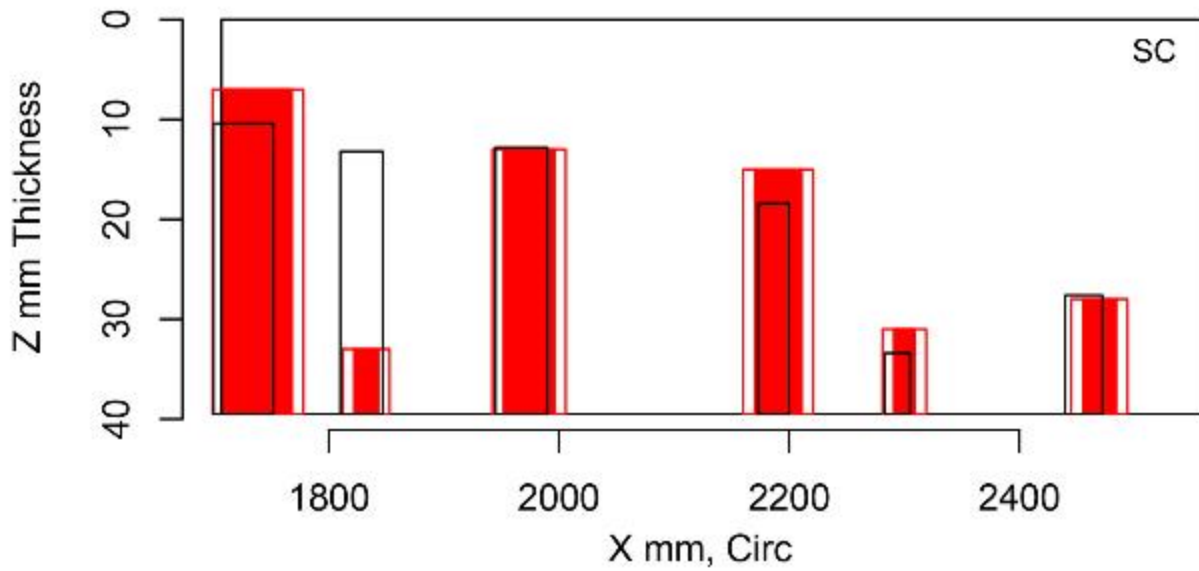


Figure E.90 Indication Plot for Procedure PAUT.108 Applied to Test Block P40 in PARENT Blind Testing (X – Z view, 1800 mm–2400 mm)

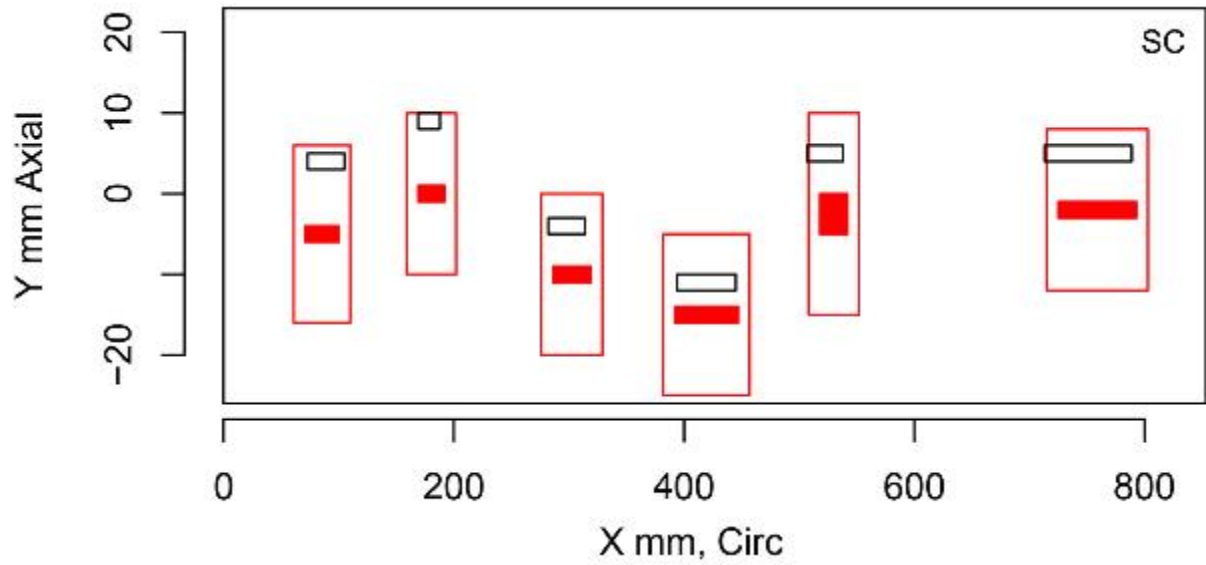


Figure E.91 Indication Plot for Procedure UT.108 Applied to Test Block P40 in PARENT Blind Testing (X – Y view, 0 mm–800 mm)

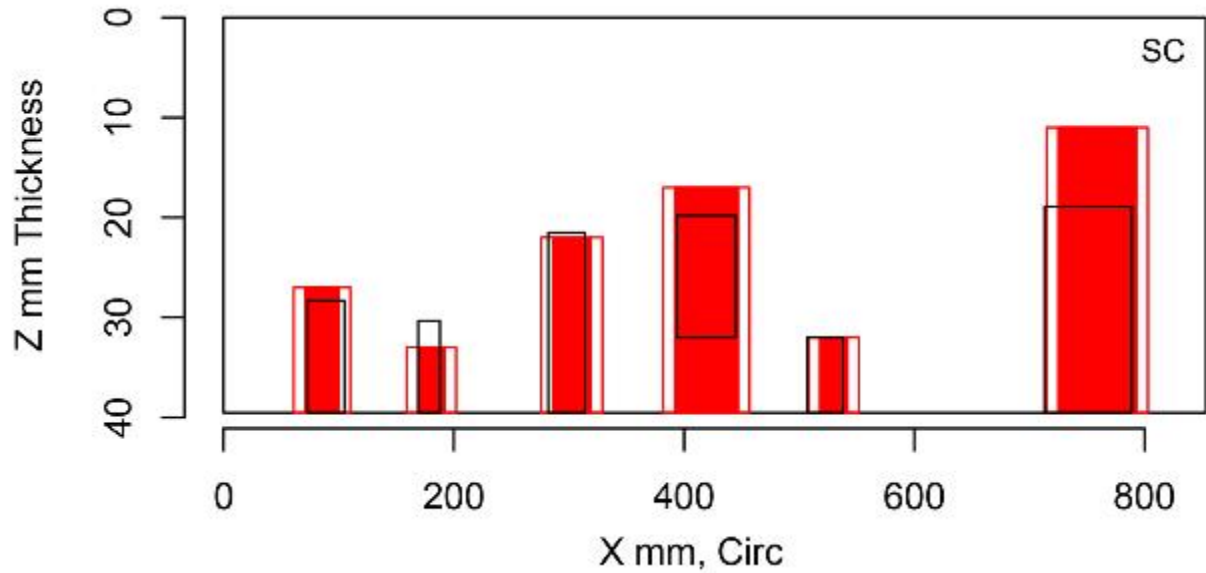


Figure E.92 Indication Plot for Procedure UT.108 Applied to Test Block P40 in PARENT Blind Testing (X – Z view, 0 mm–800 mm)

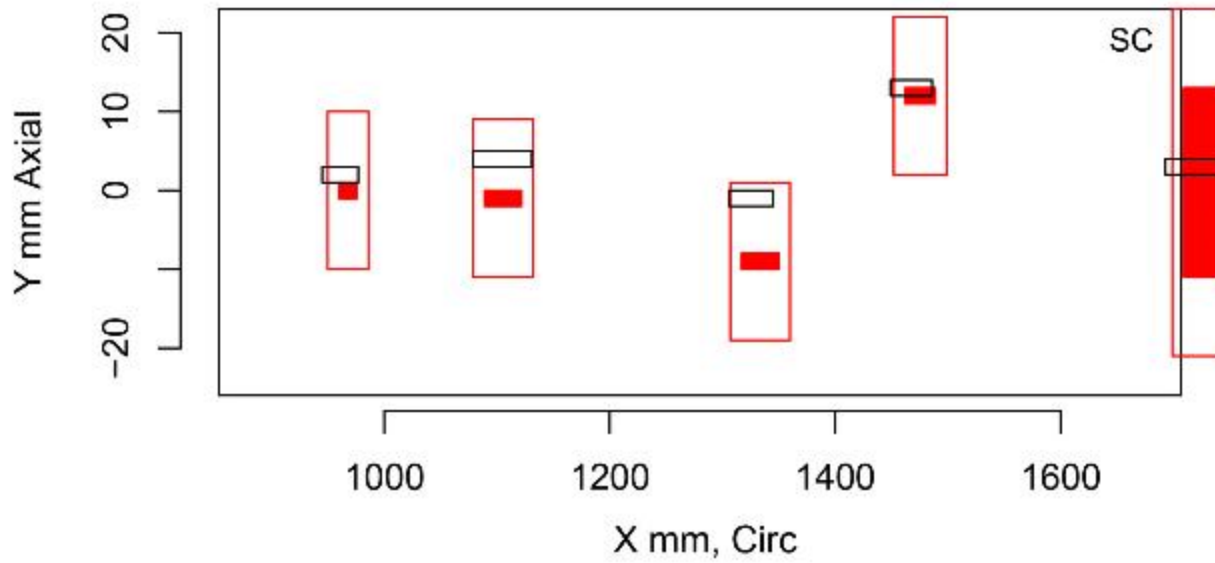


Figure E.93 Indication Plot for Procedure UT.108 Applied to Test Block P40 in PARENT Blind Testing (X – Y view, 1000 mm–1600 mm)

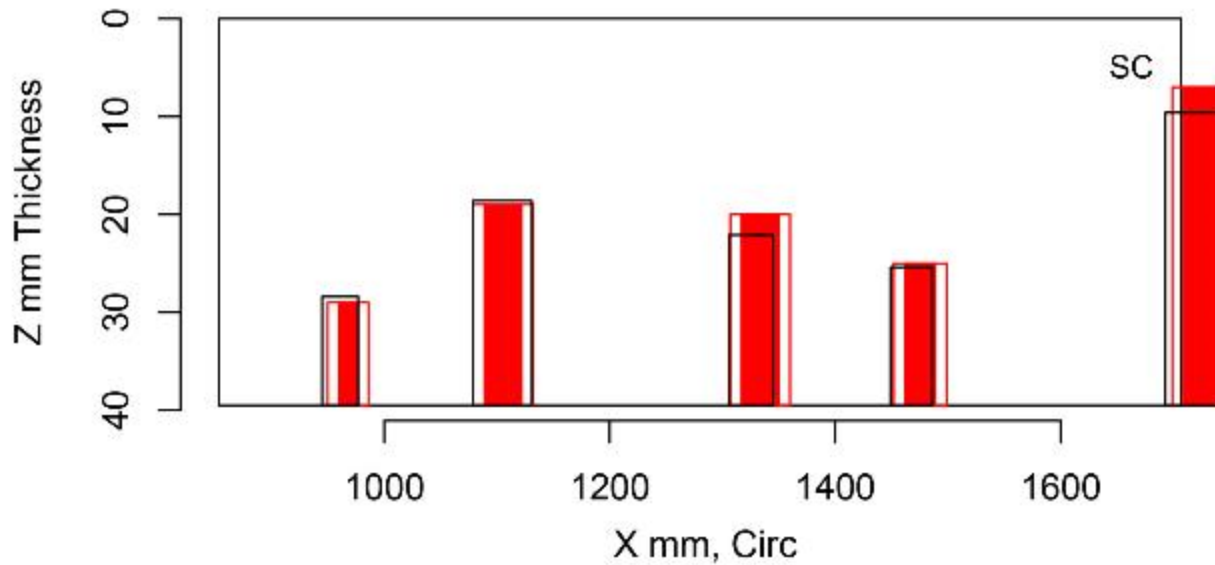


Figure E.94 Indication Plot for Procedure UT.108 Applied to Test Block P40 in PARENT Blind Testing (X – Z view, 1000 mm–1600 mm)

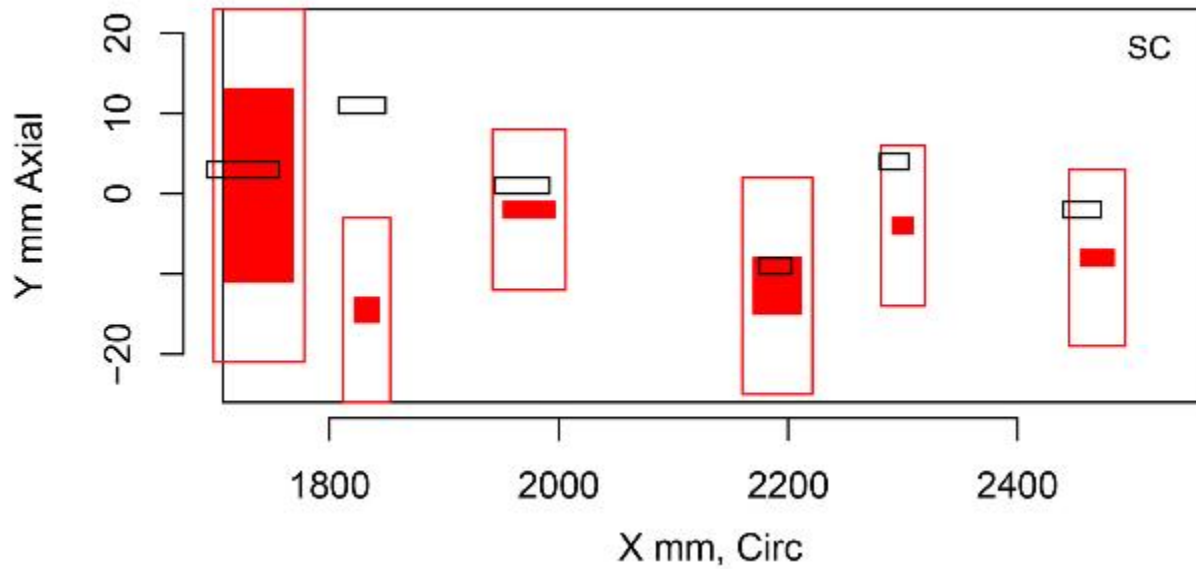


Figure E.95 Indication Plot for Procedure UT.108 Applied to Test Block P40 in PARENT Blind Testing (X – Y view, 1800 mm–2400 mm)

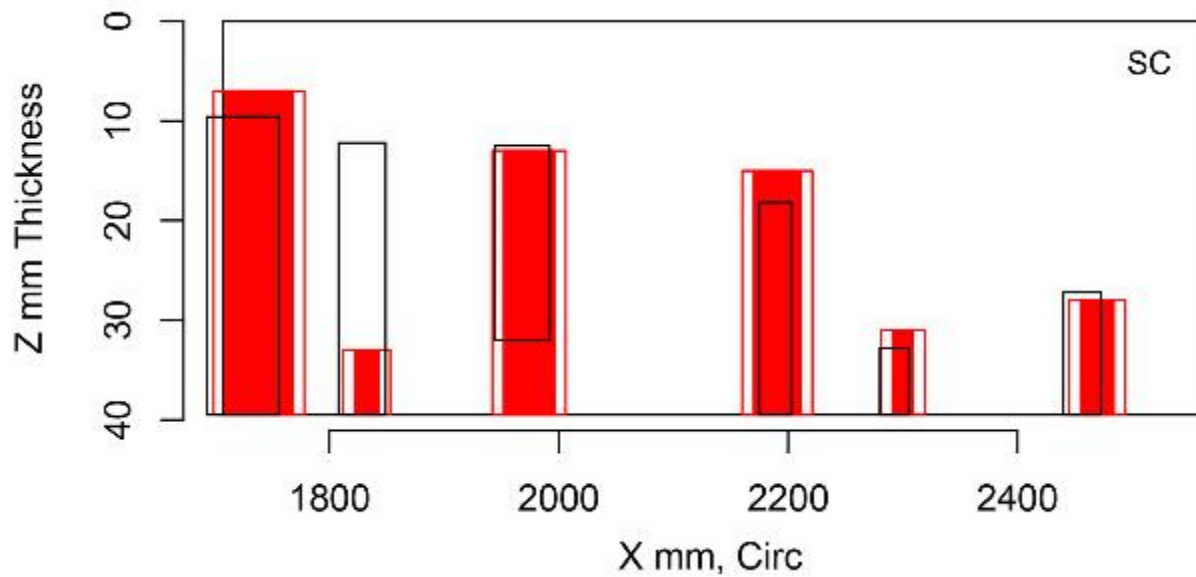


Figure E.96 Indication Plot for Procedure UT.108 Applied to Test Block P40 in PARENT Blind Testing (X – Z view, 1800 mm–2400 mm)

E.2.3 Plots for Team 113

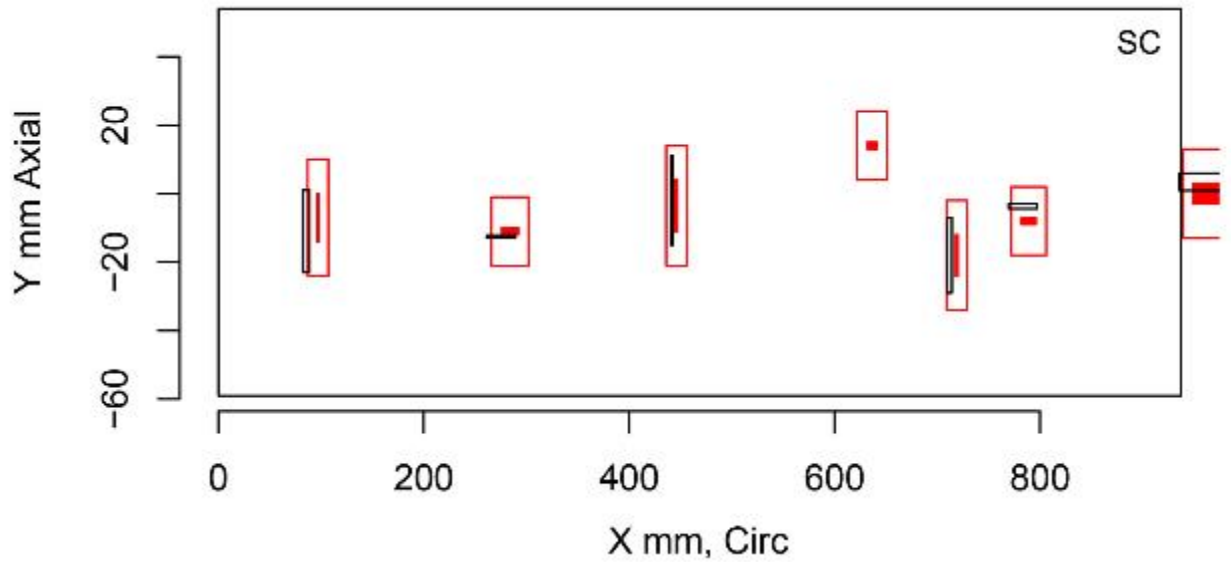


Figure E.97 Indication Plot for Procedure UT.PAUT.113 Applied to Test Block P33 in PARENT Blind Testing (X – Y view, 0 mm–800 mm)

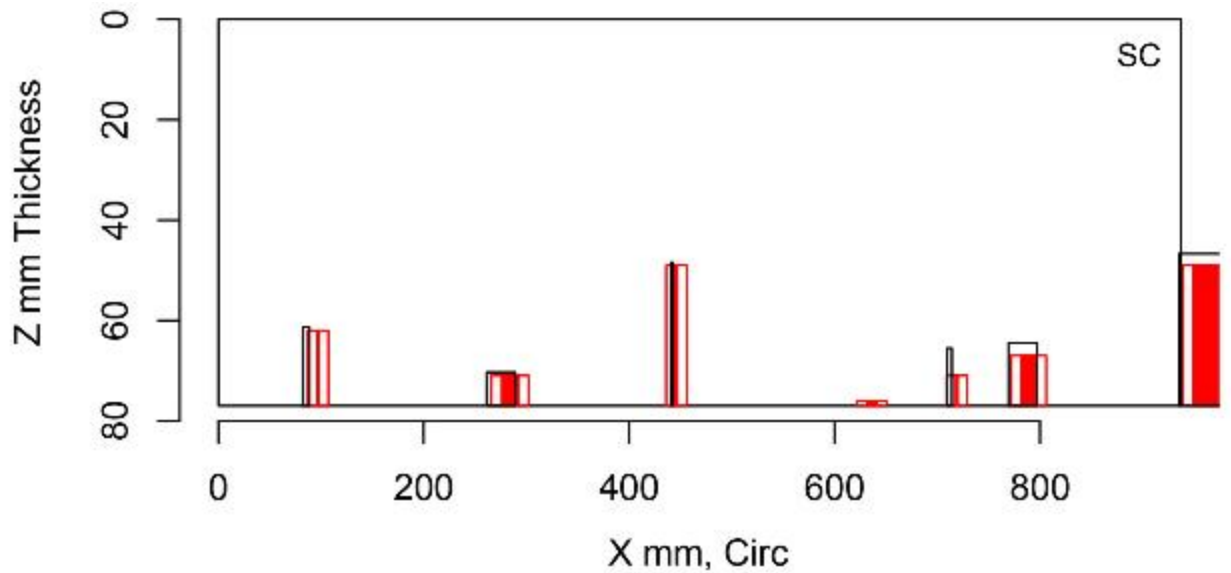


Figure E.98 Indication Plot for Procedure UT.PAUT.113 Applied to Test Block P33 in PARENT Blind Testing (X – Z view, 0 mm–800 mm)

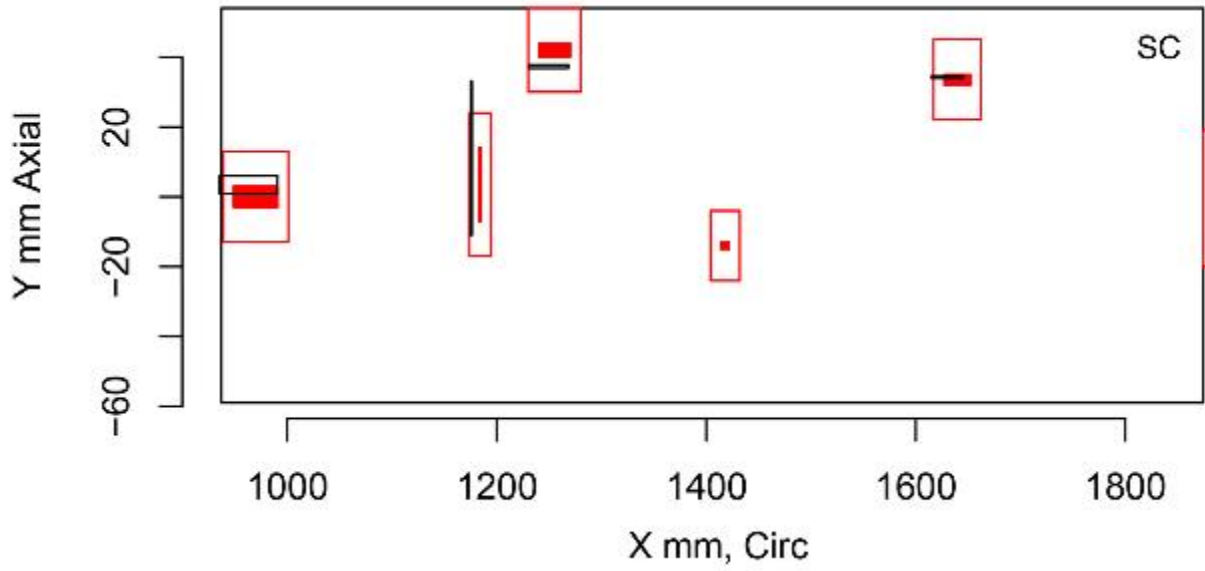


Figure E.99 Indication Plot for Procedure UT.PAUT.113 Applied to Test Block P33 in PARENT Blind Testing (X – Y view, 1000 mm–1800 mm)

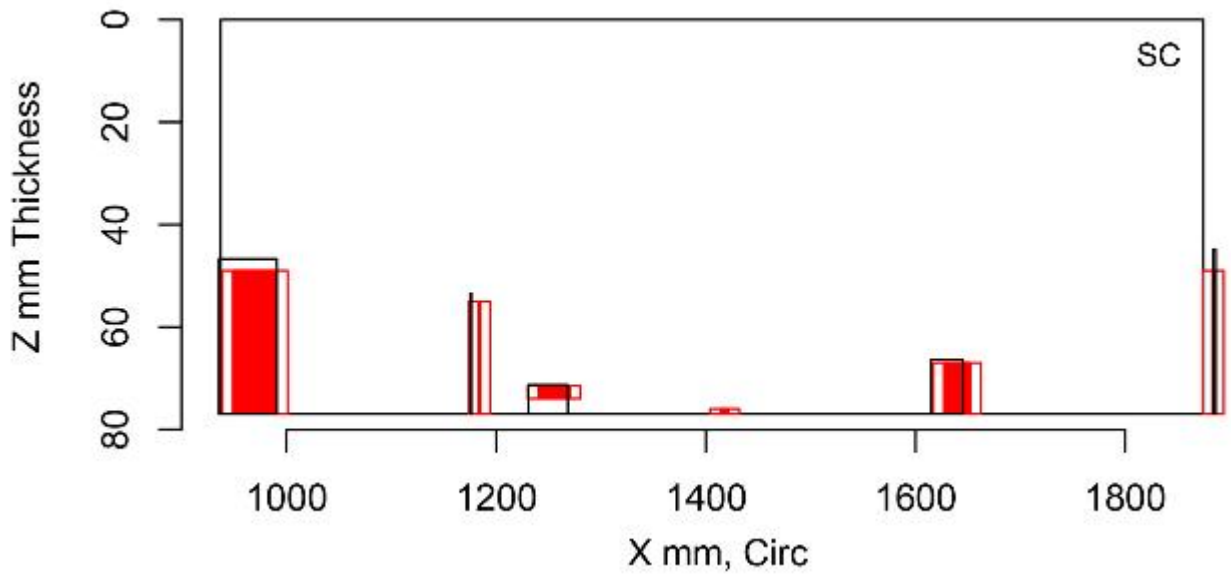


Figure E.100 Indication Plot for Procedure UT.PAUT.113 Applied to Test Block P33 in PARENT Blind Testing (X – Z view, 1000 mm–1800 mm)

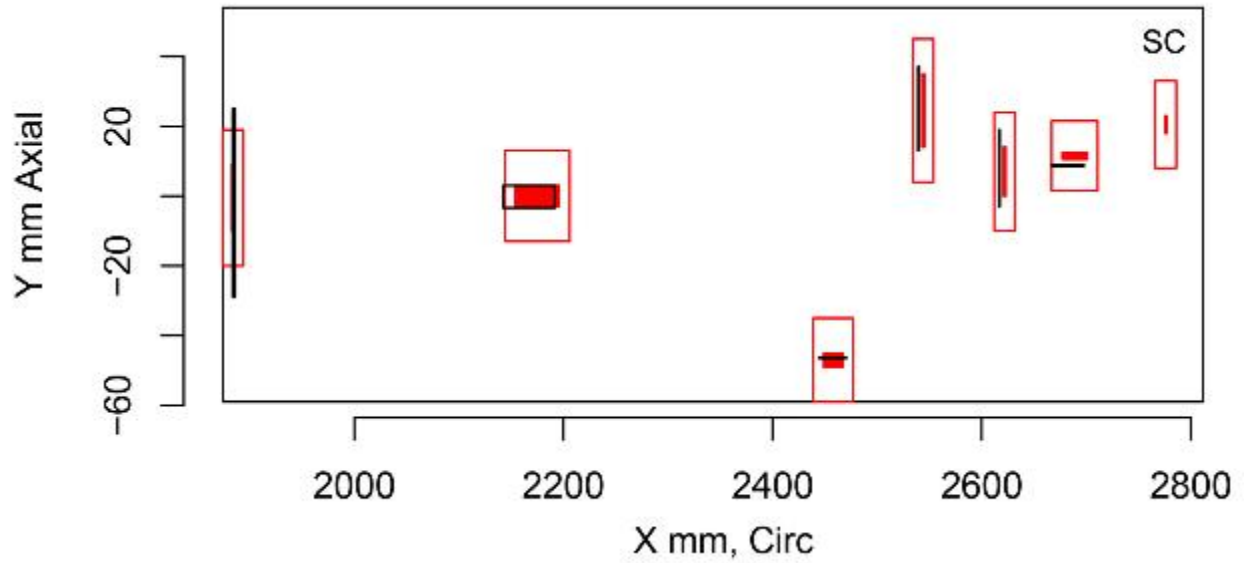


Figure E.101 Indication Plot for Procedure UT.PAUT.113 Applied to Test Block P33 in PARENT Blind Testing (X – Y view, 2000 mm–2800 mm)

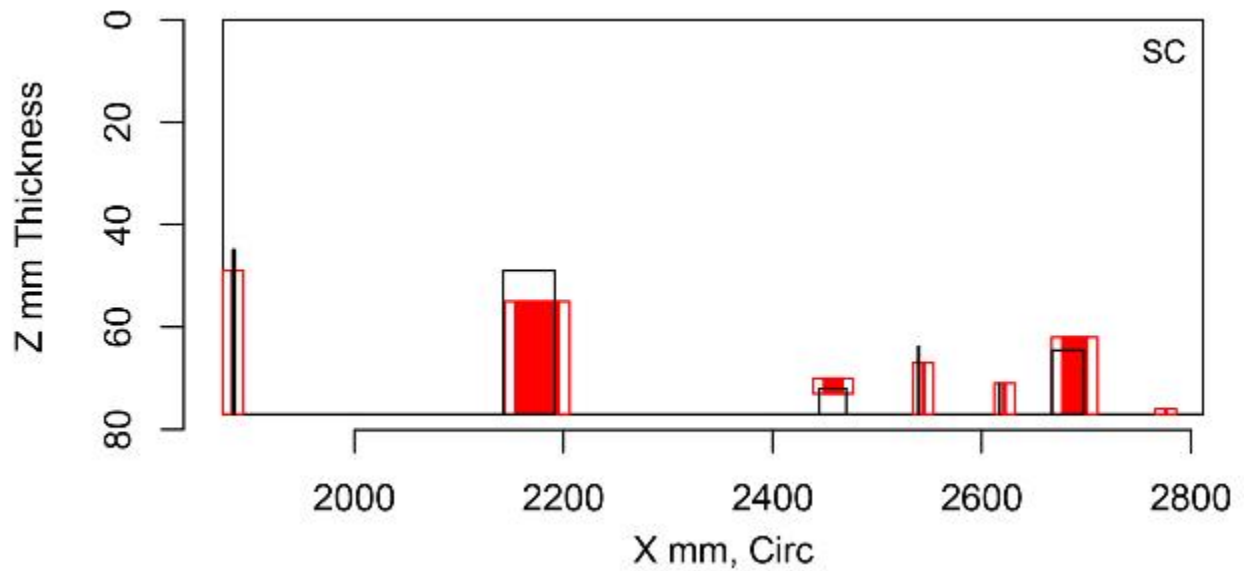


Figure E.102 Indication Plot for Procedure UT.PAUT.113 Applied to Test Block P33 in PARENT Blind Testing (X – Z view, 2000 mm–2800 mm)

E.2.4 Plots for Team 115

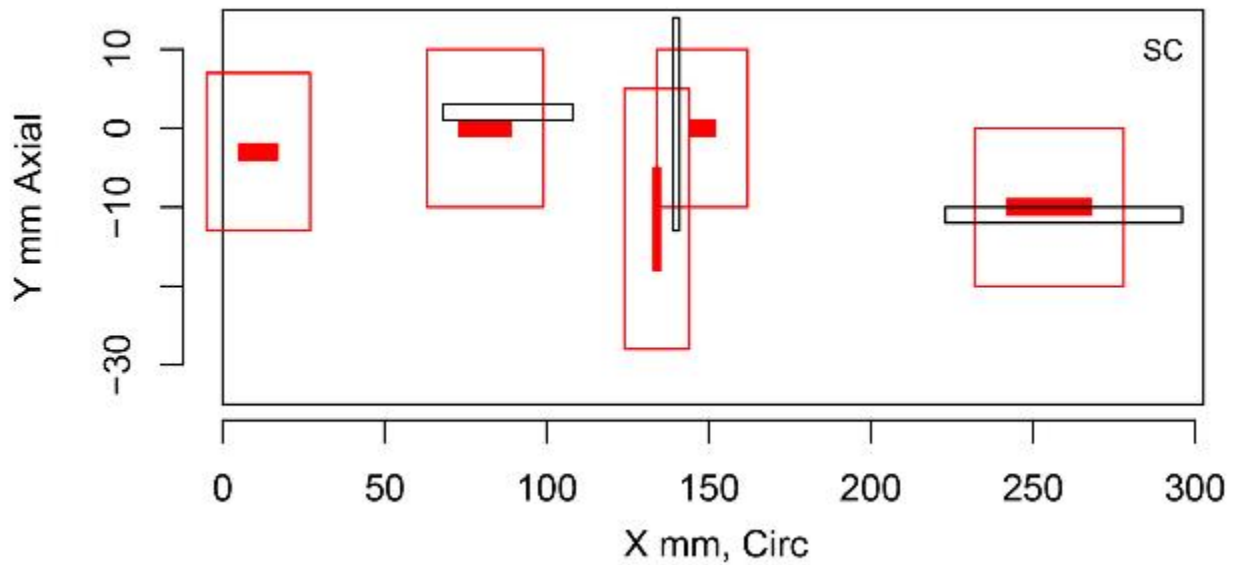


Figure E.103 Indication Plot for Procedure PAUT.115 Applied to Test Block P35 in PARENT Blind Testing (X - Y view, 0 mm-300 mm)

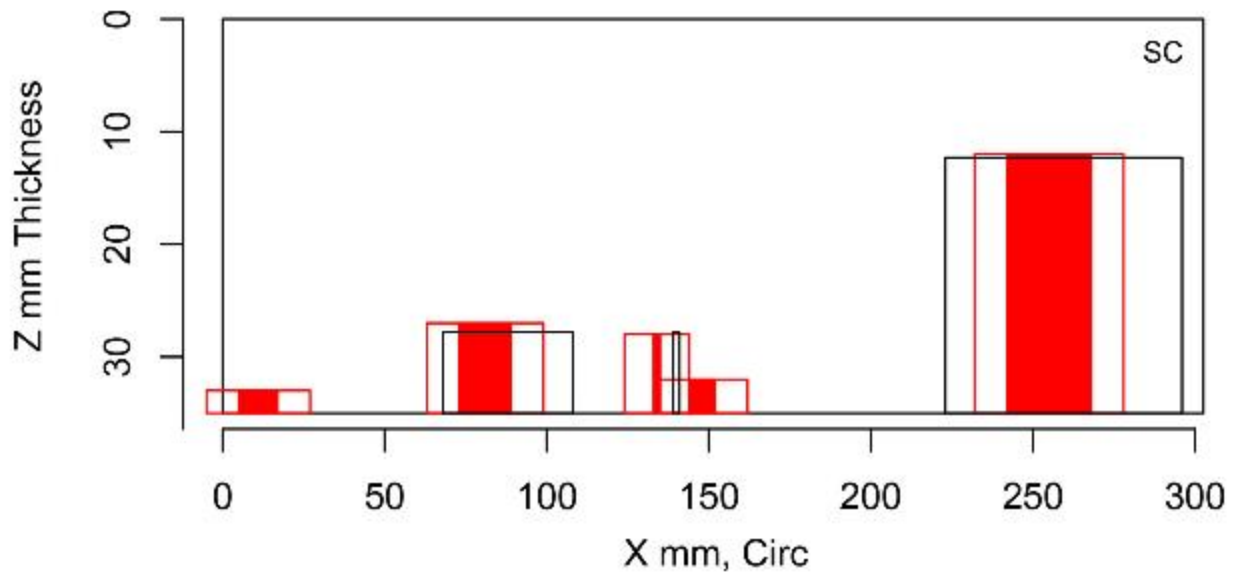


Figure E.104 Indication Plot for Procedure PAUT.115 Applied to Test Block P35 in PARENT Blind Testing (X - Z view, 0 mm-300 mm)

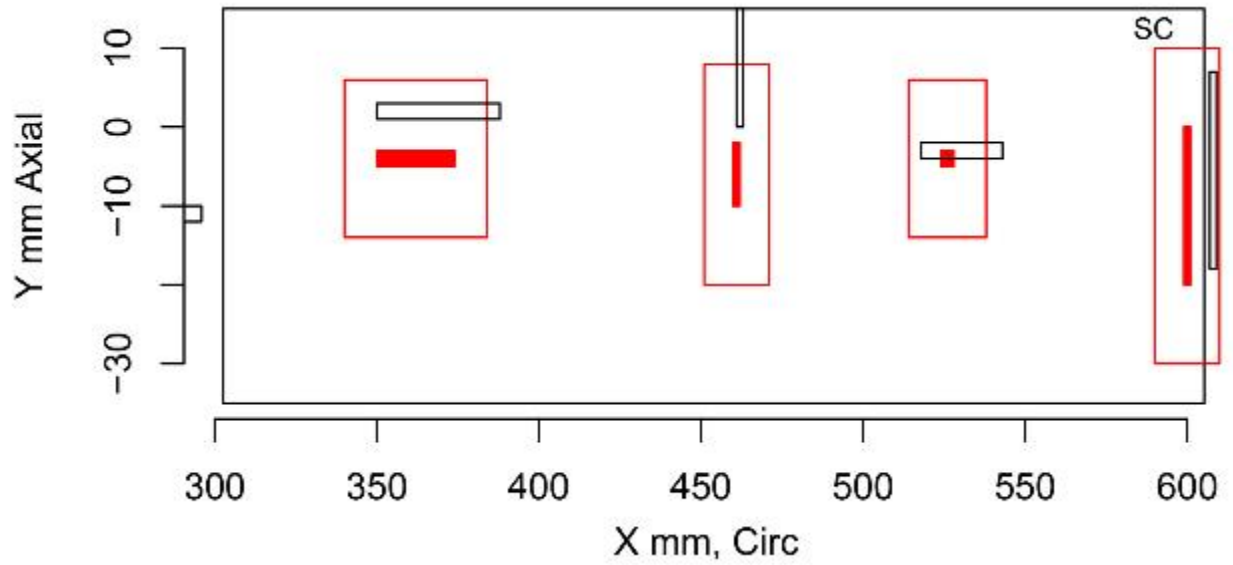


Figure E.105 Indication Plot for Procedure PAUT.115 Applied to Test Block P35 in PARENT Blind Testing (X – Y view, 300 mm–600 mm)

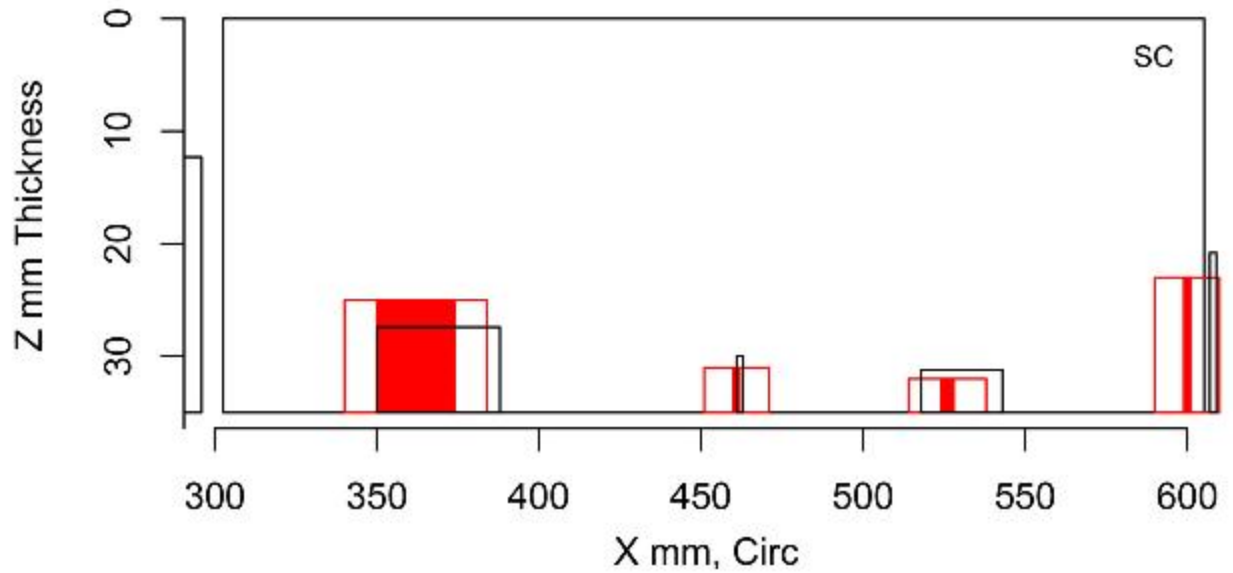


Figure E.106 Indication Plot for Procedure PAUT.115 Applied to Test Block P35 in PARENT Blind Testing (X – Z view, 300 mm–600 mm)

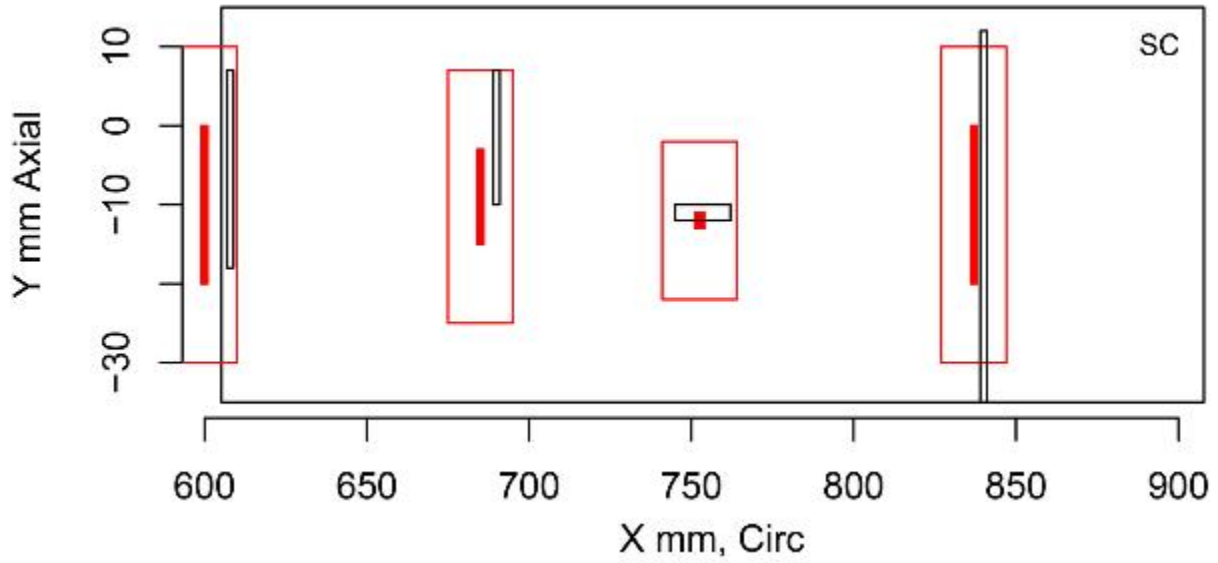


Figure E.107 Indication Plot for Procedure PAUT.115 Applied to Test Block P35 in PARENT Blind Testing (X - Y view, 600 mm-900 mm)

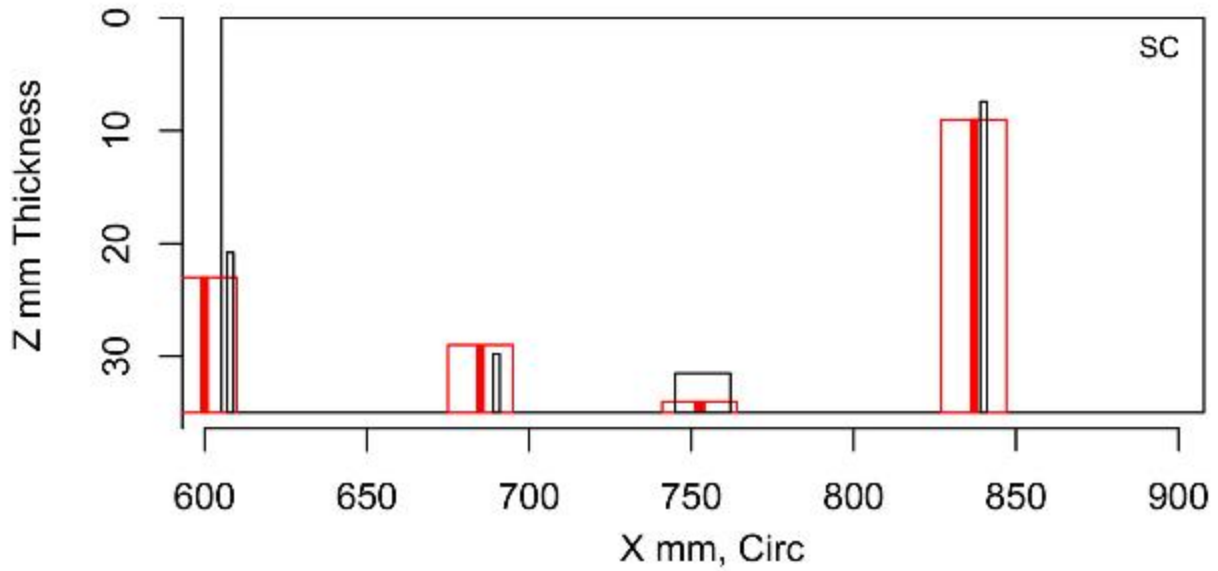


Figure E.108 Indication Plot for Procedure PAUT.115 Applied to Test Block P35 in PARENT Blind Testing (X - Z view, 600 mm-900 mm)

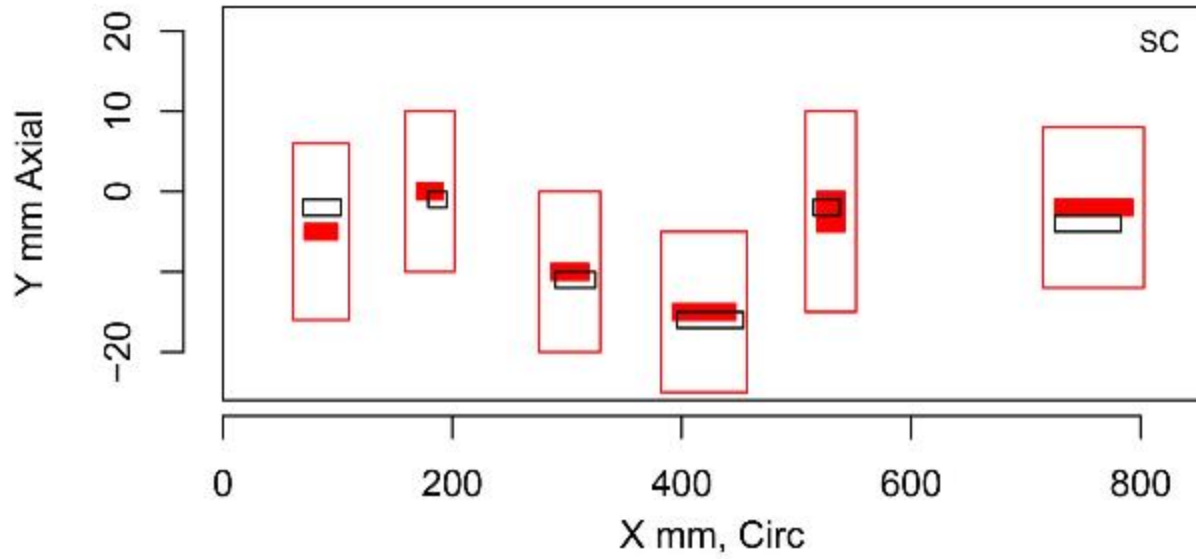


Figure E.109 Indication Plot for Procedure PAUT.115 Applied to Test Block P40 in PARENT Blind Testing (X – Y view, 0 mm–800 mm)

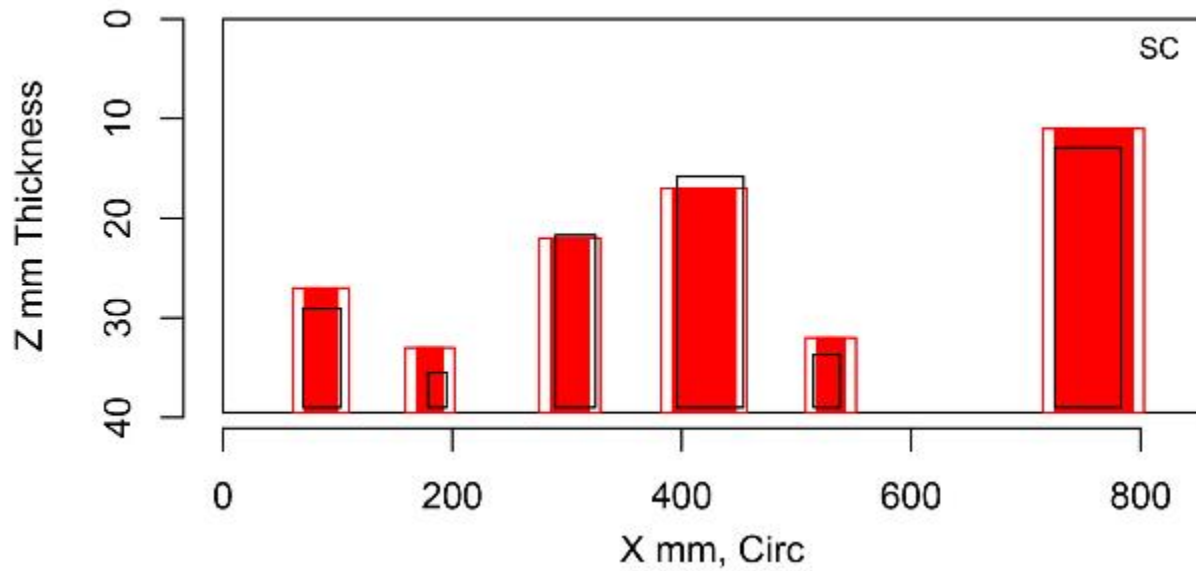


Figure E.110 Indication Plot for Procedure PAUT.115 Applied to Test Block P40 in PARENT Blind Testing (X – Z view, 0 mm–800 mm)

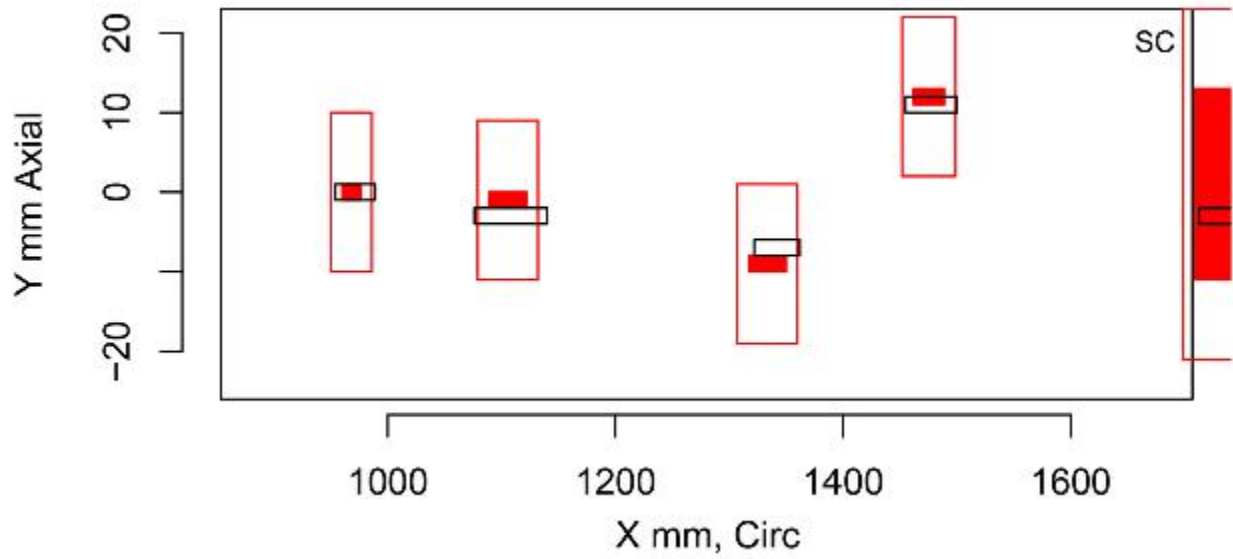


Figure E.111 Indication Plot for Procedure PAUT.115 Applied to Test Block P40 in PARENT Blind Testing (X - Y view, 1000 mm-1600 mm)

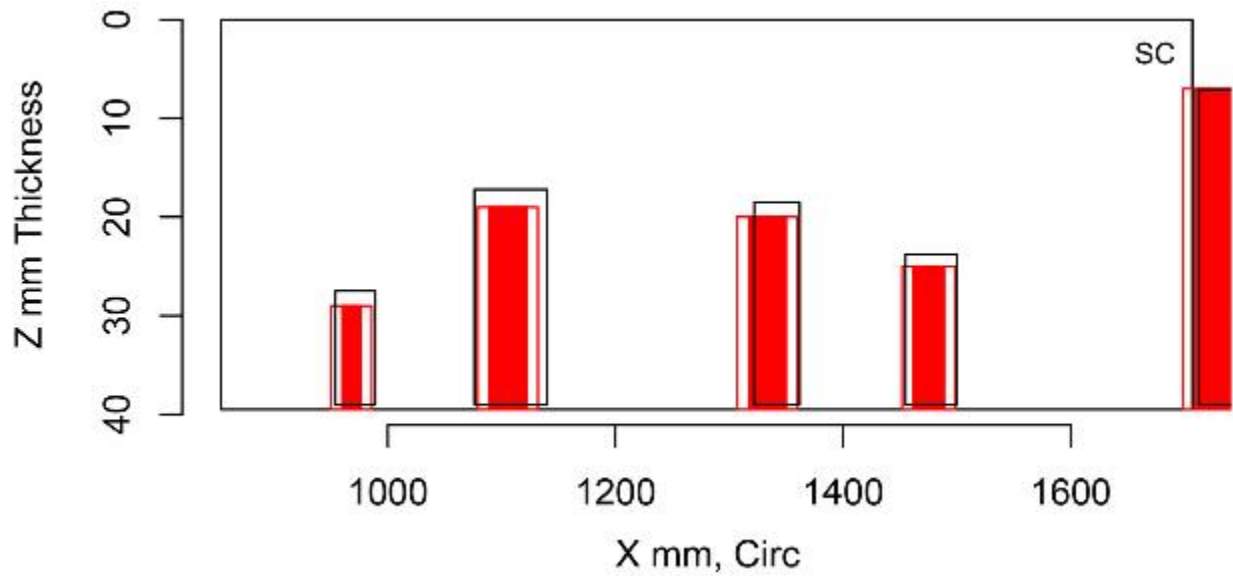


Figure E.112 Indication Plot for Procedure PAUT.115 Applied to Test Block P40 in PARENT Blind Testing (X - Z view, 1000 mm-1600 mm)

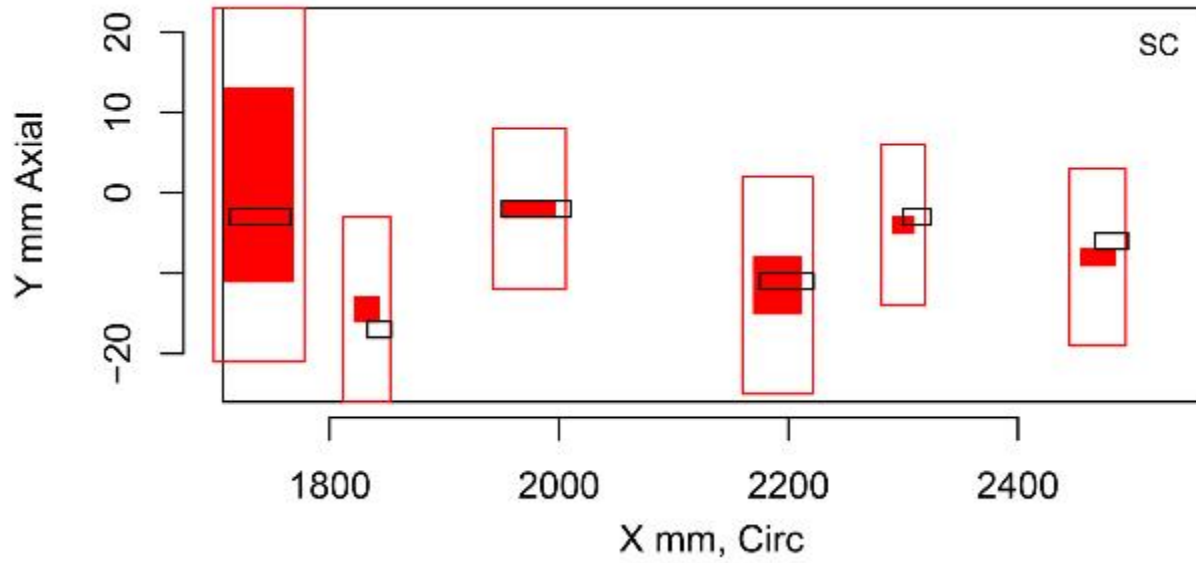


Figure E.113 Indication Plot for Procedure PAUT.115 Applied to Test Block P40 in PARENT Blind Testing (X – Y view, 1800 mm–2400 mm)

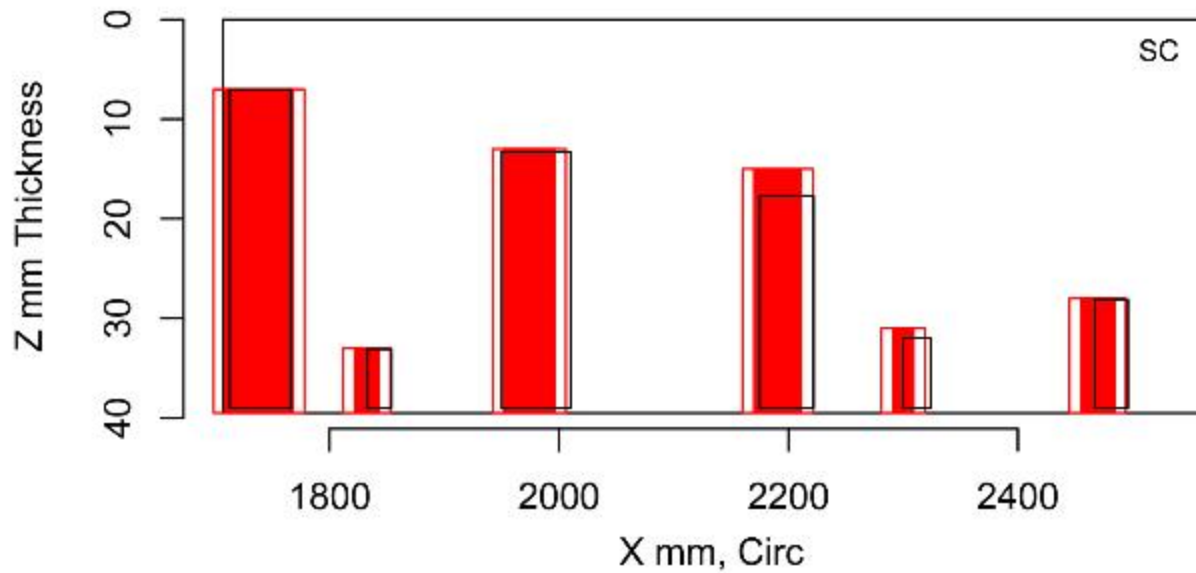


Figure E.114 Indication Plot for Procedure PAUT.115 Applied to Test Block P40 in PARENT Blind Testing (X – Z view, 1800 mm–2400 mm)

E.2.5 Plots for Team 117

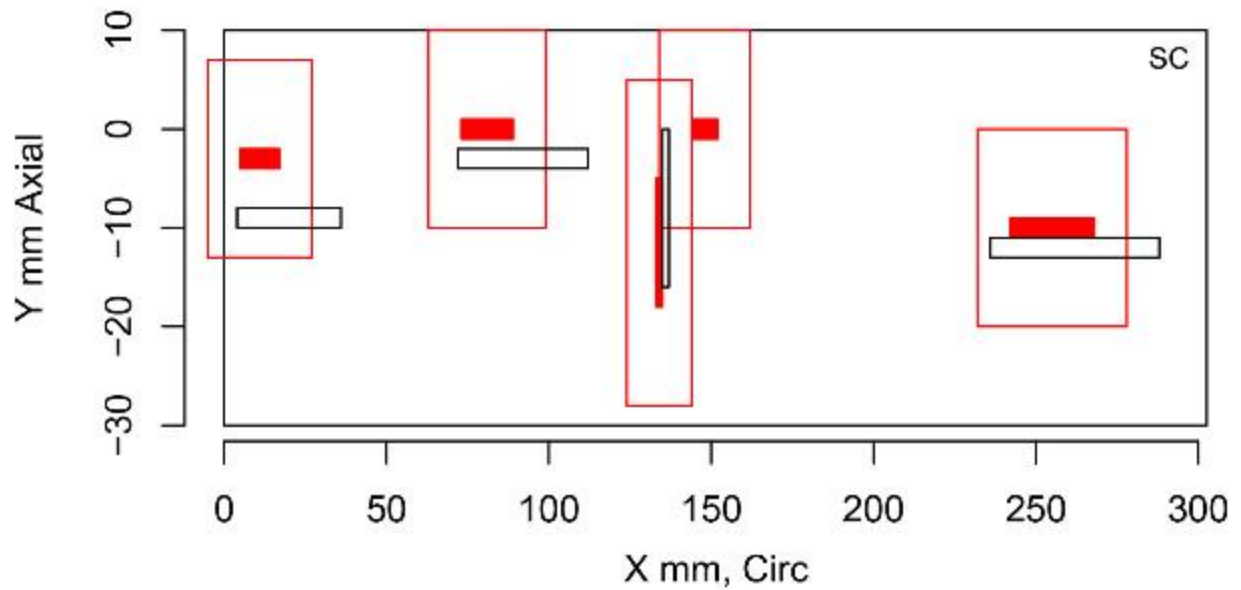


Figure E.115 Indication Plot for Procedure UT.TOFD.117 Applied to Test Block P35 in PARENT Blind Testing (X – Y view, 0 mm–300 mm)

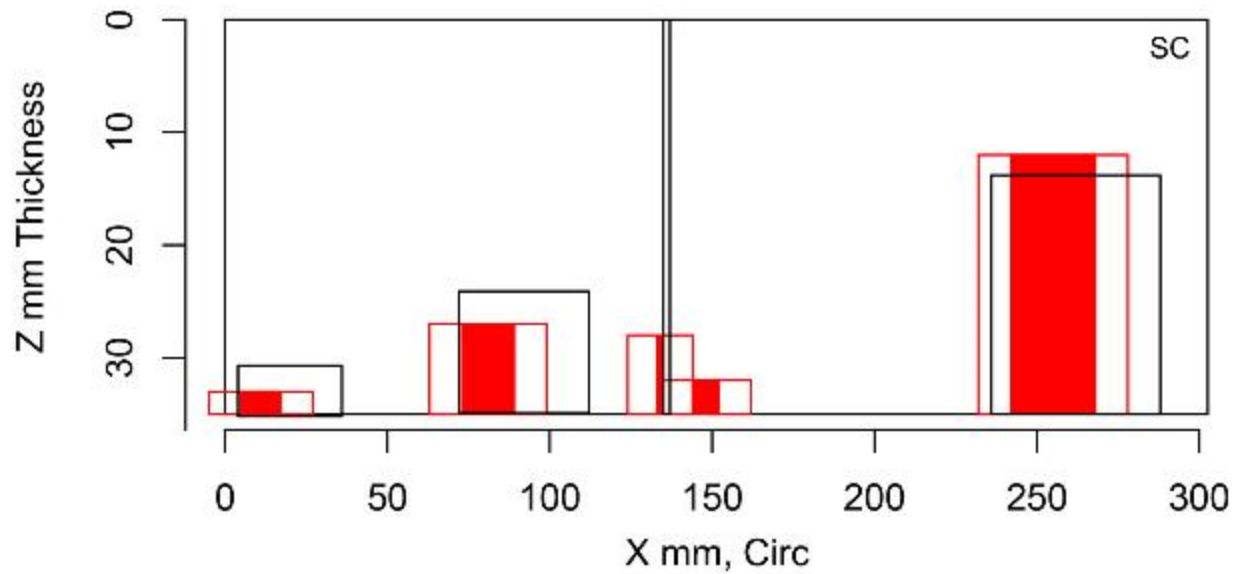


Figure E.116 Indication Plot for Procedure UT.TOFD.117 Applied to Test Block P35 in PARENT Blind Testing (X – Z view, 0 mm–300 mm)

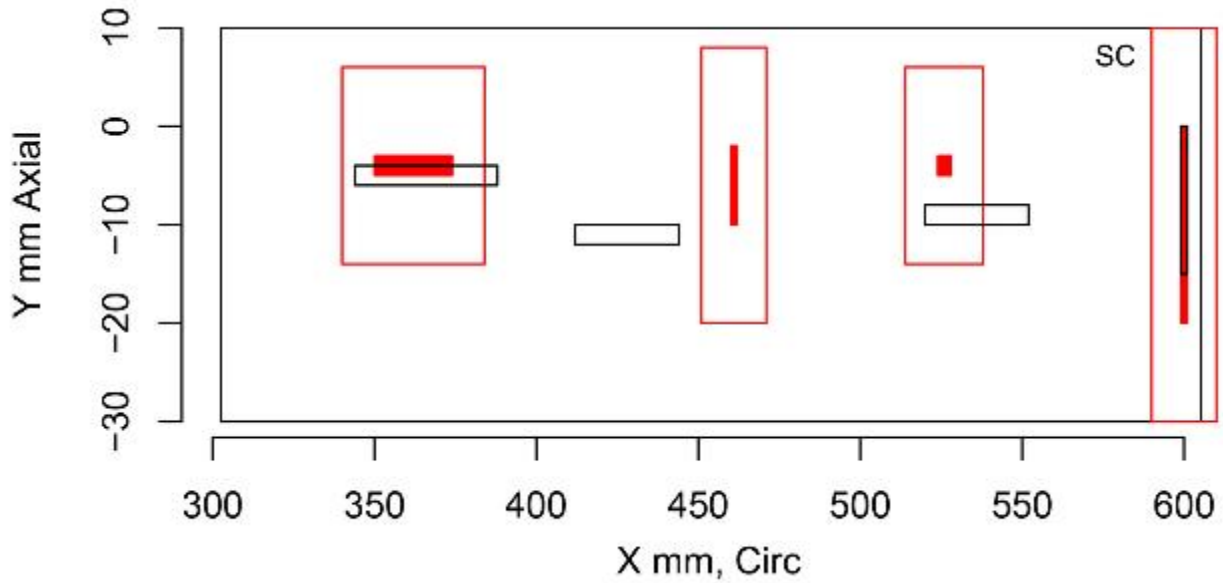


Figure E.117 Indication Plot for Procedure UT.TOFD.117 Applied to Test Block P35 in PARENT Blind Testing (X - Y view, 300 mm-600 mm)

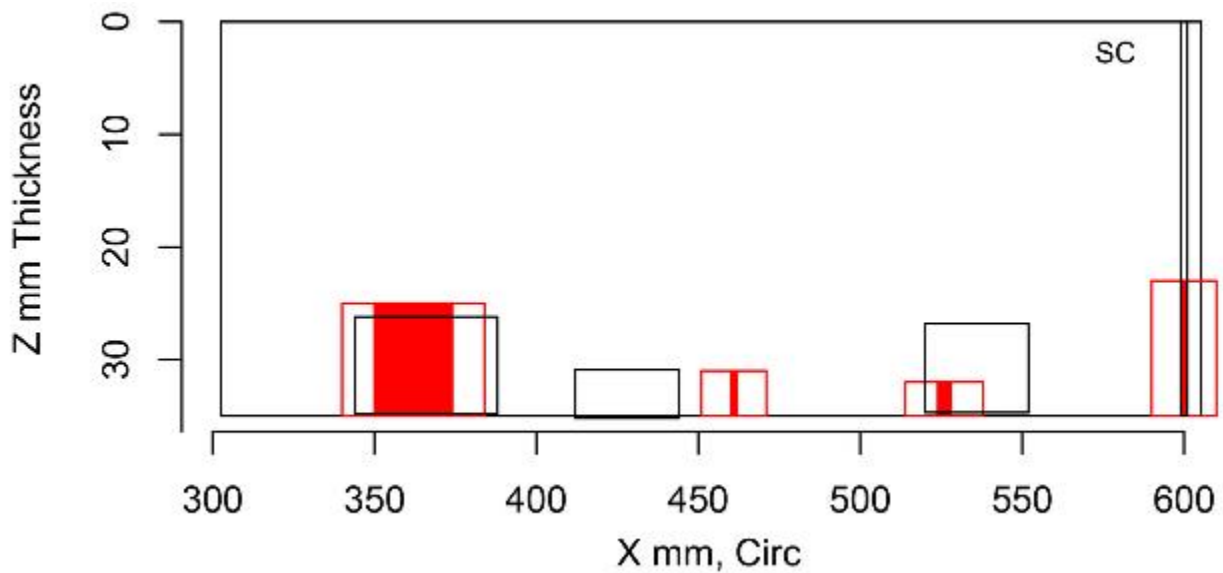


Figure E.118 Indication Plot for Procedure UT.TOFD.117 Applied to Test Block P35 in PARENT Blind Testing (X - Z view, 300 mm-600 mm)

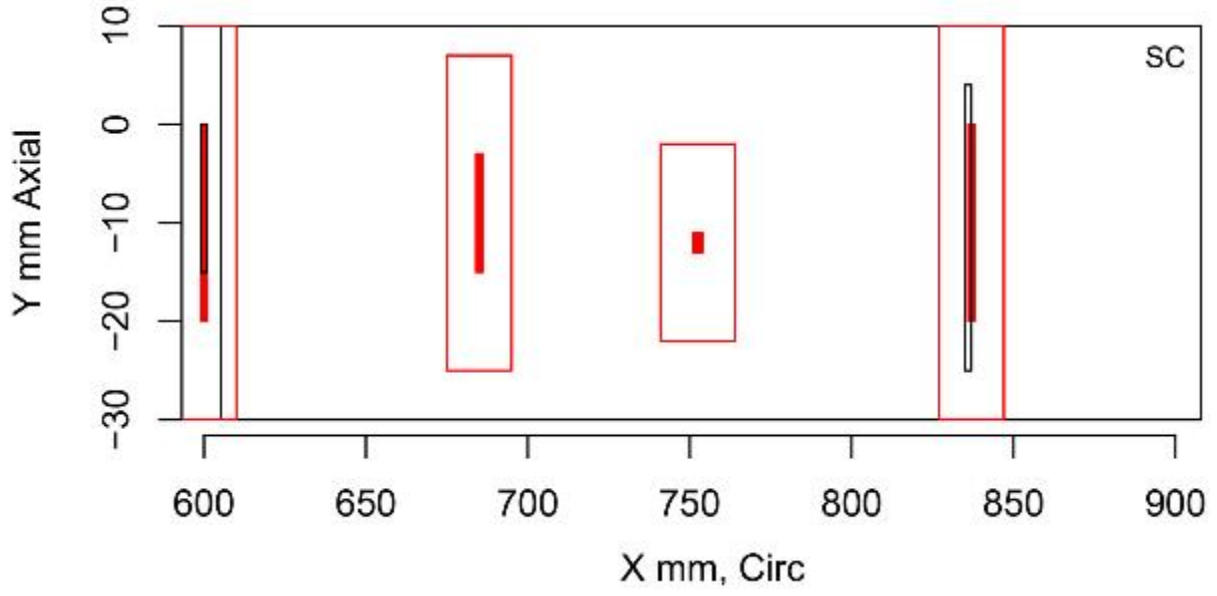


Figure E.119 Indication Plot for Procedure UT.TOFD.117 Applied to Test Block P35 in PARENT Blind Testing (X – Y view, 600 mm–900 mm)

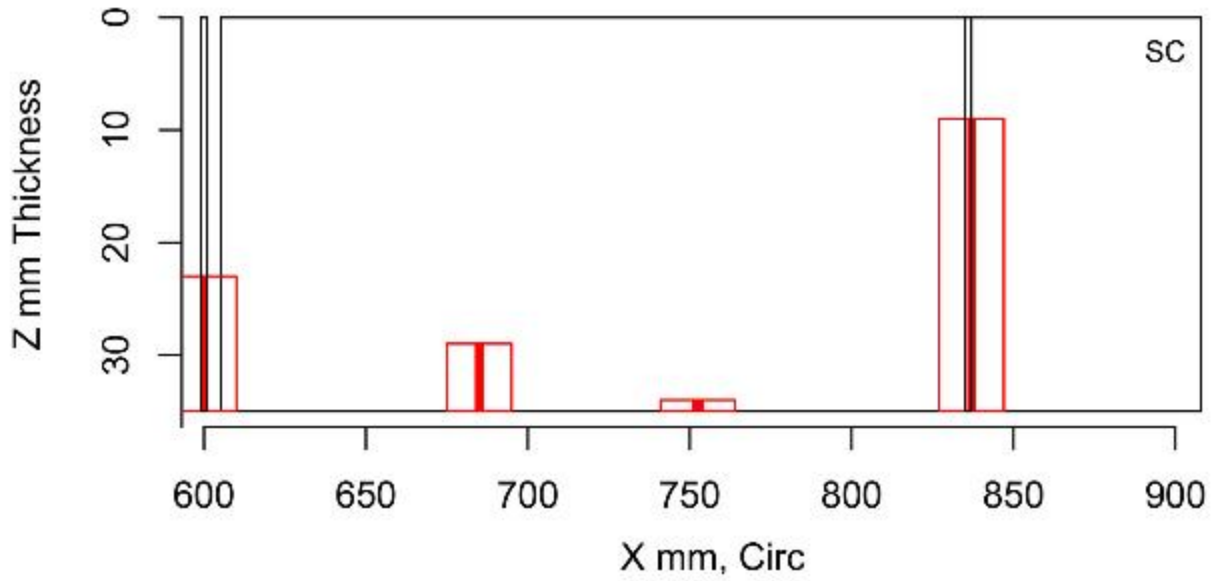


Figure E.120 Indication Plot for Procedure UT.TOFD.117 Applied to Test Block P35 in PARENT Blind Testing (X – Z view, 600 mm–900 mm)

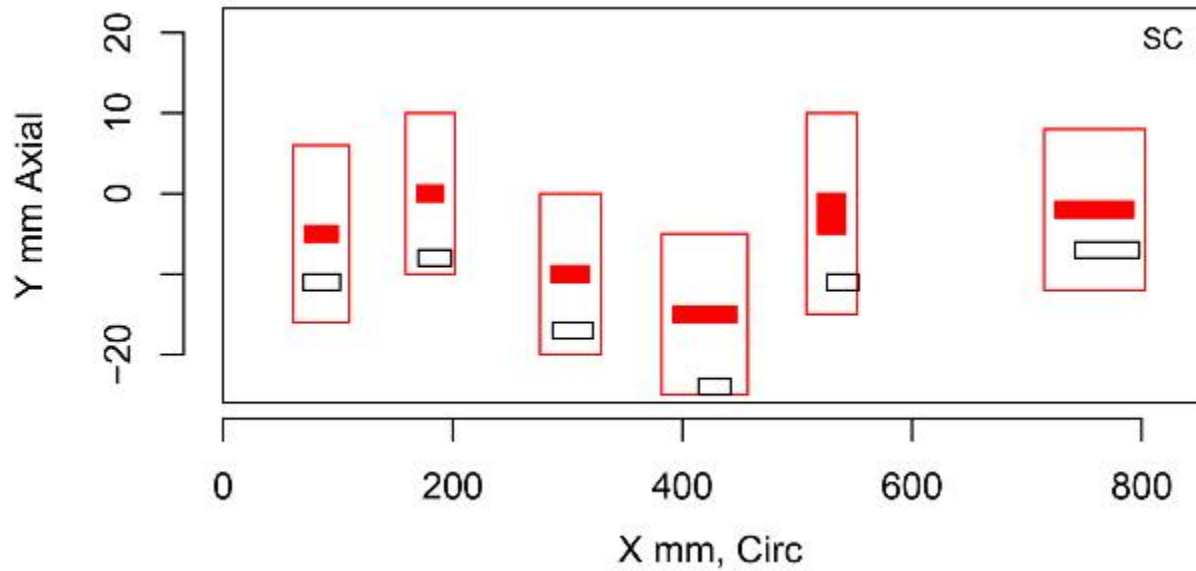


Figure E.121 Indication Plot for Procedure UT.TOFD.117 Applied to Test Block P40 in PARENT Blind Testing (X – Y view, 0 mm–800 mm)

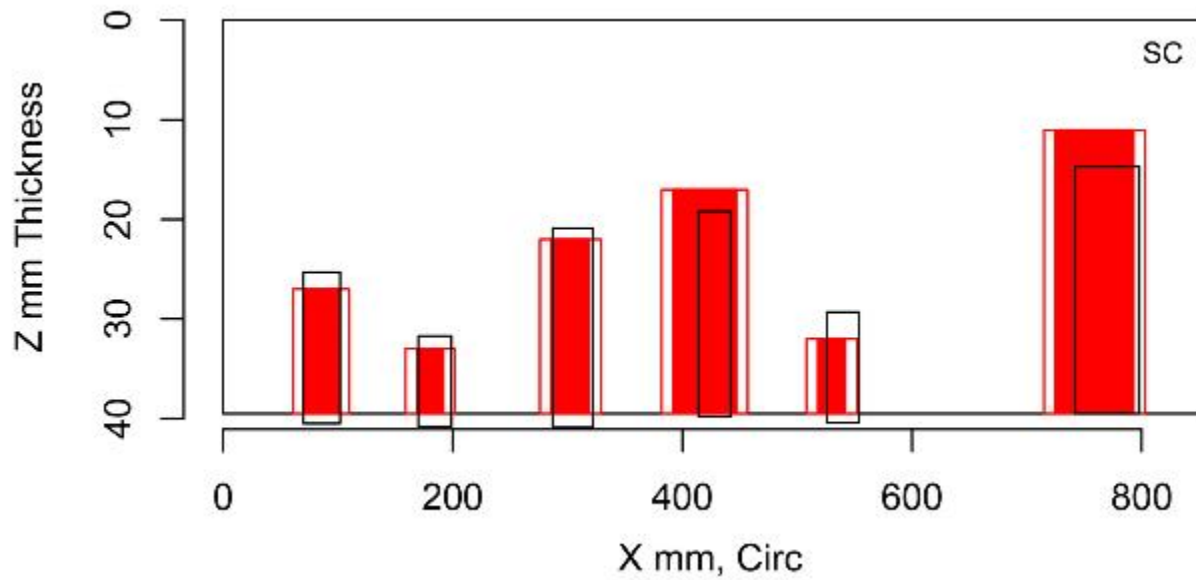


Figure E.122 Indication Plot for Procedure UT.TOFD.117 Applied to Test Block P40 in PARENT Blind Testing (X – Z view, 0 mm–800 mm)

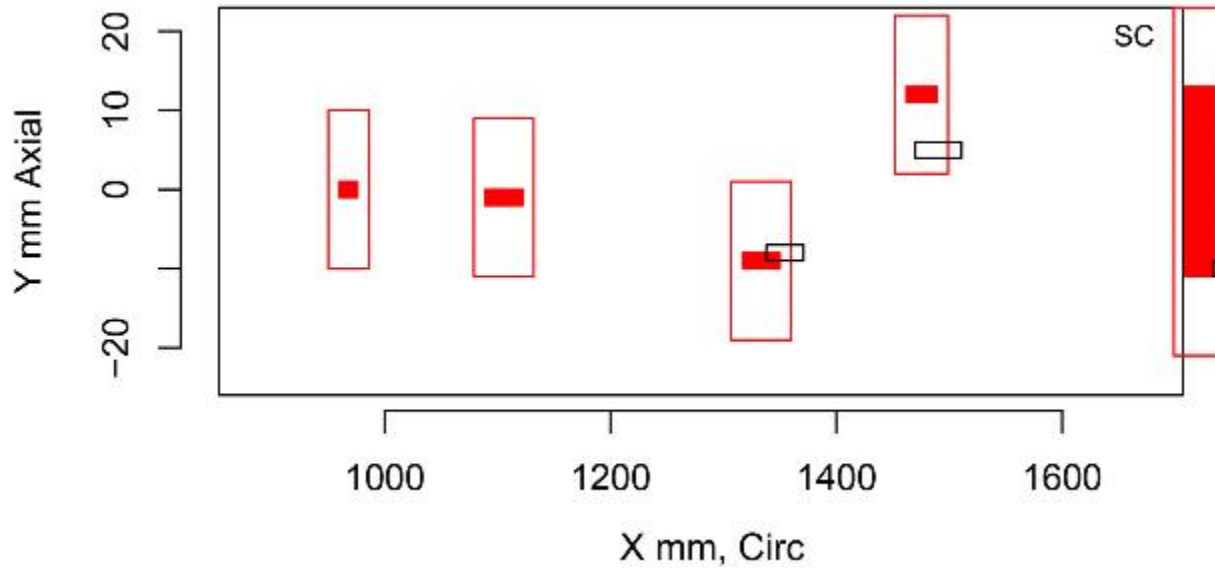


Figure E.123 Indication Plot for Procedure UT.TOFD.117 Applied to Test Block P40 in PARENT Blind Testing (X – Y view, 1000 mm–1600 mm)

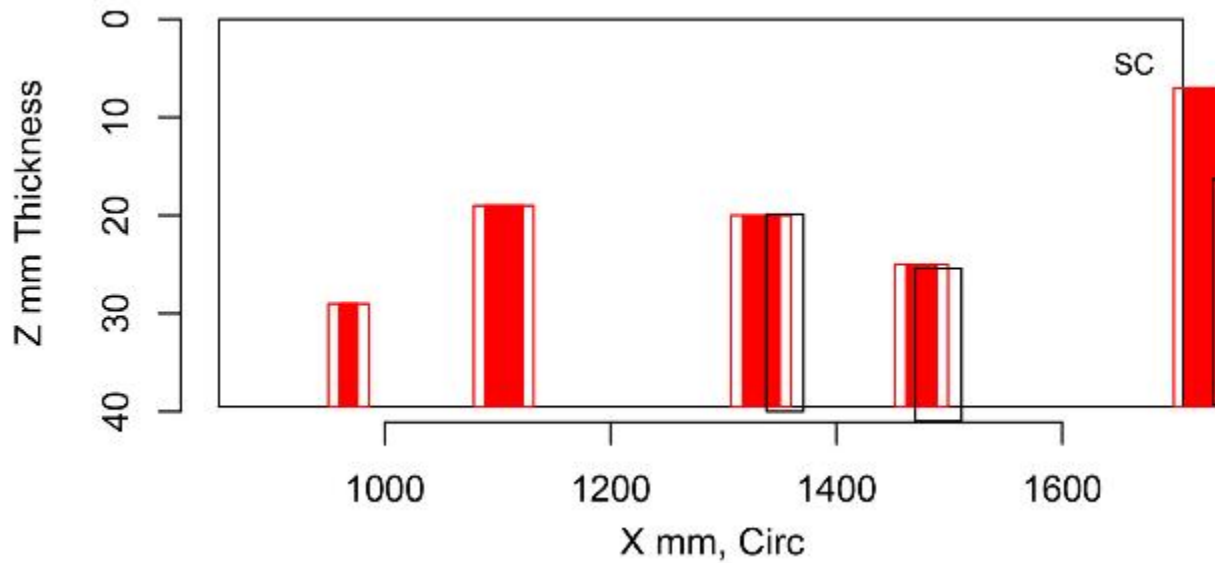


Figure E.124 Indication Plot for Procedure UT.TOFD.117 Applied to Test Block P40 in PARENT Blind Testing (X – Z view, 1000 mm–1600 mm)

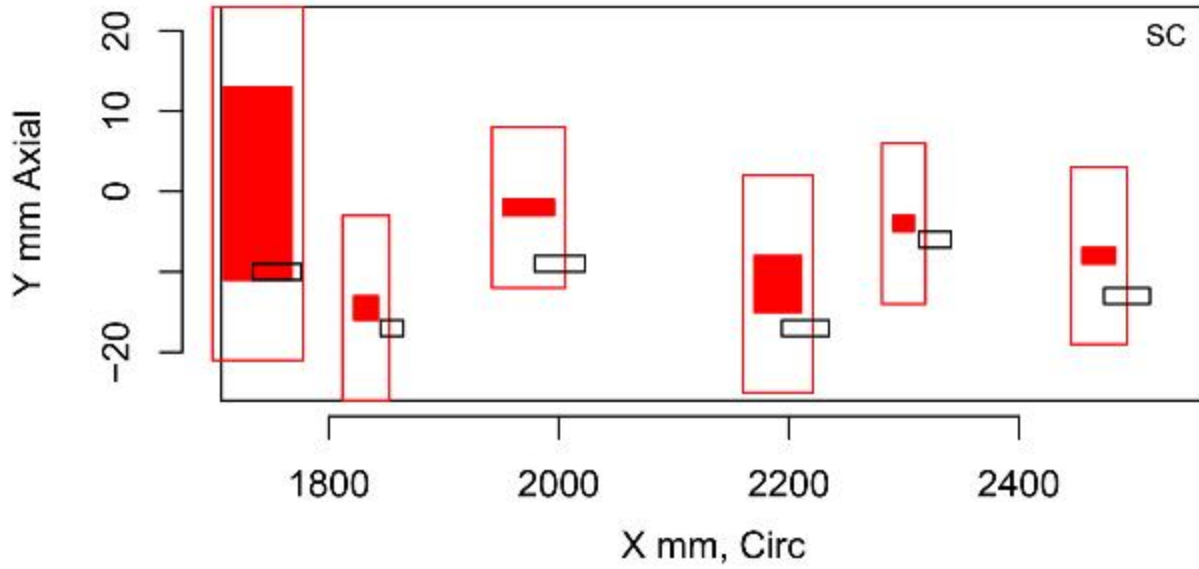


Figure E.125 Indication Plot for Procedure UT.TOFD.117 Applied to Test Block P40 in PARENT Blind Testing (X – Y view, 1800 mm–2400 mm)

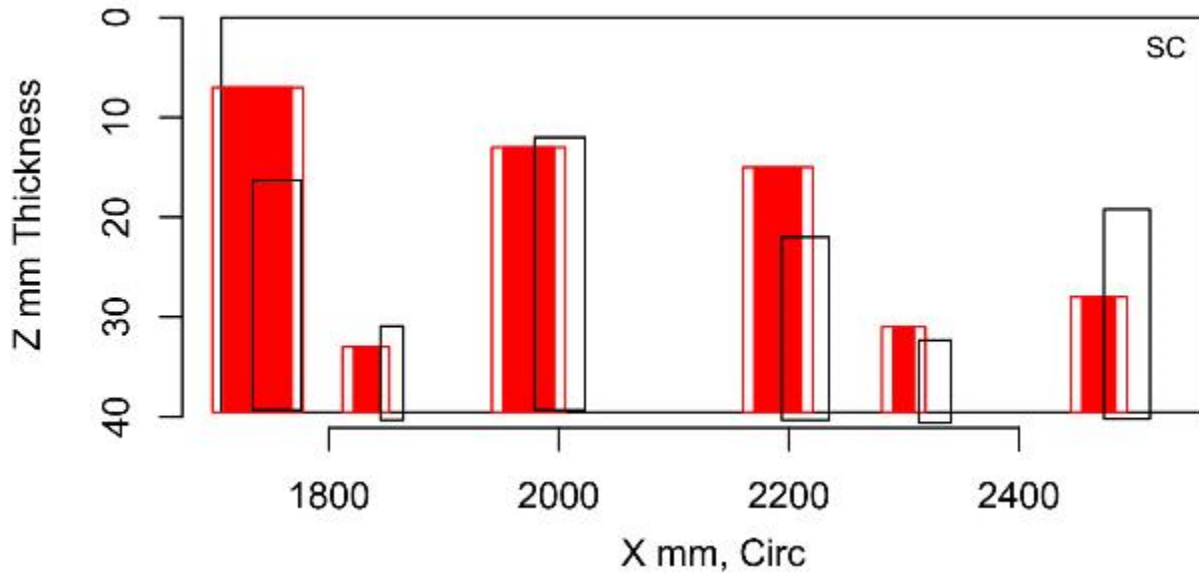


Figure E.126 Indication Plot for Procedure UT.TOFD.117 Applied to Test Block P40 in PARENT Blind Testing (X – Z view, 1800 mm–2400 mm)

E.2.6 Plots for Team 126

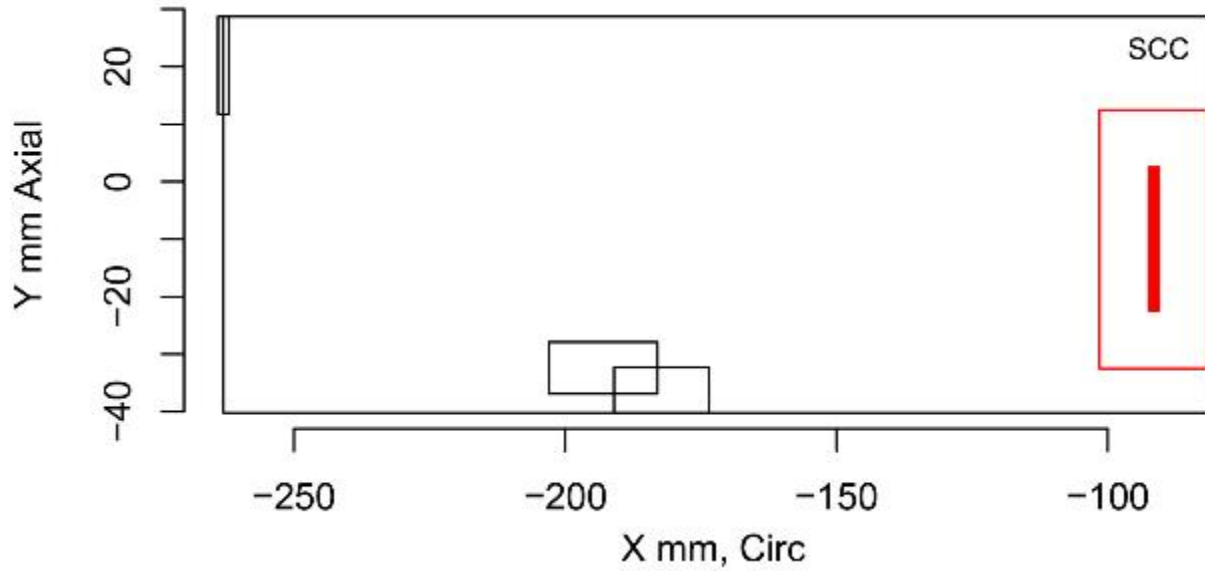


Figure E.127 Indication Plot for Procedure PAUT.126 Applied to Test Block P13 in PARENT Blind Testing (X - Y view)

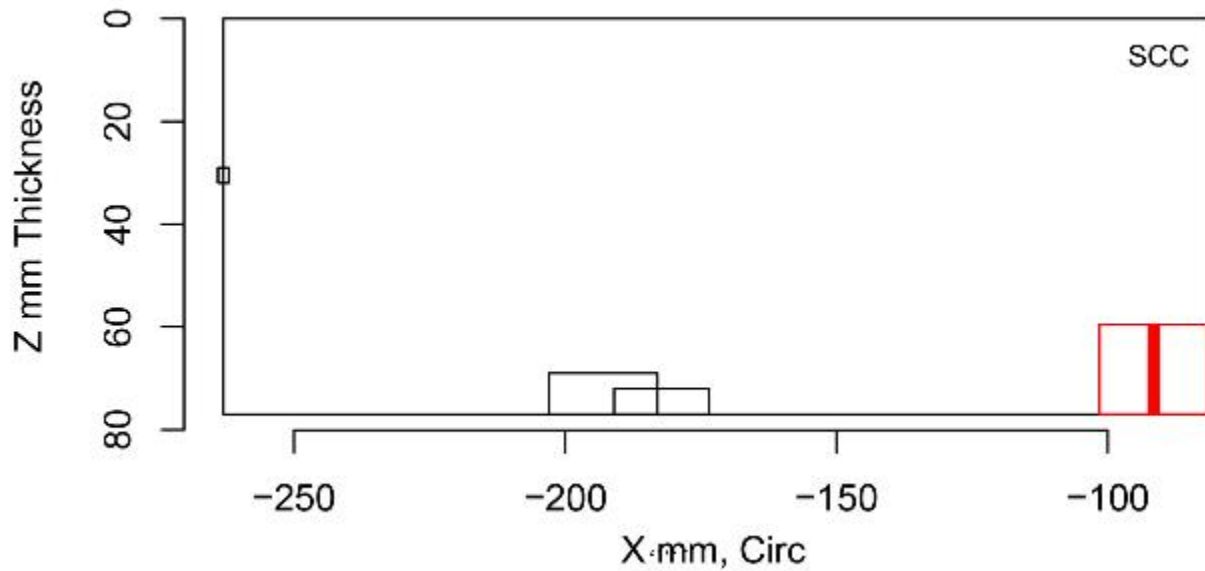


Figure E.128 Indication Plot for Procedure PAUT.126 Applied to Test Block P13 in PARENT Blind Testing (X - Z view)

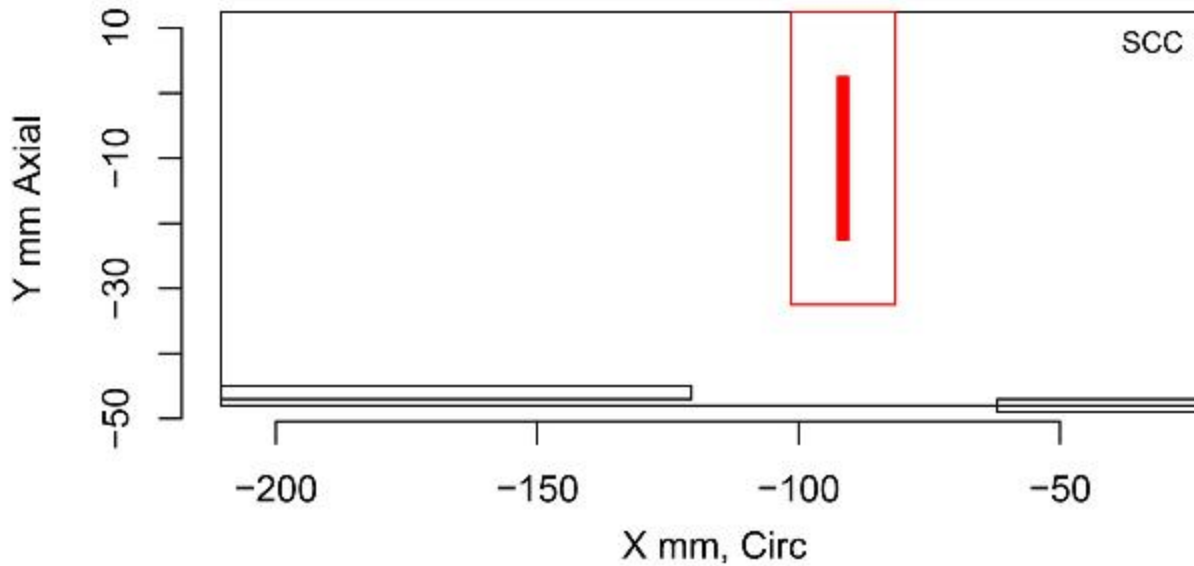


Figure E.129 Indication Plot for Procedure UT.126 Applied to Test Block P13 in PARENT Blind Testing (X – Y view)

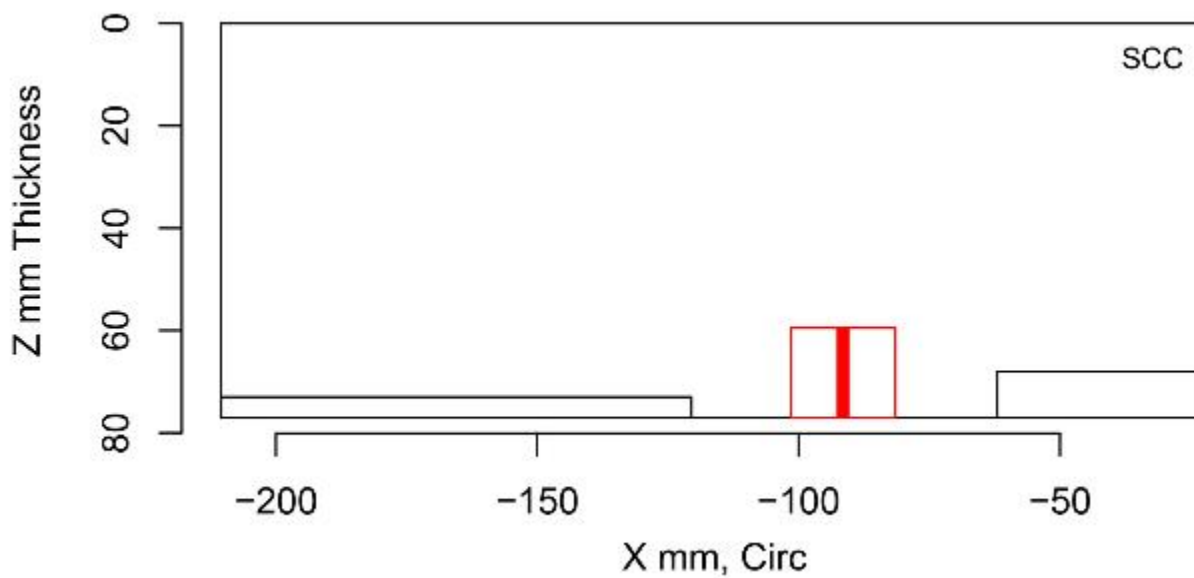


Figure E.130 Indication Plot for Procedure UT.126 Applied to Test Block P13 in PARENT Blind Testing (X – Z view)

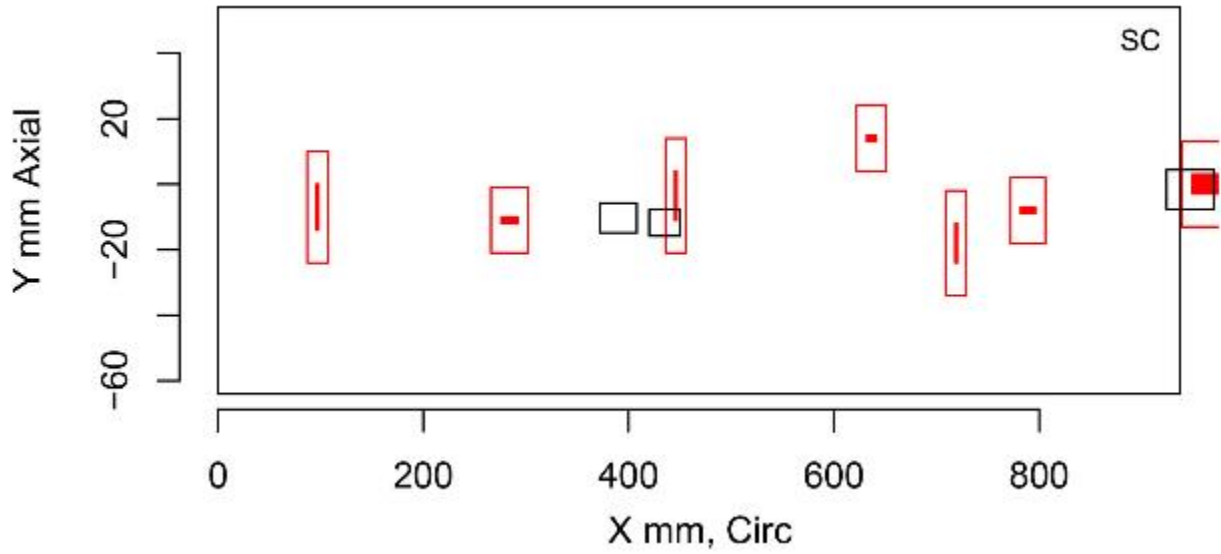


Figure E.131 Indication Plot for Procedure PAUT.126 Applied to Test Block P33 in PARENT Blind Testing (X – Y view, 0 mm–800 mm)

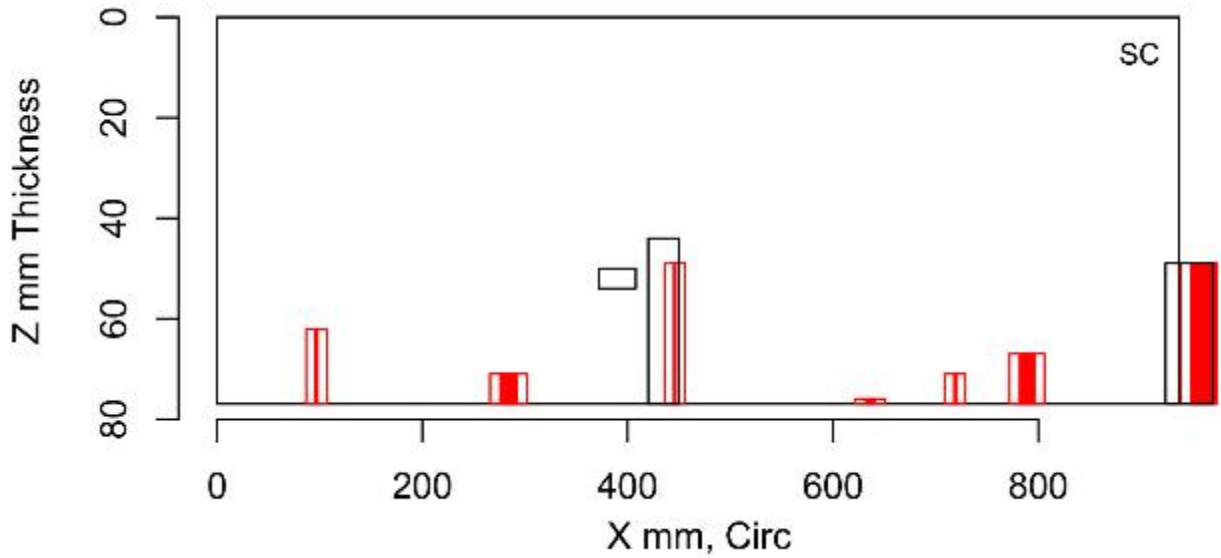


Figure E.132 Indication Plot for Procedure PAUT.126 Applied to Test Block P33 in PARENT Blind Testing (X – Z view, 0 mm–800 mm)

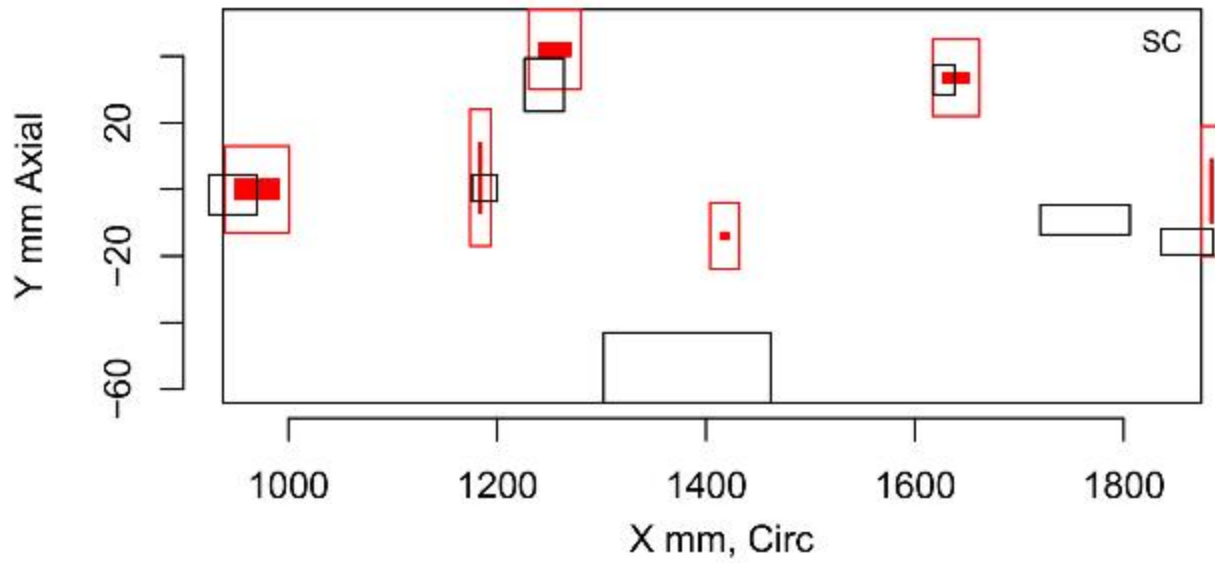


Figure E.133 Indication Plot for Procedure PAUT.126 Applied to Test Block P33 in PARENT Blind Testing (X - Y view, 1000 mm-1800 mm)

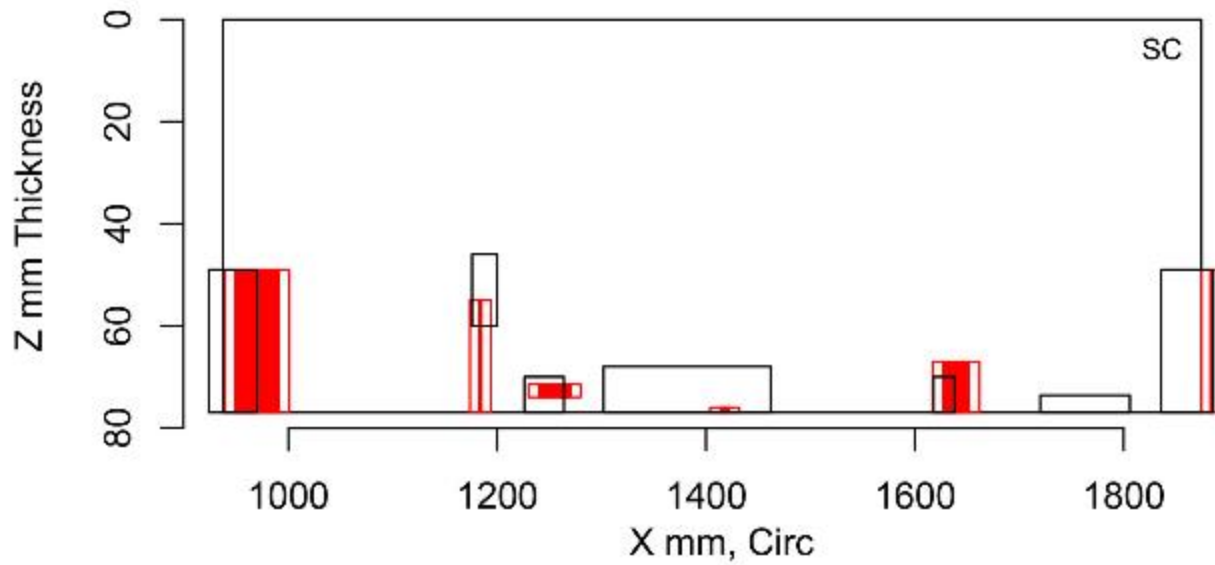


Figure E.134 Indication Plot for Procedure PAUT.126 Applied to Test Block P33 in PARENT Blind Testing (X - Z view, 1000 mm-1800 mm)

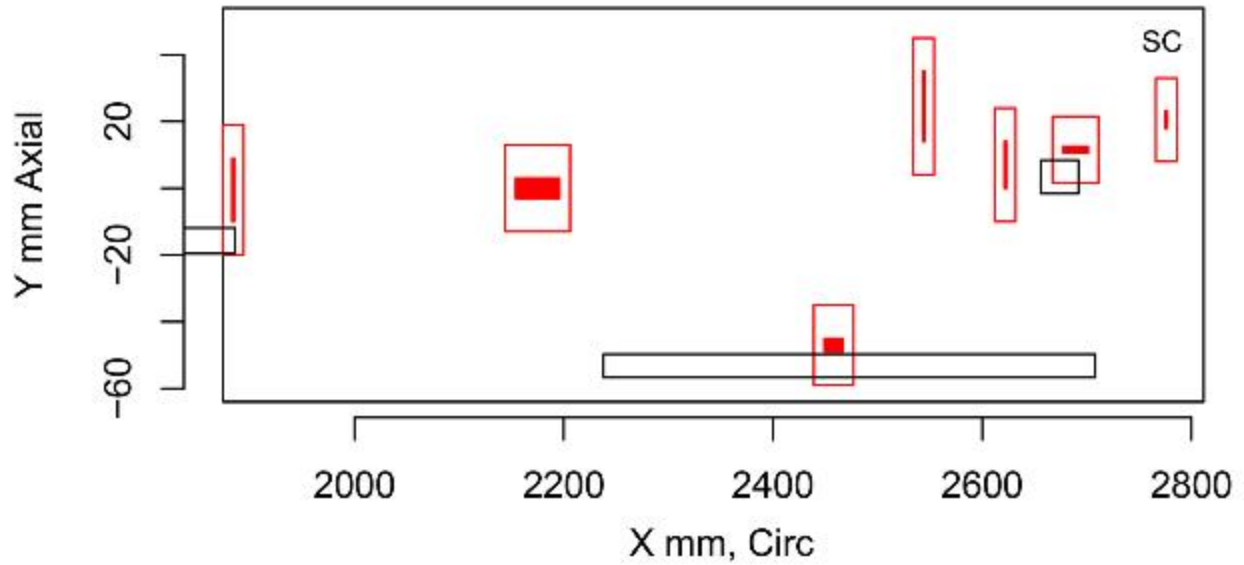


Figure E.135 Indication Plot for Procedure PAUT.126 Applied to Test Block P33 in PARENT Blind Testing (X – Y view, 2000 mm–2800 mm)

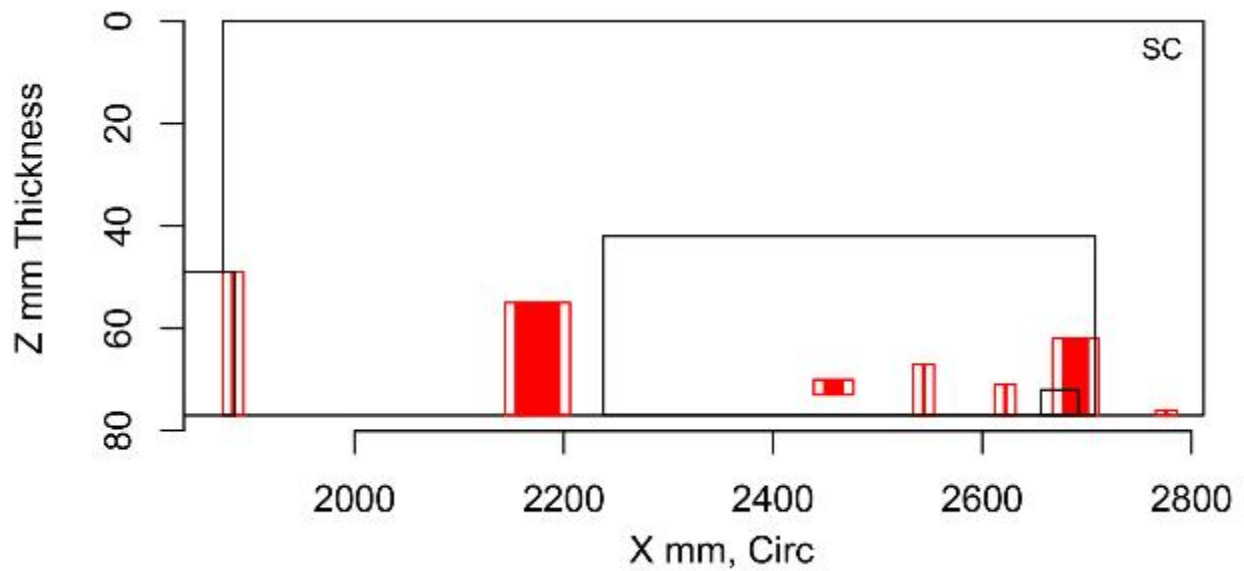


Figure E.136 Indication Plot for Procedure PAUT.126 Applied to Test Block P33 in PARENT Blind Testing (X – Z view, 2000 mm–2800 mm)

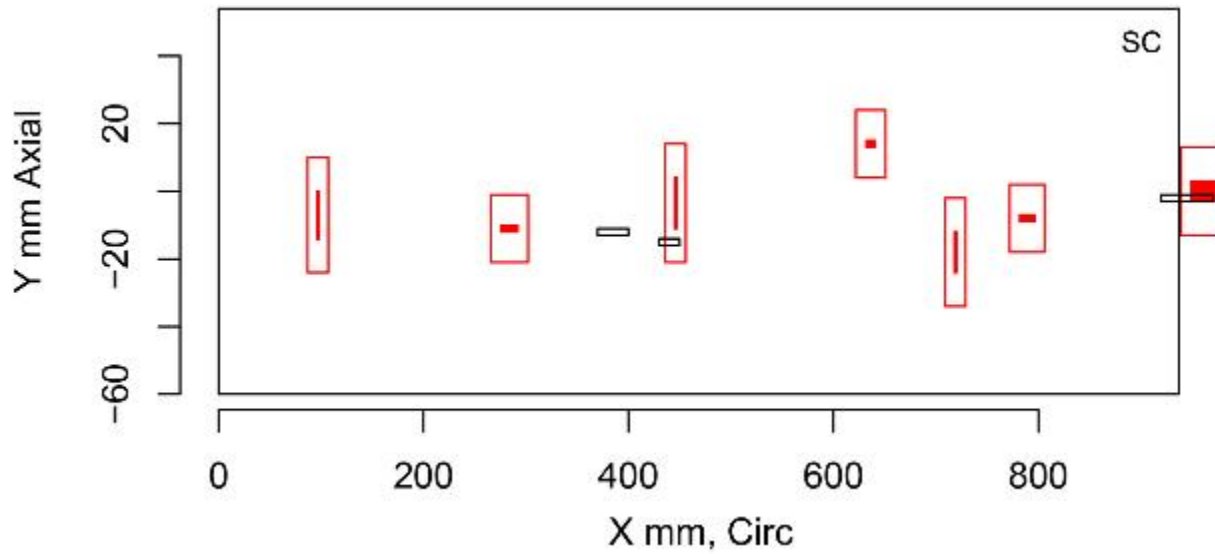


Figure E.137 Indication Plot for Procedure UT.126 Applied to Test Block P33 in PARENT Blind Testing (X - Y view, 0 mm-800 mm)

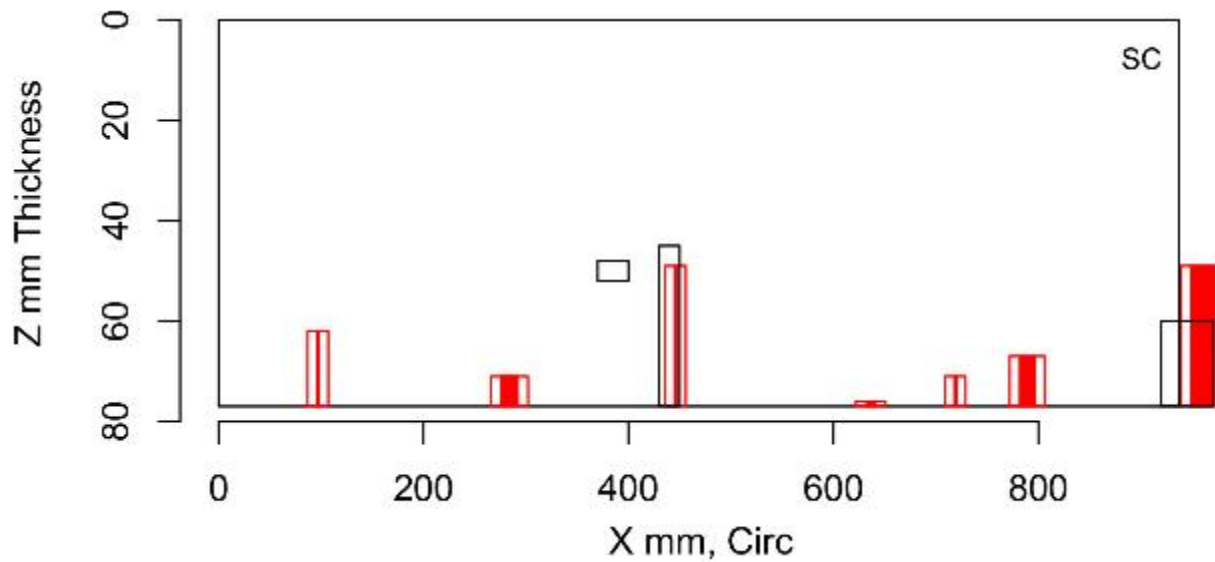


Figure E.138 Indication Plot for Procedure UT.126 Applied to Test Block P33 in PARENT Blind Testing (X - Z view, 0 mm-800 mm)

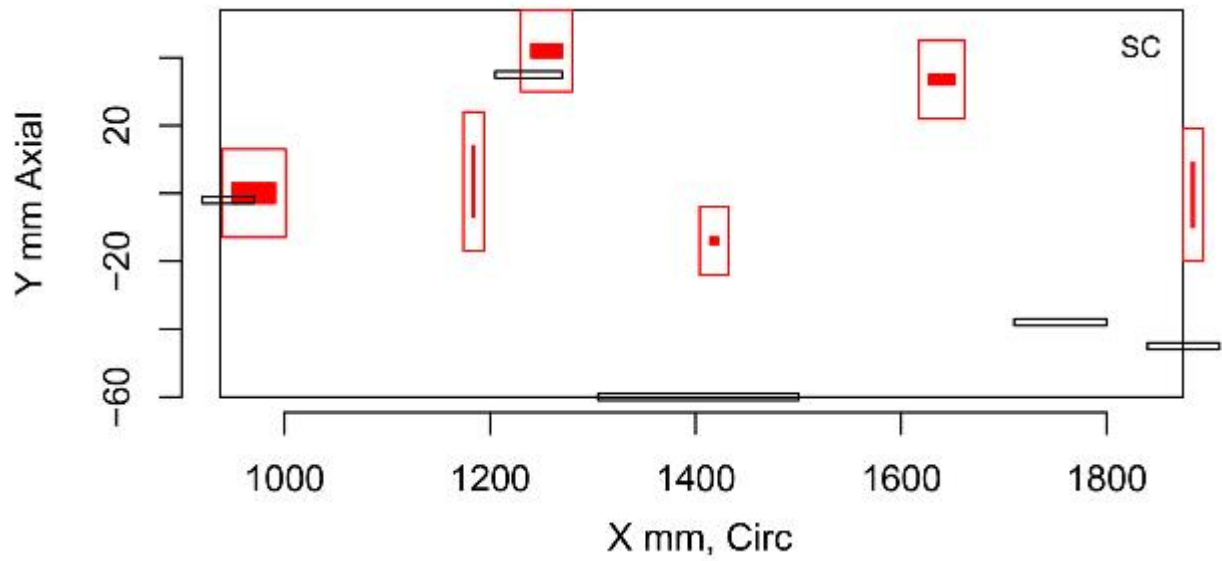


Figure E.139 Indication Plot for Procedure UT.126 Applied to Test Block P33 in PARENT Blind Testing (X – Y view, 1000 mm–1800 mm)

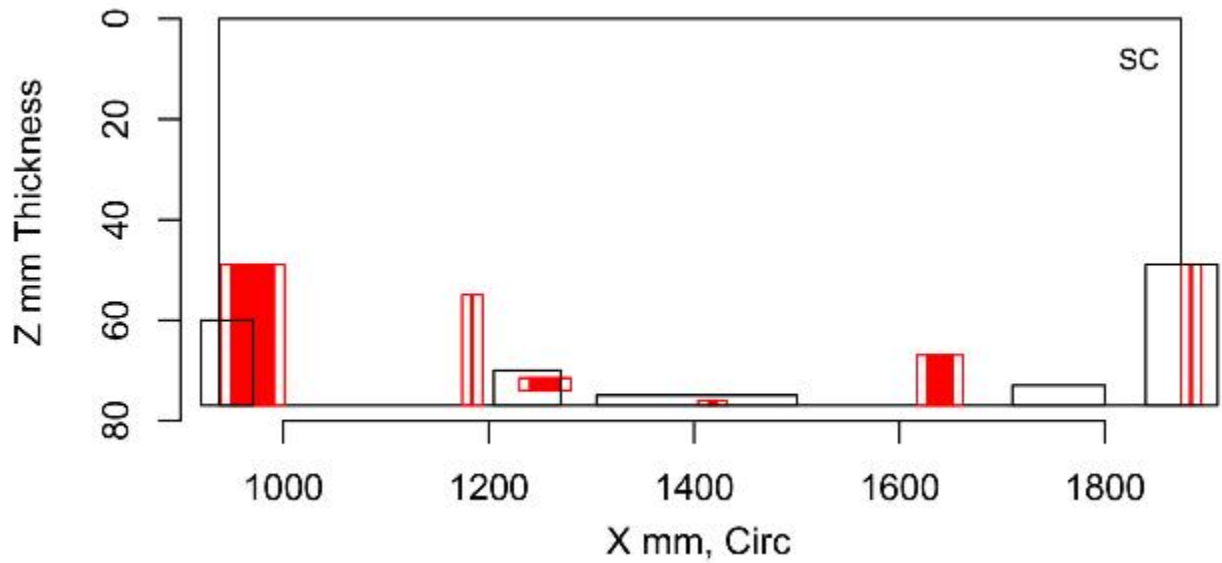


Figure E.140 Indication Plot for Procedure UT.126 Applied to Test Block P33 in PARENT Blind Testing (X – Z view, 1000 mm–1800 mm)

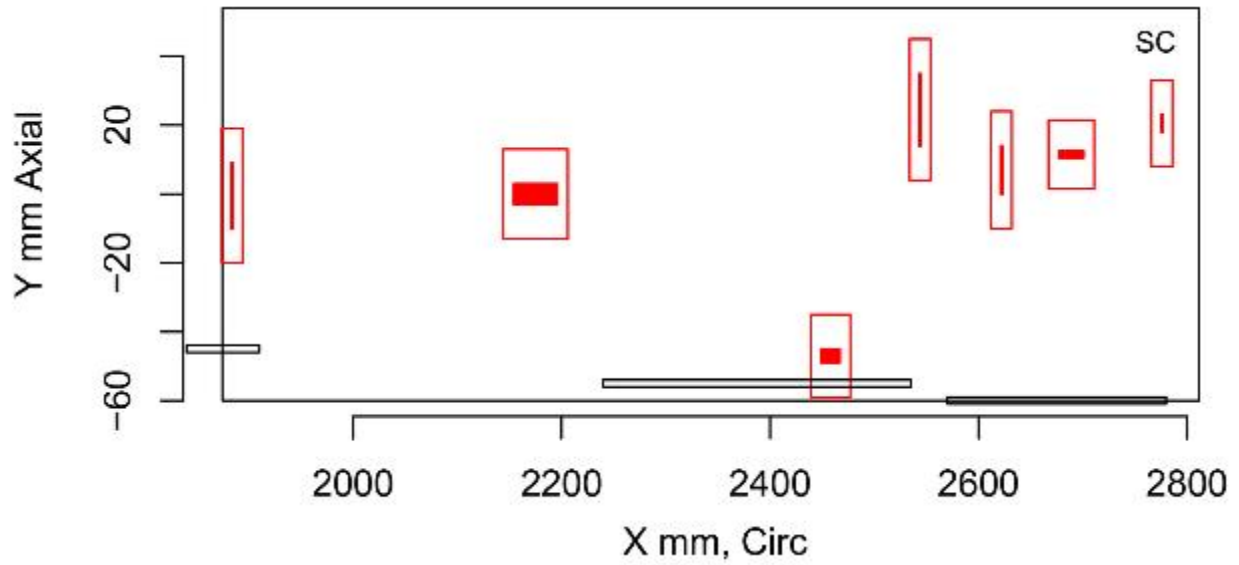


Figure E.141 Indication Plot for Procedure UT.126 Applied to Test Block P33 in PARENT Blind Testing (X - Y view, 2000 mm-2800 mm)

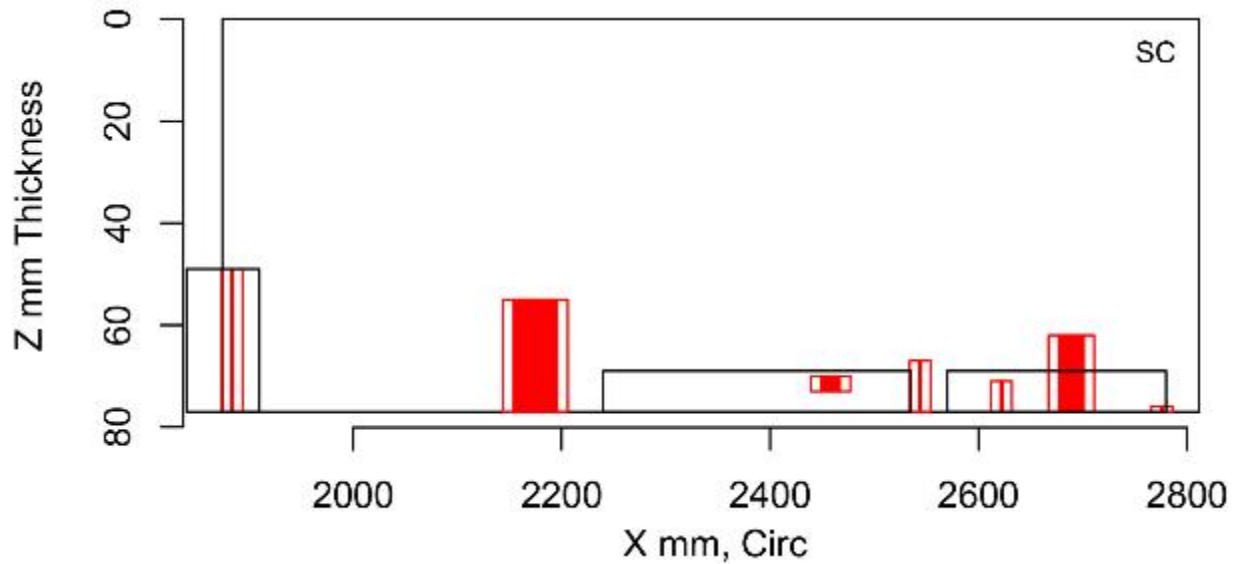


Figure E.142 Indication Plot for Procedure UT.126 Applied to Test Block P33 in PARENT Blind Testing (X - Z view, 2000 mm-2800 mm)

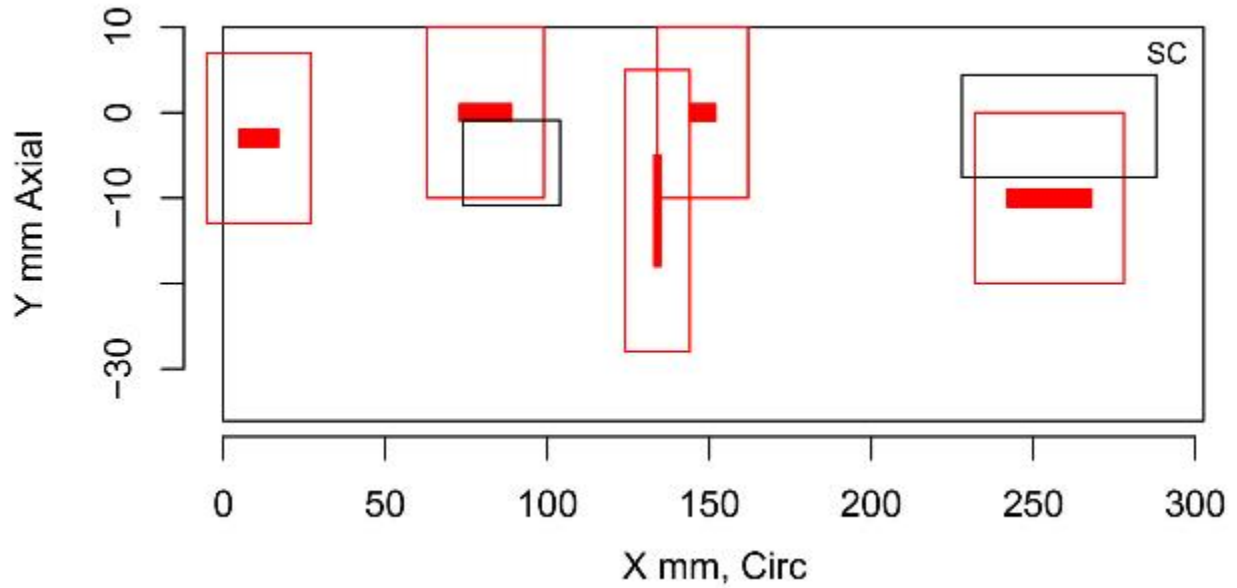


Figure E.143 Indication Plot for Procedure PAUT.126 Applied to Test Block P35 in PARENT Blind Testing (X - Y view, 0 mm-300 mm)

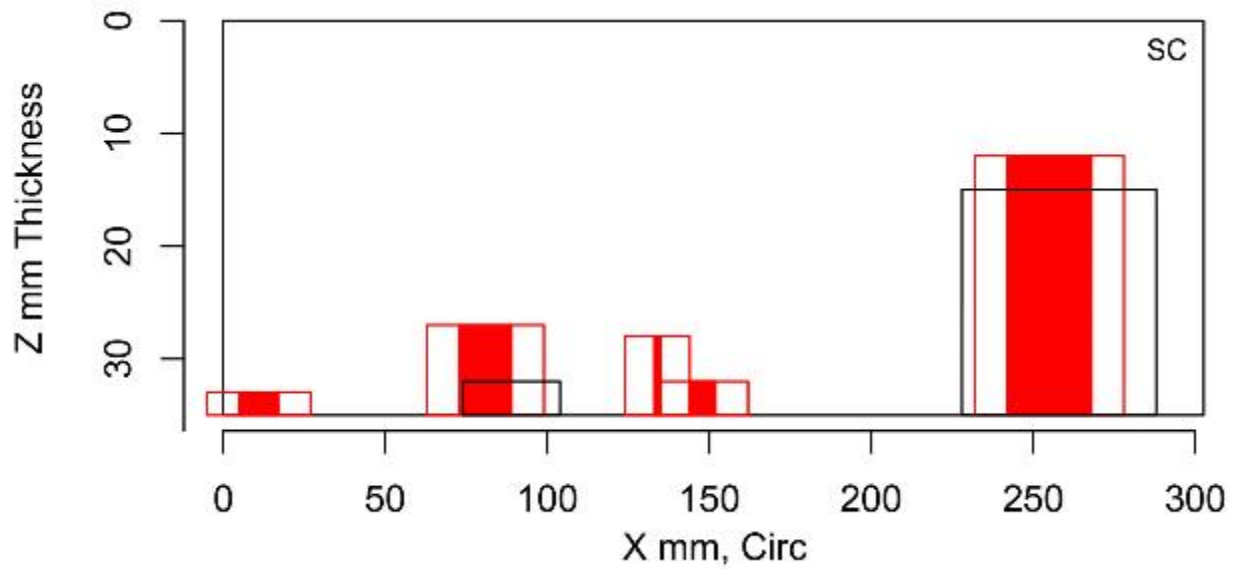


Figure E.144 Indication Plot for Procedure PAUT.126 Applied to Test Block P35 in PARENT Blind Testing (X - Z view, 0 mm-300 mm)

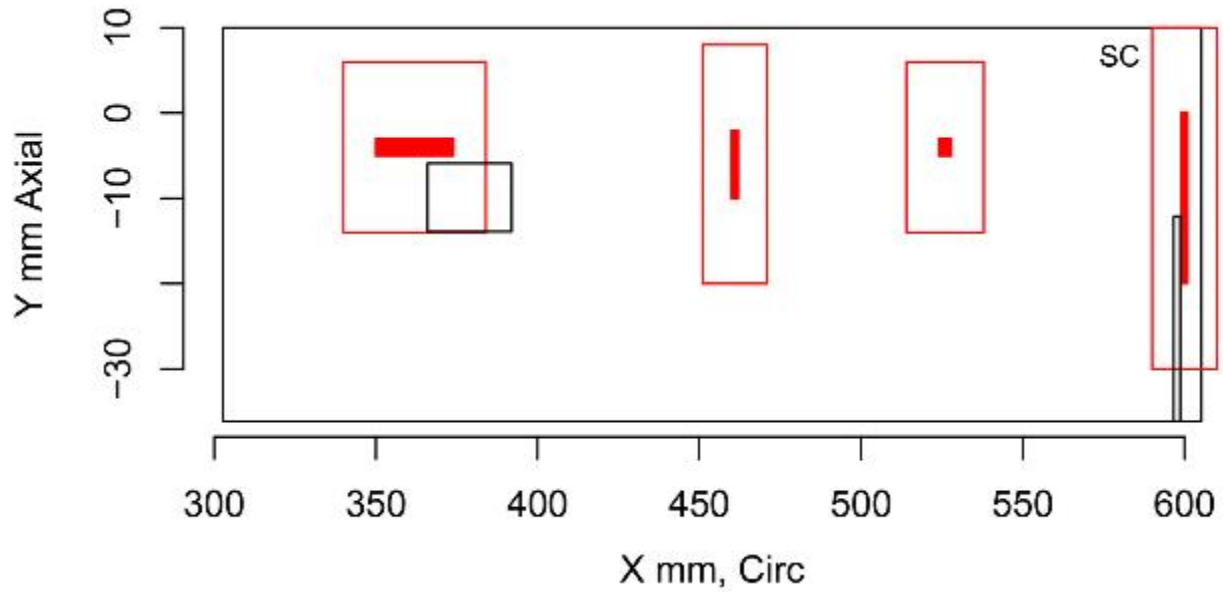


Figure E.145 Indication Plot for Procedure PAUT.126 Applied to Test Block P35 in PARENT Blind Testing (X – Y view, 300 mm–600 mm)

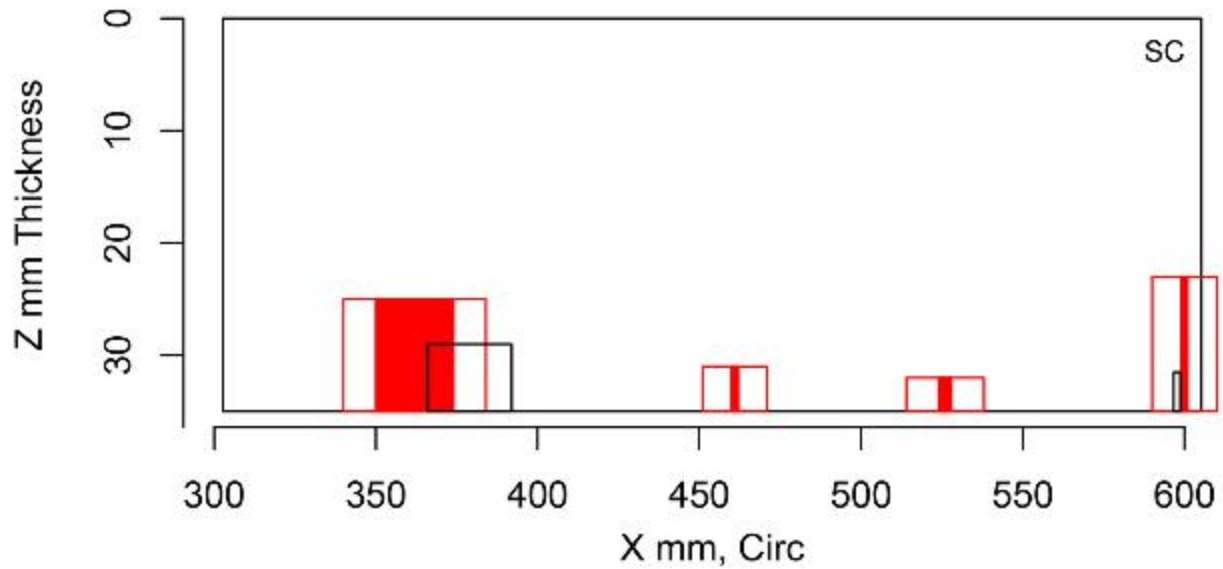


Figure E.146 Indication Plot for Procedure PAUT.126 Applied to Test Block P35 in PARENT Blind Testing (X – Z view, 300 mm–600 mm)

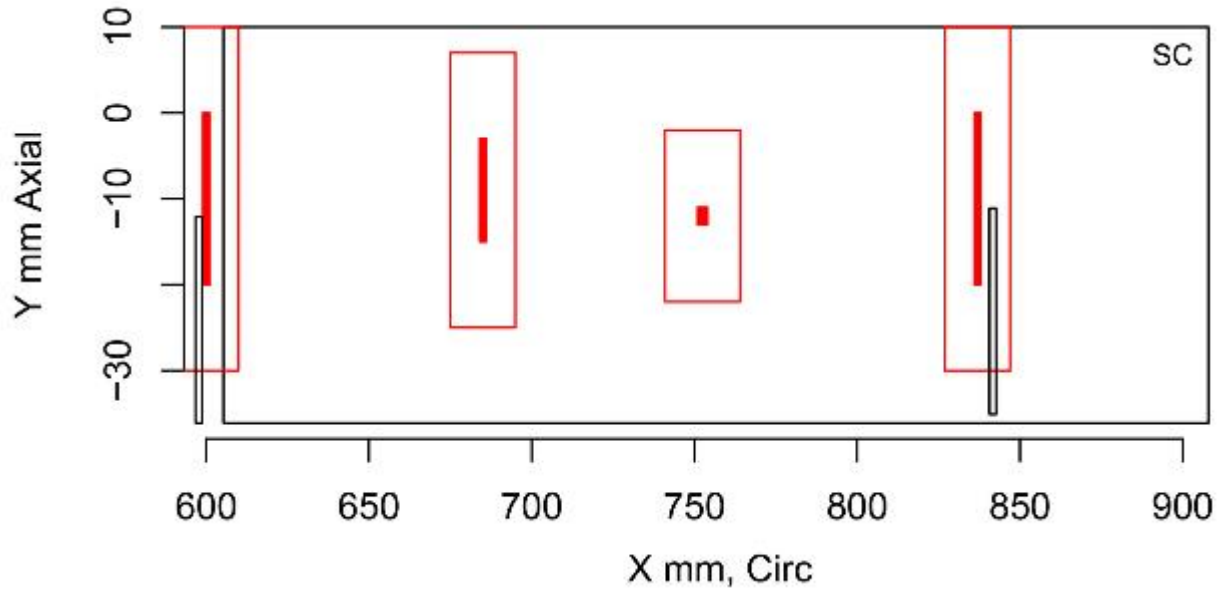


Figure E.147 Indication Plot for Procedure PAUT.126 Applied to Test Block P35 in PARENT Blind Testing (X - Y view, 600 mm-900 mm)

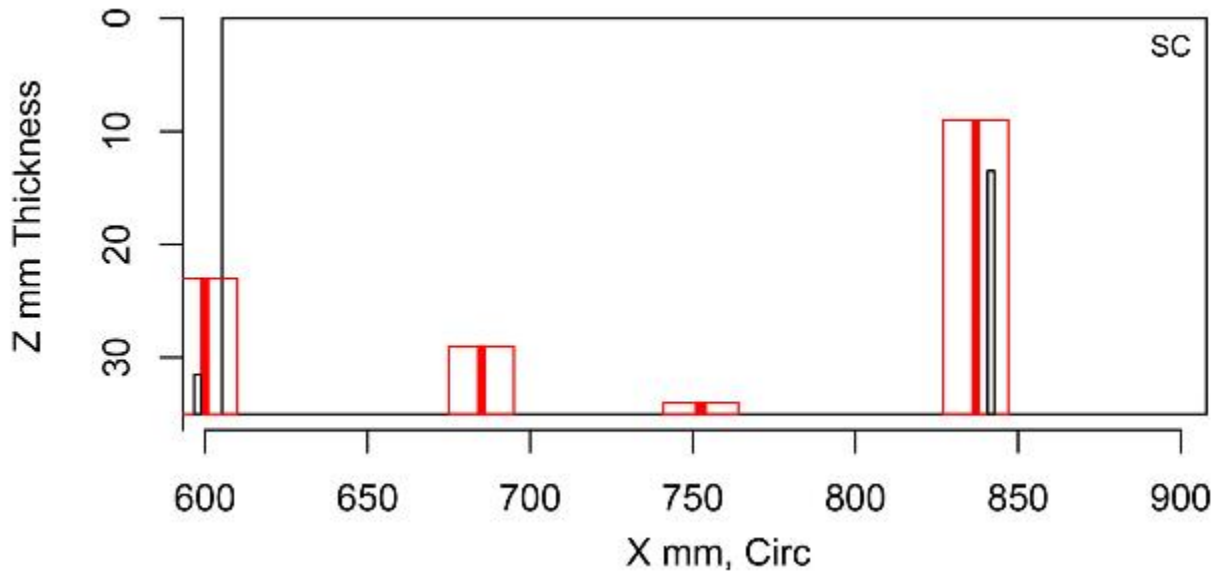


Figure E.148 Indication Plot for Procedure PAUT.126 Applied to Test Block P35 in PARENT Blind Testing (X - Z view, 600 mm-900 mm)

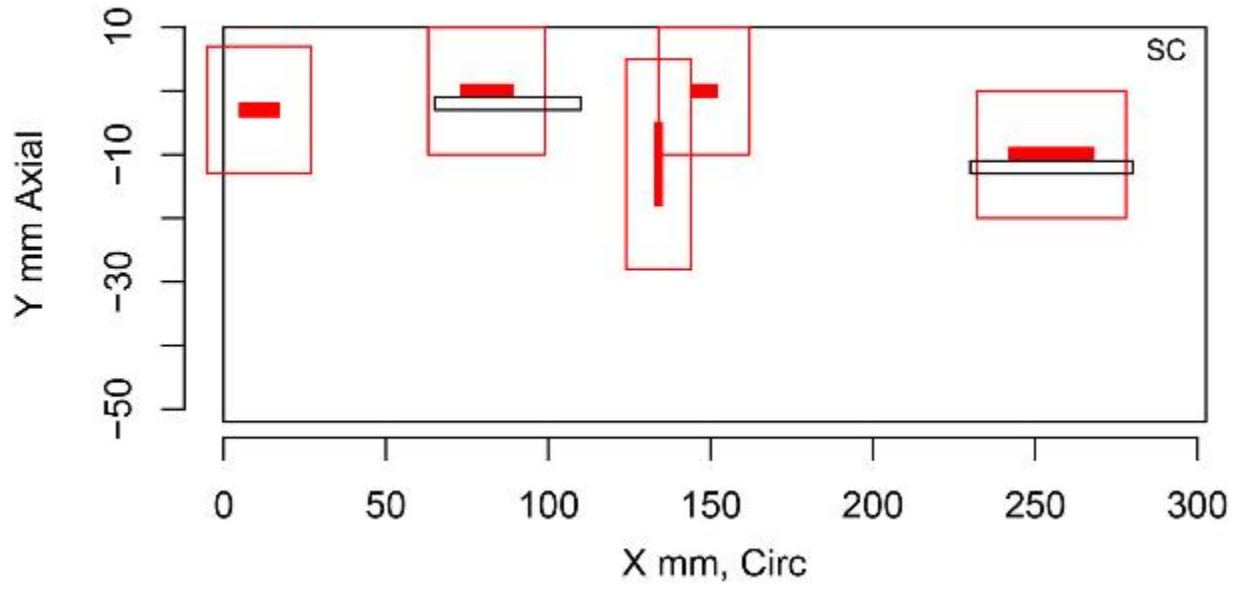


Figure E.149 Indication Plot for Procedure UT.126 Applied to Test Block P35 in PARENT Blind Testing (X – Y view, 0 mm–300 mm)

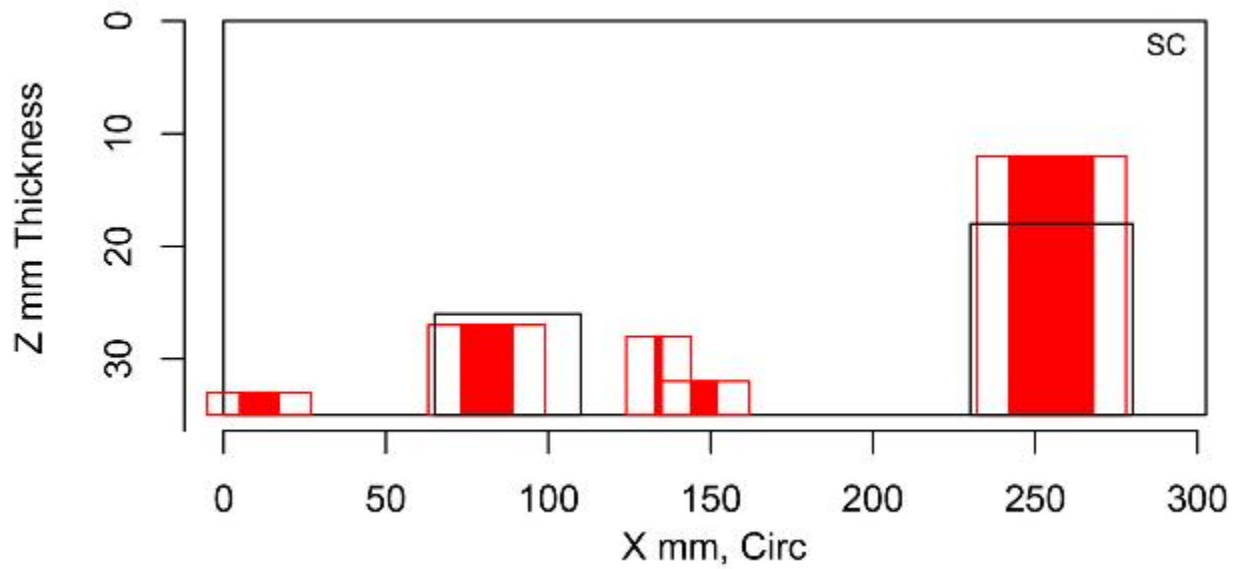


Figure E.150 Indication Plot for Procedure UT.126 Applied to Test Block P35 in PARENT Blind Testing (X – Z view, 0 mm–300 mm)

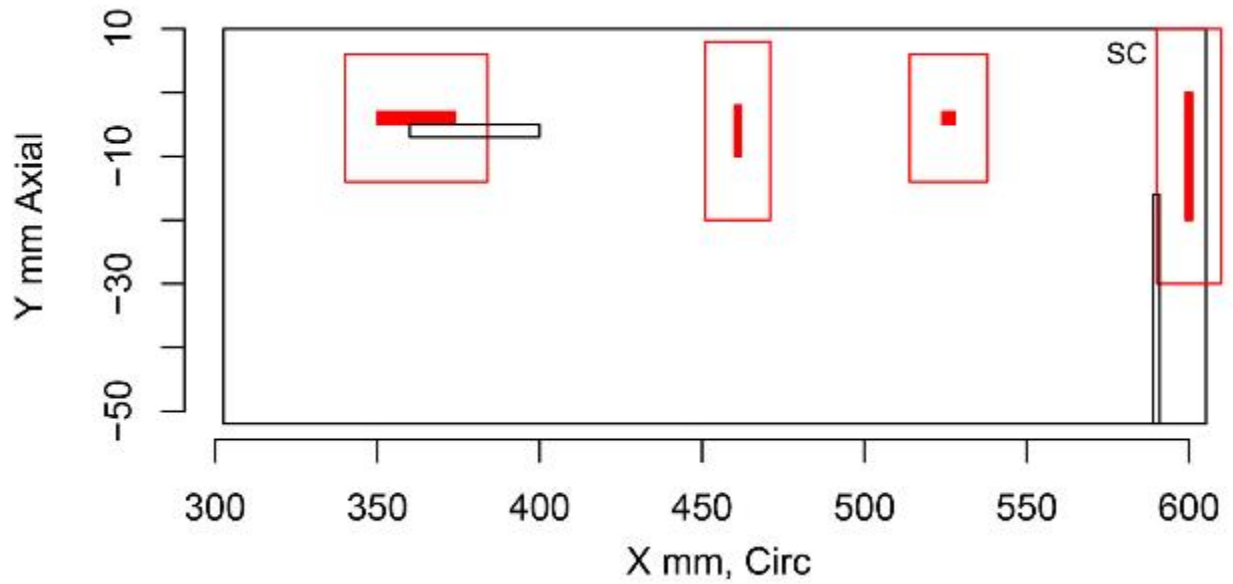


Figure E.151 Indication Plot for Procedure UT.126 Applied to Test Block P35 in PARENT Blind Testing (X – Y view, 300 mm–600 mm)

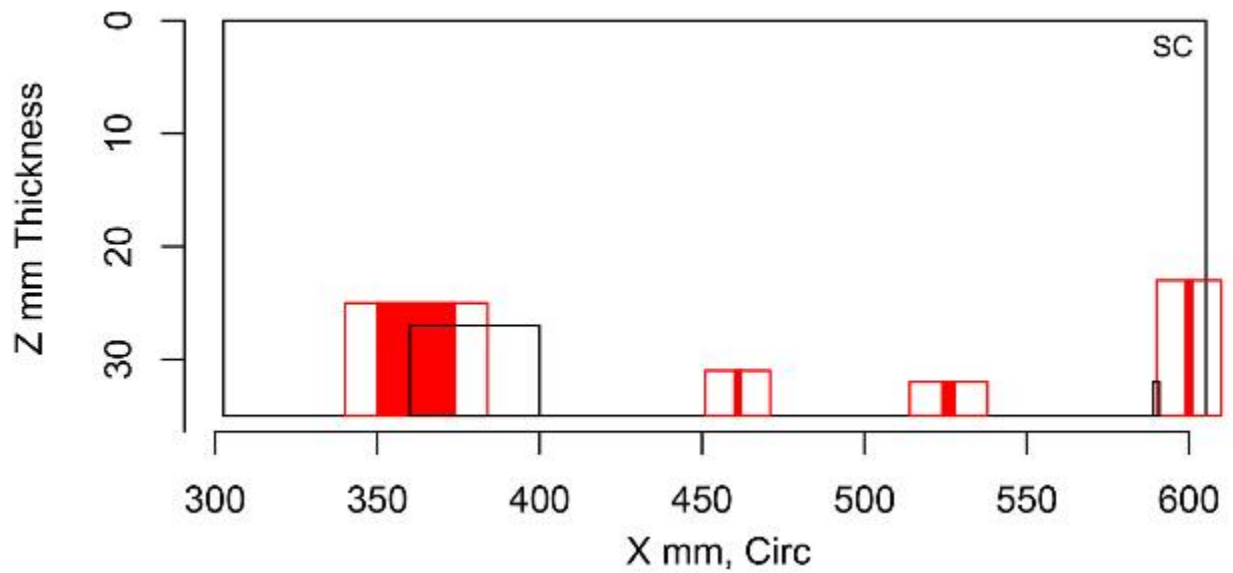


Figure E.152 Indication Plot for Procedure UT.126 Applied to Test Block P35 in PARENT Blind Testing (X – Z view, 300 mm–600 mm)

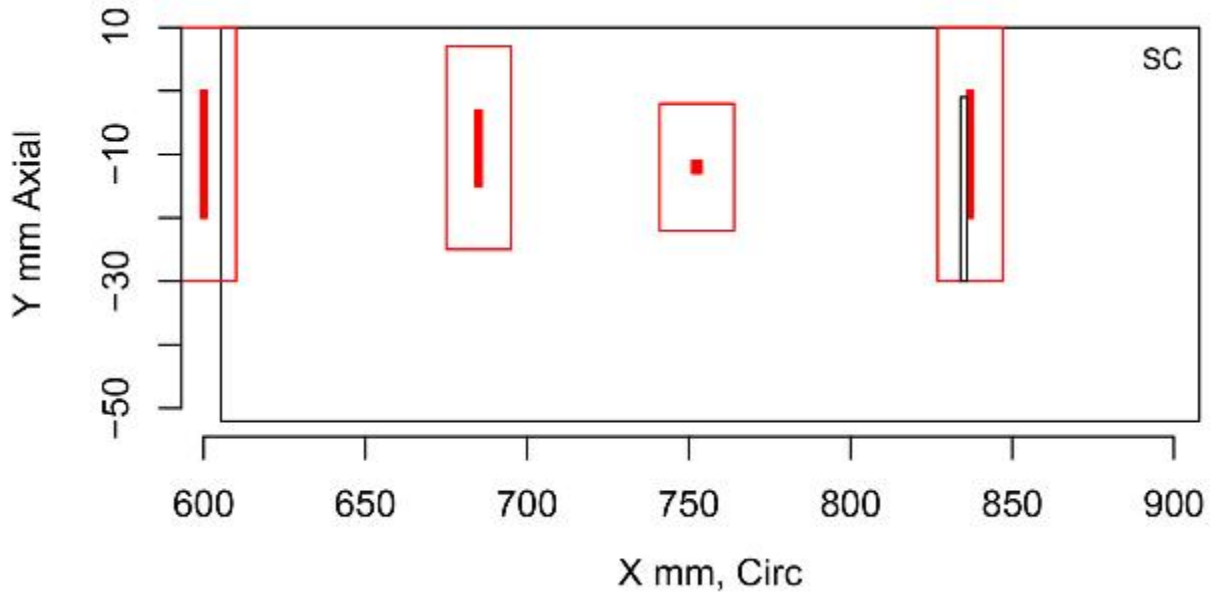


Figure E.153 Indication Plot for Procedure UT.126 Applied to Test Block P35 in PARENT Blind Testing (X – Y view, 600 mm–900 mm)

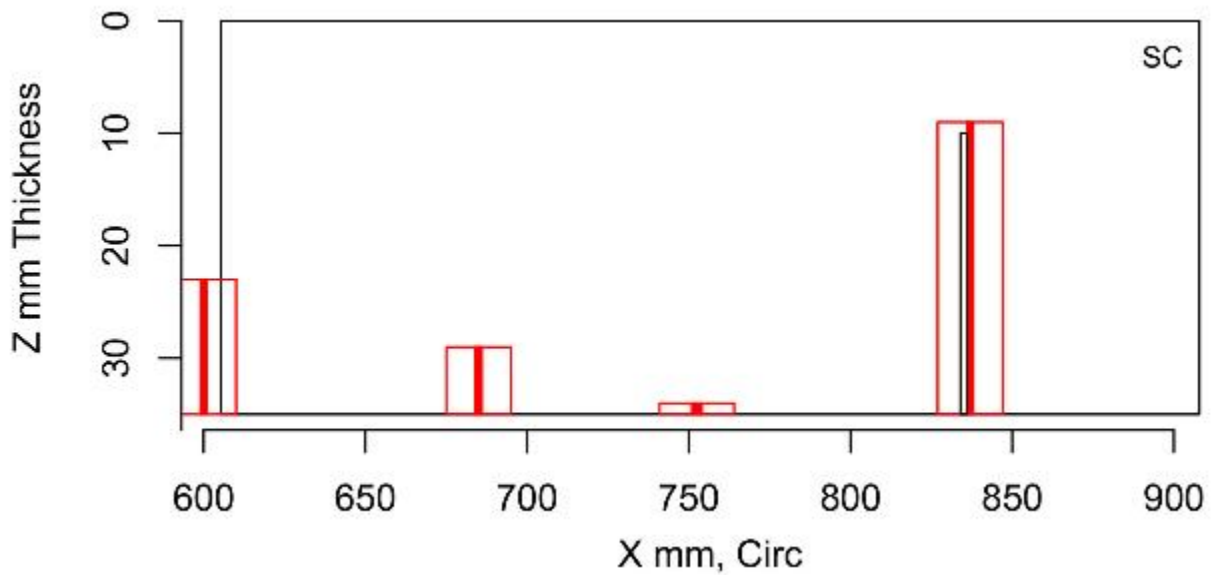


Figure E.154 Indication Plot for Procedure UT.126 Applied to Test Block P35 in PARENT Blind Testing (X – Z view, 600 mm–900 mm)

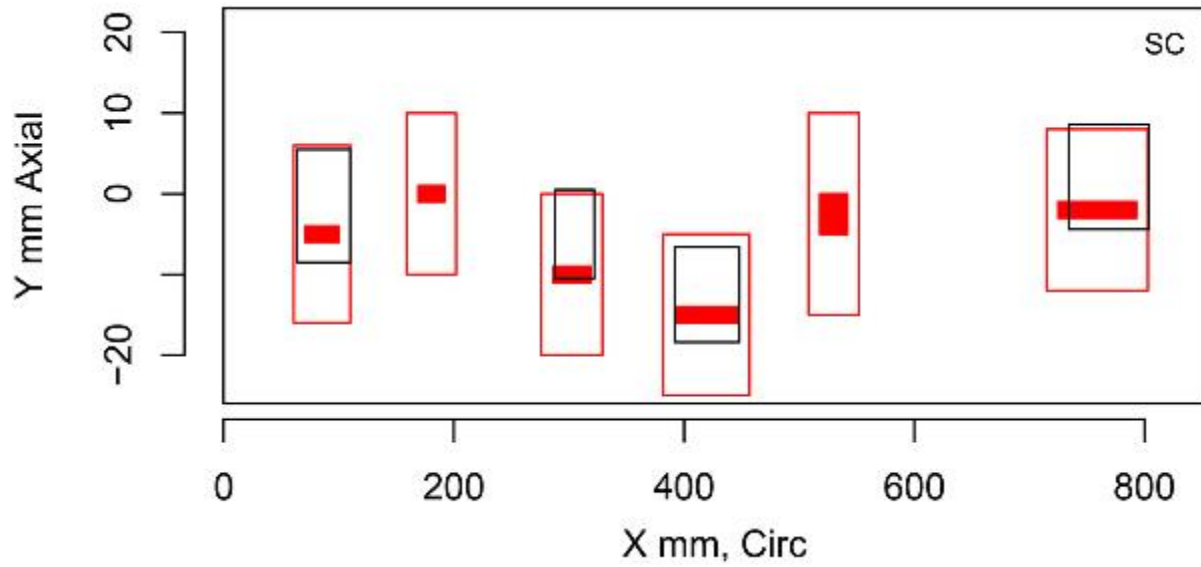


Figure E.155 Indication Plot for Procedure PAUT.126 Applied to Test Block P40 in PARENT Blind Testing (X – Y view, 0 mm–800 mm)

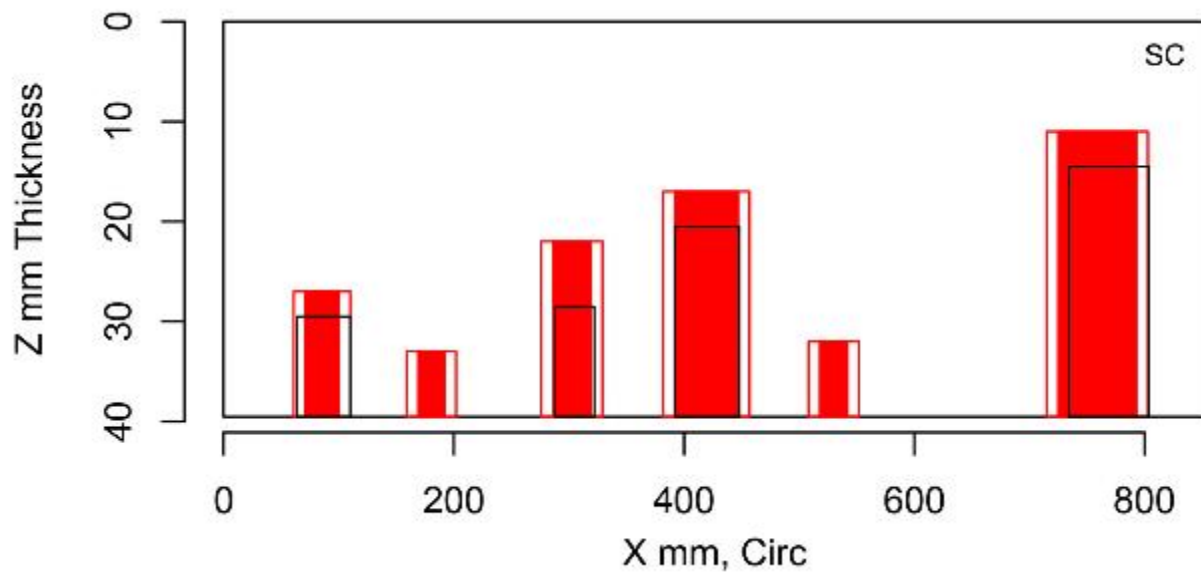


Figure E.156 Indication Plot for Procedure PAUT.126 Applied to Test Block P40 in PARENT Blind Testing (X – Z view, 0 mm–800 mm)

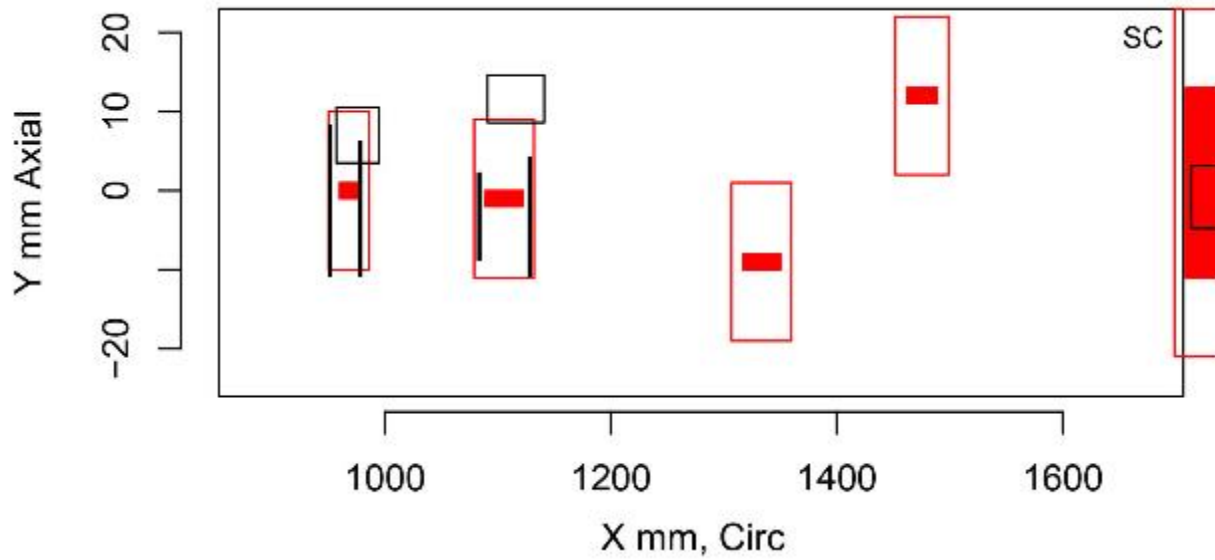


Figure E.157 Indication Plot for Procedure PAUT.126 Applied to Test Block P40 in PARENT Blind Testing (X – Y view, 1000 mm–1600 mm)

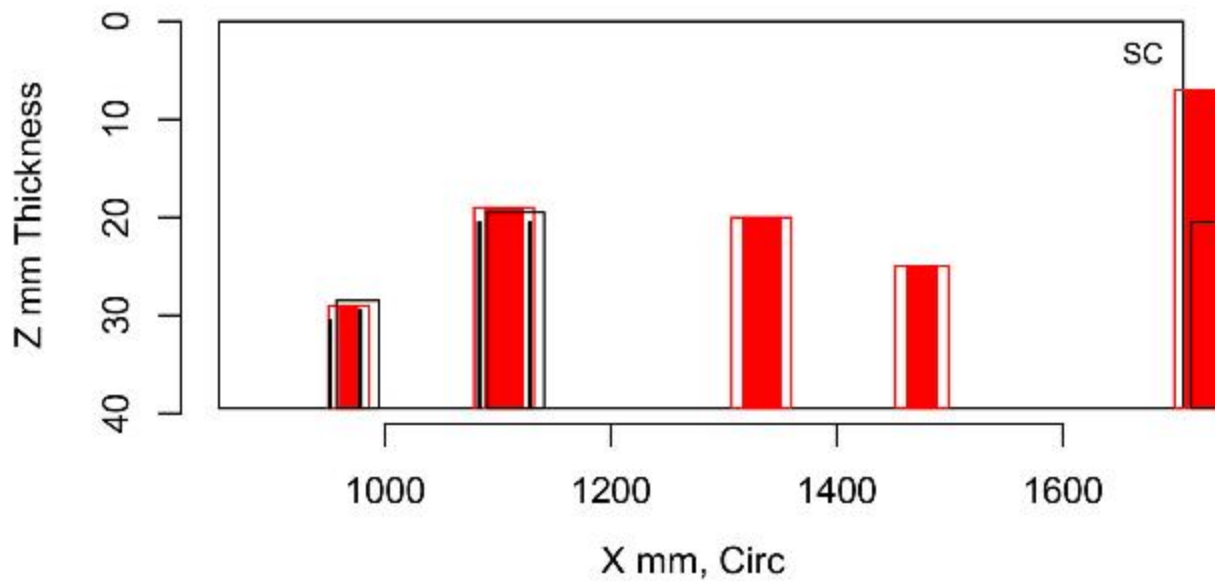


Figure E.158 Indication Plot for Procedure PAUT.126 Applied to Test Block P40 in PARENT Blind Testing (X – Z view, 1000 mm–1600 mm)

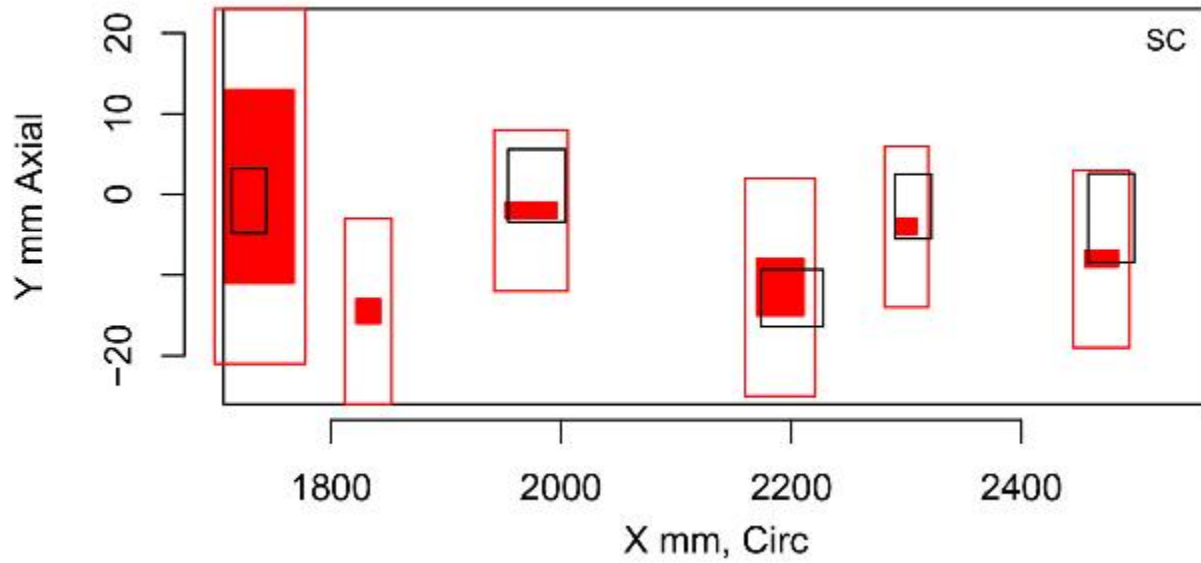


Figure E.159 Indication Plot for Procedure PAUT.126 Applied to Test Block P40 in PARENT Blind Testing (X – Y view, 1800 mm–2400 mm)

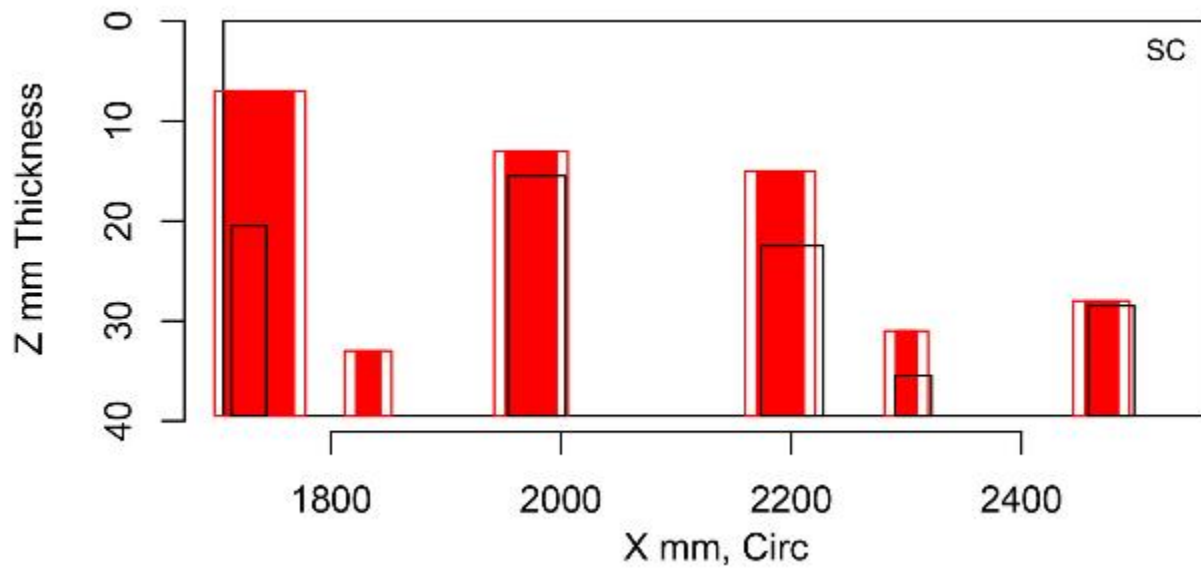


Figure E.160 Indication Plot for Procedure PAUT.126 Applied to Test Block P40 in PARENT Blind Testing (X – Z view, 1800 mm–2400 mm)

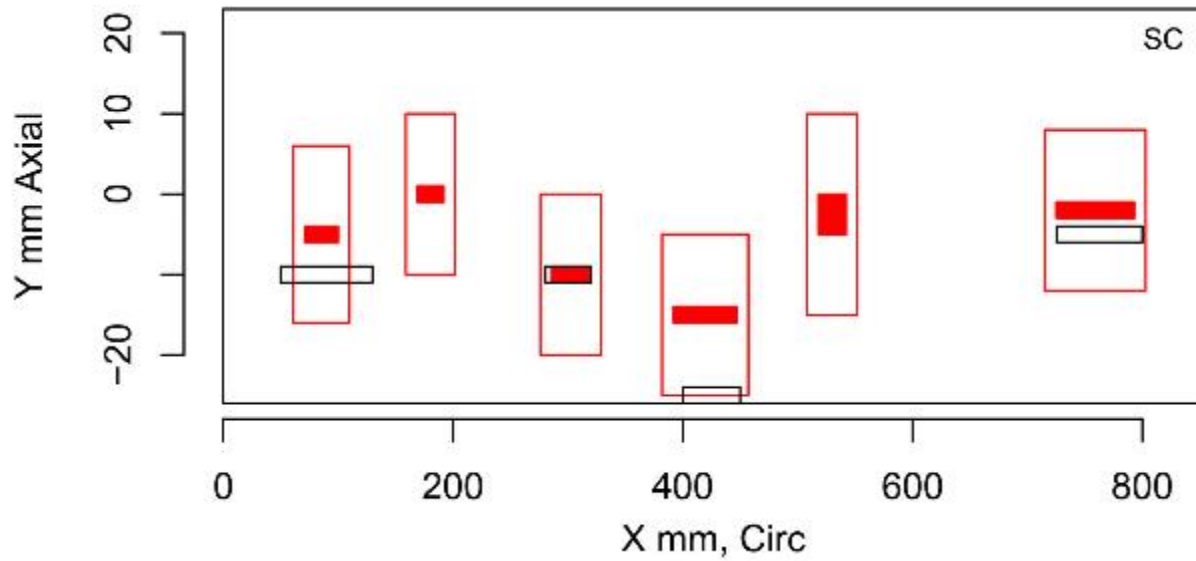


Figure E.161 Indication Plot for Procedure UT.126 Applied to Test Block P40 in PARENT Blind Testing (X – Y view, 0 mm–800 mm)

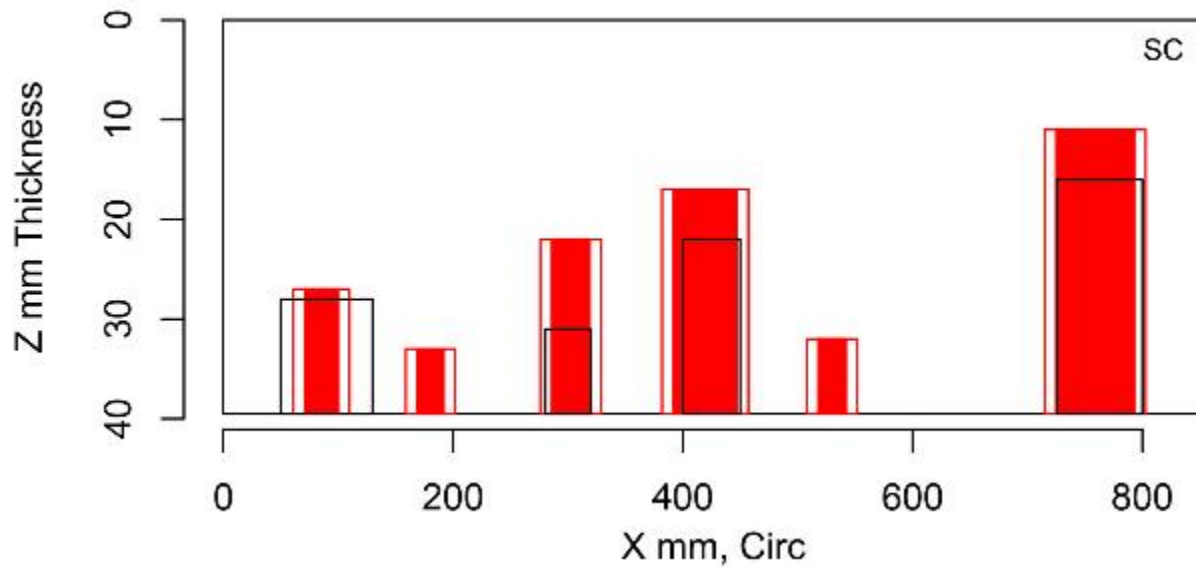


Figure E.162 Indication Plot for Procedure UT.126 Applied to Test Block P40 in PARENT Blind Testing (X – Z view, 0 mm–800 mm)

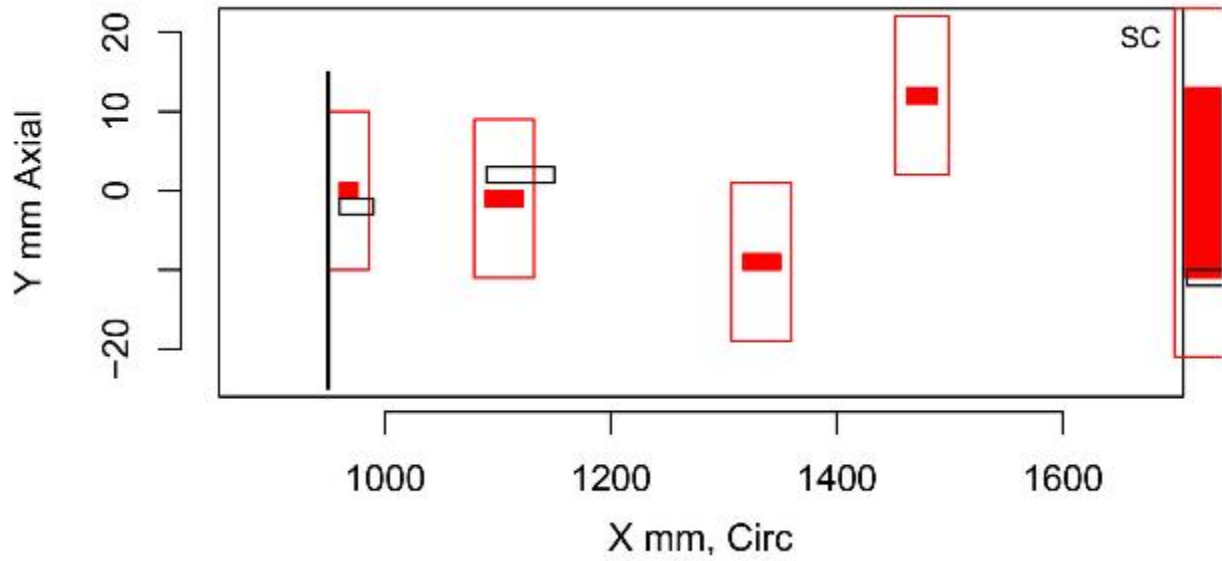


Figure E.163 Indication Plot for Procedure UT.126 Applied to Test Block P40 in PARENT Blind Testing (X – Y view, 1000 mm–1600 mm)

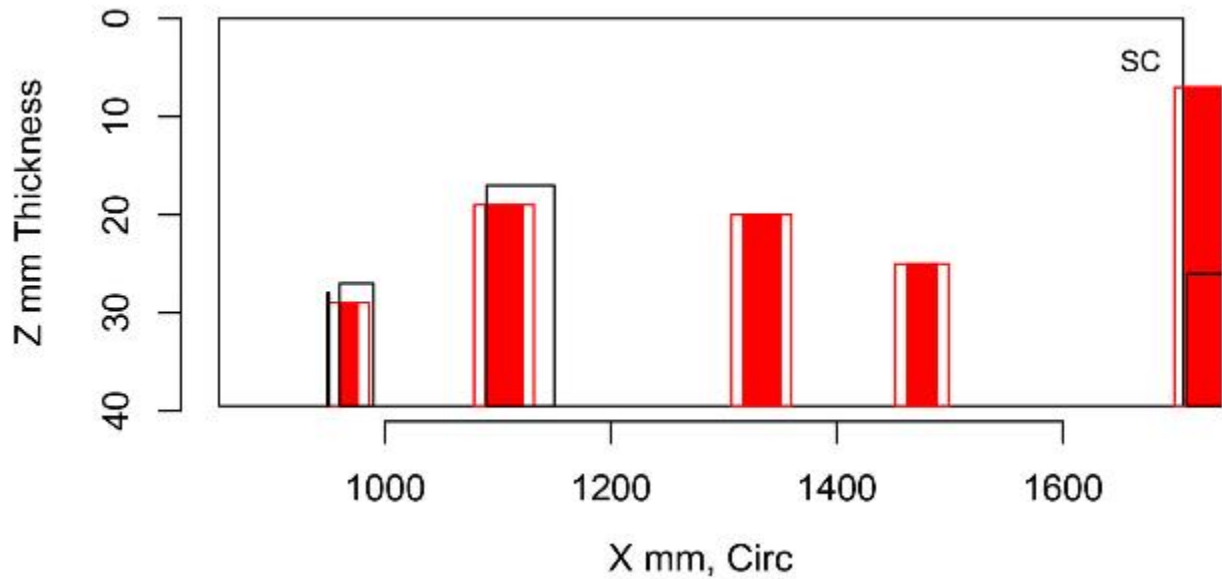


Figure E.164 Indication Plot for Procedure UT.126 Applied to Test Block P40 in PARENT Blind Testing (X – Z view, 1000 mm–1600 mm)

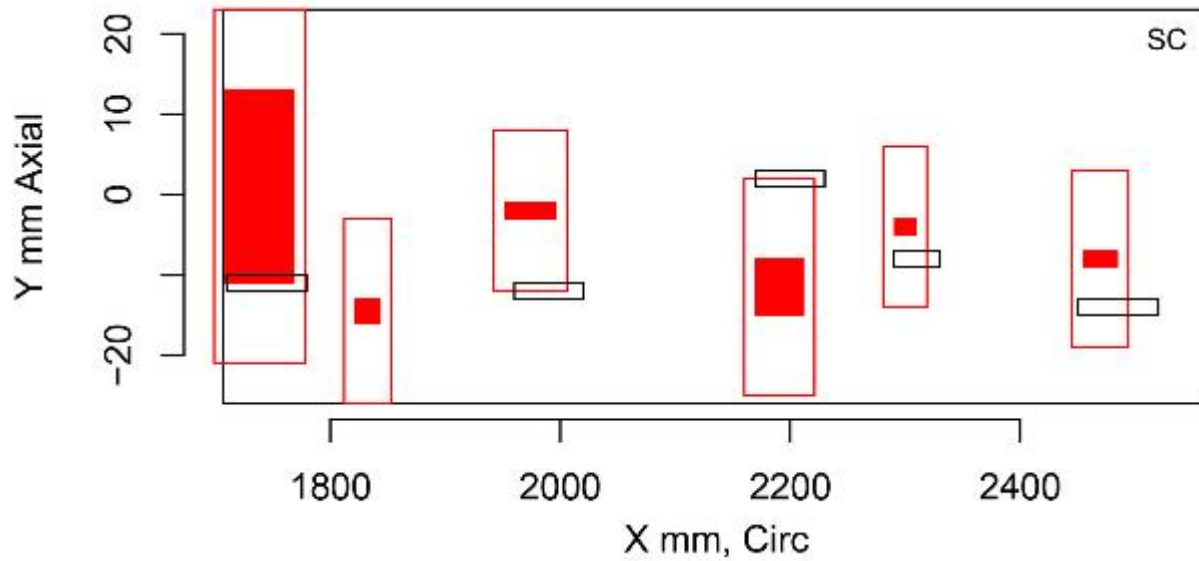


Figure E.165 Indication Plot for Procedure UT.126 Applied to Test Block P40 in PARENT Blind Testing (X – Y view, 1800 mm–2400 mm)

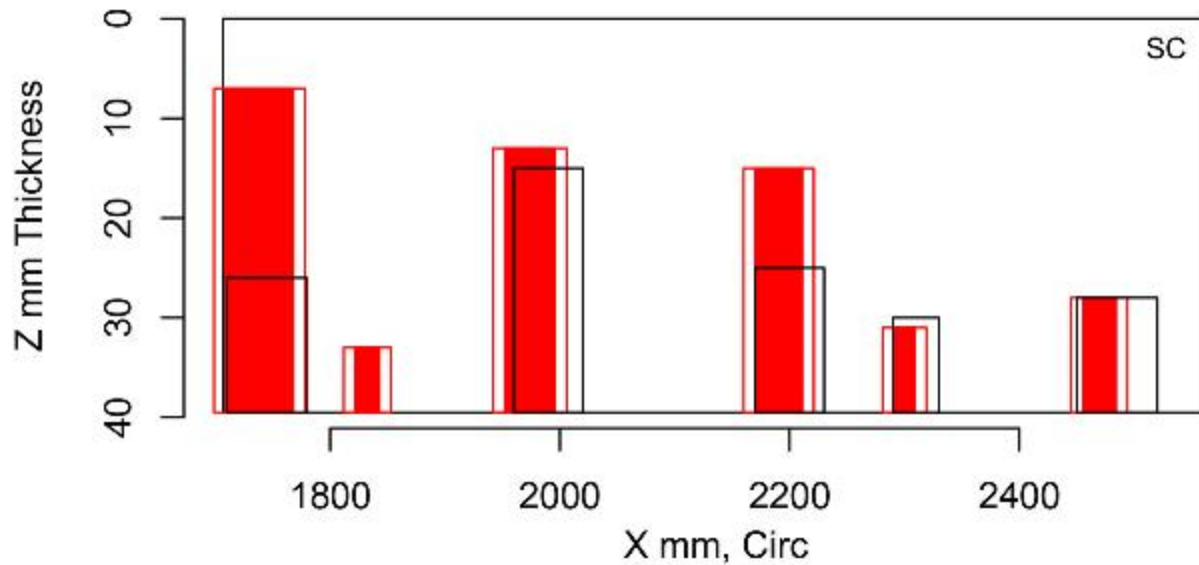


Figure E.166 Indication Plot for Procedure UT.126 Applied to Test Block P40 in PARENT Blind Testing (X – Z view, 1800 mm–2400 mm)

E.2.7 Plots for Team 128

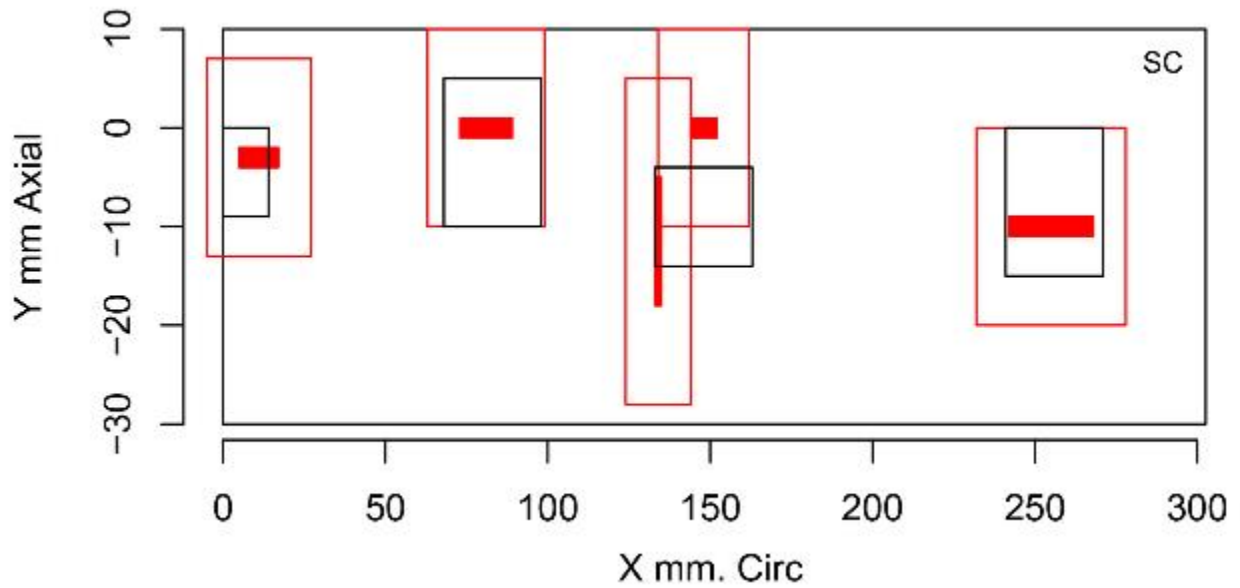


Figure E.167 Indication Plot for Procedure PAUT.128 Applied to Test Block P35 in PARENT Blind Testing (X - Y view, 0 mm-300 mm)

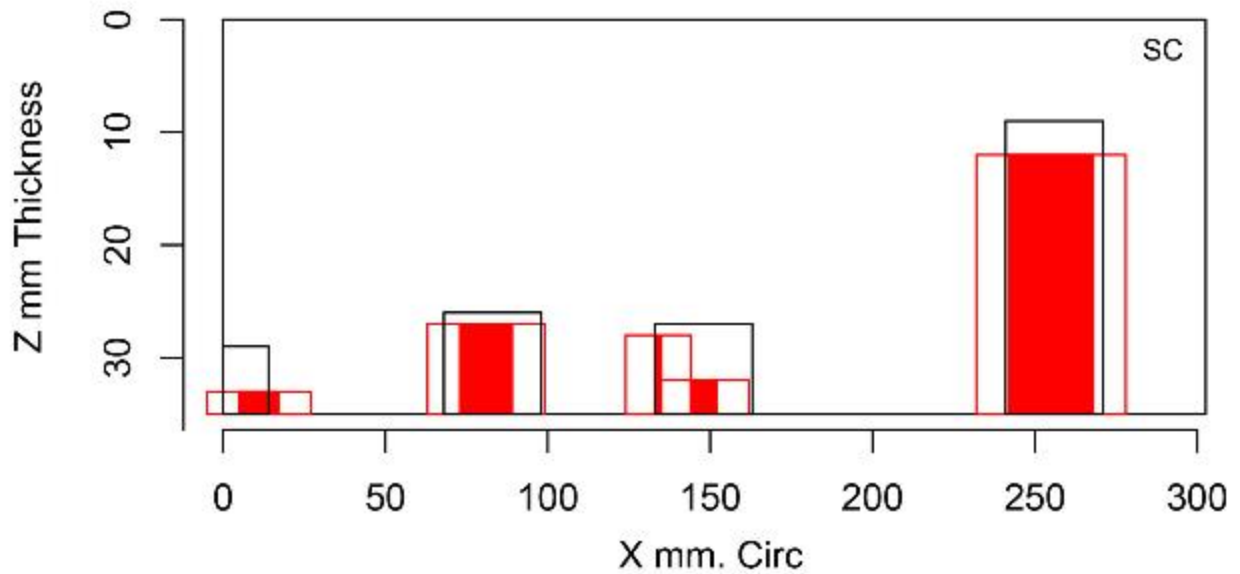


Figure E.168 Indication Plot for Procedure PAUT.128 Applied to Test Block P35 in PARENT Blind Testing (X - Z view, 0 mm-300 mm)

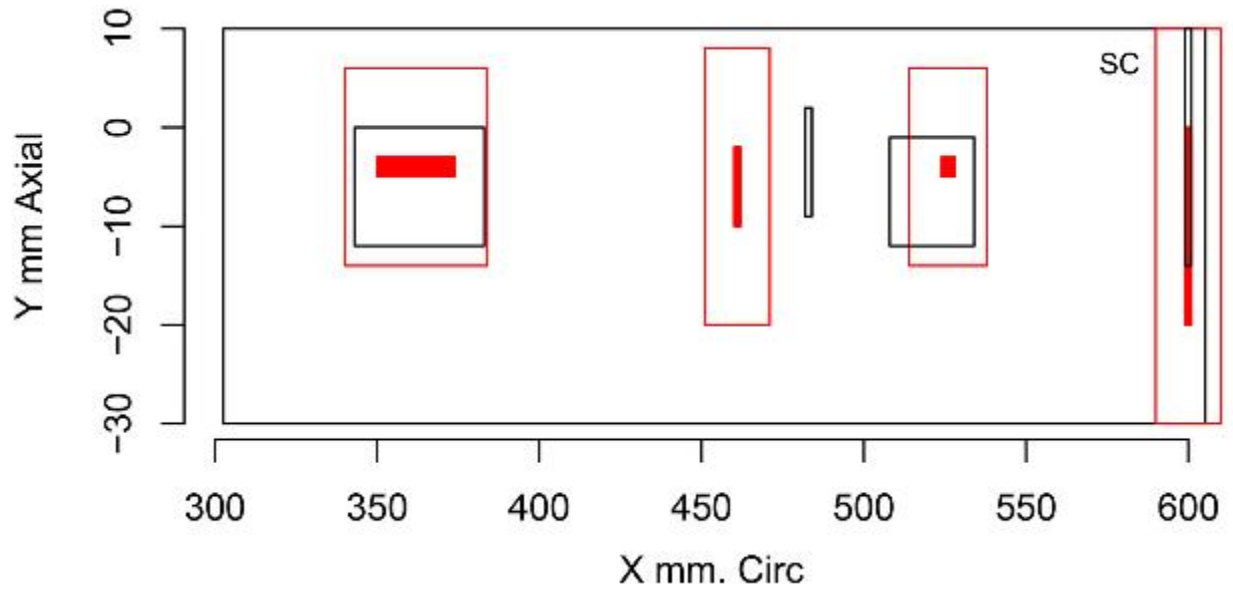


Figure E.169 Indication Plot for Procedure PAUT.128 Applied to Test Block P35 in PARENT Blind Testing (X – Y view, 300 mm–600 mm)

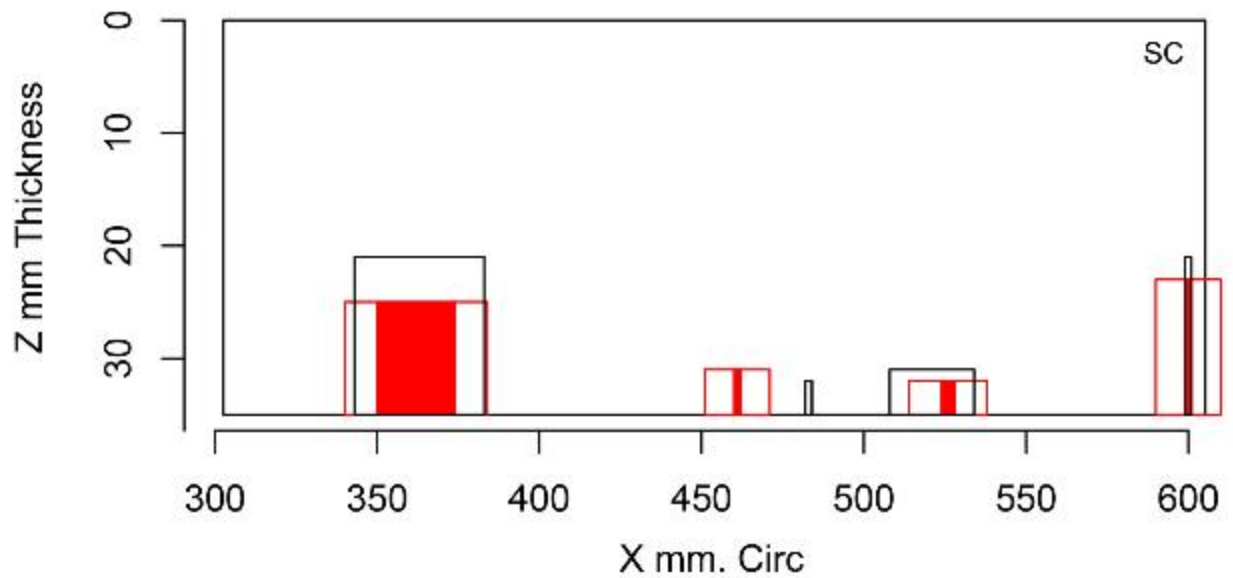


Figure E.170 Indication Plot for Procedure PAUT.128 Applied to Test Block P35 in PARENT Blind Testing (X – Z view, 300 mm–600 mm)

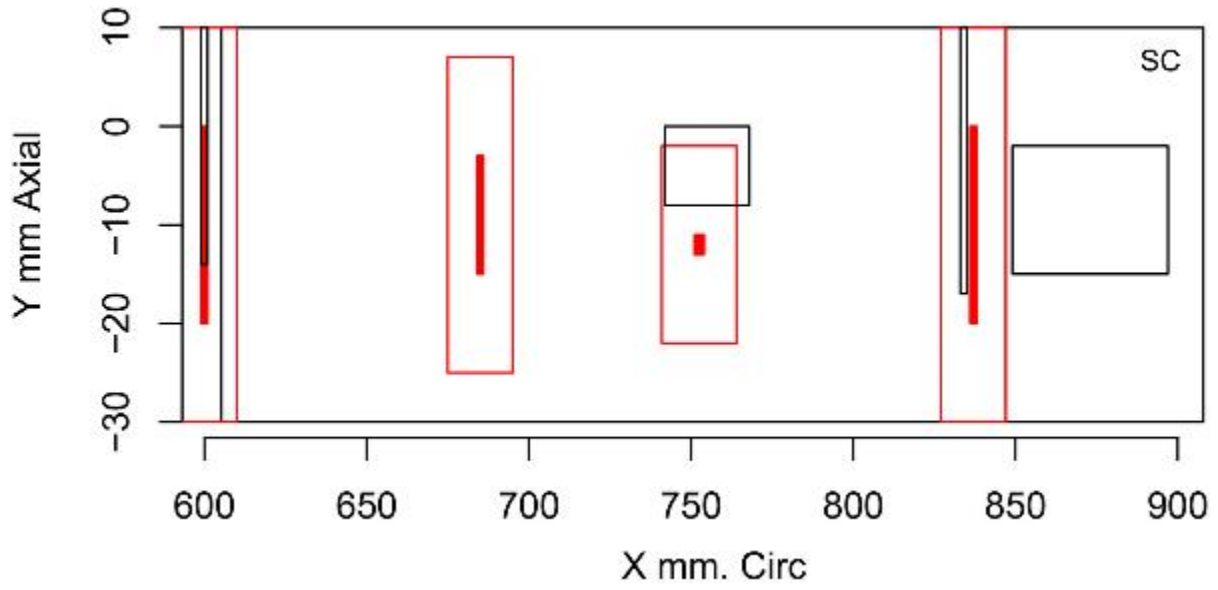


Figure E.171 Indication Plot for Procedure PAUT.128 Applied to Test Block P35 in PARENT Blind Testing (X - Y view, 600 mm-900 mm)

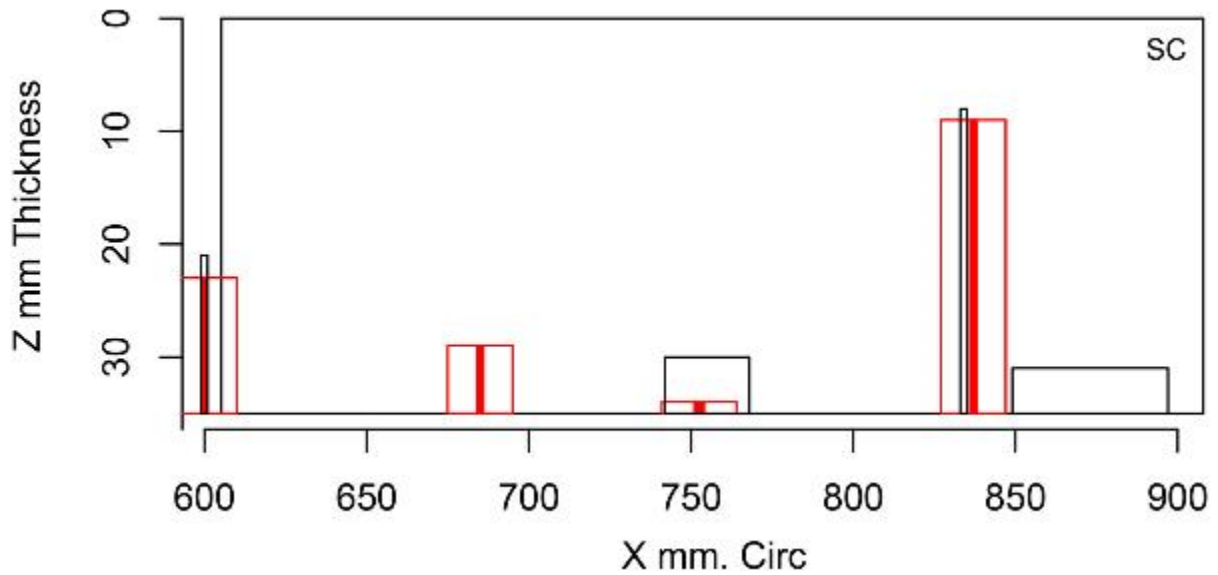


Figure E.172 Indication Plot for Procedure PAUT.128 Applied to Test Block P35 in PARENT Blind Testing (X - Z view, 600 mm-900 mm)

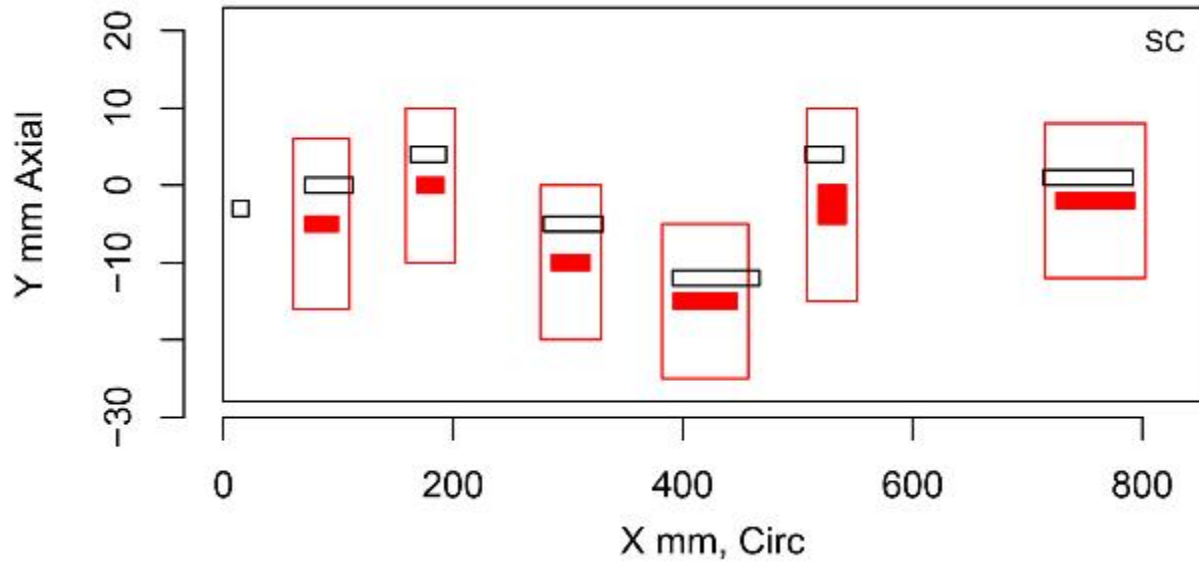


Figure E.173 Indication Plot for Procedure PAUT.128 Applied to Test Block P40 in PARENT Blind Testing (X – Y view, 0 mm–800 mm)

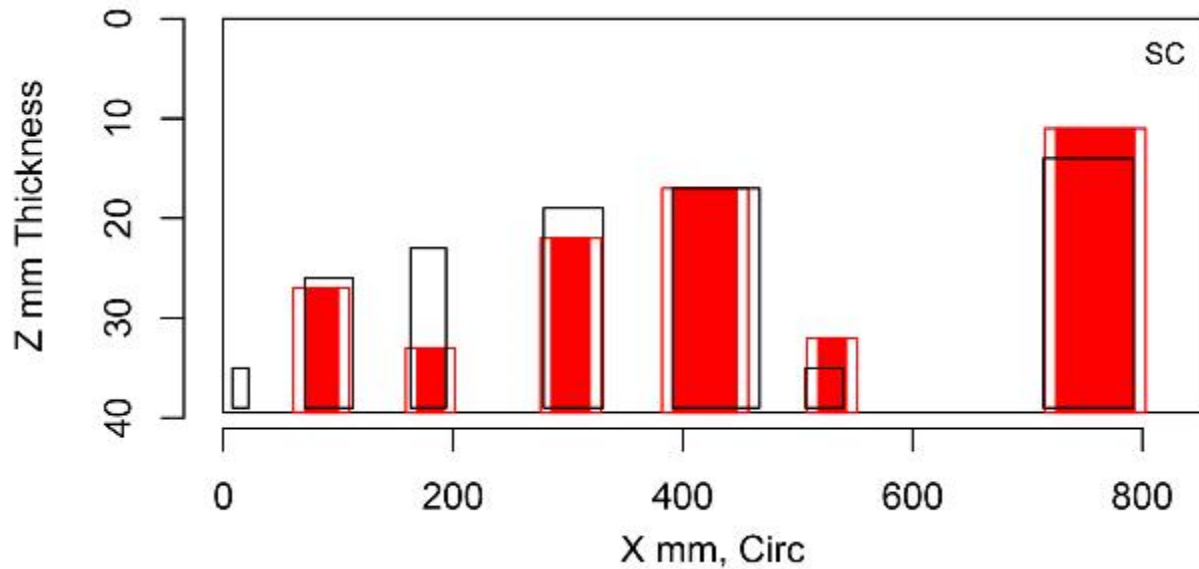


Figure E.174 Indication Plot for Procedure PAUT.128 Applied to Test Block P40 in PARENT Blind Testing (X – Z view, 0 mm–800 mm)

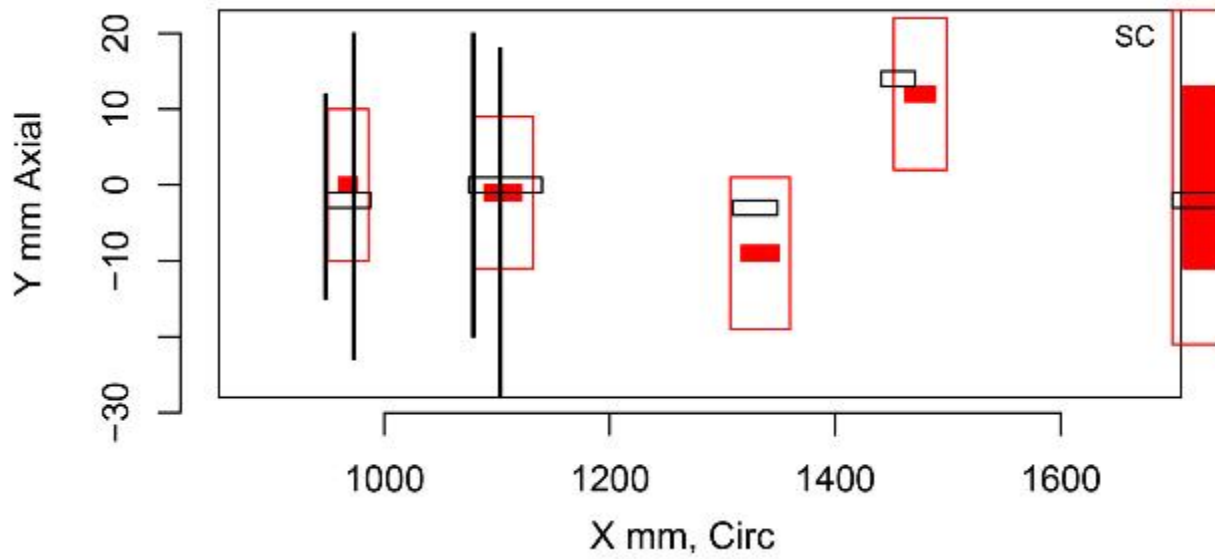


Figure E.175 Indication Plot for Procedure PAUT.128 Applied to Test Block P40 in PARENT Blind Testing (X – Y view, 1000 mm–1600 mm)

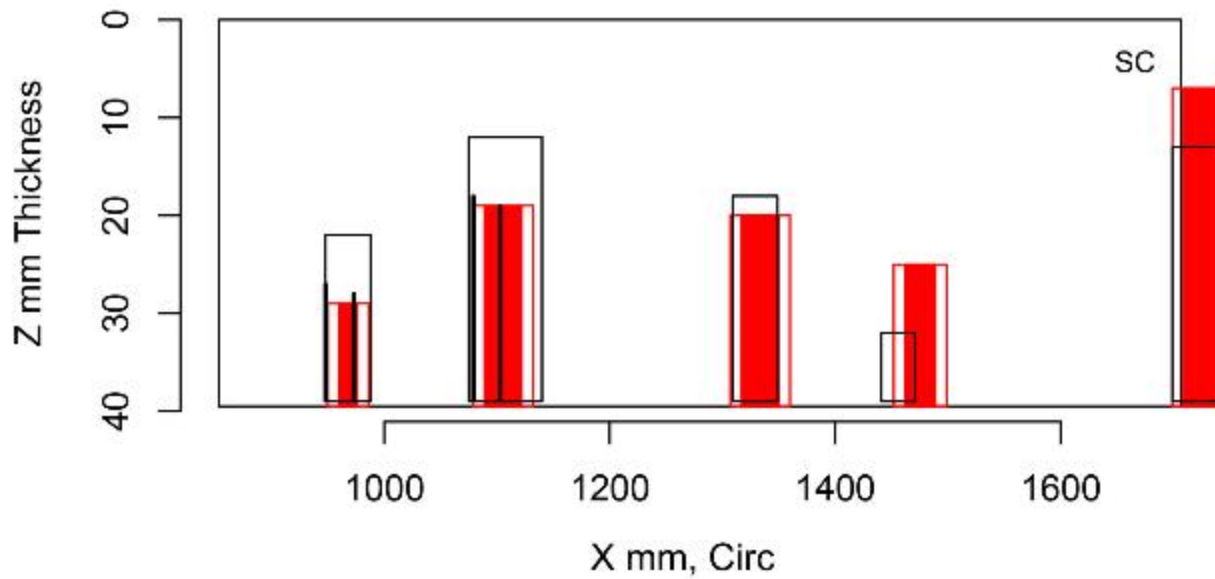


Figure E.176 Indication Plot for Procedure PAUT.128 Applied to Test Block P40 in PARENT Blind Testing (X – Z view, 1000 mm–1600 mm)

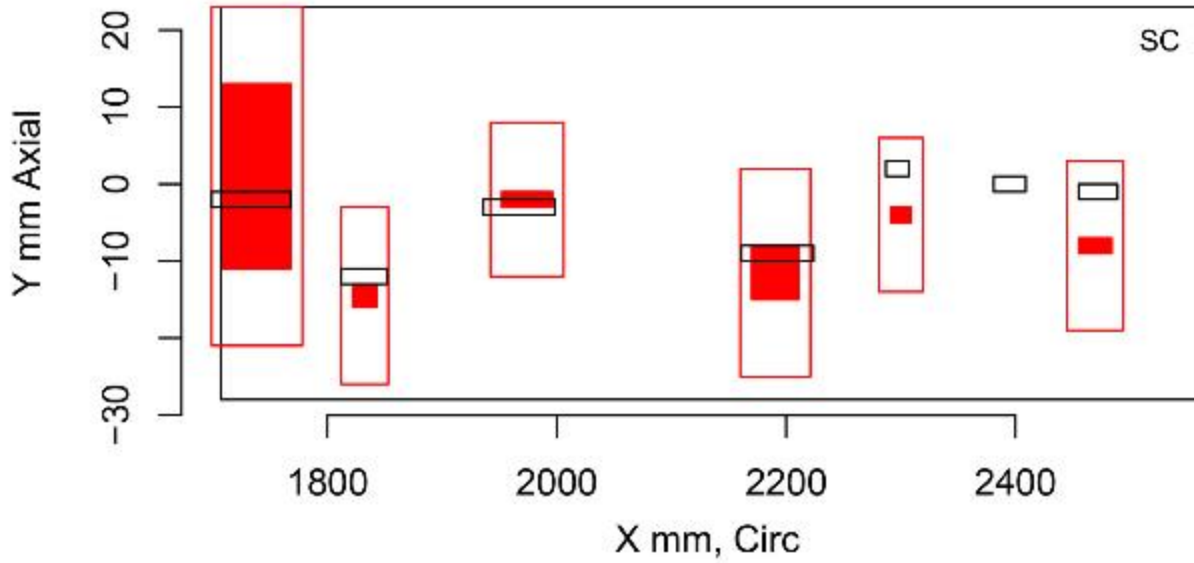


Figure E.177 Indication Plot for Procedure PAUT.128 Applied to Test Block P40 in PARENT Blind Testing (X – Y view, 1800 mm–2400 mm)

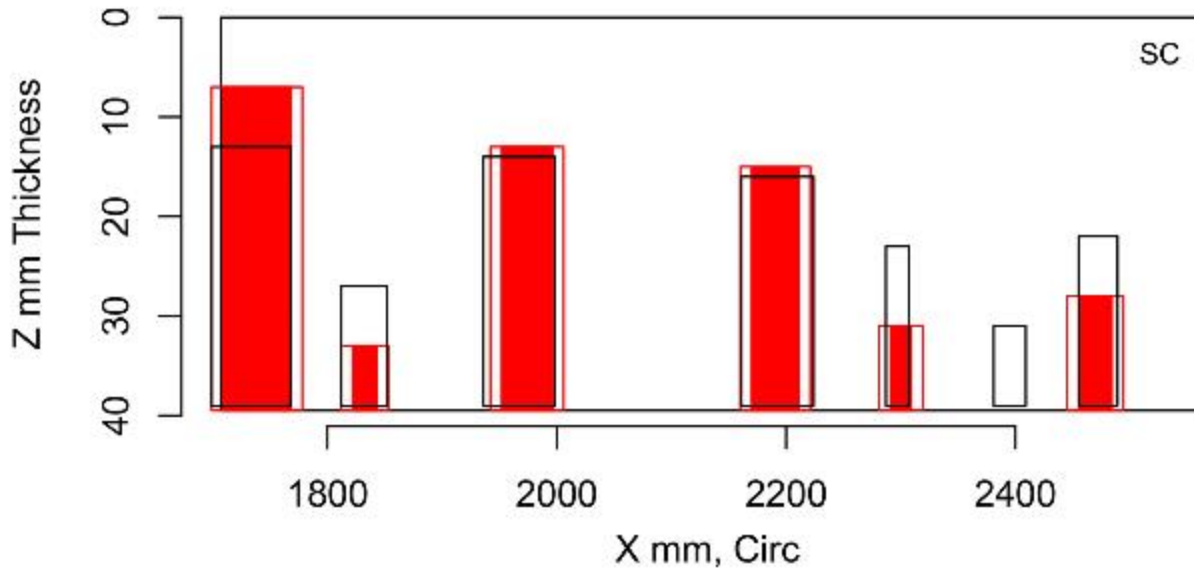


Figure E.178 Indication Plot for Procedure PAUT.128 Applied to Test Block P40 in PARENT Blind Testing (X – Z view, 1800 mm–2400 mm)

E.2.8 Plots for Team 134

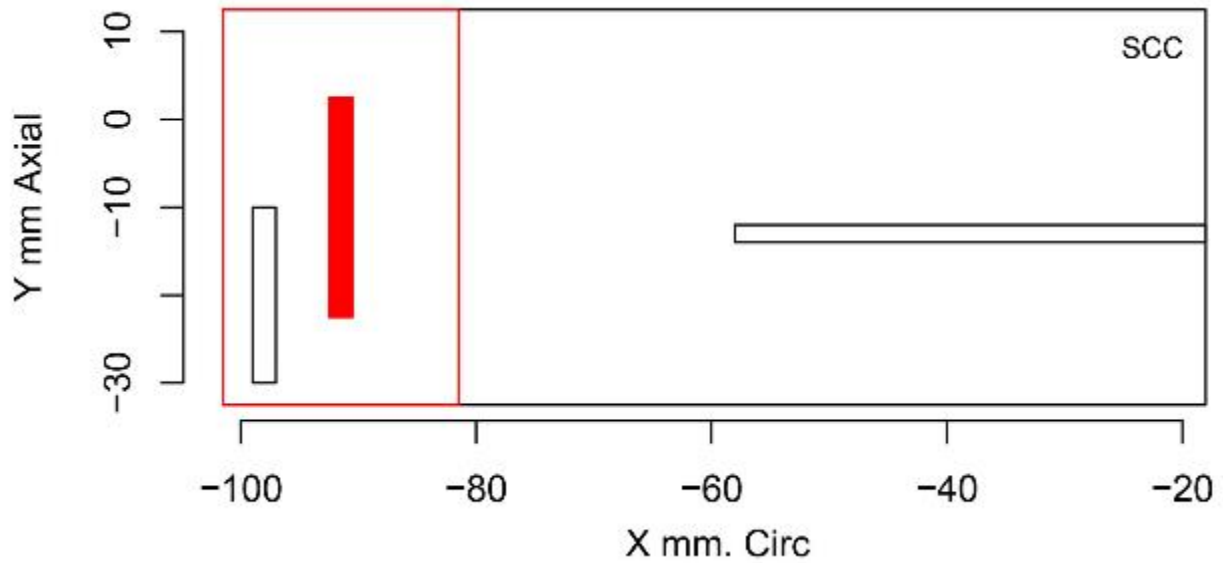


Figure E.179 Indication Plot for Procedure UT.134 Applied to Test Block P13 in PARENT Blind Testing (X – Y view)

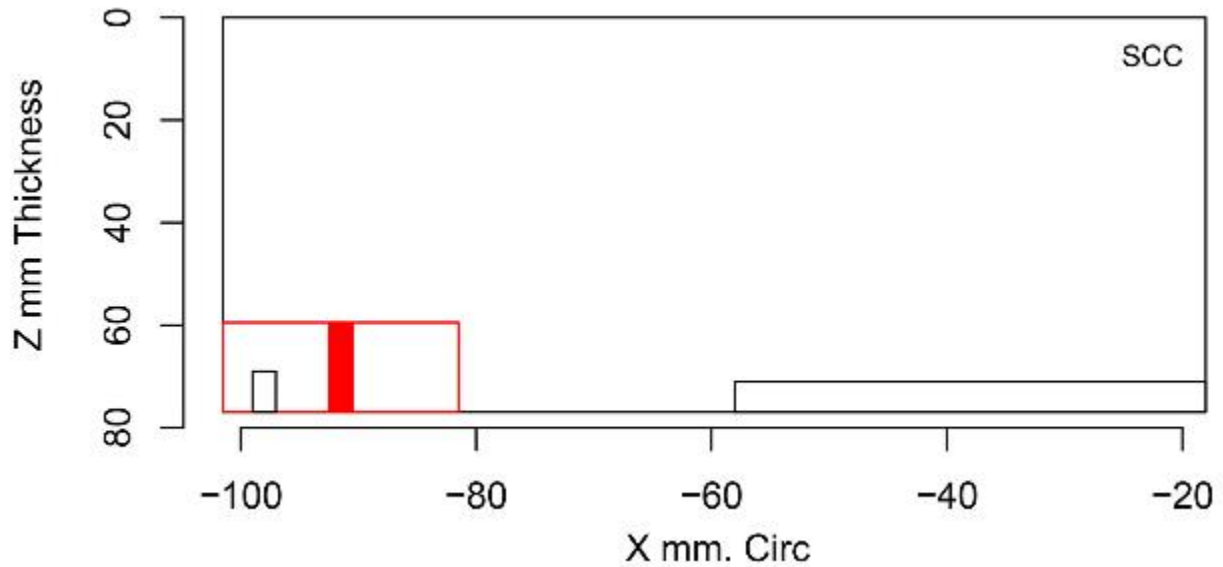


Figure E.180 Indication Plot for Procedure UT.134 Applied to Test Block P13 in PARENT Blind Testing (X – Z view)

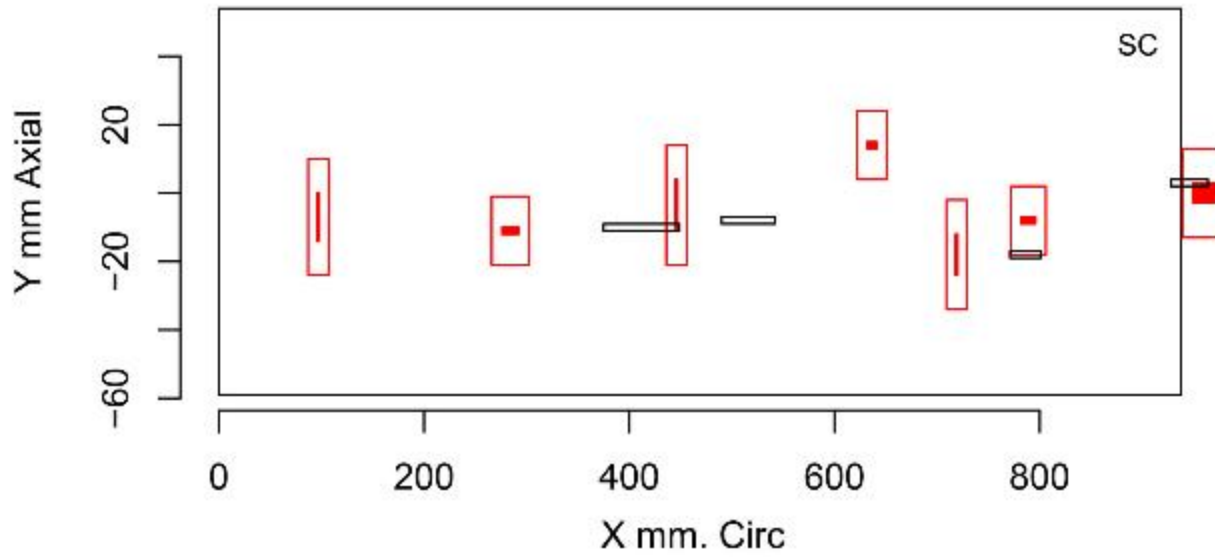


Figure E.181 Indication Plot for Procedure UT.134 Applied to Test Block P33 in PARENT Blind Testing (X - Y view, 0 mm-800 mm)

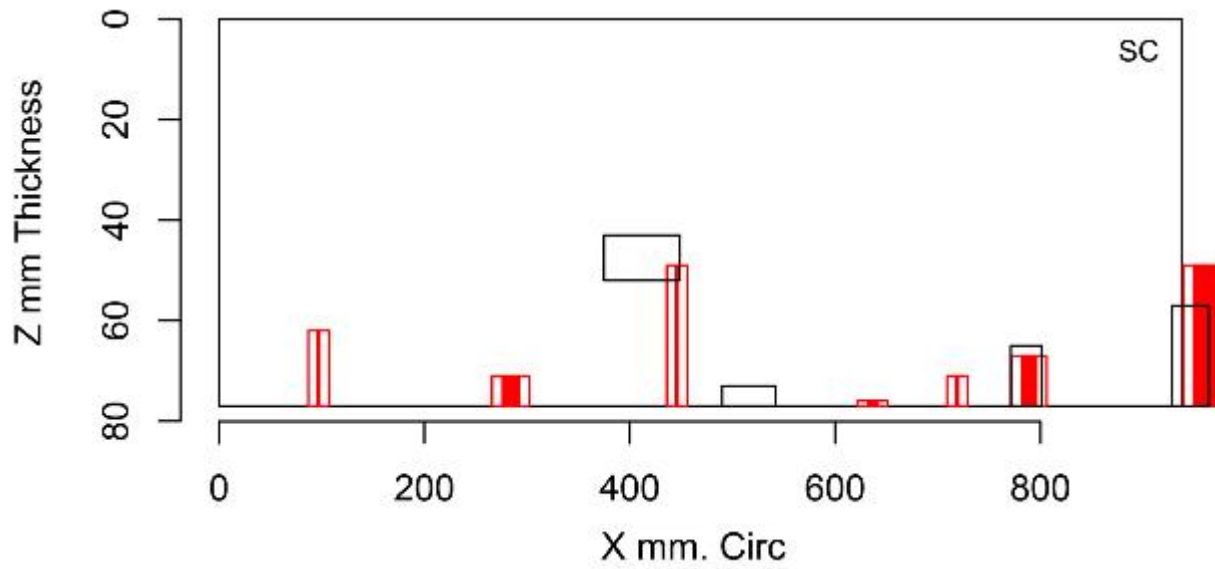


Figure E.182 Indication Plot for Procedure UT.134 Applied to Test Block P33 in PARENT Blind Testing (X - Z view, 0 mm-800 mm)

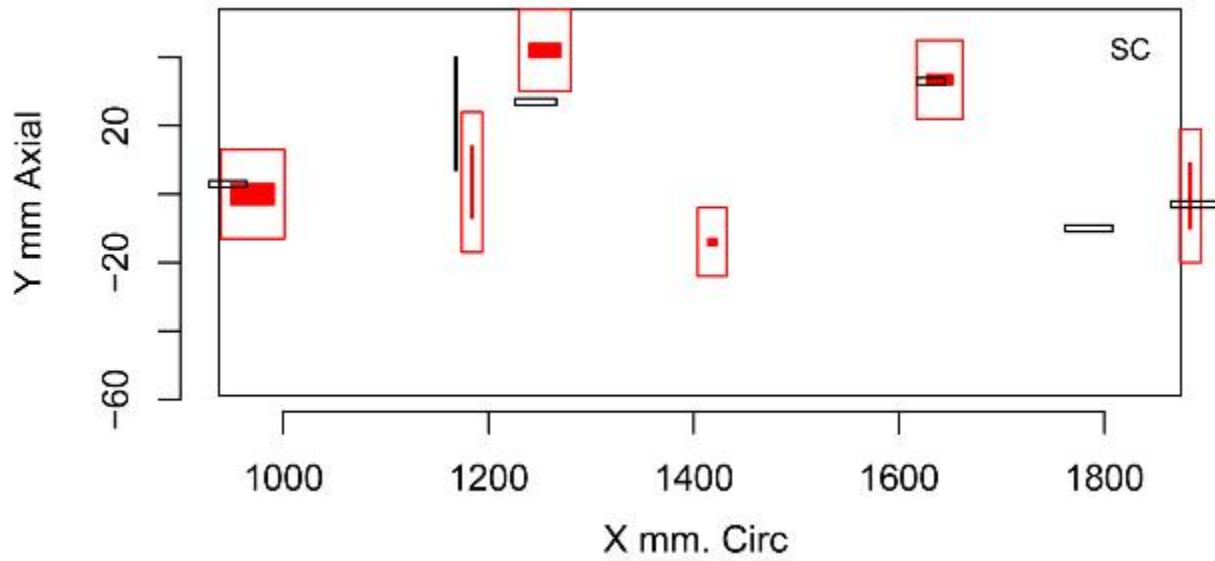


Figure E.183 Indication Plot for Procedure UT.134 Applied to Test Block P33 in PARENT Blind Testing (X – Y view, 1000 mm–1800 mm)

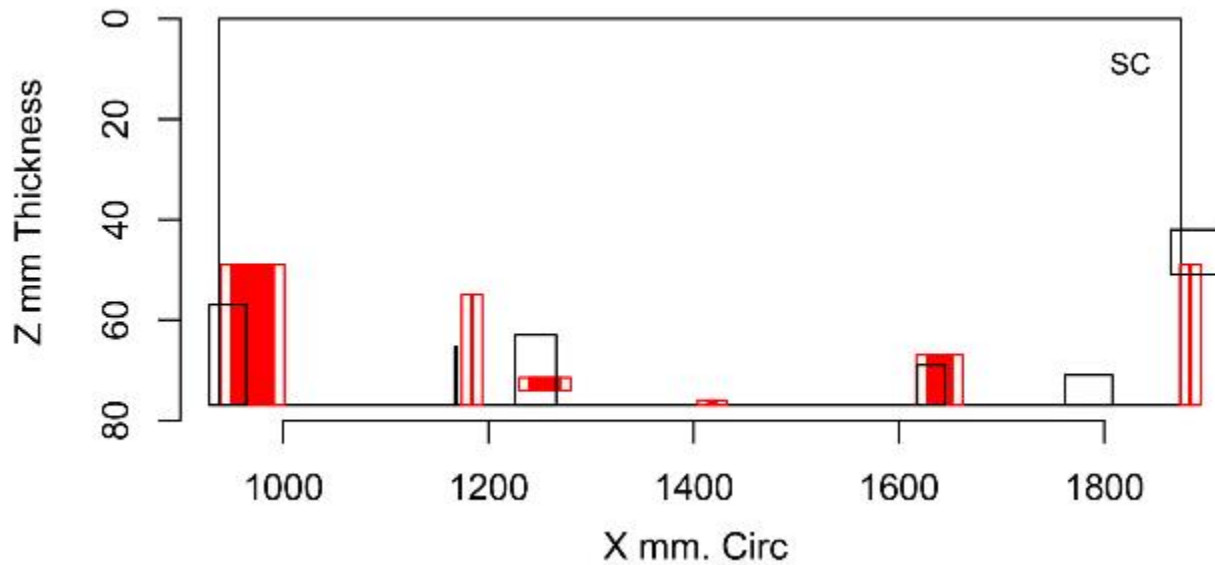


Figure E.184 Indication Plot for Procedure UT.134 Applied to Test Block P33 in PARENT Blind Testing (X – Z view, 1000 mm–1800 mm)

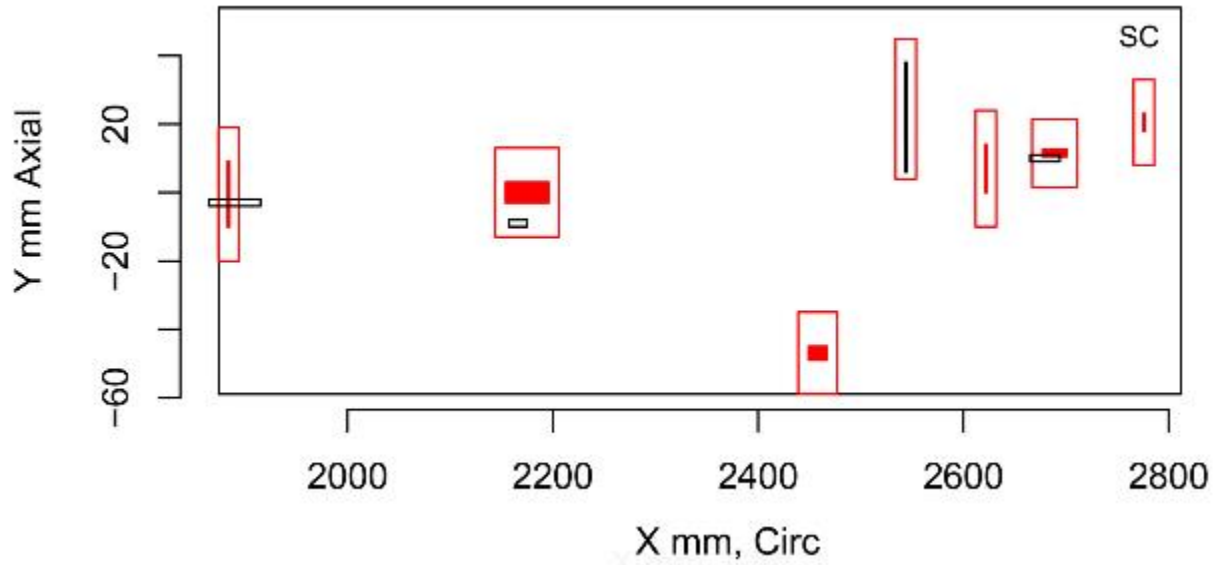


Figure E.185 Indication Plot for Procedure UT.134 Applied to Test Block P33 in PARENT Blind Testing (X – Y view, 2000 mm–2800 mm)

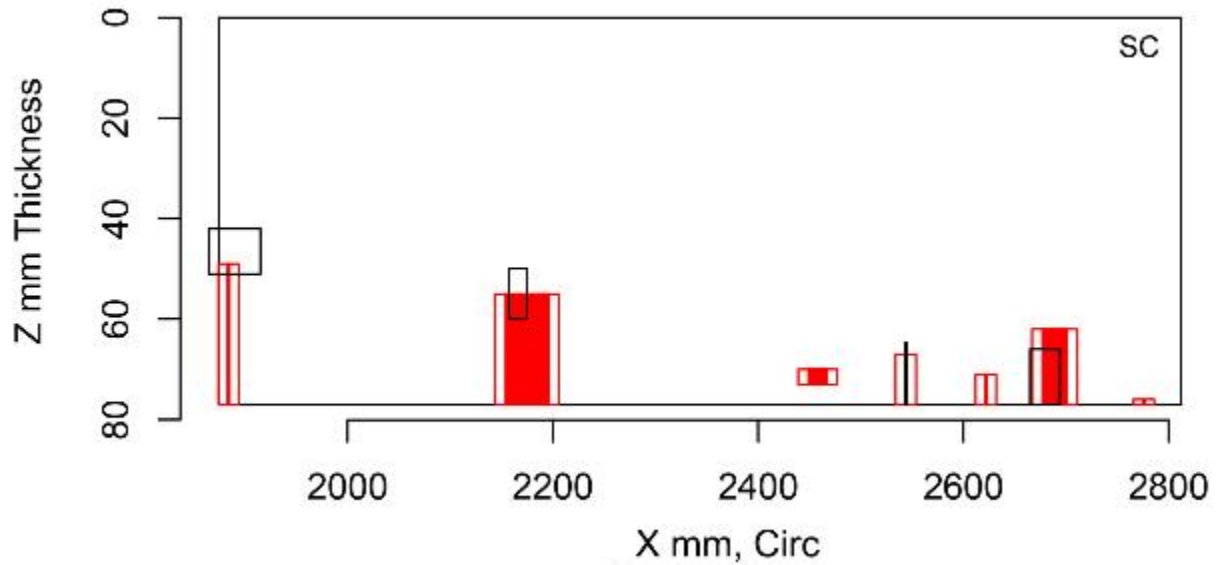


Figure E.186 Indication Plot for Procedure UT.134 Applied to Test Block P33 in PARENT Blind Testing (X – Z view, 2000 mm–2800 mm)

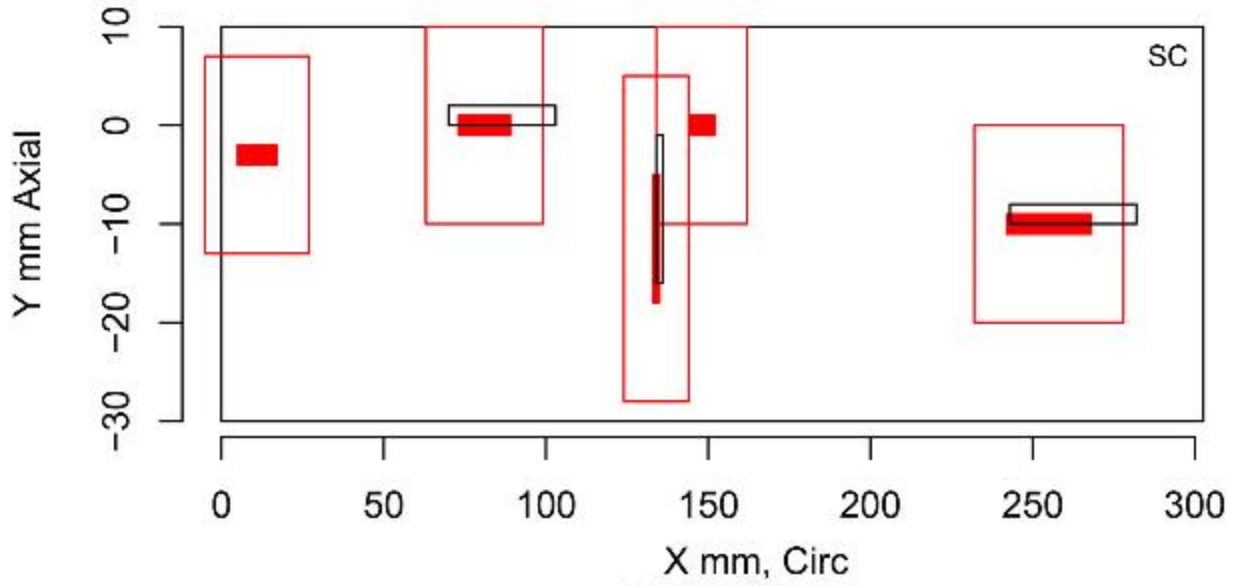


Figure E.187 Indication Plot for Procedure UT.134 Applied to Test Block P35 in PARENT Blind Testing (X – Y view, 0 mm–300 mm)

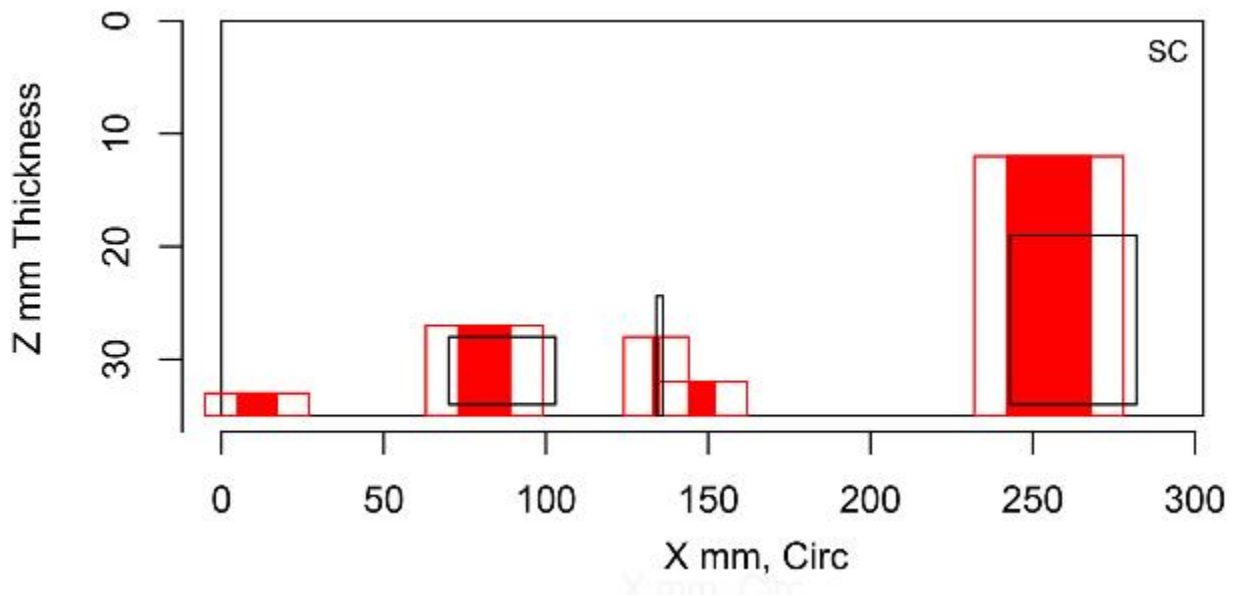


Figure E.188 Indication Plot for Procedure UT.134 Applied to Test Block P35 in PARENT Blind Testing (X – Z view, 0 mm–300 mm)

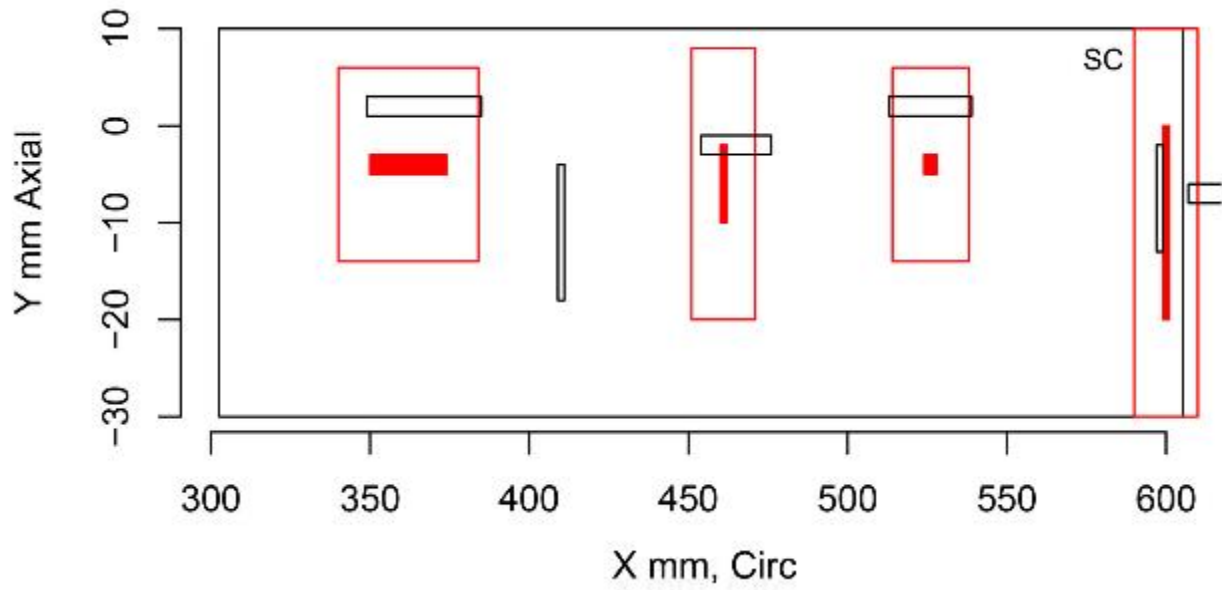


Figure E.189 Indication Plot for Procedure UT.134 Applied to Test Block P35 in PARENT Blind Testing (X – Y view, 300 mm–600 mm)

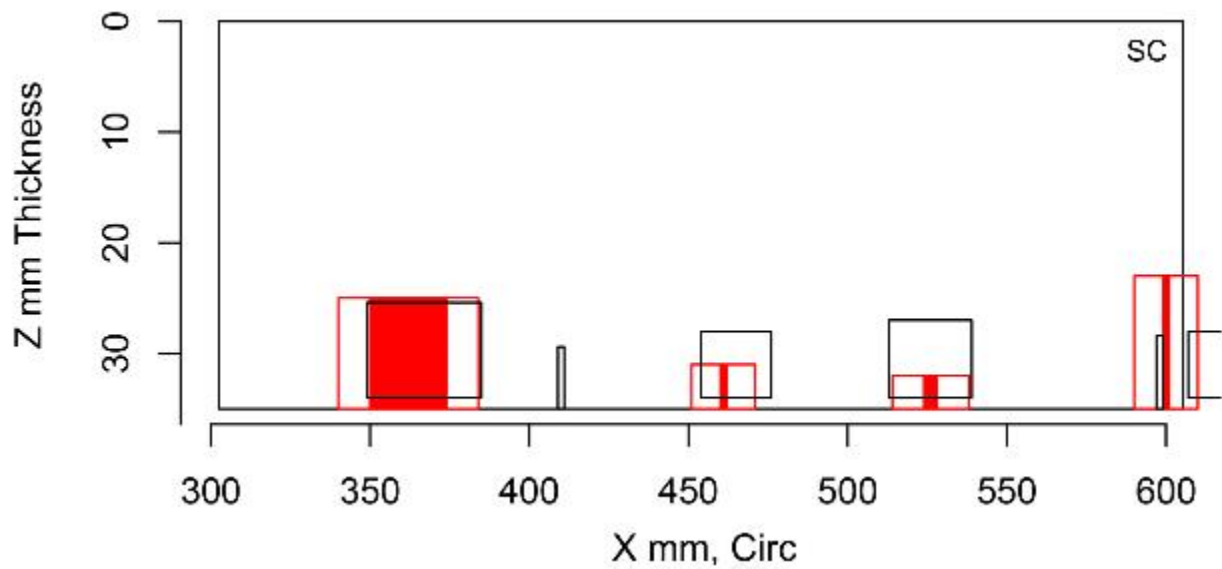


Figure E.190 Indication Plot for Procedure UT.134 Applied to Test Block P35 in PARENT Blind Testing (X – Z view, 300 mm–600 mm)

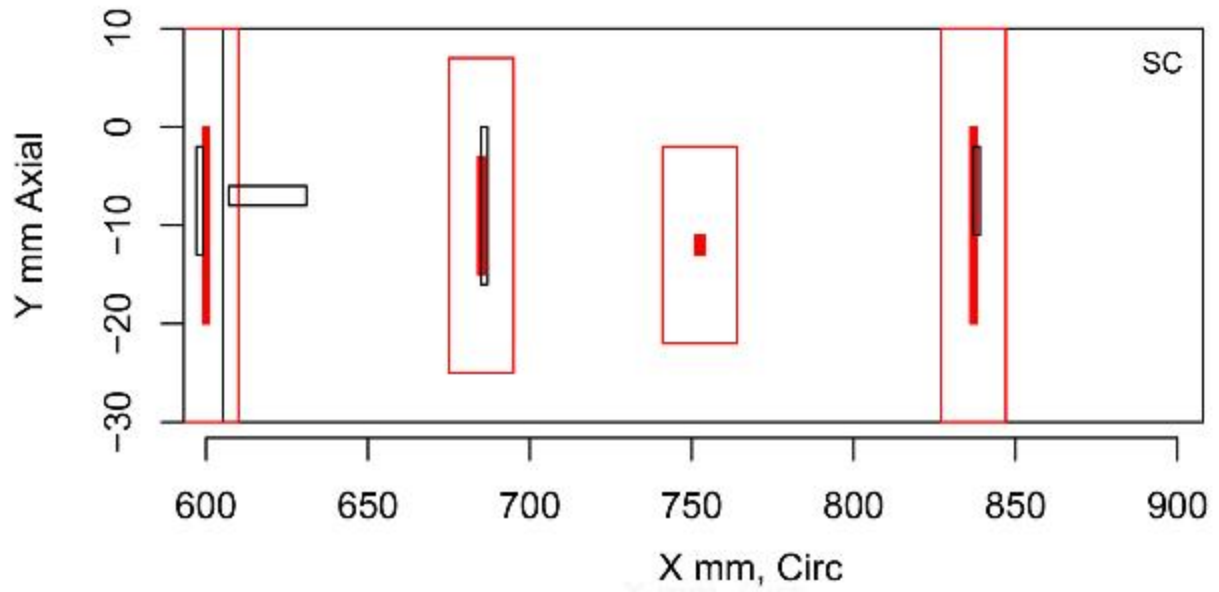


Figure E.191 Indication Plot for Procedure UT.134 Applied to Test Block P35 in PARENT Blind Testing (X – Y view, 600 mm–900 mm)

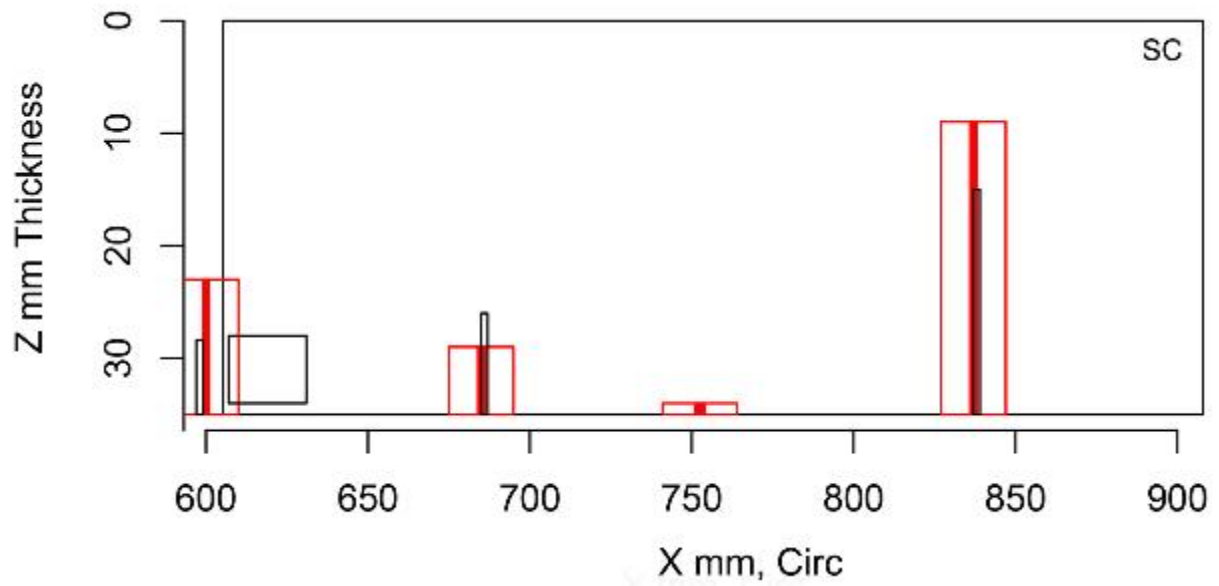


Figure E.192 Indication Plot for Procedure UT.134 Applied to Test Block P35 in PARENT Blind Testing (X – Z view, 600 mm–900 mm)

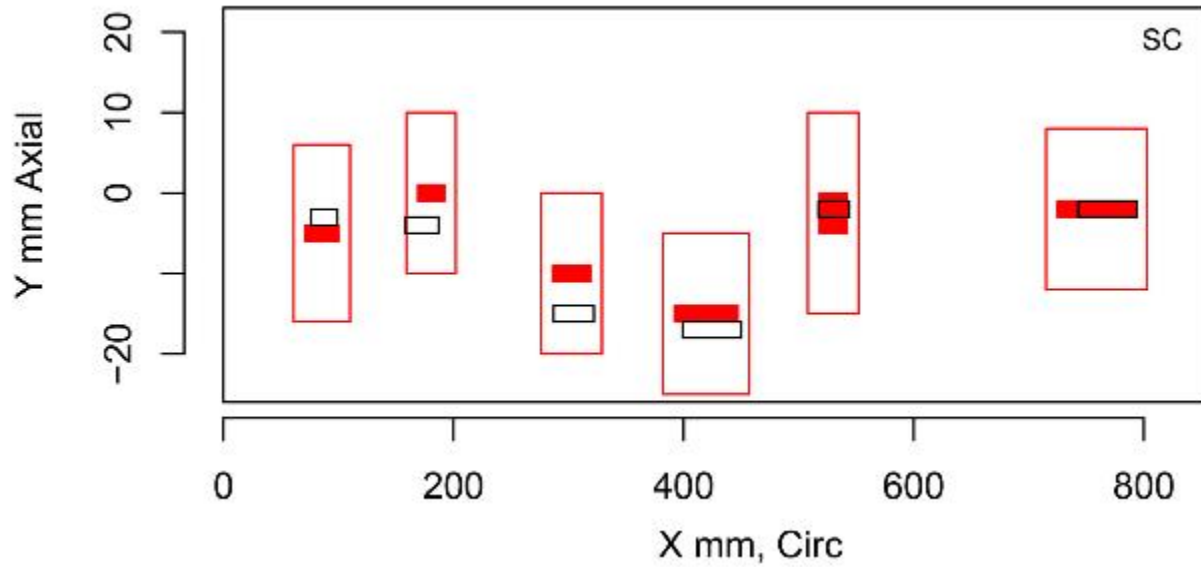


Figure E.193 Indication Plot for Procedure UT.134 Applied to Test Block P40 in PARENT Blind Testing (X – Y view, 0 mm–800 mm)

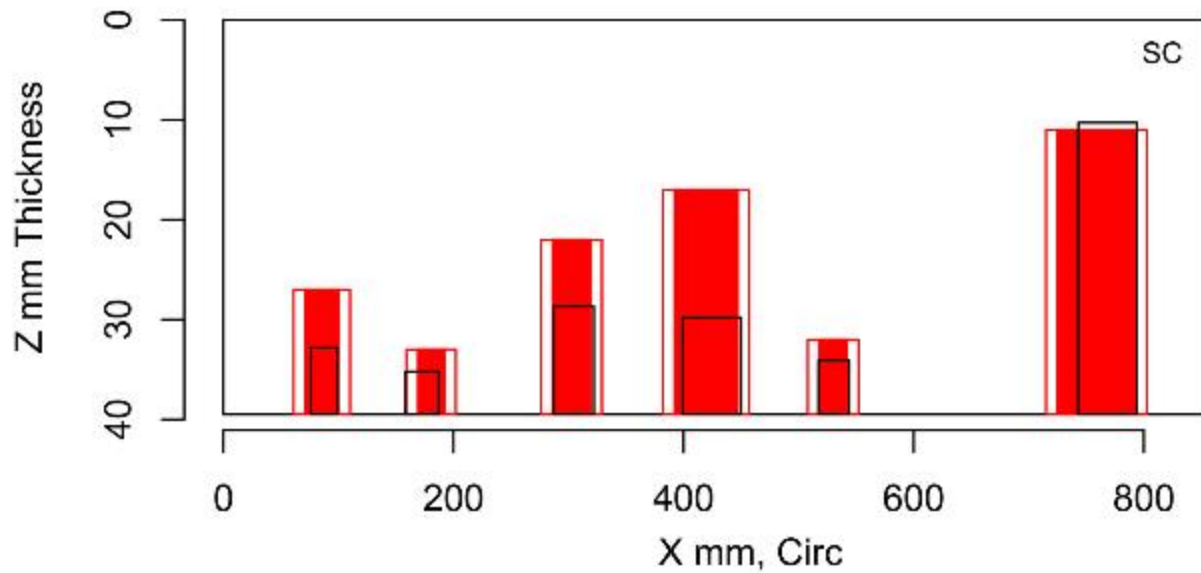


Figure E.194 Indication Plot for Procedure UT.134 Applied to Test Block P40 in PARENT Blind Testing (X – Z view, 0 mm–800 mm)

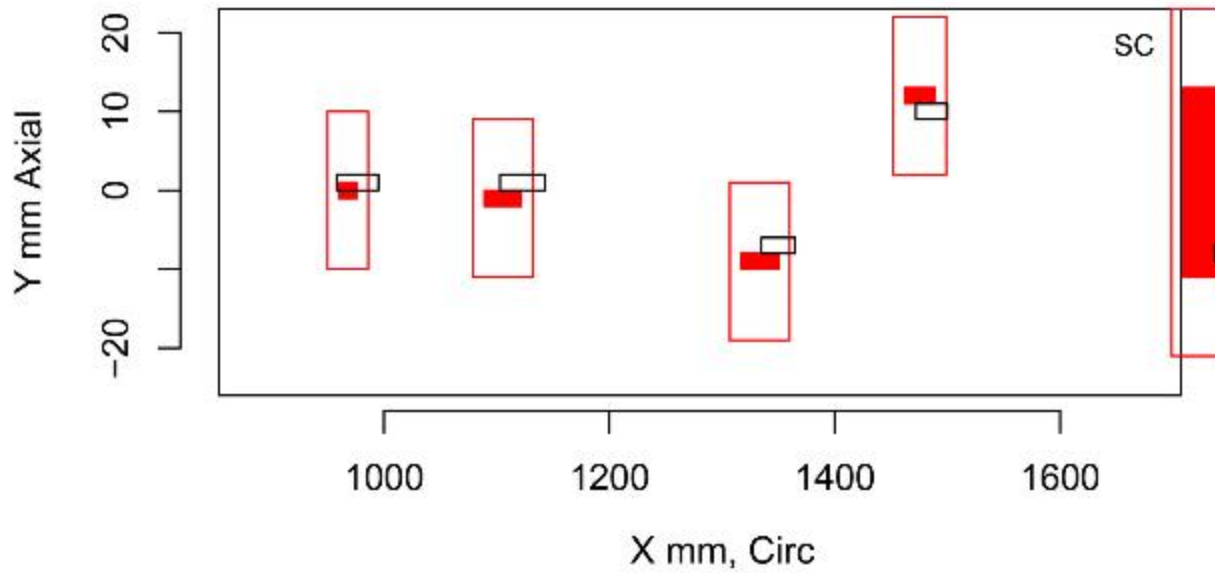


Figure E.195 Indication Plot for Procedure UT.134 Applied to Test Block P40 in PARENT Blind Testing (X – Y view, 1000 mm–1600 mm)

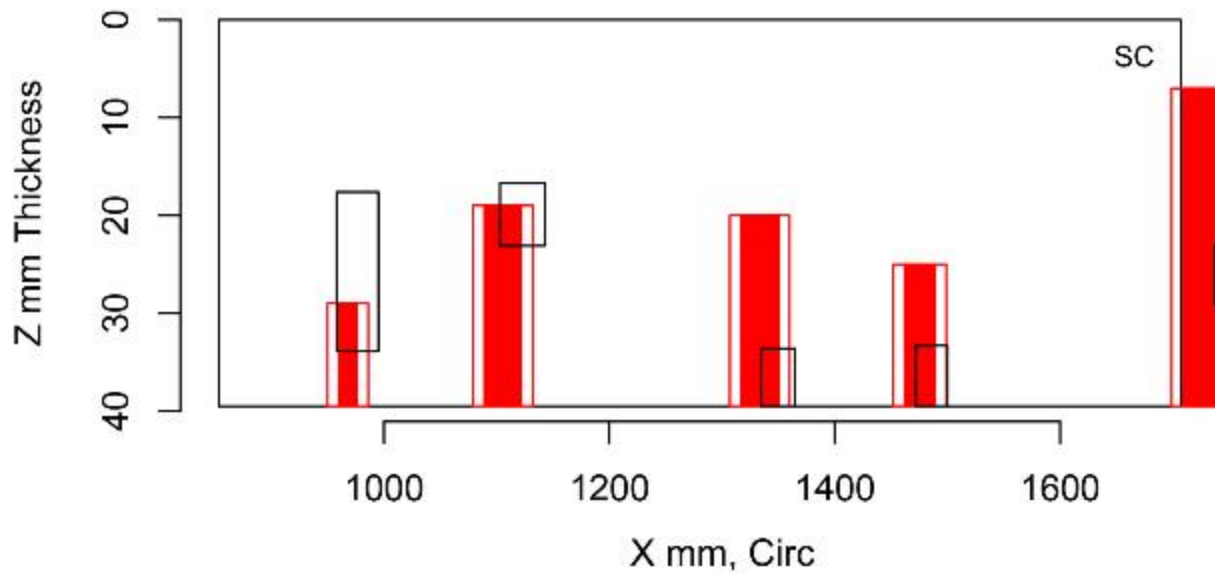


Figure E.196 Indication Plot for Procedure UT.134 Applied to Test Block P40 in PARENT Blind Testing (X – Z view, 1000 mm–1600 mm)

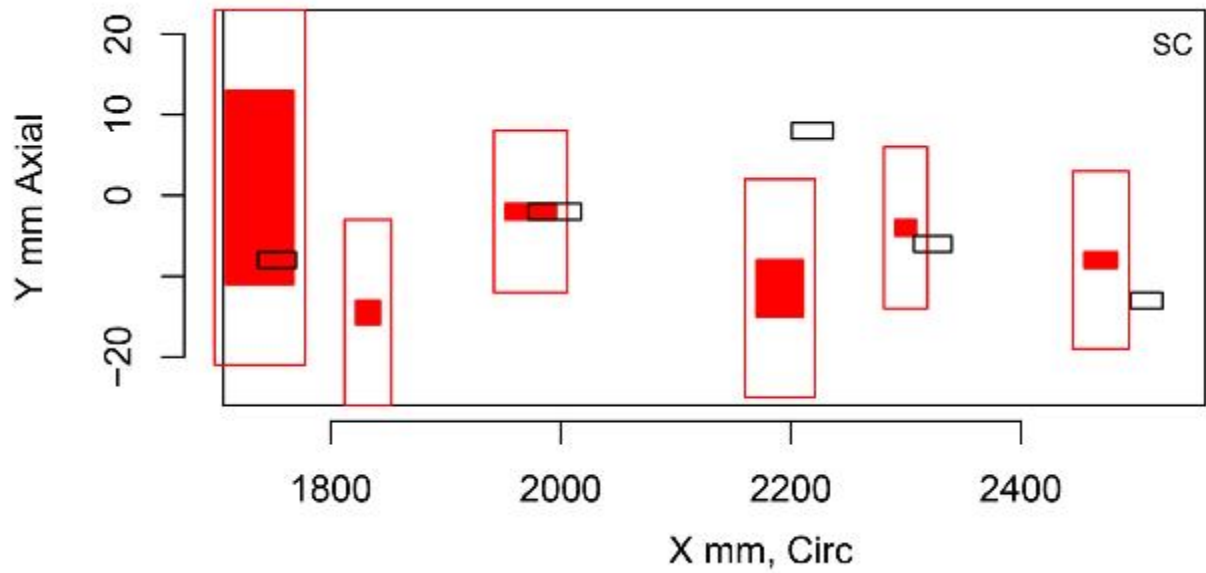


Figure E.197 Indication Plot for Procedure UT.134 Applied to Test Block P40 in PARENT Blind Testing (X – Y view, 1800 mm–2400 mm)

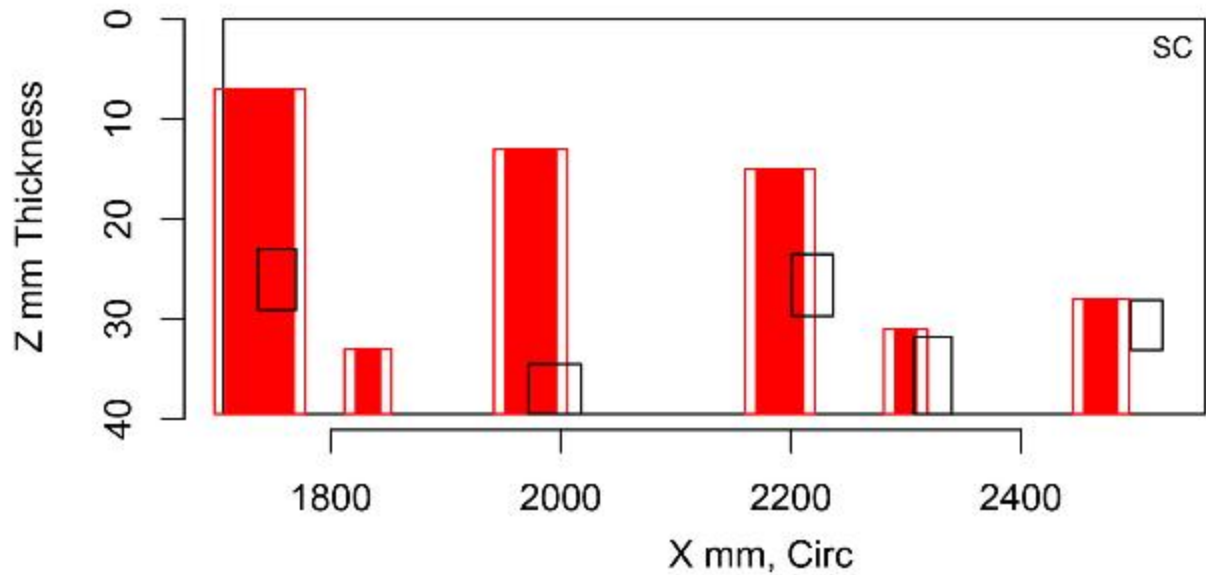


Figure E.198 Indication Plot for Procedure UT.134 Applied to Test Block P40 in PARENT Blind Testing (X – Z view, 1800 mm–2400 mm)

E.2.9 Plots for Team 135

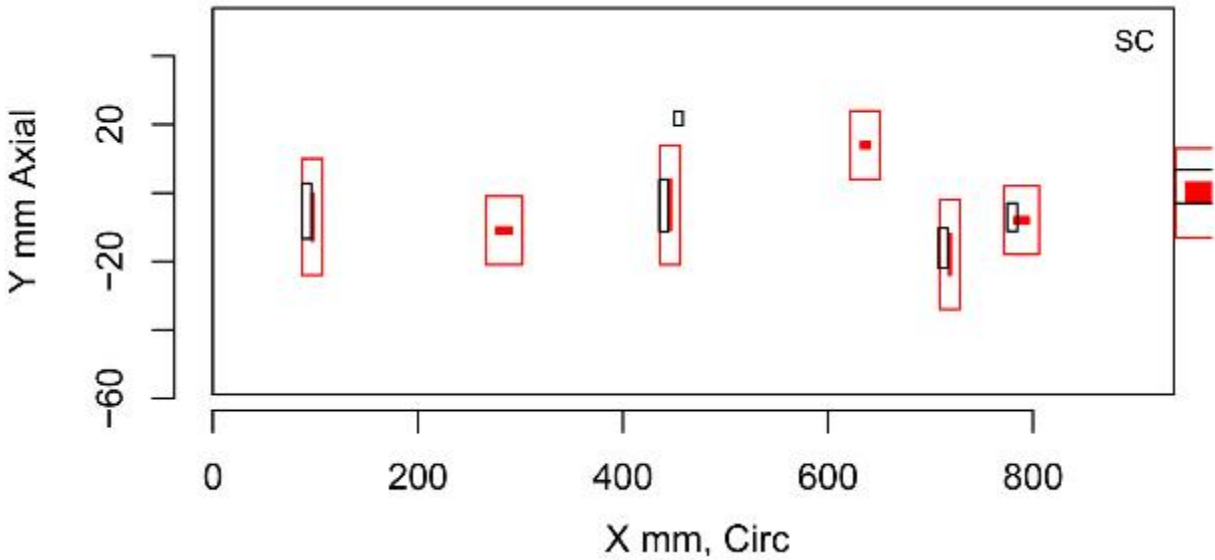


Figure E.199 Indication Plot for Procedure ECT.135 Applied to Test Block P33 in PARENT Blind Testing (X – Y view, 0 mm–800 mm)

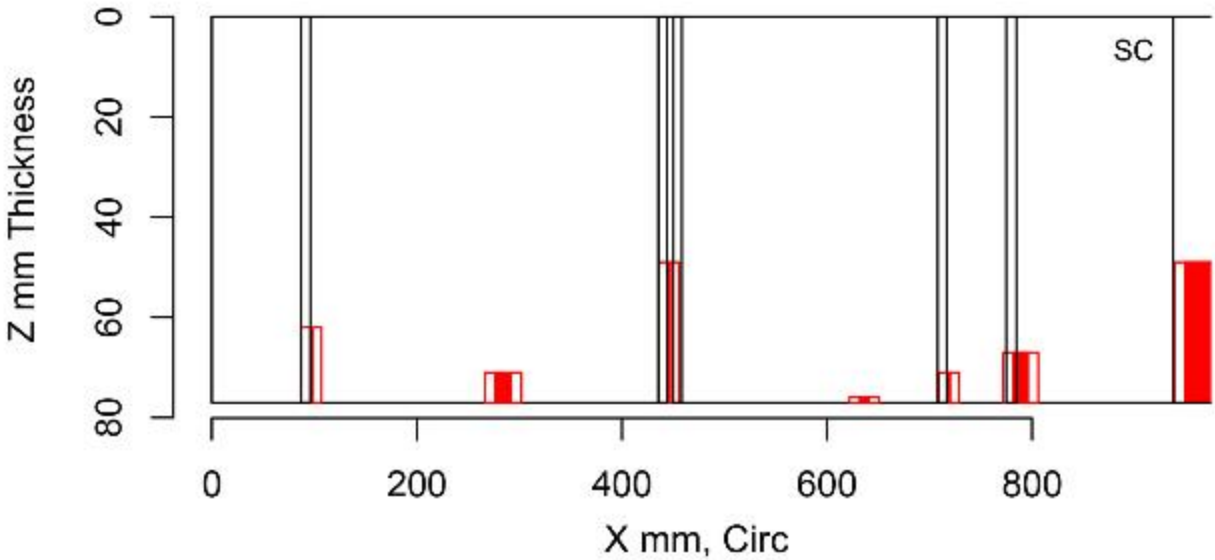


Figure E.200 Indication Plot for Procedure ECT.135 Applied to Test Block P33 in PARENT Blind Testing (X – Z view, 0 mm–800 mm)

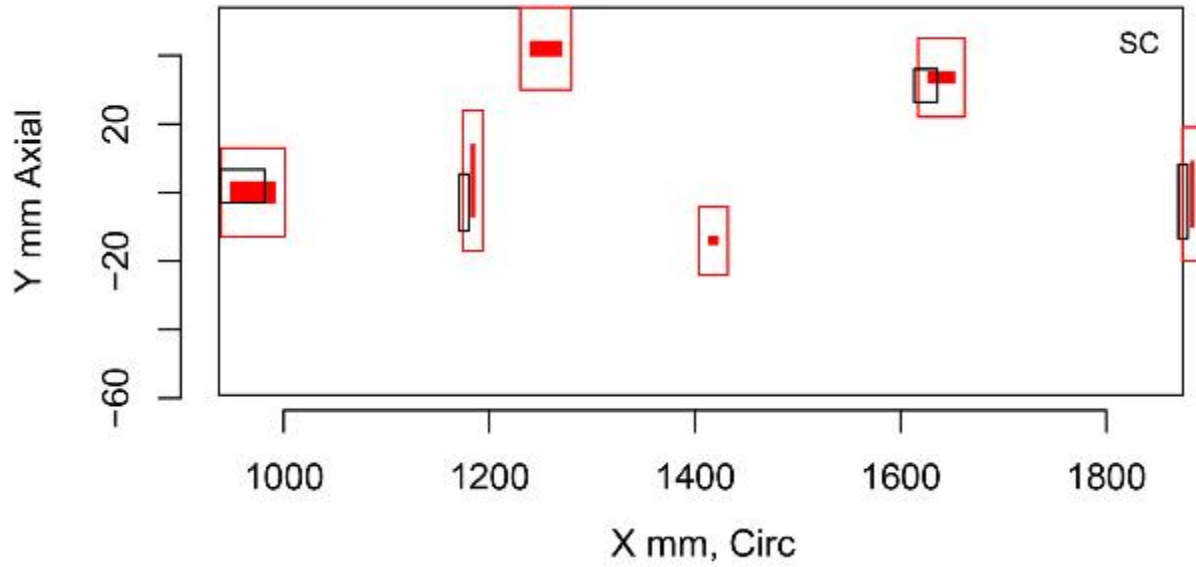


Figure E.201 Indication Plot for Procedure ECT.135 Applied to Test Block P33 in PARENT Blind Testing (X – Y view, 1000 mm–1800 mm)

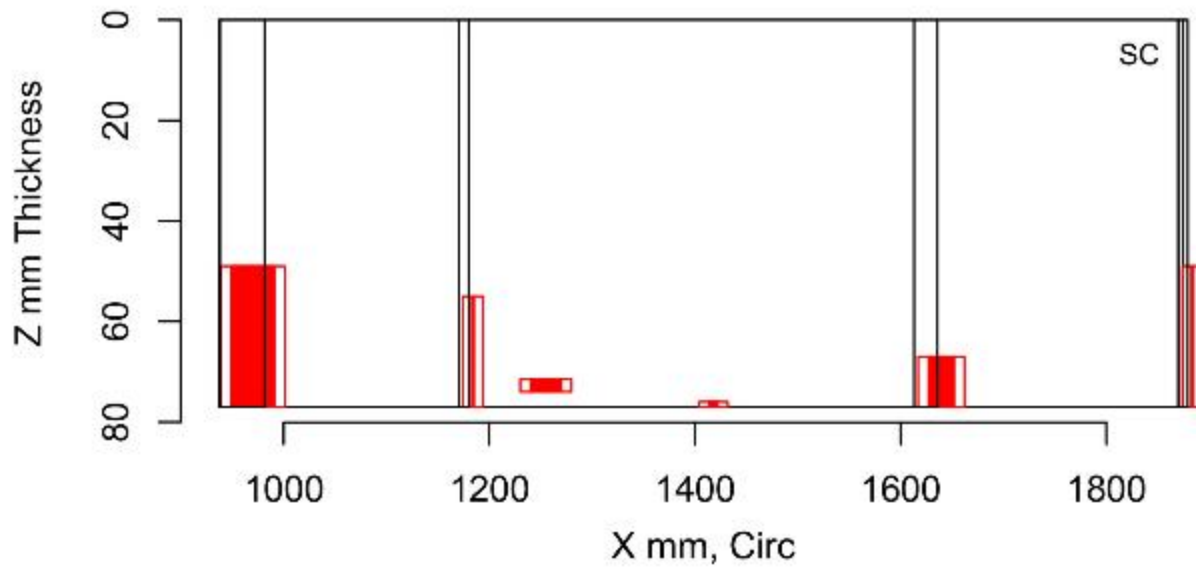


Figure E.202 Indication Plot for Procedure ECT.135 Applied to Test Block P33 in PARENT Blind Testing (X – Z view, 1000 mm–1800 mm)

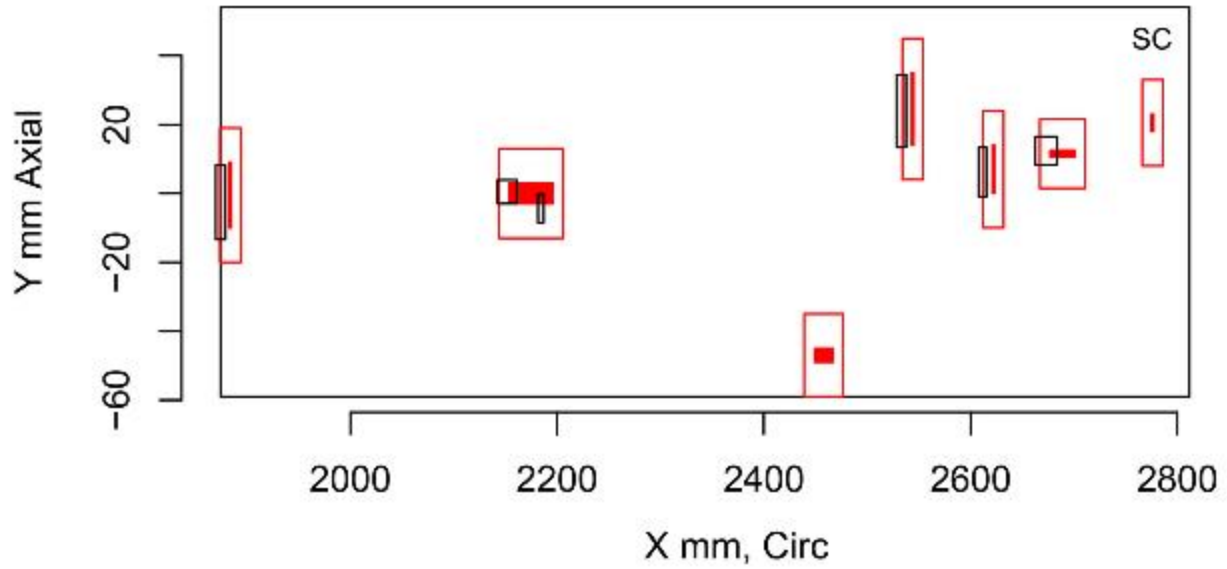


Figure E.203 Indication Plot for Procedure ECT.135 Applied to Test Block P33 in PARENT Blind Testing (X – Y view, 2000 mm–2800 mm)

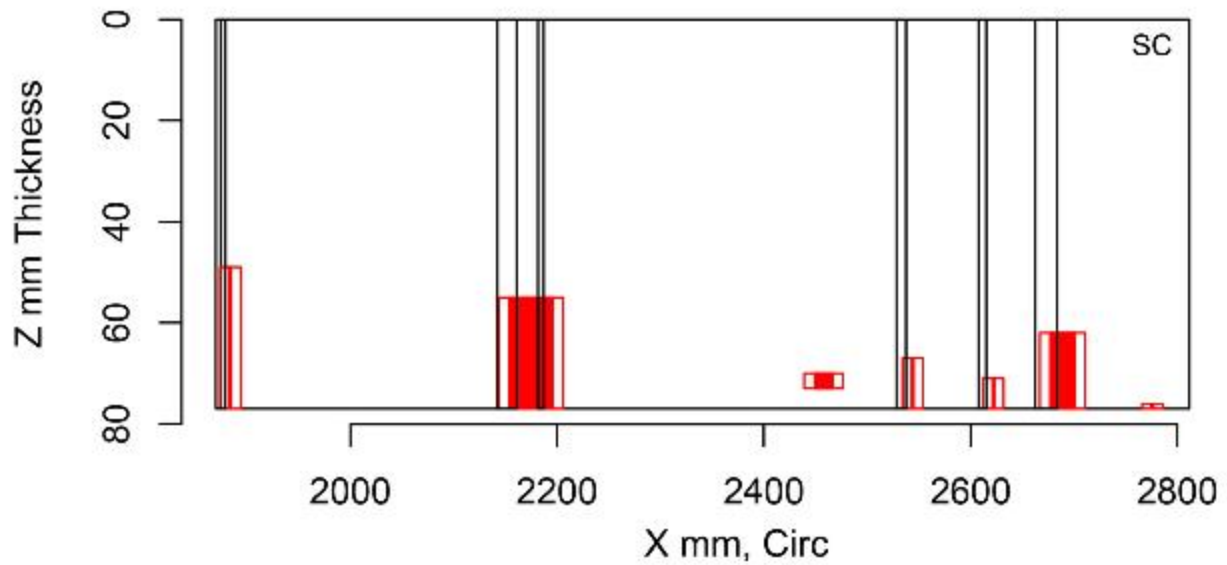


Figure E.204 Indication Plot for Procedure ECT.135 Applied to Test Block P33 in PARENT Blind Testing (X – Z view, 2000 mm–2800 mm)

E.2.10 Plots for Team 144

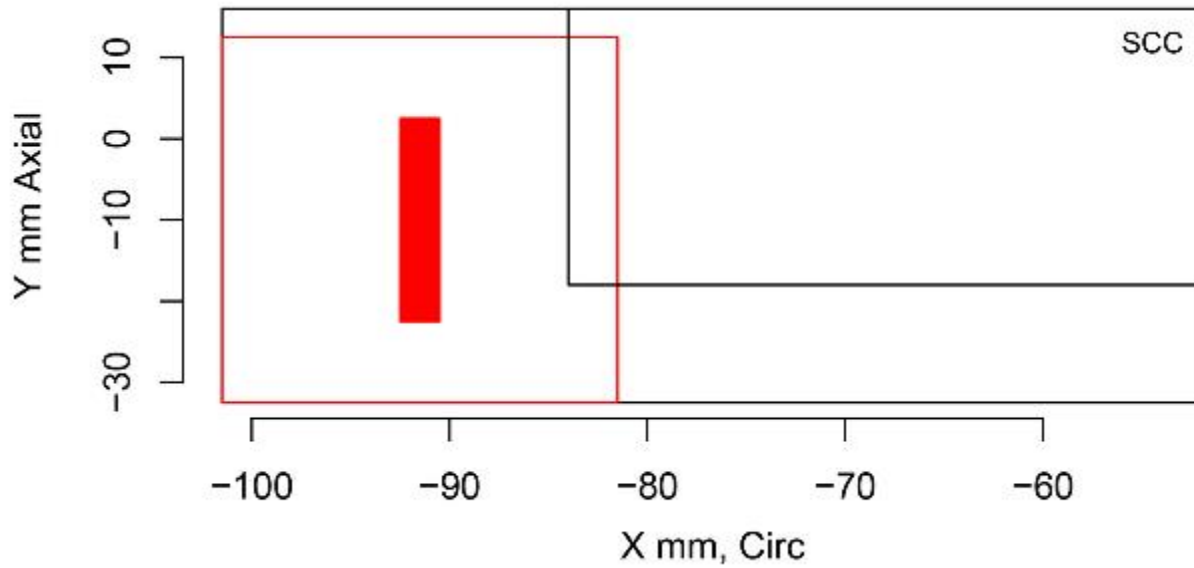


Figure E.205 Indication Plot for Procedure UT.ECT.144 Applied to Test Block P13 in PARENT Blind Testing (X - Y view)

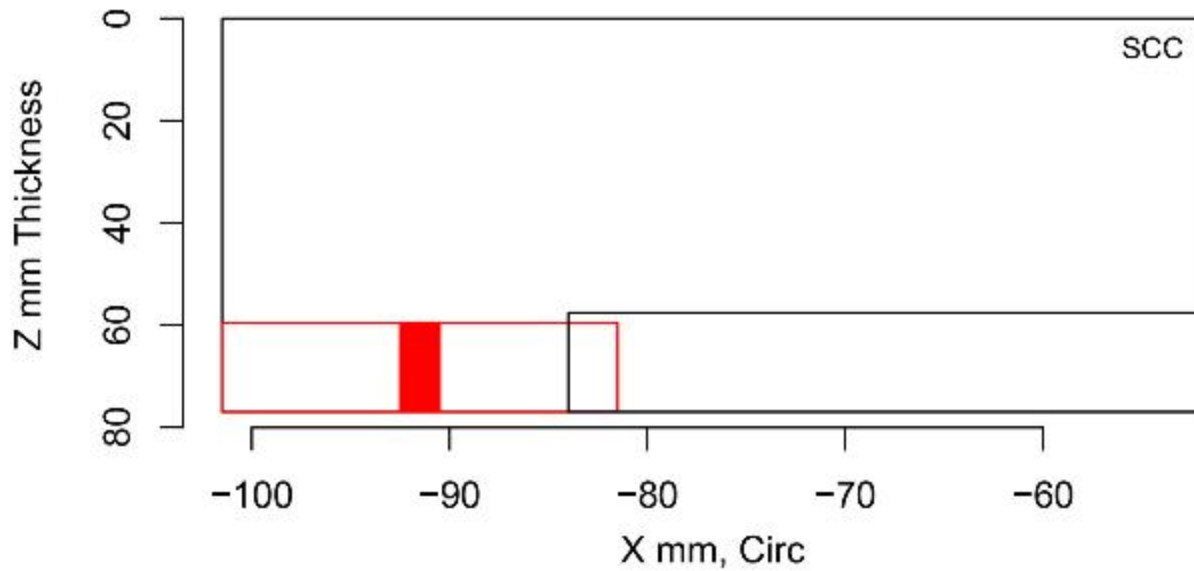


Figure E.206 Indication Plot for Procedure UT.ECT.144 Applied to Test Block P13 in PARENT Blind Testing (X - Z view)

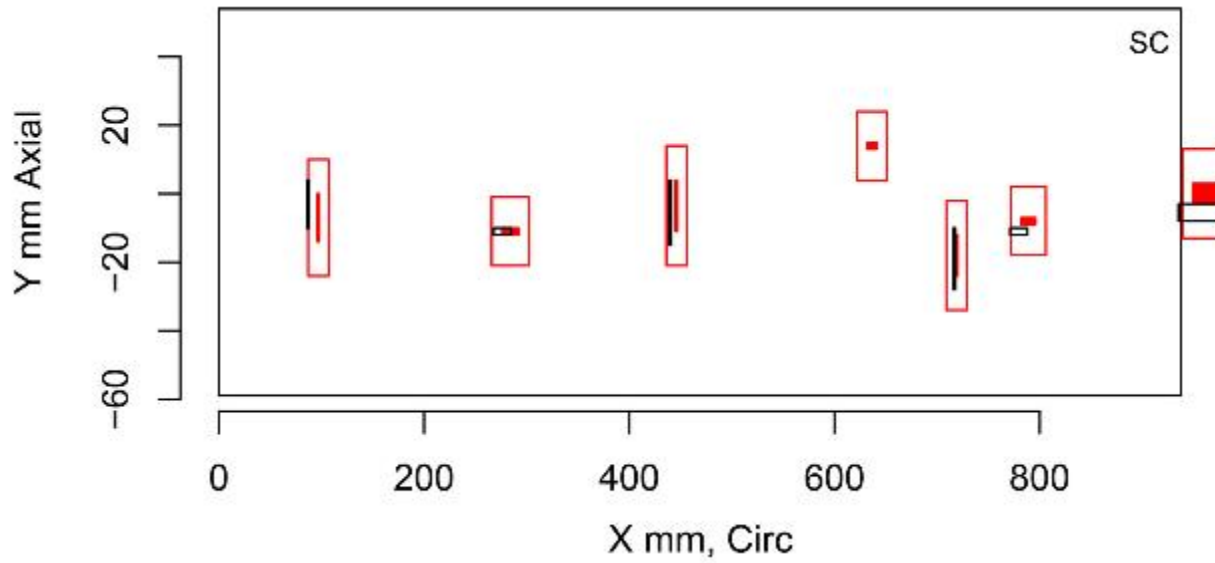


Figure E.207 Indication Plot for Procedure UT.ECT.144 Applied to Test Block P33 in PARENT Blind Testing (X – Y view, 0 mm–800 mm)

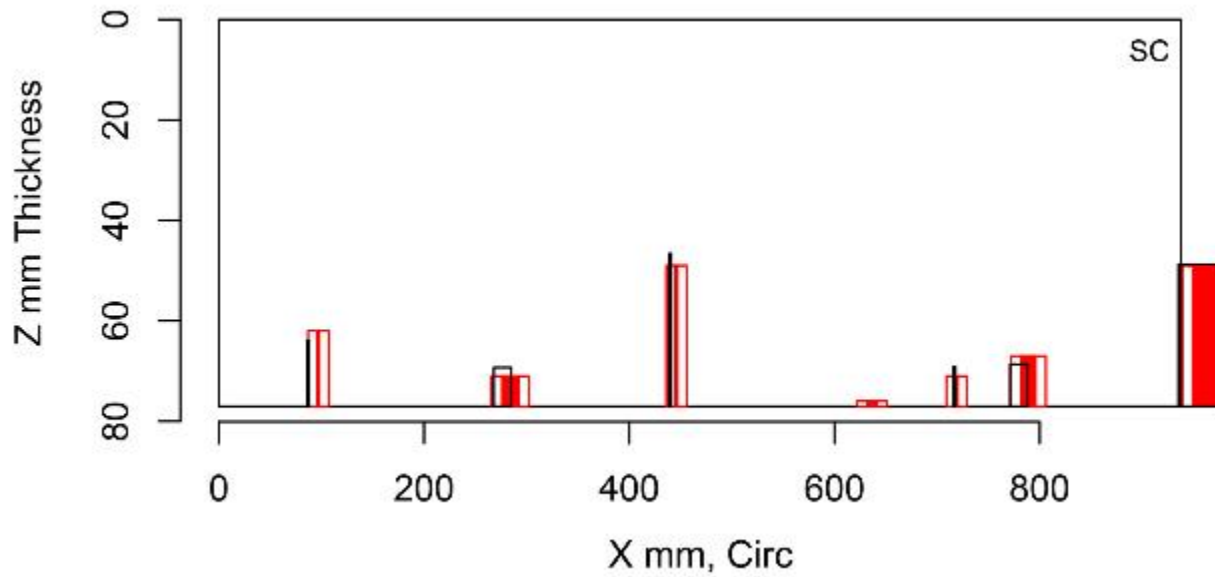


Figure E.208 Indication Plot for Procedure UT.ECT.144 Applied to Test Block P33 in PARENT Blind Testing (X – Z view, 0 mm–800 mm)

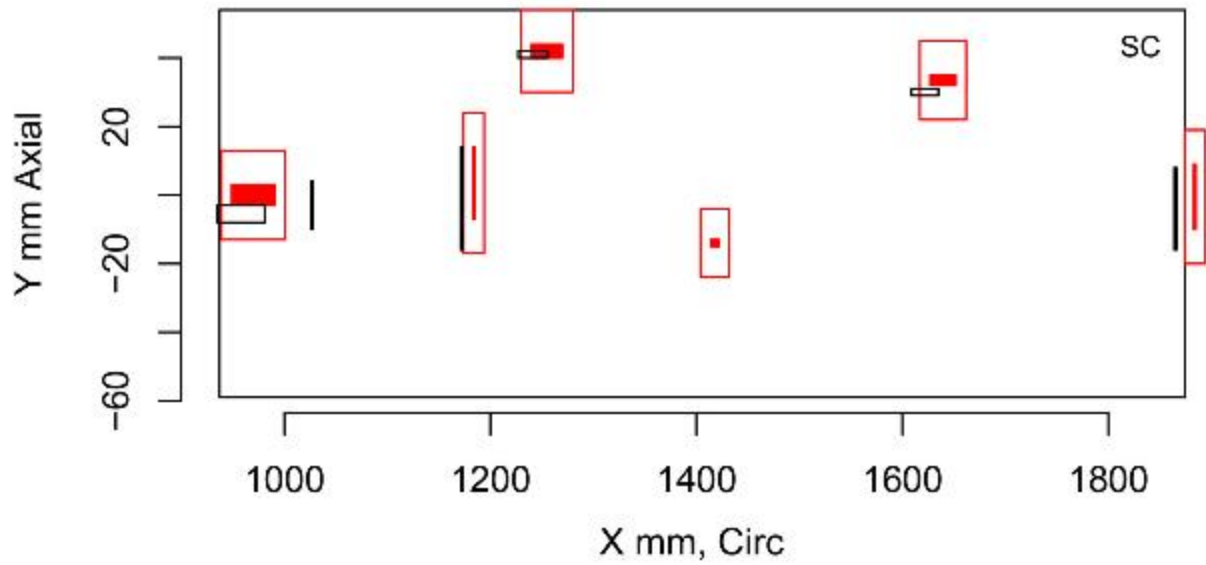


Figure E.209 Indication Plot for Procedure UT.ECT.144 Applied to Test Block P33 in PARENT Blind Testing (X – Y view, 1000 mm–1800 mm)

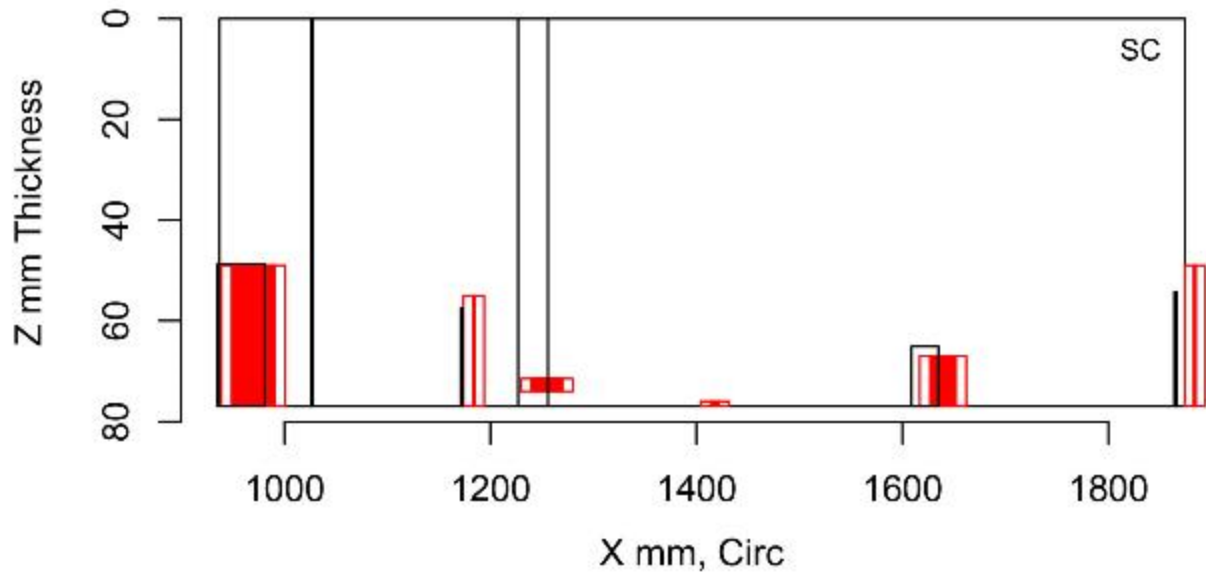


Figure E.210 Indication Plot for Procedure UT.ECT.144 Applied to Test Block P33 in PARENT Blind Testing (X – Z view, 1000 mm–1800 mm)

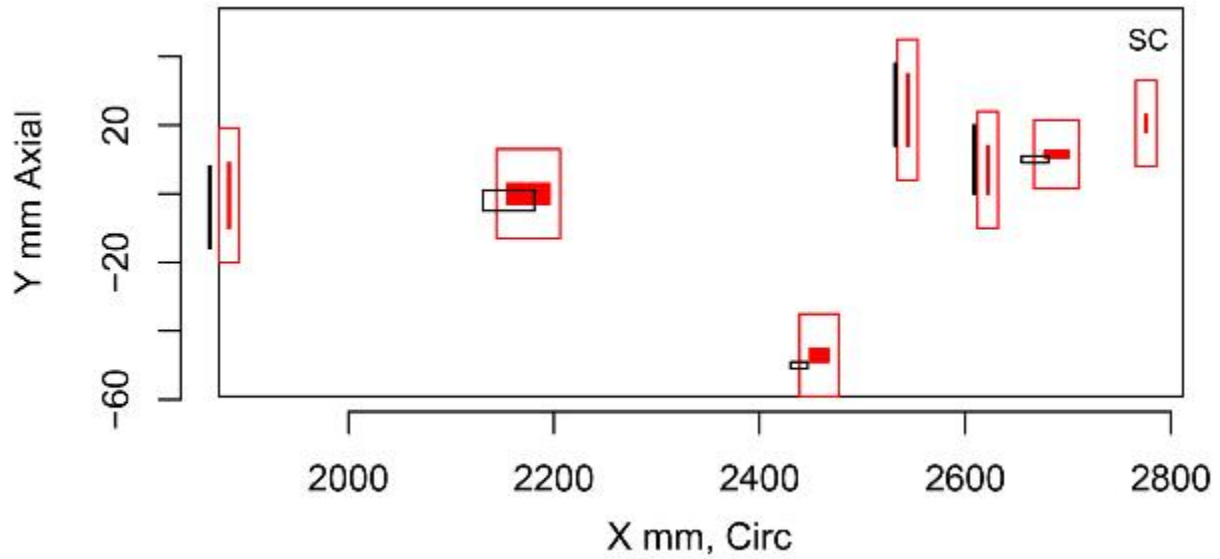


Figure E.211 Indication Plot for Procedure UT.ECT.144 Applied to Test Block P33 in PARENT Blind Testing (X – Y view, 2000 mm–2800 mm)

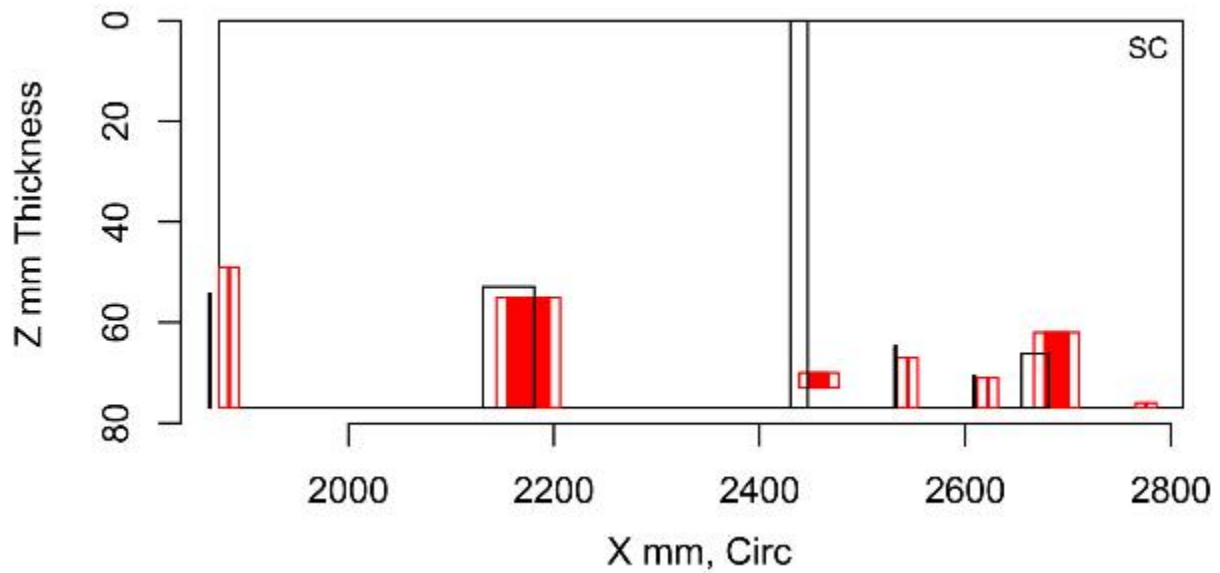


Figure E.212 Indication Plot for Procedure UT.ECT.144 Applied to Test Block P33 in PARENT Blind Testing (X – Z view, 2000 mm–2800 mm)

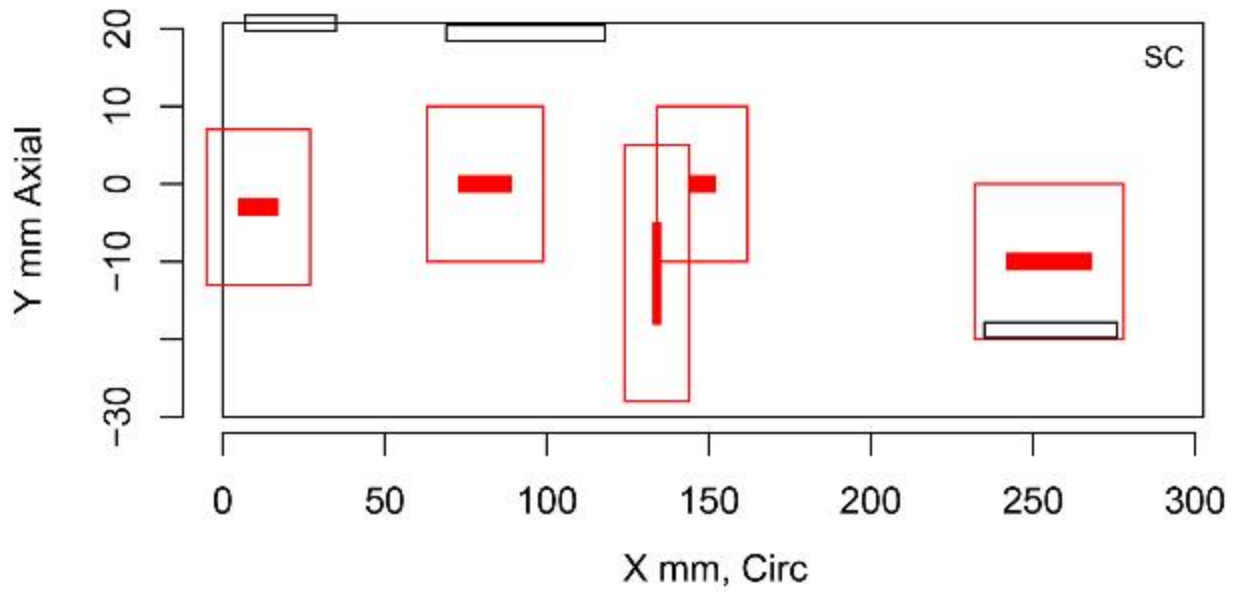


Figure E.213 Indication Plot for Procedure UT.25 Applied to Test Block P35 in PARENT Blind Testing (X – Y view, 0 mm–300 mm)

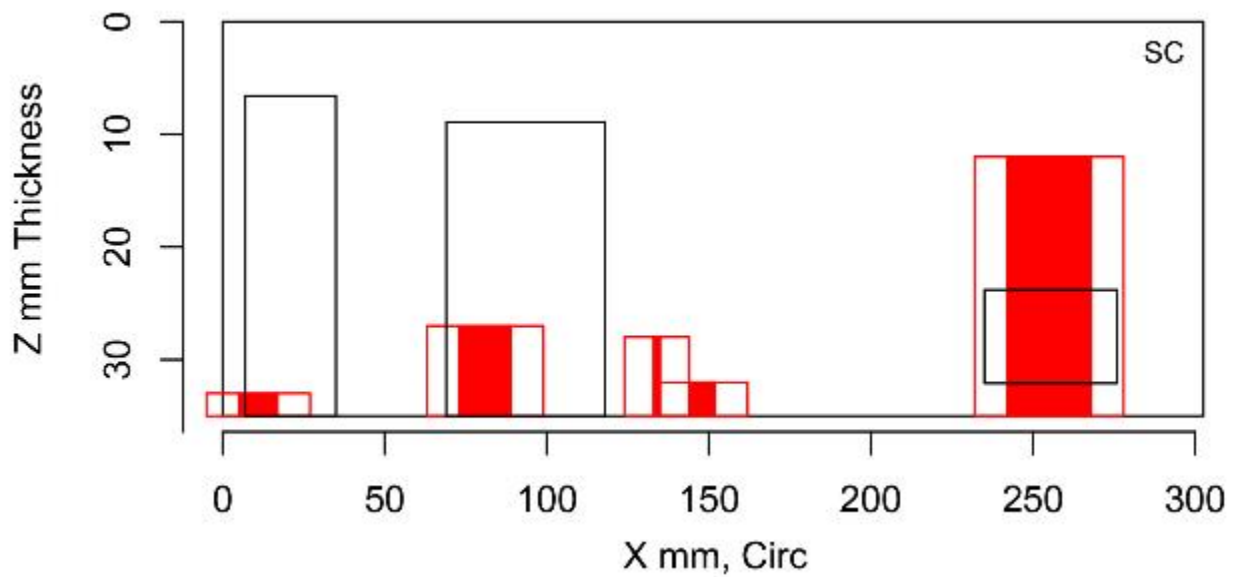


Figure E.214 Indication Plot for Procedure UT.25 Applied to Test Block P35 in PARENT Blind Testing (X – Z view, 0 mm–300 mm)

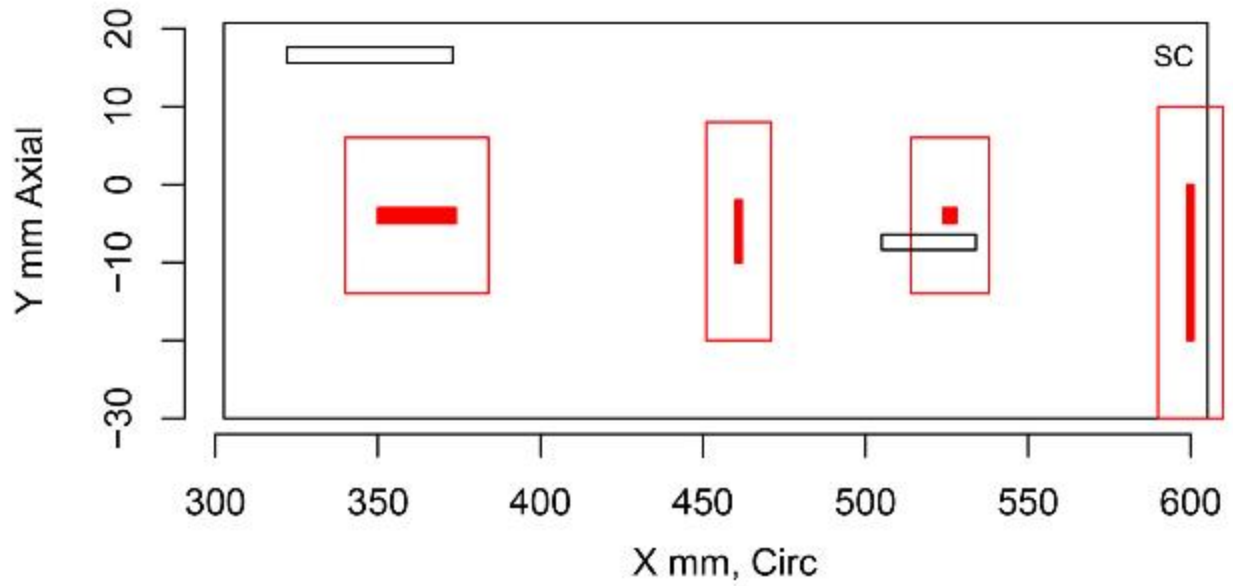


Figure E.215 Indication Plot for Procedure UT.25 Applied to Test Block P35 in PARENT Blind Testing (X – Y view, 300 mm–600 mm)

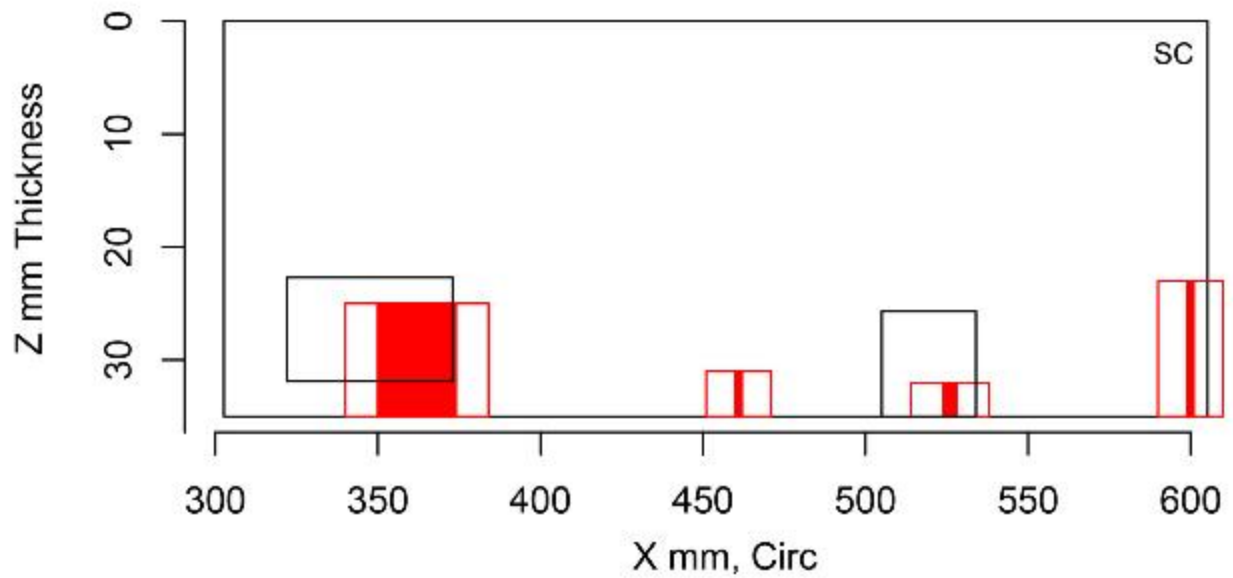


Figure E.216 Indication Plot for Procedure UT.25 Applied to Test Block P35 in PARENT Blind Testing (X – Z view, 300 mm–600 mm)

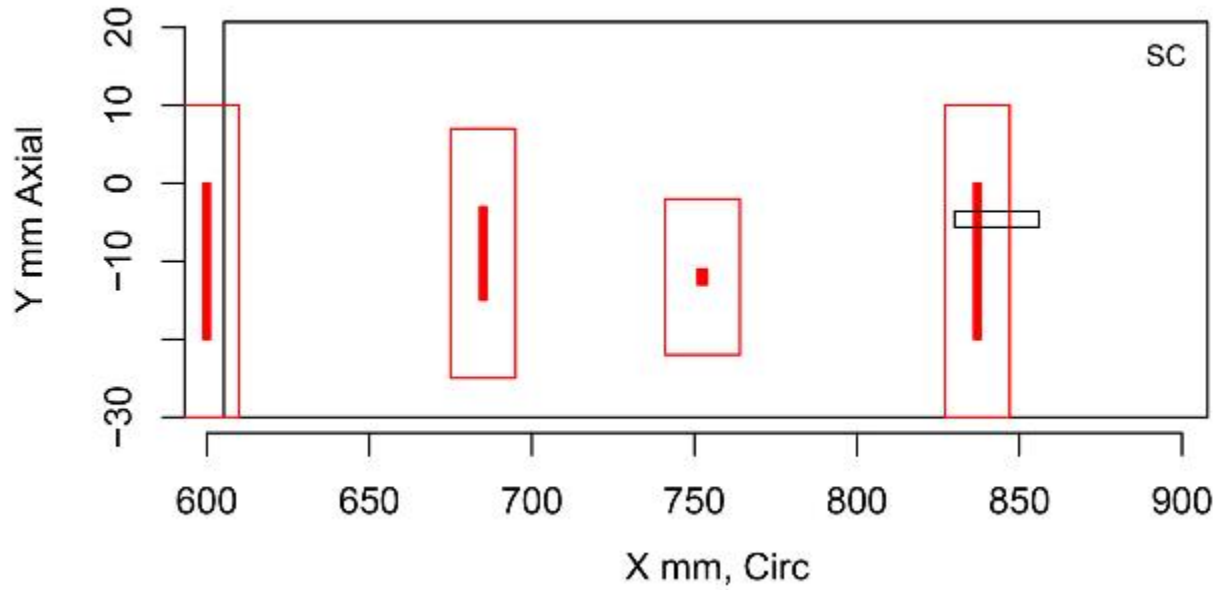


Figure E.217 Indication Plot for Procedure UT.25 Applied to Test Block P35 in PARENT Blind Testing (X - Y view, 600 mm-800 mm)

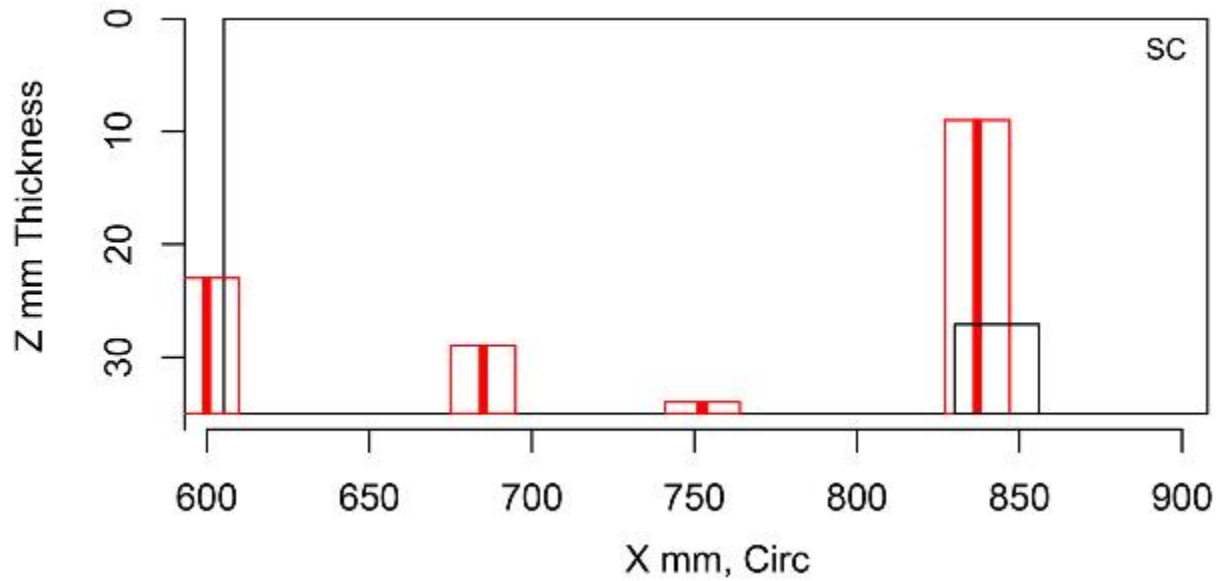


Figure E.218 Indication Plot for Procedure UT.25 Applied to Test Block P35 in PARENT Blind Testing (X - Z view, 600 mm-800 mm)

E.3 BMI Inspection Summary Results

E.3.1 Plots for Team 108

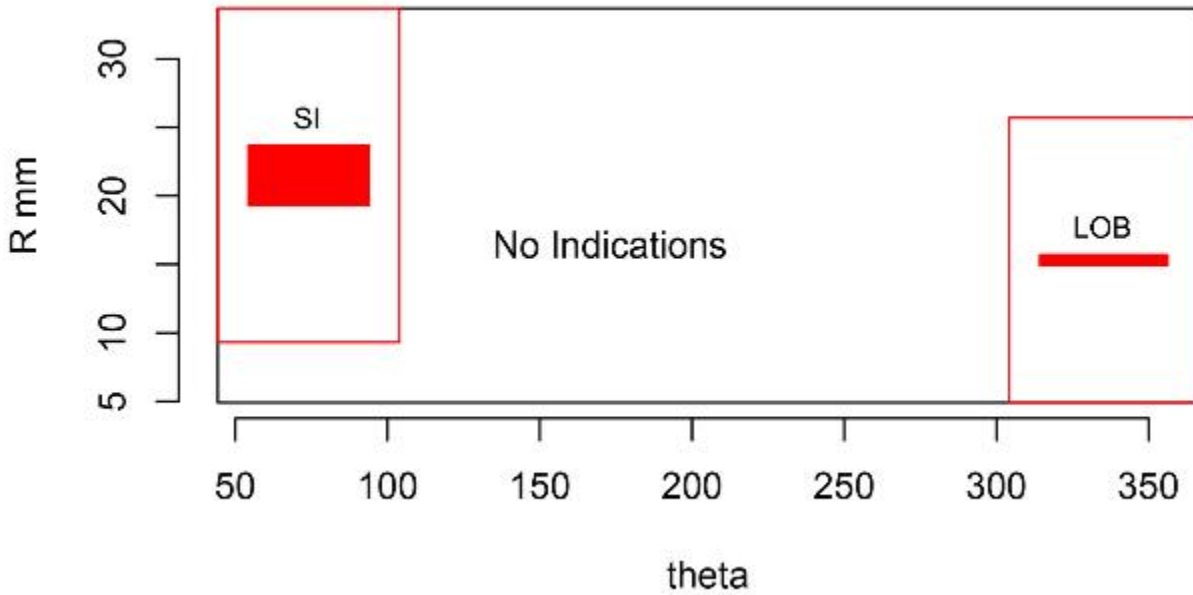


Figure E.219 Indication Plot for Procedure ECT.108 Applied to Test Block P25 in PARENT Blind Testing (theta – R view)

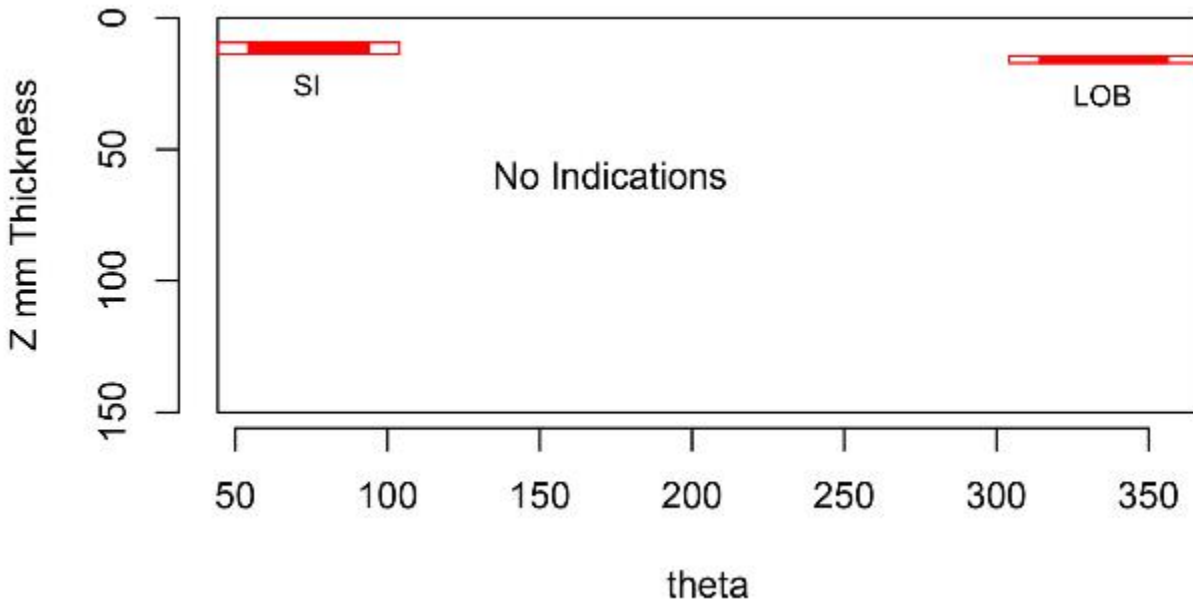


Figure E.220 Indication Plot for Procedure ECT.108 Applied to Test Block P25 in PARENT Blind Testing (theta – Z view)

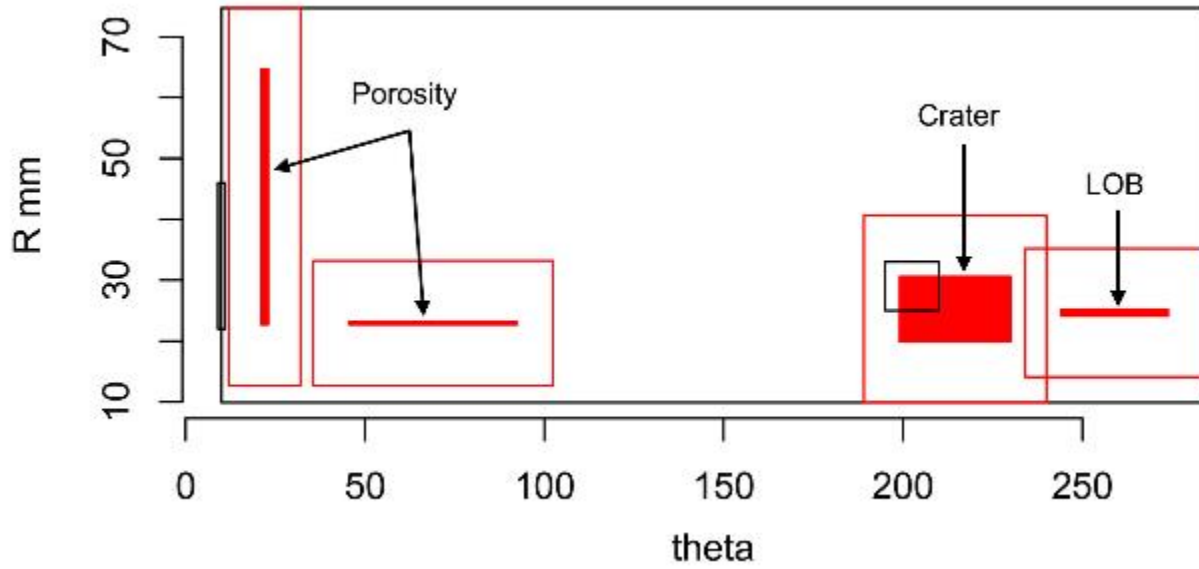


Figure E.221 Indication Plot for Procedure ECT.108 Applied to Test Block P26 in PARENT Blind Testing (theta - R view)

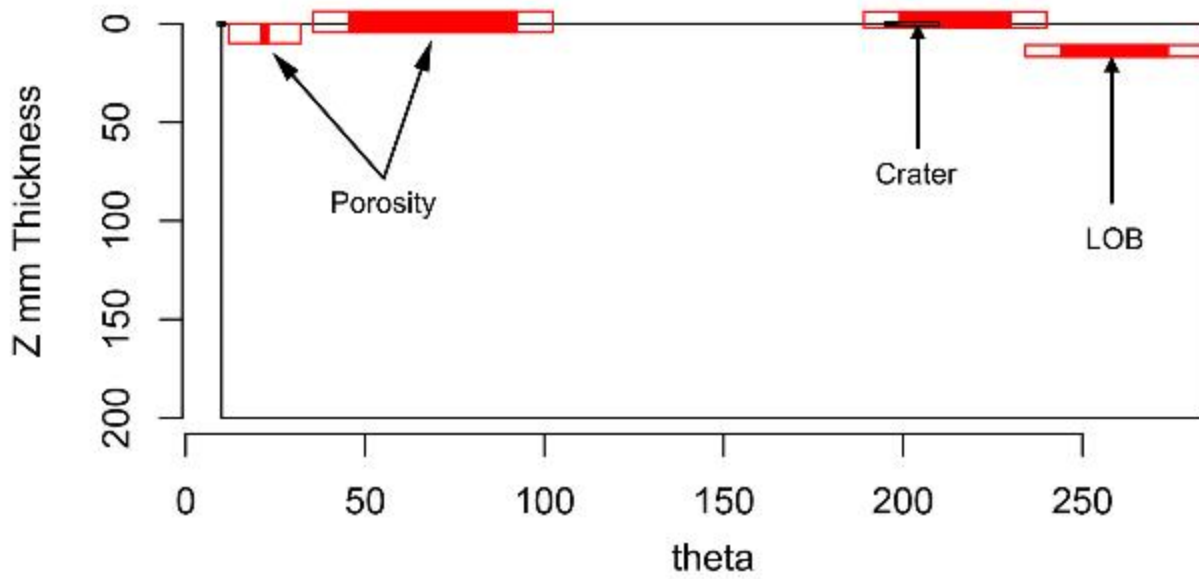


Figure E.222 Indication Plot for Procedure ECT.108 Applied to Test Block P26 in PARENT Blind Testing (theta - Z view)

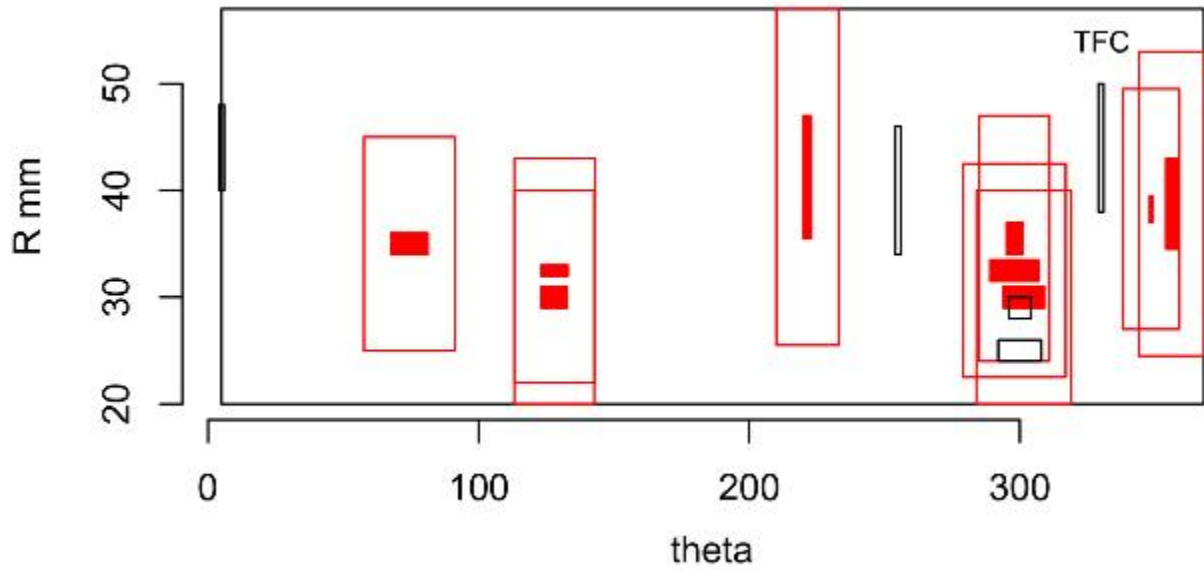


Figure E.223 Indication Plot for Procedure ECT.108 Applied to Test Block P6 in PARENT Blind Testing (theta - R view)

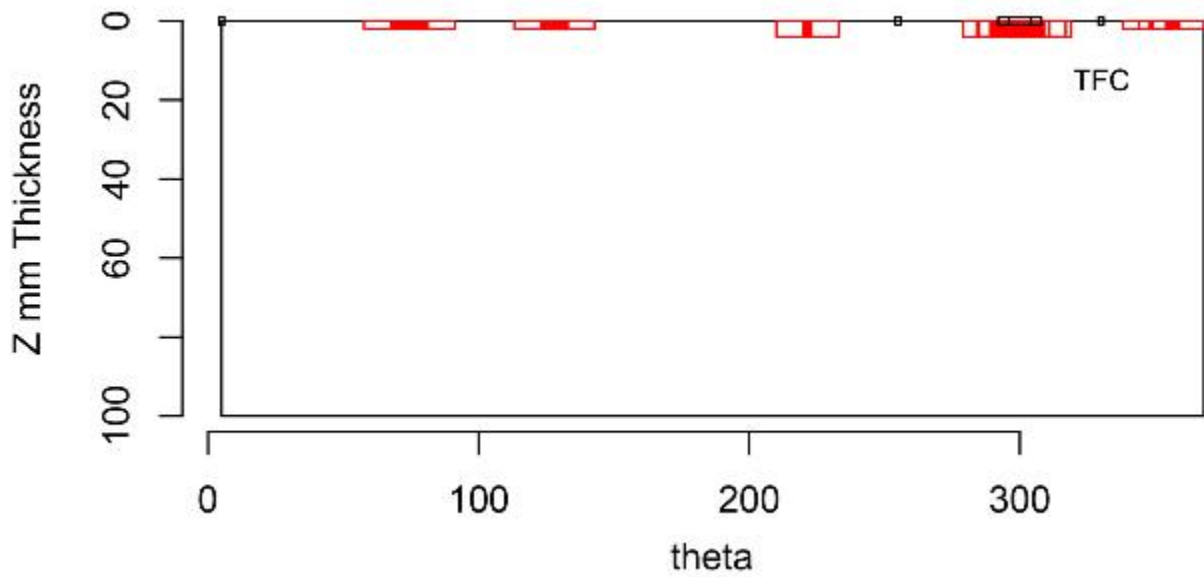


Figure E.224 Indication Plot for Procedure ECT.108 Applied to Test Block P6 in PARENT Blind Testing (theta - Z view)

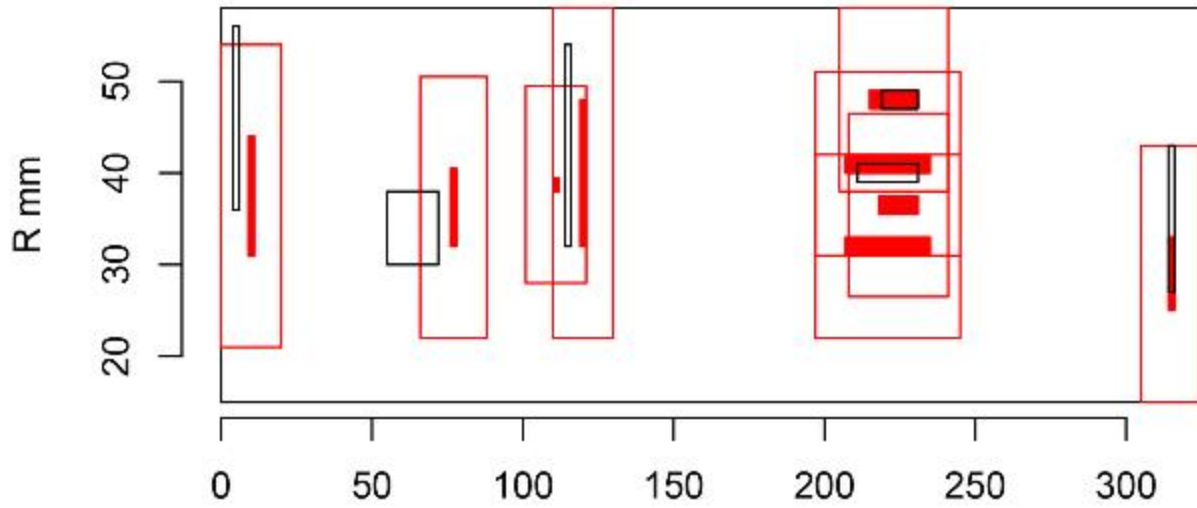


Figure E.225 Indication Plot for Procedure ECT.108 Applied to Test Block P8 in PARENT Blind Testing (theta – R view)

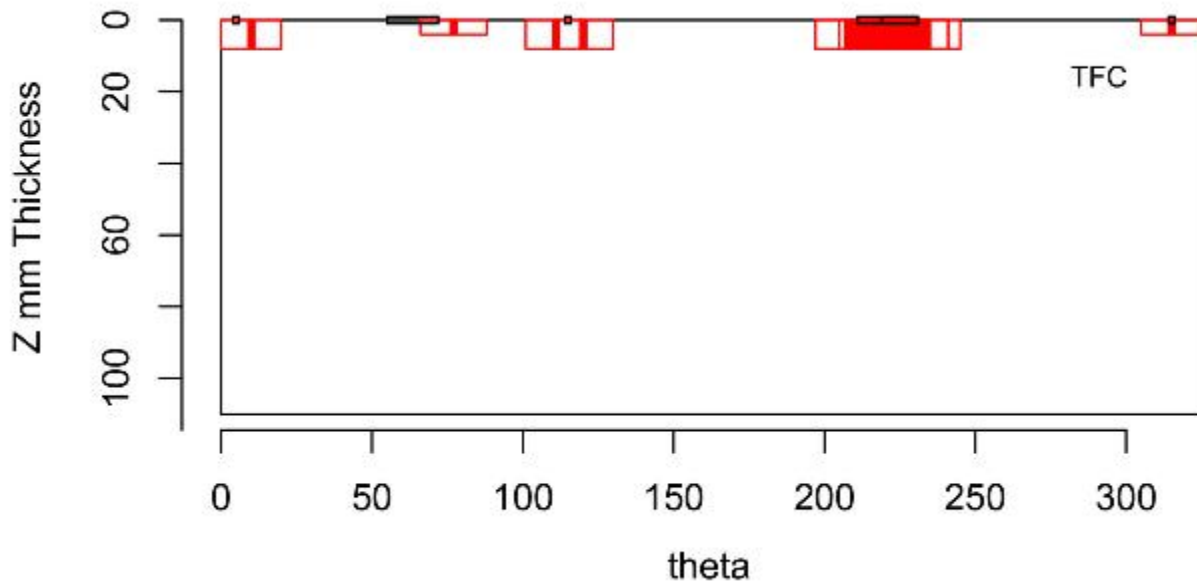


Figure E.226 Indication Plot for Procedure ECT.108 Applied to Test Block P8 in PARENT Blind Testing (theta – Z view)

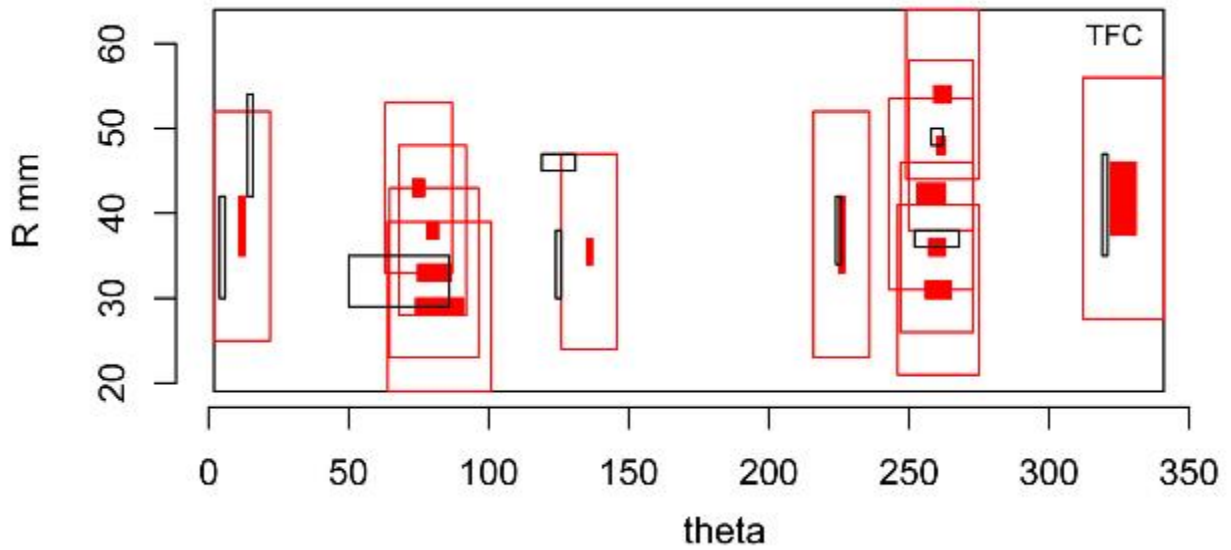


Figure E.227 Indication Plot for Procedure ECT.108 Applied to Test Block P9 in PARENT Blind Testing (theta - R view)

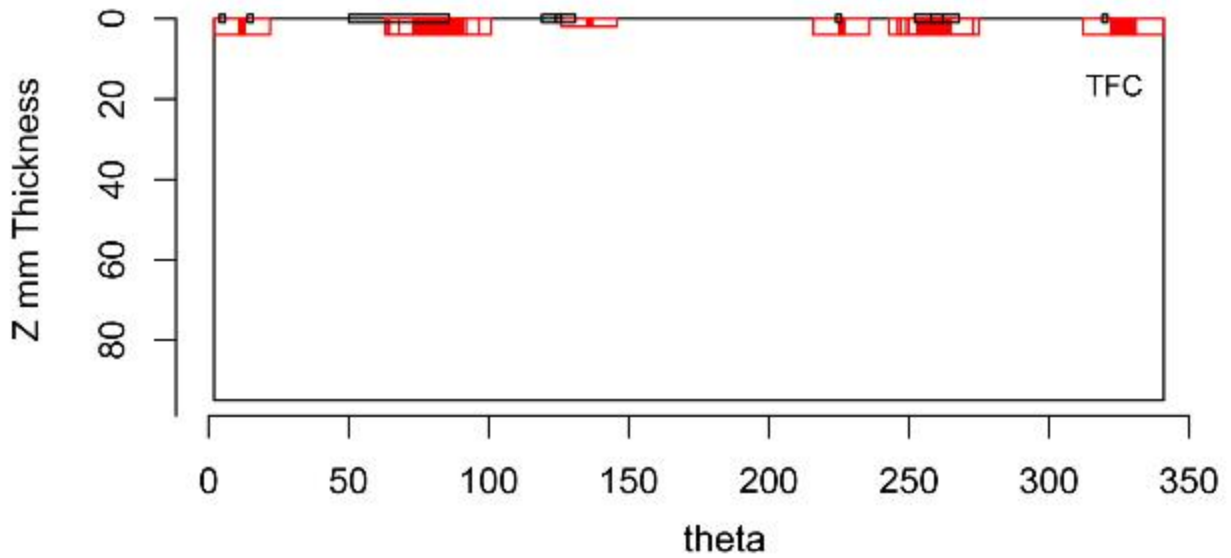


Figure E.228 Indication Plot for Procedure ECT.108 Applied to Test Block P9 in PARENT Blind Testing (theta - Z view)

E.3.2 Plots for Team 124

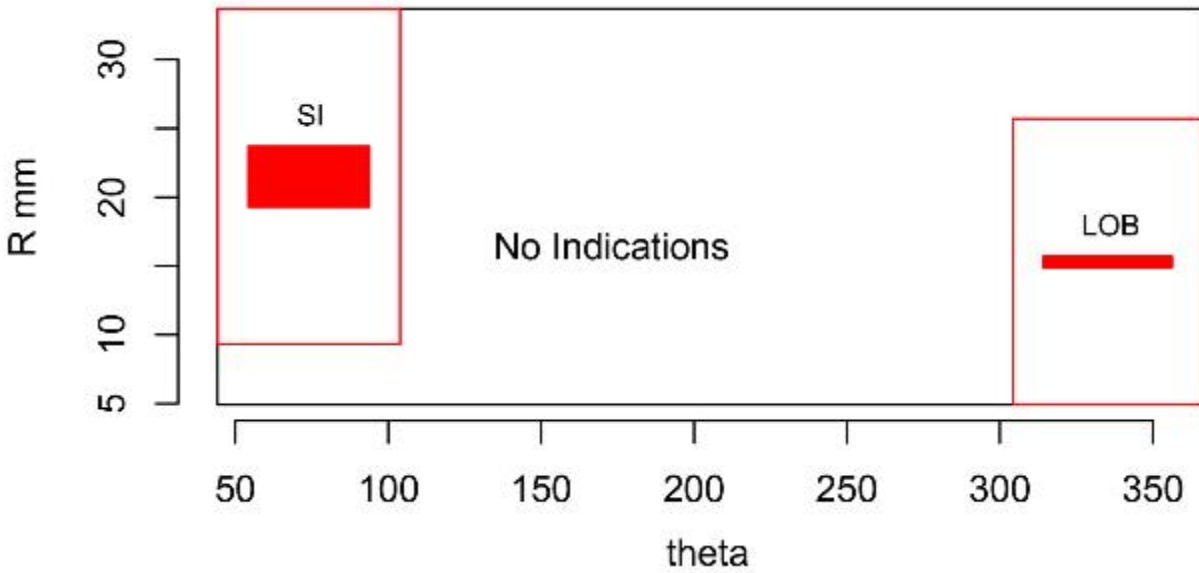


Figure E.229 Indication Plot for Procedure ECT.124 Applied to Test Block P25 in PARENT Blind Testing (theta - R view)

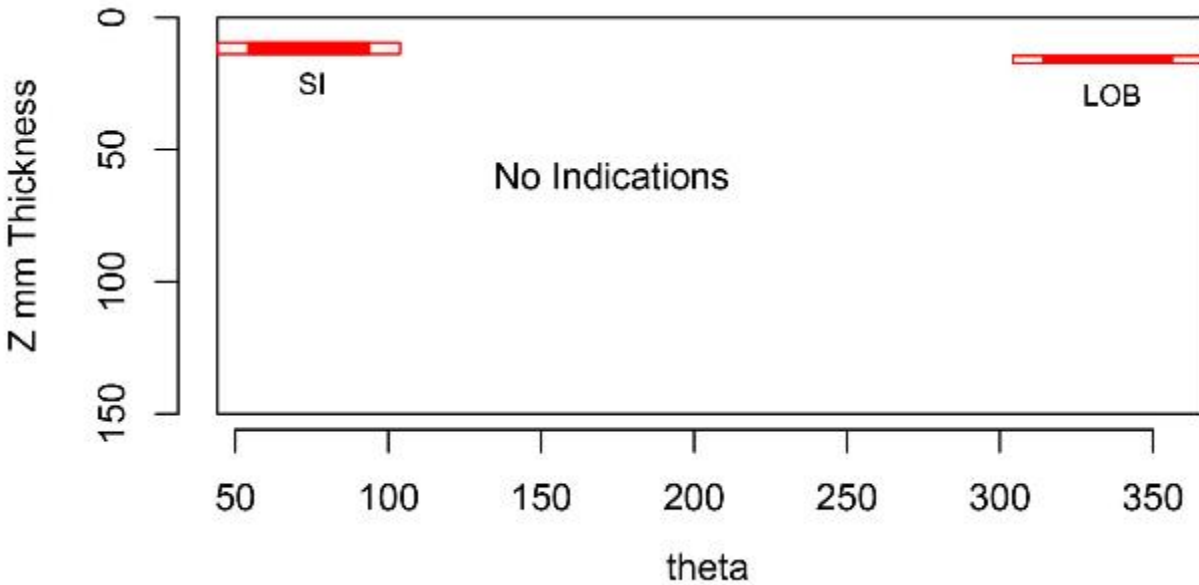


Figure E.230 Indication Plot for Procedure ECT.124 Applied to Test Block P25 in PARENT Blind Testing (theta - Z view)

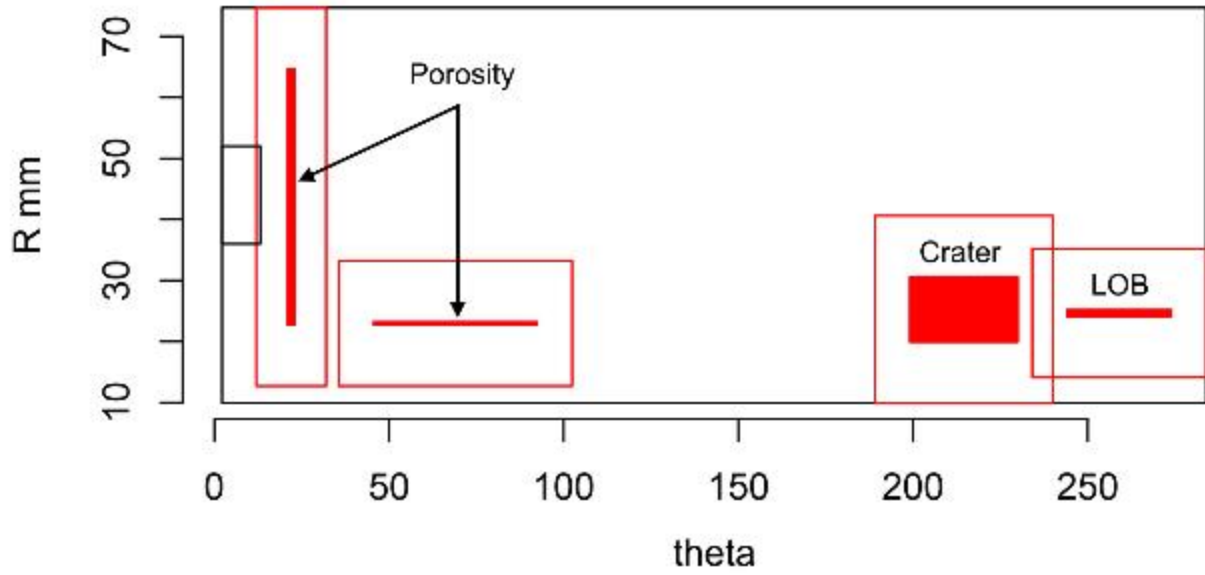


Figure E.231 Indication Plot for Procedure ECT.124 Applied to Test Block P26 in PARENT Blind Testing (theta – R view)

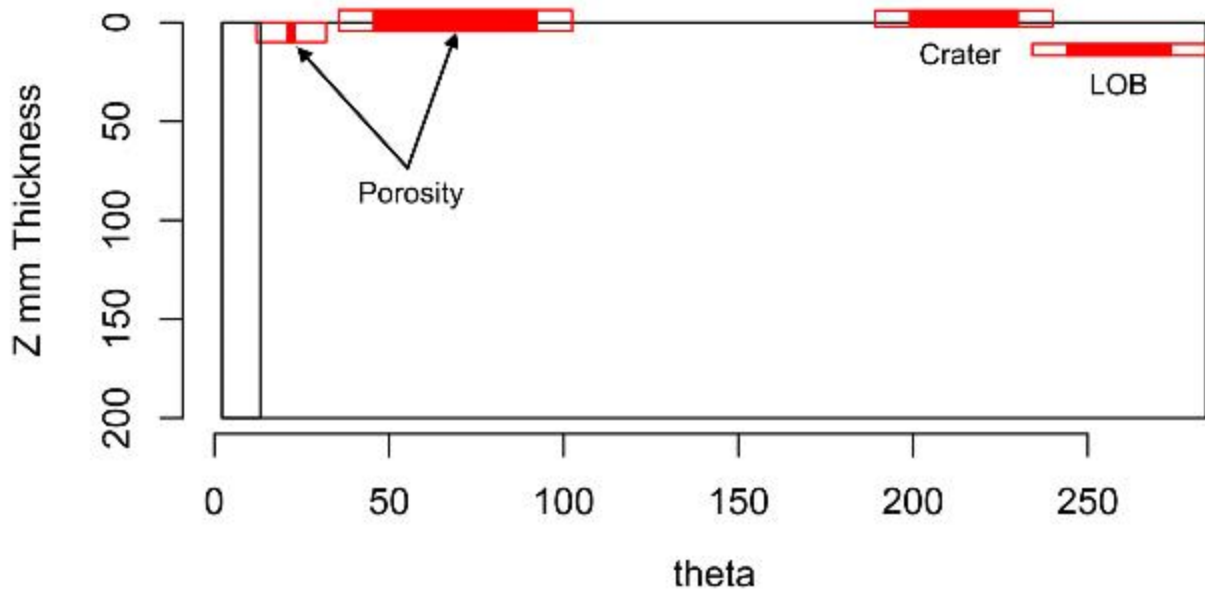


Figure E.232 Indication Plot for Procedure ECT.124 Applied to Test Block P26 in PARENT Blind Testing (theta – Z view)

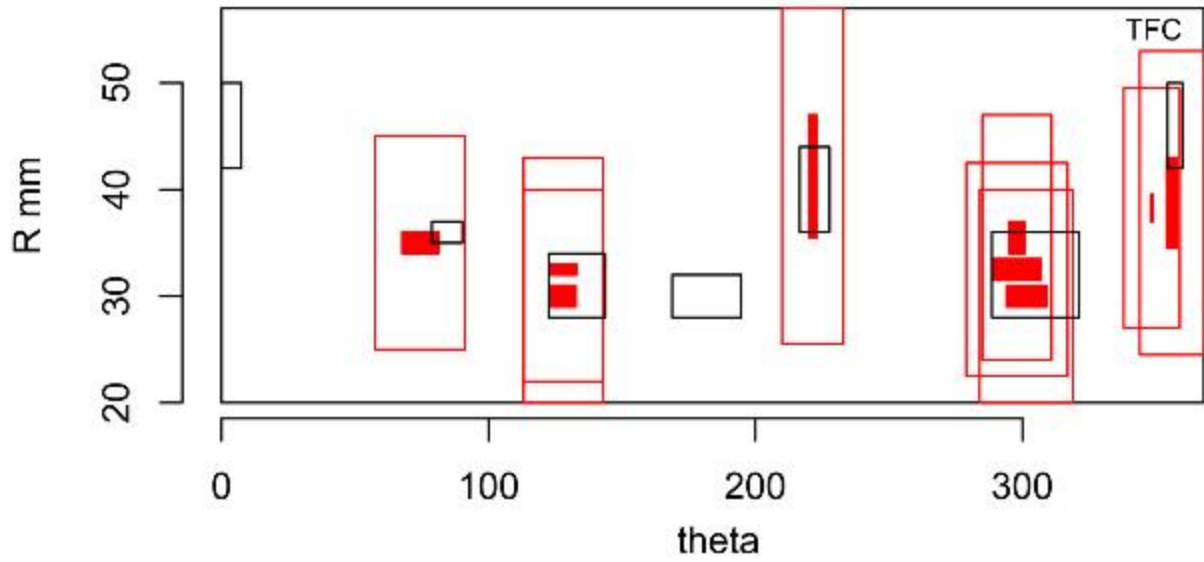


Figure E.233 Indication Plot for Procedure ECT.124 Applied to Test Block P6 in PARENT Blind Testing (theta – R view)

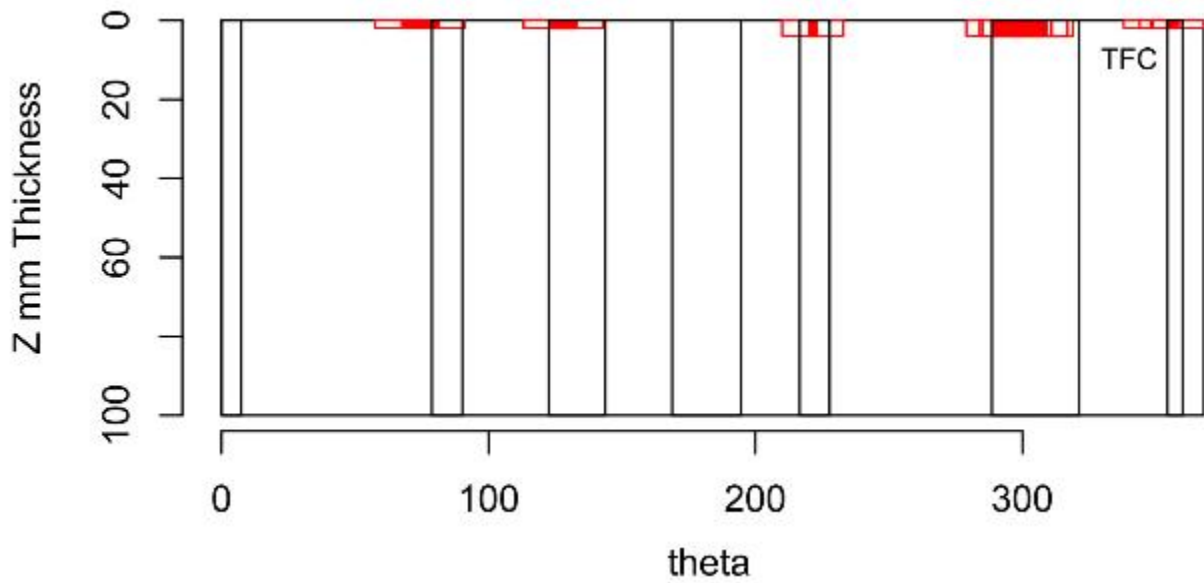


Figure E.234 Indication Plot for Procedure ECT.124 Applied to Test Block P6 in PARENT Blind Testing (theta – Z view)

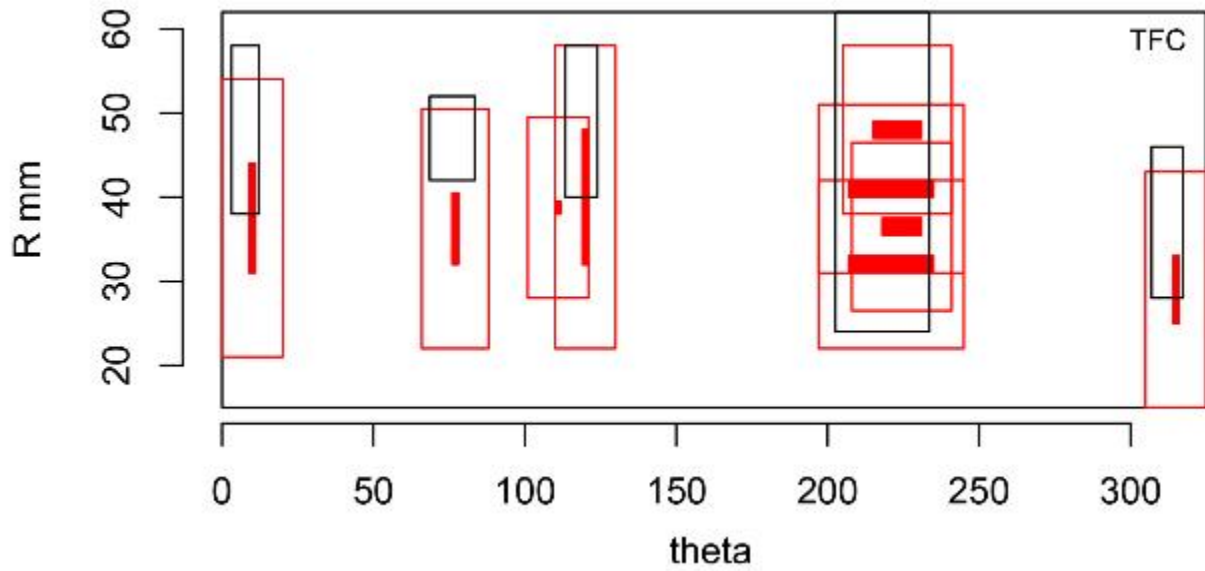


Figure E.235 Indication Plot for Procedure ECT.124 Applied to Test Block P8 in PARENT Blind Testing (theta - R view)

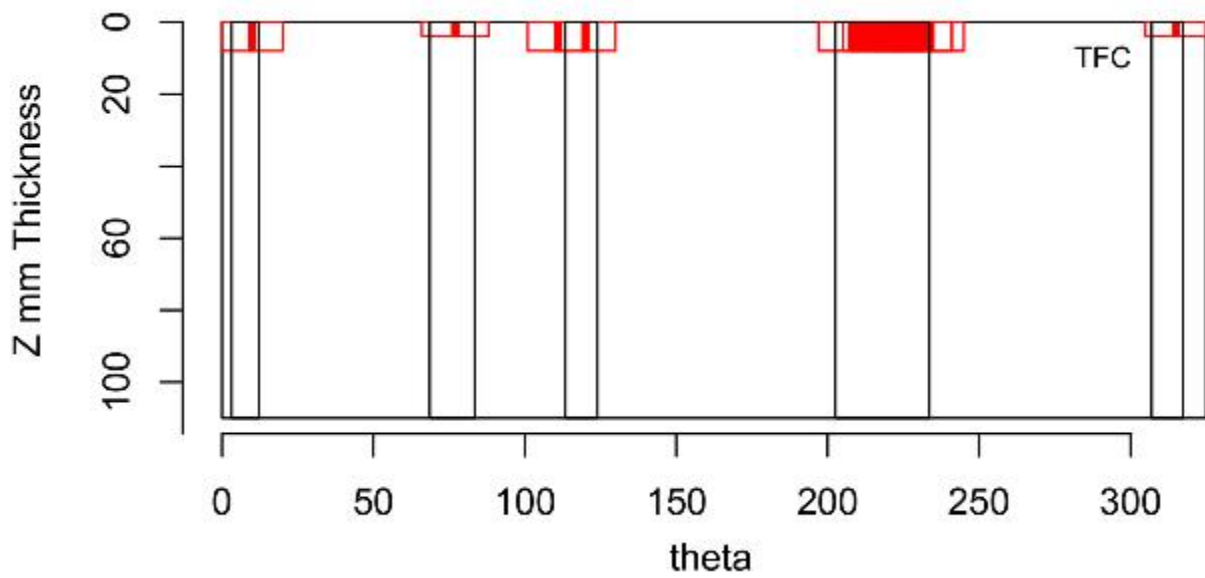


Figure E.236 Indication Plot for Procedure ECT.124 Applied to Test Block P8 in PARENT Blind Testing (theta - Z view)

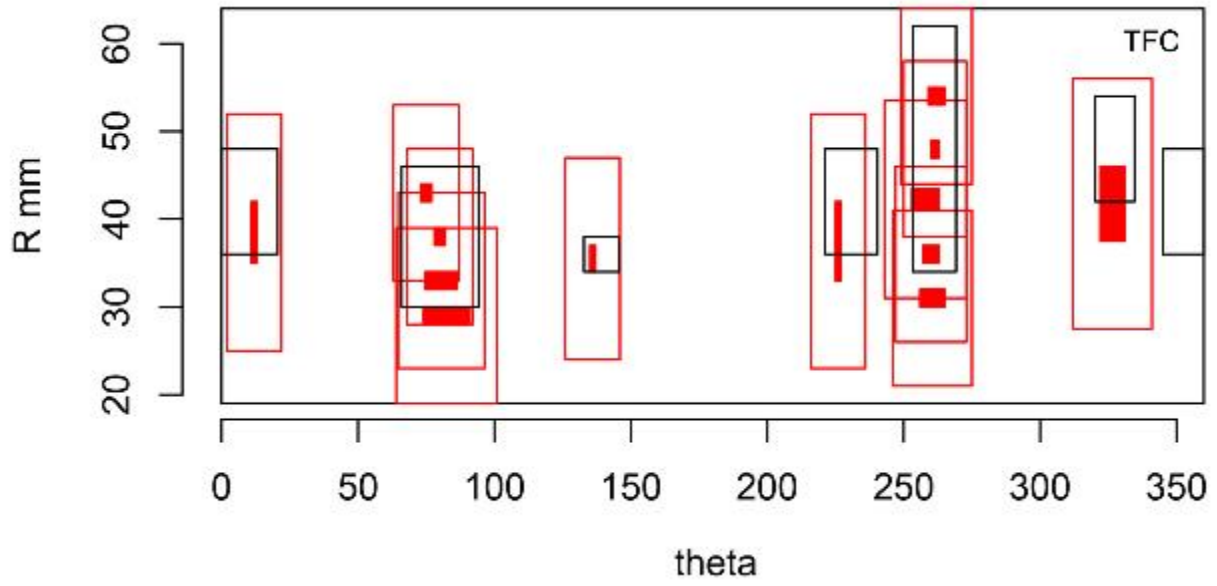


Figure E.237 Indication Plot for Procedure ECT.124 Applied to Test Block P9 in PARENT Blind Testing (theta – R view)

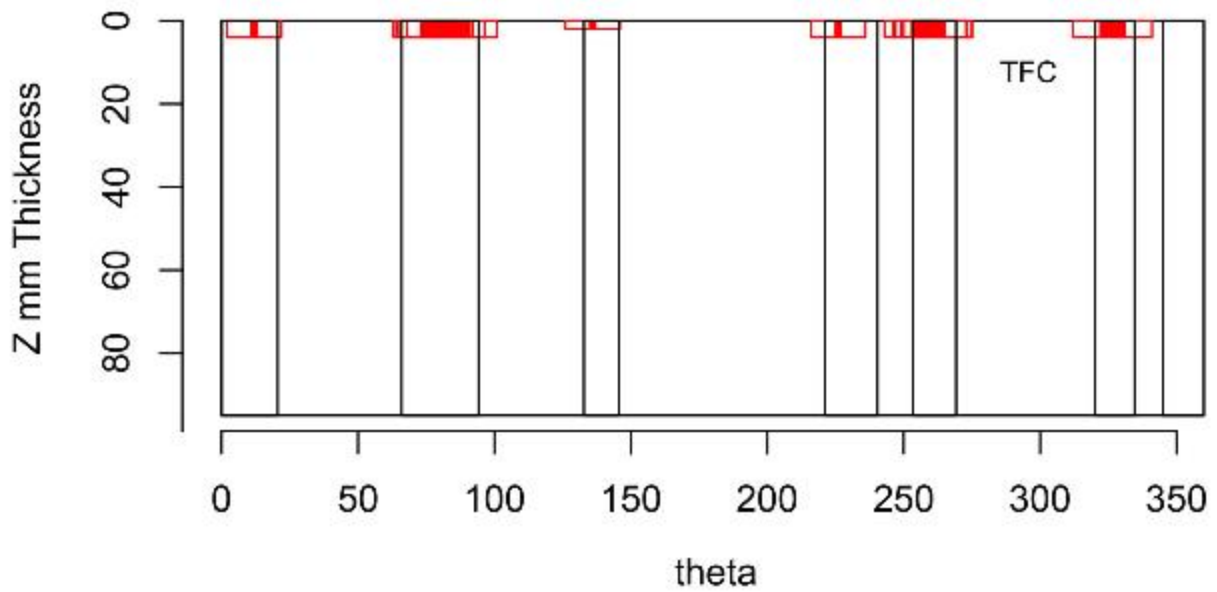


Figure E.238 Indication Plot for Procedure ECT.124 Applied to Test Block P9 in PARENT Blind Testing (theta – Z view)

E.3.3 Plots for Team 126

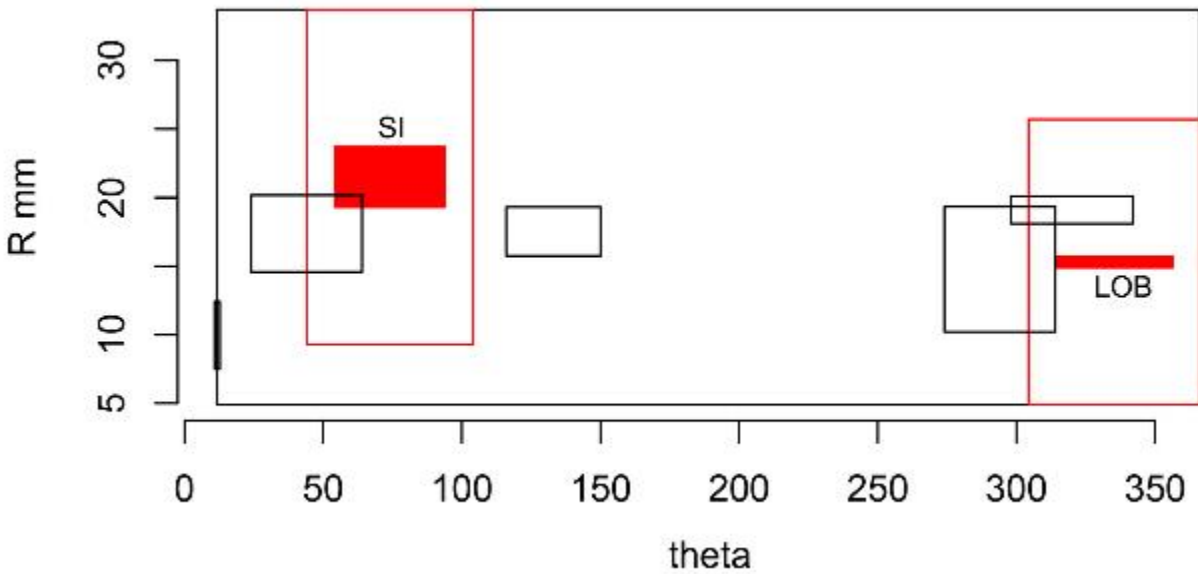


Figure E.239 Indication Plot for Procedure TOFD.ECT.126 Applied to Test Block P25 in PARENT Blind Testing (theta - R view)

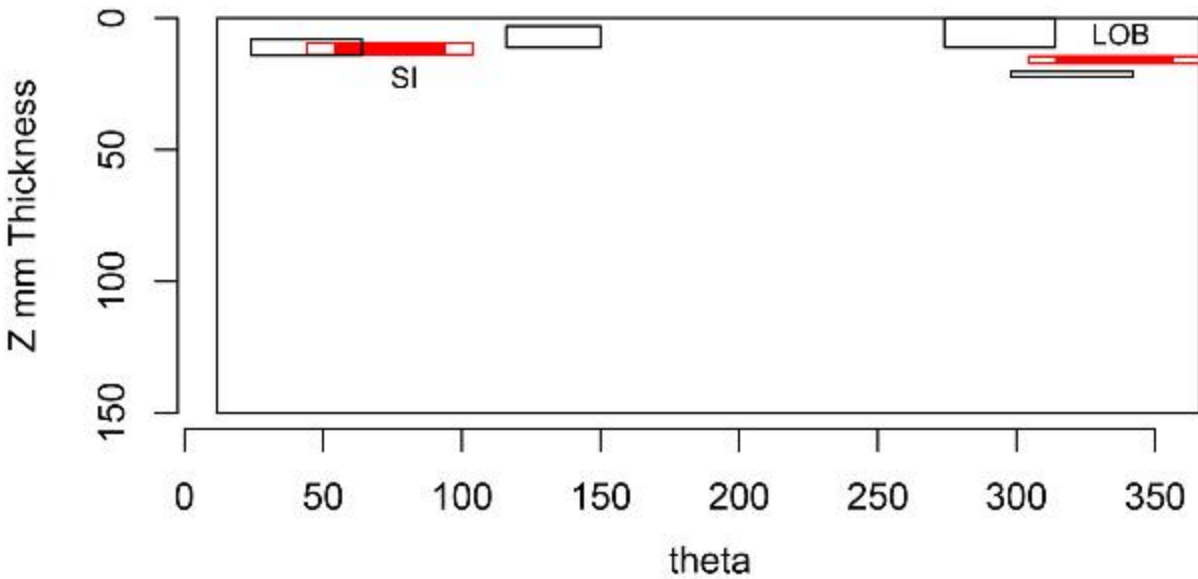


Figure E.240 Indication Plot for Procedure TOFD.ECT.126 Applied to Test Block P25 in PARENT Blind Testing (theta - Z view)

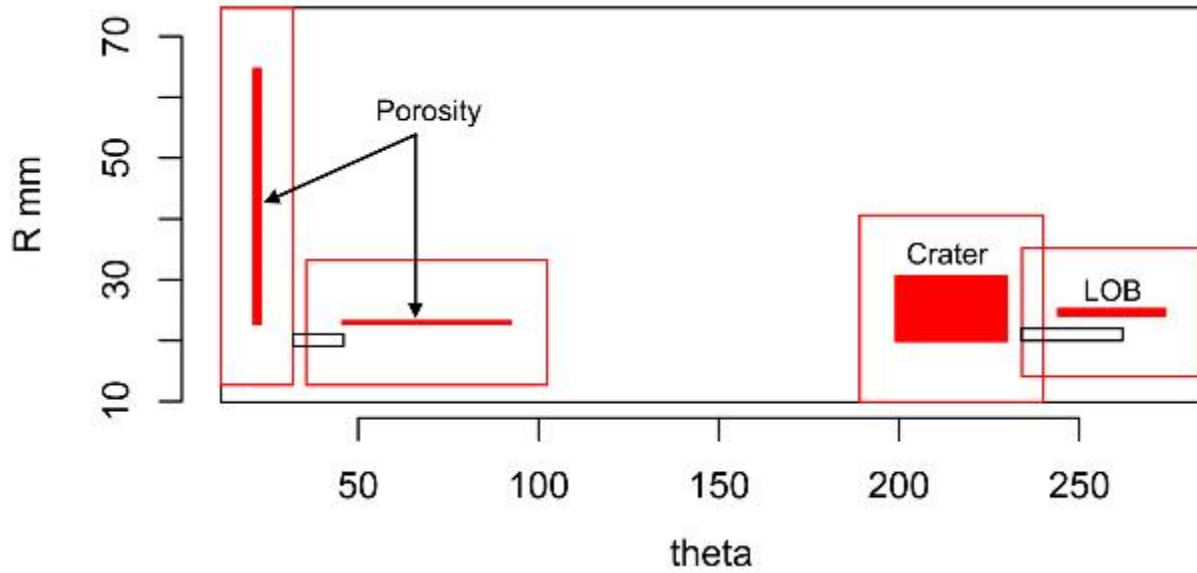


Figure E.241 Indication Plot for Procedure TOFD.ECT.126 Applied to Test Block P26 in PARENT Blind Testing (theta - R view)

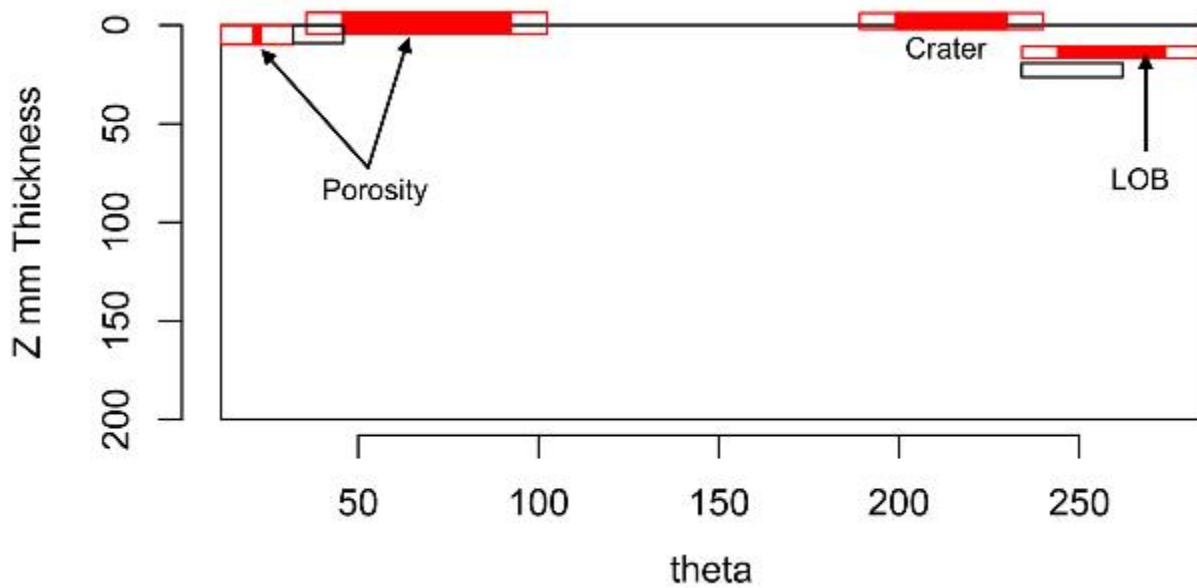


Figure E.242 Indication Plot for Procedure TOFD.ECT.126 Applied to Test Block P26 in PARENT Blind Testing (theta - Z view)

E.4 WOL Inspection Summary Results

E.4.1 Plots for Team 108

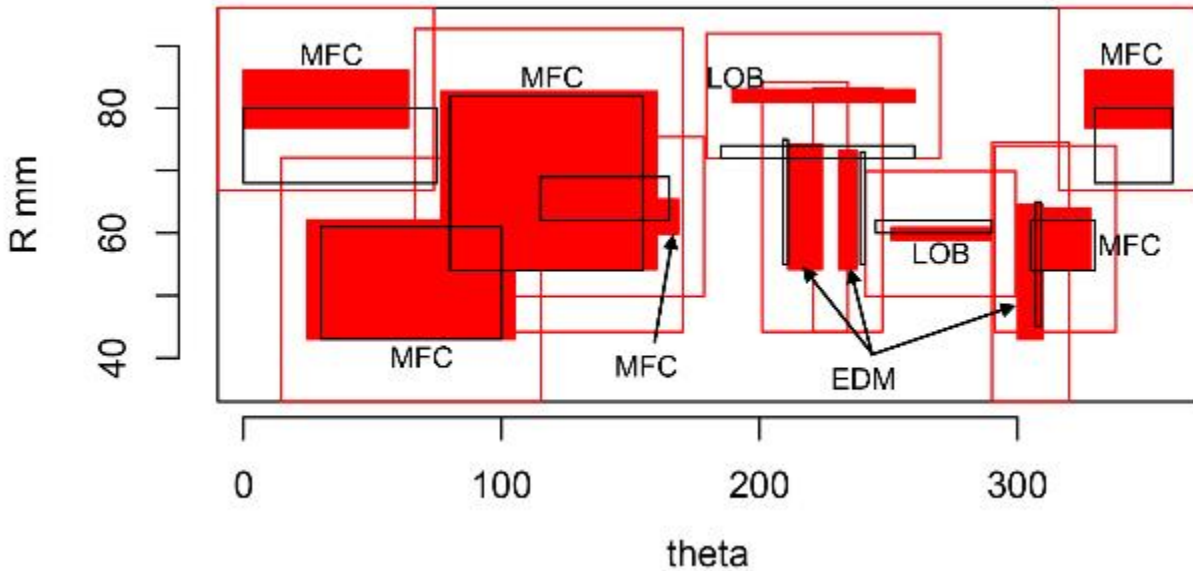


Figure E.243 Indication Plot for Procedure PAUT.108.WOL Applied to Test Block P27 in PARENT Blind Testing (theta - R view)

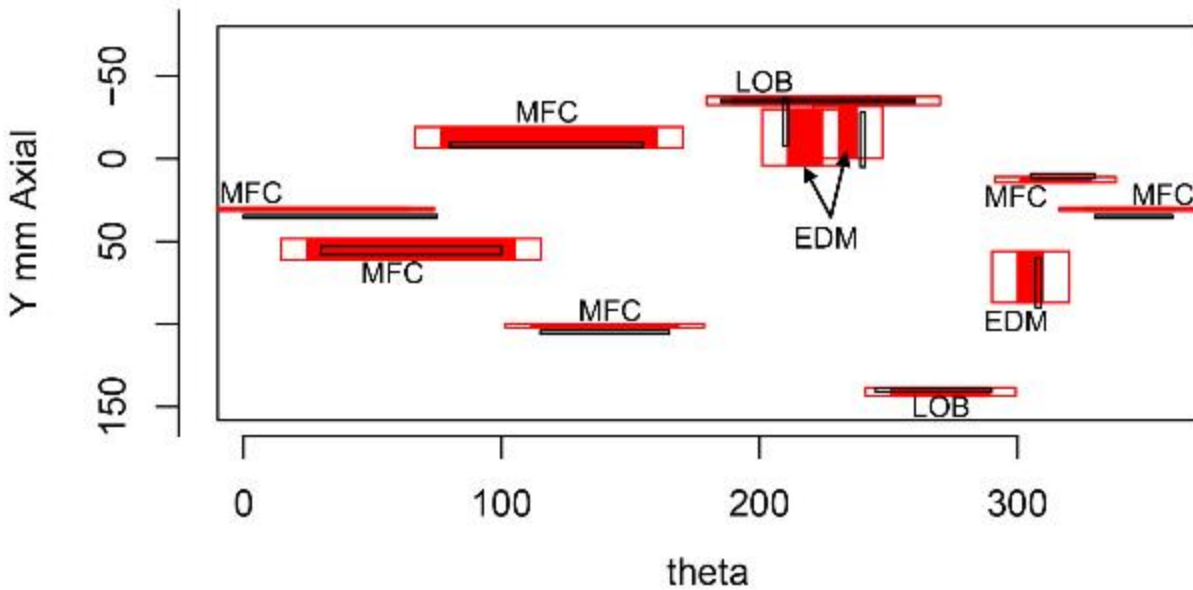


Figure E.244 Indication Plot for Procedure PAUT.108.WOL Applied to Test Block P27 in PARENT Blind Testing (theta - Z view)

E.4.2 Plots for Team 126

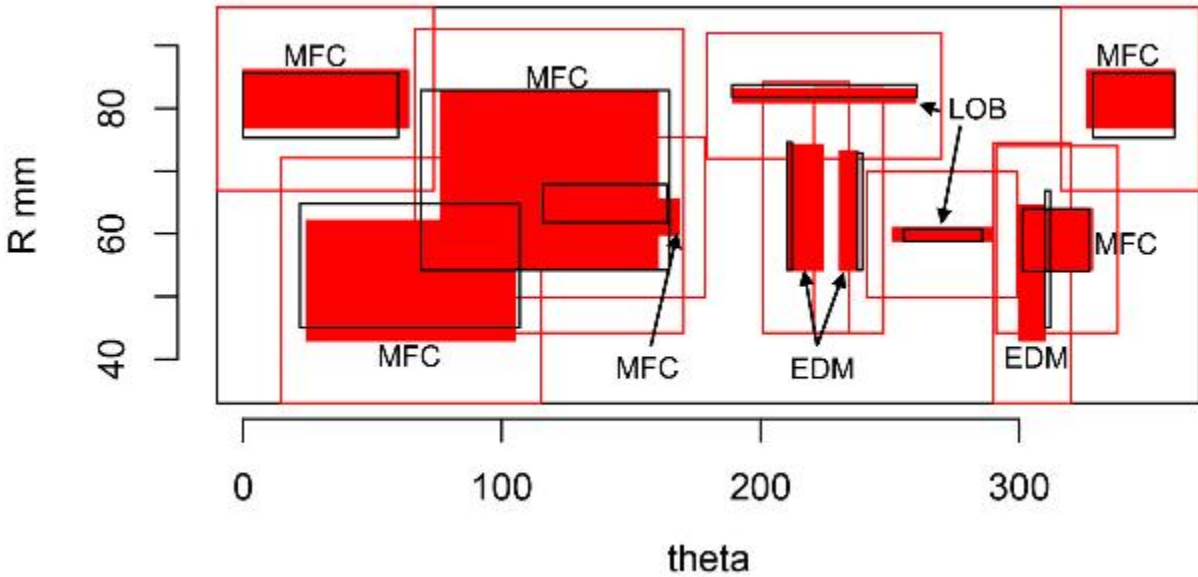


Figure E.245 Indication Plot for Procedure PAUT.126.WOL Applied to Test Block P27 in PARENT Blind Testing (theta - R view)

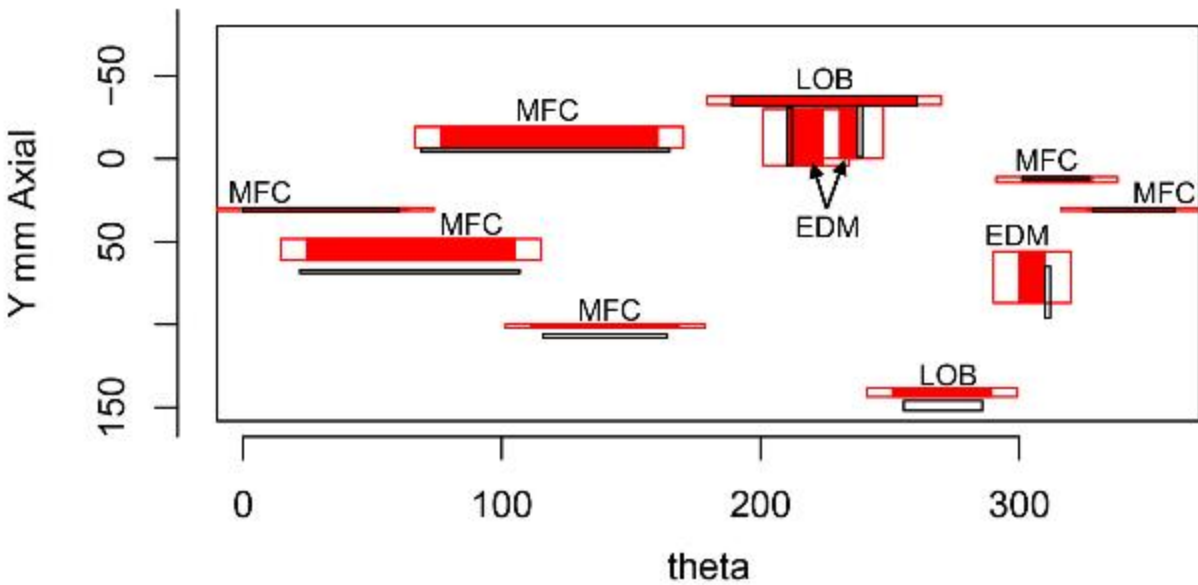


Figure E.246 Indication Plot for Procedure PAUT.126.WOL Applied to Test Block P27 in PARENT Blind Testing (theta - Z view)

APPENDIX F

PROBABILITY OF DETECTION CURVES

APPENDIX F

PROBABILITY OF DETECTION CURVES

Contents

F.1	Probability of Detection Curves	F-2
F.1.1	POD vs. Flaw Depth Results	F-2
F.1.1.1	POD vs. Flaw Depth Results for LBDMWs (I.D. Access)	F-2
F.1.1.2	POD vs. Depth Results for LBDMWs (O.D. Access)	F-5
F.1.1.3	POD vs. Depth Results for SBDMWs	F-6
F.1.1.4	POD vs. Depth Results for BMIs (Tube I.D. Access)	F-8
F.1.2	POD vs. Length Results	F-10
F.1.2.1	POD vs. Length Results for LBDMWs (I.D. Access)	F-10
F.1.2.2	POD vs. Length Results for LBDMWs (O.D. Access)	F-13
F.1.2.3	POD vs. Length Results for SBDMWs	F-14
F.1.2.4	POD vs. Length Results for BMIs (J-Groove Surface)	F-16
F.2	Probability of Detection Curves (Blind + Quick-blind)	F-18
F.2.1	POD vs. Depth Results	F-18
F.2.1.1	POD vs. Depth Results for LBDMWs (I.D. Access)	F-18
F.2.1.2	POD vs. Depth Results for LBDMWs (O.D. Access)	F-20
F.2.2	POD vs. Length Results	F-22
F.2.2.1	POD vs. Length Results for LBDMWs (I.D. Access)	F-22
F.2.2.2	POD vs. Length Results for LBDMWs (O.D. Access)	F-24

F.1 Probability of Detection Curves

F.1.1 POD vs. Flaw Depth Results

F.1.1.1 POD vs. Flaw Depth Results for LBDMWs (I.D. Access)

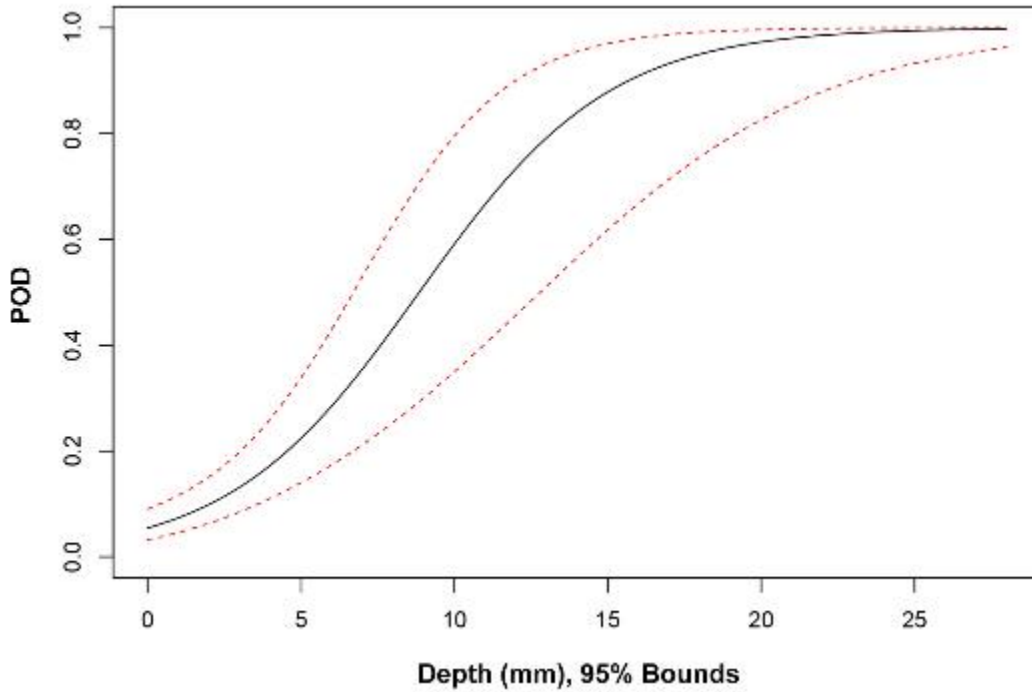


Figure F.1 POD versus Depth (mm) for All Procedures Applied to LBDMW Test Blocks with I.D. Access

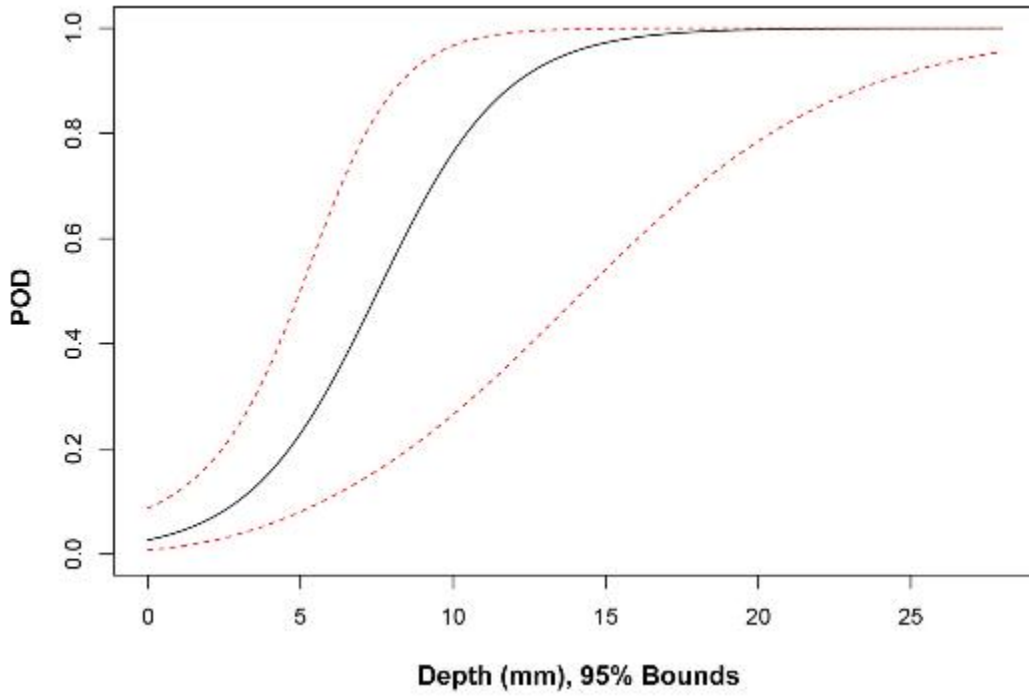


Figure F.2 POD versus Depth (mm) for ECT Procedures Applied to LBDMW Test Blocks with I.D. Access

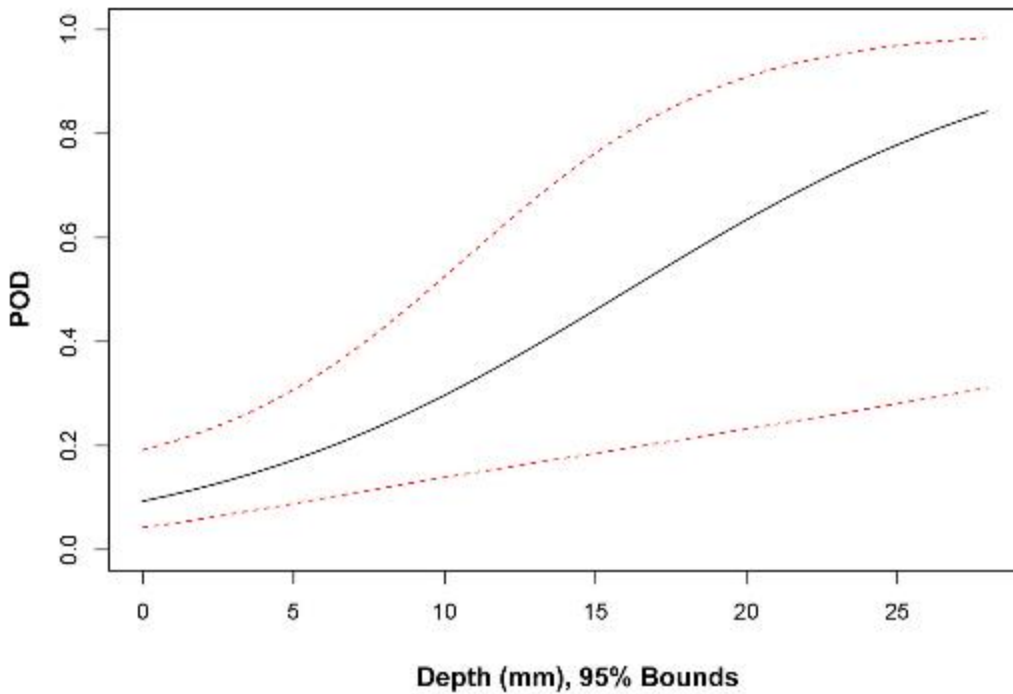


Figure F.3 POD versus Depth (mm) for UT.ECT Procedures Applied to LBDMW Test Blocks with I.D. Access

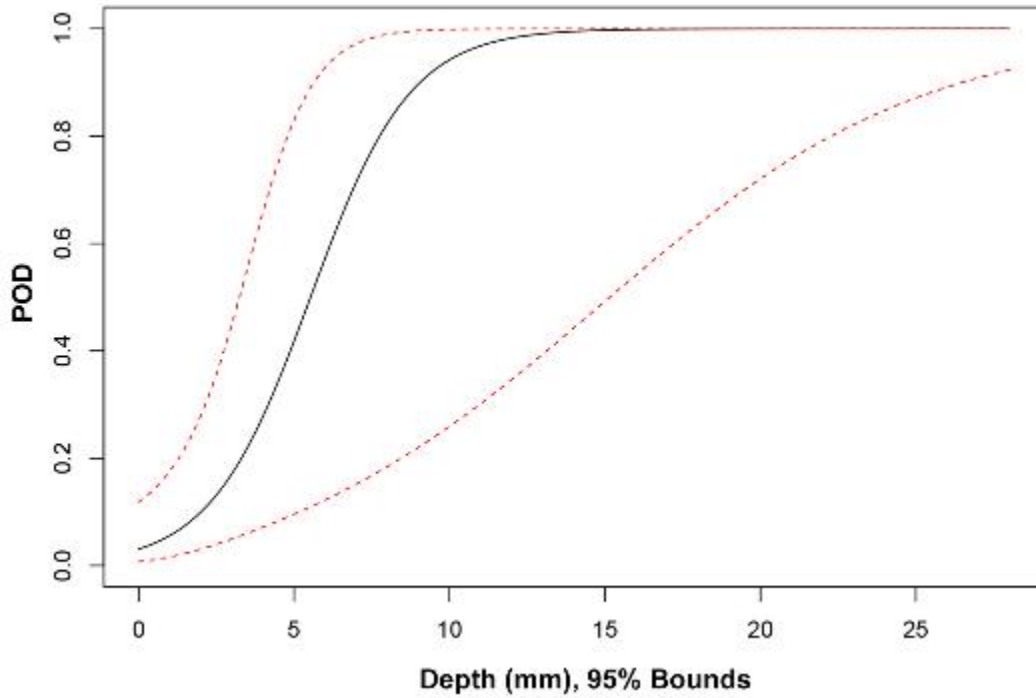


Figure F.4 POD versus Depth (mm) for UT.PAUT Procedures Applied to LBDMW Test Blocks with I.D. Access

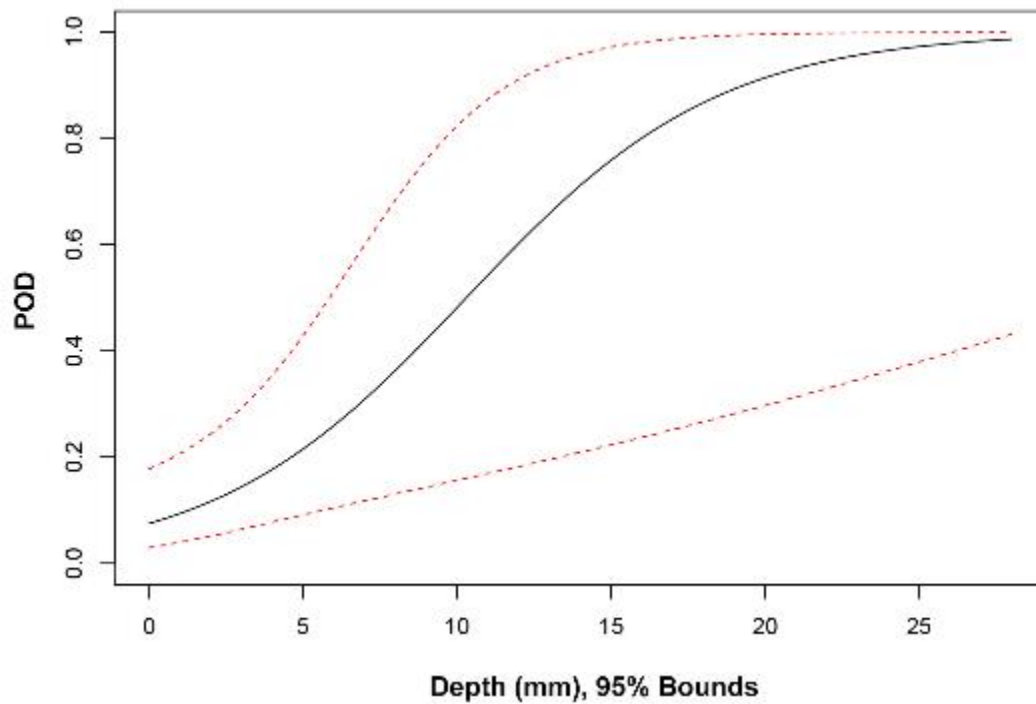


Figure F.5 POD versus Depth (mm) for UT.TOFD.ECT Procedures Applied to LBDMW Test Blocks with I.D. Access

F.1.1.2 POD vs. Depth Results for LBDMWs (O.D. Access)

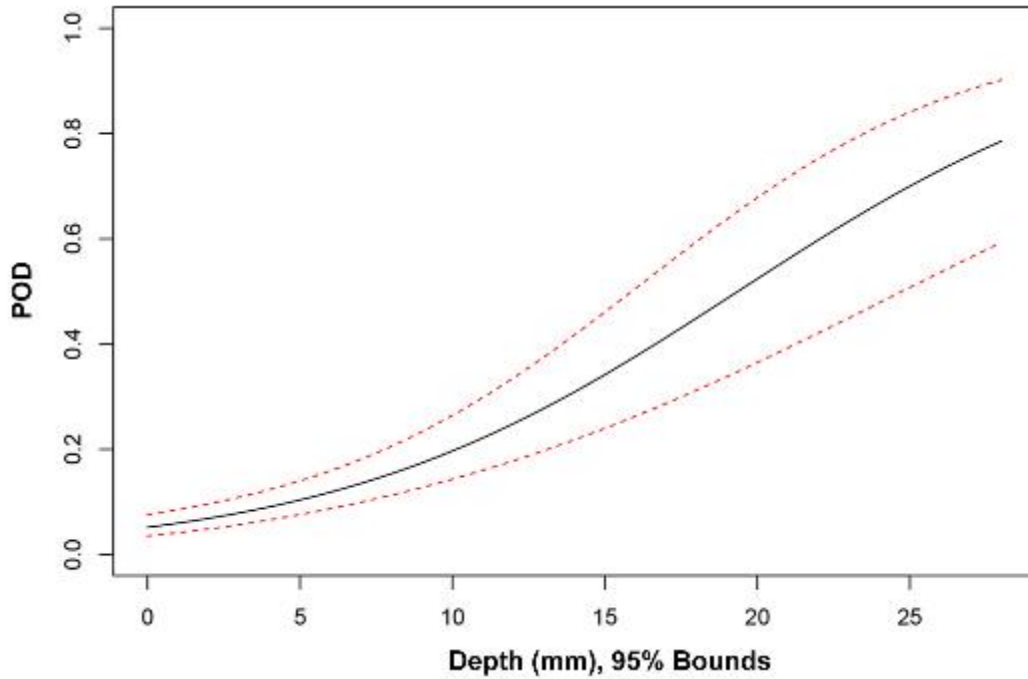


Figure F.6 POD versus Depth (mm) for All Procedures Applied to LBDMW Test Blocks with O.D. Access

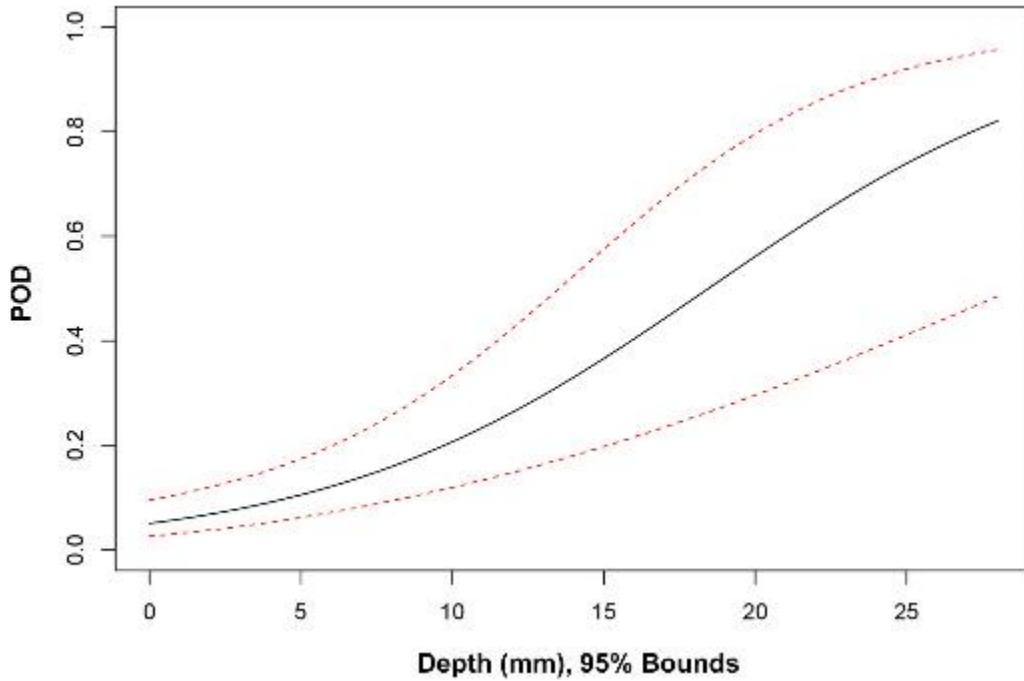


Figure F.7 POD versus Depth (mm) for PAUT Procedures Applied to LBDMW Test Blocks with O.D. Access

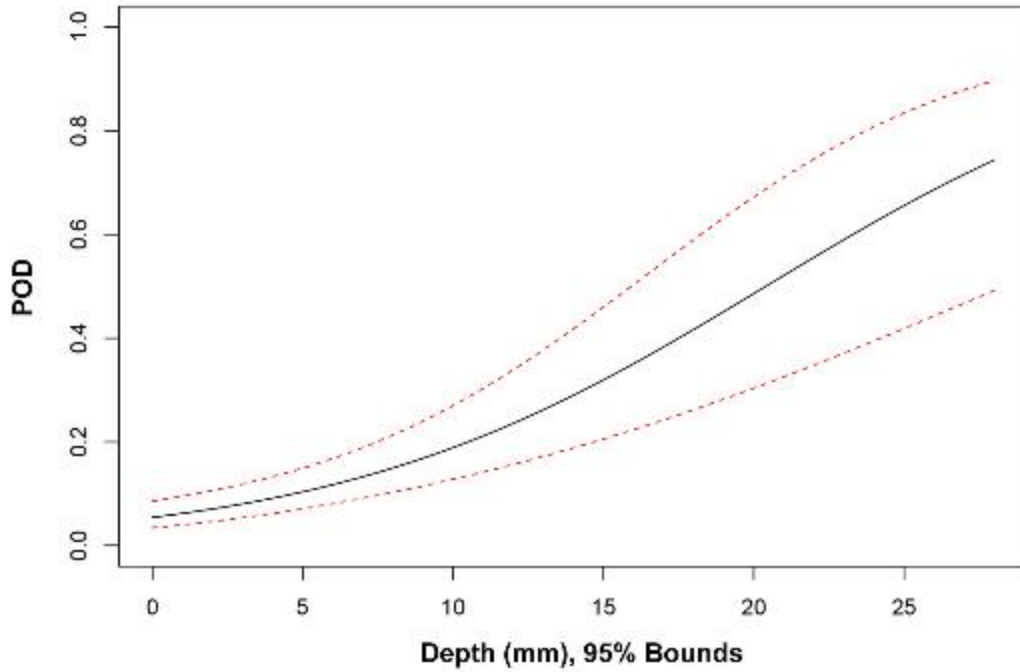


Figure F.8 POD versus Depth (mm) for UT Procedures Applied to LBDMW Test Blocks with O.D. Access

F.1.1.3 POD vs. Depth Results for SBDMWs

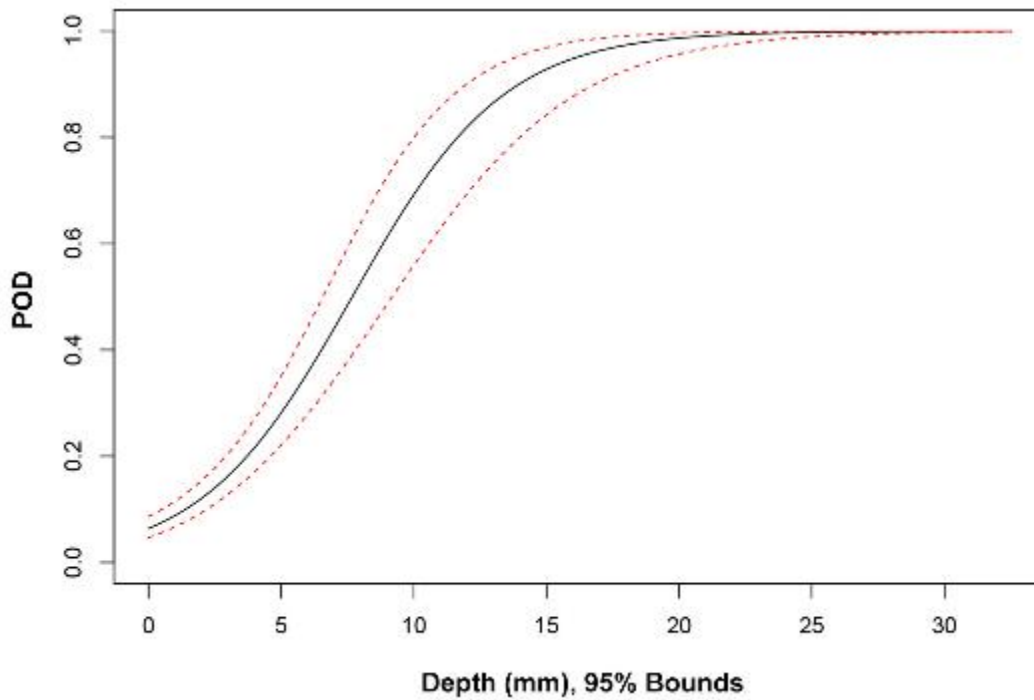


Figure F.9 POD versus Depth (mm) for All Procedures Applied to SBDMW Test Blocks

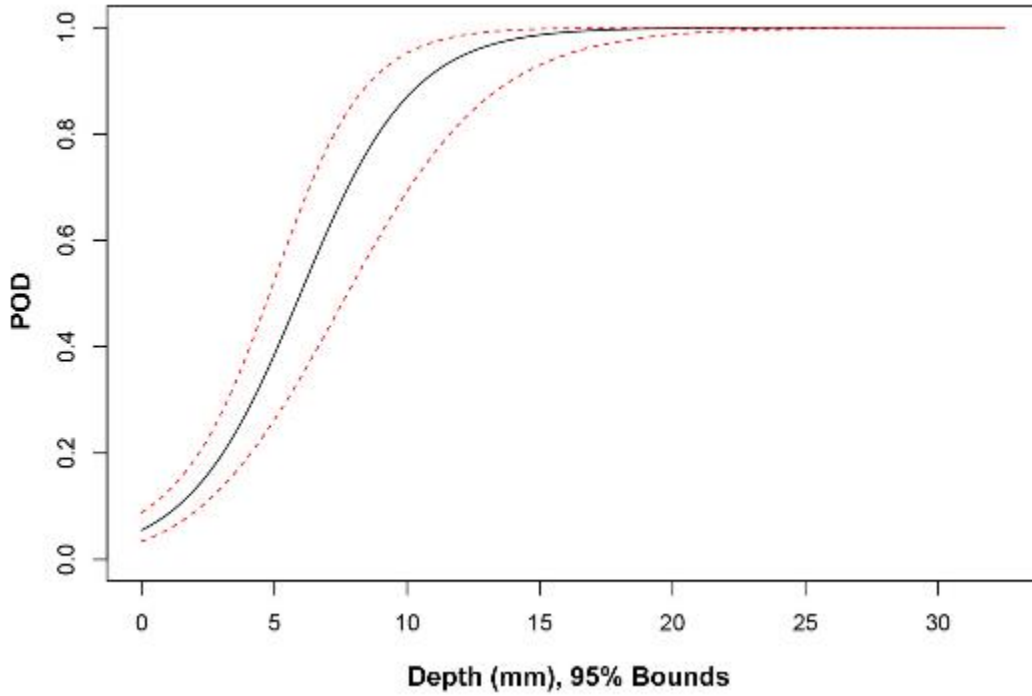


Figure F.10 POD versus Depth (mm) for PAUT Procedures Applied to SBDMW Test Blocks

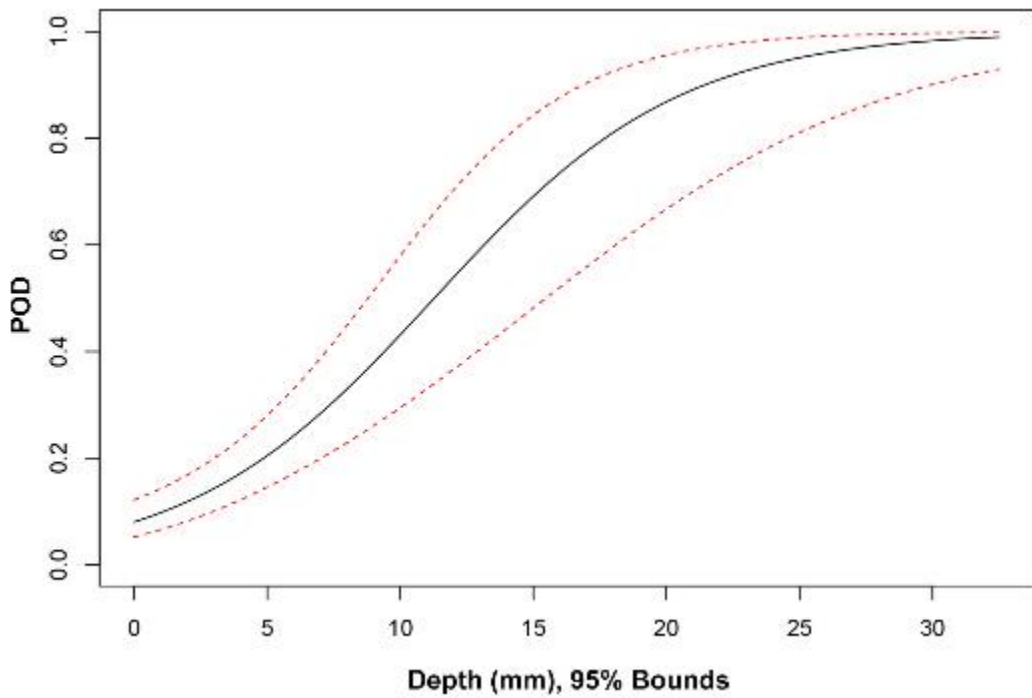


Figure F.11 POD versus Depth (mm) for UT Procedures Applied to SBDMW Test Blocks

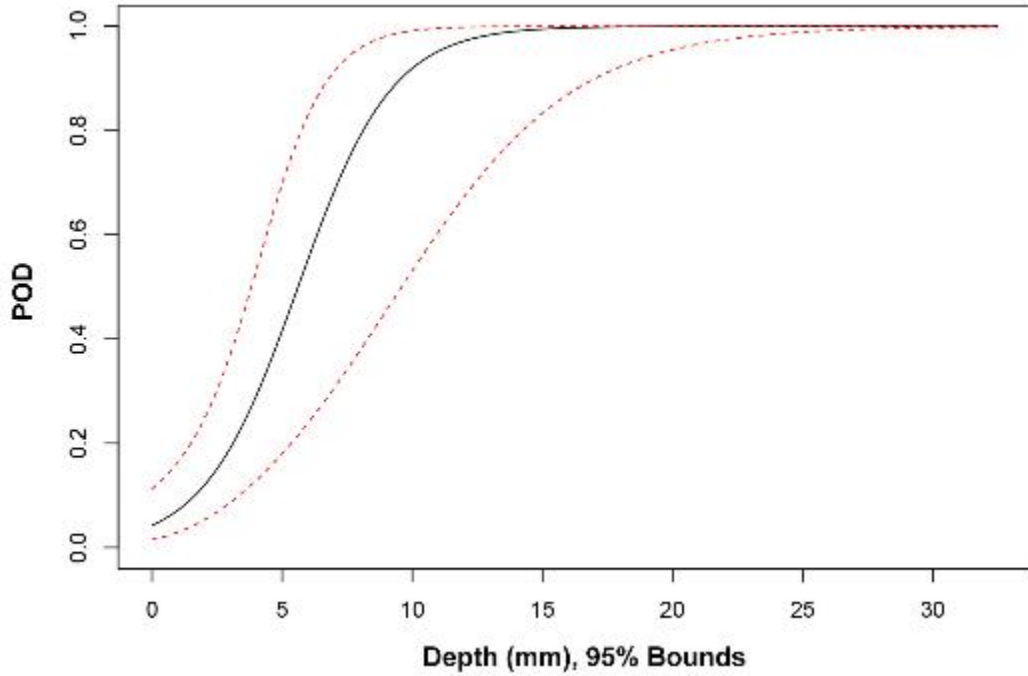


Figure F.12 POD versus Depth (mm) for UT.TOFD Procedures Applied to SBDMW Test Blocks

F.1.1.4 POD vs. Depth Results for BMIs (Tube I.D. Access)

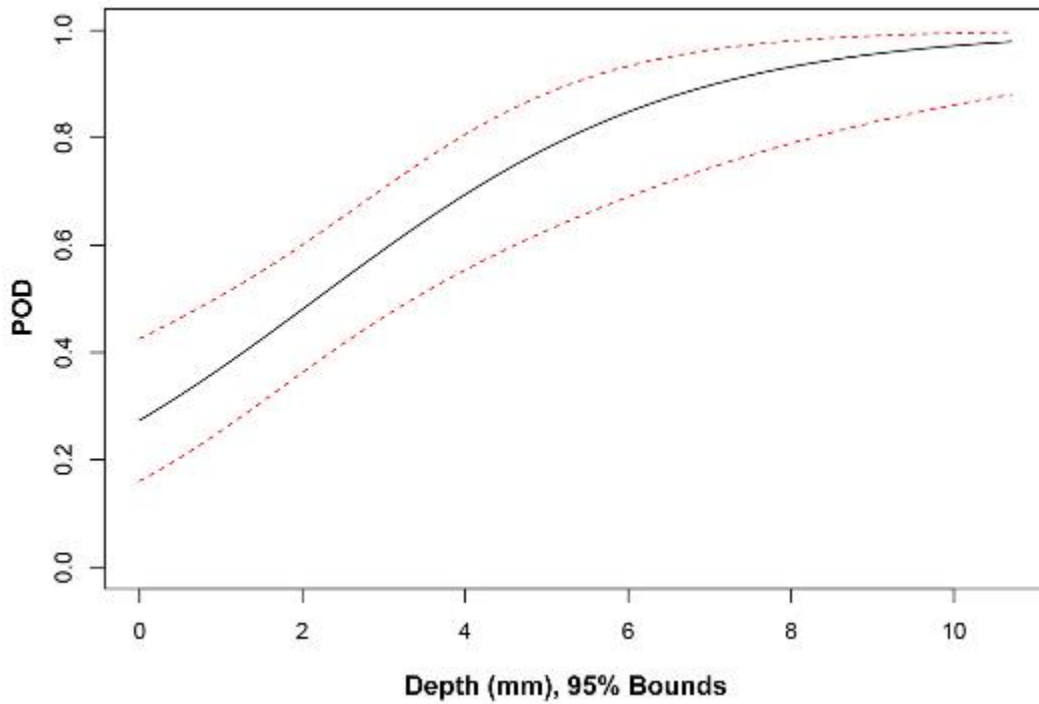


Figure F.13 POD versus Depth (mm) for ECT Procedures Applied to BMI Test Blocks

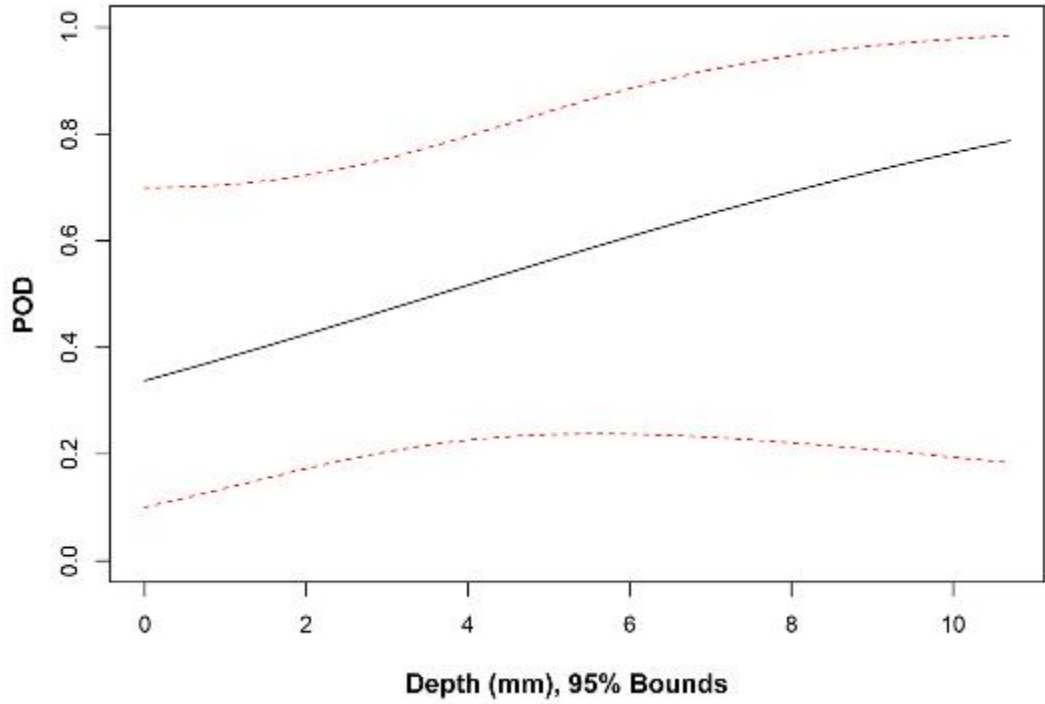


Figure F.14 POD versus Depth (mm) for TOFD Procedures Applied to BMI Test Blocks

F.1.2 POD vs. Length Results

F.1.2.1 POD vs. Length Results for LBDMWs (I.D. Access)

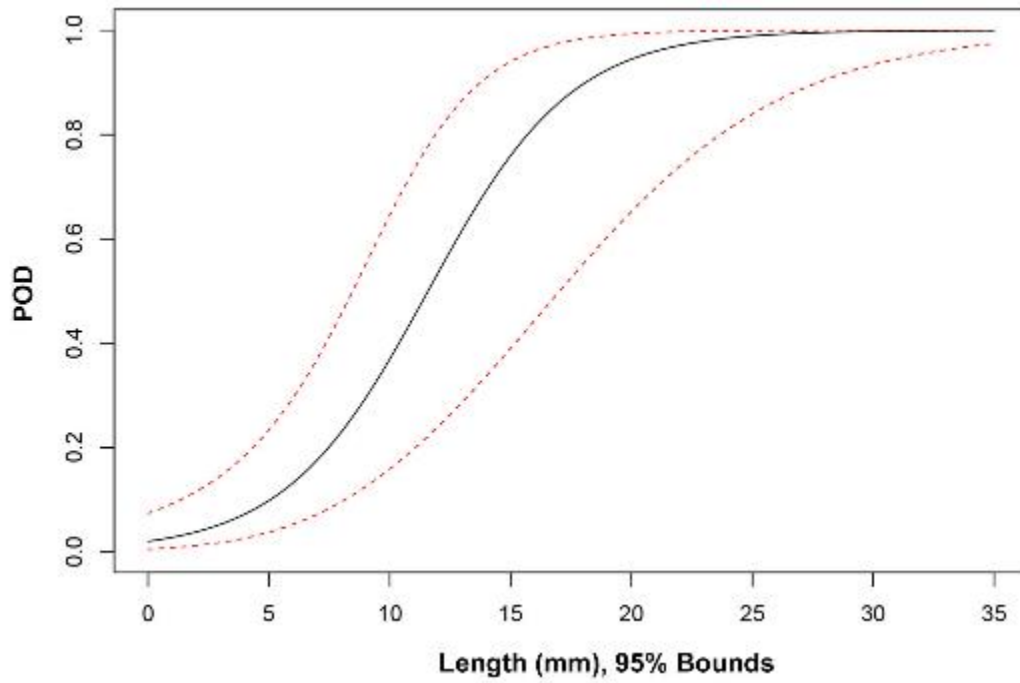


Figure F.15 POD versus Length (mm) for All Procedures Applied to LBDMW Test Blocks with I.D. Access

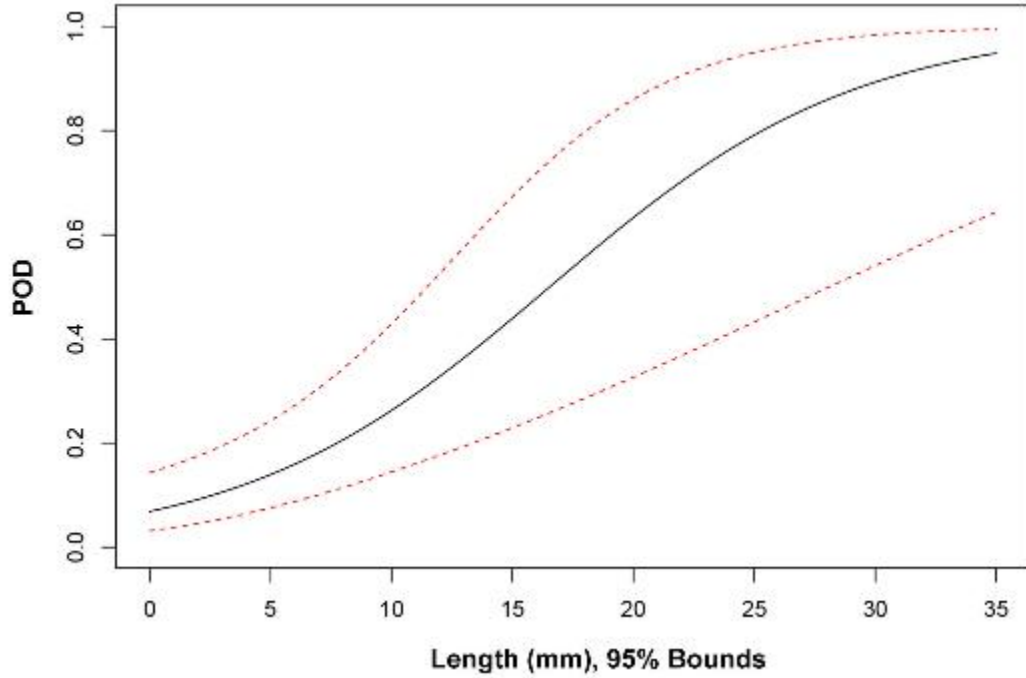


Figure F.16 POD versus Length (mm) for ECT Procedures Applied to LBDMW Test Blocks with I.D. Access

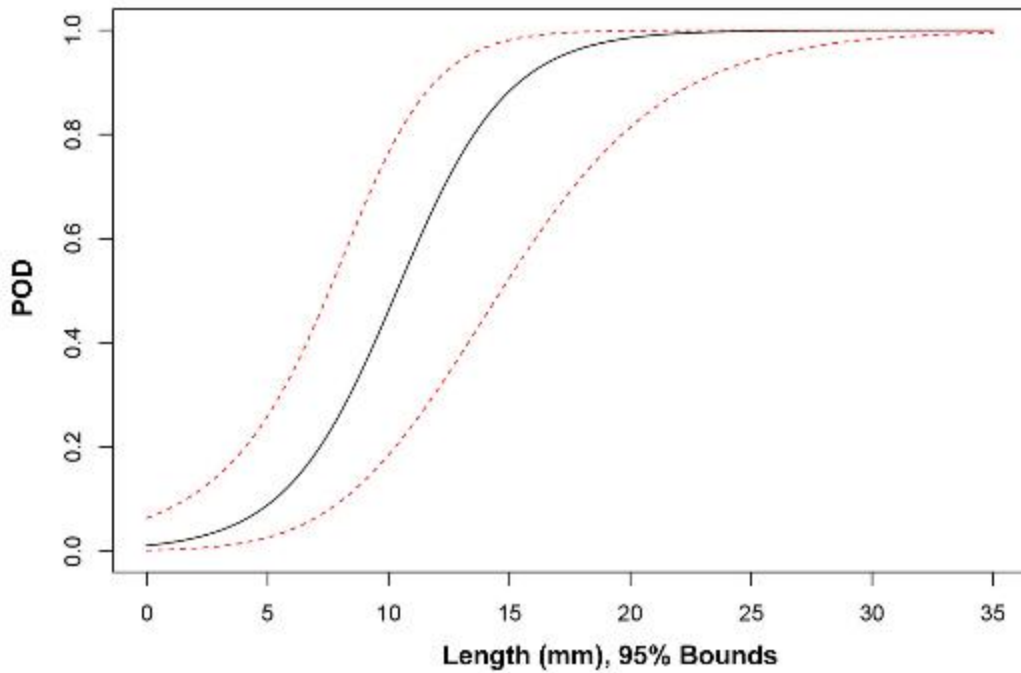


Figure F.17 POD versus Length (mm) for UT.ECT Procedures Applied to LBDMW Test Blocks with I.D. Access

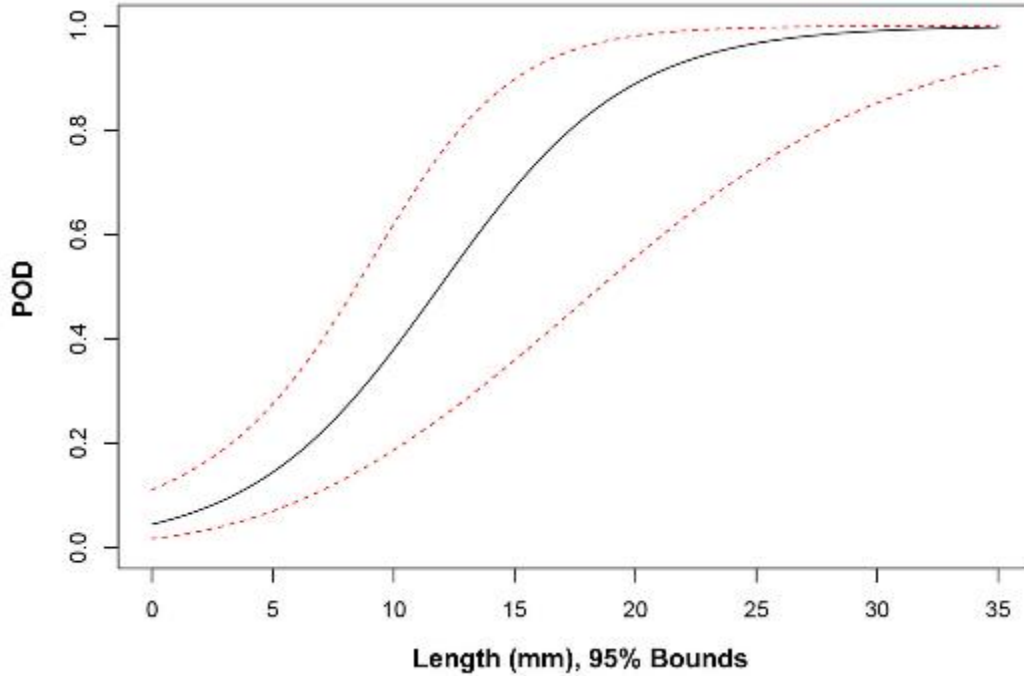


Figure F.18 POD versus Length (mm) for UT.PAUT Procedures Applied to LBDMW Test Blocks with I.D. Access

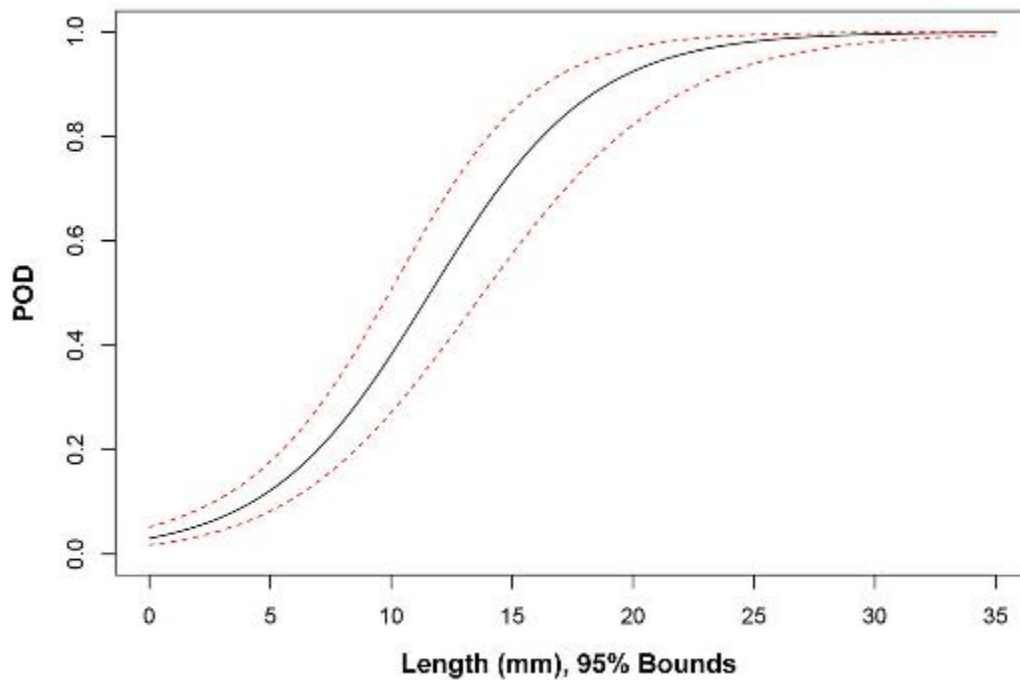


Figure F.19 POD versus Length (mm) for UT.TOFD.ECT Procedures Applied to LBDMW Test Blocks with I.D. Access

F.1.2.2 POD vs. Length Results for LBDMWs (O.D. Access)

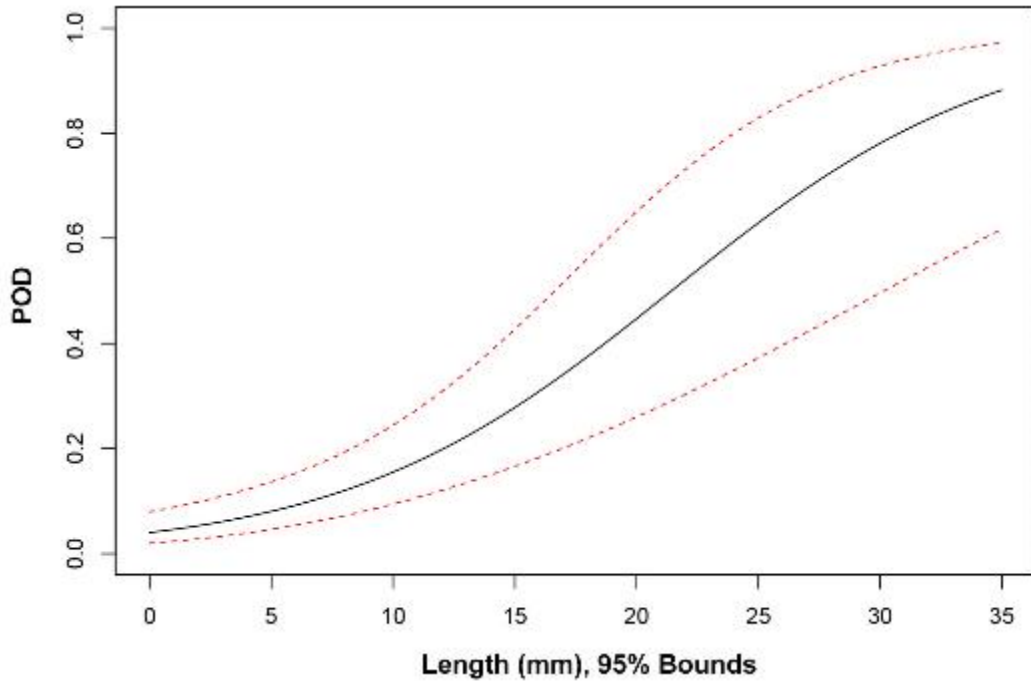


Figure F.20 POD versus Length (mm) for All Procedures Applied to LBDMW Test Blocks with O.D. Access

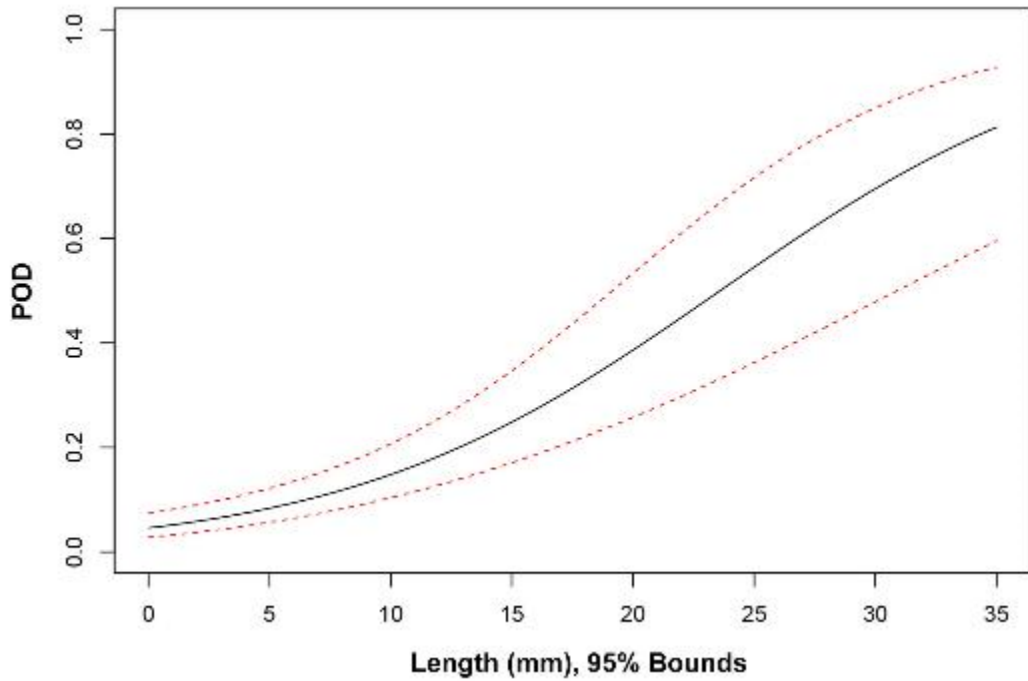


Figure F.21 POD versus Length (mm) for PAUT Procedures Applied to LBDMW Test Blocks with O.D. Access

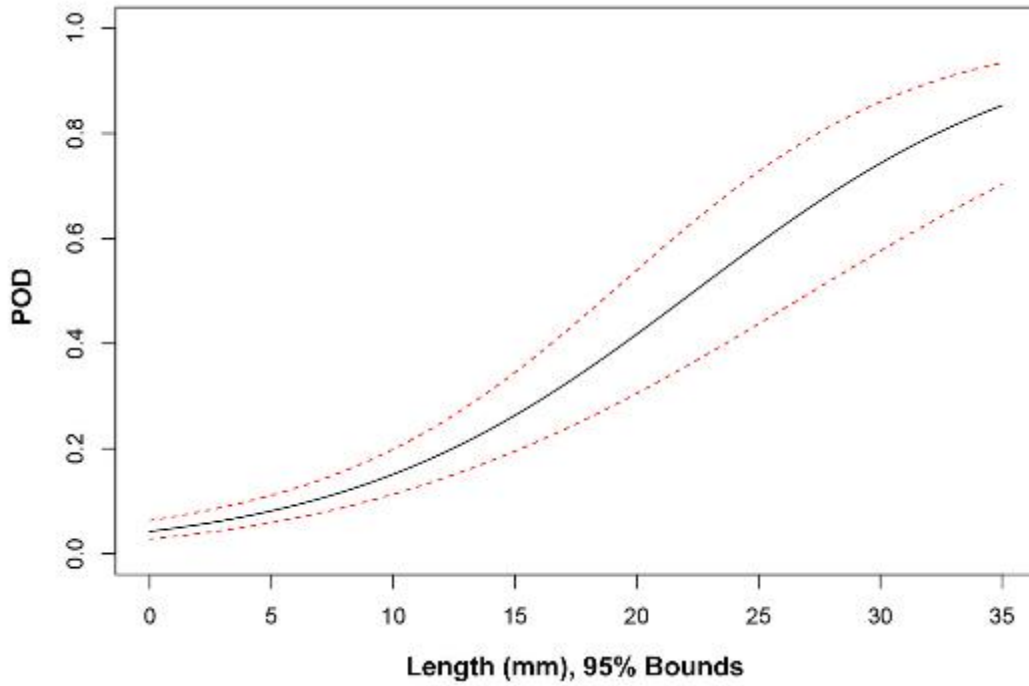


Figure F.22 POD versus Length (mm) for UT Procedures Applied to LBDMW Test Blocks with O.D. Access

F.1.2.3 POD vs. Length Results for SBDMWs

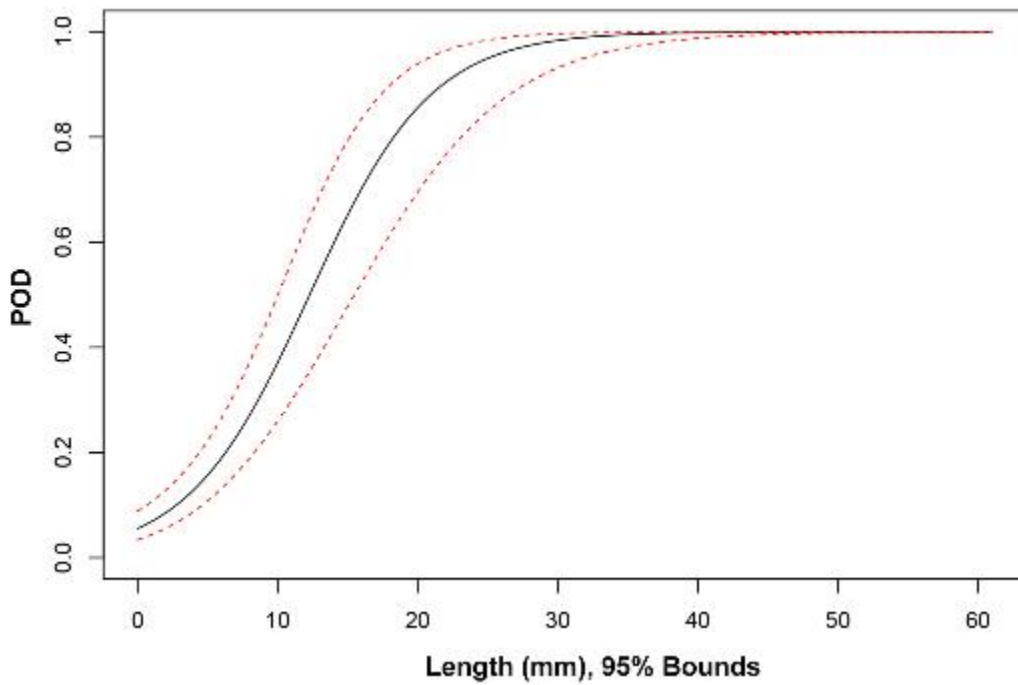


Figure F.23 POD versus Length (mm) for All Procedures Applied to SBDMW Test Blocks

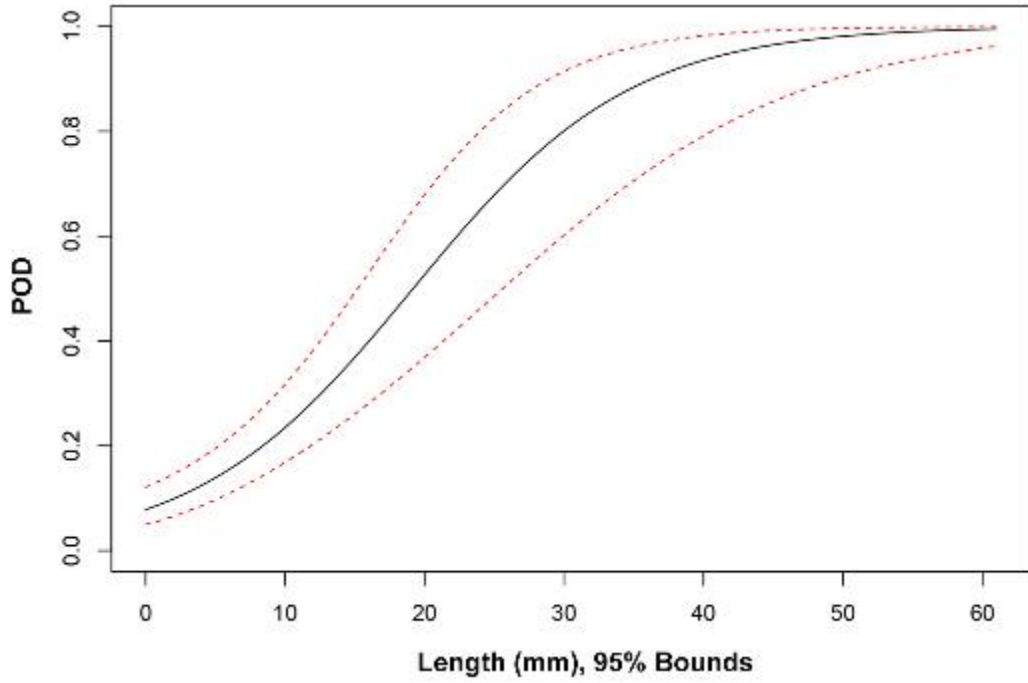


Figure F.24 POD versus Length (mm) for PAUT Procedures Applied to SBDMW Test Blocks

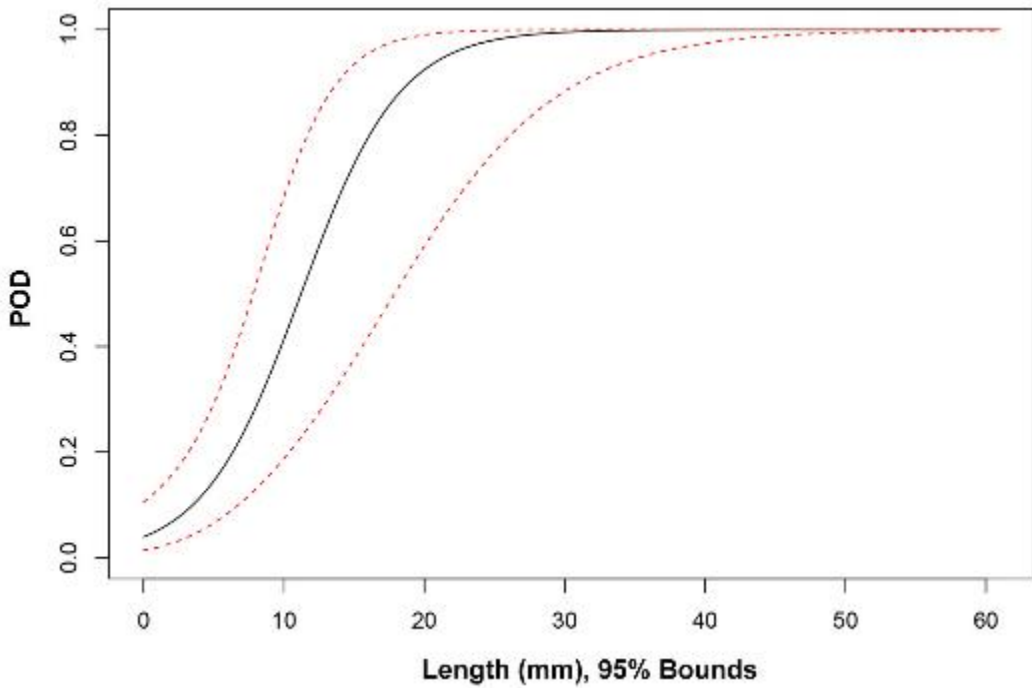


Figure F.25 POD versus Length (mm) for UT Procedures Applied to SBDMW Test Blocks

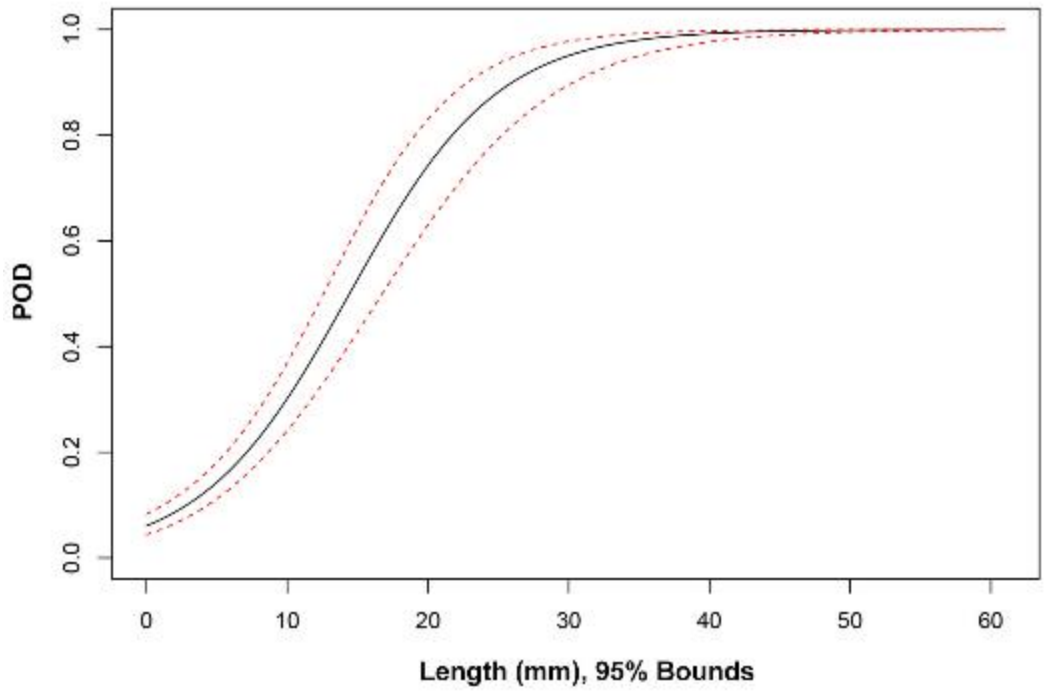


Figure F.26 POD versus Length (mm) for UT.TOFD Procedures Applied to SBDMW Test Blocks

F.1.2.4 POD vs. Length Results for BMIs (J-Groove Surface)

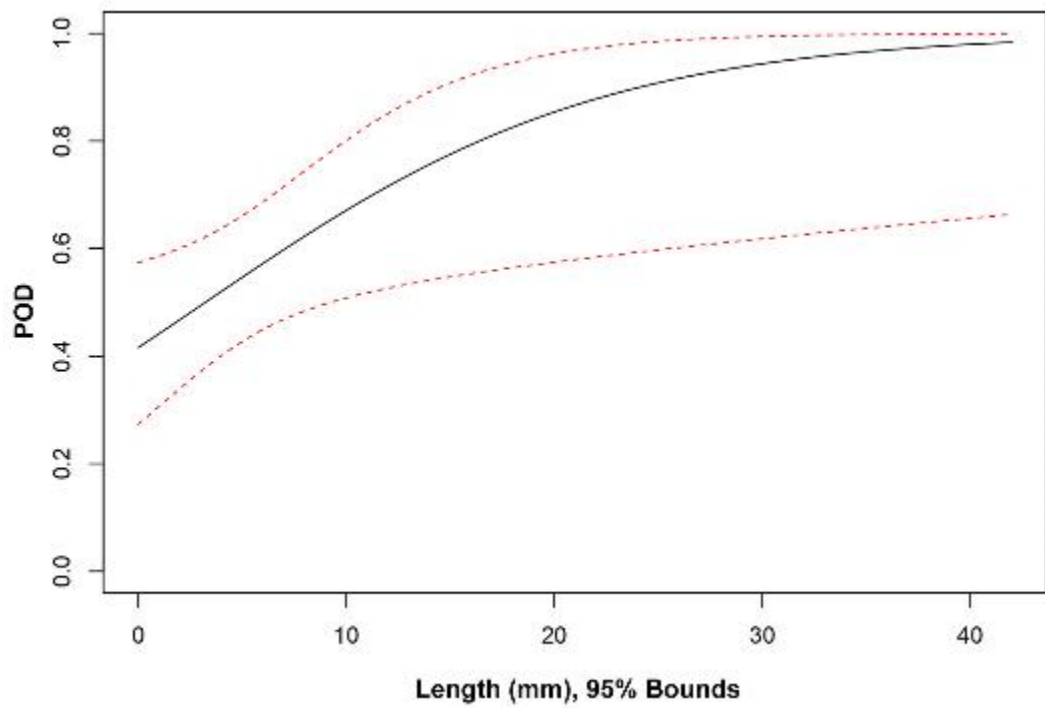


Figure F.27 POD versus Length (mm) for ECT Procedures Applied to BMI Test Blocks

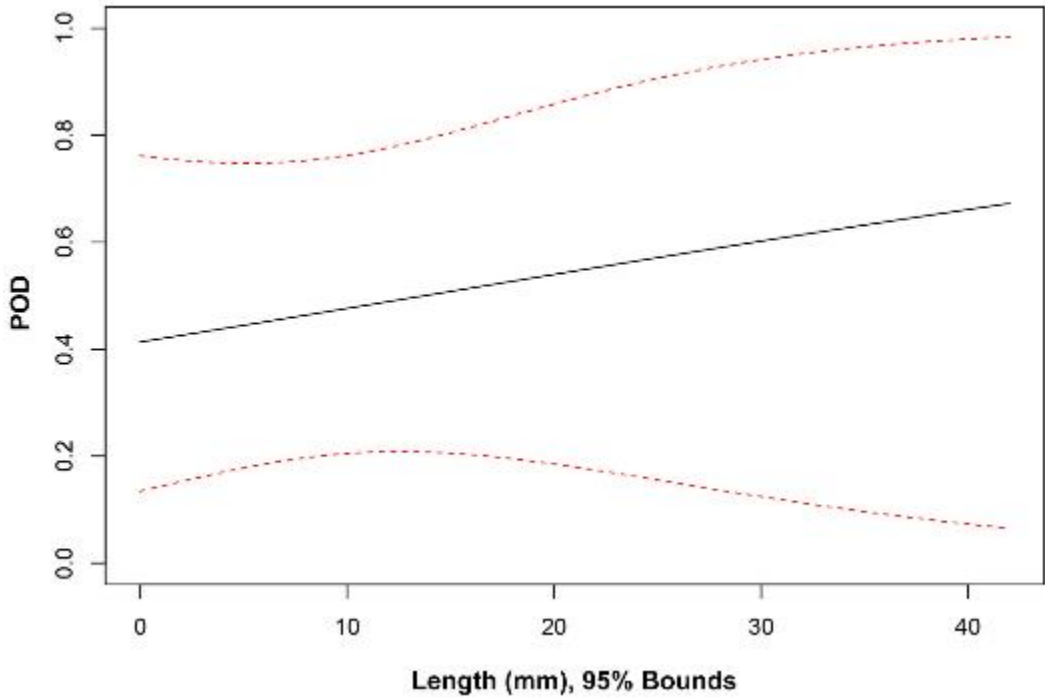


Figure F.28 POD versus Length (mm) for TOFD Procedures Applied to BMI Test Blocks

F.2 Probability of Detection Curves (**Blind + Quick-blind**)

F.2.1 POD vs. Depth Results

F.2.1.1 POD vs. Depth Results for LBDMWs (I.D. Access)

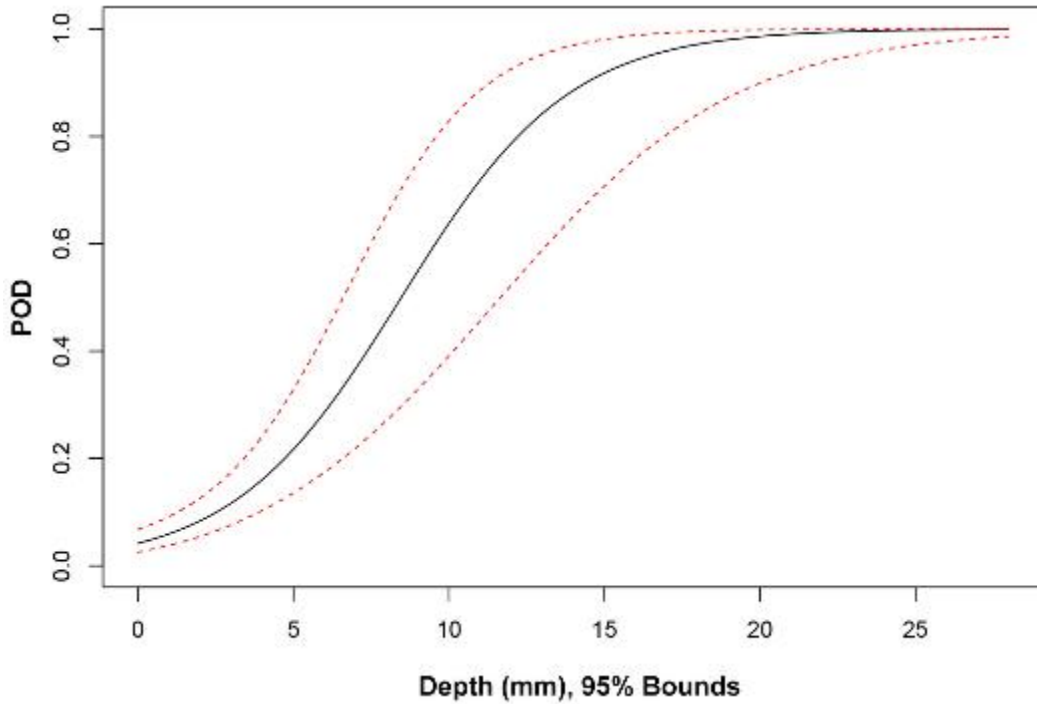


Figure F.29 POD versus Depth (mm) for All Procedures Applied to LBDMW Test Blocks with I.D. Access (**Blind + Quick-blind**)

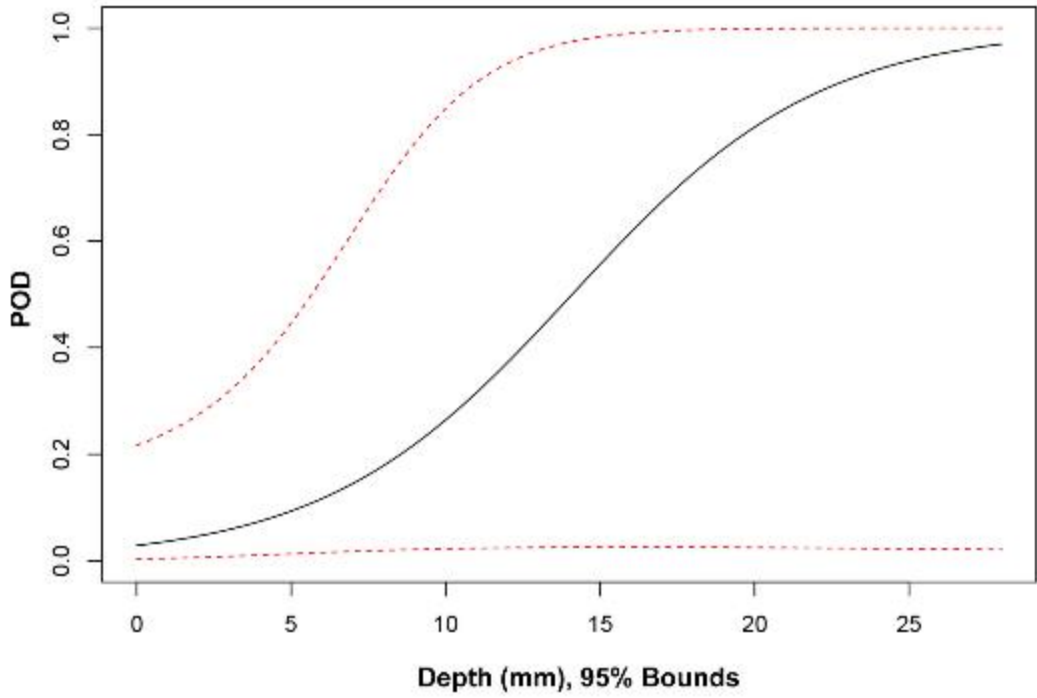


Figure F.30 POD versus Depth (mm) for PAUT Procedures Applied to LBDMW Test Blocks with I.D. Access (Blind + Quick-blind)

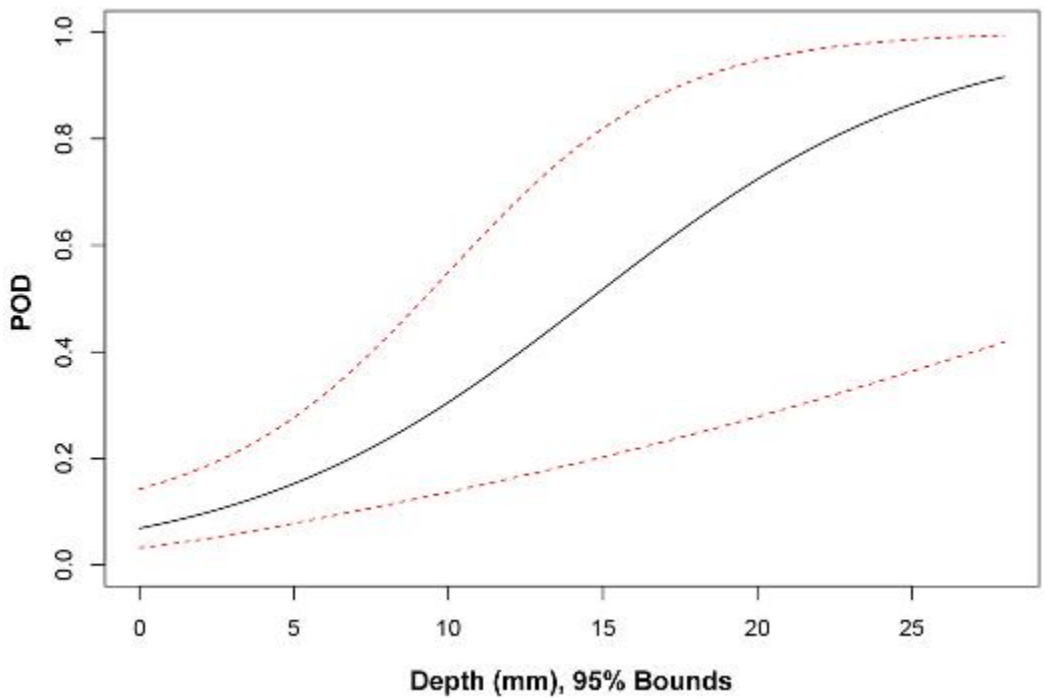


Figure F.31 POD versus Depth (mm) for UT.ECT Procedures Applied to LBDMW Test Blocks with I.D. Access (Blind + Quick-blind)

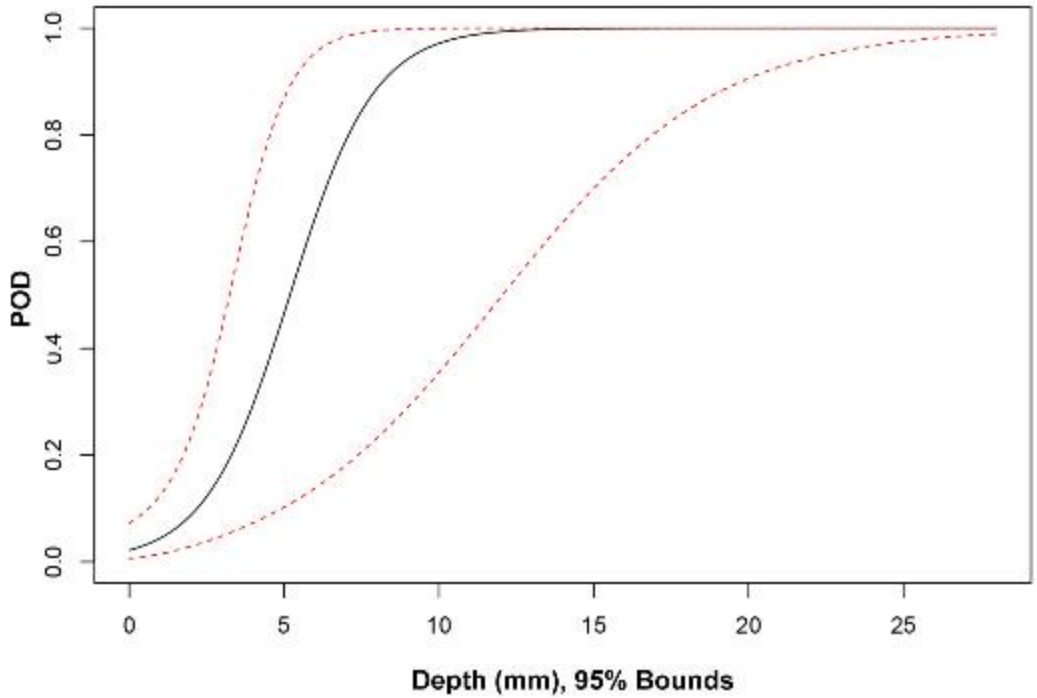


Figure F.32 POD versus Depth (mm) for UT.PAUT Procedures Applied to LBDMW Test Blocks with I.D. Access (**Blind + Quick-blind**)

F.2.1.2 POD vs. Depth Results for LBDMWs (O.D. Access)

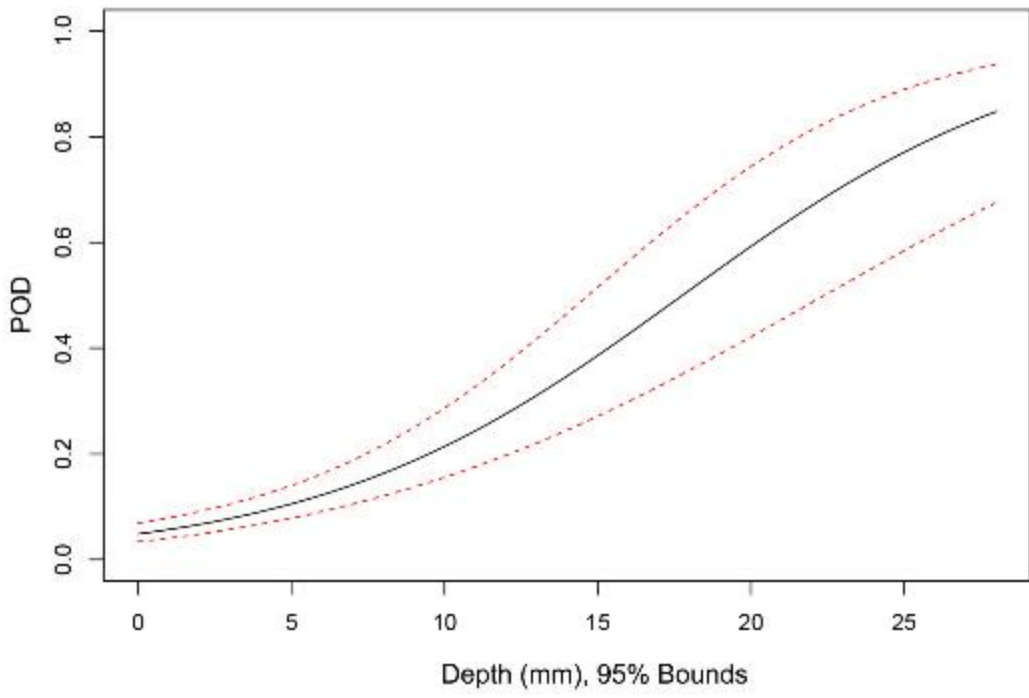


Figure F.33 POD versus Depth (mm) for All Procedures Applied to LBDMW Test Blocks with O.D. Access (**Blind + Quick-blind**)

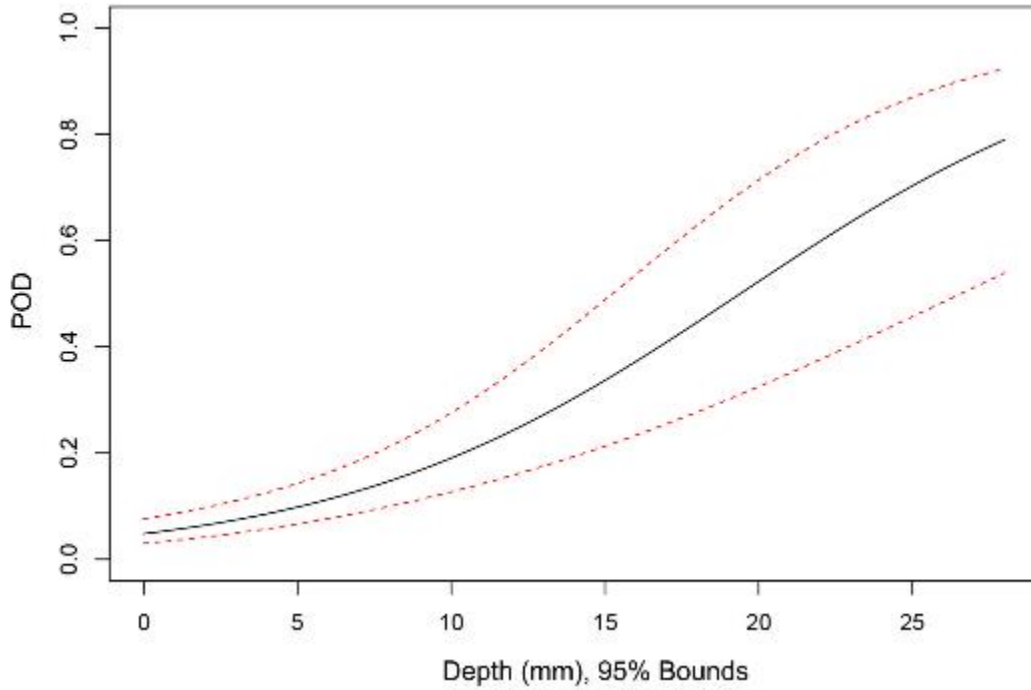


Figure F.34 POD versus Depth (mm) for UT Procedures Applied to LBDMW Test Blocks with O.D. Access (**Blind + Quick-blind**)

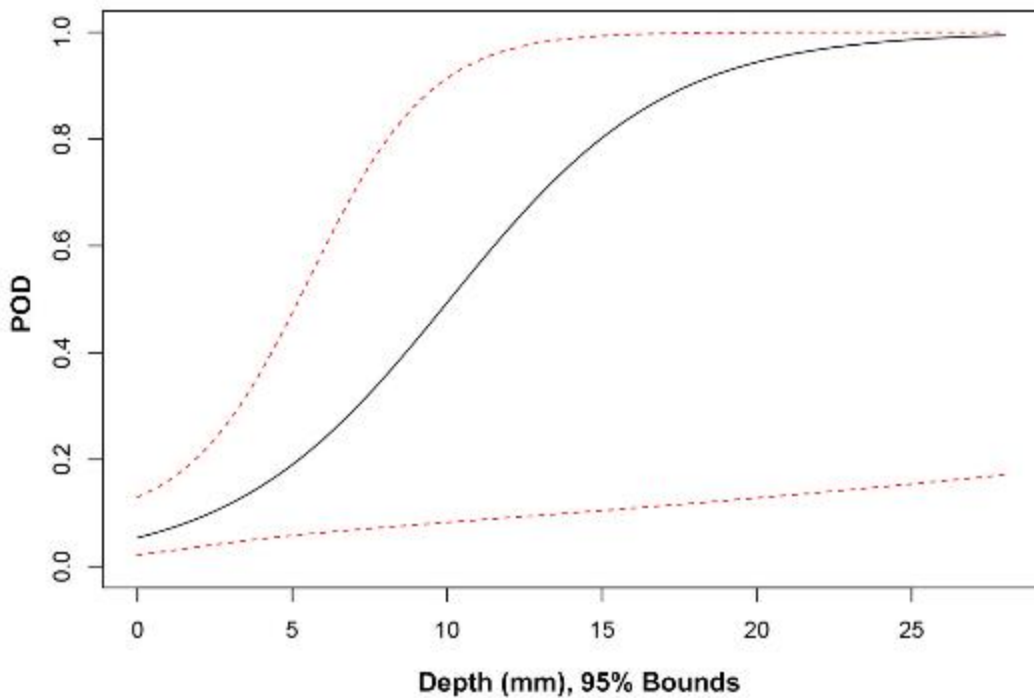


Figure F.35 POD versus Depth (mm) for UT.PAUT Procedures Applied to LBDMW Test Blocks with O.D. Access (**Blind + Quick-blind**)

F.2.2 POD vs. Length Results

F.2.2.1 POD vs. Length Results for LBDMWs (I.D. Access)

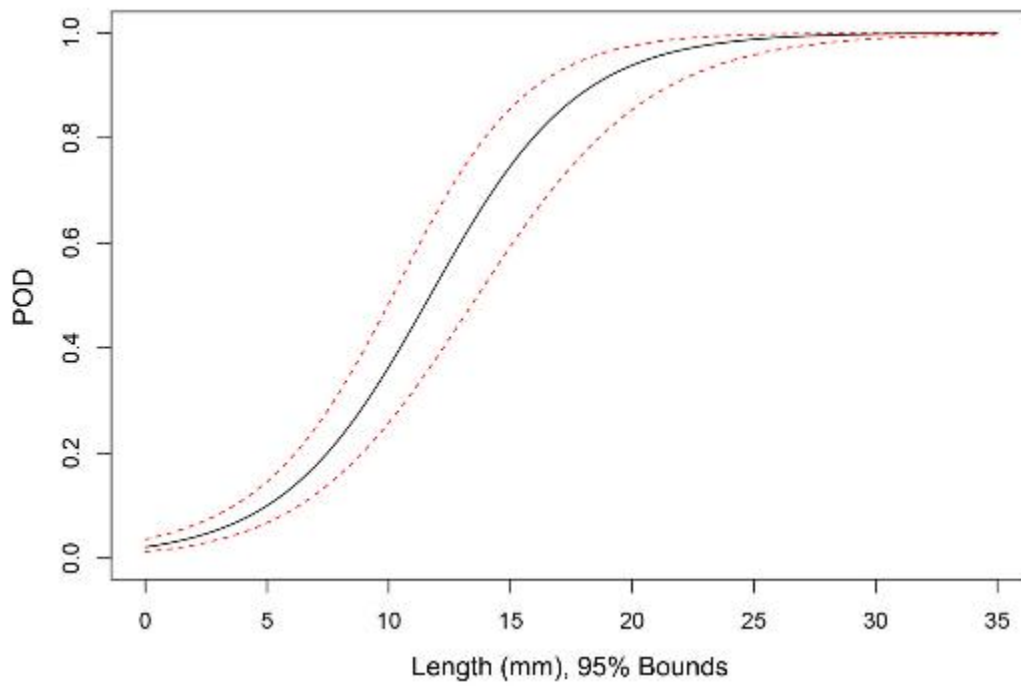


Figure F.36 POD versus Length (mm) for All Procedures Applied to LBDMW Test Blocks with I.D. Access (**Blind + Quick-blind**)

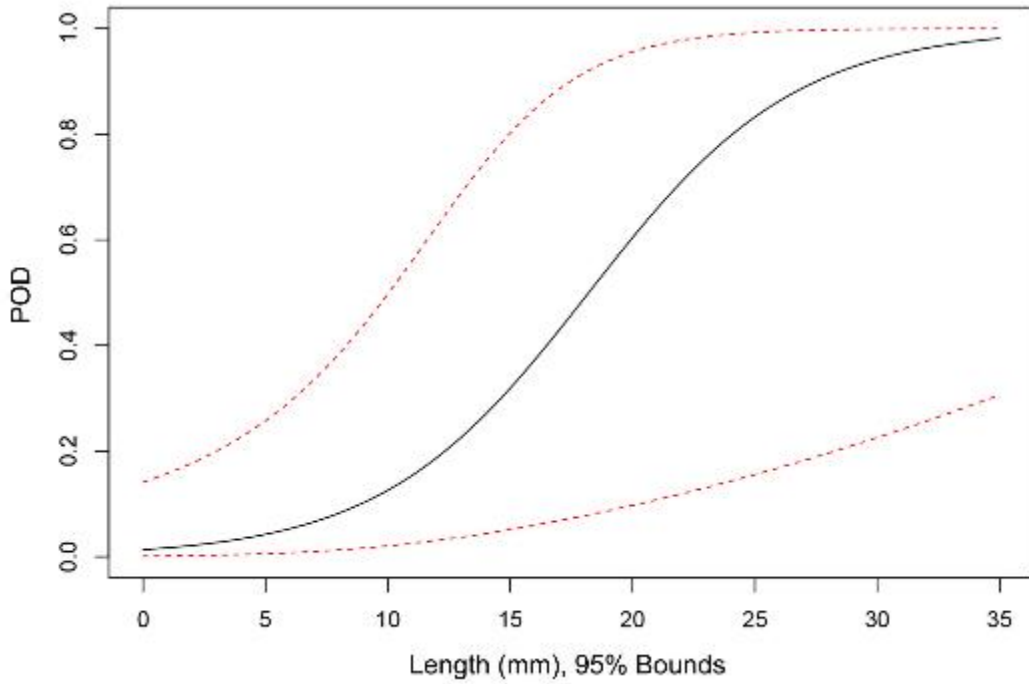


Figure F.37 POD versus Length (mm) for PAUT Procedures Applied to LBDMW Test Blocks with I.D. Access (Blind + Quick-blind)

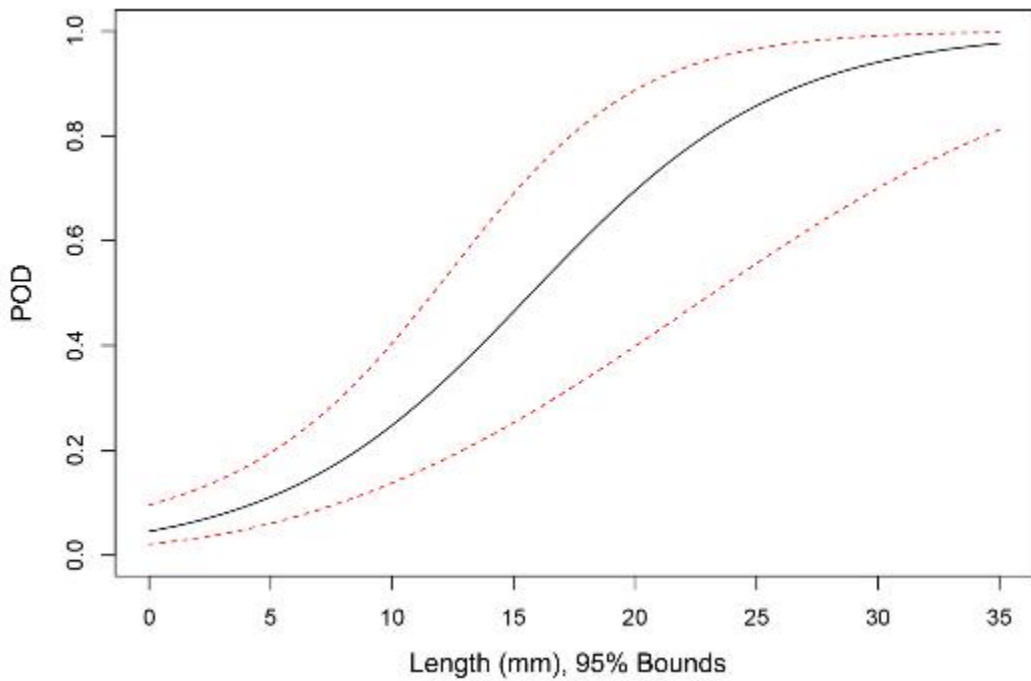


Figure F.38 POD versus Length (mm) for UT.ECT Procedures Applied to LBDMW Test Blocks with I.D. Access (Blind + Quick-blind)

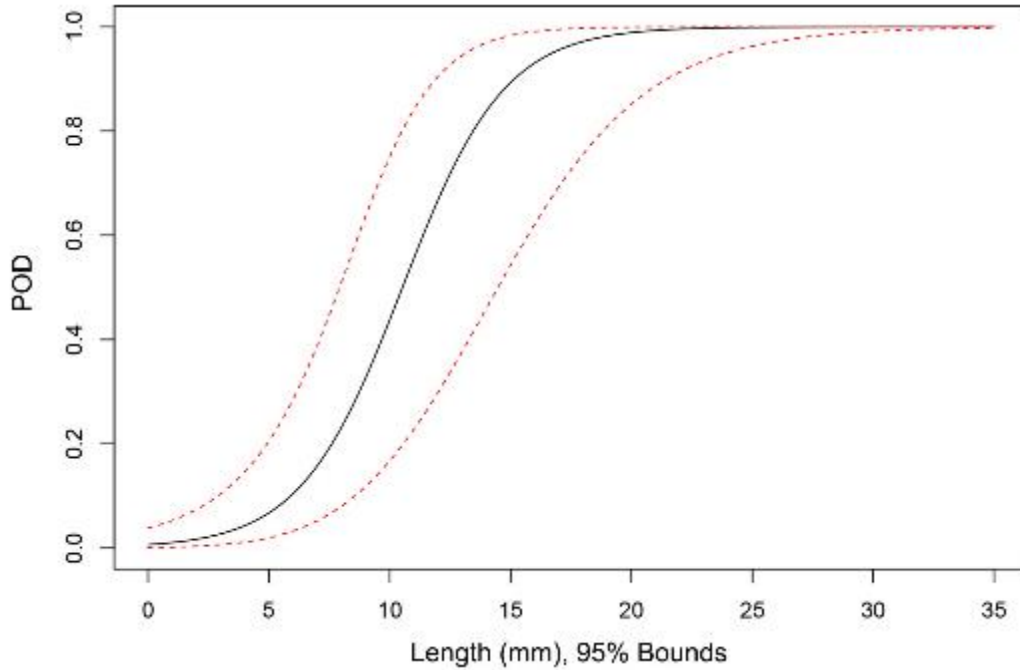


Figure F.39 POD versus Length (mm) for UT.PAUT Procedures Applied to LBDMW Test Blocks with I.D. Access (Blind + Quick-blind)

F.2.2.2 POD vs. Length Results for LBDMWs (O.D. Access)

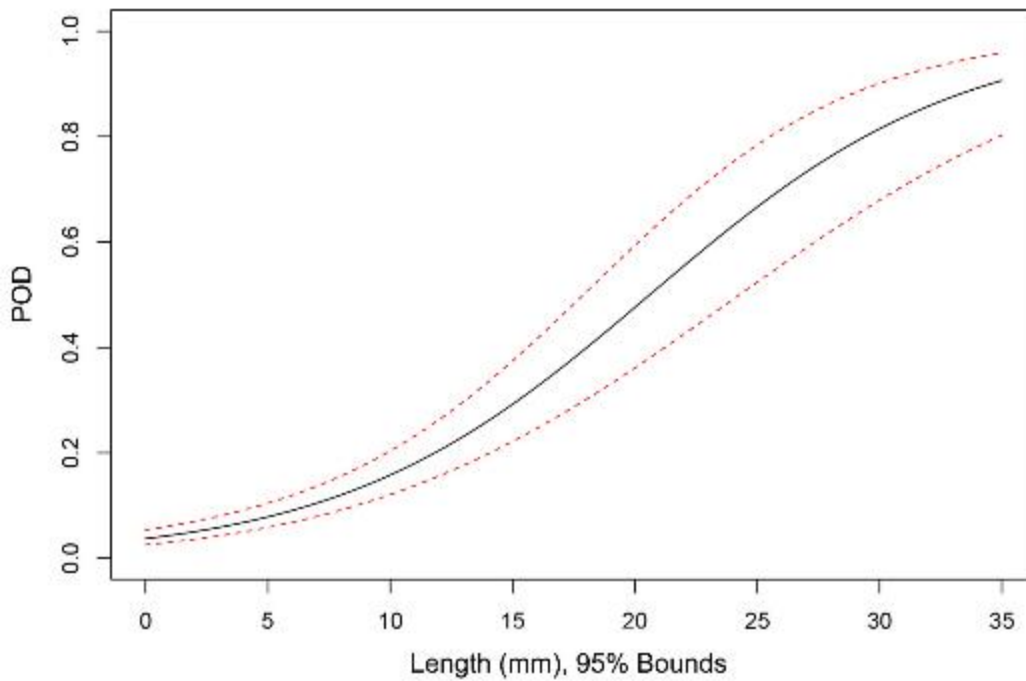


Figure F.40 POD versus Length (mm) for All Procedures Applied to LBDMW Test Blocks with O.D. Access (Blind + Quick-blind)

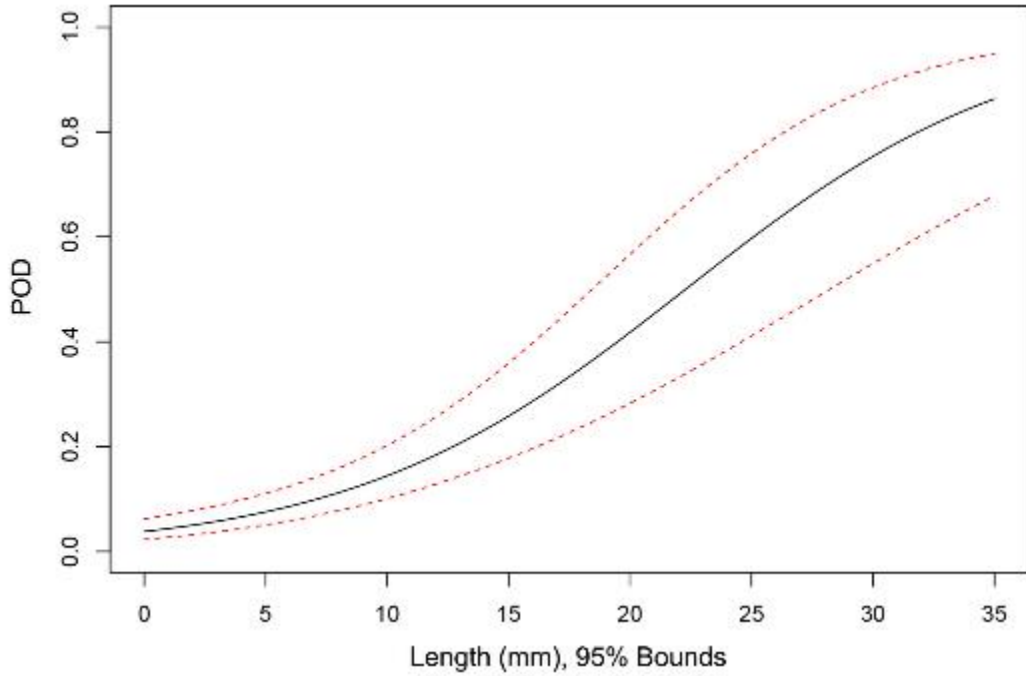


Figure F.41 POD versus Length (mm) for UT Procedures Applied to LBDMW Test Blocks with O.D. Access (**Blind + Quick-blind**)

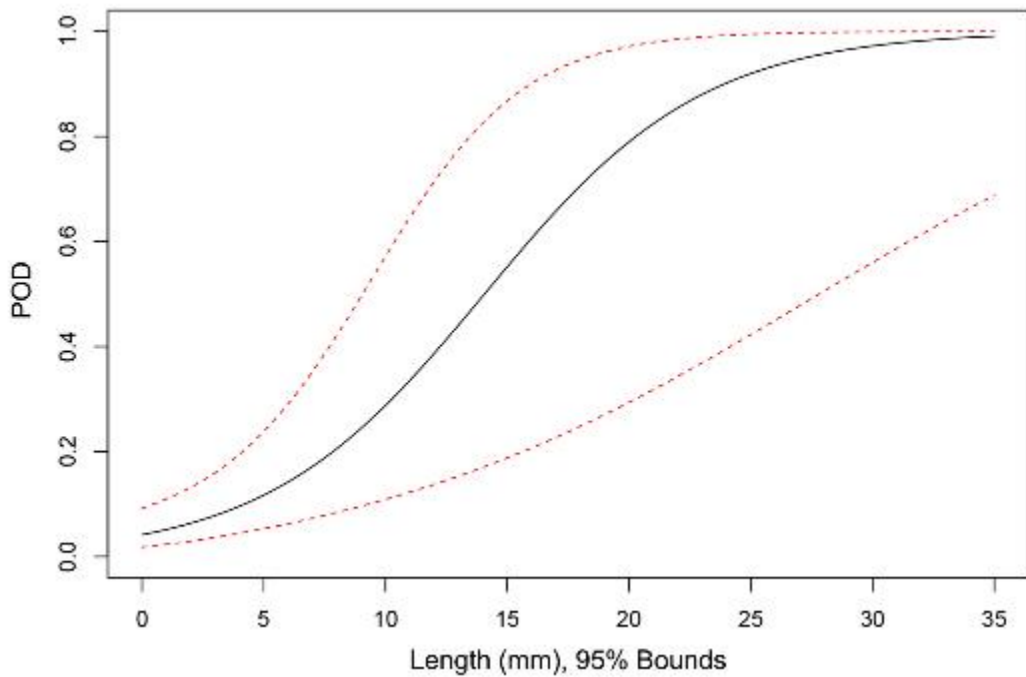


Figure F.42 POD versus Length (mm) for UT.PAUT Procedures Applied to LBDMW Test Blocks with O.D. Access (**Blind + Quick-blind**)

APPENDIX G
SIZING REGRESSION PLOTS

APPENDIX G|

SIZING REGRESSION PLOTS

Contents

G.1	Sizing Results	G-2
G.1.1	Depth Sizing Results	G-2
G.1.1.1	Depth Sizing Results for LBDMWs (I.D. Access)	G-2
G.1.1.2	Depth Sizing Results for LBDMWs (O.D. Access)	G-8
G.1.1.3	Depth Sizing Results for SBDMWs	G-15
G.1.1.4	Depth Sizing Results for BMIs (Tube I.D. Access)	G-27
G.1.2	Length Sizing Results	G-28
G.1.2.1	Length Sizing Results for LBDMWs (I.D. Access)	G-28
G.1.2.2	Length Sizing Results for LBDMWs (O.D. Access)	G-36
G.1.2.3	Length Sizing Results for SBDMWs	G-43
G.1.2.4	Length Sizing Results for BMIs (J-Groove Surface)	G-55
G.2	Sizing Results (Blind + Quick-blind)	G-58
G.2.1	Depth Sizing Results	G-58
G.2.1.1	Depth Sizing Results for LBDMWs (I.D. Access)	G-58
G.2.1.2	Depth Sizing Results for LBDMWs (O.D. Access)	G-64
G.2.2	Length Sizing Results	G-69
G.2.2.1	Length Sizing Results for LBDMWs (I.D. Access)	G-69
G.2.2.2	Length Sizing Results for LBDMWs (O.D. Access)	G-73

G.1 Sizing Results

G.1.1 Depth Sizing Results

G.1.1.1 Depth Sizing Results for LBDMWs (I.D. Access)

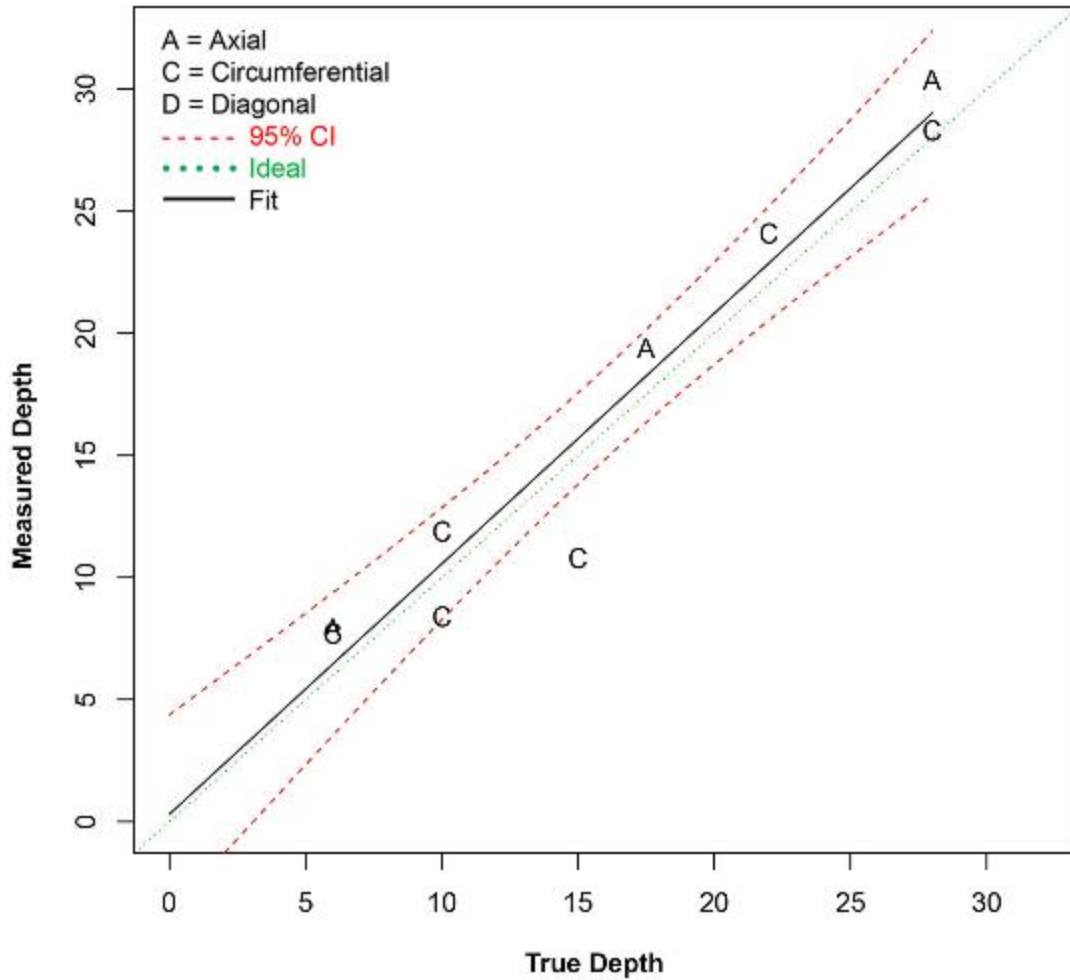


Figure G.1 Depth Sizing Regression (in mm) for UT.ECT Procedures on LBDMW Test Blocks in PARENT Blind Testing (I.D. Access)

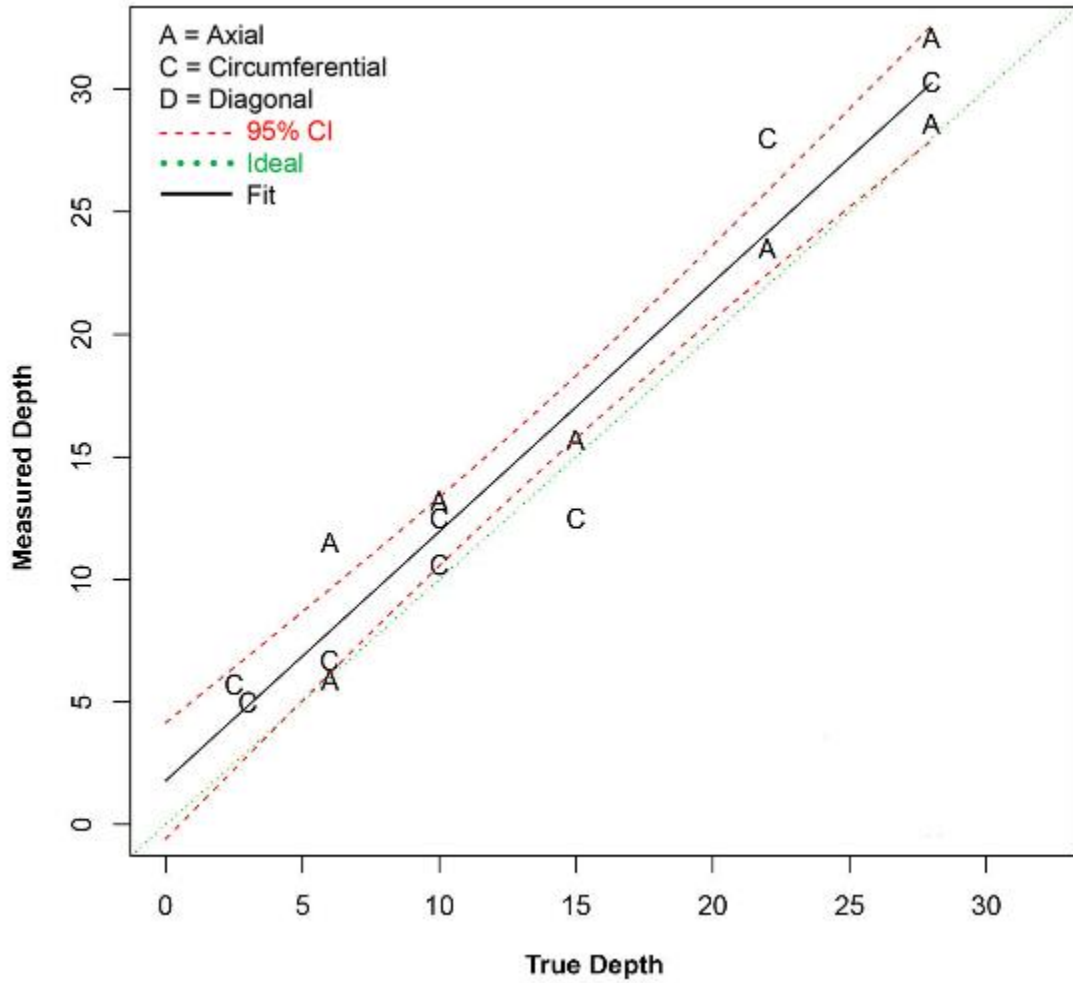


Figure G.2 Depth Sizing Regression (in mm) for UT.PAUT Procedures on LBDMW Test Blocks in PARENT Blind Testing (I.D. Access)

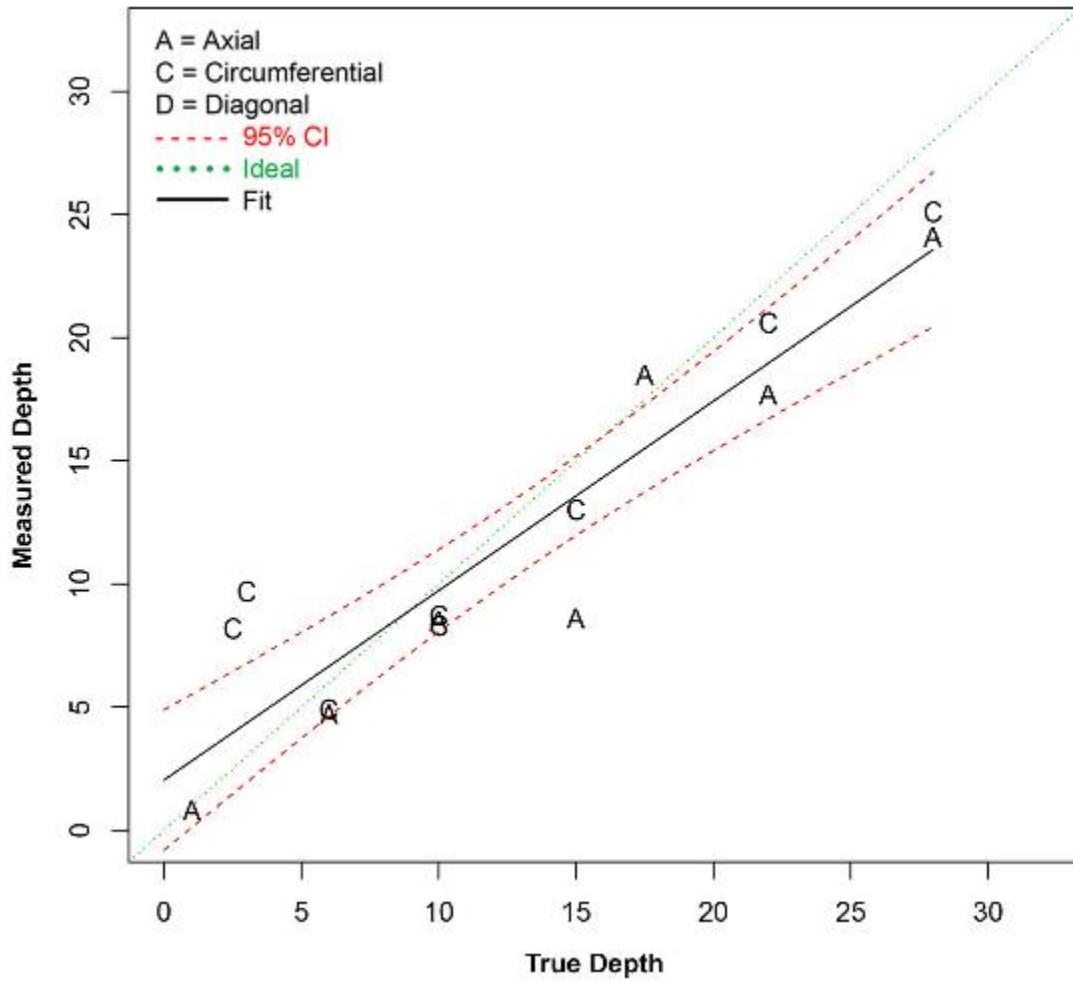


Figure G.3 Depth Sizing Regression (in mm) for UT, TOFD, ECT Procedures on LBDMW Test Blocks in PARENT Blind Testing (I.D. Access)

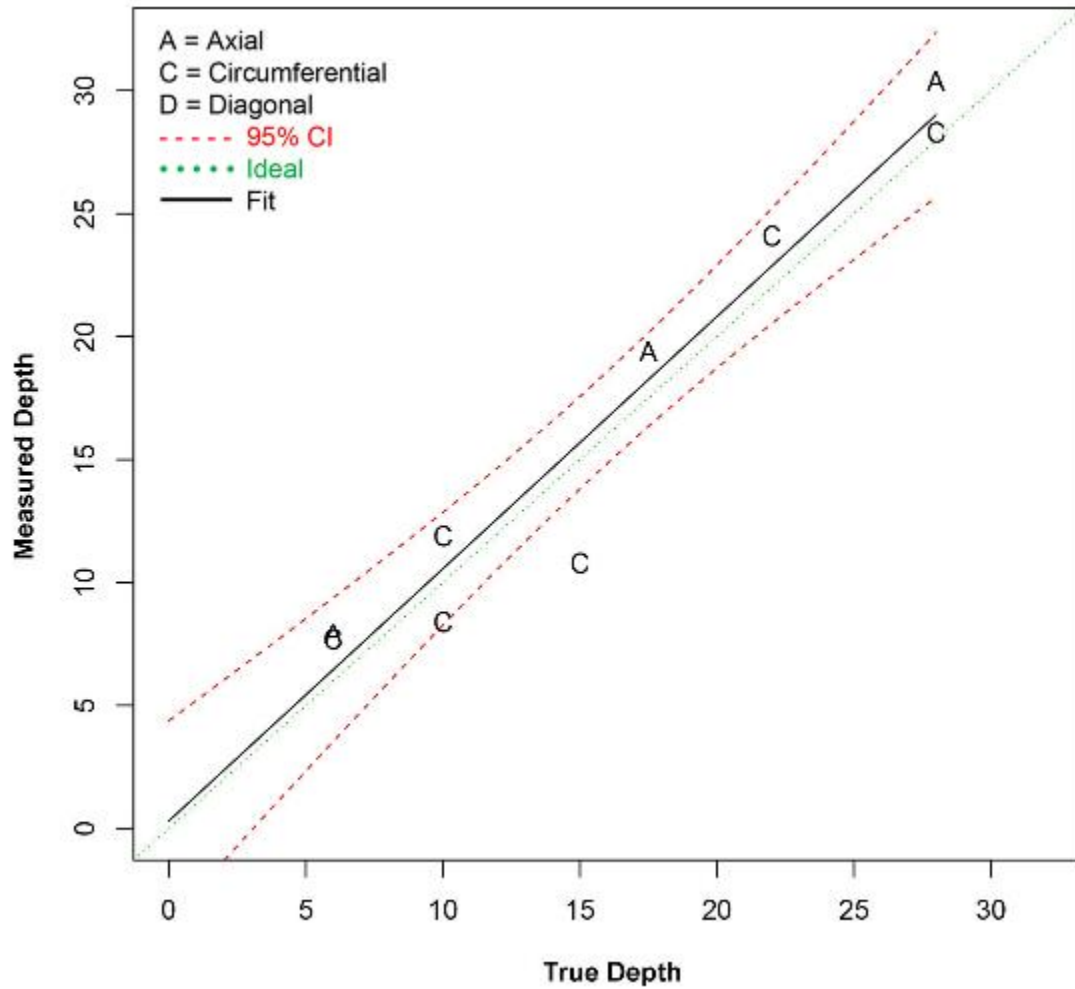


Figure G.4 Depth Sizing Regression (in mm) for Procedure UT.ECT.144 on LBDMW Test Blocks in PARENT Blind Testing (I.D. Access)

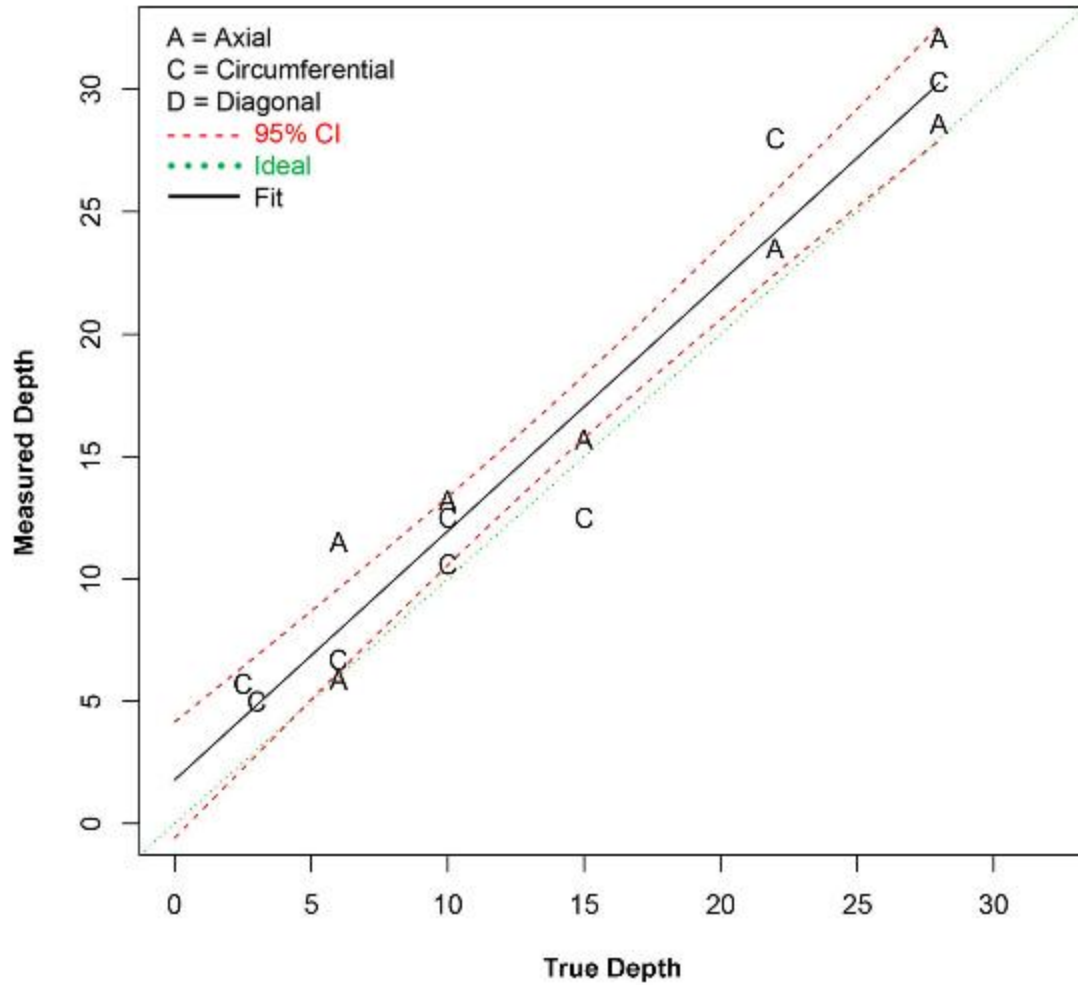


Figure G.5 Depth Sizing Regression (in mm) for Procedure UT.PAUT.113 on LBDMW Test Blocks in PARENT Blind Testing (I.D. Access)

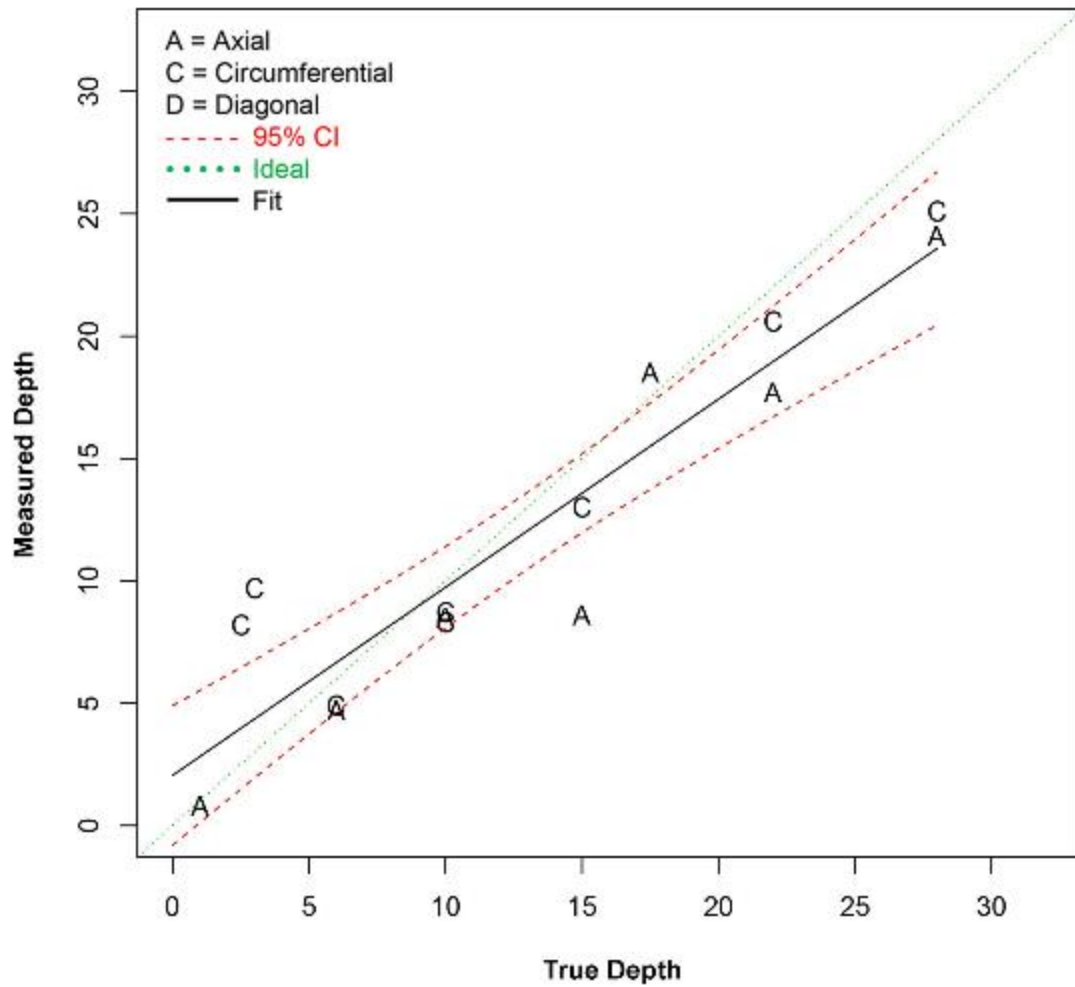


Figure G.6 Depth Sizing Regression (in mm) for Procedure UT.TOFD.ECT.101 on LBDMW Test Blocks in PARENT Blind Testing (I.D. Access)

G.1.1.2 Depth Sizing Results for LBDMWs (O.D. Access)

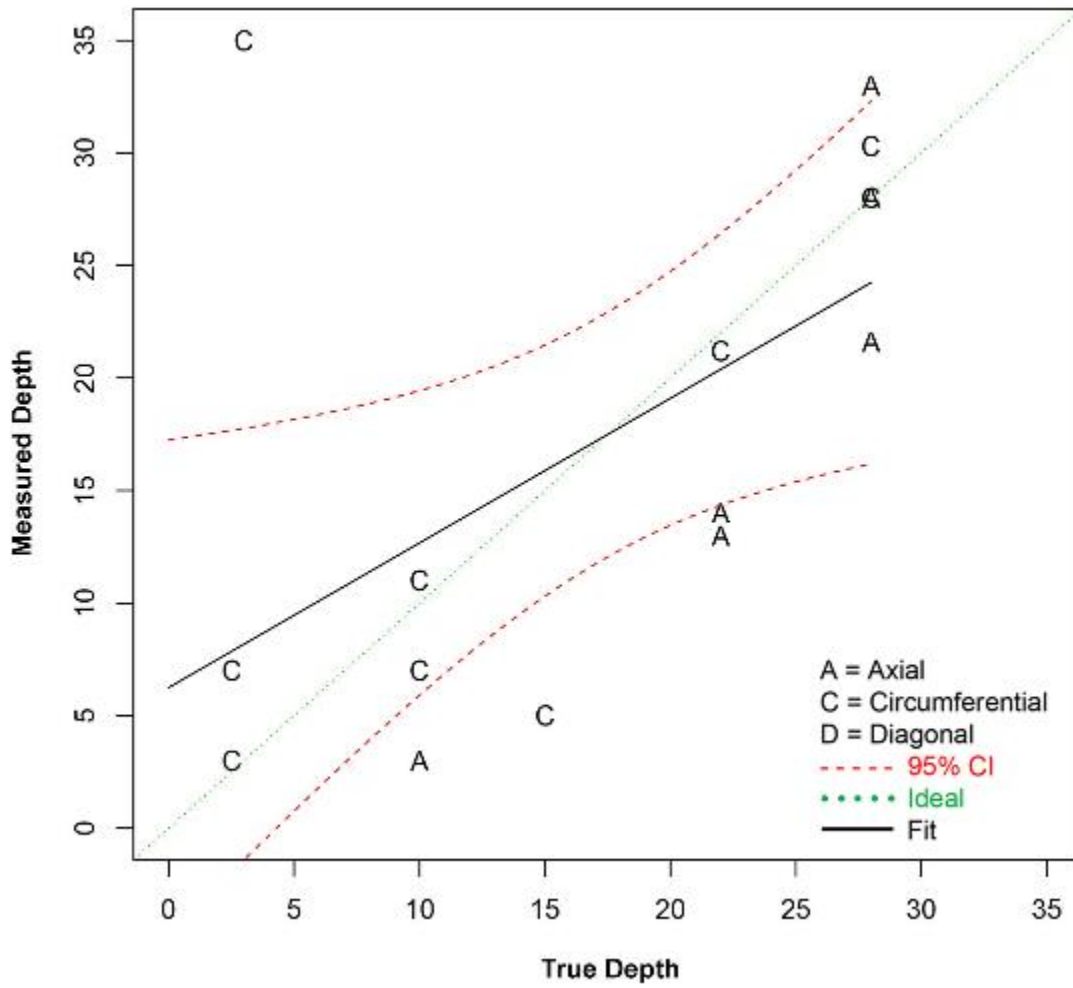


Figure G.7 Depth Sizing Regression (in mm) for Procedure PAUT on LBDMW Test Blocks in PARENT Blind Testing (O.D. Access)

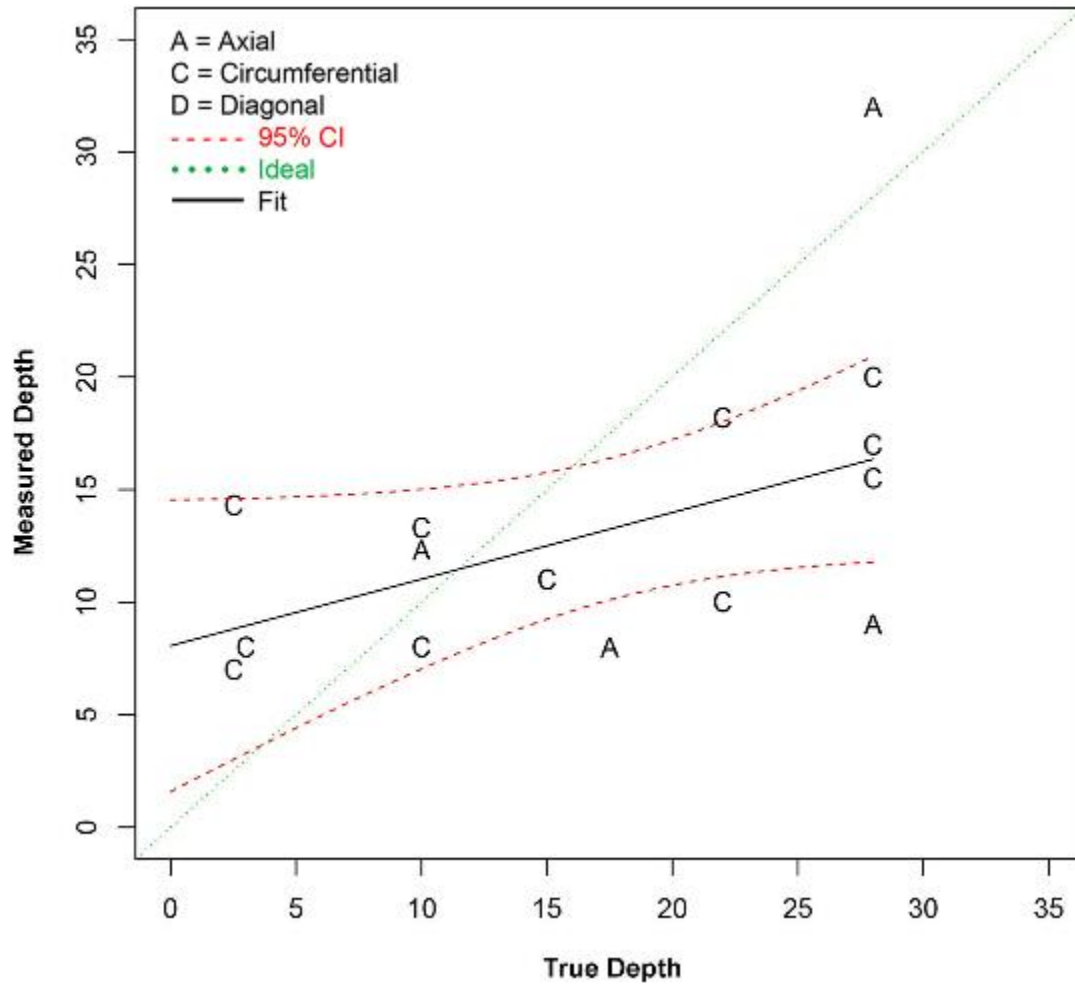


Figure G.8 Depth Sizing Regression (in mm) for Procedure UT on LBDMW Test Blocks in PARENT Blind Testing (O.D. Access)

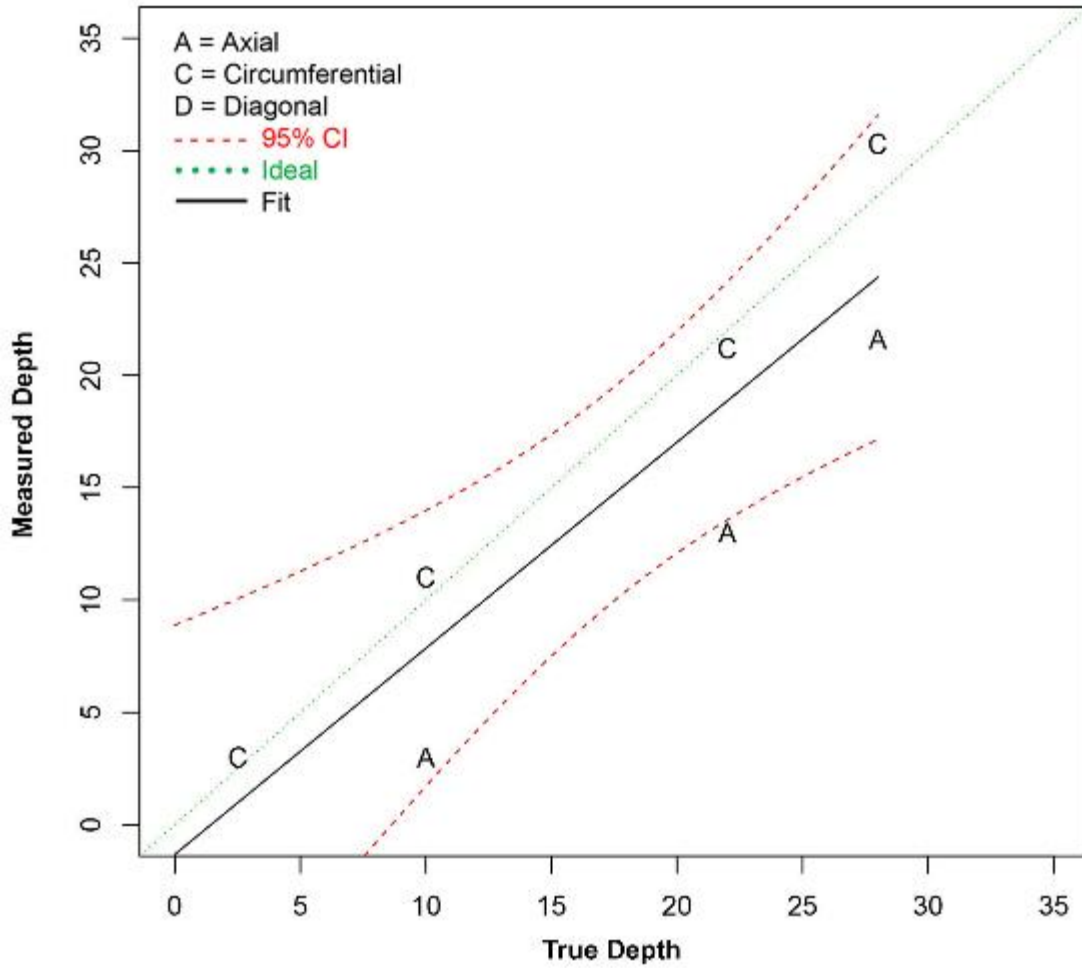


Figure G.9 Depth Sizing Regression (in mm) for Procedure PAUT.108 on LBDMW Test Blocks in PARENT Blind Testing (O.D. Access)

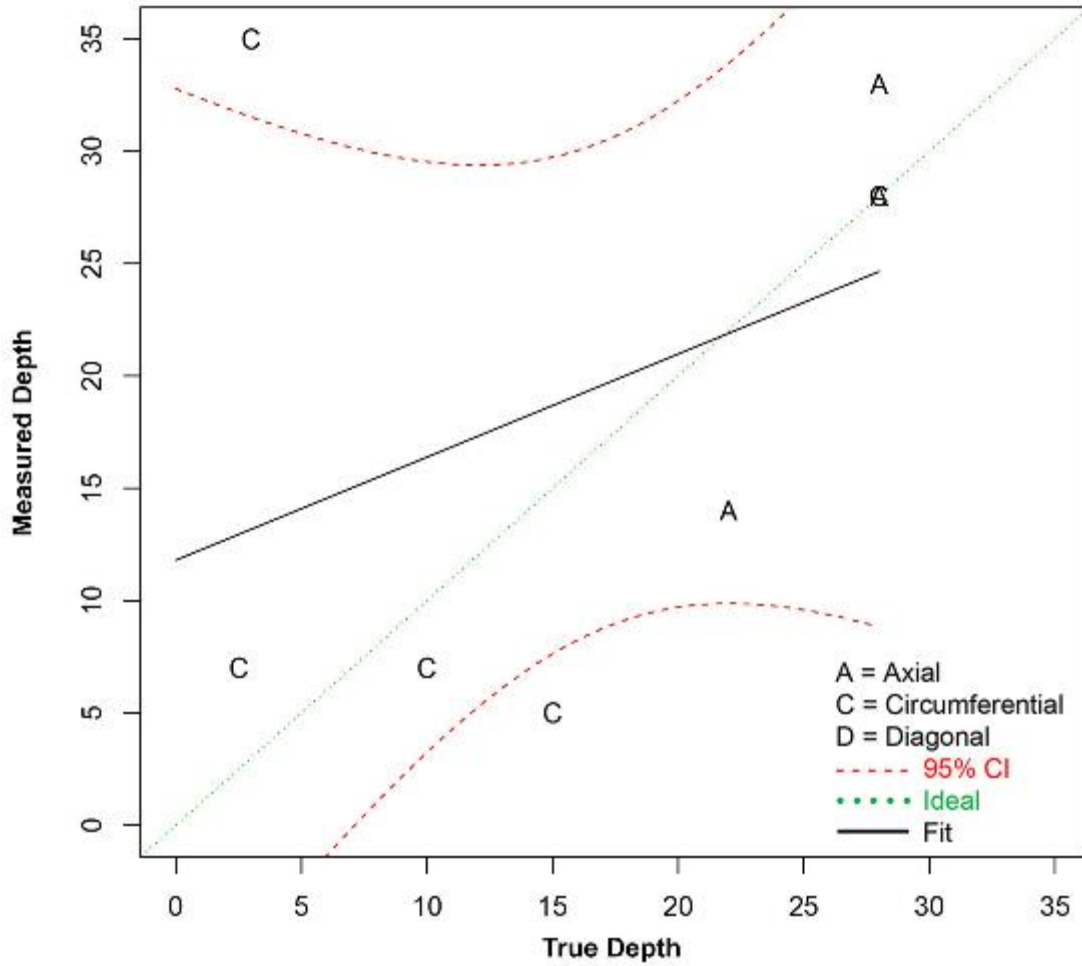


Figure G.10 Depth Sizing Regression (in mm) for Procedure PAUT.126 on LBDMW Test Blocks in PARENT Blind Testing (O.D. Access)

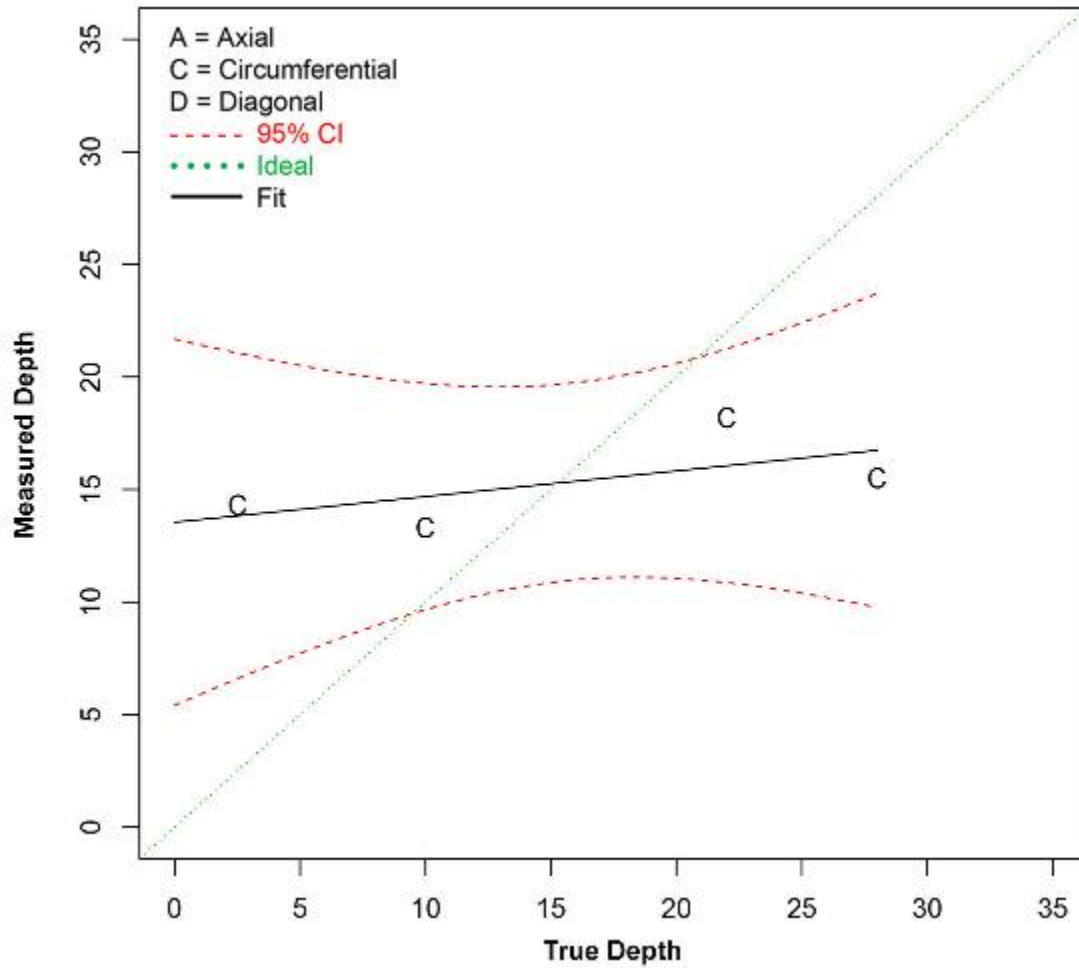


Figure G.11 Depth Sizing Regression (in mm) for Procedure UT.108 on LBDMW Test Blocks in PARENT Blind Testing (O.D. Access)

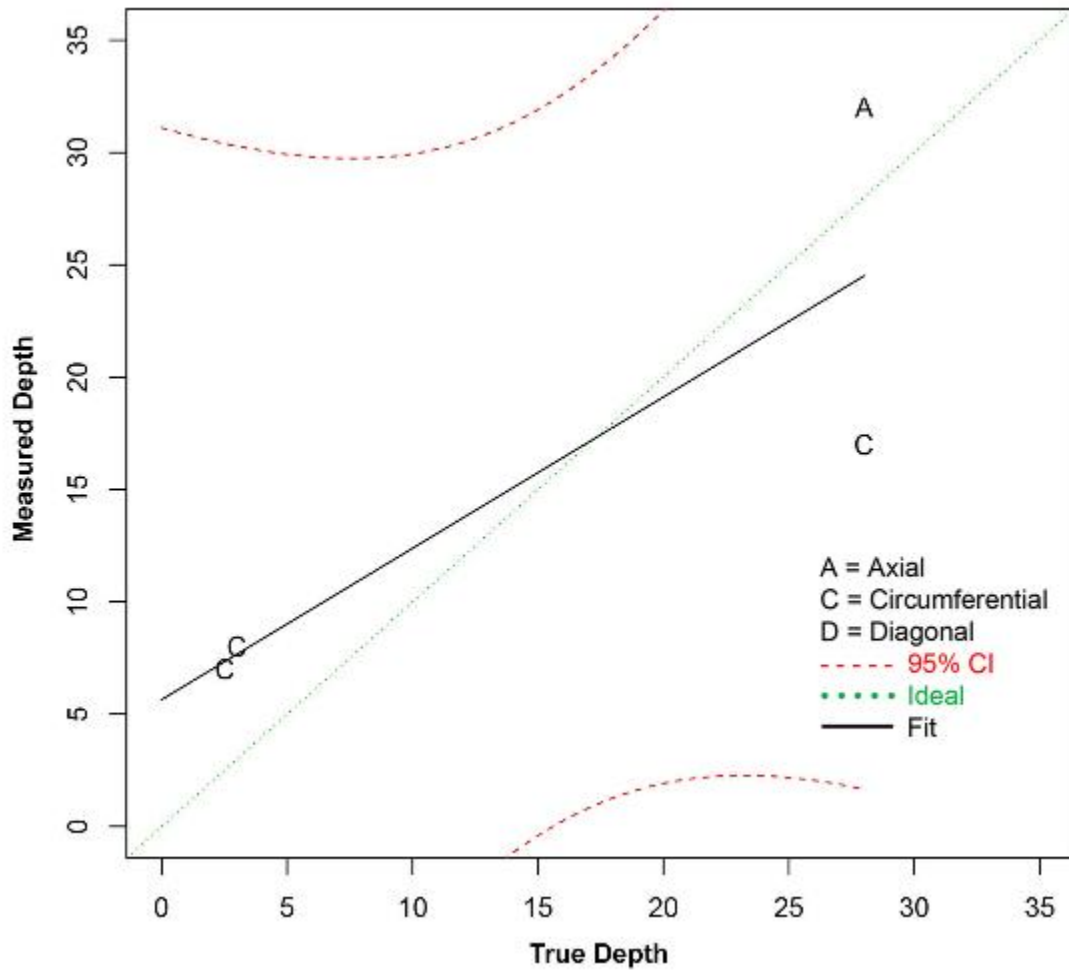


Figure G.12 Depth Sizing Regression (in mm) for Procedure UT.126 on LBDMW Test Blocks in PARENT Blind Testing (O.D. Access)

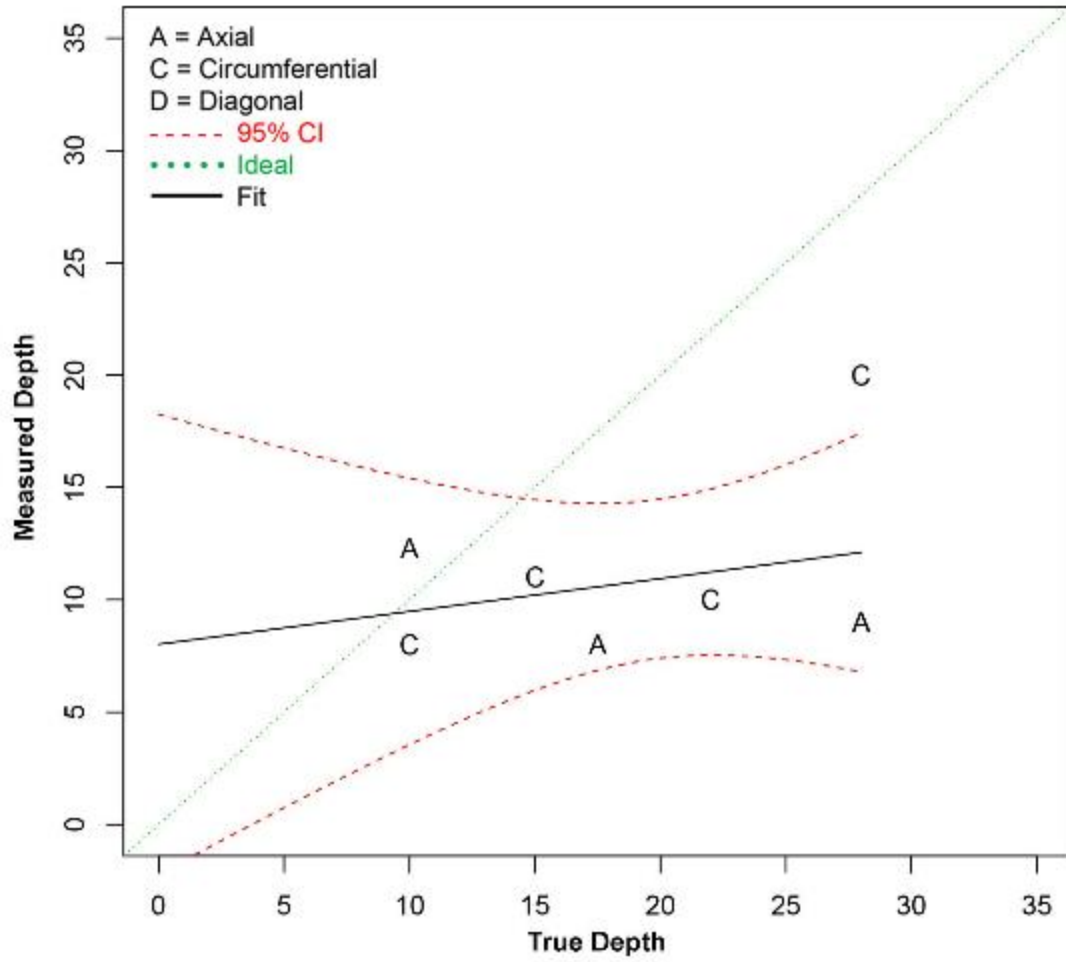


Figure G.13 Depth Sizing Regression (in mm) for Procedure UT.134 on LBDMW Test Blocks in PARENT Blind Testing (O.D. Access)

G.1.1.3 Depth Sizing Results for SBDMWs

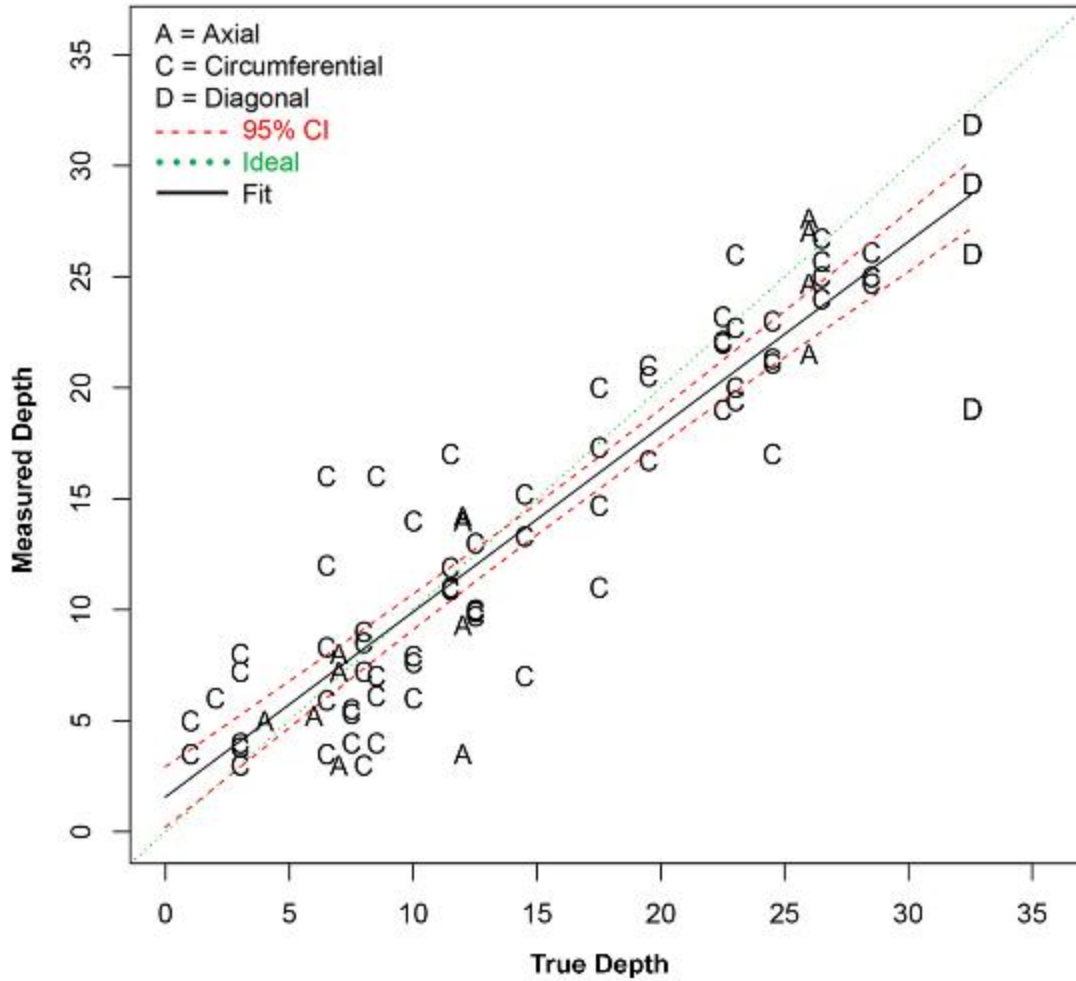


Figure G.14 Depth Sizing Regression (in mm) for Procedure PAUT on SBDMW Test Blocks in PARENT Blind Testing (O.D. Access)

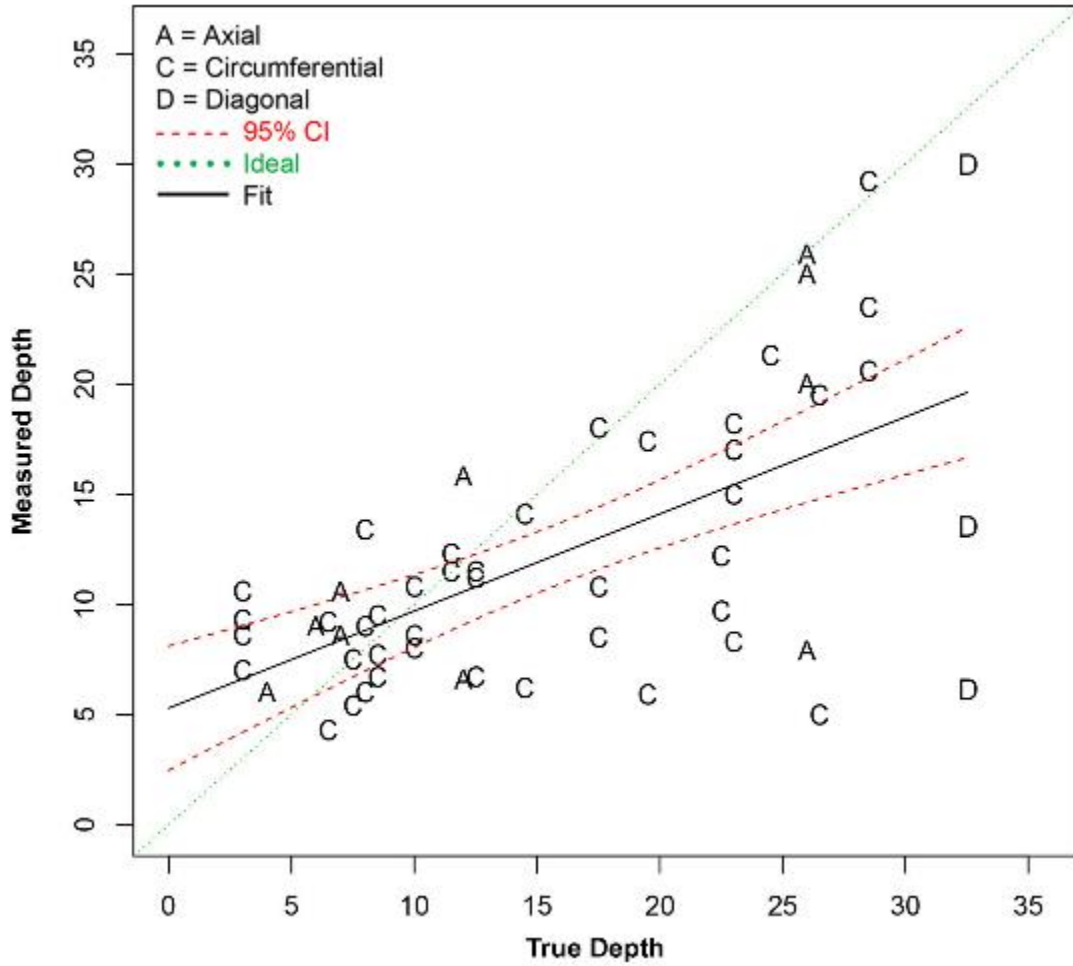


Figure G.15 Depth Sizing Regression (in mm) for Procedure UT on SBDMW Test Blocks in PARENT Blind Testing (O.D. Access)

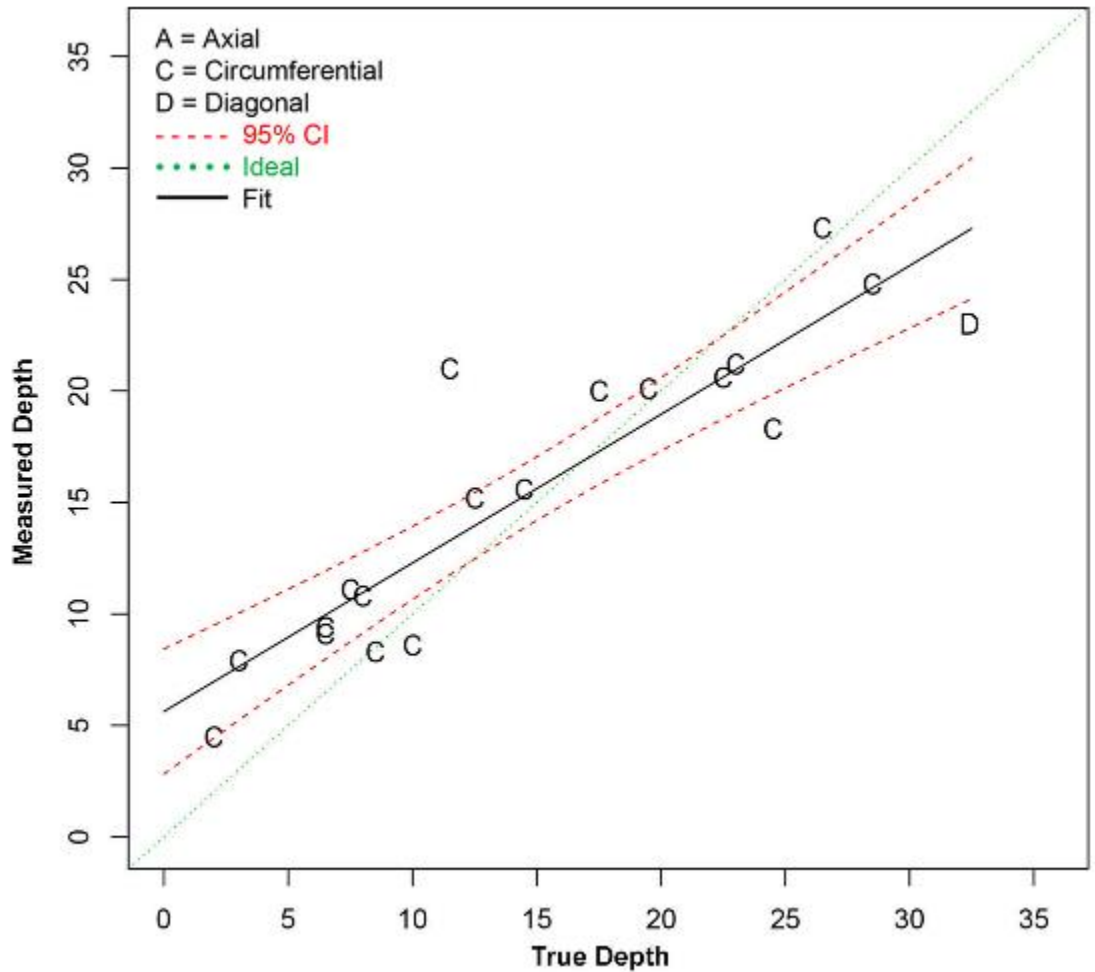


Figure G.16 Depth Sizing Regression (in mm) for Procedure UT.TOFD on SBDMW Test Blocks in PARENT Blind Testing (O.D. Access)

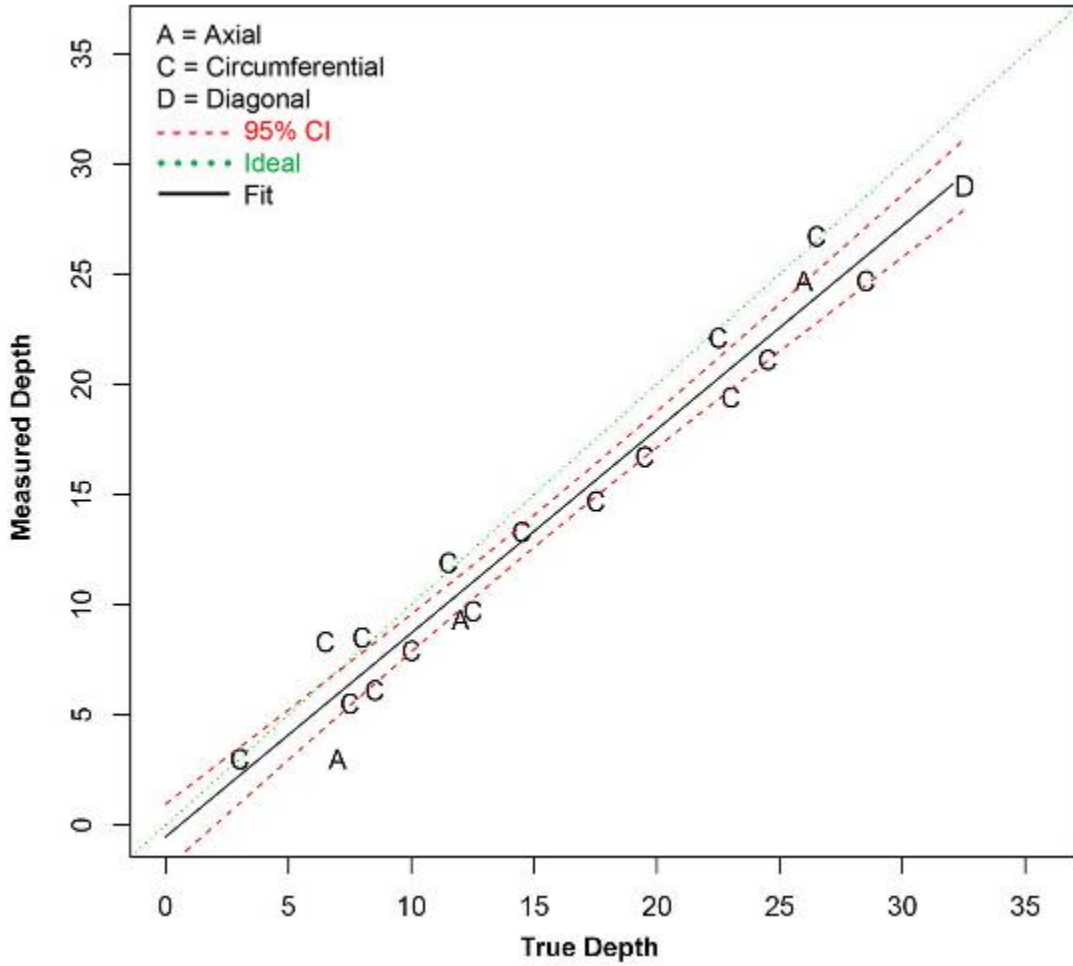


Figure G.17 Depth Sizing Regression (in mm) for Procedure PAUT.108 on SBDMW Test Blocks in PARENT Blind Testing (O.D. Access)

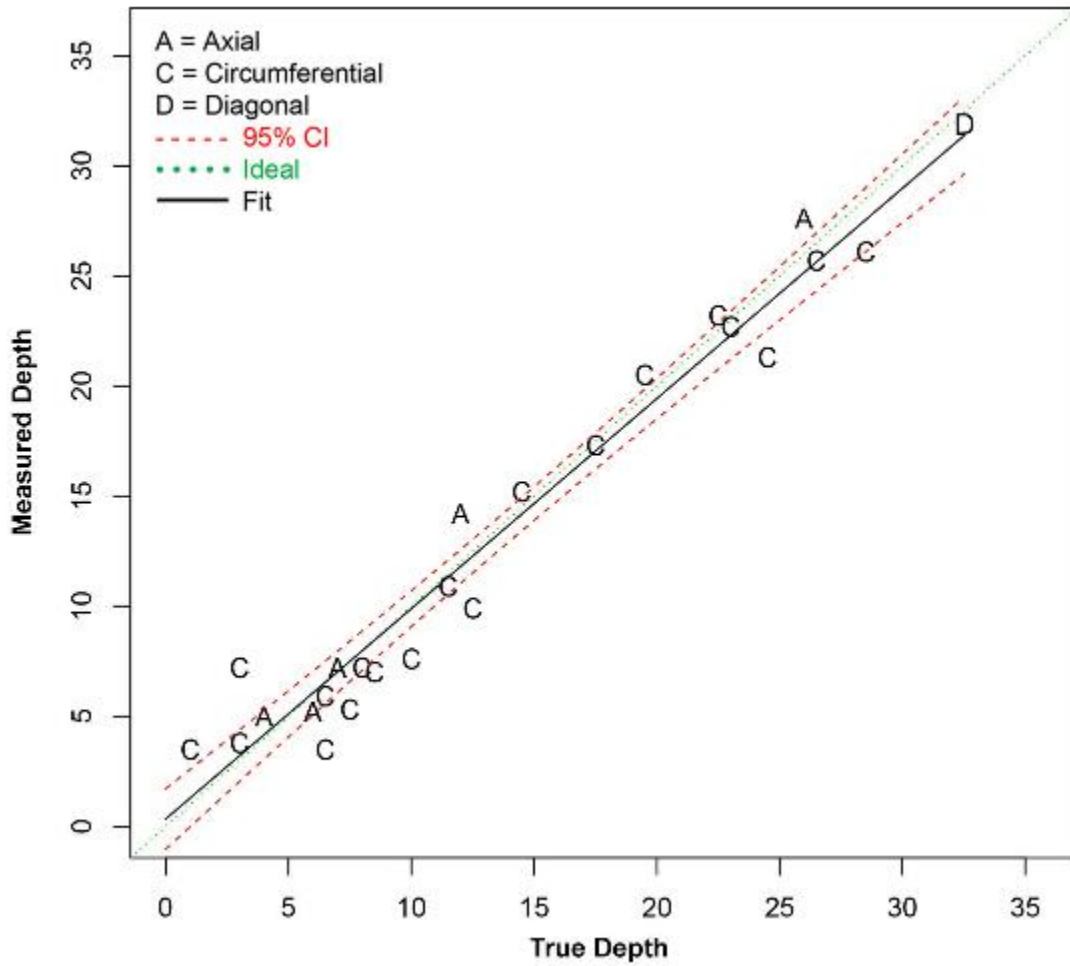


Figure G.18 Depth Sizing Regression (in mm) for Procedure PAUT.115 on SBDMW Test Blocks in PARENT Blind Testing (O.D. Access)

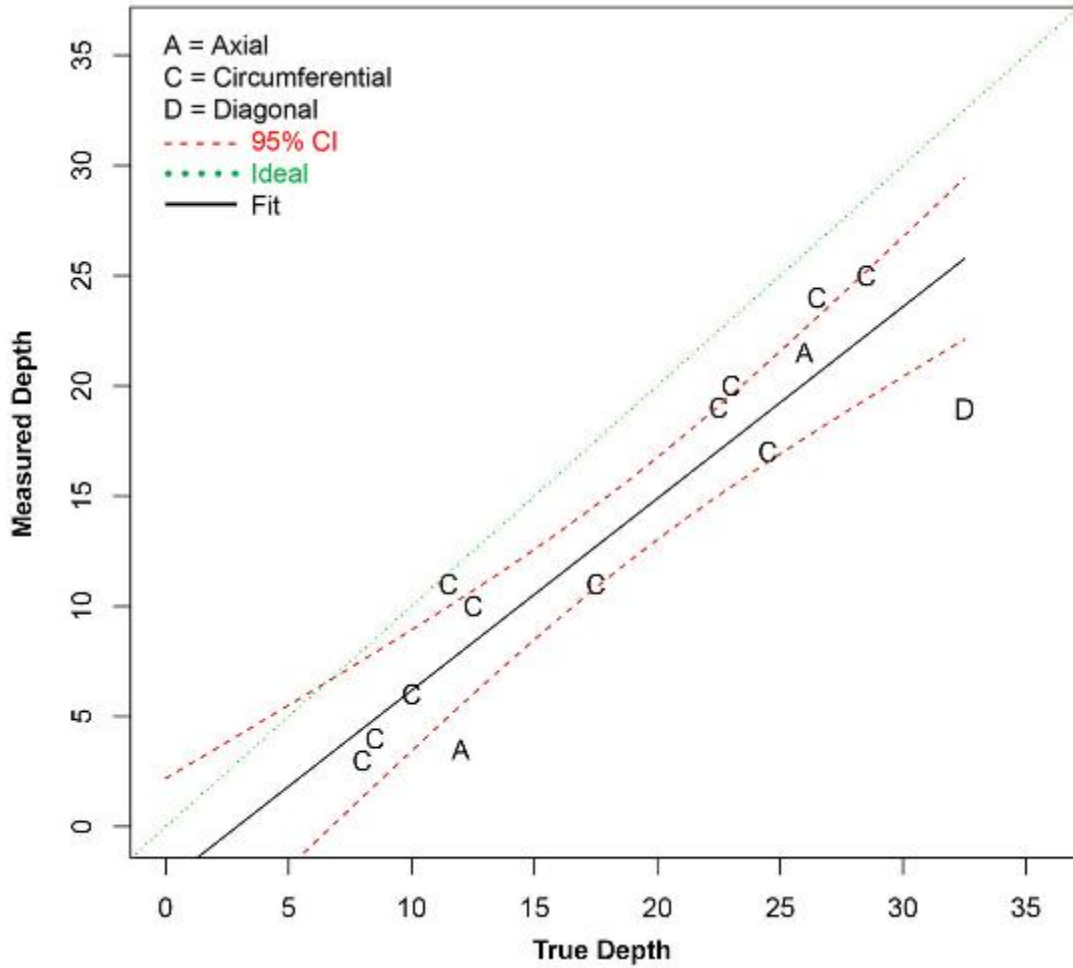


Figure G.19 Depth Sizing Regression (in mm) for Procedure PAUT.126 on SBDMW Test Blocks in PARENT Blind Testing (O.D. Access)

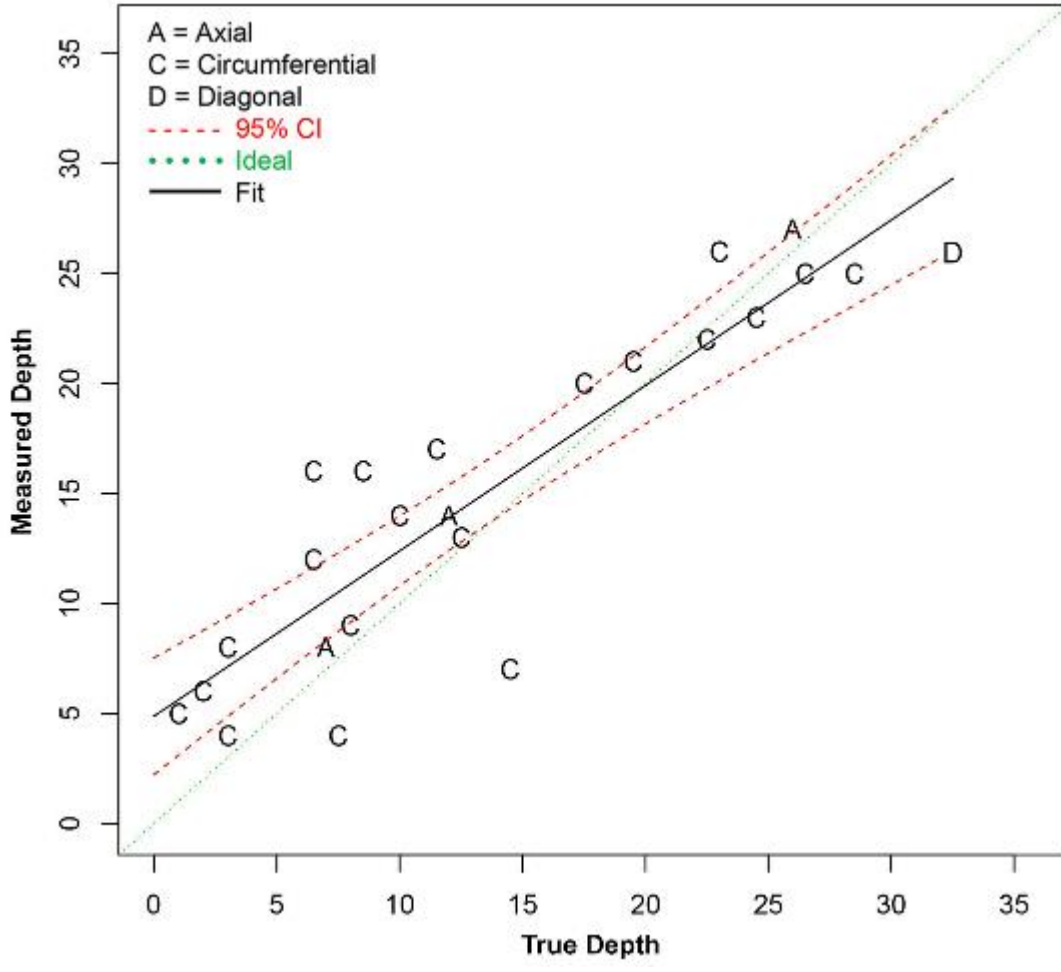


Figure G.20 Depth Sizing Regression (in mm) for Procedure PAUT.128 on SBDMW Test Blocks in PARENT Blind Testing (O.D. Access)

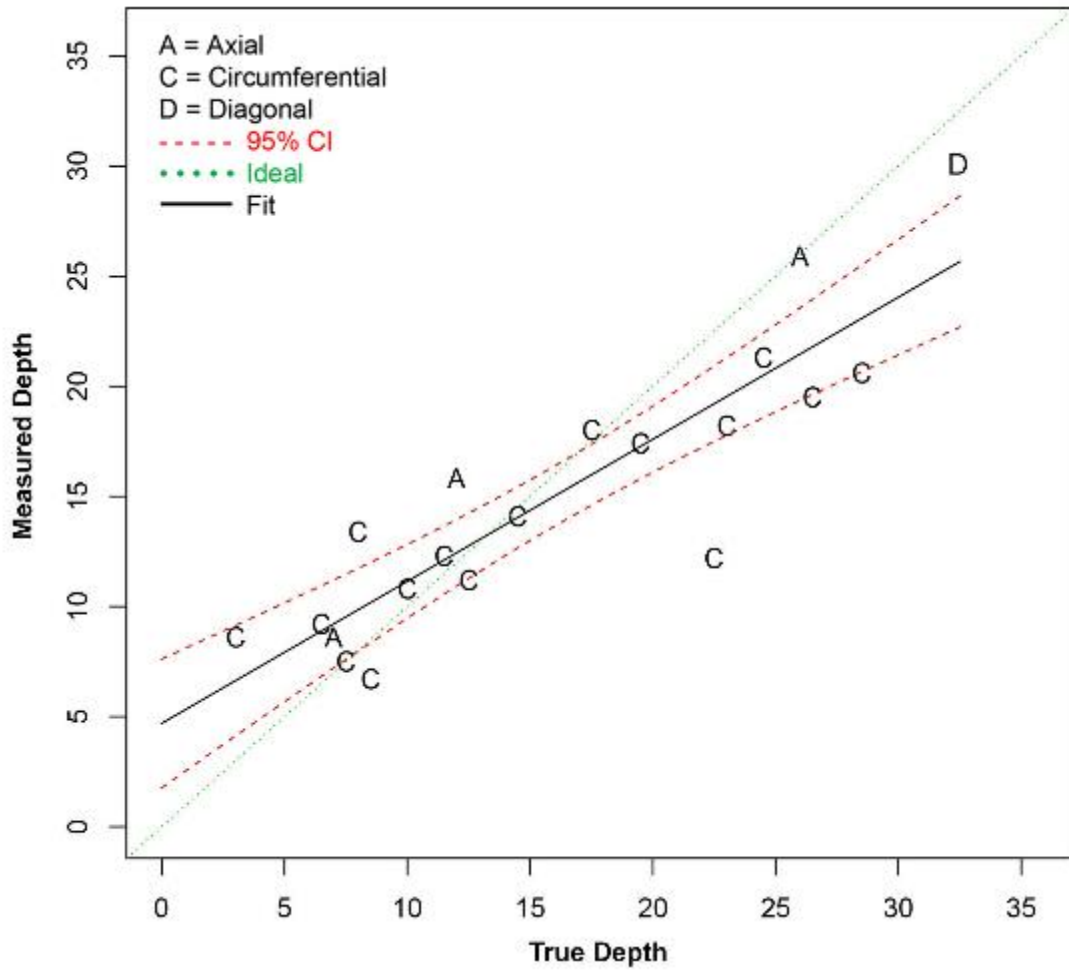


Figure G.21 Depth Sizing Regression (in mm) for Procedure UT.108 on SBDMW Test Blocks in PARENT Blind Testing (O.D. Access)

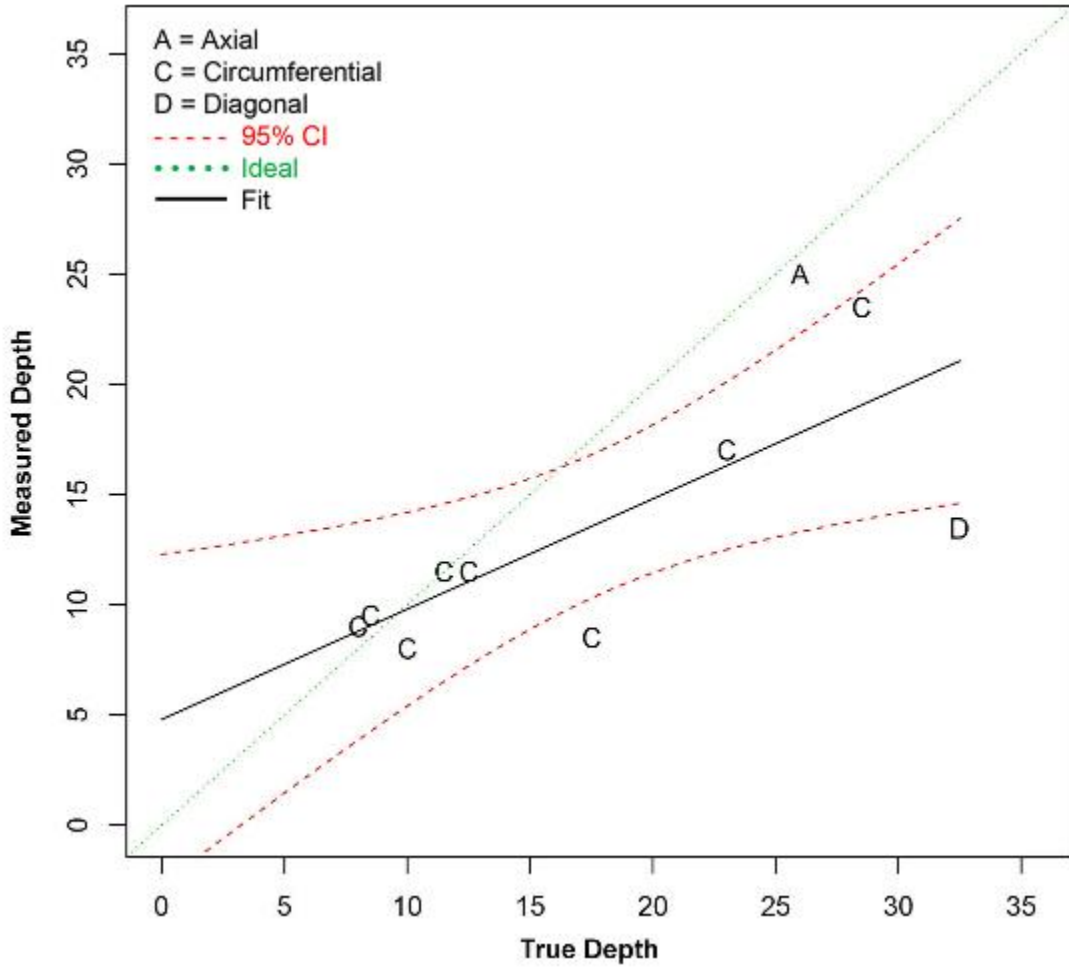


Figure G.22 Depth Sizing Regression (in mm) for Procedure UT.126 on SBDMW Test Blocks in PARENT Blind Testing (O.D. Access)

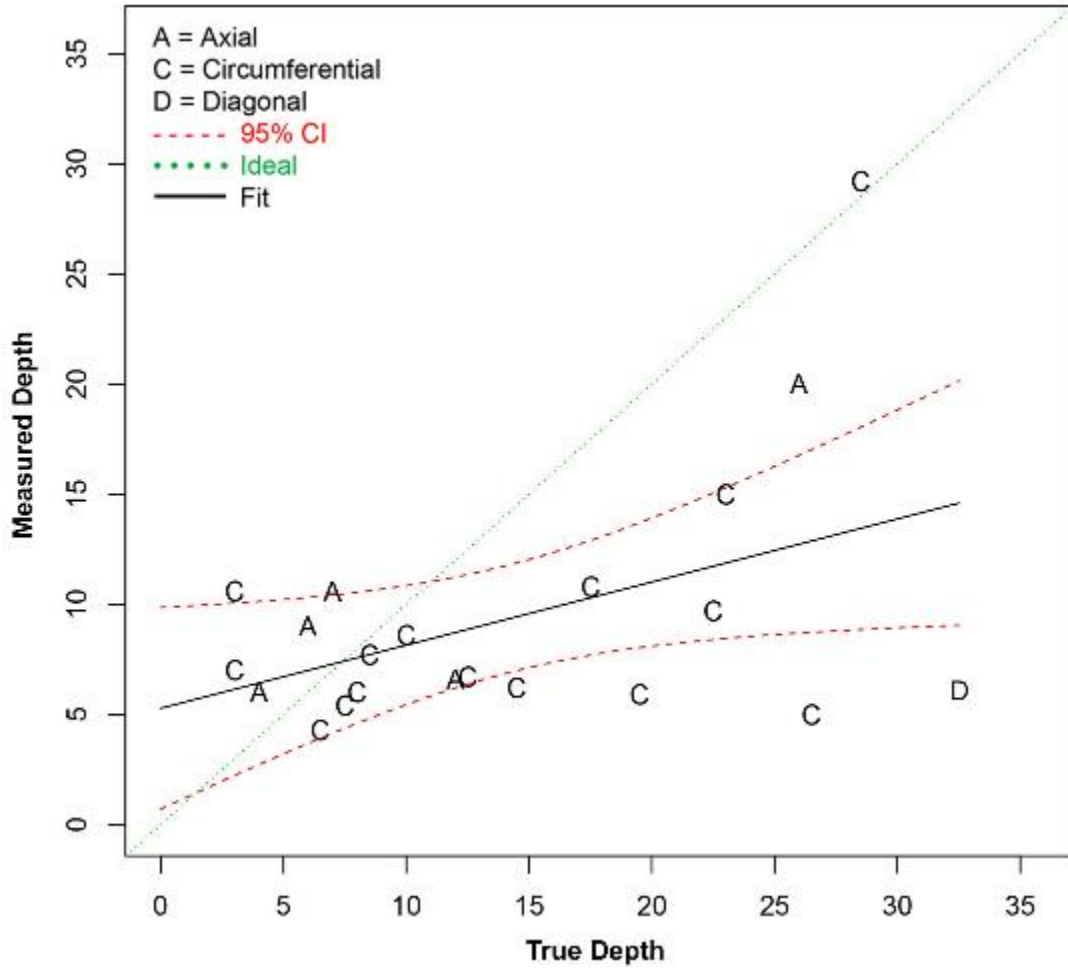


Figure G.23 Depth Sizing Regression (in mm) for Procedure UT.134 on SBDMW Test Blocks in PARENT Blind Testing (O.D. Access)

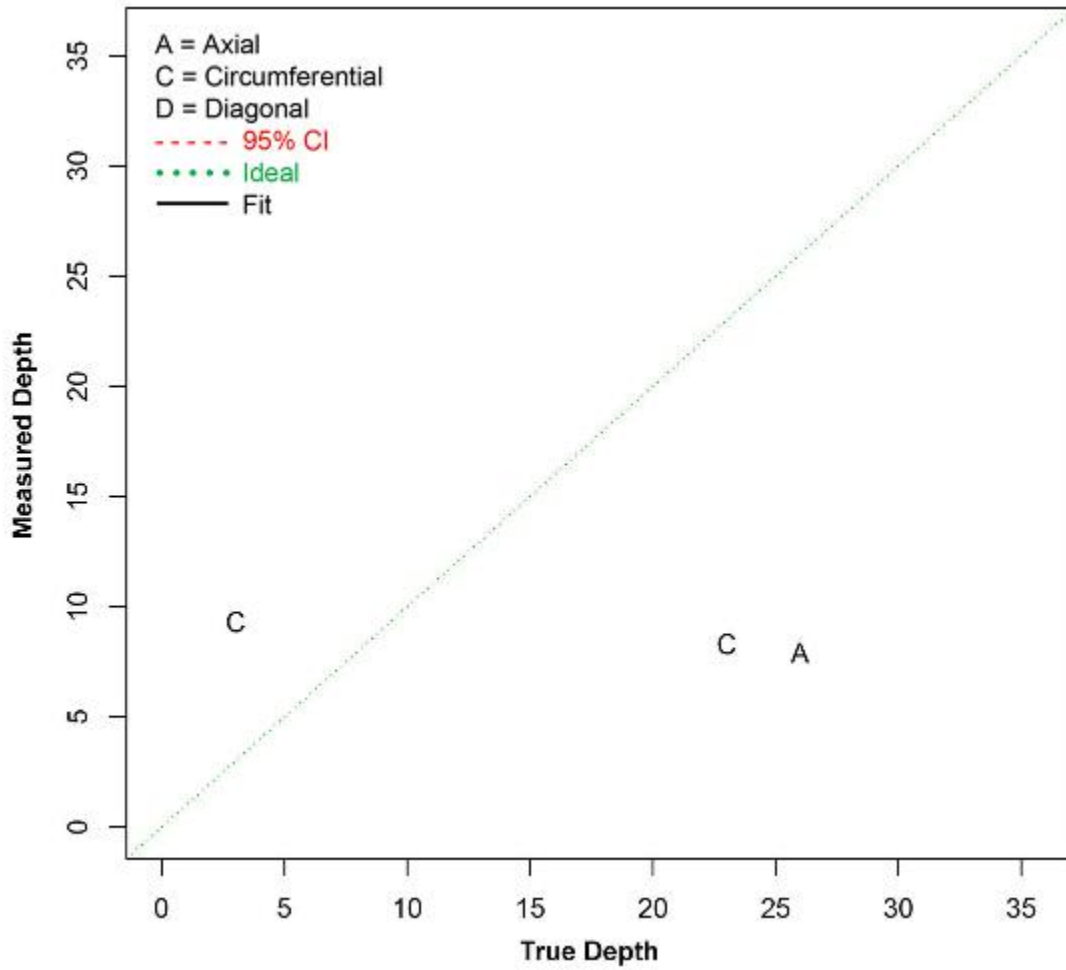


Figure G.24 Depth Sizing Regression (in mm) for Procedure UT.25 on SBDMW Test Blocks in PARENT Blind Testing (O.D. Access)

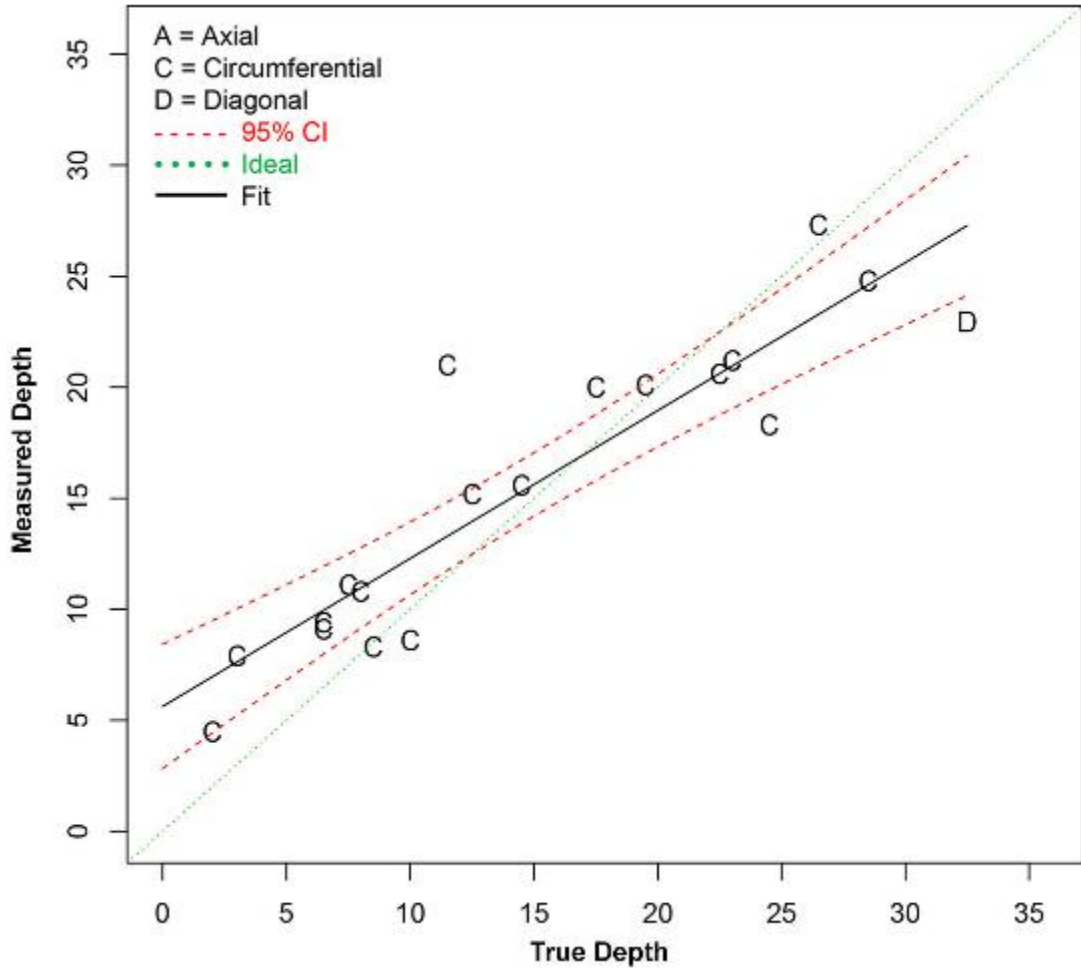


Figure G.25 Depth Sizing Regression (in mm) for Procedure UT.TOFD.117 on SBDMW Test Blocks in PARENT Blind Testing (O.D. Access)

G.1.1.4 Depth Sizing Results for BMIs (Tube I.D. Access)

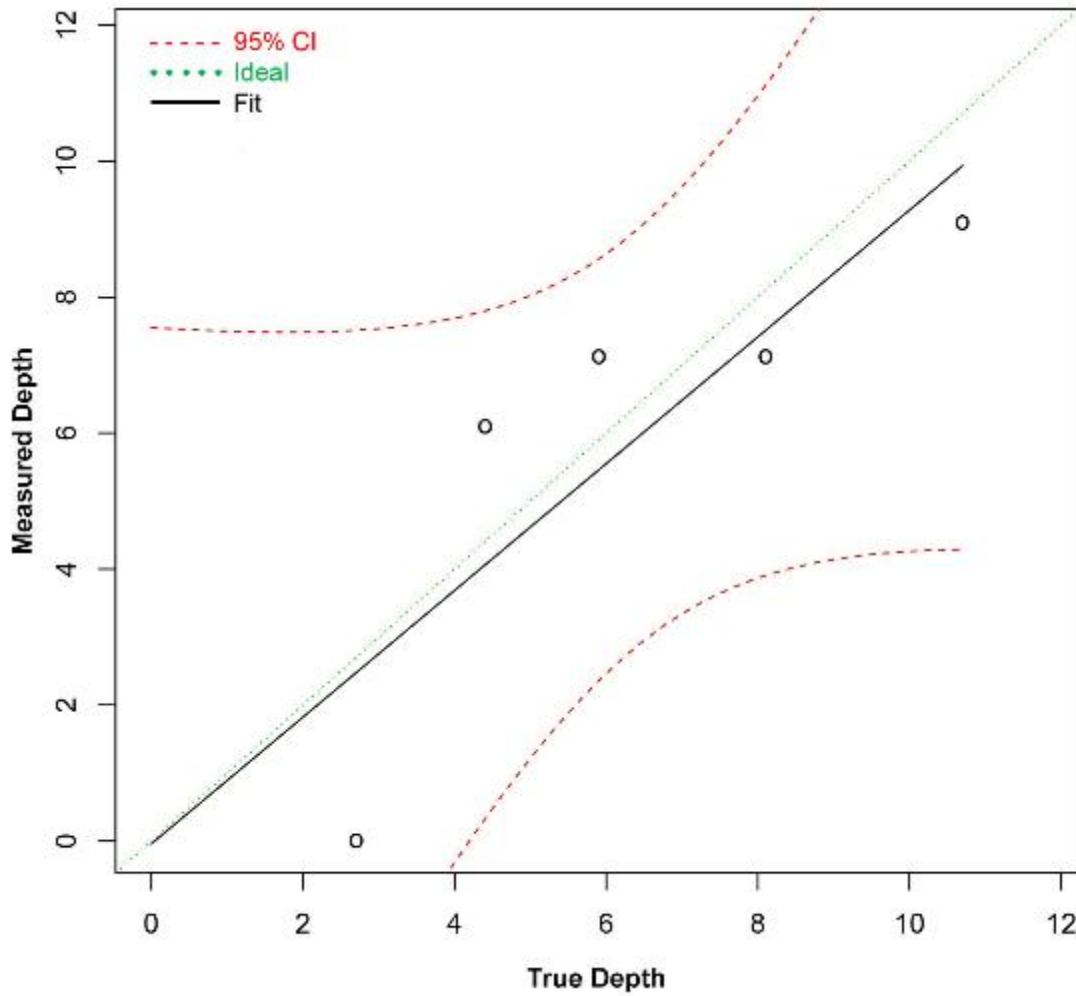


Figure G.26 Depth Sizing Regression (in mm) for Procedure TOFD.ECT.126 on BMI Test Blocks in PARENT Blind Testing

G.1.2 Length Sizing Results

G.1.2.1 Length Sizing Results for LBDMWs (I.D. Access)

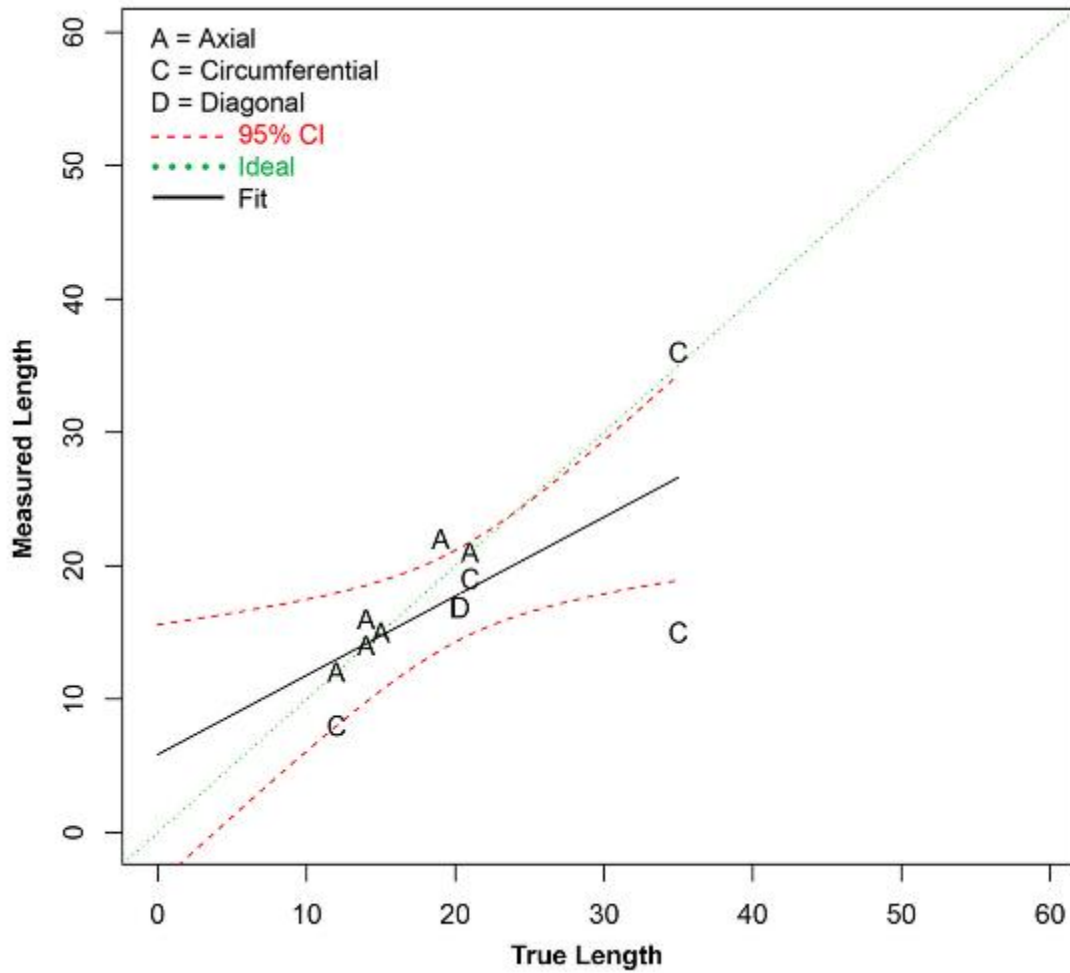


Figure G.27 Length Sizing Regression (in mm) for ECT Procedures on LBDMW Test Blocks in PARENT Blind Testing (I.D. Access)

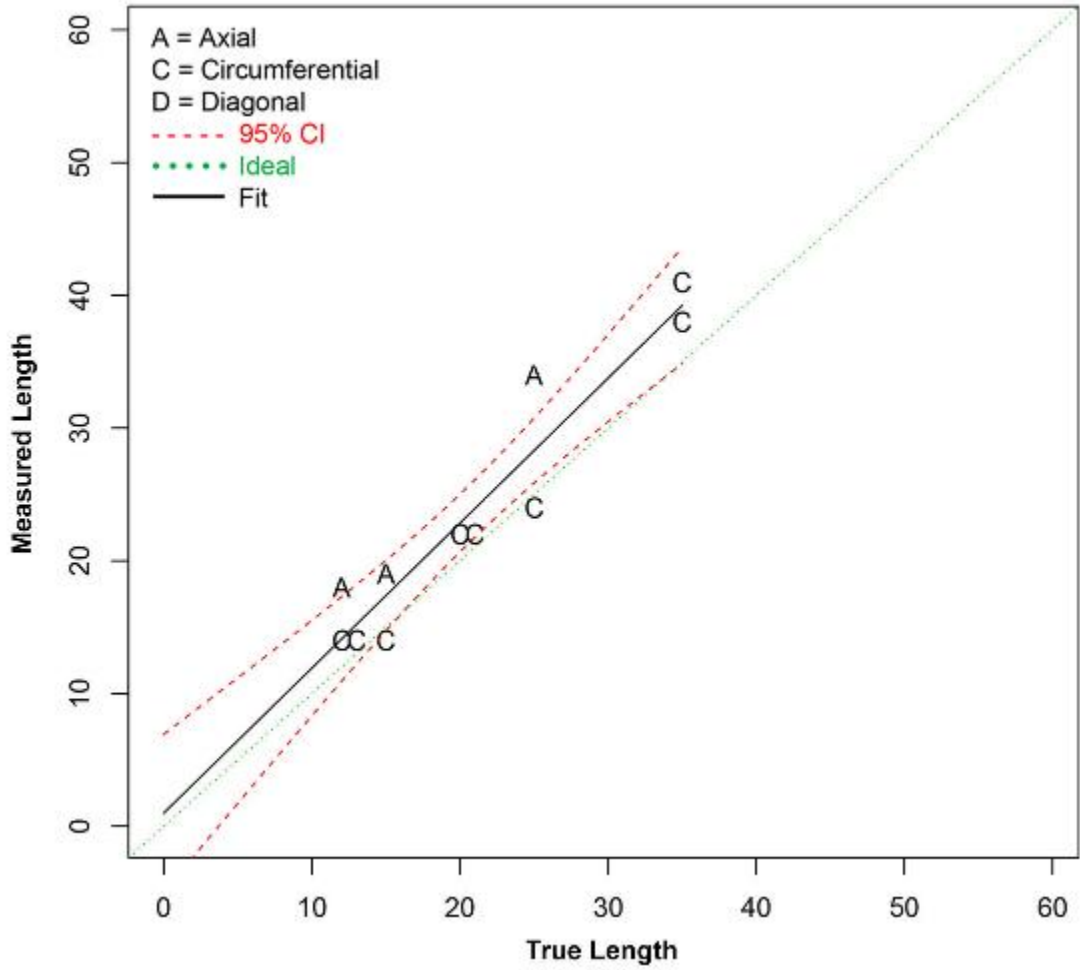


Figure G.28 Length Sizing Regression (in mm) for UT.ECT Procedures on LBDMW Test Blocks in PARENT Blind Testing (I.D. Access)

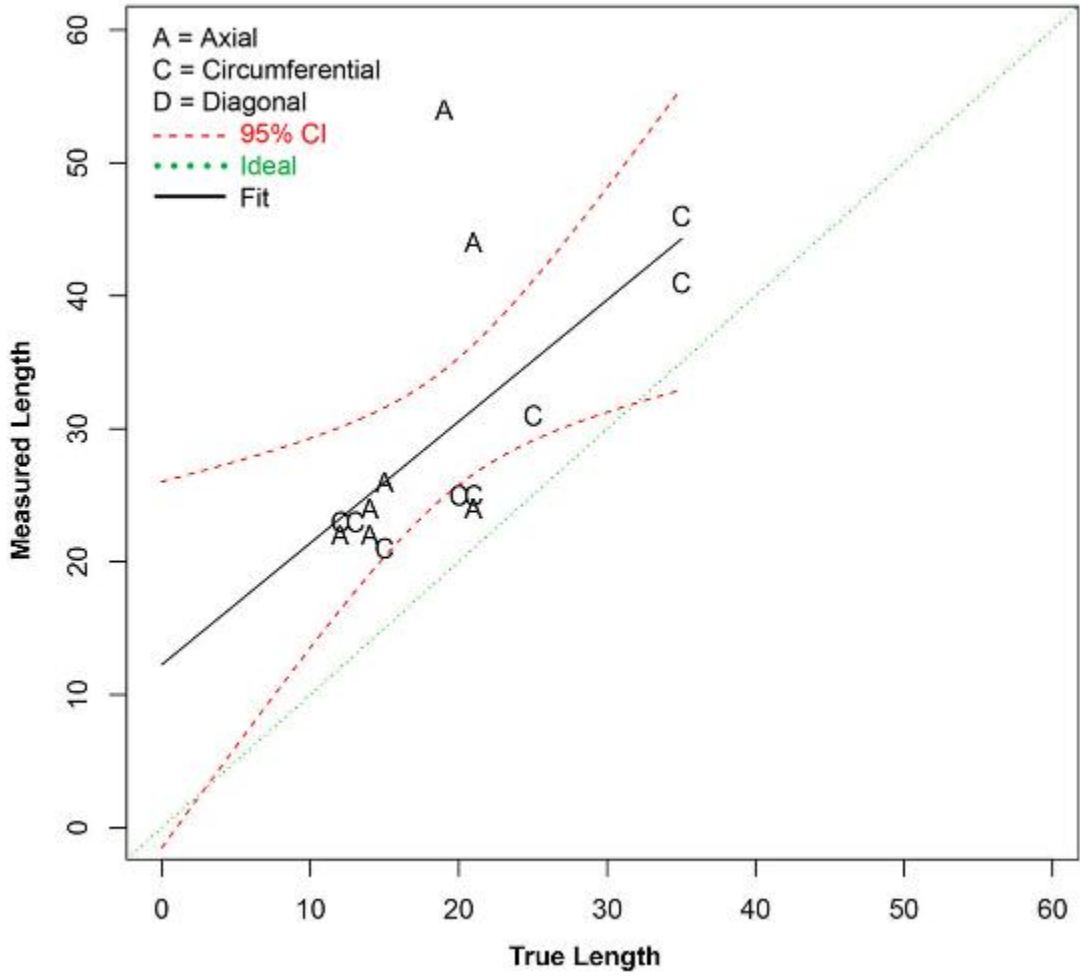


Figure G.29 Length Sizing Regression (in mm) for UT.PAUT Procedures on LBDMW Test Blocks in PARENT Blind Testing (I.D. Access)

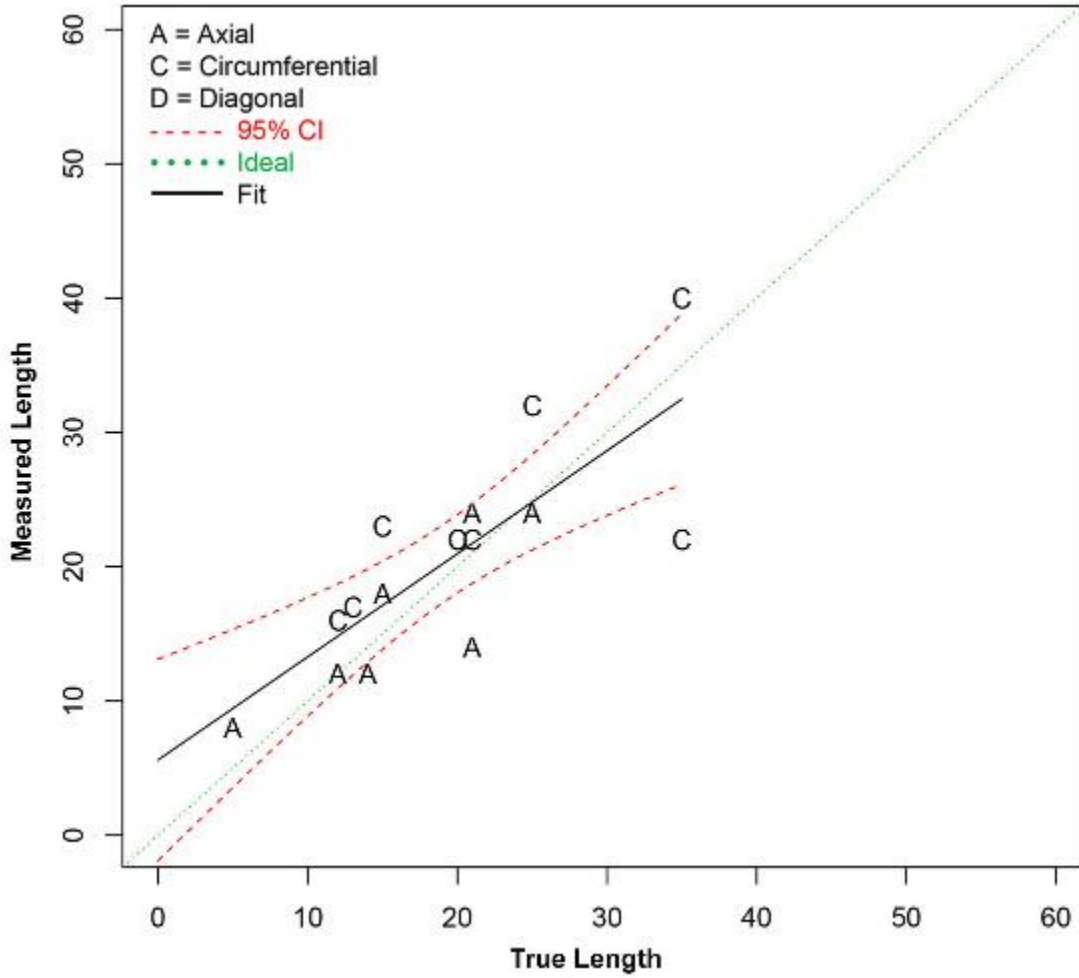


Figure G.30 Length Sizing Regression (in mm) for UT.TOFD.ECT Procedures on LBDMW Test Blocks in PARENT Blind Testing (I.D. Access)

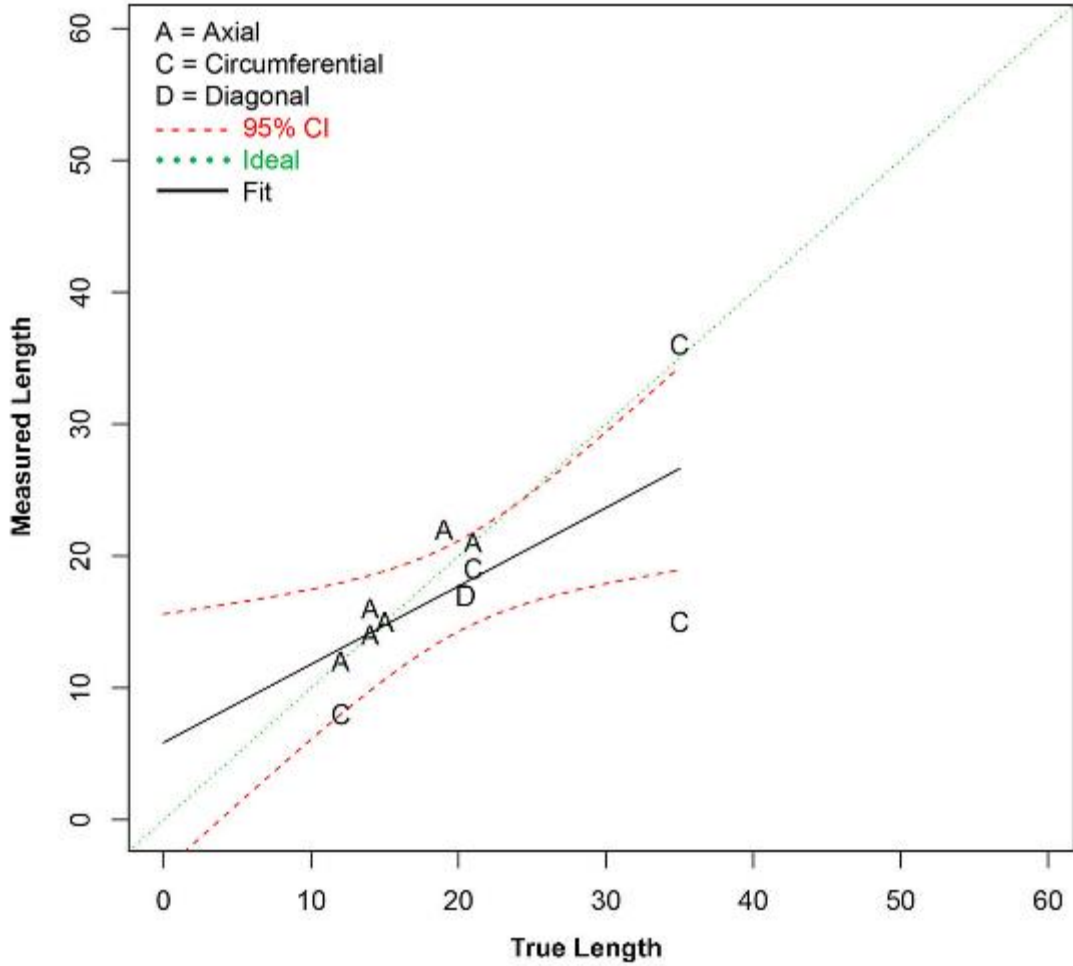


Figure G.31 Length Sizing Regression (in mm) for Procedure ECT.135 on LBDMW Test Blocks in PARENT Blind Testing (I.D. Access)

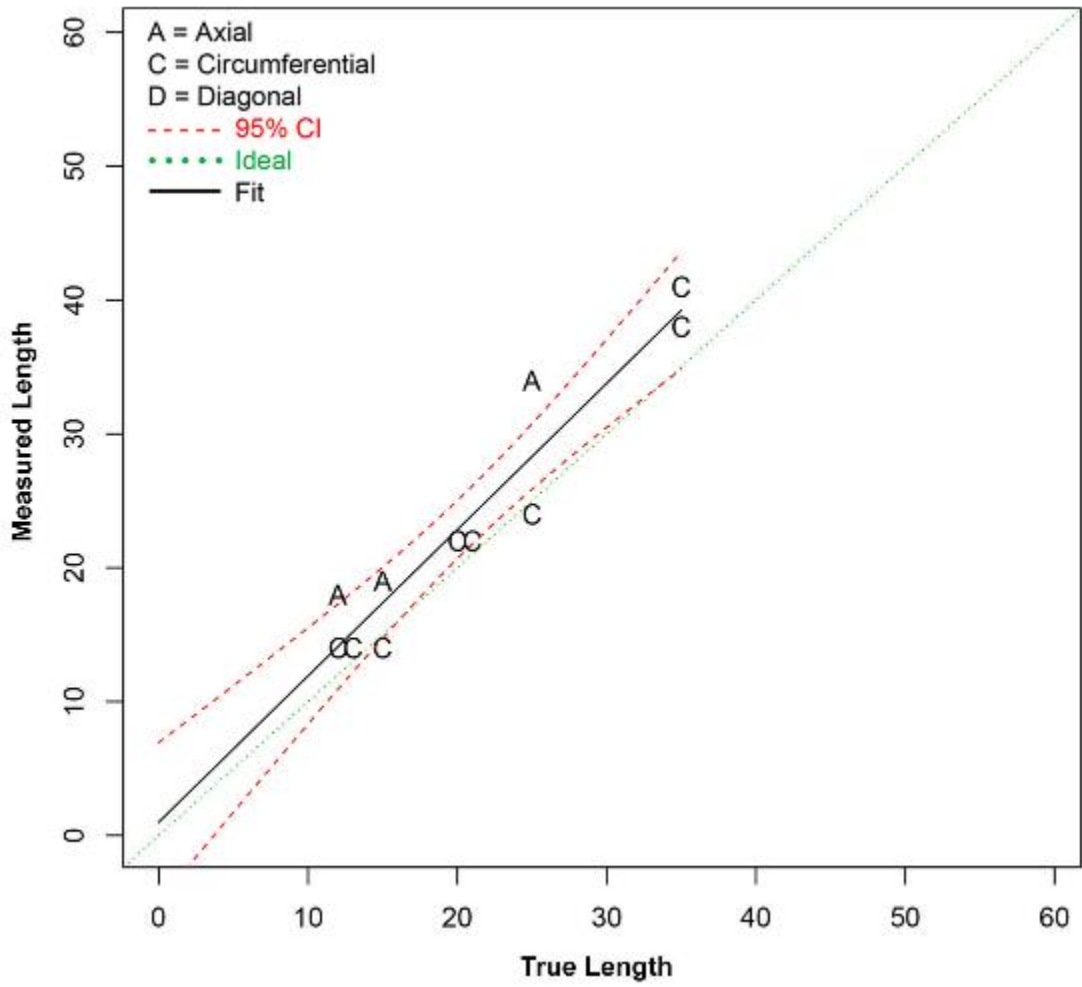


Figure G.32 Length Sizing Regression (in mm) for Procedure UT.ETC.144 on LBDMW Test Blocks in PARENT Blind Testing (I.D. Access)

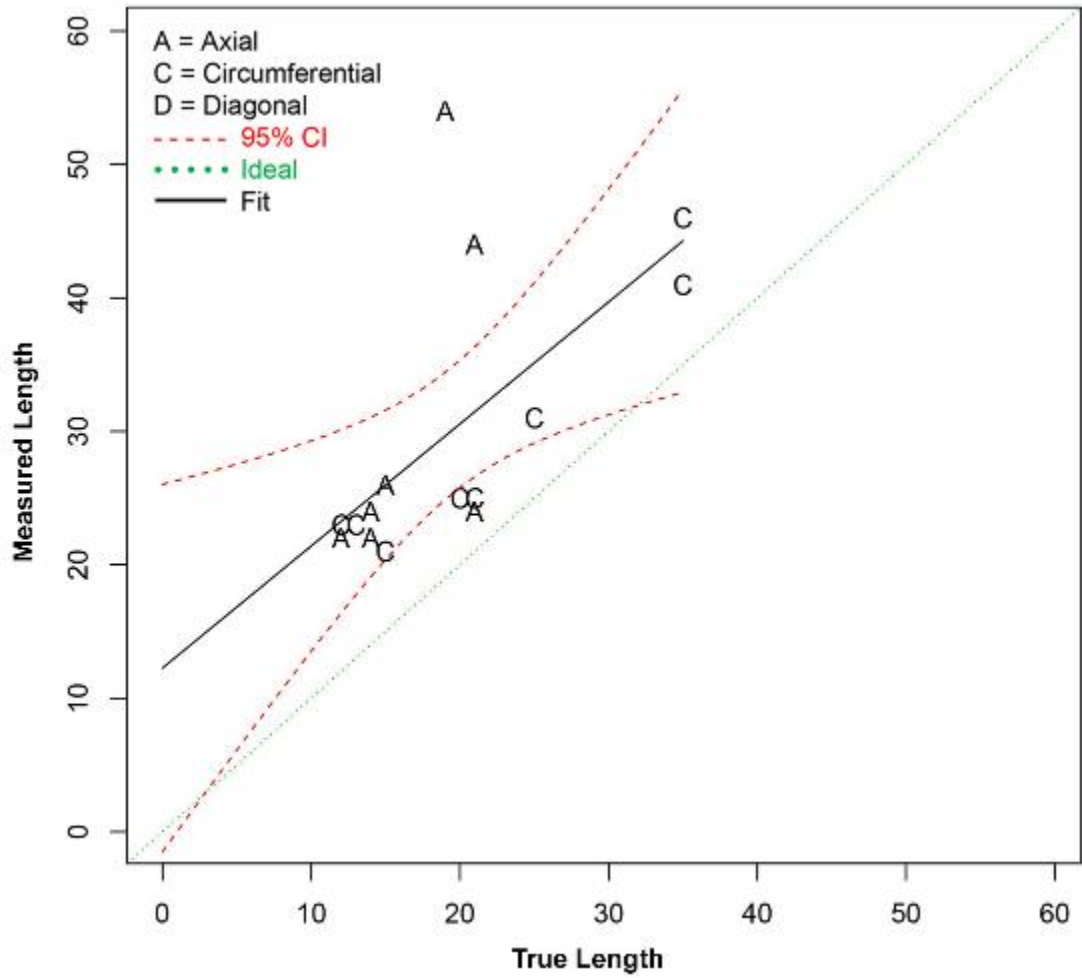


Figure G.33 Length Sizing Regression (in mm) for Procedure UT.PAUT.113 on LBDMW Test Blocks in PARENT Blind Testing (I.D. Access)

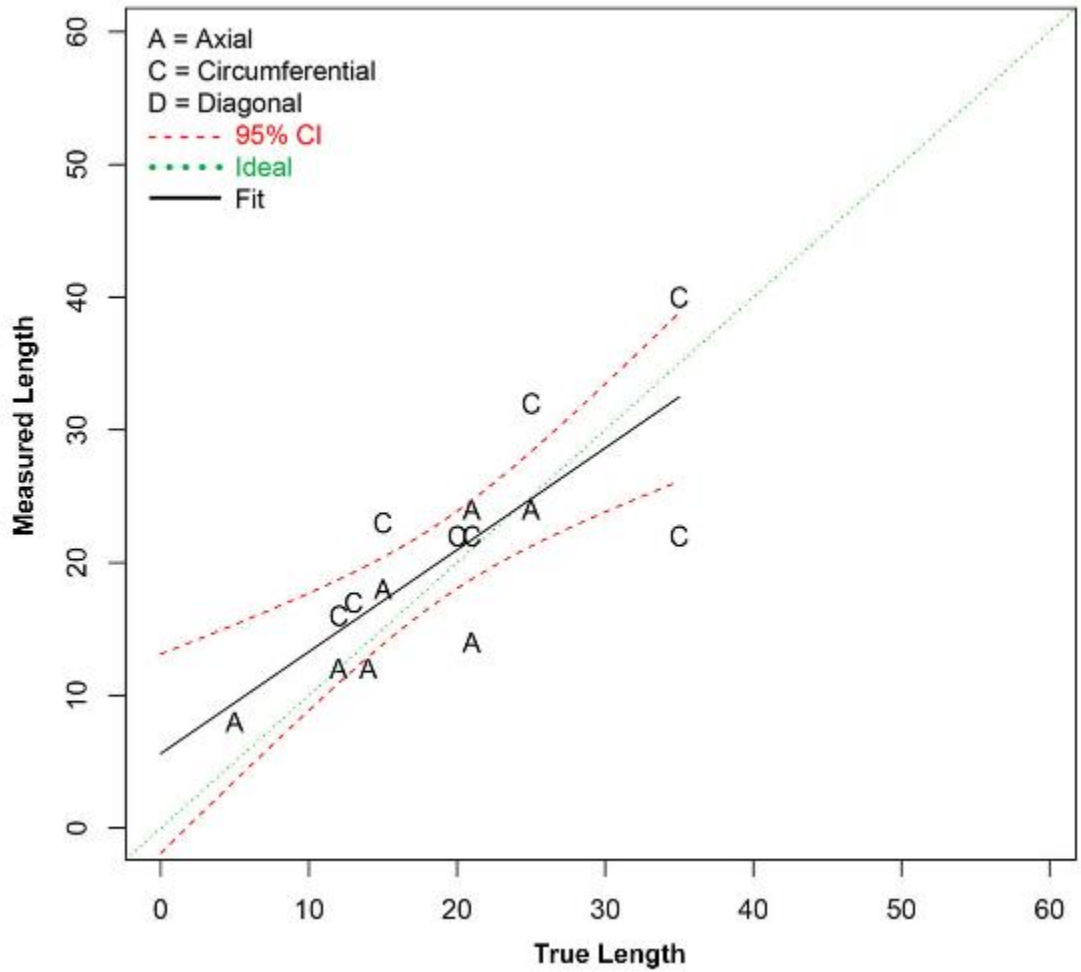


Figure G.34 Length Sizing Regression (in mm) for Procedure UT.TOFD.ECT.101 on LBDMW Test Blocks in PARENT Blind Testing (I.D. Access)

G.1.2.2 Length Sizing Results for LBDMWs (O.D. Access)

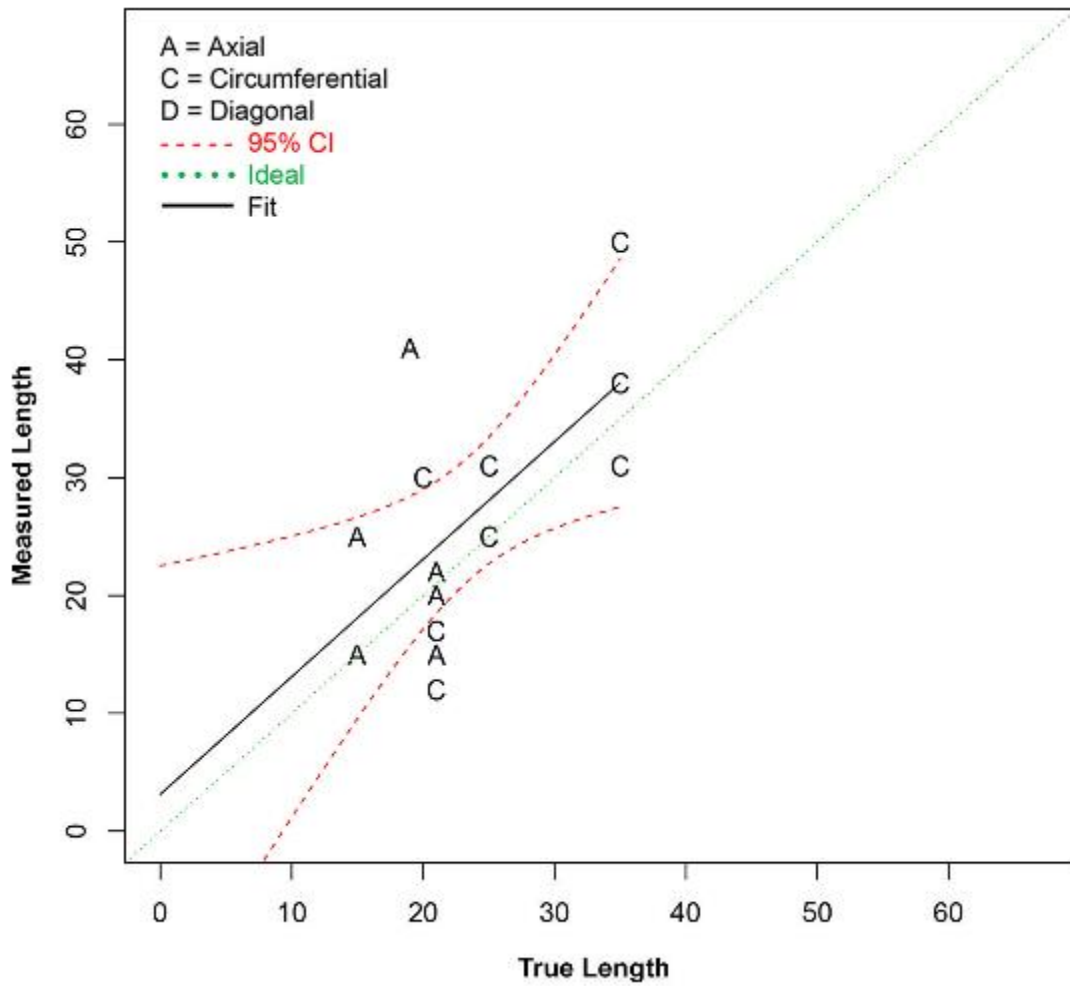


Figure G.35 Length Sizing Regression (in mm) for PAUT Procedures on LBDMW Test Blocks in PARENT Blind Testing (O.D. Access)

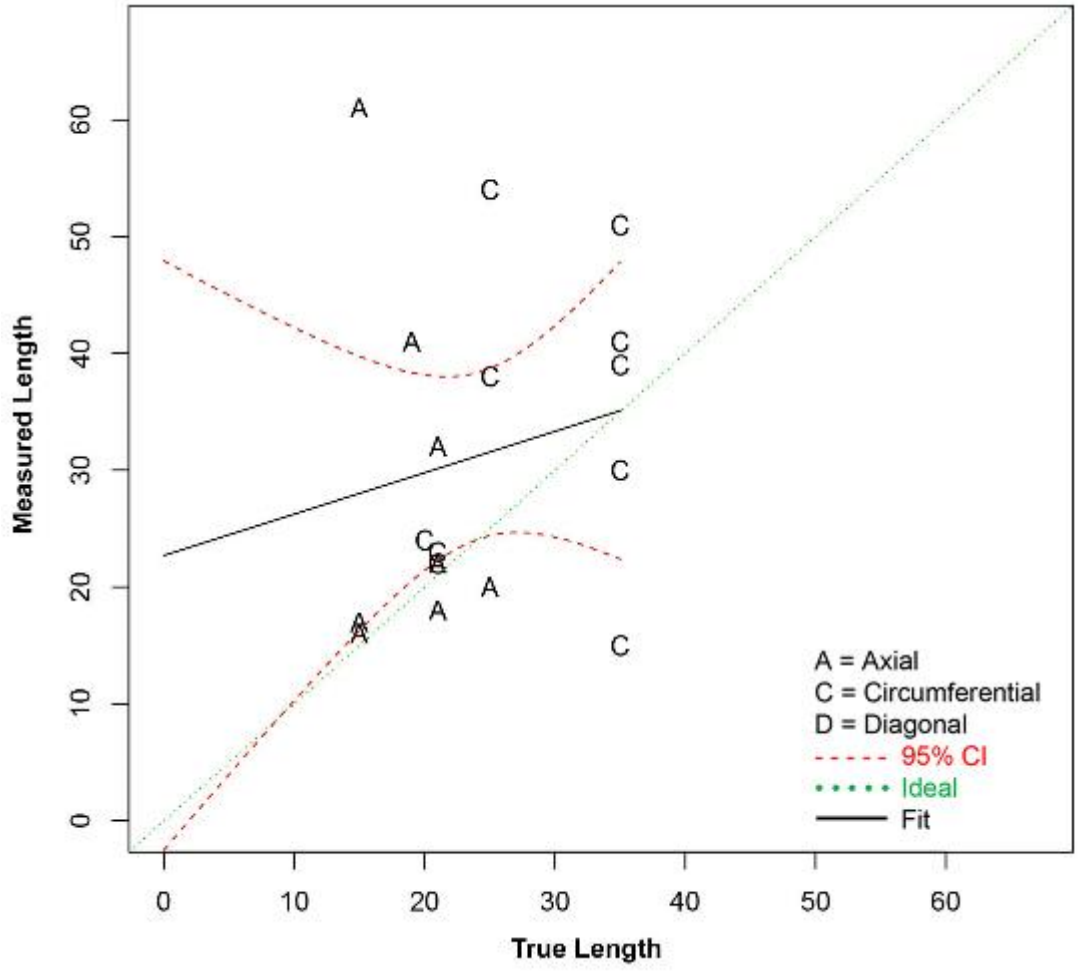


Figure G.36 Length Sizing Regression (in mm) for UT Procedure on LBDMW Test Blocks in PARENT Blind Testing (O.D. Access)

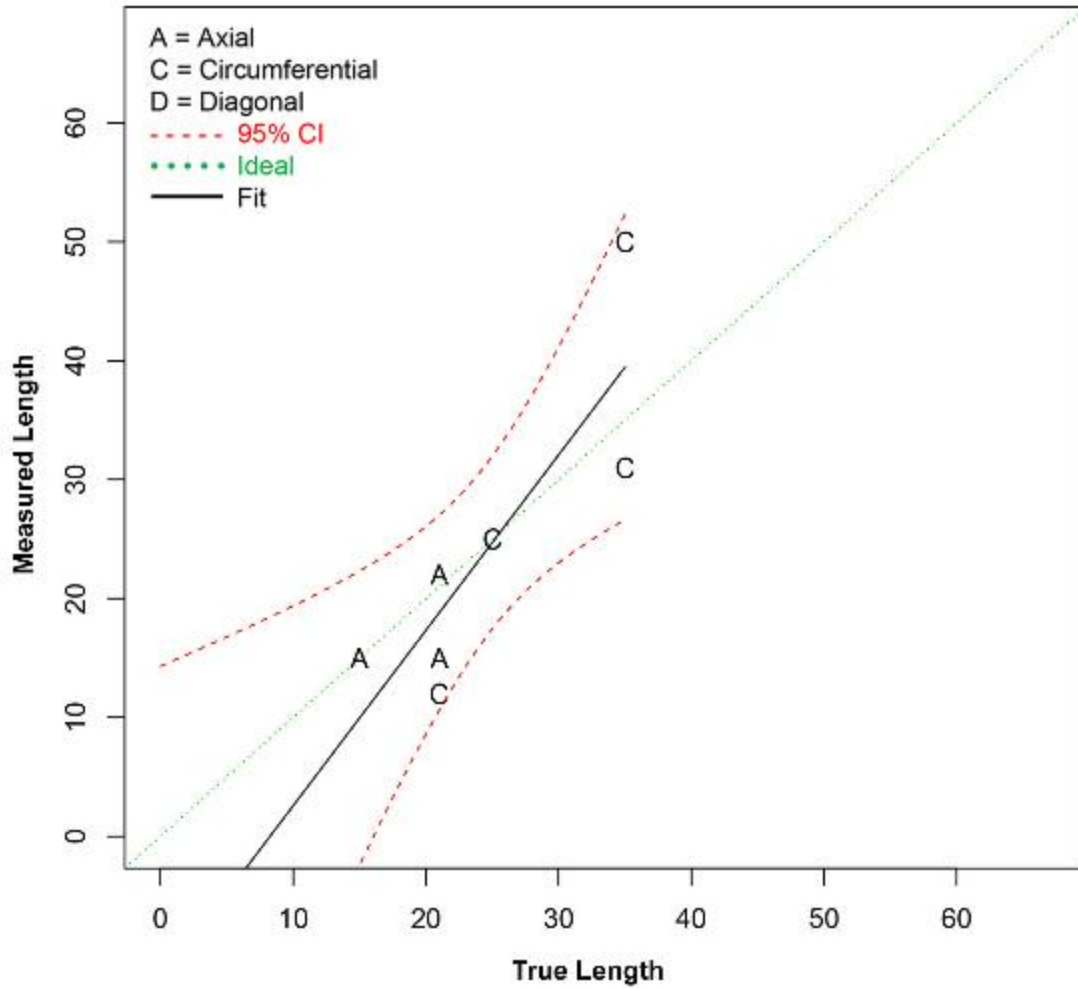


Figure G.37 Length Sizing Regression (in mm) for Procedure PAUT.108 on LBDMW Test Blocks in PARENT Blind Testing (O.D. Access)

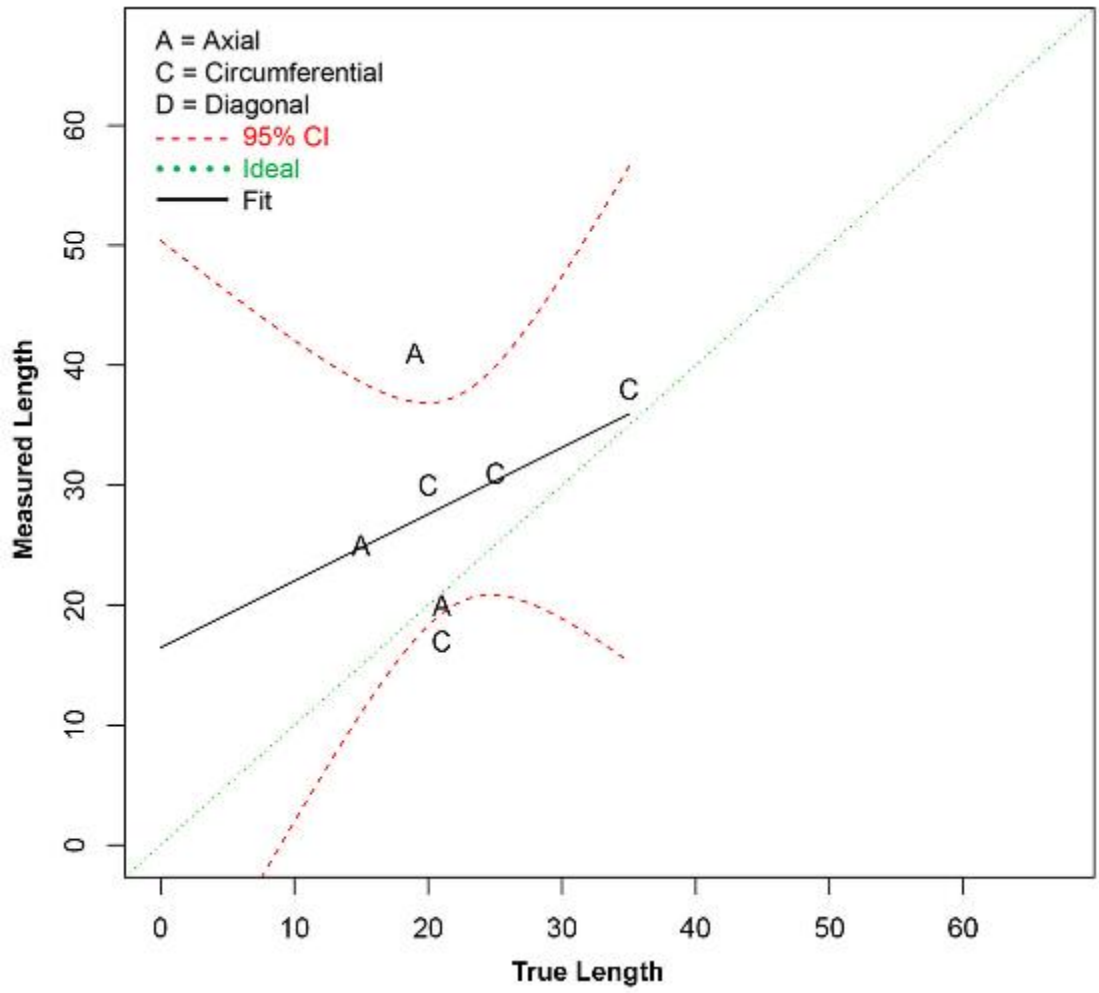


Figure G.38 Length Sizing Regression (in mm) for Procedure PAUT.126 on LBDMW Test Blocks in PARENT Blind Testing (O.D. Access)

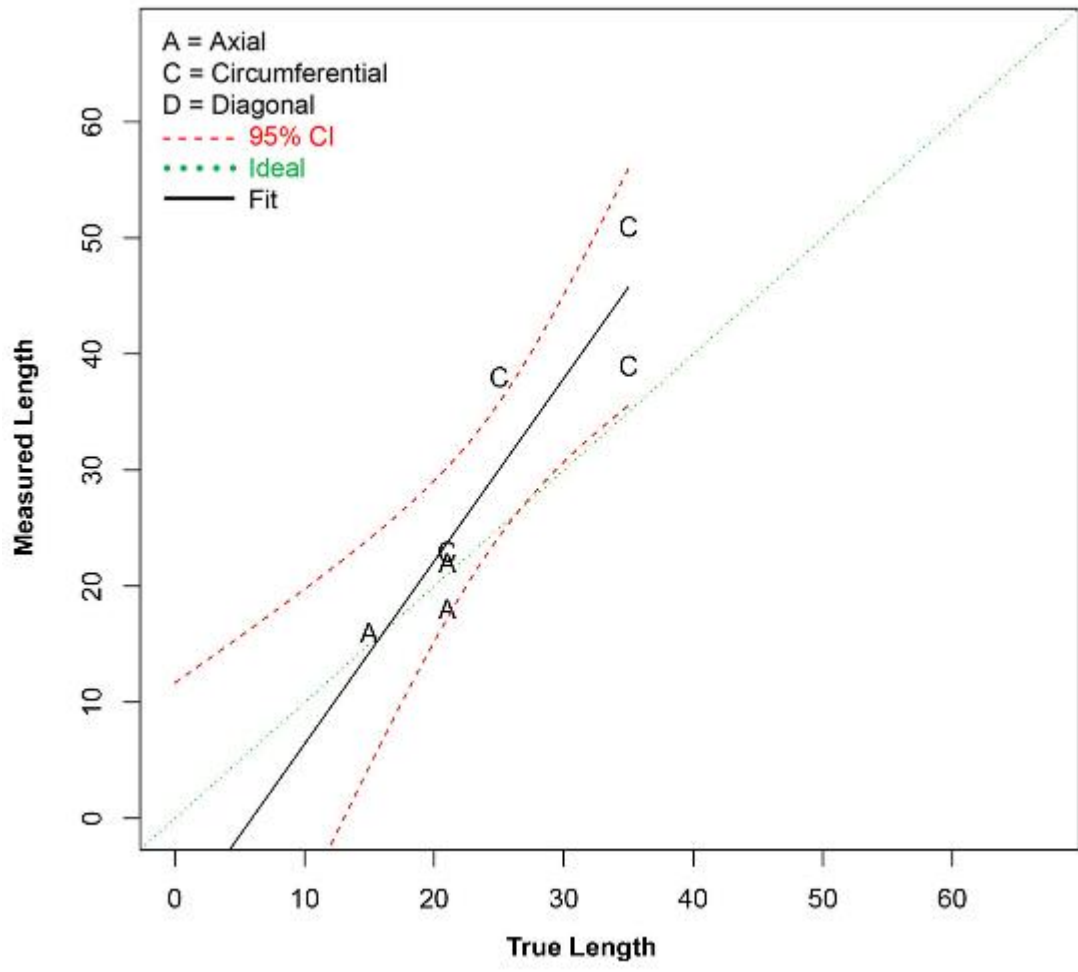


Figure G.39 Length Sizing Regression (in mm) for Procedure UT.108 on LBDMW Test Blocks in PARENT Blind Testing (O.D. Access)

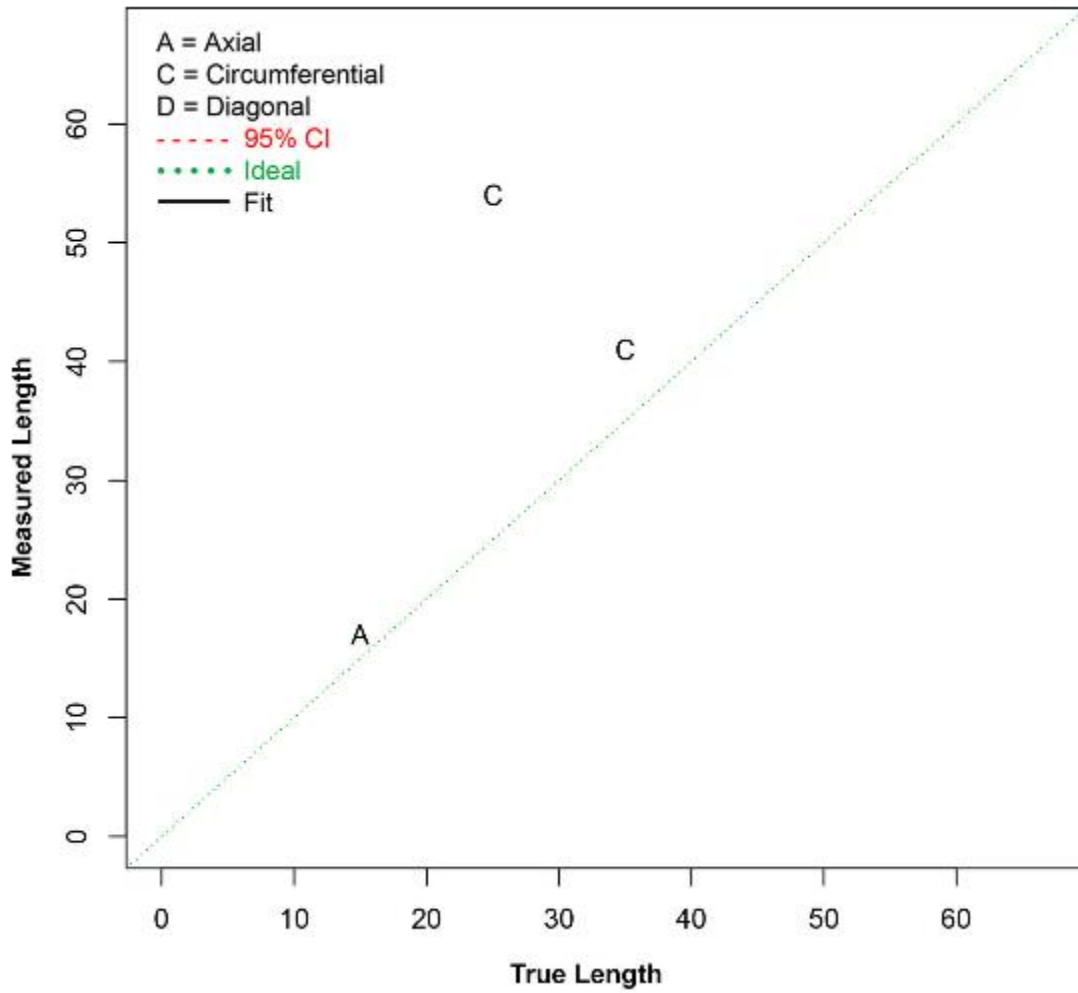


Figure G.40 Length Sizing Regression (in mm) for Procedure UT.126 on LBDMW Test Blocks in PARENT Blind Testing (O.D. Access)

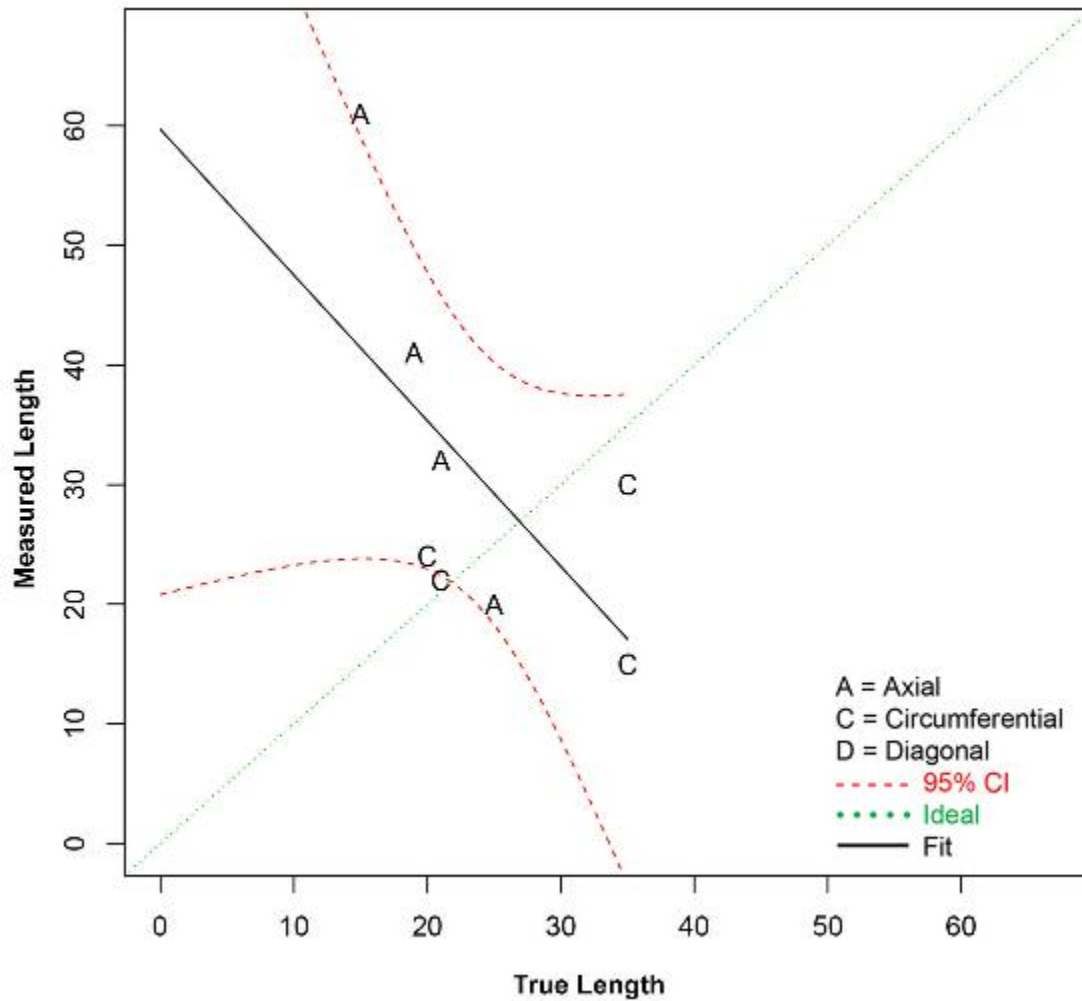


Figure G.41 Length Sizing Regression (in mm) for Procedure UT.134 on LBDMW Test Blocks in PARENT Blind Testing (O.D. Access)

G.1.2.3 Length Sizing Results for SBDMWs

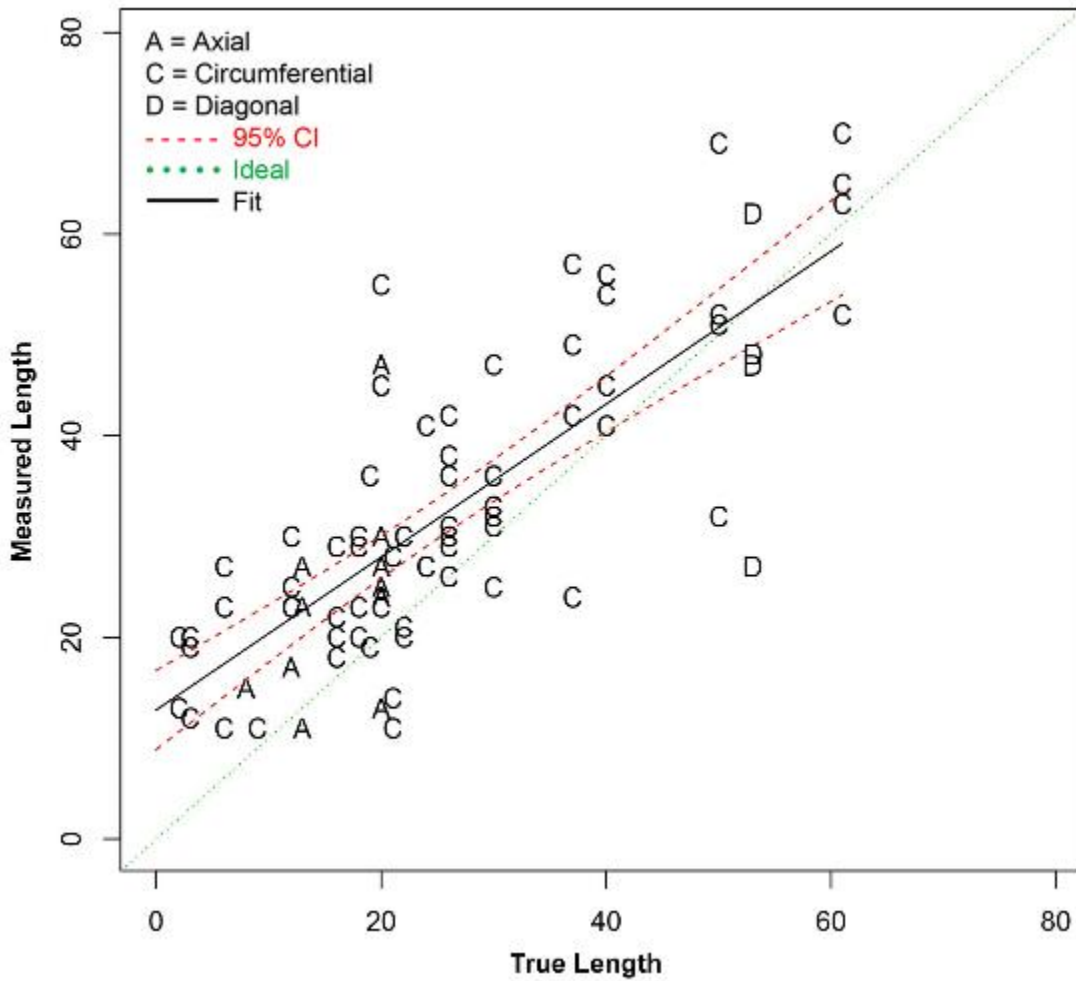


Figure G.42 Length Sizing Regression (in mm) for PAUT Procedure on SBDMW Test Blocks in PARENT Blind Testing

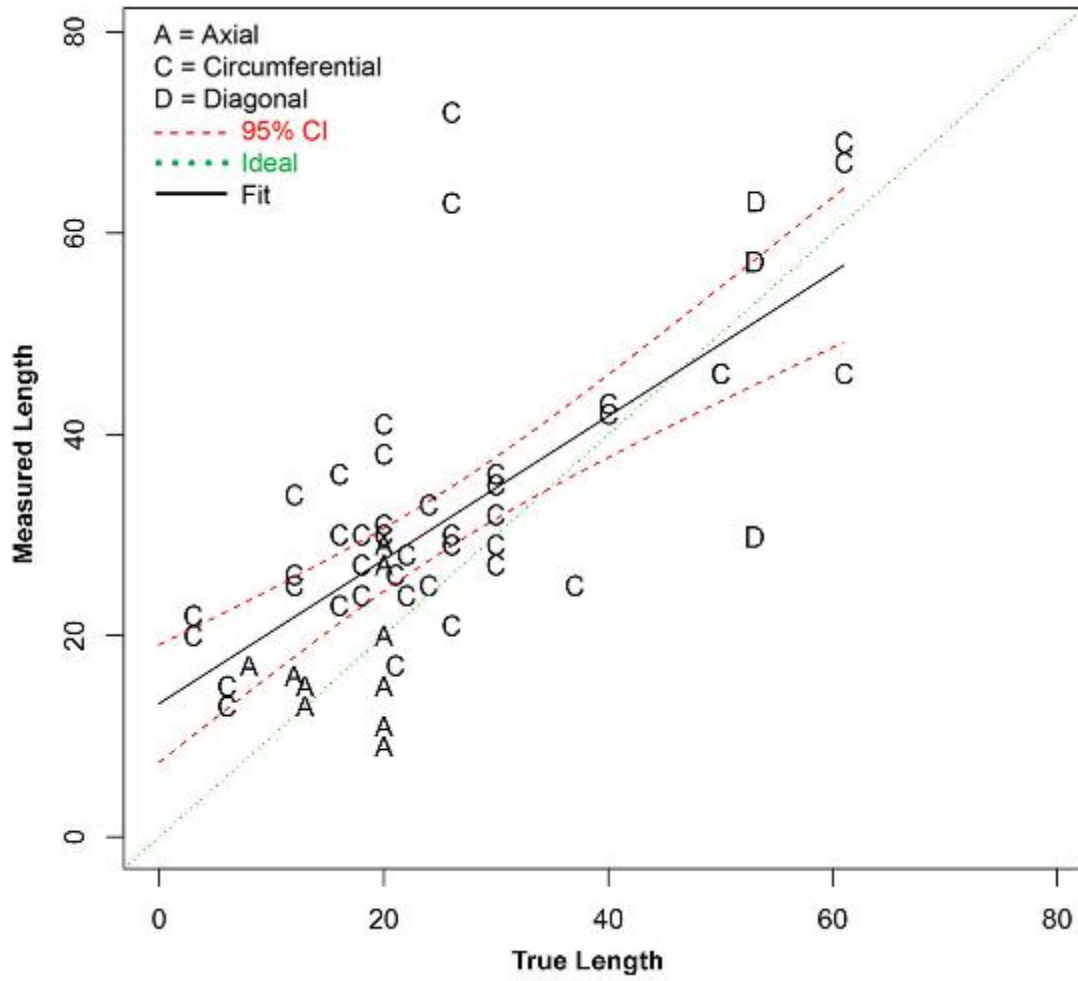


Figure G.43 Length Sizing Regression (in mm) for UT Procedure on SBDMW Test Blocks in PARENT Blind Testing

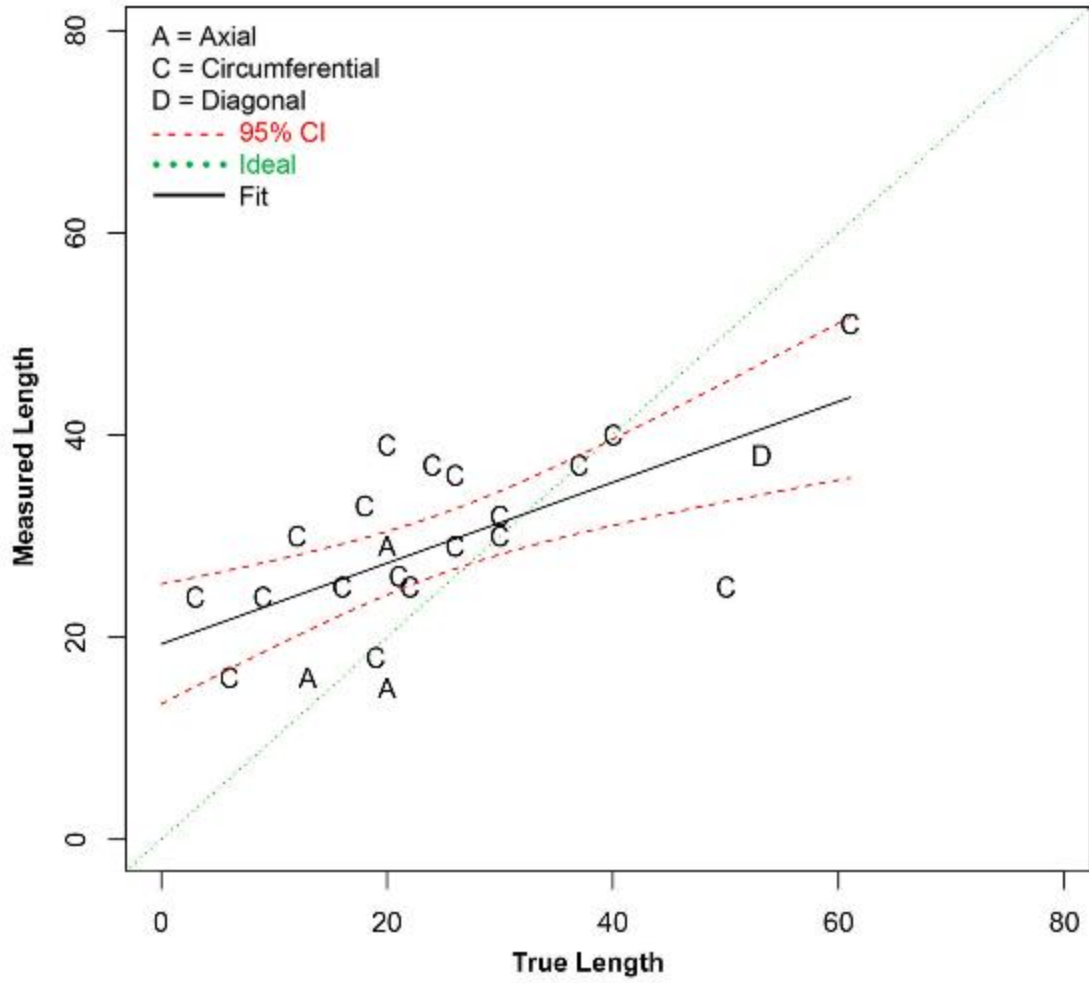


Figure G.44 Length Sizing Regression (in mm) for UT.TOFD Procedure on SBDMW Test Blocks in PARENT Blind Testing

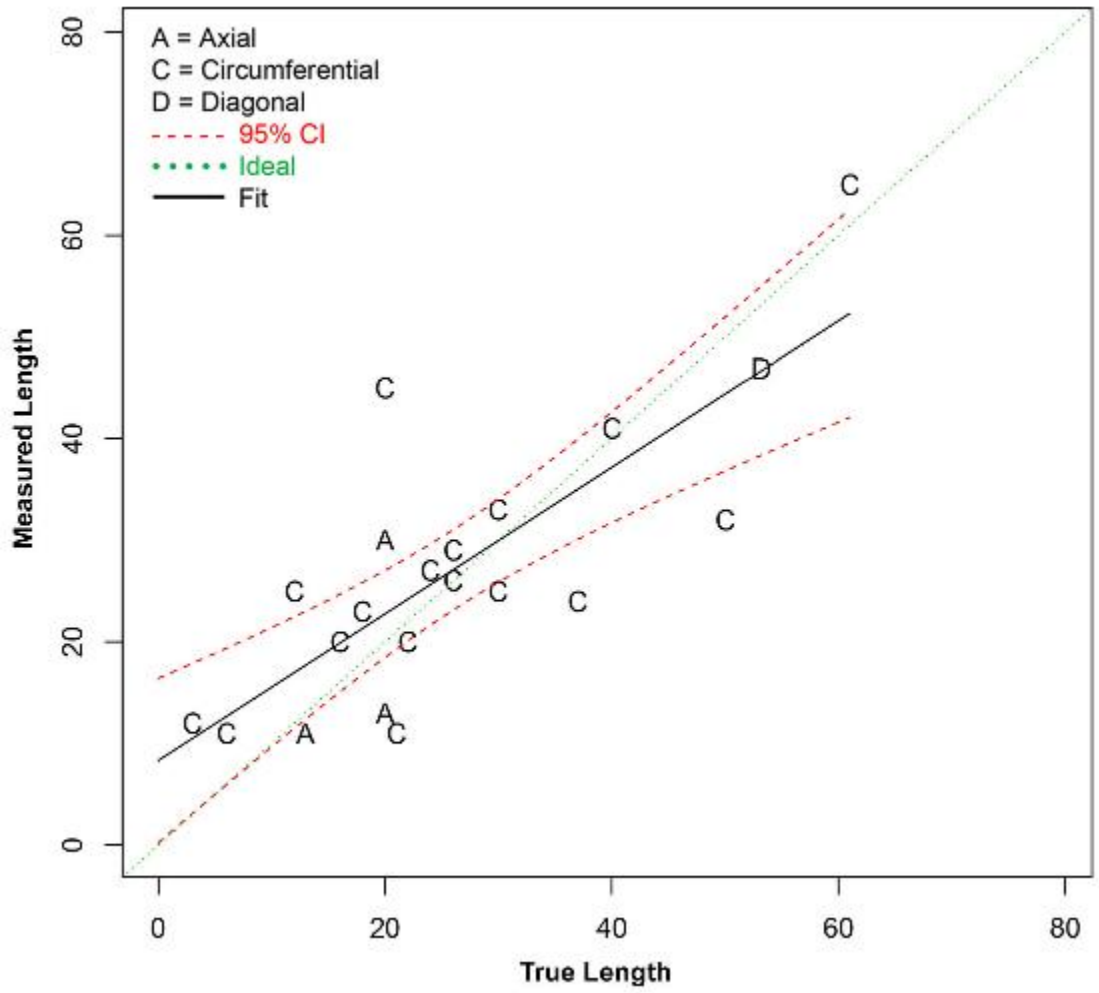


Figure G.45 Length Sizing Regression (in mm) for Procedure PAUT.108 on SBDMW Test Blocks in PARENT Blind Testing

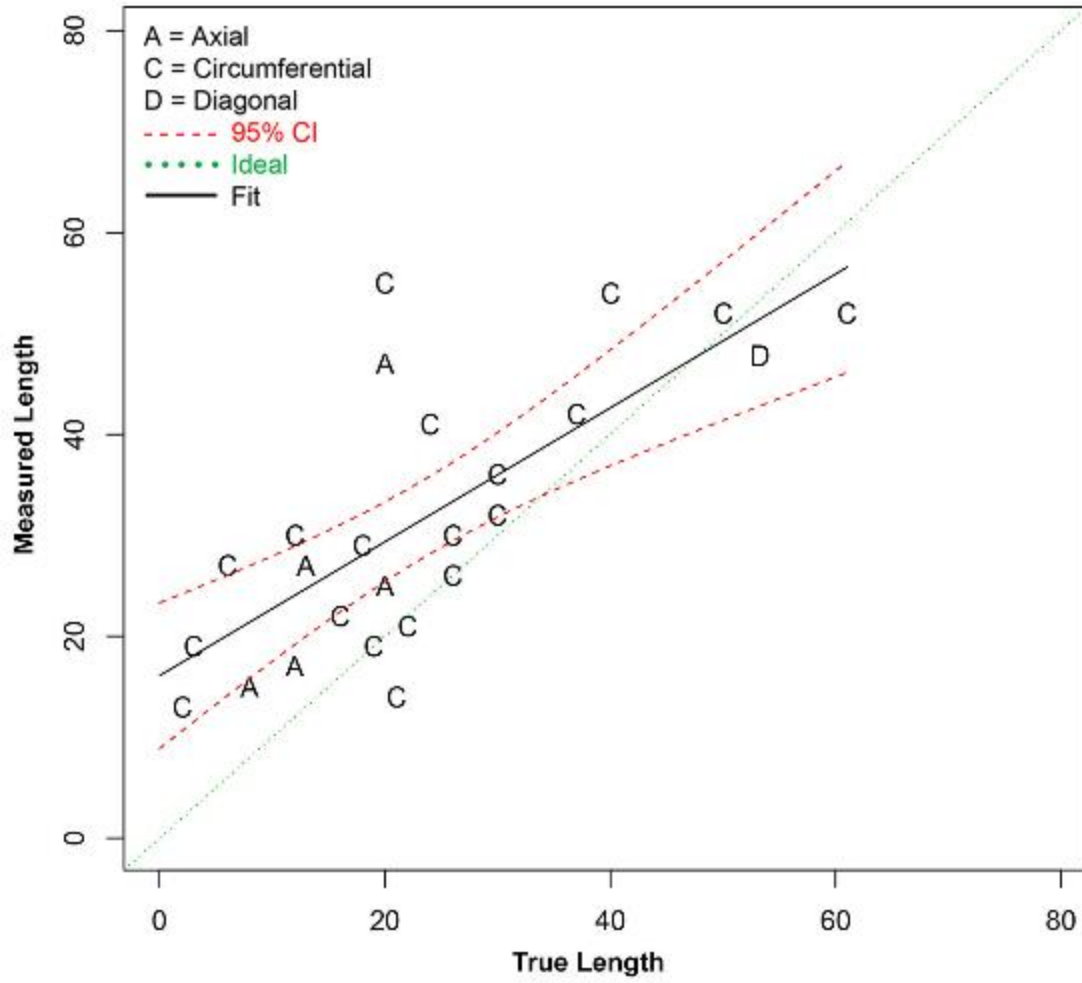


Figure G.46 Length Sizing Regression (in mm) for Procedure PAUT.115 on SBDMW Test Blocks in PARENT Blind Testing

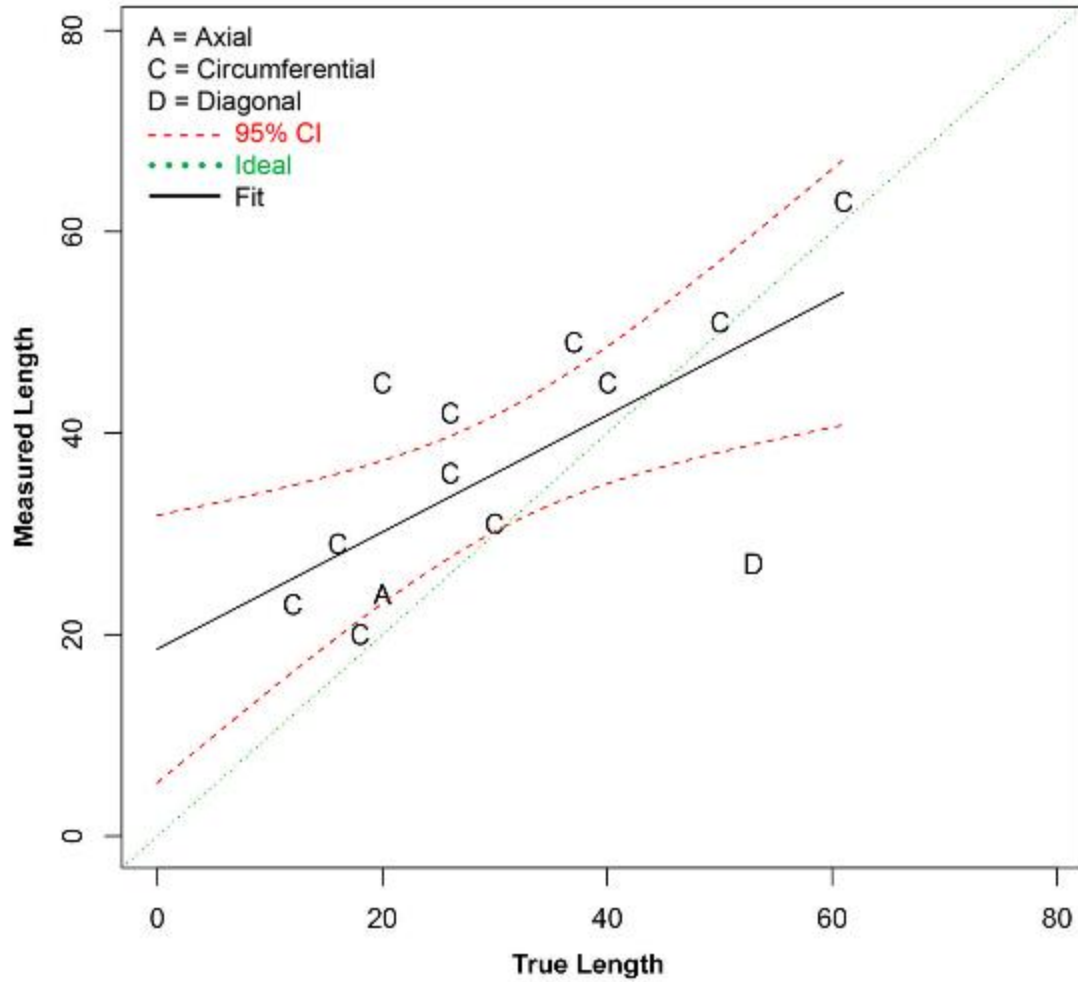


Figure G.47 Length Sizing Regression (in mm) for Procedure PAUT.126 on SBDMW Test Blocks in PARENT Blind Testing

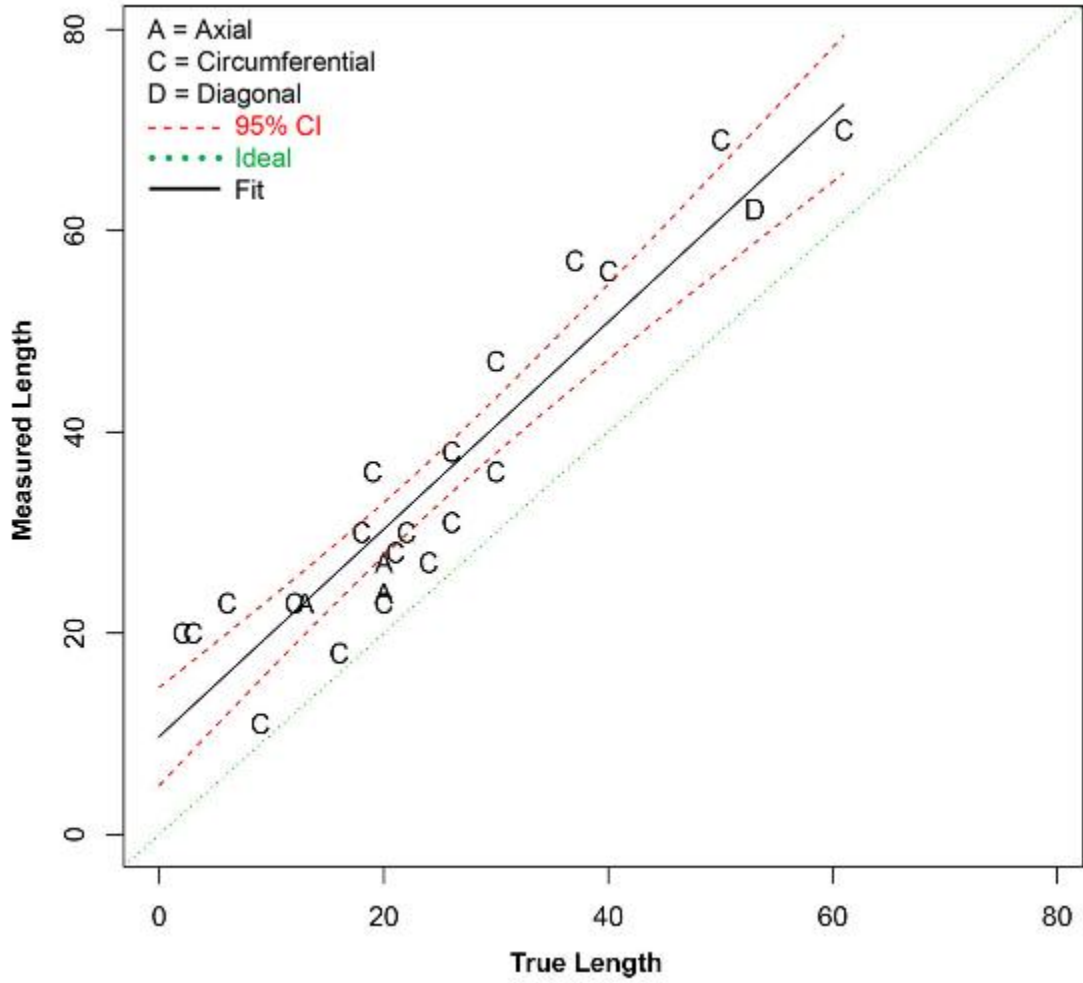


Figure G.48 Length Sizing Regression (in mm) for Procedure PAUT.128 on SBDMW Test Blocks in PARENT Blind Testing

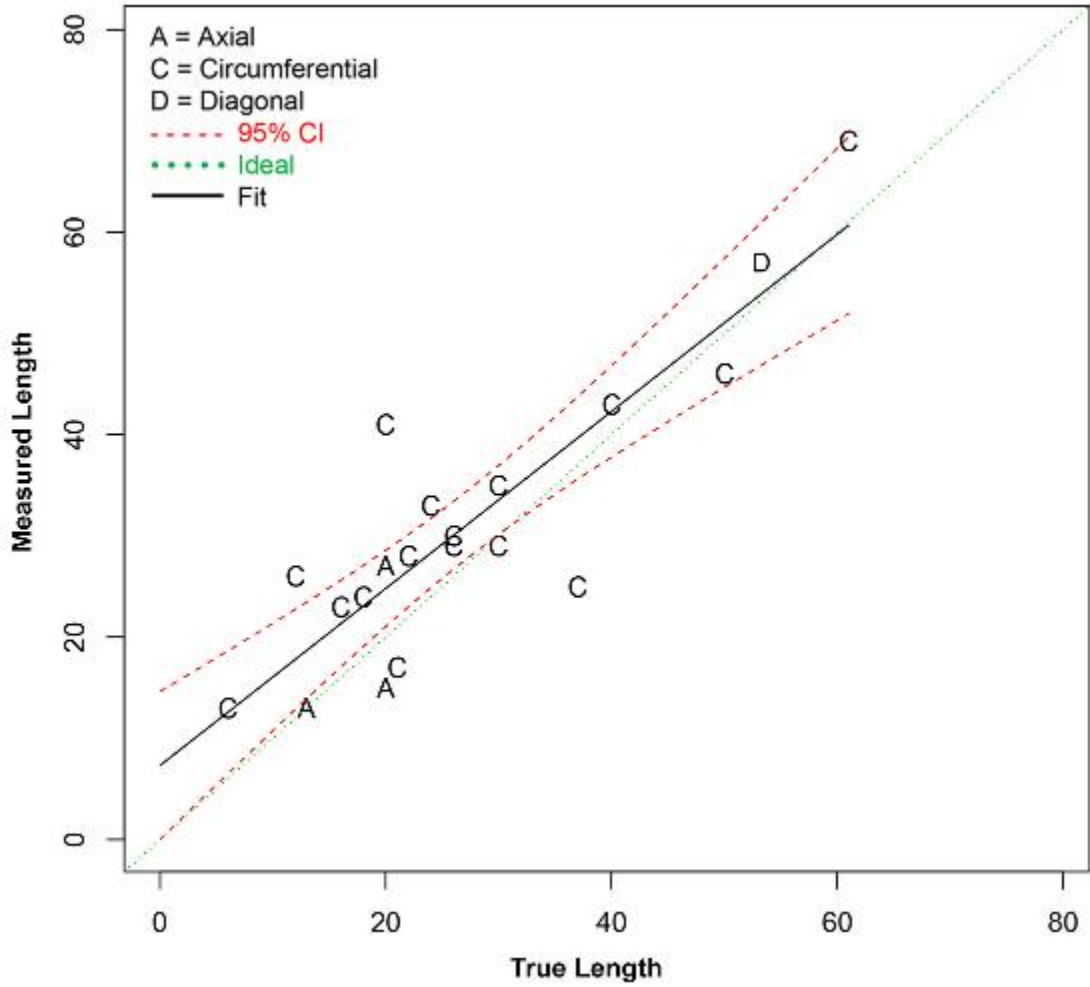


Figure G.49 Length Sizing Regression (in mm) for Procedure UT.108 on SBDMW Test Blocks in PARENT Blind Testing

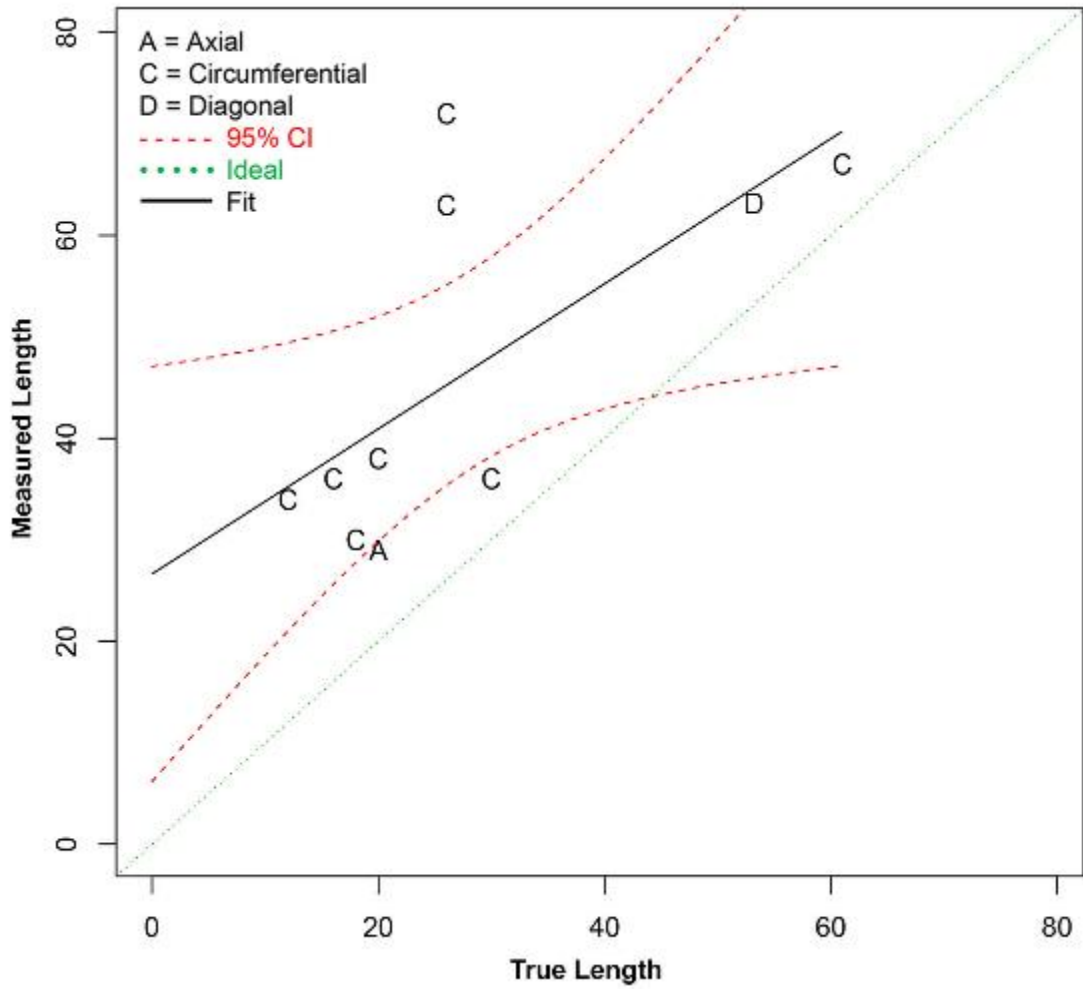


Figure G.50 Length Sizing Regression (in mm) for Procedure UT.126 on SBDMW Test Blocks in PARENT Blind Testing

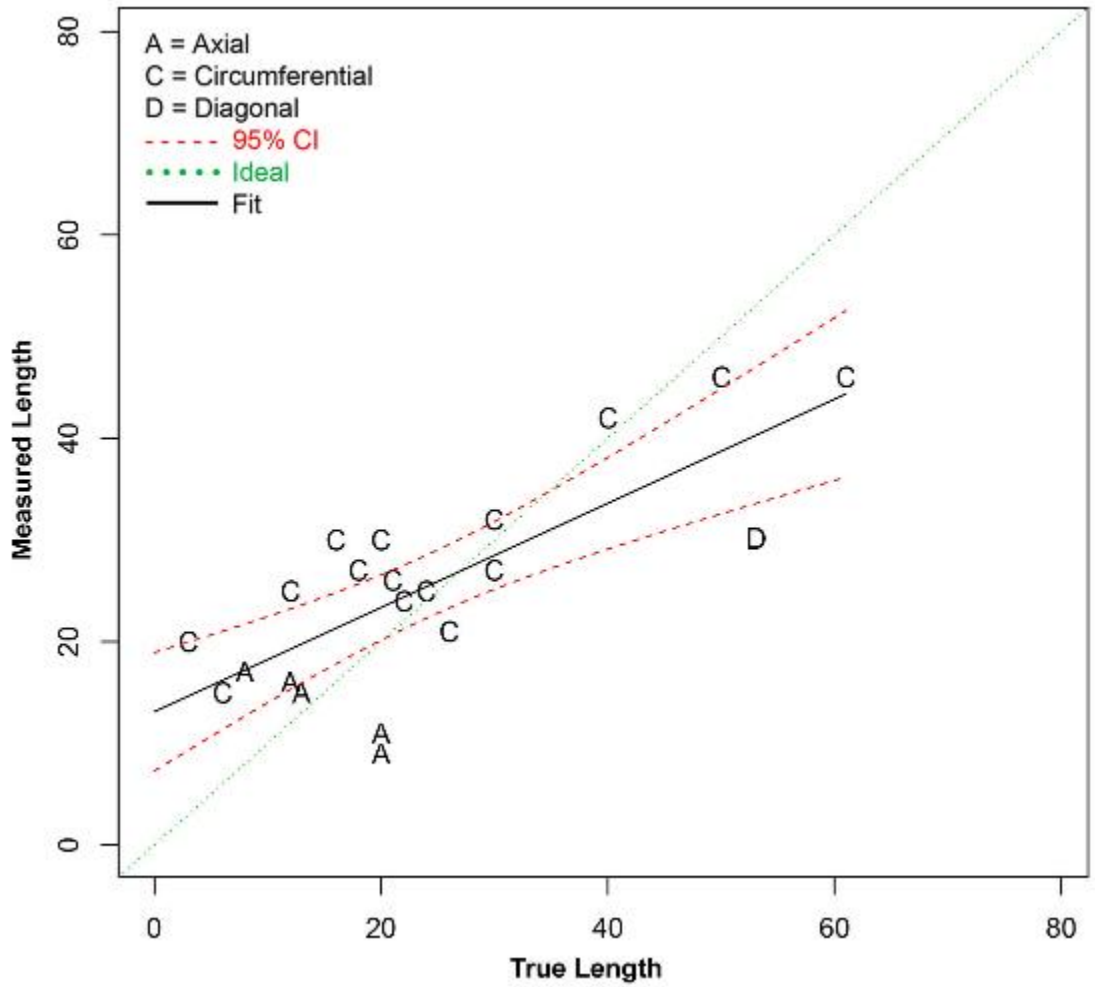


Figure G.51 Length Sizing Regression (in mm) for Procedure UT.134 on SBDMW Test Blocks in PARENT Blind Testing

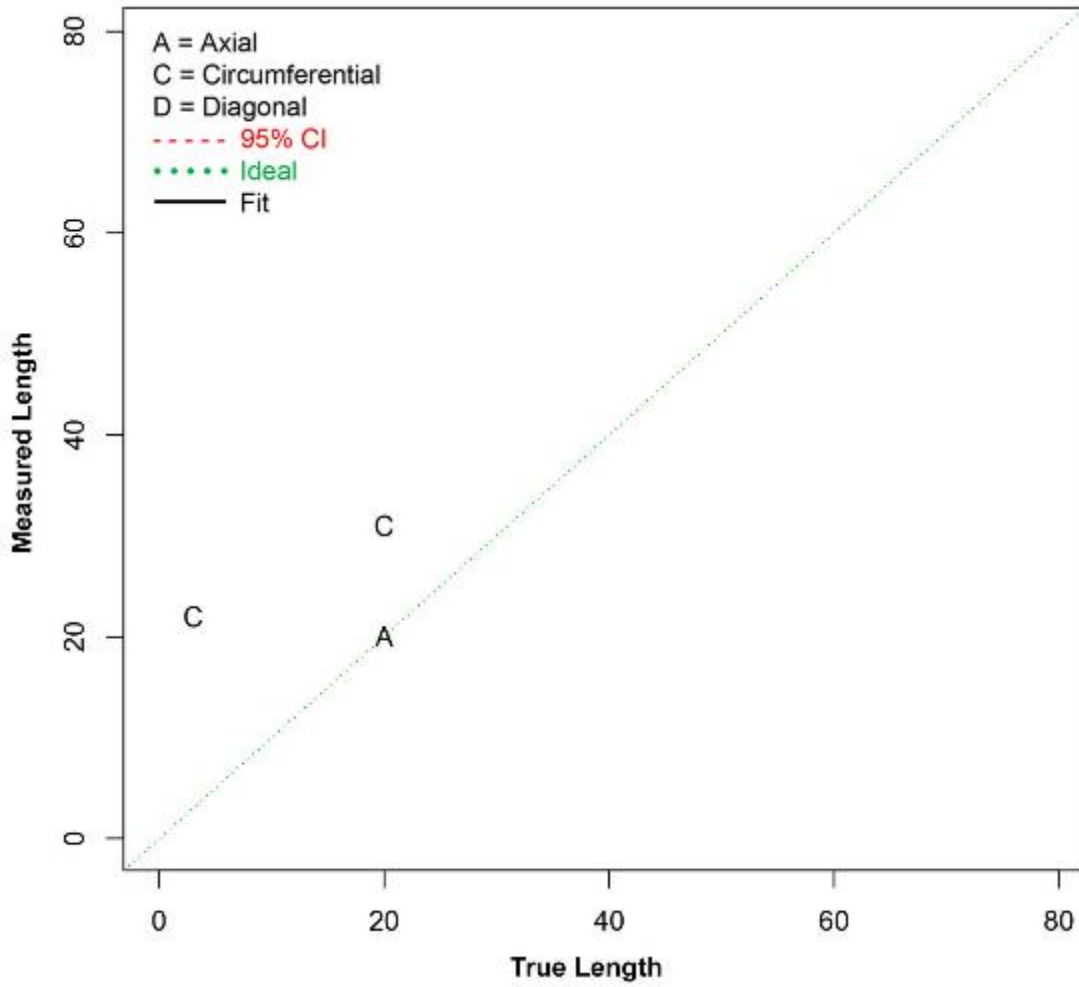


Figure G.52 Length Sizing Regression (in mm) for Procedure UT.25 on SBDMW Test Blocks in PARENT Blind Testing

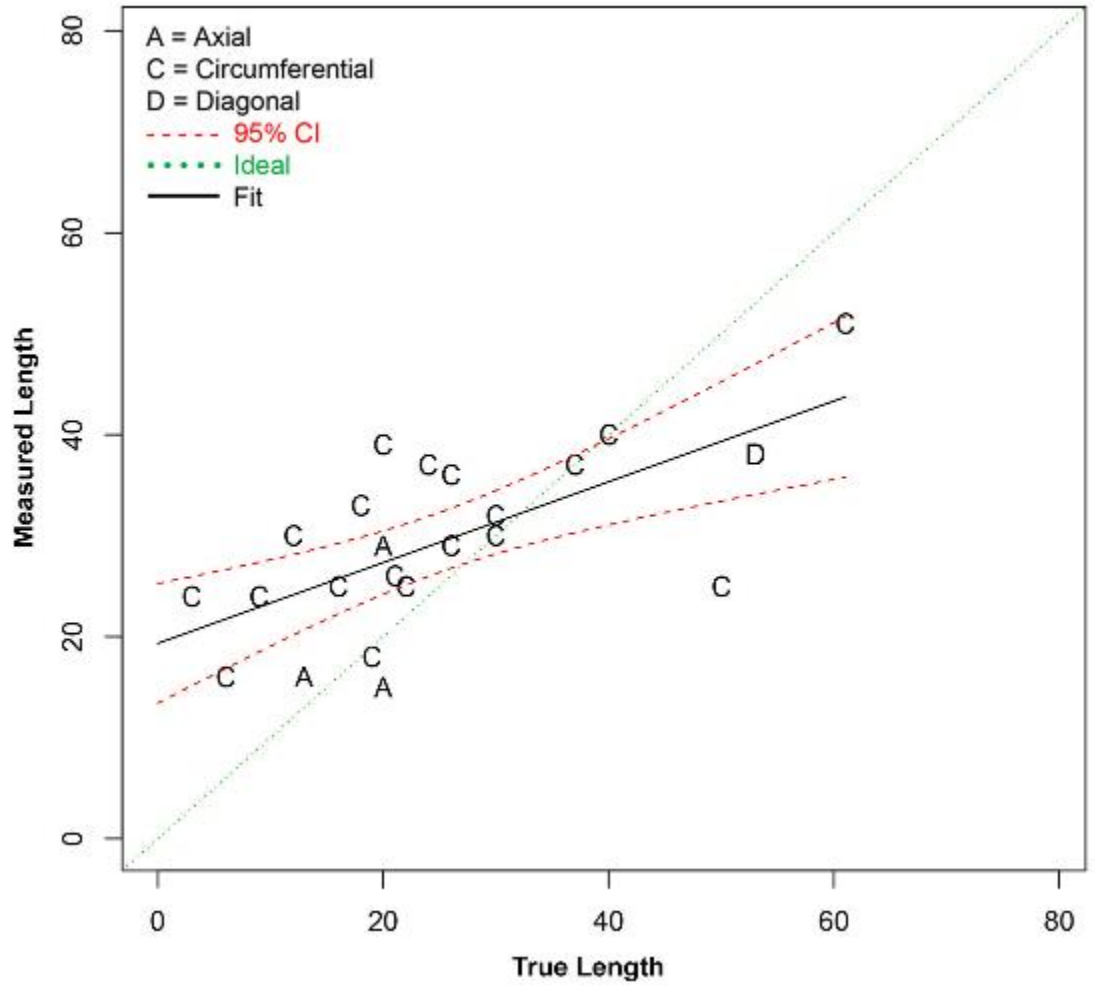


Figure G.53 Length Sizing Regression (in mm) for Procedure UT.TOFD.117 on SBDMW Test Blocks in PARENT Blind Testing

G.1.2.4 Length Sizing Results for BMIs (J-Groove Surface)

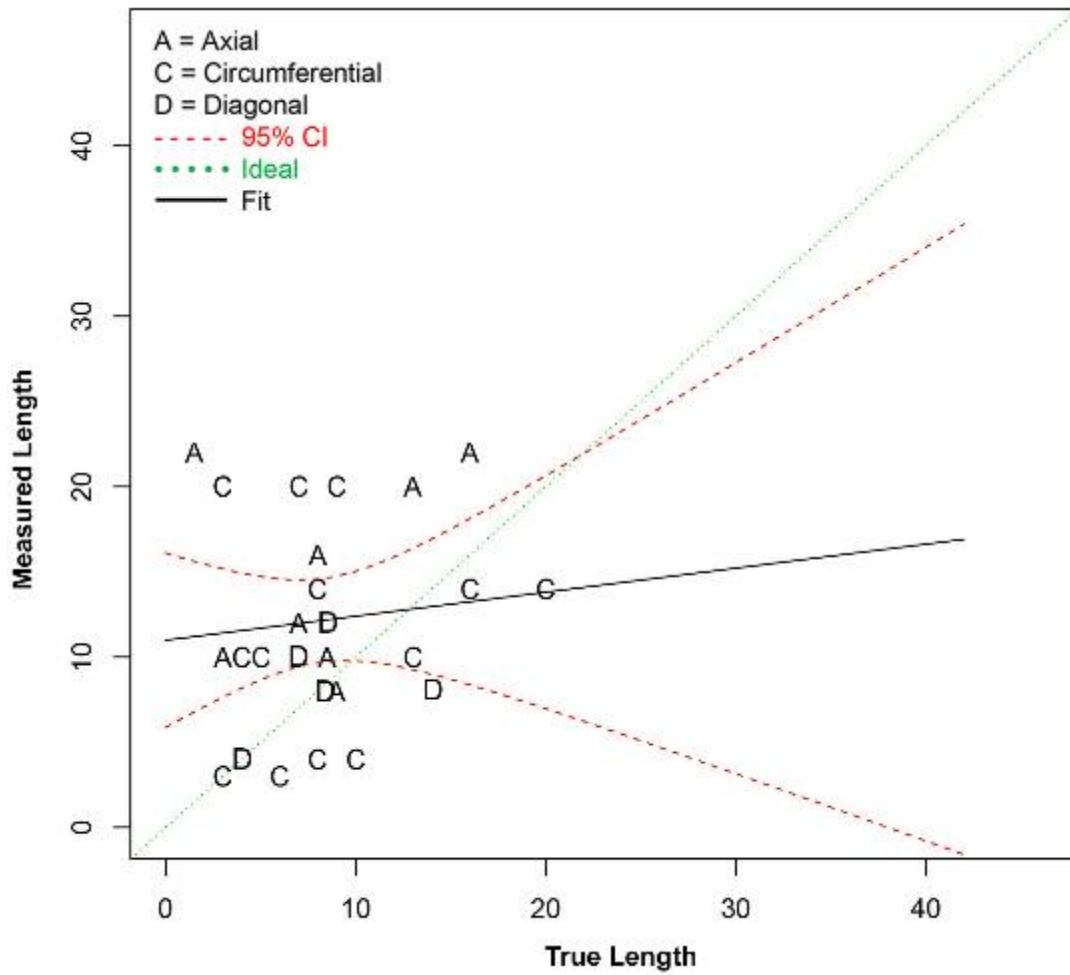


Figure G.54 Length Sizing Regression (in mm) for Procedure ECT.108 on BMI Test Blocks in PARENT Blind Testing

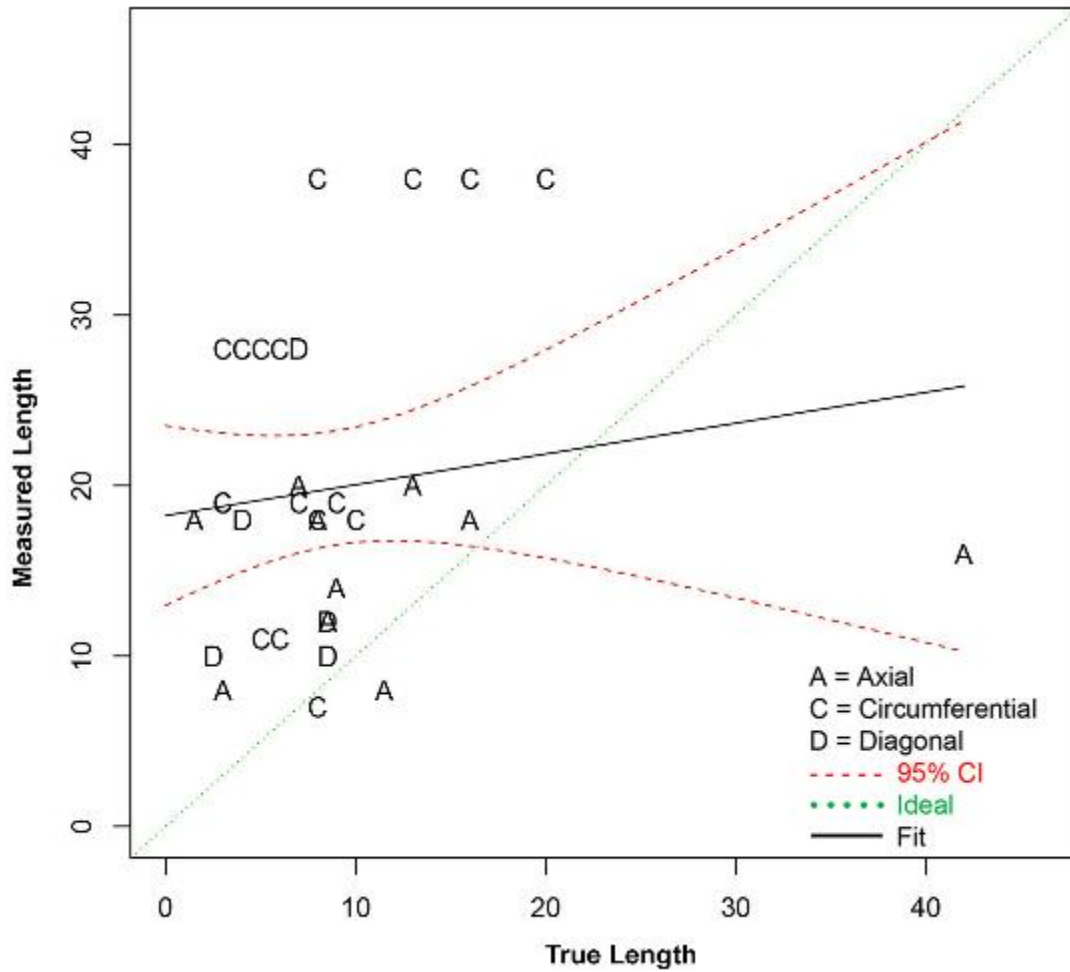


Figure G.55 Length Sizing Regression (in mm) for Procedure ECT.124 on BMI Test Blocks in PARENT Blind Testing

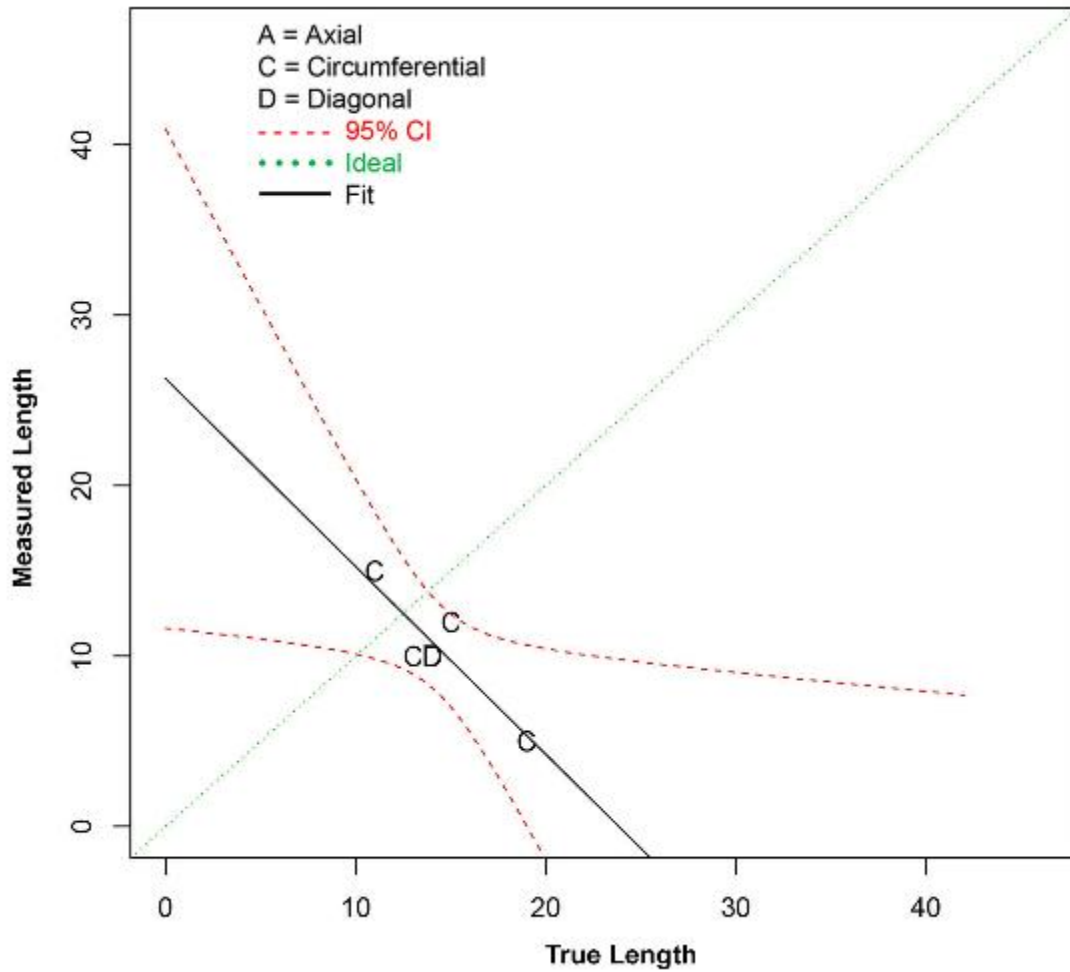


Figure G.56 Length Sizing Regression (in mm) for Procedure TOFD.ECT.126 on BMI Test Blocks in PARENT Blind Testing

G.2 Sizing Results (Blind + Quick-blind)

G.2.1 Depth Sizing Results

G.2.1.1 Depth Sizing Results for LBDMWs (I.D. Access)

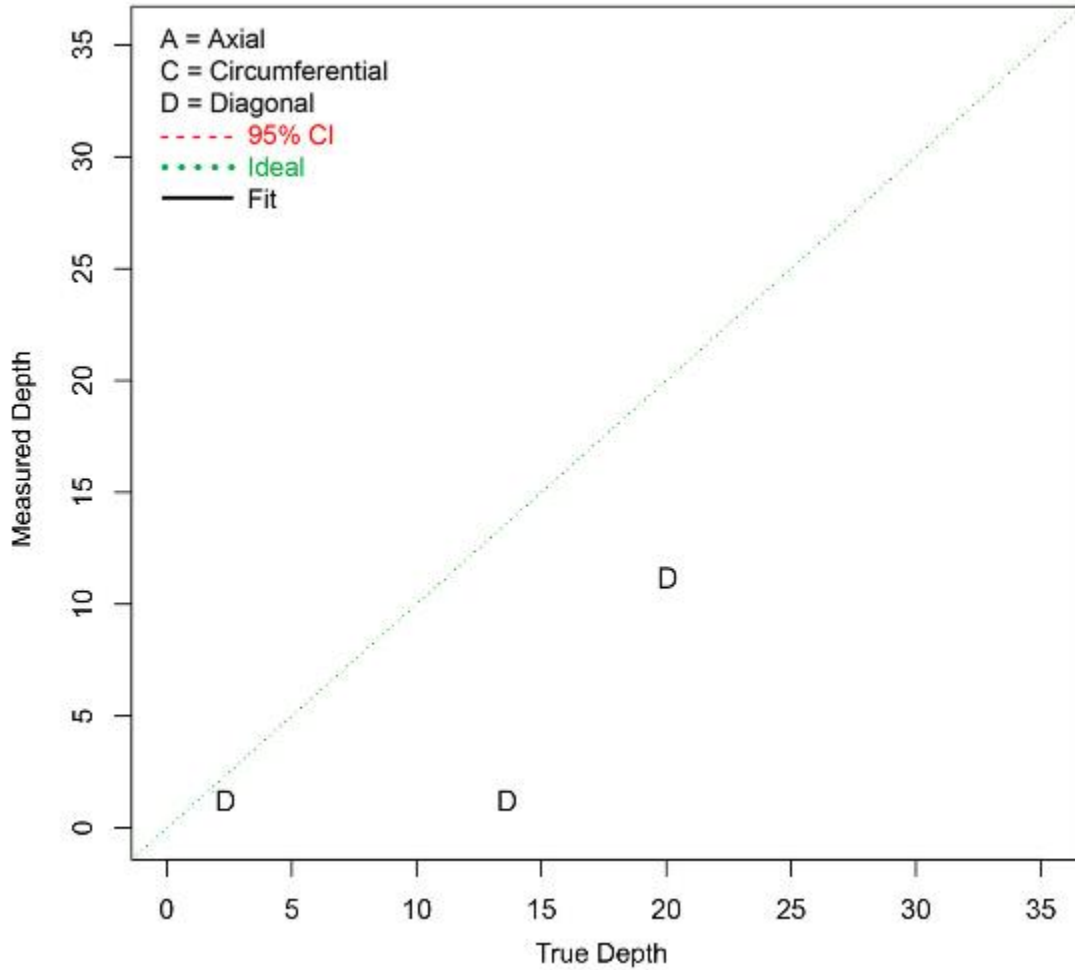


Figure G.57 Depth Sizing Regression (in mm) for PAUT Procedures on LBDMW Test Blocks in PARENT Blind Testing (I.D. Access – Quick-blind)

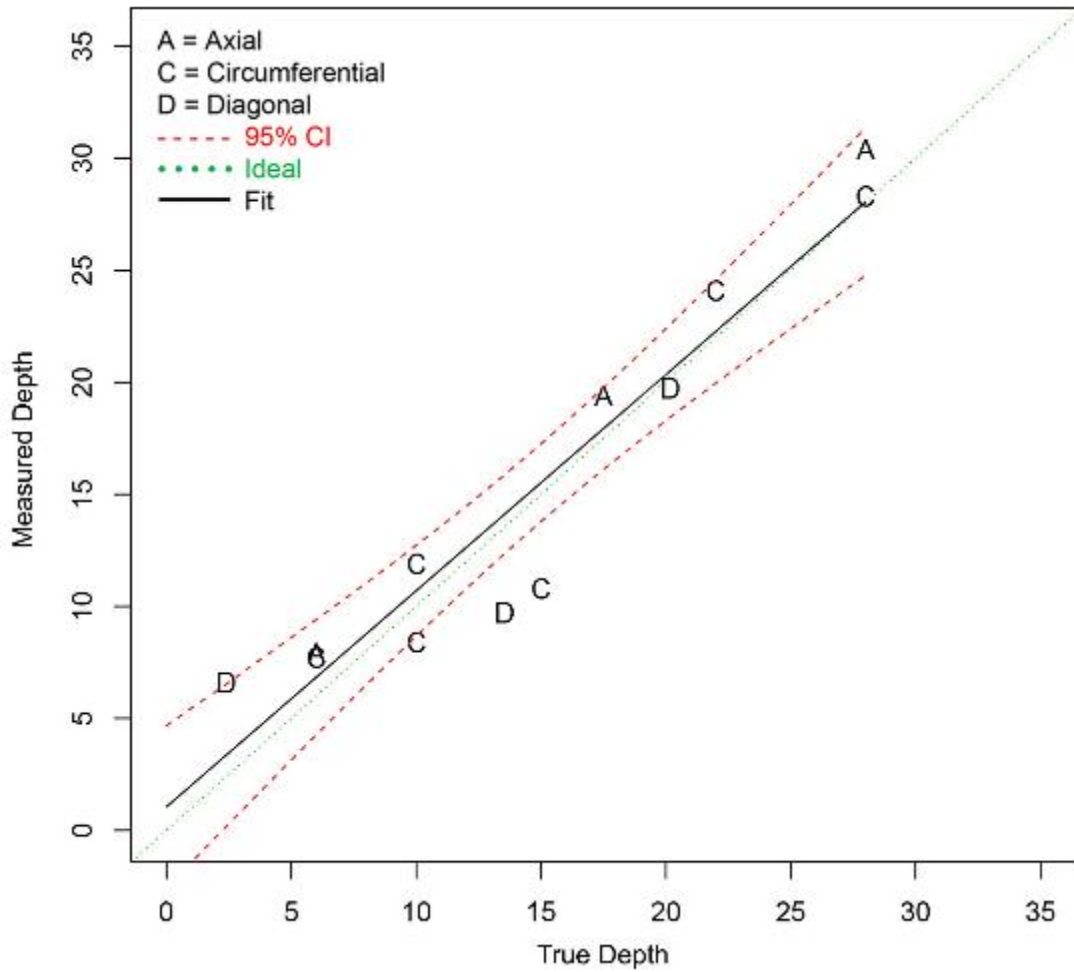


Figure G.58 Depth Sizing Regression (in mm) for UT.ECT Procedures on LBDMW Test Blocks in PARENT Blind Testing (I.D. Access – **Blind + Quick-blind**)

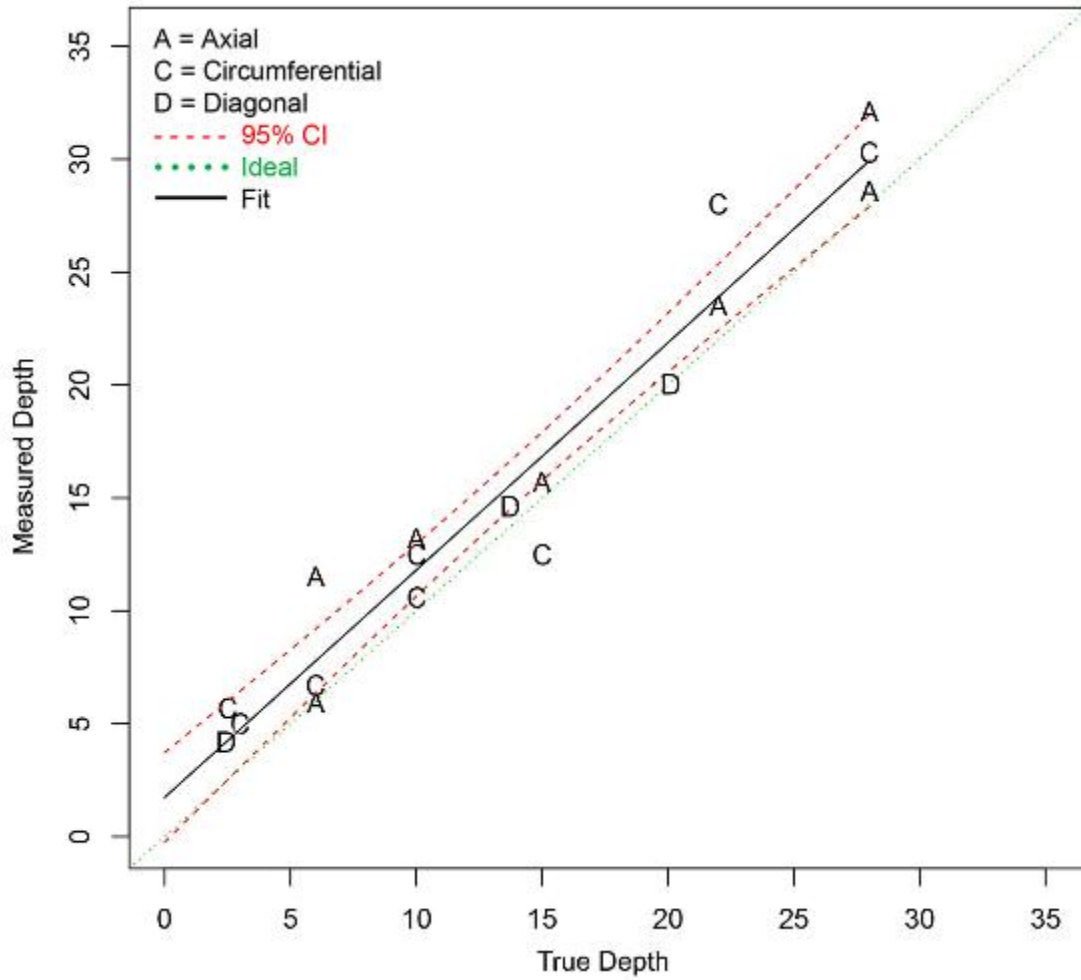


Figure G.59 Depth Sizing Regression (in mm) for UT.PAUT Procedures on LBDMW Test Blocks in PARENT Blind Testing (I.D. Access – **Blind + Quick-blind**)

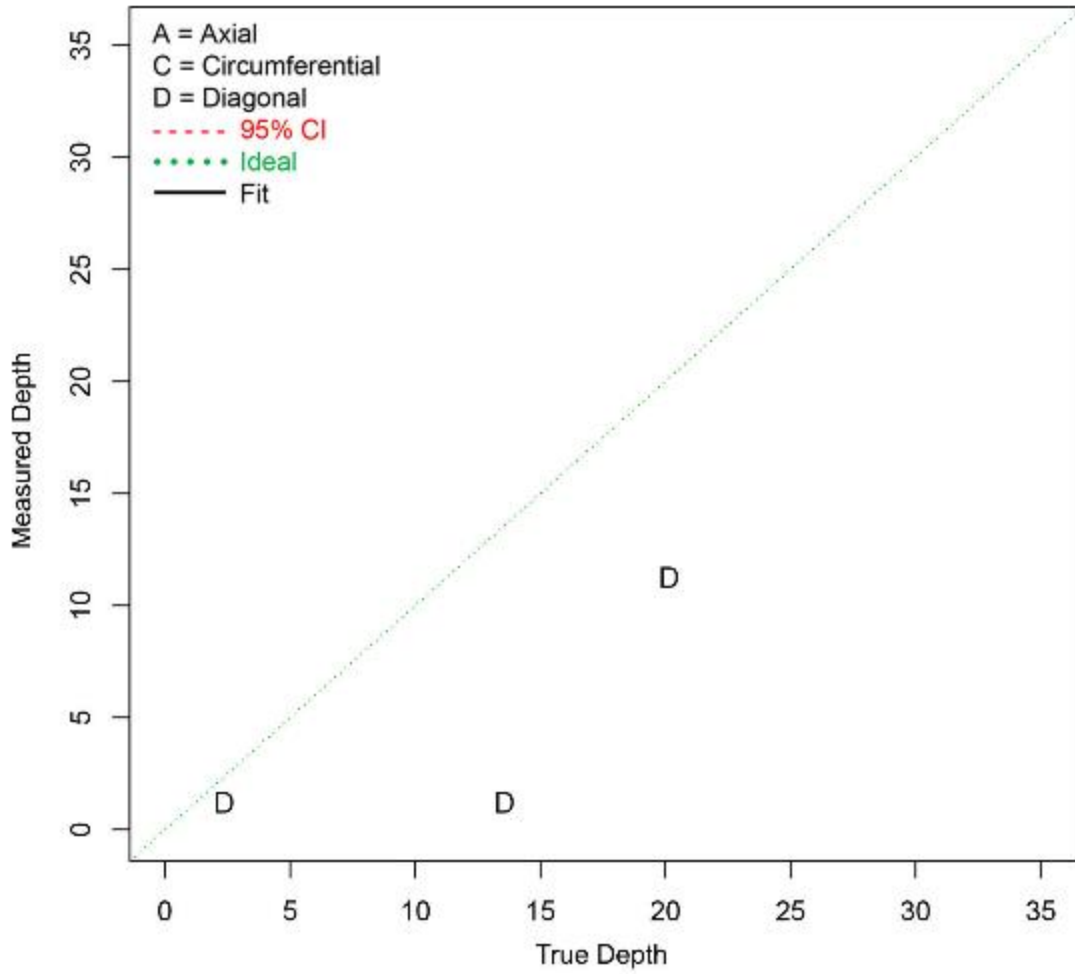


Figure G.60 Depth Sizing Regression (in mm) for PAUT.132 Procedures on LBDMW Test Blocks in PARENT Blind Testing (I.D. Access – **Quick-blind**)

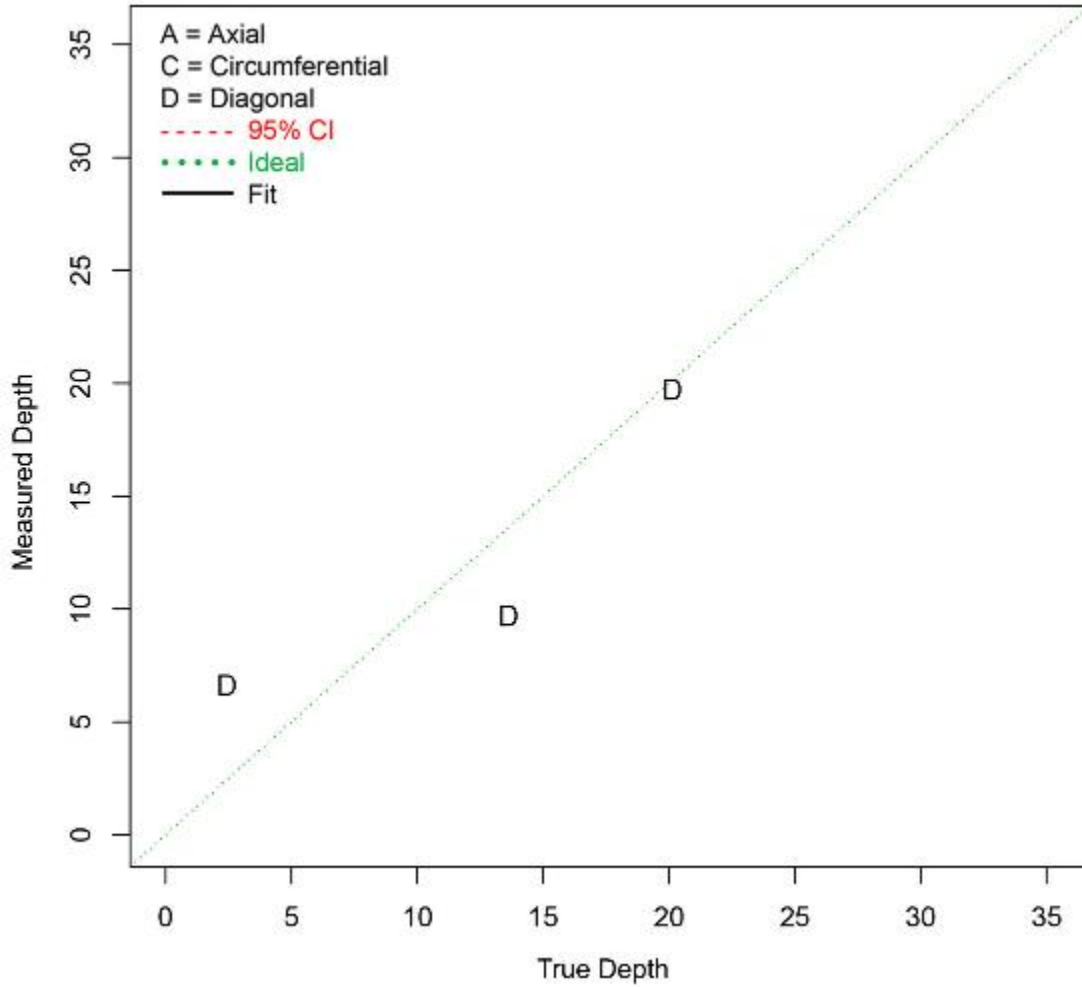


Figure G.61 Depth Sizing Regression (in mm) for UT.ECT.106 Procedures on LBDMW Test Blocks in PARENT Blind Testing (I.D. Access – Quick-blind)

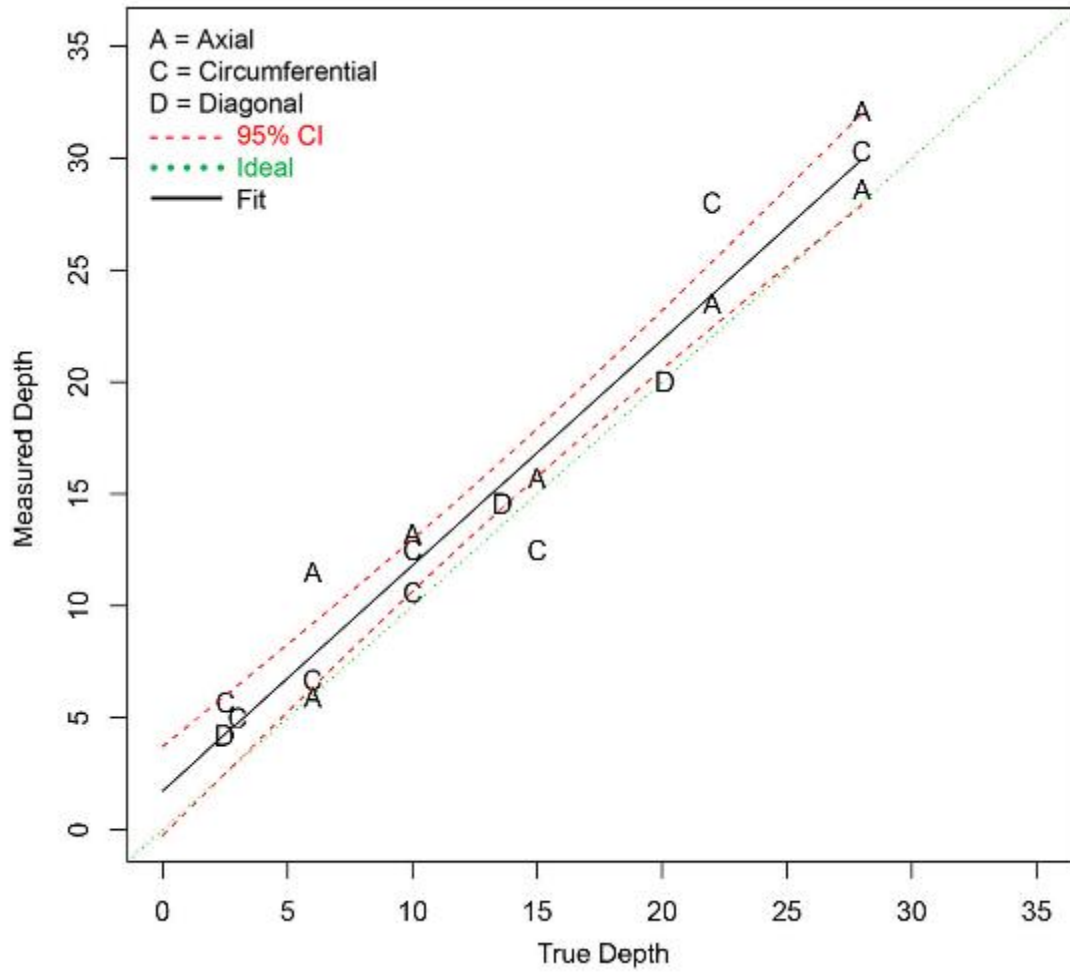


Figure G.62 Depth Sizing Regression (in mm) for UT.PAUT.113 Procedures on LBDMW Test Blocks in PARENT Blind Testing (I.D. Access – **Blind + Quick-blind**)

G.2.1.2 Depth Sizing Results for LBDMWs (O.D. Access)

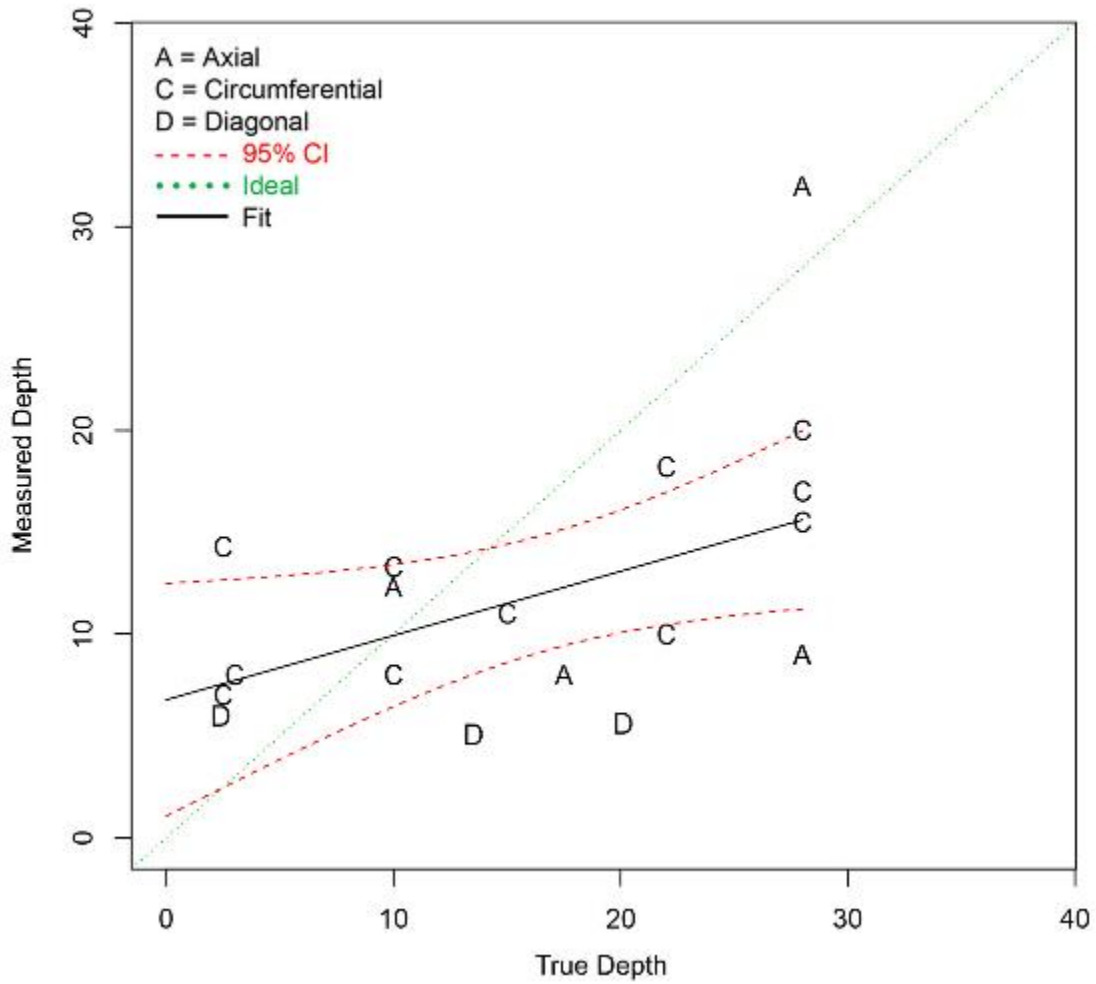


Figure G.63 Depth Sizing Regression (in mm) for UT Procedures on LBDMW Test Blocks in PARENT Blind Testing (O.D. Access – **Blind + Quick-blind**)

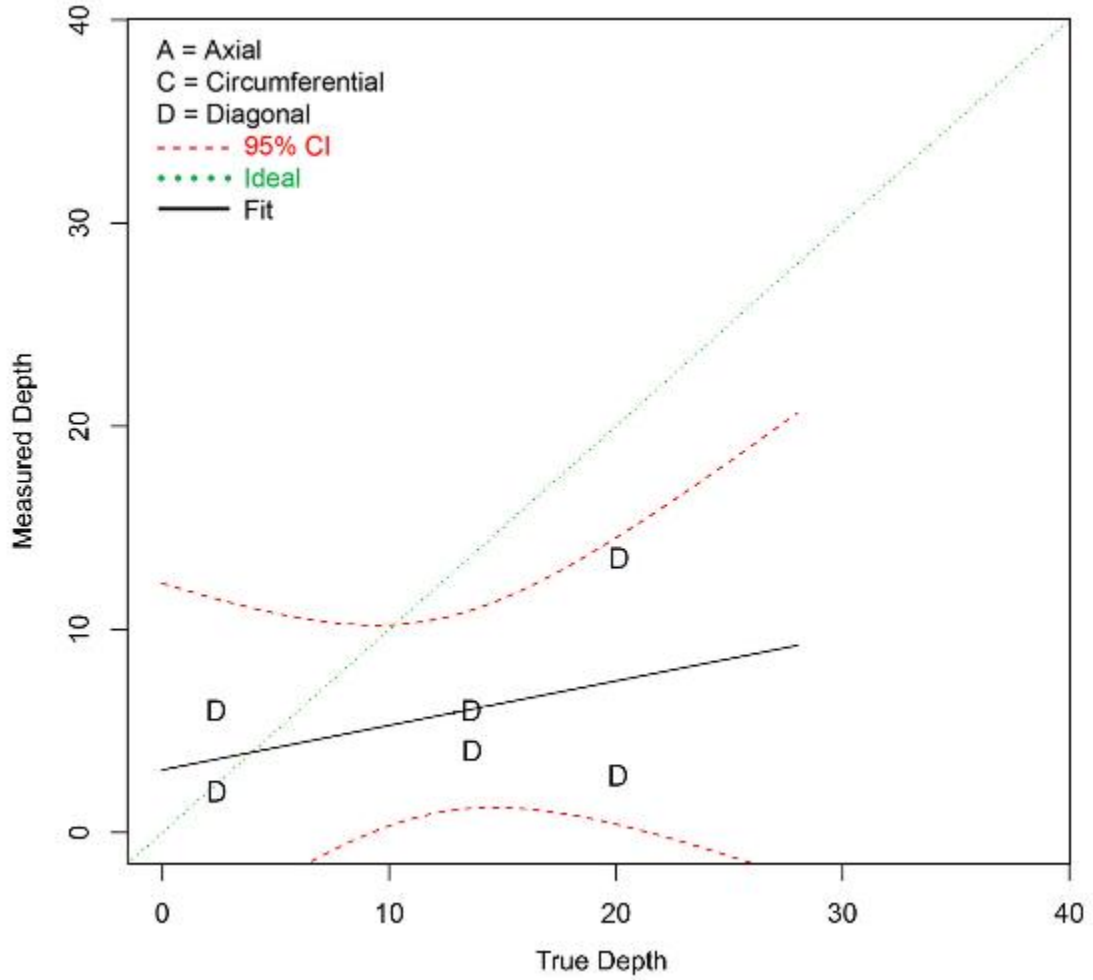


Figure G.64 Depth Sizing Regression (in mm) for UT.PAUT Procedures on LBDMW Test Blocks in PARENT Blind Testing (O.D. Access – Quick-blind)

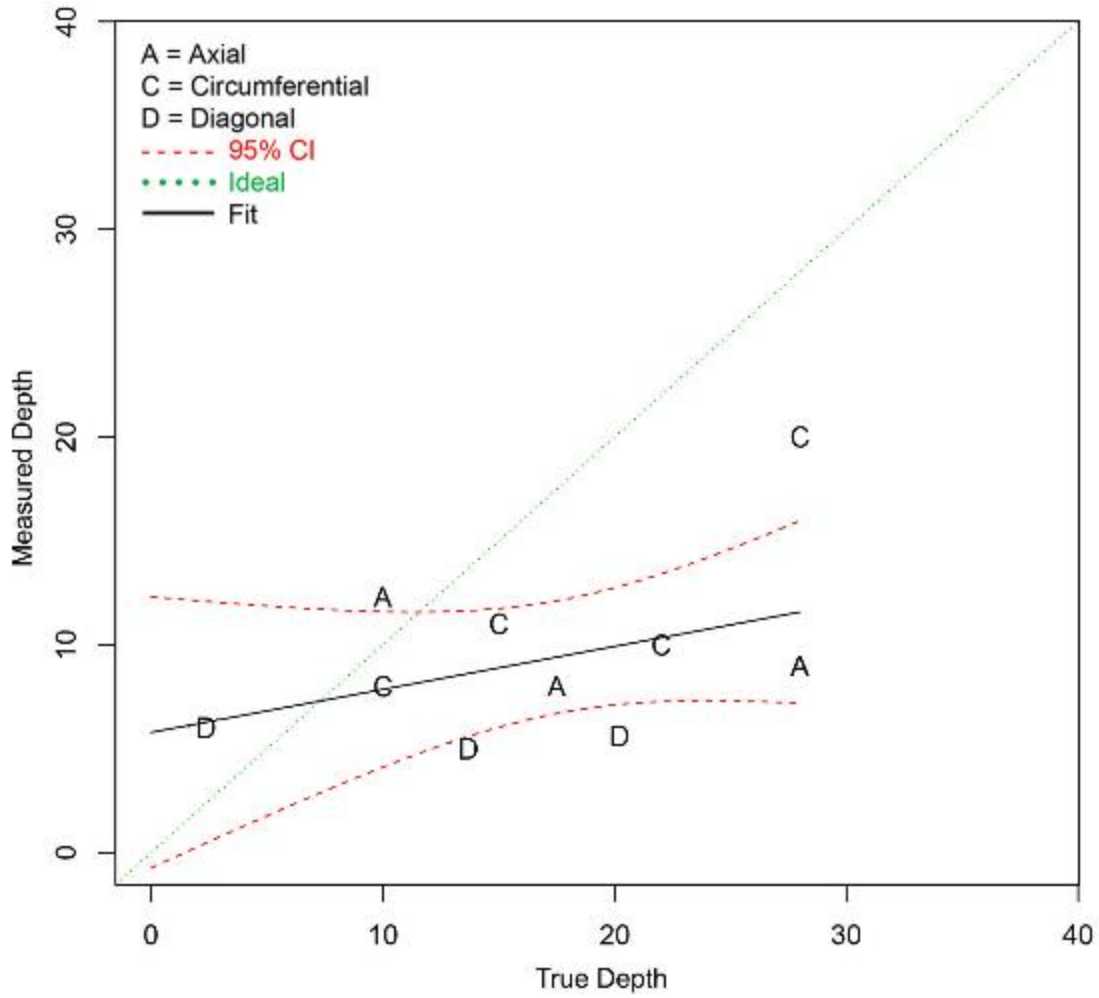


Figure G.65 Depth Sizing Regression (in mm) for UT.134 Procedures on LBDMW Test Blocks in PARENT Blind Testing (O.D. Access – **Blind + Quick-blind**)

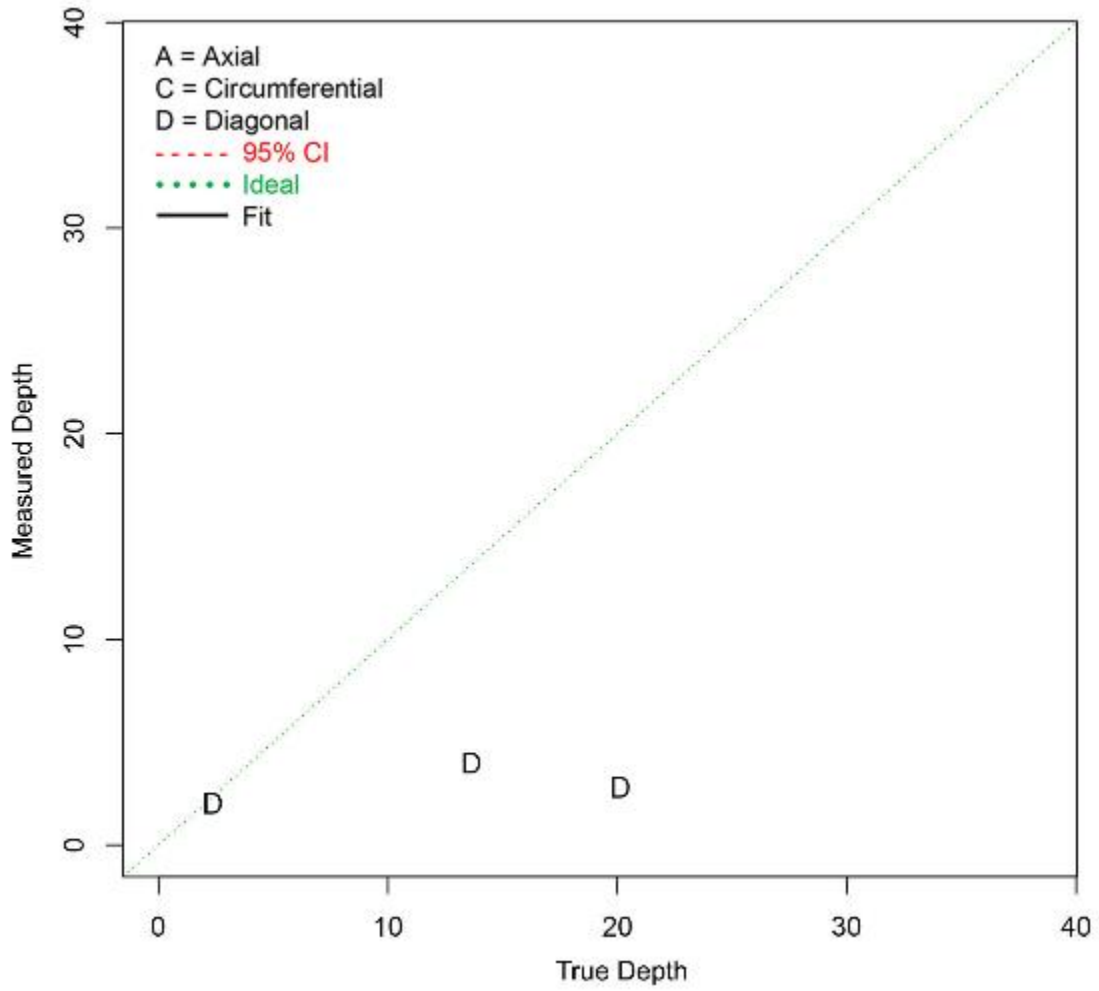


Figure G.66 Depth Sizing Regression (in mm) for UT.PAUT.108 Procedures on LBDMW Test Blocks in PARENT Blind Testing (O.D. Access – Quick-blind)

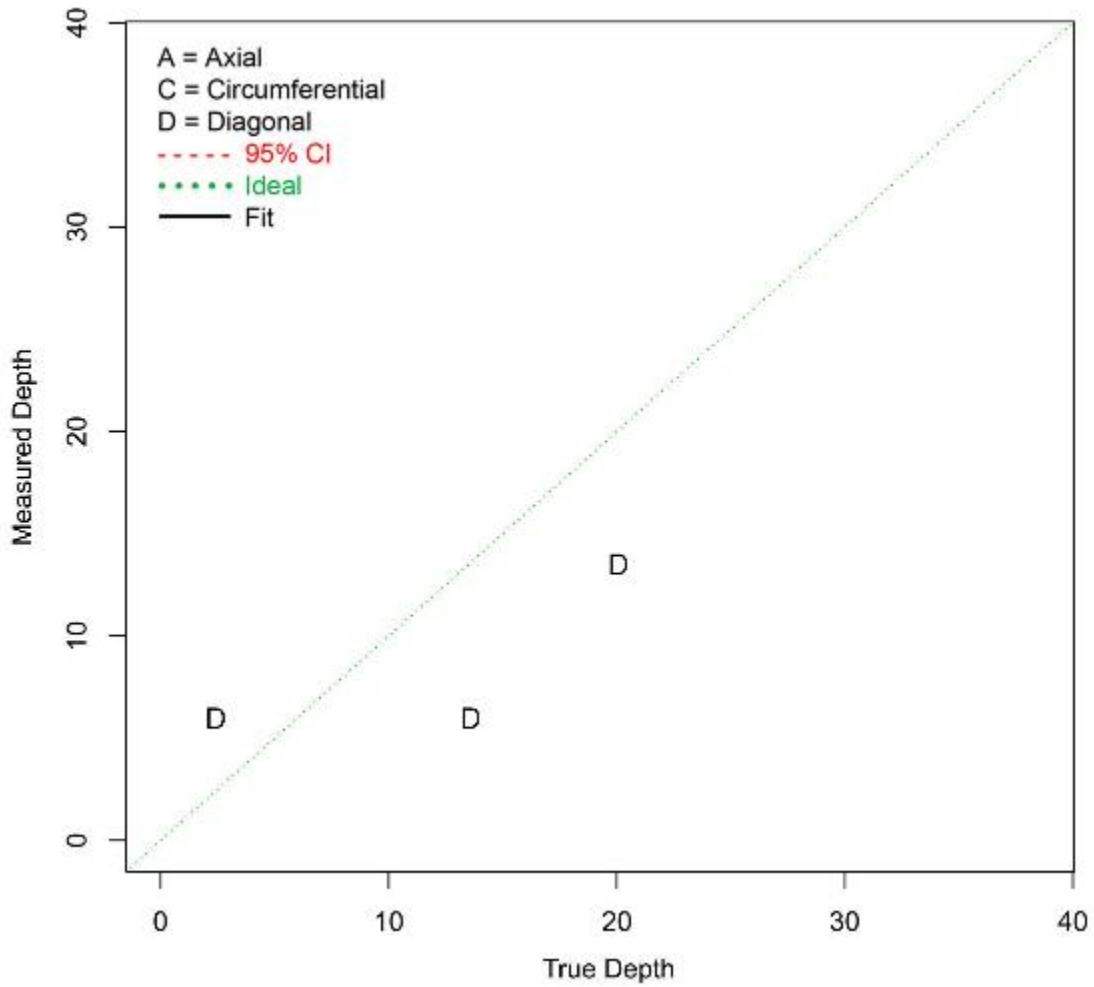


Figure G.67 Depth Sizing Regression (in mm) for UT.PAUT.126 Procedures on LBDMW Test Blocks in PARENT Blind Testing (O.D. Access – **Quick-blind**)

G.2.2 Length Sizing Results

G.2.2.1 Length Sizing Results for LBDMWs (I.D. Access)

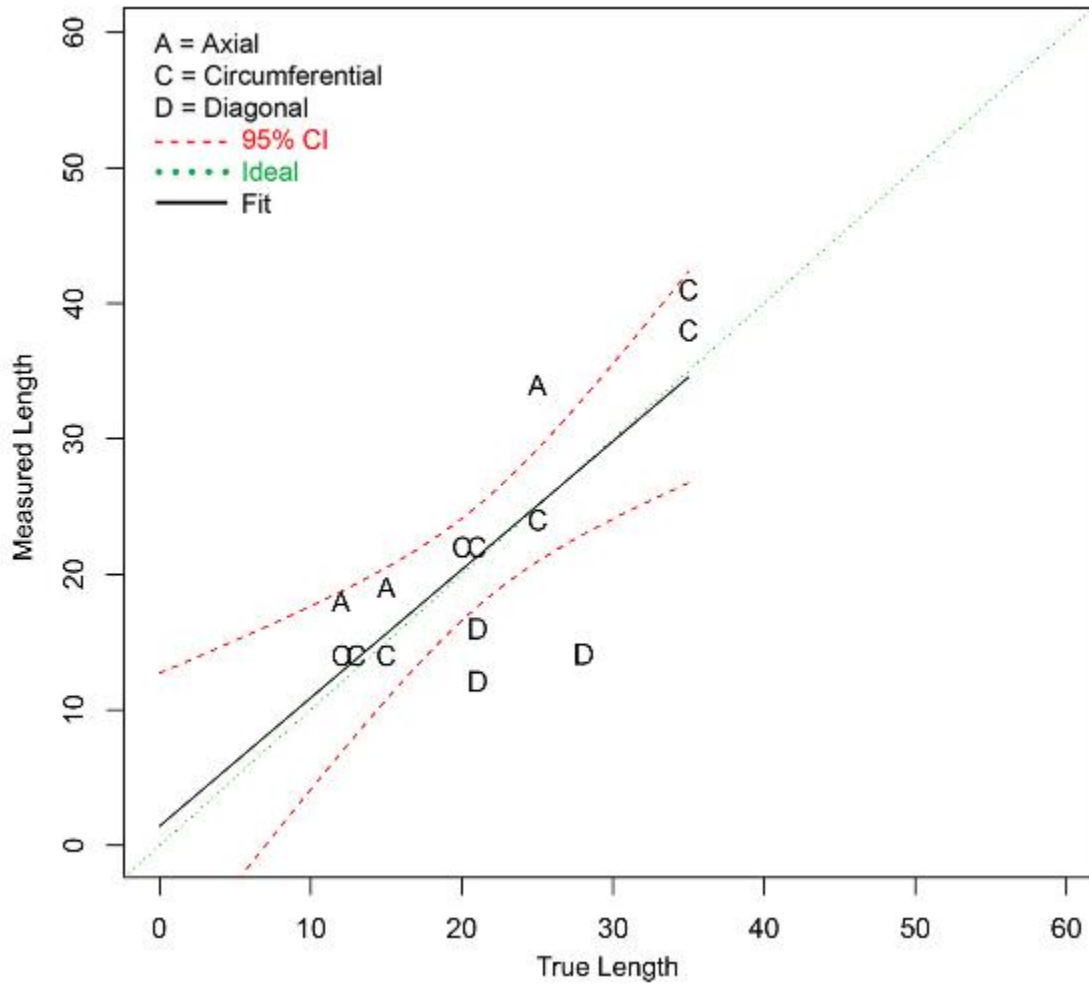


Figure G.68 Length Sizing Regression (in mm) for UT.ECT Procedure on LBDMW Test Blocks in PARENT Blind Testing (I.D. Access – **Blind + Quick-blind**)

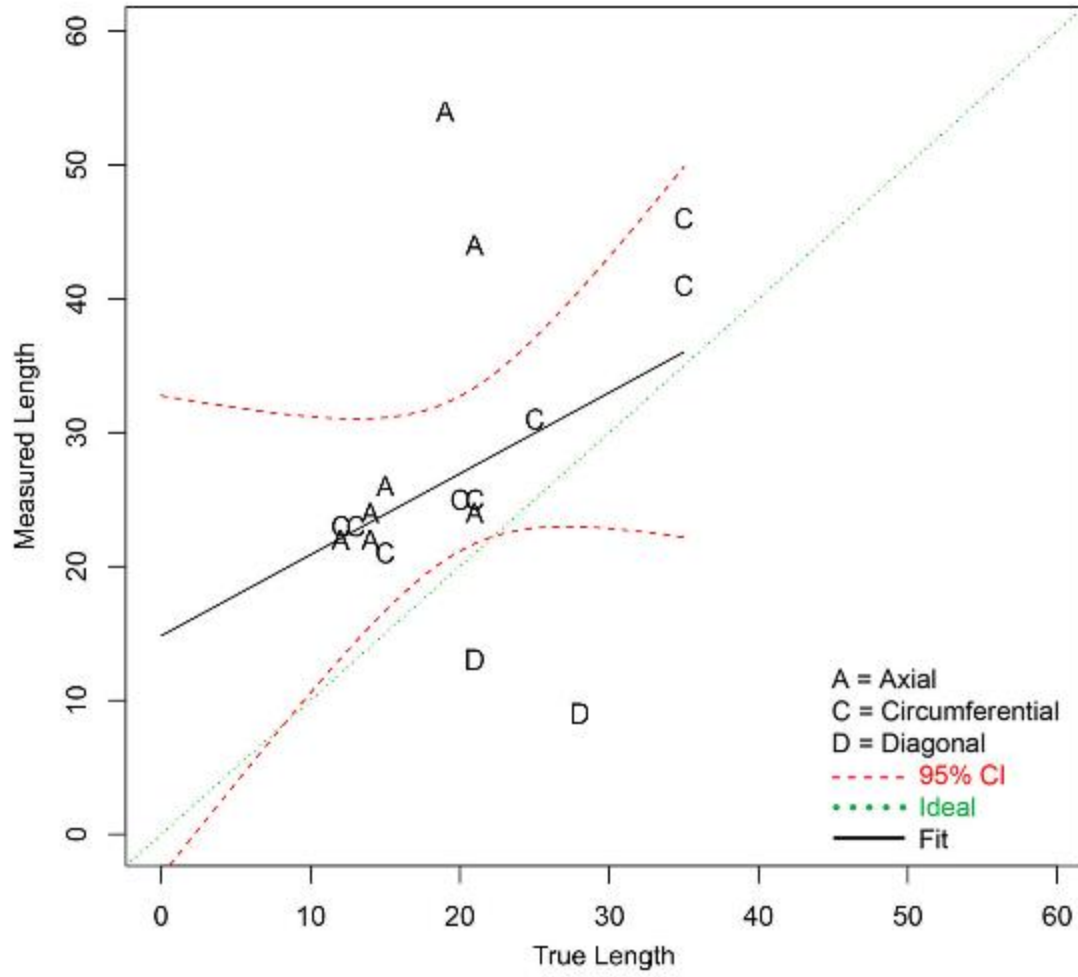


Figure G.69 Length Sizing Regression (in mm) for UT.PAUT Procedure on LBDMW Test Blocks in PARENT Blind Testing (I.D. Access – **Blind + Quick-blind**)

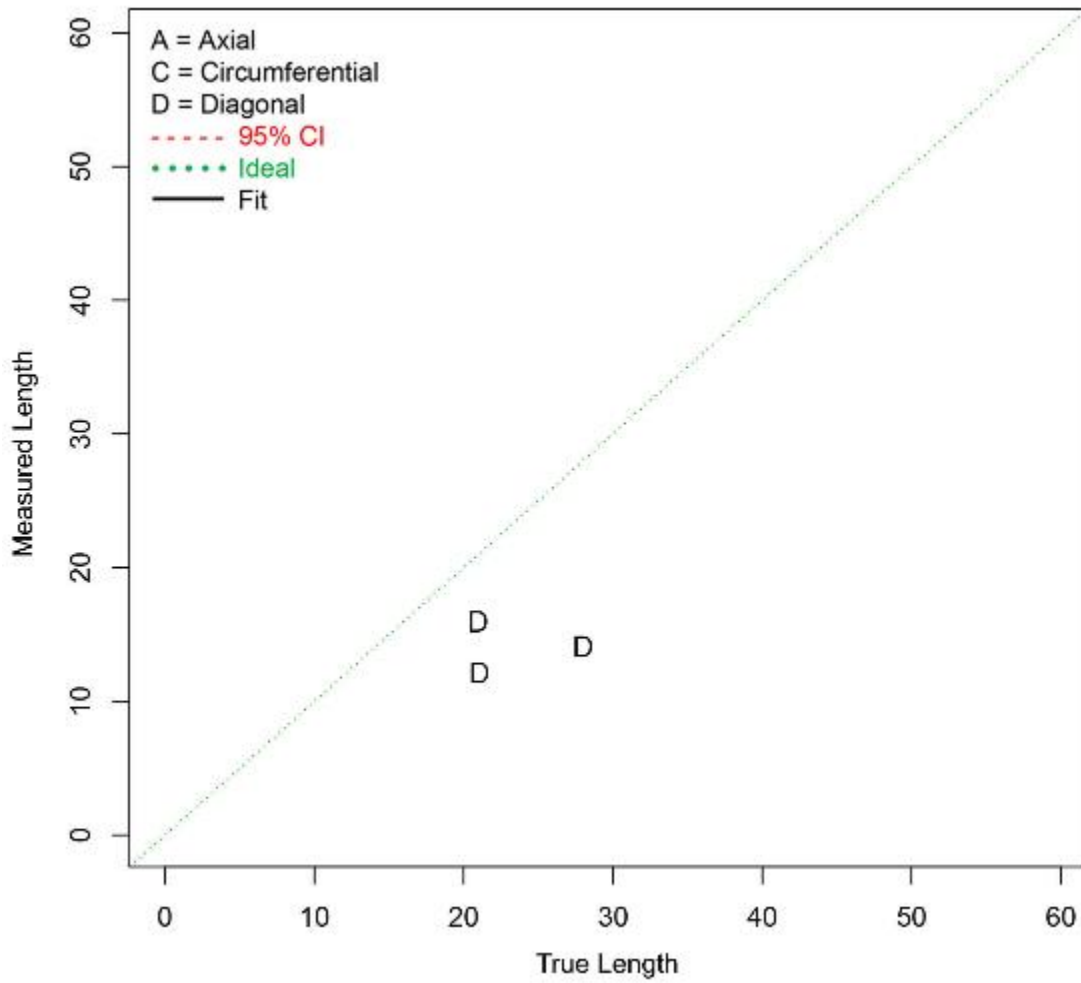


Figure G.70 Length Sizing Regression (in mm) for Procedure UT.ECT.106 on LBDMW Test Blocks in PARENT Blind Testing (I.D. Access – **Quick-blind**)

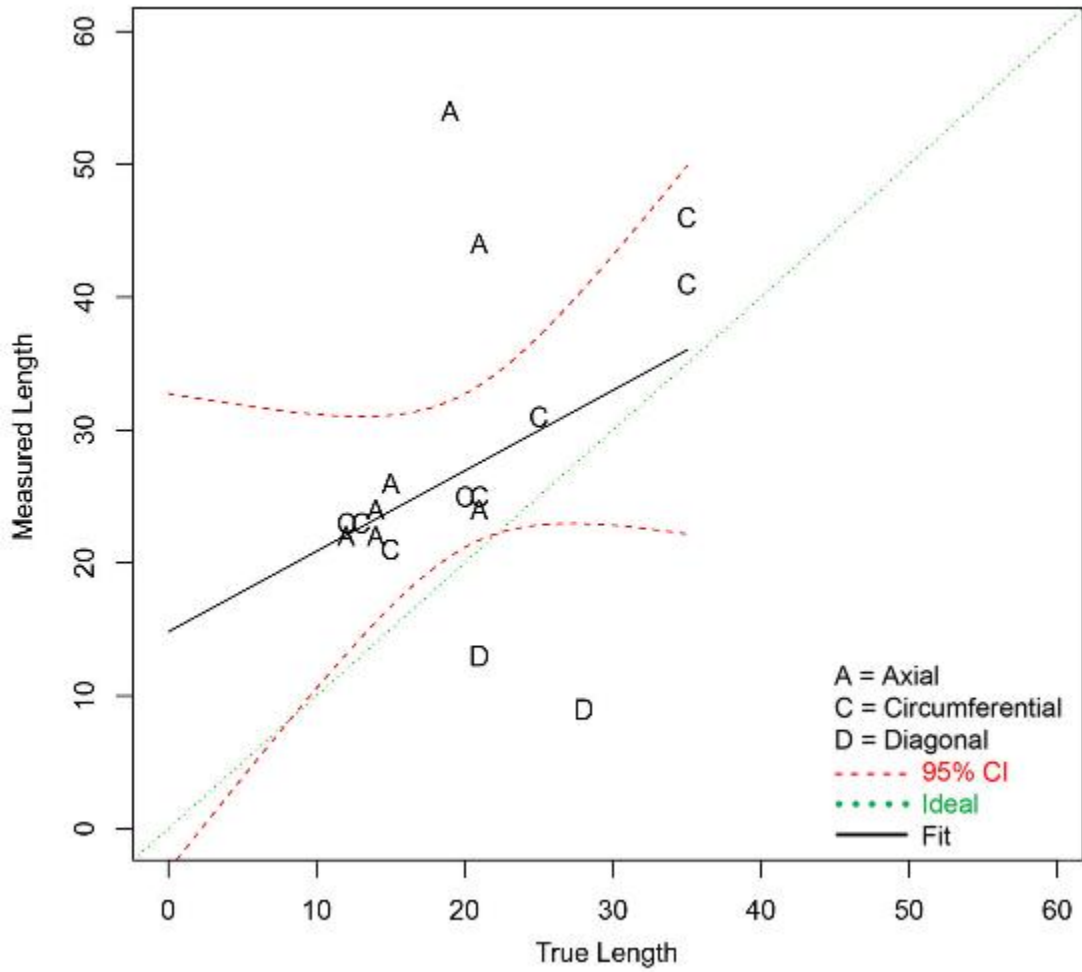


Figure G.71 Length Sizing Regression (in mm) for Procedure UT.PAUT.113 on LBDMW Test Blocks in PARENT Blind Testing (I.D. Access – **Blind + Quick-blind**)

G.2.2.2 Length Sizing Results for LBDMWs (O.D. Access)

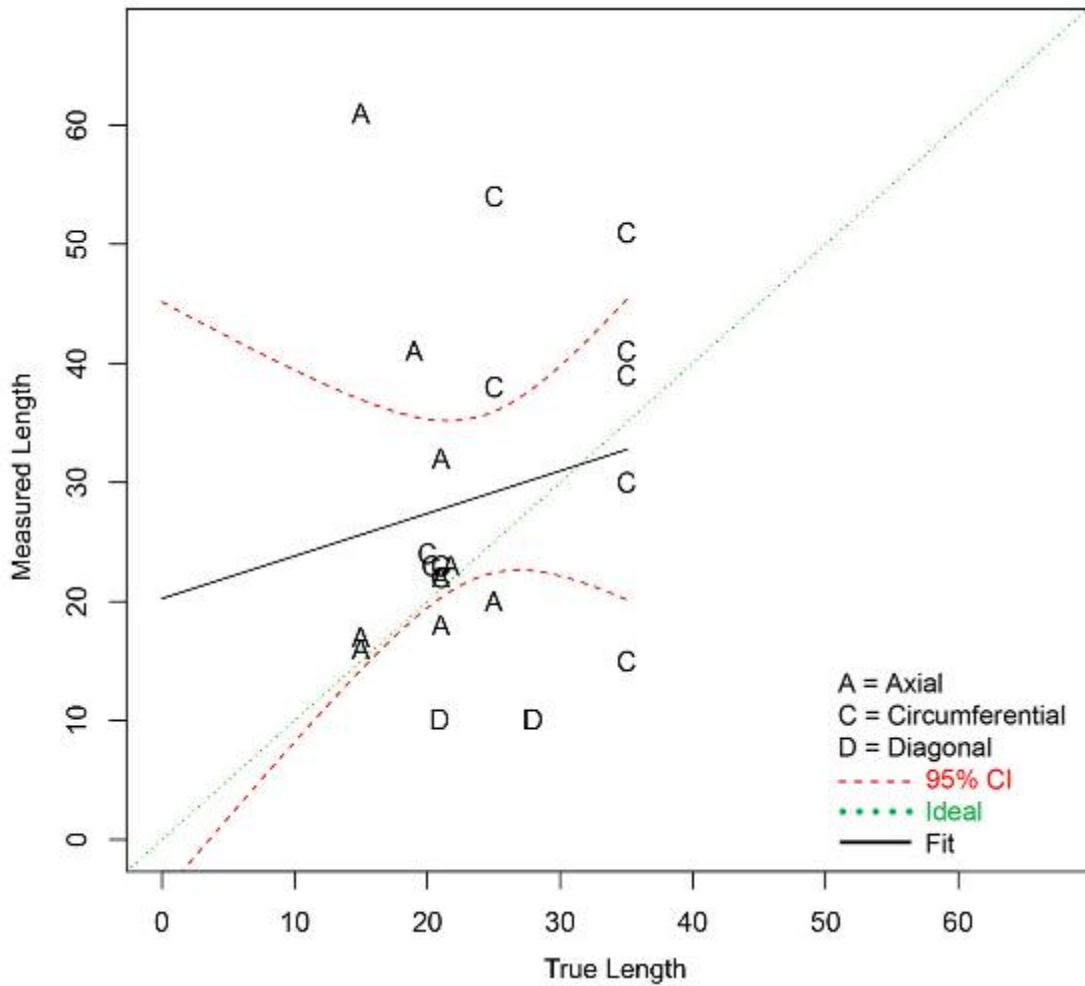


Figure G.72 Length Sizing Regression (in mm) for UT Procedure on LBDMW Test Blocks in PARENT Blind Testing (O.D. Access – **Blind + Quick-blind**)

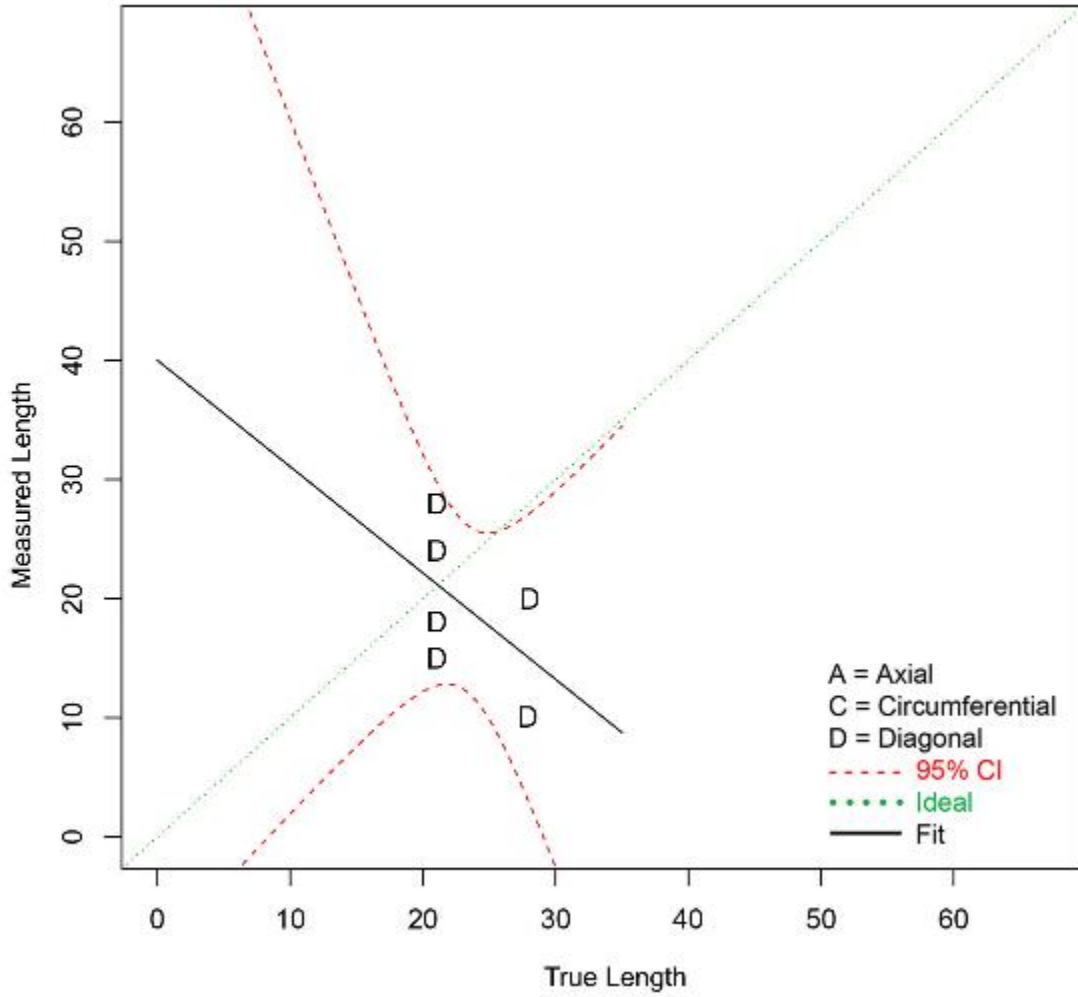


Figure G.73 Length Sizing Regression (in mm) for UT.PAUT Procedure on LBDMW Test Blocks in PARENT Blind Testing (O.D. Access – Quick-blind)

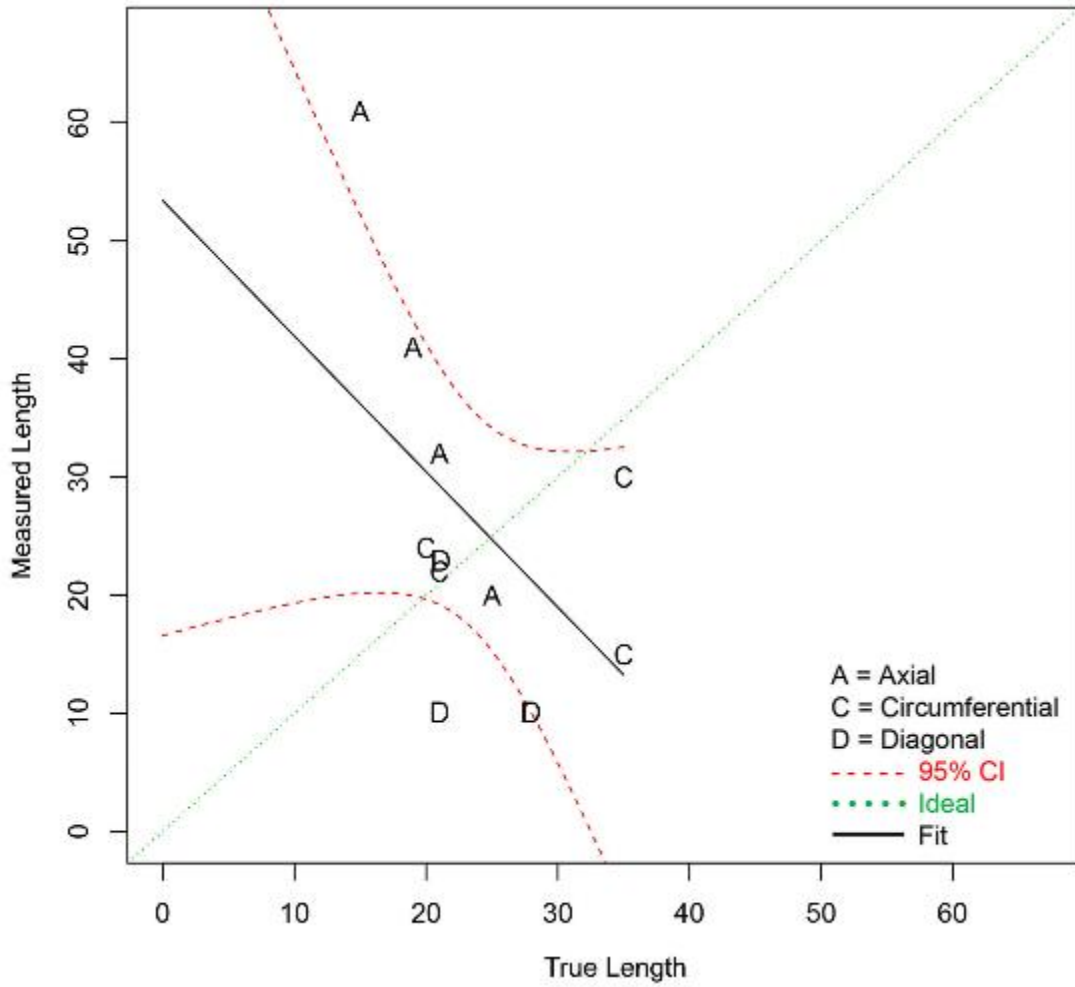


Figure G.74 Length Sizing Regression (in mm) for Procedure UT.134 on LBDMW Test Blocks in PARENT Blind Testing (O.D. Access – Blind + Quick-blind)

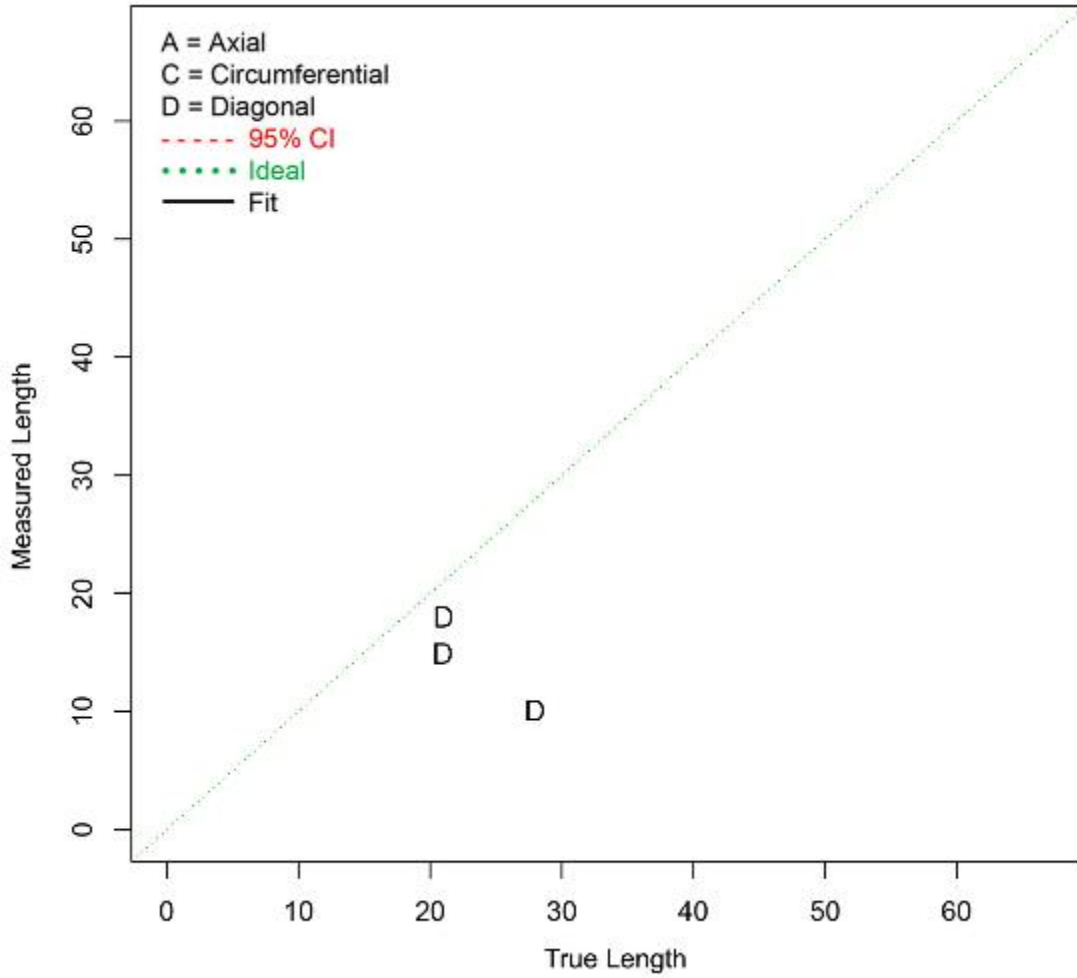


Figure G.75 Length Sizing Regression (in mm) for Procedure UT.PAUT.108 on LBDMW Test Blocks in PARENT Blind Testing (O.D. Access – Quick-blind)

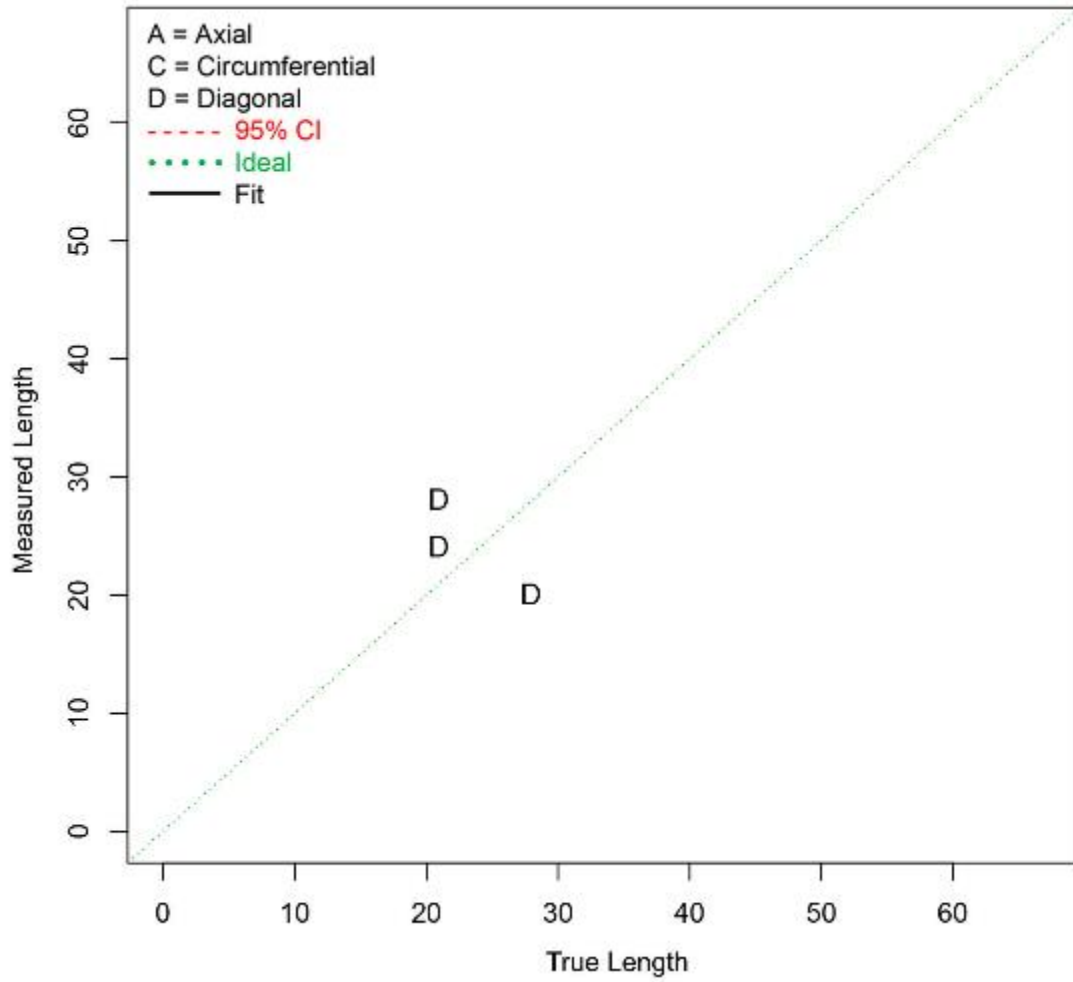


Figure G.76 Length Sizing Regression (in mm) for Procedure UT.PAUT.126 on LBDMW Test Blocks in PARENT Blind Testing (O.D. Access – **Quick-blind**)

APPENDIX H

EFFECTIVENESS EVOLUTION OF DMW INSPECTION TECHNIQUES ASSESSED THROUGH THREE INTERNATIONAL RRTs

APPENDIX H

EFFECTIVENESS EVOLUTION OF DMW INSPECTION TECHNIQUES ASSESSED THROUGH THREE INTERNATIONAL RRTs

¹Tommy Zettervall, ²Steven R Doctor

¹SQC Swedish Qualification Centre,
P.O.Box 519, 183 25 Täby, Sweden

²Pacific Northwest National Laboratory PNNL,
P.O. Box 999, MSIN K5-26, Richland, WA 99352, USA

E-mail address: tommy.zetterwall@sqc.se; steven.doctor@pnnl.gov

Abstract

Nickel-based alloy cracking of reactor pressure boundary components has been a worldwide concern for about 25 years. Increased inspection frequencies, improved inspection practices, and increased licensee vigilance continue to identify nickel-based alloy cracking in vessel penetrations and various components of the primary coolant loop. To address the issue of quantifying the effectiveness of NDE, a number of international Round-Robin Tests (RRT) have been conducted since 1986.

The first RRT was PISC III Action No. 3 which was initiated in 1986 with the objective to evaluate the non-destructive examination (NDE) performance capability of in-service inspection (ISI) procedures used for structural integrity assessment of safe-end welds in power plants. A number of test pieces were manufactured with state of the art techniques at that time for implanting flaws simulating the NDE response expected from service degradation.

The next RRT was the PINC project initiated in 2005 addressing the problem of primary water stress corrosion cracking/interdendritic stress corrosion cracking (PWSCC/IDSCC), which is a form of degradation observed in some reactor piping and pressure vessel components. PINC was designed to understand the crack morphology and to assess the NDE evaluation of procedures/techniques for the detection, characterization and sizing of SCC. PINC provided data that enabled a quantitative assessment of both commercially available and evolving laboratory NDE techniques. Two types of nickel-alloy components were studied, bottom-mounted instrumentation penetrations (BMI) and dissimilar metal piping welds (DMWs).

An on-going RRT is PARENT that was initiated in 2010 as a follow-up to the PINC RRT and is planned to be finished in 2015. The PARENT RRT comprises a study of the efficiency of NDE techniques for detecting, characterizing and sizing SCC defect types in nickel-based materials. Emerging techniques were demonstrated in open tests and commercial techniques in blind tests.

The objectives of this paper is to compare results, make conclusions and propose future activities based upon these three international RRT's conducted over the past three decades. The paper will also include a comparison of field experience from detected PWSCC/IDSCC at power plants in the USA and Sweden. One focus is the NDE signal responses versus the crack morphology that have been simulated in test pieces with respect to real crack morphologies.

H.1 Objectives

Nickel-based alloy cracking of reactor pressure boundary components has been a worldwide concern for about 25 years. Increased inspection frequencies, improved inspection practices, and increased licensee vigilance continue to identify nickel-based alloy cracking in vessel penetrations and various other piping components of the primary coolant loop. To address the issue of quantifying the effectiveness of NDE, a number of international RRTs have been conducted since 1986.

The objectives of this paper is to compare results, make conclusions and propose future activities based upon these three international RRT's conducted over the past three decades. The paper will also include a comparison of field experience from detected PWSCC/IDSCC at power plants in the USA and Sweden. One focus is the NDE signal responses versus the crack morphology that have been simulated in test pieces with respect to real crack morphologies.

The first RRT was PISC III Action No. 3 (Programme for the Inspection of Steel Components) which was initiated in 1986 and ended in 1993 with the objective to evaluate the NDE performance capability of ISI procedures used for structural integrity assessment of dissimilar metal safe-end welds in nuclear power plants. A number of test pieces were manufactured with state of the art techniques at that time for implanting flaws simulating the NDE response expected from service degradation.

The next RRT was the PINC project (Programme for the Inspection of Nickel-Alloy Components) initiated in 2005 addressing the problem of primary water stress corrosion cracking (PWSCC/IDSCC), which is a form of degradation observed in some reactor piping and pressure vessel components. PINC was designed to understand the crack morphology and to assess the NDE performance of procedures/techniques for the detection, characterization and sizing of SCC. PINC provided data that enabled a quantitative assessment of both commercially available and evolving laboratory NDE techniques. Two types of nickel-alloy components were studied—BMI and DMWs.

An on-going RRT is PARENT (Program to Assess the Reliability of Emerging Non-destructive Techniques) that was initiated in 2010 as a follow-up to the PINC RRT and is planned to be finished in 2015. The PARENT RRT comprises a study of the efficiency of NDE techniques for detecting, characterizing and sizing SCC defect types in nickel-based materials. Emerging techniques were demonstrated in open tests and commercial techniques in blind tests. The test assemblies included large-bore DMWs, small-bore DMWs, BMIs and a weld overlay configuration.

H.2 PISC III Action No. 3

H.2.1 General

The PISC Program (Program for the Inspection of Steel Components) had the general objective of assessing procedures and techniques in use for the inspection of nuclear power plant pressurized components.

The third phase of PISC III consisted of eight actions and Action No. 3 was dealing with the evaluation of the effectiveness and reliability of NDE procedures on, at that time, realistic defects in dissimilar metal weldments. This phase was conducted during the years 1986 to 1993 as an international RRT.

Action No. 3 consisted of RRT on three test assemblies that were representative of safe-end weldments in both BWR and PWR designs based in general on the drawings, materials and

manufacturing procedures actually used in the nuclear industry. All nozzle ends were clad with stainless steel and buttered and welded with Ni-alloy (Inconel). A total of 25 flaws were intentionally introduced, these flaws having a through-wall depth size ranging from 10% to 50% of the local wall thickness.

The products of the exercise focused on the capability of procedures and techniques for detection and sizing, assessment of inspections on the most difficult cases and evaluation of the false calls probabilities in safe-end welds.

Each of the test assemblies was given a blind examination by 20 teams in 10 different countries using a range of industrial and laboratory methods that included the best method currently available. Most of teams used ultrasonic techniques, both with compression and shear wave probes, with manual or automated scanning. Two teams also provided radiography inspection results for detection. The flaw detection rate capability for radiography was similar to the average of UT, but with a higher false call rate (FCR). For classification and sizing, teams used a variety of different techniques including tandem, focusing probes, mode conversion and time-of-flight-diffraction (TOFD).

H.2.2 Test Pieces in PISC III Action No. 3

Three test assemblies were available for Action No. 3 having representative drawings, materials and manufacturing procedures typical of those employed in the nuclear industry. The three test assemblies were named Assembly 20, 24 and 25. However, Assembly 20 contains two safe-end pipe configurations, referred as Assemblies No. 21 and No. 22. Assemblies No. 21 and 22 were based on a BWR pressure vessel including nozzle to safe-end welds and safe-end to pipe welds. Only Assembly 21 is of interest for this study and comparison with other RRT's due to the flaw simulations that it contained.

H.2.2.1 Assembly No. 20, 21 and 22

Welds in Assembly 21 (PISC 1993a) included crack simulations utilizing both machining and welding processes. Two crack simulations were of PISC Type A, which was a machining process coupled with electrical discharge machining (EDM). These flaws represent a smooth crack with sharp tip.

The four welding flaws were introduced by ENSA and represent surface breaking smooth cracks. These cracks were obtained by welding and modifying the welding process or by including poisoning material during welding, and were placed in the weld fusion line. The wall thickness at the nozzle to safe-end weld was 40 mm and at the safe-end to pipe weld it was 35 mm.

Welds in Assembly 22 contained lack of root penetration, several groups of porosities, and lack of fusion. These flaws are not of interest in this study for the evaluation of procedures/ techniques to detect and size PWSCC/IDSCC and thus, this assembly is not included in this evaluation.

H.2.2.2 Assembly No. 24

Assembly 24 (PISC 1993b) was a precise copy of a BWR nozzle to safe-end weld and was manufactured with Inconel 182 buttering and weld. Fifteen intentional flaws were introduced using different methods, such as welding process errors, welding of implants and three were the PISC Type A machined flaws.

H.2.2.3 Assembly No. 25

Assembly No. 25 (PISC 1993c) was intended to simulate a PWR safe-end area. The ferritic nozzle pipe was clad with stainless steel and joined to a cast pipe using Inconel 182 weld and

buttering. Nine flaws were intentionally introduced by different implanting techniques, where five of them were located in the fusion line or in the weld material of the safe-end weld. Fabrication was performed with machined slots and then filled using crack type electrodes, e.g., doped electrodes.

H.2.3 Results of PISC III Action No. 3

The first important conclusion to be noted is that only a few of the teams reached a flaw detection frequency (FDF) of 80%. Moreover the results were further marred by the large number of false calls. Considering the effectiveness of through-wall depth sizing there was, on average an overall slight tendency to oversize along with a comparatively large standard deviation. The overall dispersion of sizing error was of the order of ± 5 mm.

The effectiveness of correctly classifying flaws, the correct rejection frequency (CRF), was on average below 70%. It was found that teams that achieved a high CRF also showed a tendency to oversize flaws leading to incorrect rejection of acceptable flaws and also to high FCRs.

It was also found that the overall effectiveness was somewhat lower for the inspections conducted on Assembly 20. This was explained by the existence of many natural occurring welding flaws and the smaller size of the intended flaws in the complex heterogeneous weldment.

Figure H.1 (European Communities 1994; Dombret 1995) illustrates the average flaw detection and correct rejection performance of the procedure families A–H, versus their FCRs. Table H.1 (Dombret 1995) specifies the acronyms used in the evaluation principles of inspection results and the Procedure families that were used.

Table H.1 Procedure Families and Acronyms of Evaluation Principles

Procedure Families		Evaluation Principles	
A:	Manual scanning	FDF:	Reference flaws that are detected by a team
B:	Automatic scanning	CRF	Rejectable defects that are correctly rejected by a team
C:	Recording at noise level	CAF	Acceptable flaws that are correctly accepted by a team
D:	Recording at 10 – 25% DAC	MESZ	Mean error of sizing in the depth direction
E:	Recording at 50% DAC	SESZ	Standard deviation of sizing in depth direction
F:	Manual scanning at noise level	FCRD	No. of false calls in the total number of detected flaws
G:	Automatic scanning at noise level	FCRR	No. of false calls in rejectable number of detected flaws
H:	Focusing probes, with high sensitivity from I.D.		

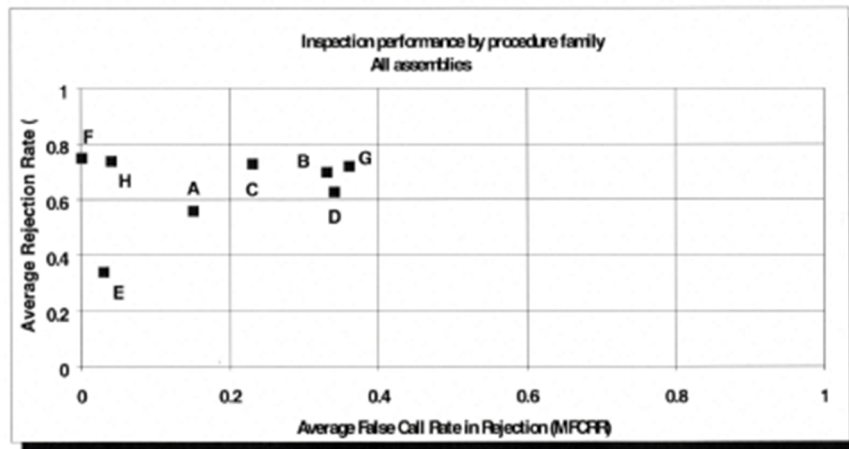
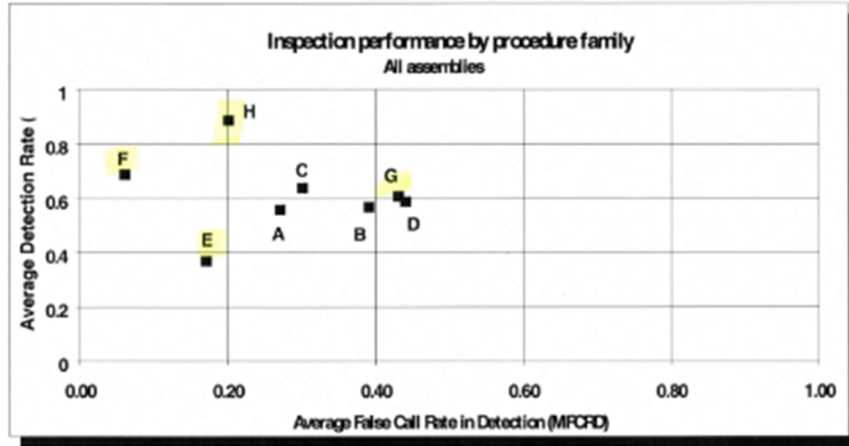


Figure H.1 PISC III Action No. 3 Results of Inspection Procedure Families

Considering the relevant points in Figure H.1, it is clearly seen that those techniques which recorded all the indications that were above the level of the general background noise, i.e. those which did not make use of an amplitude threshold (F, C, G, H) were more efficient than those (D,E) which only recorded indications which exceeded a threshold in the range 10% to 25% or 50% of the standard level. Techniques which limited their reports to only indications which exceeded 50% DAC gave unsatisfactory results as seen from Table H.2.¹

¹ Nichols RW. 1999. "Some Achievements of the Third Part of the OECD/CEC Program for the Inspection of Steel Components (PISC III)."

Table H.2 PISC III Action No. 3 Results for Different Reporting Levels

Evaluation	Assembly	FDF	CRF	FCRD	FCRR	MESZ	SESZ
Noise Level	20	0,33	0,65	0,29	0,24	3,3	7
	24	0,73	0,77	0,35	0,30	1,5	4
	25	0,78	0,64	0,13	0,08	-2,5	5
10–25% DAC	20	0,32	0,27	0,47	0,39	4,0	5
	24	0,54	0,59	0,49	0,38	0,0	5
	25	0,82	0,78	0,24	0,07	-0,3	6
50% DAC	20	0,18	0,10	0,17	0,5	-0,5	2
	24	0,34	0,28	0,28	0,0	-1,3	7
	25	0,73	0,62	0,07	0,0	-2,0	5

It should be noted that each team in presenting its results took account of evidence from more than one technique and only a few teams provided detailed results for each of their individual techniques. This limits the conclusions on technique effectiveness to stating that the compression wave techniques made an essential and important contribution to getting good results. It was also noted that the same flaws that proved difficult for X-rays were also difficult for UT examination.

At first sight a comparison of the effectiveness of those UT examinations that were made from the outside surface with those made from the inner surface, as seen from Table H.3⁴ shows a small preference for the I.D. scanning, especially in respect to FCRs and for scatter in sizing.

Table H.3 PISC III Action No. 3 Average Results Comparing Scanning from O.D. and I.D. with Focus on DMWs

Surface	Weld	FDF	CRF	FCRD	FCRR	MESZ	SESZ
O.D.	DW	0,80	0,75	0,12	0,04	-2,5	6,3
I.D.	DW	0,75	0,70	0,17	0,03	-3,2	3,5

With focus on the safe-end welds and buttering, i.e. Ni-based alloy materials, flaws located in those materials appear to give the greatest difficulties, compared with flaws located in carbon steel or wrought stainless steel materials.

Another parameter to evaluate is whether the NDE effectiveness depends on the flaw type, flaw size or the location of the flaw being examined. The frequency of detection and the frequency of correct rejection, shows that the effectiveness of detection was higher for flaw depth dimensions exceeding 40% of wall thickness. Detection of reflectors smaller than 2 mm, about 5% of wall thickness, lies beyond the reach of the common technology employed at that time.

An overall result of FDF, CRF and SESZ, i.e., flaw detection, FCR and standard deviation in sizing, shows a better result in scanning from the I.D. than from the O.D. Not surprisingly, the essential contribution of compression wave techniques gave better results compared with those using shear wave probes. Also combinations of different techniques show better results for classification and sizing than procedures using only a single technique.

Teams that reached a FDF of 1,0 and had a low rate of false call, used a combination of different techniques like compression and shear wave transducers or TOFD and mode conversion techniques. Flaws that were correctly rejected were also ones that had a high level NDE response producing a CRF >0,8. Procedures applied on all assemblies that were characterized by using focusing probes with automated scanning from the I.D. and with a noise level reporting threshold was the best combination.

A systemic trend was that shallow flaws were consistently oversized and large flaws were consistently undersized. In general the same performance was found for height sizing of PISC Type A machined slots with the height sizing of welding flaws.

H.3 PINC

H.3.1 General

The next large international RRT was the PINC (Program for the Inspection of Nickel-Alloy Components) program (Cumblidge et al. 2010) between 2005 and 2008 with the objectives to join together for cooperation research and to address the problem of primary water stress corrosion cracking PWSCC/IDSCC in pressurized nuclear reactor components. The research was designed to understand the morphology of PWSCC/IDSCC and to assess NDE techniques for detection, characterization and sizing cracks with such morphology.

The PINC project (Cumblidge et al. 2010) was focused on two areas—penetration BMI and DMWs. The DMW round-robin exercises that were conducted as part of the PINC program was an important part of the process in assessing nondestructive testing methods because the data that is developed in the round-robin testing offers insight into the capabilities of “current” field nondestructive methods used to detect, characterize and size PWSCC and to provide insight into the capabilities of more “experimental” laboratory evolving nondestructive methods.

H.3.2 Test Pieces in PINC

Participants in PINC offered more than 30 test blocks for use in round-robin tests of NDE effectiveness. The test blocks had more than 130 cracks in nickel-base weld metal that were intended to simulate PWSCC in a variety of component configurations and geometries. The project divided the test blocks into two categories that would be circulated, inspected, and analyzed separately. These two categories were mid-thickness DMW with a wall thickness range of 41 mm to 47 mm, and BMI with a tube I.D. less than 28 mm. The BMIs were ranked as top priority, but dissimilar metal piping welds were considered to also be very important based on the cracking that had been experienced at some NPPs.

Cracks in DMW piping and BMI test blocks were produced as weld solidification cracks and as laboratory-grown PWSCC through using a corrosive environment while tensile loading and bending. The laboratory-grown cracks were used to simulate medium depth and shallow cracks.

H.3.3 Result of PINC

The 16 teams conducting the DMW examinations used a wide mix of nondestructive techniques, ranging from standard methods such as conventional ultrasonic inspection to experimental techniques such as potential drop. As there was a wide variety of techniques and the application of those techniques, comparing the effectiveness of the individual techniques would result in a very complex matrix. PNNL divided the different techniques used in the DMW round robin into two broad categories, ultrasonic and electromagnetic.

Within the ultrasonic category the following methods were used:

- Conventional ultrasonic (UT) methods
- Phased-array UT methods
- TOFD methods

Within the electromagnetic category the following methods were used:

- Eddy current methods
- Potential-drop methods, both direct current (DC) method, alternating current (AC) method, and modified variations of these methods.

One of the objectives of the round-robin test is to estimate the probability of detection (POD) as a function of crack size. All flaws in the test blocks simulated service-induced cracks and thus, were surface breaking in axial or circumferential directions, so the most important variables for the detection and sizing probability was the variation of flaw length and flaw depth. Another important variable in any round-robin test is the skill level of the team performing the test.

The POD results sorted by procedures and by flaw depth are shown in Table H.4. The procedures are grouped by detection technique to allow for an easy comparison of procedures performance within the different techniques. The POD is given for 5-mm deep flaws, 10-mm deep flaws, and 15-mm deep flaws, along with the FCR.

Table H.4 PINC POD Summary for Procedures

Procedure Families	POD for Flaw Depth of			False Call Rate	I.D./O.D.
	5 mm	10 mm	15 mm		
Eddy Current	0,89	1,00	1,00	0,17	I.D.
Conventional UT and Phased Array	0,62	0,94	0,99	0,14	O.D.
Conventional UT	0,36	0,51	0,67	0,23	O.D.
Phased Array	0,36	0,51	0,66	0,24	O.D.
Conventional UT and TOFD	0,44	0,53	0,61	0,35	O.D.
Potential Drop	0,29	0,33	0,38	0,25	I.D./O.D.

Eddy current had the highest performance in detection of surface breaking cracks and making the fewest false calls. Conventional UT in combination with phased array gave similar effective performance results. Performance was reduced for conventional UT alone or phased array alone while the potential-drop technique showed an even lower performance.

When looking at the POD of shallow cracks with a depth about 4 to 5 mm, approximately 10% of wall thickness, the eddy current technique achieved the highest performance.

As some techniques are more easily applied along the length of a pipe as opposed to around a pipe, it is important to examine the POD of flaws based on their orientation. The POD results are shown in Table H.5 and Table H.6.

Table H.5 PINC POD for Circumferential Flaws as Function of Flaw Depth

Procedure	POD for Flaw Depth of			False Call Rate
	5 mm	10 mm	15 mm	
Eddy Current	0,92	1,00	1,00	0,17
UT	0,41	0,61	0,61	0,23
Potential Drop	0,28	0,36	0,43	0,23

Table H.6. PINC POD for Axial Flaws as Function of Flaw Depth

Procedure	POD for Flaw Depth of			False Call Rate
	5 mm	10 mm	15 mm	
Eddy Current	0,80	0,99	1,00	0,17
UT	0,32	0,45	0,59	0,21
Potential Drop	0,24	0,27	0,32	0,20

The results show that circumferential flaws in these blocks were somewhat easier to detect than axial flaws using ultrasound UT, especially for cracks close to 10-mm deep. Eddy current was largely unaffected, but does show an 11% greater chance of detecting a 5 mm deep circumferential flaw than a 5 mm deep axial flaw. Circumferential flaws were somewhat more detectable with the potential-drop technique as well. It was also shown that a higher frequency on ECT, 400 KHz gave a better result than for instance of a 100 KHz ECT probe.

One of the goals of the PINC project was to determine which techniques are the most effective at characterizing the through-wall depth and length of PWSCC. Phased-array UT and tip diffraction techniques performed well in both detection and sizing. Only one PAUT team had an RMSE of 3.18 mm and another PAUT was 4.01 mm while all the remainder had substantially larger depth sizing RMSE values. However, it needs to be pointed out that the RMSE value is a useful metric but the flaws used in PINC were not selected to meet the sizing requirements in ASME Boiler and Pressure Vessel Code (ASME Code), Section XI, Division 1, Appendix VIII so having a small RMSE value is insightful but does not necessarily reflect desired performance. Therefore, when reviewing the sizing results, all teams that used the phased-array UT technology performed better than teams that only used conventional ultrasonic methods.

None of the NDE techniques in this round robin demonstrated the capability to accurately depth-size flaws in DMWs. The average depth sizing for all teams and techniques tended to slightly undersize the flaws and had standard deviations and root mean square error (RSME) of approximately 7 mm. The ASME Code requires a RSME of 0.125 inches (3.2 mm) for depth sizing to successfully pass a performance demonstration. No team performed depth sizing to this level of accuracy. The depth sizing of flaws could be improved. The use of phased-array UT and conventional ultrasound together showed the most promise. This study showed that what is important for depth sizing is that the diffracted signals from the crack tip can be detected. Due to the fragmented but unbroken ligaments in depth of PWSCC/IDSCC, the challenge is to find the deepest through-wall crack tip while only detecting shallower tips leads to systematically under sizing the flaw depth.

A review of the information shows that eddy current techniques performed the best for length sizing flaws followed by phased-array ultrasonic techniques. Conventional ultrasonic and potential-drop techniques were poor at length sizing. Appendix VIII of Section XI of the ASME Code states that examination procedures, equipment, and personnel be qualified for length sizing when the RMSE of the flaw length measurements in the test set compared to the true flaw lengths, does not exceed 0.75 in. (19 mm). A review of the data shows that half (8 out of the 16 teams) would have passed an Appendix VIII type performance demonstration test for length sizing.

H.4 PARENT

H.4.1 General

The third large international RRT is the PARENT program (Program to Assess the Reliability of Emerging Nondestructive Techniques) (Braatz et al. 2014) initiated in 2010 and plans to be finished in 2015. The objectives of PARENT is to continue the work begun in PINC and apply the lessons learned to a series of open and blind international round-robin tests that will be conducted on a new set of piping components including large-bore (≈ 900 -mm diameter) DMWs, small-bore DMWs, and BMIs.

The project has objectives to:

- Pool International expertise and resources to evaluate the inspectability of Ni-alloy components and welds.
- Identify and quantitatively assess NDE methods for accurately detecting, characterizing, and sizing PWSCC/IDSCC cracks.
 - A. Blind Round-Robin Testing
 - 1. Evaluate commercially used inspection techniques
 - 2. Evaluate the effectiveness of qualified procedures and inspectors
 - 3. Evaluate which commercial techniques are the most effective for different components
 - B. Open Round-Robin Testing
 - 1. Evaluate emerging non-destructive testing techniques, which could be used in the future
 - 2. Evaluate how effective novel techniques are for detecting flaws in Ni-alloy welds
 - 3. Evaluate the characteristics of each emerging technique for further improvements
- Investigate and document field locations and crack morphologies for PWSCC and their observed NDE responses in an electronic database "ATLAS".
- Utilize lessons learned from PINC to employ techniques to manufacture representative NDE mock-ups with flaws that simulate real field PWSCC/IDSCC NDE signal responses.

The blind testing was conducted in two phases, one was called Quick-Blind and the other was called Blind. The reason for the Quick-Blind testing was that test blocks had been provided by Japan from an on-going program and they needed to be returned to Japan for destructive analysis as required by the Japan program when these blocks were provided.

Six testing organizations representing Japan, South Korea, Sweden, and the USA applied NDE test procedures that employed conventional ultrasonic, phased-array ultrasonic, and eddy current NDE techniques in the Quick-Blind testing. The objective of the tests was to learn how the NDE procedures applied performed from the standpoint of flaw detection, flaw depth sizing, and flaw length sizing.

Approximately 170 inspections were scheduled to be performed on 19 test blocks for the open testing portion of PARENT by 23 teams from Japan, Europe (Sweden, Finland, Spain, Denmark), South Korea, and the USA. Of the 19 open test blocks, only two were BMIs. The NDE techniques used in the open portion of study are broadly categorized as ultrasonic techniques, eddy current techniques, and other techniques. Motivations for developing many of the open NDE techniques can be characterized as addressing one or more of the following challenges: (1) to more accurately characterize large defects, (2) to enable inspections of difficult-to-access regions, and (3) to improve detectability of small defects.

H.4.2 Test Pieces in PARENT

H.4.2.1 Open Trials

The open trials consisted of four BMI test assemblies, 11 small-bore DMW test assemblies and four large-bore DMW test assemblies. A variety of flaw types and locations were included but since the flaw locations were provided to the inspection teams, the results are biased and the current status of data analysis is in progress and not available when this paper was in preparation. These trials were pursued to assess a wide variety of non-standard techniques such as higher harmonic UT and nonlinear resonant ultrasound spectroscopy for specific problematic issues including detection of small defects, access to challenging geometries and accurately characterizing large flaws. There were 209 inspections conducted on DMW test assemblies by these techniques. Thus, these open trial studies may provide some important insights as the analysis proceeds.

H.4.2.2 Blind Trials

The blind trials consisted of a number of test assemblies with five being BMIs, two were small-bore DMWs, six were large-bore DMWs, and there was one weld overlay sample. As already noted there were several blind trial inspection sequences conducted based on test assembly availability. For use in the Quick-Blind tests, four large-bore DMW test block segments were provided. Three of these test blocks contained laboratory-grown axially oriented stress corrosion crack flaws and the fourth test block was blank. The other assemblies contained weld solidification cracks and repairs. The techniques employed were able to be classified as conventional UT, phased-array UT (PAUT), TOFD, or eddy current testing (ECT). Since these are all techniques that are commercially available and the examiners have been qualified within their respective countries to inspect NPPs, the trials represent current field practice and quality of ISI. In summary there were a total of 20 procedures applied by 14 inspection teams. The bulk of the inspections were conducted on the small-bore and large-bore DMW test assemblies providing 421 flaw observations with 124 of these for axial flaws, 271 for circumferential flaws and 26 for volumetric flaws.

H.4.3 Result of PARENT

As already noted, since this paper is comparing the results and trends from PISC and PINC with those from PARENT, only the blind trials on the small-bore and large-bore DMWs will be overviewed in this section. There is substantial data available but when it is broken down to

address specific performance issues for four different inspection techniques (UT, PAUT, TOFD and ECT), inspection frequencies, inspection angles, crack location, crack orientation, manual inspection, encoded inspection, inside surface versus outside surface for inspection etc. it is challenging to address the measurement uncertainties to make definitive conclusions. But it needs to be noted that this is the same issue all RRTs have to deal with. The following are global numbers obtained by collapsing all data into the four generic categories. The first is looking at the data for all flaw types and orientations in Table H.7.

Table H.7 Summary of PARENT Probability of Detection as a Function of Flaw Depth in DMW Test Assemblies for Some Procedure Families

Procedure Families	POD for Flaw Depth of			False Call Rate
	5 mm	10 mm	15 mm	
Eddy Current	0,22	0,72	0,96	0,03
UT	0,15	0,31	0,67	0,07
PAUT	0,23	0,58	0,87	0,06
UT + ECT	0,15	0,30	0,50	0,07
UT + PAUT	0,55	0,98	1,00	0,03
UT + TOFD	0,37	0,90	0,99	0,04
UT + TOFD + ECT	0,21	0,46	0,74	0,08

Additional data analysis of the PARENT database is in progress and this work needs to be completed in order to understand further insights into what can be learned from this RRT.

H.5 Results from ISI at NPPs

H.5.1 Background

Cracking observed in the early 1990s in reactor components in France and other countries was attributed to PWSCC, leading to replacement of reactor vessel heads, piping, etc. The problem resurfaced in 2000 when, at the Oconee plant in the United States, leakage was discovered from a control rod drive mechanism (CRDM) penetration fabricated using Alloy 600, resulting in deposits of boric-acid crystals on the vessel head. Further investigation led to the identification of PWSCC cracks in the reactor penetration tubes and attachment J-groove welds. Circumferential cracking of CRDM nozzles has been identified at Oconee Units 2 and 3 and Crystal River Unit 3. An extreme consequence of such cracking was illustrated by the discovery of wastage on the Davis-Besse reactor vessel head. More recently, boric-acid deposits and NDE indications found at the South Texas Project BMI nozzles have been attributed to PWSCC.

Cracks also have been found in reactor nozzle hot leg DMWs at the V.C. Summer plant in the United States and at the Ringhals plant in Sweden, providing further evidence that PWSCC is a generic concern.

H.5.2 Experience from Sweden

In the outage of year 2000 a number of surface breaking transverse defects were detected during the ISI of dissimilar connection welds (Alloy 182) in the RC-loops at Ringhals 4 (PWR), Figure H.2. The defects were detected with an inspection system qualified for that type of welds, but the qualified inspection system did not perform as expected regarding characterization with ET and

sizing utilizing UT. One part of the problem was the defect simulation techniques used in the test specimens used for qualification of procedures, equipment and personnel. The defects in the test specimens did not give a realistic signal response for the techniques used; ET for detection/characterization and UT for sizing of longitudinal and transverse defects in Alloy 182/82 weld material.

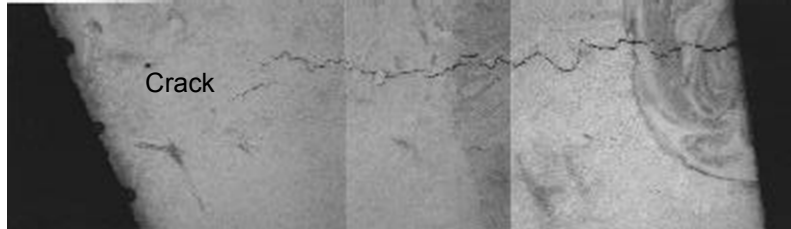


Figure H.2 Cut-out of a Typical PWSCC with a Depth of Approximately 11 mm from Ringhals

The reported height of defects from the qualified inspection system was outside the specified tolerances for 2 of the 4 defects. Detection with ET failed due to the unbroken ligaments and small crack openings at the component surface.

An attempt to summarize the main findings are made in the following conclusions.

- The cracks were, with one exception, oriented across the weld at an angle close to 90°. The exception is the V.C. Summer where a crack occurs parallel to the weld.
- In the boat sample from Ringhals 4 and Barsebäck 1, IDSCC appear in the weld metal, primarily consisting of Alloy 182. The V.C. Summer PWSCC occurred in weld metal with the essential element being Alloy 82. It was not possible to determine if the crack was initiated in weld metal/Alloy 82 or buttering/Alloy 182.
- The cracks in the Ringhals 4 and V.C. Summer DMWs occurred as a result of internal welding repairs. Three of the cracks in the Barsebäck 1 occurred in welding repairs while information is missing for the other two crack locations.
- An unusual feature of PWSCC/IDSCC is that crack width decreases in an area near the intersection of the crack with the component surface. Simulated cracks have given a relevant signal response with crack widths of approximately 10–35 micrometre. For other crack types, the crack width will typically increase at the intersection of the crack with the component surface.
- Result of further investigations showed that some defect parameters must be taken into account when simulating PWSCC/IDSCC in test assemblies that have to be used in qualification activities, see Table H.8 (SQC 2003).

Table H.8 Sizes of Defect Parameters that have to be Taken into Account to Get a Relevant Signal Response of PWSCC

Defect parameter	Parameter Values to be Simulated in Test Assemblies, which gives Relevant Signal Response on UT and ECT	
	UT	ECT
Defect width at the surface	10–35 μm	10–35 μm
Unbroken ligaments at the surface	Length = 1–4 mm; Depth = 0.6–2 mm	Length = 1–4 mm Depth = 0.6–2 mm
Defect width in depth	Min/max value > 5 μm –0.287 mm Average value 0.025–0.060 mm	-
Unbroken ligaments in depth	Number: 4–17 Size: 0.14–0.80 mm	Number: 2–9 Size: 0.14–0.80 mm
Crack shape in depth	Winding	Winding
Crack shape in length	-	Winding
Crack tip radius	7–40 μm	-
Crack roughness	$R_z = 187\text{--}471 \mu\text{m}$	-
Branching	0.25–0.60 /mm	-

H.5.3 Experience from United States

In the USA there have been a number of events related to PWSCC in DMWs (Grimmel 2005). A recent report by Sullivan and Anderson (2014) examined the management of PWSCC in butt welds by mitigation and inspection. The report provides details and extensive references for these events in the USA as well as those that have been reported worldwide. The reader is directed to the US NRC website where this report can be downloaded (<http://www.nrc.gov/reading-rm/doc-collections/nuregs/contract/cr7187/>). The intent in this paper is to just highlight some of the salient features of these events that are relevant. The events in the USA began in 1993 at Palisades with PWSCC in the heat-affected zone of a power-operated relief valve Alloy 600 safe-end located near the pressurizer. The most recent event occurred at the North Anna Power Station, Unit 1 in the "B" reactor coolant loop hot-leg-to-steam generator nozzle weld in 2012.

There have been 17 events reported for butt weld PWSCC from 1993 through 2012. It is interesting to note that nearly one-half of these events involved PWSCC that had circumferential flaw orientation. Only one of these circumferential cracks had significant depth that was estimated to be 65% through wall in one location. The axial flaws were typically deeper in through-wall extent than the circumferential flaws. Furthermore, a number of these PWSCC were discovered by non-NDE methods such as, water on the floor, accumulated boric-acid deposits or leakage uncovered when the mitigation was being applied. This has raised some important questions about the effectiveness of the NDE being applied to detect PWSCC in DMWs and was one of the driving forces for the PINC and the PARENT programs. Since many of these examinations were conducted under the requirements of ASME Code, Section XI, Division 1, Appendix VIII, questions for why the PWSCC have been missed remain. Many factors such as the NDE methods and technology being employed and the representativeness of the simulated PWSCC and component configurations in the Appendix VIII testing are being assessed to try to understand where improvements need to be made. The PINC and PARENT program results will hopefully, answer some of these questions and provide direction on what needs to be done so that there will be fewer events in U.S. NPPs. Thus, in the future NDE will find these conditions before leakage occurs and in a timely manner so that appropriate mitigation can be deployed.

H.6 Conclusion and Lessons Learned

The conclusions from PISC III Action 3 was that this action clearly confirmed that the examination of safe-end weldment provides some of the most difficult and challenging NDE problems to reliably inspect pressurized DMW piping circuit configurations. The effectiveness of focused probe techniques was also apparent. Most difficulties were found with flaws which lay in and especially those neighboring alongside the weld materials and safe-end fusion line. Detection of reflectors smaller than 2 mm, about 5% of wall thickness, lies beyond the reach of the inspection technology available at that time. An overall result of flaw detection, FCR and standard deviation in sizing, shows a better result in scanning from I.D. than from O.D. A combination of different techniques shows a better result in classification and sizing than the use of a single technique. Procedures from all assemblies characterized by the use of focusing probes with automatic scanner from I.D. and with a reporting at noise level was the best combination. The most frequent trend was that shallow flaws were oversized and large flaws were undersized. In general it was the same result for height sizing for PISC Type A slots and height sizing for welding flaws.

The results also clearly indicate that Performance Demonstrations and Qualification tests for each industrial application are desirable to check that satisfactory effectiveness can be achieved.

- The PINC study focused on efforts to characterize PWSCC and the NDE responses that real service-induced PWSCC have. This guidance was then reflected in the selection of the methods to introduce simulated and realistic PWSCC in the PINC test assemblies. The conclusions that were drawn from PINC for piping DMWs and summarized below were extracted from Cumblidge et al. (2010). Eddy current inspections from the cracked surface demonstrated the highest POD for all flaws in the DMW test assemblies.
- The POD results for the DMW round robin show significant variability in detection performance based upon the technique, procedure and inspection team.
- None of the NDE techniques in PINC demonstrated the capability to accurately depth-size flaws in DMWs to the requirements specified in ASME Code, Section XI, Division 1, Appendix VIII. The average depth sizing for all techniques in PINC tended to slightly undersize the flaws and had standard deviations and RSMEs of approximately 7 mm.
- Eight teams length-sized flaws with an RMSE within the ASME Code, Section XI, Division 1, Appendix VIII requirement of 0.75 inch (19 mm). Teams that used PAUT and ECT achieved higher accuracy than teams using conventional UT and potential-drop techniques.
- The surface conditions, access to both sides of the weld, and inspection conditions for the PINC test assemblies provided the inspectors with less challenging conditions than would be inspected in field inspections of NPP components. Thus, the results in PINC should be considered upper bounds for the inspection techniques.
- The inspection procedures and inspection teams participating in PINC with formal qualifications tended to have higher POD values and lower FCRs than the teams and procedures with no formal qualifications.

The PARENT study was conducted as a second phase of the studies initiated under the PINC trials while taking advantage of the lessons learned from PINC. The PARENT test assemblies contained smaller (both depth and length) simulated PWSCC than what was used in the PINC assemblies. Thus, PARENT trials were more challenging for the inspection procedure and teams participating in PARENT. The majority of the results from PINC were confirmed by the PARENT

RRT results. One of the significant differences with PARENT was that there were many more - procedures that combined a variety of techniques. This was important to gain insights to the effectiveness of these combinations but because of this diversity, the data was limited in achieving small confidence bounds on performance. All of the conclusions summarized above for PINC were supported by the PARENT results. However there are some differences in that procedures which employed multiple techniques tended to perform better (higher POD or small sizing RMSE values). Complete analysis of all of the PARENT data needs to be completed to fully quantify all performance data and to provide insights to what conclusions can be drawn from the data.

There are differences between the types, number, orientation and sizes of simulated cracks in PARENT, PINC and PISC test assemblies. This means that the comparisons between these three studies must proceed cautiously to insure that one is making a fair and defensible comparison along with drawing accurate conclusions. PARENT included smaller flaws than the smallest in PINC (both depth and length) and the largest flaws in both depth and length were also in the PINC flaws. However, having stated this there are some observations that can be made at this time. There appears to be higher POD performance for the ECT and conventional UT for PINC which is probably what should be expected for larger flaws. On the other hand the PAUT performance improved for PARENT flaws versus that found in PINC. PAUT is a more commonly used NDE technique today than during PINC, and many advances and insights are being gained as it evolves. In contrast at the time of PISC III Action No. 3, the dominate inspection methods were conventional UT at different sensitivity thresholds with by far the most effective being working down to the noise level of the materials being inspected. There were also significant differences in the flaw types used in PISC III since at that time PWSCC/IDSCC had not occurred and thus only tight fatigue type cracks were employed.

H.7 Recommendations for Future Activities

One of the significant differences between PISC III Action 3 and the PINC and PARENT trials is that there was considerable experience with PWSCC at the time of PINC and PARENT and that got reflected in how the simulated PWSCC were created in the test assemblies as well as their NDE response properties. Most of the inspection techniques (except for immersion focused probes) employed amplitude response criteria in the PISC III Action 3 studies while these later studies focused on advanced methods such as PAUT. Thus, there are significant differences between these studies and this makes it challenging to draw definitive conclusions. However, there are a number of conclusions that all three studies support:

- The use of a diversity of techniques tended to improve performance for detection, depth sizing and length sizing.
- The advances in the use and deployment of PAUT are significant and procedures including this technology tended to perform better than those relying on conventional UT using one or only a few inspection angles.
- Having access to the surface from which PWSCC initiates for complex DMW configurations, is preferred. Some techniques such as ECT require this access.
- There was a wide variety of scatter in the performance data; thus, all three studies recommend the need for procedure, equipment and personnel qualification.
- DMWs are very complex because of geometry and metallurgy, making them one of the most challenging NPP components that need to be reliably inspected during ISI.

- Length sizing accuracy appears to support the needed level of performance required by current code and standards particularly when the PWSCC initiation surface is available for inspection.
- All three RRT represent an upper bound of performance since many factors of the test assemblies and test environment do not reflect the challenges associated with field conditions.
- All three RRTs support using correct flaw simulation techniques in test assemblies as important to get a realistic signal response compared with real PWSCC/IDSCC.

These conclusions support that improvements are occurring in procedures, equipment and personnel conducting ISI on NPP DMW components. They all conclude that DMWs are very challenging to inspect and that qualified procedures, equipment and personnel need to be employed for ISI. However, in examining the data, it is clear that a very wide range of techniques are being pursued which leads to large uncertainty in the quantitative performance values being measured since there is limited data about each technique and no ability to collapse data across multiple teams basically using very similar techniques. One recommendation for future work would be to select some of the best procedures and conduct much more extensive laboratory testing, modeling and blind assessment to provide more definitive data with small measurement uncertainty on the “true” performance capability of them to reliably inspect DMWs. This work needs to be conducted using realistic PWSCC with NDE responses reflecting the properties of service degradation. Future work should be conducted to evaluate methods to make these realistic defects in a cost effective manner to enhance training and refining the evolution of techniques to improve detection, characterization and sizing.

Efforts should continue to accumulate NDE response data on PWSCC as it occurs in-service to augment existing databases, to provide more input to PWSCC simulation methods and to insure that future studies are using the “best” flaw simulations known.

H.8 References

Braatz BG, PG Heasler and RM Meyer. 2014. *PARENT Quick Blind Round-Robin Test Report*. PNNL-22677, Pacific Northwest National Laboratory, Richland, Washington. ADAMS Accession No. ML14276A052.

Cumblidge SE, SR Doctor, PG Heasler and TT Taylor. 2010. *Results of the Program for the Inspection of Nickel Alloy Components*. NUREG/CR-7019; PNNL-18713, Rev. 1, U.S. Nuclear Regulatory Commission, Washington, D.C.

European Commission. 1994. *Non-Destructive Examination Practice and Results, State of the Art and PISC III Results, Proceedings of the Joint CEC OECD IAEA Specialists Meeting, March 8–10, 1994*. Report No. EUR 15906 EN, NEA/CSN/R(94)/23, Commission of the European Communities, Luxembourg, Petten, The Netherlands.

Dombret P. 1995. "PISC III Results on Action 3 'Nozzles and Dissimilar Welds'." In *Non-destructive Examination Practice and Results; State of the Art and PISC III Results, Proceedings of the Joint CEC OECD IAEA Specialists Meeting*, pp. 11-31. March 8-10, 1994, Petten, The Netherlands. Commission of the European Communities, Luxembourg.

Grimmel B. 2005. *U.S. Plant Experience with Alloy 600 Cracking and Boric Acid Corrosion of Light-Water Reactor Pressure Vessel Materials*. NUREG-1823, U.S. Nuclear Regulatory Commission, Washington, D.C.

PISC. 1993a. Evaluation of the Inspection Results of the PISC III Safe-end Assembly No. 20, Safe-ends Nos. 21 and 22. PISC III Report No. 20, EUR 15558 EN, Commission of the European Communities, Joint Research Centre, Ispra Site.

PISC. 1993b. Evaluation of the Inspection Results of the Safe-end Areas of the PISC III Assembly No. 24. PISC III Report No. 24, EUR 15369 EN, Commission of the European Communities, Joint Research Centre, Ispra Site.

PISC. 1993c. Evaluation of the Inspection Results of the PISC III Safe-end Assembly No. 25. PISC III Report No. 25, EUR 15370 EN, Commission of the European Communities, Joint Research Centre, Ispra Site.

SQC. 2003. Project PostDAS - Final Report, Test Specimen Report. Report Nr RAPP0115/03A, Swedish Qualification Center (SQC), Stockholm, Sweden.

Sullivan EJ and MT Anderson. 2014. *Managing PWSCC in Butt Welds by Mitigation and Inspection*. NUREG/CR-7187, PNNL-23659, U.S. Nuclear Regulatory Commission, Washington, D.C.

BIBLIOGRAPHIC DATA SHEET

(See instructions on the reverse)

NUREG/CR-7235

2. TITLE AND SUBTITLE

Results of Blind Testing for the Program to Assess the Reliability of Emerging Nondestructive Techniques

3. DATE REPORT PUBLISHED

MONTH

June

YEAR

2017

4. FIN OR GRANT NUMBER

V6286

5. AUTHOR(S)

R.M. Meyer and P.G. Heasler

6. TYPE OF REPORT

Technical

7. PERIOD COVERED (Inclusive Dates)

8. PERFORMING ORGANIZATION - NAME AND ADDRESS (If NRC, provide Division, Office or Region, U. S. Nuclear Regulatory Commission, and mailing address; if contractor, provide name and mailing address.)

Pacific Northwest National Laboratory
P.O. Box 999
Richland WA 99352

9. SPONSORING ORGANIZATION - NAME AND ADDRESS (If NRC, type "Same as above", if contractor, provide NRC Division, Office or Region, U. S. Nuclear Regulatory Commission, and mailing address.)

Division of Engineering
Office of Nuclear Regulatory Research
U.S. Nuclear Regulatory Commission
Washington, DC 20555-0001

10. SUPPLEMENTARY NOTES

11. ABSTRACT (200 words or less)

The U.S. Nuclear Regulatory Commission (NRC) conducted agreements with organizations in Finland, Japan, South Korea, Sweden and Switzerland to establish the Program to Assess the Reliability of Emerging Nondestructive Techniques (PARENT) whose goal was to investigate the performance of current and emerging nondestructive examination (NDE) procedures and techniques to find flaws in nickel-alloy welds and base materials. This was performed by conducting a series of open and blind international round-robin tests on a set of nickel alloy piping components that included large-bore dissimilar metal welds (LBDMW), small-bore dissimilar metal welds (SBDMW), and bottom-mounted instrumentation (BMI) penetration welds. The project was divided into open and blind testing to separate the evaluation of novel techniques implemented by nonqualified teams (open testing) from the evaluation of more established techniques implemented by commercial inspection service providers (blind testing). The objective of blind testing was to obtain quantitative estimates of the performance of the latest NDE inspection techniques used commercially in the field for detection and accurate sizing of primary water stress corrosion cracks (PWSCC) or interdendritic stress corrosion cracks (IDSCC). The report documents the results of the detection and sizing analyses performed on data collected in blind testing for PARENT.

12. KEY WORDS/DESCRIPTORS (List words or phrases that will assist researchers in locating the report.)

Nondestructive Examination, Stress Corrosion Cracking, Dissimilar Metal Welds, Ultrasonic Testing, Probability of Detection

13. AVAILABILITY STATEMENT

unlimited

14. SECURITY CLASSIFICATION

(This Page)

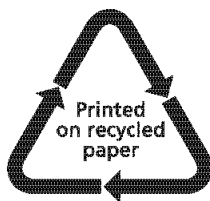
unclassified

(This Report)

unclassified

15. NUMBER OF PAGES

16. PRICE



Federal Recycling Program



UNITED STATES
NUCLEAR REGULATORY COMMISSION
WASHINGTON, DC 20555-0001

OFFICIAL BUSINESS



NUREG/CR-7235

**Results of Blind Testing for the Program to Assess the
Reliability of Emerging Nondestructive Techniques**

June 2017